EMERGING INFECTIOUS DISEASES®

Vectors

February 2024

Karl Bitter (1867–1915), *Spirit of Transportation* (1895) relief sculpture. William H. Gray III 30th Street Station (moved from Broad Street Station), Philadelphia, Pennsylvania, United States. Craig Jack Photographic/Almay Stock Photo.

EMERGING INFECTIOUS DISEASES®

Emerging Infectious Diseases is published monthly by the Centers for Disease Control and Prevention, 1600 Clifton Rd NE, Mailstop H16-2, Atlanta, GA 30329-4018, USA. Telephone 404-639-1960; email, eideditor@cdc.gov

EMERGING INFECTIOUS DISEASES®

Vectors

February 2024

On the Cover

Karl Bitter (1867–1915), Spirit of Transportation (1895) relief sculpture. William H. Gray III 30th Street Station (moved from Broad Street Station), Philadelphia, Pennsylvania, United States. Craig Jack Photographic/Almay Stock Photo

About the Cover p. 406

Synopses

Medscape EDUCATION ACTIVITY

Research

EMERGING INFECTIOUS DISEASES®
February 2024

Medscape EDUCATION ACTIVITY

Dispatches

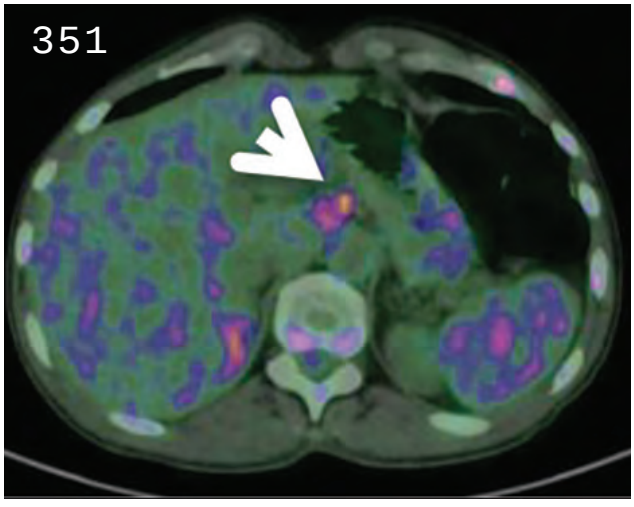

EMERGING INFECTIOUS DISEASES®
February 2024

Research Letters

Comment Letters

Book Review

About the Cover

Online Report

Etymologia

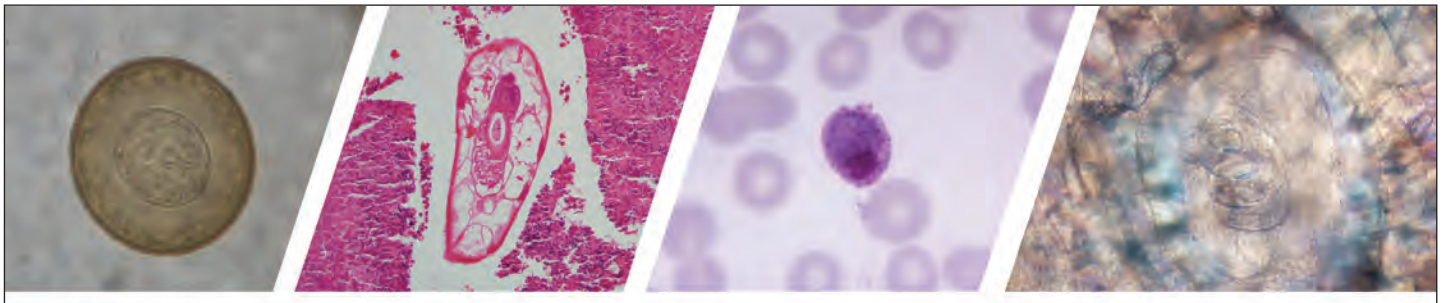

DPDx

Diagnostic Assistance and Training in Laboratory Identification of Parasites

A free service of CDC available to laboratorians, pathologists, and other health professionals in the United States and abroad

- Diagnosis from photographs of worms, histological sections, fecal, blood, and other specimen types
- Expert diagnostic review
- Formal diagnostic laboratory report
- Submission of samples via secure file share

Visit the DPDx website for information on laboratory diagnosis, geographic distribution, clinical features, parasite life cycles, and training via Monthly Case Studies of parasitic diseases.

www.cdc.gov/dpdx
dpdx@cdc.gov

U.S. Department of Health and Human Services
Centers for Disease Control and Prevention

CS272346-DE

Multicenter Retrospective Study of Invasive Fusariosis in Intensive Care Units, France

Jordane Demonchy, Lucie Biard, Raphaël Clere-Jehl, Florent Wallet, Djamel Mokart, Anne-Sophie Moreau, Laurent Argaud, Camille Verlhac, Frédéric Pène, Alexandre Lautrette, Naïke Bige, Audrey de Jong, Emmanuel Canet, Jean-Pierre Quenot, Nahéma Issa, Yoann Zerbib, Inès Bouard, Muriel Picard, Lara Zafrani

In support of improving patient care, this activity has been planned and implemented by Medscape, LLC and Emerging Infectious Diseases. Medscape, LLC is jointly accredited with commendation by the Accreditation Council for Continuing Medical Education (ACCME), the Accreditation Council for Pharmacy Education (ACPE), and the American Nurses Credentialing Center (ANCC), to provide continuing education for the healthcare team.

Medscape, LLC designates this Journal-based CME activity for a maximum of 1.00 ***AMA PRA Category 1 Credit(s)™***. Physicians should claim only the credit commensurate with the extent of their participation in the activity.

Successful completion of this CME activity, which includes participation in the evaluation component, enables the participant to earn up to 1.0 MOC points in the American Board of Internal Medicine's (ABIM) Maintenance of Certification (MOC) program. Participants will earn MOC points equivalent to the amount of CME credits claimed for the activity. It is the CME activity provider's responsibility to submit participant completion information to ACCME for the purpose of granting ABIM MOC credit.

All other clinicians completing this activity will be issued a certificate of participation. To participate in this journal CME activity: (1) review the learning objectives and author disclosures; (2) study the education content; (3) take the post-test with a 75% minimum passing score and complete the evaluation at http://www.medscape.org/journal/eid; and (4) view/print certificate. For CME questions, see page 410.

NOTE: It is Medscape's policy to avoid the use of brand names in accredited activities. However, in an effort to be as clear as possible, the use of brand names should not be viewed as a promotion of any brand or as an endorsement by Medscape of specific products.

Release date: January 22, 2024; Expiration date: January 22, 2025

Learning Objectives

Upon completion of this activity, participants will be able to:

- Assess clinical risk factors for invasive fusariosis (IF) in the current study.
- Evaluate the rate of complications of IF in the current study.
- Identify methods for mycological diagnosis.
- Analyze risk factors for mortality associated with IF in the current study.

CME Editor

Amy J. Guinn, BA, MA, Technical Writer/Editor, Emerging Infectious Diseases. *Disclosure: Amy J. Guinn, BA, MA, has no relevant financial relationships.*

CME Author

Charles P. Vega, MD, Health Sciences Clinical Professor of Family Medicine, University of California, Irvine School of Medicine, Irvine, California. *Disclosure: Charles P. Vega, MD, has the following relevant financial relationships: served as consultant or advisor for Boehringer Ingelheim; GlaxoSmithKline.*

Authors

Jordane Demonchy, MD; Lucie Biard, MD, PhD; Raphaël Clere-Jehl, MD; Florent Walle, MD; Djamel Mokart, MD, PhD; Anne-Sophie Moreau, MD; Laurent Argaud, MD, PhD; Camille Verlhac, MD; Frédéric Pène MD, PhD; Alexandre Lautrette, MD, PhD; Naïke Bige, MD, PhD; Audrey de Jong, MD, PhD; Emmanuel Canet, MD, PhD; Jean-Pierre Quenot, MD, PhD; Nahéma Issa, MD; Yoann Zerbib, MD; Inès Bouard, MS; Muriel Picard, MD; Lara Zafrani, MD, PhD.

Invasive fusariosis can be life-threatening, especially in immunocompromised patients who require intensive care unit (ICU) admission. We conducted a multicenter retrospective study to describe clinical and biologic characteristics, patient outcomes, and factors associated with death and response to antifungal therapy. We identified 55 patients with invasive fusariosis from 16 ICUs in France during 2002–2020. The mortality rate was high (56%). Fusariosis-related pneumonia occurred in 76% of patients, often leading to acute respiratory failure. Factors associated with death included elevated sequential organ failure assessment score at ICU admission or history of allogeneic hematopoietic stem cell transplantation or hematologic malignancies. Neither voriconazole treatment nor disseminated fusariosis were strongly associated with response to therapy. Invasive fusariosis can lead to multiorgan failure and is associated with high mortality rates in ICUs. Clinicians should closely monitor ICU patients with a history of hematologic malignancies or stem cell transplantation because of higher risk for death.

Invasive fungal infections are common, and severe complications can occur in immunocompromised patients, especially in patients with hematologic malignancies who require intensive care unit (ICU) admission (*1*,*2*). Invasive fusariosis is a mycosis caused by infection with *Fusarium* spp. (*3*). *Fusarium* are ubiquitous filamentous fungi that can cause a range of infections, from localized lesions due to penetrating trauma in healthy persons, to acute invasive or disseminated infection in immunocompromised patients (*3*–*6*). Most frequent clinical manifestations of invasive fusariosis are fever refractory to antimicrobial drugs, pneumonia, metastatic skin lesions of a disseminated infection, and sinusitis (*3*,*4*,*6*).

The European Organization for Research and Treatment of Cancer/Invasive Fungal Infections Cooperative Group and the US National Institute of Allergy and Infectious Diseases Mycoses Study Group (EORTC/MSG) published definitions for proven and probable invasive fusariosis in immunocompromised patients (*7*). Although proven infection requires microscopic analysis or culture of a sterile material, probable infection is based on host factors, clinical features, and mycologic criteria (Appendix Table 1, https://wwwnc.cdc.gov/EID/article/30/2/23-1221-App1.pdf). Despite progress in managing invasive fungal infections in recent decades, including the widespread use of antifungal prophylaxis in immunocompromised patients and improved treatment strategies, invasive fusariosis remains a serious and potentially life-threatening infection. Invasive fusariosis can lead to severe organ failure and has been associated with mortality rates ranging from 40% to 70% (*8*–*11*). Even when amphotericin B and voriconazole are the first drugs of choice, sometimes in combination, the best antifungal treatment remains unclear (*12*).

Data focusing on fusariosis rely mainly on case reports (*13*–*15*), studies based on selected populations (*9*–*11*,*16*,*17*), or epidemiologic studies (*18*,*19*). None of those studies focused on critically ill patients with invasive fusariosis. We conducted a multicenter retrospective study to describe the characteristics and outcomes of invasive fusariosis in ICU patients in France and to identify the main risk factors associated with death and response to therapy.

Methods

Ethics

This observational study was based on anonymized hospitalization reports and was in strict compliance with the reference methodology MR-004 of France. The study was approved by the data protection authority, Commission Nationale de l'Informatique et des Libertés (registration no. 2220799v0), and received a favorable opinion from the Comité Ethique de la Société de Réanimation de Langue Française institutional review board (approval no. 20–95). The study was conducted in accordance with principles of the Declaration of Helsinki (World Medical Association, https://www.wma.net).

Study Population

We retrospectively included in the study adult ICU patients with a diagnosis of invasive fusariosis during

Author affiliations: Centre Hospitalier Universitaire de Lille, Lille, France (J. Demonchy, A.-S. Moreau); Institut national de la santé et de la recherche médicale (INSERM), University of Paris Cité, Paris, France (J. Demonchy, L. Zafrani); Hôpital Saint-Louis, Paris (L. Biard, I. Bouard, L. Zafrani); Centre Hospitalier Universitaire de Strasbourg, Strasbourg, France (R. Clere-Jehl); Centre Hospitalier Universitaire de Lyon, Lyon, France (F. Wallet, L. Argaud); Institut Paoli-Calmettes, Marseille, France (D. Mokart); Centre Hospitalier Universitaire de Clermont-Ferrand, Clermont-Ferrand, France (C. Verlhac, A. Lautrette); Hôpital Cochin, Paris (F. Pène); Hôpital Saint-Antoine, Paris (N. Bige); Montpellier University, INSERM, and St-Eloi Hospital, Montpellier, France (A. de Jong); Centre Hospitalier Universitaire de Nantes, Nantes, France (E. Canet); Centre Hospitalier Universitaire de Dijon Bourgogne, Dijon, France (J.-P. Quenot); Centre Hospitalier Universitaire de Bordeaux, Bordeaux, France (N. Issa); Centre Hospitalier Universitaire de Amiens-Picardie, Amiens, France (Y. Zerbib); Centre Hospitalier Universitaire de Toulouse, Toulouse, France (M. Picard)

DOI: https://doi.org/10.3201/eid3002.231221

January 1, 2002–December 31, 2020. We used a modified EORTC/MSG criteria to determine diagnosis of proven or probable invasive fusariosis (*7*) (Appendix Table 1). We identified patients by reviewing medical records, microbiologic databases, or both. To identify patients eligible for our study, we conducted a comprehensive screening of all ICUs and parasitology and mycology departments in France from which *Fusarium* species had been identified. Of 47 screened ICUs, only 16 had patients with a positive *Fusarium* microbiologic documentation during the inclusion period. We assessed a total of 120 patients for eligibility. We excluded 53 patients with *Fusarium* colonization and ultimately included 55 patients in the study (Figure 1).

We collected data from anonymized hospitalization reports, including information on patient age, sex, underlying disease conditions, history of immunodeficiency, clinical and microbiologic characteristics of the *Fusarium* infection, any co-infections, antifungal treatment, need for organ support, and outcomes. For each patient, simplified acute physiology score (SAPS II) and sequential organ failure assessment (SOFA) scores were collected at admission, as previously defined (*20*,*21*). For response to therapy, we defined progression as clinical deterioration or death after antifungal treatment. We considered response complete if clinical improvement occurred, biological samples became sterile, and computed tomography (CT) features cleared. When all the complete response criteria were not met, we considered response to therapy to be partial.

Outcomes

Our primary objective was to identify factors associated with ICU mortality rates. Our secondary objective was to identify factors associated with response to therapy.

Statistical Analyses

We reported continuous variables as medians and interquartile ranges (IQRs) and categorical variables as numbers and percentages. We considered response to treatment, death in the ICU, death in the hospital, and death within 1 year as binary endpoints for the main analysis. We compared continuous variables by using Wilcoxon rank-sum test and compared categorical variables by using Fisher exact test. We performed adjusted analyses to evaluate factors associated with treatment response and death by using multivariable logistic regression models. We estimated cumulative incidence of death in the ICU by using standard methods for competing events and considered discharged alive as a competing outcome to ICU death.

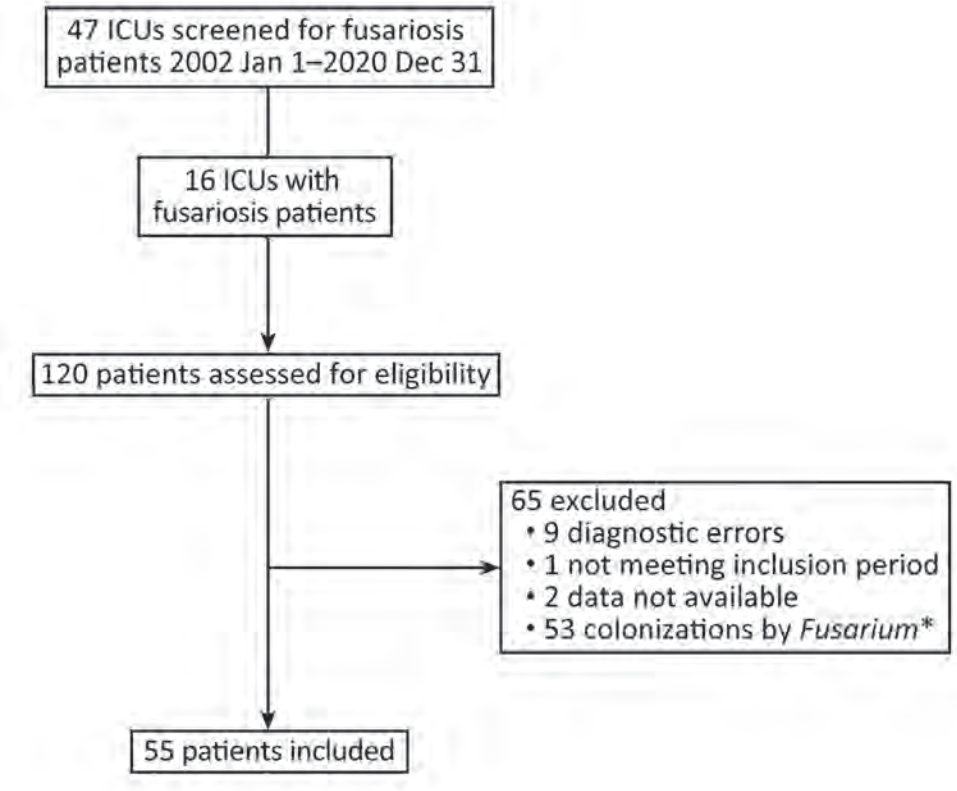

Figure 1. Flowchart for patient inclusion in a multicenter retrospective study of invasive fusariosis in ICUs, France. *Colonization by *Fusarium* defined as patient not meeting the European Organization for Research and Treatment of Cancer/Invasive Fungal Infections Cooperative Group or National Institute of Allergy and Infectious Diseases Mycoses Study Group criteria for proven or probable invasive fungal diseases (*7*). ICU, intensive care unit.

We performed all tests 2-sided at the 5% significance level. We performed all analyses on the R statistical platform (The R Foundation for Statistical Computing, https://www.r-project.org).

Results

Patient Characteristics

We identified 55 patients with invasive fusariosis in 16 ICUs during the inclusion period (Table 1). The median age was 61 (IQR 52–67) years; 80% (n = 44) were immunocompromised, most (n = 32) of whom had active hematologic malignancies (36%, n = 16) or underwent a recent (<1 year) allogeneic hematopoietic stem cell transplantation (allo-HSCT) (36%, n = 16). Eleven (25%) immunocompromised patients had a medical history of solid organ transplantation. Of 11 (20%) immunocompetent patients, all had invasive fusariosis diagnosed during a prolonged (>2 weeks) ICU hospitalization, including hospitalization for septic shock (n = 7), acute respiratory distress syndrome (n = 2), and multiple traumatic injuries (n = 2). Only 24% (n = 13) of patients had an antifungal prophylaxis at ICU admission. Patients admitted to the ICU had severe illness as indicated by elevated median SAPS II and SOFA scores.

Table 1. Clinical and biologic characteristics among 55 patients in a multicenter retrospective study of invasive fusariosis in intensive care units, France*

Characteristics	Value
Median age, y (IQR)	61 (52–67)
Sex	
M	39 (71)
F	26 (29)
Immunocompromise type	44 (80)
Hematologic malignancy	16 (36)
Allo-HSCT	16 (36)
Solid organ transplant	11 (20)
Kidney transplant	2 (18)
Liver transplant	4 (36)
Kidney-liver transplant	1 (9)
Lung transplant	3 (27)
Heart transplant	1 (9)
Rheumatoid arthritis with corticosteroids	1 (2)
Diabetes mellitus	10 (18)
Immunosuppressive agents	
Corticosteroids >3 weeks	12 (22)
Other immunosuppressive therapy	22 (40)
Chemotherapy <3 mo	21 (38)
Biologic data	
Neutropenia, neutrophil <0.5 G/L	22 (40)
Lymphopenia, lymphocytes <1 G/L	47 (85)
Hypoalbuminemia, albumin <35 g/L	48 (87)
Antifungal prophylaxis	13 (24)
Posaconazole	9 (16)
Voriconazole	2 (4)
Fluconazole	2 (4)
Performance status at admission	
>2	30 (55)
≤2	25 (45)
Median prognostic scores at admission (IQR)	
SAPS II	54 (40–65)
SOFA at admission	9 (6–13)

*Values are no. (%) except as indicated. Allo-HSCT, allogeneic hematopoietic stem cell transplantation; IQR, interquartile range; SAPS II, simplified acute physiology score II; SOFA, sequential organ failure assessment.

Table 2. Organ failure and outcomes among 55 patients in a multicenter retrospective study of invasive fusariosis in intensive care units, France*

Characteristics	Value
Invasive mechanical ventilation†	44 (80)
Median days (IQR)	16 (9–39)
Noninvasive ventilation	18 (33)
High flow nasal oxygen therapy	11 (20)
Prone position	5 (9)
Neuromuscular blockers	13 (24)
Nasal oxygenotherapy	49 (89)
Vasopressors	38 (69)
Acute kidney injury	40 (73)
Renal-replacement therapy	29 (53)
Acute liver failure	18 (33)
Median length of stay, d (IQR)	17 (6–37)
Death in ICU	31 (56)

*Values are no. (%) except as indicated. IQR, interquartile range.
†With orotracheal intubation cannula or tracheotomy.

During ICU stays, acute respiratory failure was the main organ failure in patients with invasive fusariosis; 80% (n = 44) of patients required invasive mechanical ventilation (Table 2). Furthermore, acute kidney injury was observed in 73% (n = 40) of patients, among whom 29 (72.5%) required renal-replacement therapy, such as continuous venovenous hemofiltration and hemodialysis. The incidence of acute kidney injury was notably higher (100%) for the 11 patients with solid organ transplant than for the patients with hematologic malignancies (44%, n = 7), allo-HSCT (69%, n = 11), and other patients (92%, n = 11) (p = 0.003) (Appendix Table 2).

Patients experienced prolonged ICU hospitalizations; median length of stay was 17 (IQR 6–37) days, and the mortality rate was high (56%, n = 31). Of 31 ICU patients who died, 18 (58.1%) deaths were considered directly related to invasive fusariosis and 13 (41.9%) deaths were not considered directly related to invasive fusariosis. Of those 13 deaths, causes were multivisceral organ failures related to secondary infections (n = 6), severe graft versus host disease (n = 1), progression of the underlying malignancy (n = 2), hemorrhagic shock (n = 1), or withdrawal of life-sustaining treatment (n = 3). Among ICU survivors, 1 (4%) patient died in the hospital and 3 (4%) patients died within 1 year of diagnosis.

Invasive Fusariosis in ICUs

Using EORTC/MSG criteria, we classified a total of 32 (58%) cases as probable invasive fusariosis and 23

cases (42%) as proven invasive fusariosis (Table 3). Among invasive fusariosis patients, 53% of diagnoses were established after admission to the ICU; median time from ICU admission to invasive fusariosis diagnosis was 9 (IQR 1–16) days. Mycologic diagnosis was achieved through culture of various biologic samples and was guided by the patients' clinical signs and symptoms. Blood cultures (22%, n = 12) were used for cases of fever and disseminated invasive fusariosis, biopsies (29%, n = 10) were taken from skin lesions, sputum (29%, n = 16) and bronchoalveolar lavage fluid (22%, n = 12) were collected for pneumonia cases, sinus aspirate samples (5%, n = 3) were obtained for sinusitis, joint fluid (5%, n = 3) was examined for arthritis, and pancreatic fluid (2%, n = 1) collections were analyzed for suspected infection (Figure 2). Pathologic examination of skin or sinus biopsies revealed *Fusarium* associated with tissue damage in 10 (18%) patients.

Results of serum galactomannan test were available for 50 (90.9%) patients and 15 (30%) of them had a positive serum galactomannan test on the day of invasive fusariosis diagnosis. Among those patients, 4 also had concomitant aspergillosis diagnosed. Other observed co-infections included bacterial co-infection in 58% (n = 32), viral co-infection in 35% (n = 19), and fungal co-infection in 34% (n = 19) of invasive fusariosis patients (Appendix Table 3).

Pneumonia was the most prevalent clinical manifestation, accounting for 76% (n = 42) of the cases. Consistent with the EORTC/MSG criteria, the diagnosis of fungal lung disease primarily relied on thoracic CT. Among the patients, fusariosis-related pneumonia exhibited a wide range of thoracic CT patterns (Figure 3): 43% (n = 16) had pulmonary consolidations, 32% (n = 12) had nodules and micronodules, 24% (n = 9) had ground glass opacities, 16% (n = 6) had pleural effusion, and 8% (n = 3) had excavated pulmonary lesions. Moreover, the incidence of disseminated invasive fusariosis was notably higher (44%, n = 7) in patients with hematologic malignancies than in patients who had allo-HSCT (25%, n = 4) or solid organ transplants (9%, n = 1) (p = 0.03) (Appendix Table 2).

Two thirds of invasive fusariosis patients received antifungal monotherapy. The 2 primary drugs used were voriconazole (62%, n = 34) and amphotericin B (60%, n = 33). Four (7%) patients died before invasive fusariosis diagnosis and did not receive treatment. Granulocyte colony-stimulating factor was administered to 55% (n = 12) of the neutropenic patients, and surgical debridement of localized lesions was performed in 13% (n = 7) of patients. Half of the patients experienced disease progression despite receiving adequate therapy.

Table 3. Characteristics of *Fusarium* infections and co-infections in among 55 patients in a multicenter retrospective study of invasive fusariosis in intensive care units, France

Infections and co-infections	No. (%) patients
Fusariosis diagnosis	
Probable	32 (58)
Proven	23 (42)
Fusarium species	
Fusarium spp.	38 (69)
F. oxysporum	5 (9)
F. proliferatum	4 (7)
F. solani	3 (5)
F. fujikuroi	2 (4)
F. dimerum	1 (2)
F. monoliforme	1 (2)
F. keratoplasticum	1 (2)
Mycologic diagnosis	
Mycologic culture of biologic samples*	55 (100)
Pathologic examination of biopsies†	10 (18)
Positive serum galactomannan	15 (27)
Time of diagnosis from intensive care admission	
Before admission	12 (22)
Day of admission	12 (22)
After admission	29 (53)
Clinical manifestation	
Disseminated infection	12 (22)
Skin lesions	14 (25)
Pneumonia	42 (76)
Sinusitis	3 (5)
Arthritis	3 (5)
Infection of pancreatic fluid collections	1 (2)
Thoracic computed tomography patterns of pneumonia, n = 37	
Pulmonary consolidations	16 (43)
Nodules and micronodules	12 (32)
Excavated pulmonary lesions	3 (8)
Ground glass opacities	9 (24)
Pleural effusion	6 (16)
Missing data	5 (14)
Co-infections	
Bacterial	32 (58)
Viral	19 (35)
Fungal	27 (49)
Antifungal treatment‡	
Monotherapy	46 (84)
Voriconazole	23 (42)
Amphotericin B	21 (38)
Isavuconazole	1 (2)
Terbinafine	1 (2)
Combination therapy	
Voriconazole + amphotericin B	11 (20)
Isavuconazole + micafungin	1 (2)
None	4 (7)
Missing data	1 (2)
Granulocyte colony-stimulating factor	12 (22)
Surgical debridement of localized infection	7 (13)
Response to therapy	
Progression	28 (51)
Partial or complete	14 (25)
Missing data	13 (24)

*Biologic samples included blood cultures, skin biopsies, sputum, bronchoalveolar lavage fluid, sinus aspirate samples, joint fluid, and pancreatic fluid collections.
†Pathologic examination of skin or sinus biopsies in which *Fusarium* are seen and accompanied by tissue damage.
‡Some patients first received a monotherapy and then a combination of 2 drugs because of refractory disease.

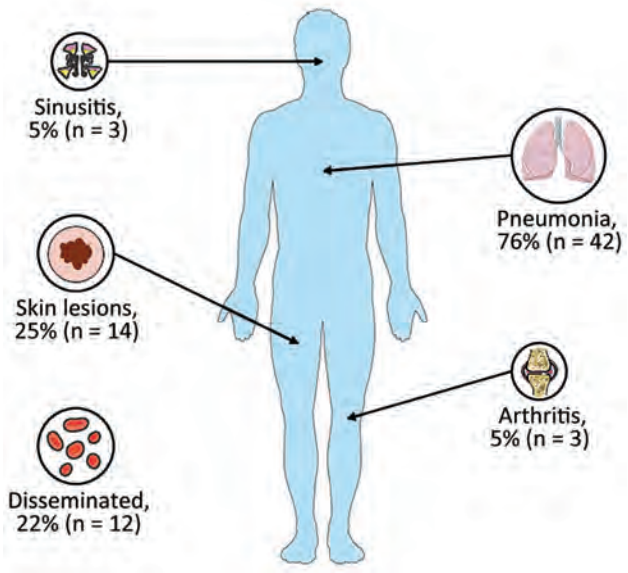

Figure 2. Main clinical manifestations among patients in a multicenter retrospective study of invasive fusariosis in intensive care units, France. The figure was partly generated using Servier Medical Art (https://smart.servier.com), licensed under a Creative Commons Attribution 3.0 unported license.

Factors Associated with Response to Therapy

Factors associated with invasive fusariosis progression under therapy in all 55 patients by univariate analysis were history of recent (<1 year) and past (>1 year) allo-HSCT (p = 0.049), corticosteroid therapy for >3 weeks (p = 0.019), a higher SOFA score at admission (p = 0.002), performance status >2 at admission (p = 0.022), and pulmonary consolidations on thoracic CT for fusariosis-related pneumonia (p = 0.001) (Appendix Table 4). Conversely, nodules and micronodules on thoracic CT were significantly associated with partial and complete response (p = 0.001). By multivariate analysis, none of the following were significantly associated with response to therapy: voriconazole treatment (odds ratio [OR] 3.55, 95% CI 0.72–17.6; p = 0.12), history of allo-HSCT (OR 0.21, 95% CI 0.036–1.24; p = 0.086), and disseminated fusariosis (OR 0.15, 95% CI 0.015–1.42; p = 0.098).

Factors Associated with Death

By univariate analysis, signs and symptoms significantly associated with death in the ICU included history of hematologic malignancies and allo-HSCT (p = 0.017), immunosuppressive therapy other than corticosteroids (p = 0.036), elevated SAPS II (p = 0.007) or SOFA (p = 0.001) score at admission, and neutropenia (neutrophils <0.5 G/L) (p = 0.05) (Appendix Table 5). Among patients with organ failure, only vasopressors were associated with death (p = 0.006). Conversely, surgical debridement of localized lesion was associated with ICU survival (p = 0.014).

By multivariate analysis, the factors associated with death in the ICU were higher SOFA score (OR 1.51, 95% CI 1.15–1.98; p = 0.003) and history of hematologic malignancy or allo-HSCT (OR 8.28, 95% CI 1.26–54.2; p = 0.027). Cumulative incidence of ICU death showed a 50% (95% CI 31.4%–66%) ICU mortality rate at 28 days for patients with hematologic malignancies or allo-HSCT compared with 26.1% (95% CI 10.3%–45.3%) for patients without hematologic malignancy and allo-HSCT (Figure 4). Multivariate analyses on factors associated with death in the hospital and within 1 year of admission were similar to the results of the analyses for factors associated with death in the ICU. Indeed, higher SOFA score was associated with death in the hospital (OR 1.50, 95% CI 1.14–1.97; p = 0.004), death within 1 year of admission (OR 1.66 95% CI 1.16–2.36; p = 0.005), history of hematologic malignancy (OR 7.87, 95% CI 1.18–52.6; p = 0.033), or allo-HSCT (OR 15.3, 95% CI 1.60–145.7; p = 0.018).

Discussion

We conducted a large retrospective study to describe the clinical characteristics and outcomes of patients

Figure 3. Thoracic computed tomography scans from patients included in a multicenter retrospective study of invasive fusariosis in intensive care units, France, showing findings of fusariosis-related pneumonia. A) Unilateral consolidations (asterisk); B) ground glass opacities (triangle); C) 7-mm nodule (arrow) and bilateral pleural effusion.

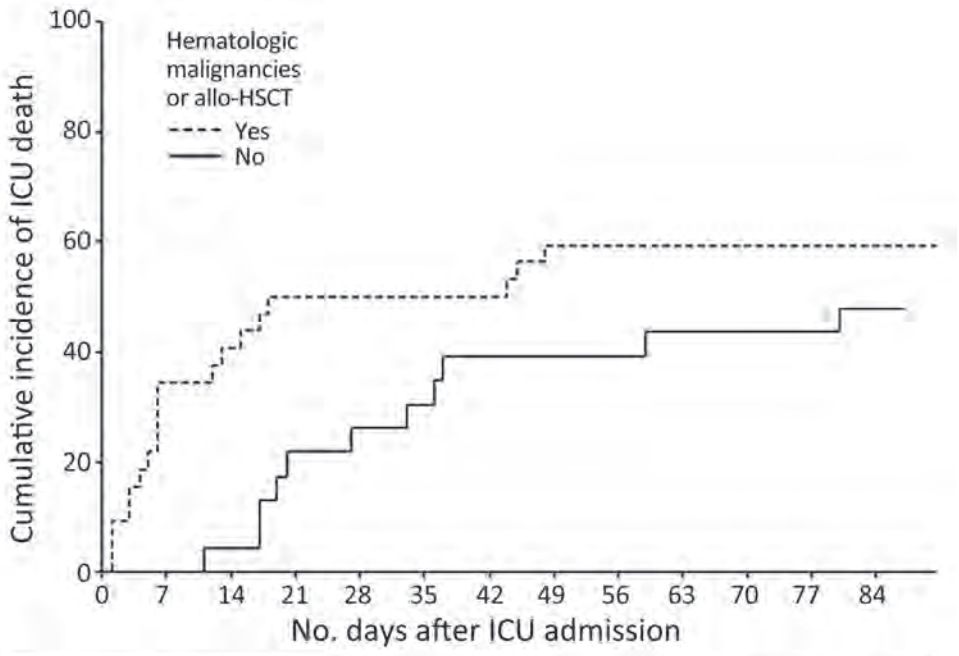

	Hematologic malignancies or allo-HSCT	No hemotologic malignancy or allo-HSCT
14 days	40.6% (95% CI 23.5%–57.1%)	4.3% (95% CI 0.3%–18.7%)
28 days	50.6% (95% CI 31.4%–66.0%)	26.1% (95% CI 10.3%–45.3%)

Figure 4. Cumulative incidence of death among patients with and without history of hematologic malignancies and allo-HSCT in a multicenter retrospective study of invasive fusariosis in ICUs, France. Calculations used Fisher exact test (p = 0.017). Chart shows 14-day and 28-day death rates. Allo-HSCT, allogeneic hematopoietic stem cell transplant; ICU, intensive care unit.

with invasive fusariosis admitted to ICUs in France. We found that invasive fusariosis can be life-threatening; often is associated with bacterial, viral, and fungal co-infections; and occurs mainly in immunocompromised patients or patients enduring extended ICU stays. Pneumonia is the prevailing clinical manifestation in ICU patients. Despite ICU hospitalization, organ support, and adequate treatment, the fusariosis mortality rate remains high. SOFA score and a history of allo-HSCT or hematologic malignancies, or both, are significantly associated with death in the ICU.

The available medical literature on invasive fusariosis remains scarce, and a paucity of studies specifically focused on invasive fusariosis in the ICU setting. The few studies dedicated to invasive fungal infections in ICU patients included <5 patients with invasive fusariosis (*2*,*22*). Our study provides a comprehensive description of clinical, biologic, and microbiologic characteristics of critically ill invasive fusariosis patients.

Previous studies indicate that most invasive fusariosis patients have immunocompromising conditions, including hematologic malignancies, recent allo-HSCT, or solid organ transplantation (*9*,*11*,*17*,*19*,*23*). However, we found that one fifth of patients with invasive fusariosis in the ICU are considered immunocompetent at ICU admission but experienced a prolonged ICU hospitalization, mainly because of septic shock. That finding supports the concept of sepsis-induced immunosuppression, wherein an imbalanced inflammatory state contributes to immunoparalysis and increases the risk for nosocomial infections (*24*). Therefore, physicians should investigate the possibility of invasive fusariosis in patients with prolonged ICU hospitalization, especially in cases of a secondary sepsis unresponsive to antimicrobial agents and clinical manifestations consistent with invasive fusariosis.

The clinical manifestations we observed in our cohort align with those from previous reports (*3*,*4*,*6*). However, a notable finding in our study was identification of *Fusarium* in mycologic culture (semiquantitative results showing numerous *Fusarium* colonies) from pancreatic fluid collected in a case of suspected infection from a site that has not been previously described. That novel observation highlights the importance of considering *Fusarium* as a potential pathogen in unusual infection sites and expands our understanding of clinical manifestations

of fusariosis. In addition, our study revealed a lower prevalence of disseminated infection, affecting only one fifth of patients, in contrast to reports from previous publications focusing on non-ICU patients (*8*,*11*,*17*). However, patients with hematologic malignancies in our study exhibited much higher rates of disseminated infections. That finding aligns with a hypothesis proposed by others that suggests the larger proportion of neutropenia in fusariosis patients might contribute to the increased susceptibility to disseminated infection (*17*).

We noted a marked predominant prevalence of pneumonia (76%) among our study population. That finding highlights that fusariosis-related pneumonia can lead to acute respiratory failure, often necessitating invasive mechanical ventilation. Thoracic CT patterns of fusariosis-related pneumonia included pulmonary consolidations, micronodules and nodules, and ground-glass opacities. Excavations and pleural effusions have also been observed, but proportions of those CT patterns vary across different publications, mainly due to the small number of patients included (*25*–*27*). In addition, the timing of imaging and presence of neutropenia or co-infections might influence those patterns. Many patients in our study had co-infections; thus, we cannot attribute their CT patterns solely to invasive fusariosis.

All patients in our study who had solid organ transplants also had acute kidney injury. That difference varied from previous reports and could be explained mainly by the presence of calcineurin inhibitor, well known for its nephrotoxicity (*28*). In addition, one third of solid organ transplant patients in our study had undergone a kidney transplant, which might have contributed to the increased susceptibility to acute kidney injury in this subgroup.

Despite identifying various factors associated with treatment response in the univariate analysis, the multivariate analysis in our study did not reveal any independent risk factors. However, the small number of patients included in our study might have limited the statistical power of the analysis. Moreover, we considered all non-ICU survivors to be nonresponders and 4 patients died before receiving treatment, findings others should consider when interpreting our results but that further emphasize the need for larger studies among more extensive patient populations to better elucidate the independent risk factors associated with treatment response in invasive fusariosis.

The optimal antifungal treatment for invasive fusariosis remains uncertain (*29*). The heterogeneity of treatments administered to patients across different centers in our study further complicates the interpretation of our results. However, our analysis was underpowered to detect a favorable response with voriconazole. Conversely, a previous study reported a 90-day survival rate of 60% with voriconazole monotherapy (*8*), surpassing the outcomes associated with liposomal or deoxycholate amphotericin B. Another study demonstrated an overall response rate of 47% with voriconazole (*10*). Nevertheless, because the current literature primarily consists of case reports and small retrospective studies, determining the optimal antifungal regimen for such patients remains challenging.

The mortality rate observed for ICU patients with invasive fusariosis in our study was notably high, reaching 56%. That finding is consistent with previous studies reporting mortality rates ranging from 40% to 70% in patients with invasive fusariosis, although those studies did not specifically focus on ICU patients (*8*–*11*). In univariate analysis, the observed association between surgical debridement and survival could be attributed to the fact that patients were well enough, and possibly had less severe and fewer disseminated infections, to undergo debridement. By multivariate analysis, we identified history of hematologic disease, including active hematologic malignancy or recent allo-HSCT, as an independent risk factor for death. Patients with hematologic malignancies and those who have undergone allo-HSCT are more likely to experience neutropenia. Persistent neutropenia has been identified as a factor associated with increased mortality rates among invasive fusariosis patients in several previous studies (*8*,*16*,*17*,*30*).

One limitation in our study is the lack of assessment of persistent neutropenia during hospitalization because of missing data on hospitalization reports; those missing data prevented a comprehensive analysis of the effects of persistent neutropenia on patient outcomes in our study population. Also, because we did not have access to the total number of immunocompromised patients admitted to ICUs during the entire study period, we were unable to estimate the prevalence of invasive fusariosis in this population. Finally, the variability in ICU admitting policies across different centers might have influenced our study results. Some patients with invasive fusariosis and underlying conditions or poor prognosis related to hematologic malignancies might have been denied ICU admission. That potential selection bias could affect the generalizability of our findings and should be considered when interpreting the results.

In conclusion, invasive fusariosis is a severe condition that can lead to multiorgan failure and is associated with high mortality rates in the ICU. Clinicians should consider invasive fusariosis as a potential diagnosis in immunocompromised patients who have pneumonia or persistent fever unresponsive to antimicrobial agents. Treatment for invasive fusariosis includes antifungal therapy, rapid reversal of neutropenia, and surgical debridement for localized lesions. Further research is warranted to optimize diagnostic strategies and treatment approaches for this challenging and life-threatening infection. However, clinicians should closely monitor ICU patients with a history of hematologic malignancies or allo-HSCT because of significantly higher invasive fusariosis ICU mortality rates among those patients.

L.Z. reports receiving fees for lectures for MSD and Sanofi and her institution received a research grant from Jazz Pharmaceuticals. E.C. received fees for lectures and conference talks and had travel and accommodation expenses related to attending scientific meetings covered by Gilead, Shionogi B.V., and Sanofi-Genzyme. N.B. reports fees and reimbursements for national congresses from Sanofi. F.P. report receiving fees for lectures and consulting from Gilead and an institutional grant from ALEXION Pharma. A.D.J. reports receiving remuneration for presentations from Medtronic, Drager, Viatris, and Fisher & Paykel. Other authors declare no conflict of interest.

About the Author

Dr. Demonchy is a specialist in intensive care at the Medical Intensive Care Unit, Critical Care Center, University Hospital of Lille, France. Her primary interest is in infectious diseases and immunocompromised patients, especially patients with hematologic malignancies.

References

1. Pagano L, Caira M, Candoni A, Offidani M, Fianchi L, Martino B, et al. The epidemiology of fungal infections in patients with hematologic malignancies: the SEIFEM-2004 study. Haematologica. 2006;91:1068–75.
2. Borjian Boroujeni Z, Shamsaei S, Yarahmadi M, Getso MI, Salimi Khorashad A, Haghighi L, et al. Distribution of invasive fungal infections: molecular epidemiology, etiology, clinical conditions, diagnosis and risk factors: a 3-year experience with 490 patients under intensive care. Microb Pathog. 2021;152:104616. https://doi.org/10.1016/j.micpath.2020.104616
3. Nucci M, Barreiros G, Akiti T, Anaissie E, Nouér SA. Invasive fusariosis in patients with hematologic diseases. J Fungi (Basel). 2021;7:815. https://doi.org/10.3390/jof7100815
4. Dignani MC, Anaissie E. Human fusariosis. Clin Microbiol Infect. 2004;10(Suppl 1):67–75. https://doi.org/10.1111/j.1470-9465.2004.00845.x
5. Nucci M, Anaissie E. *Fusarium* infections in immunocompromised patients. Clin Microbiol Rev. 2007;20:695–704. https://doi.org/10.1128/CMR.00014-07
6. Tortorano AM, Richardson M, Roilides E, van Diepeningen A, Caira M, Munoz P, et al.; European Society of Clinical Microbiology and Infectious Diseases Fungal Infection Study Group; European Confederation of Medical Mycology. ESCMID and ECMM joint guidelines on diagnosis and management of hyalohyphomycosis: *Fusarium* spp., *Scedosporium* spp. and others. Clin Microbiol Infect. 2014;20(Suppl 3):27–46. https://doi.org/10.1111/1469-0691.12465
7. De Pauw B, Walsh TJ, Donnelly JP, Stevens DA, Edwards JE, Calandra T, et al.; European Organization for Research and Treatment of Cancer/Invasive Fungal Infections Cooperative Group; National Institute of Allergy and Infectious Diseases Mycoses Study Group (EORTC/MSG) Consensus Group. Revised definitions of invasive fungal disease from the European Organization for Research and Treatment of Cancer/Invasive Fungal Infections Cooperative Group and the National Institute of Allergy and Infectious Diseases Mycoses Study Group (EORTC/MSG) Consensus Group. Clin Infect Dis. 2008;46:1813–21. https://doi.org/10.1086/588660
8. Nucci M, Marr KA, Vehreschild MJGT, de Souza CA, Velasco E, Cappellano P, et al. Improvement in the outcome of invasive fusariosis in the last decade. Clin Microbiol Infect. 2014;20:580–5. https://doi.org/10.1111/1469-0691.12409
9. Horn DL, Freifeld AG, Schuster MG, Azie NE, Franks B, Kauffman CA. Treatment and outcomes of invasive fusariosis: review of 65 cases from the PATH Alliance® registry. Mycoses. 2014;57:652–8. https://doi.org/10.1111/myc.12212
10. Lortholary O, Obenga G, Biswas P, Caillot D, Chachaty E, Bienvenu AL, et al.; French Mycoses Study Group. International retrospective analysis of 73 cases of invasive fusariosis treated with voriconazole. Antimicrob Agents Chemother. 2010;54:4446–50. https://doi.org/10.1128/AAC.00286-10
11. Campo M, Lewis RE, Kontoyiannis DP. Invasive fusariosis in patients with hematologic malignancies at a cancer center: 1998–2009. J Infect. 2010;60:331–7. https://doi.org/10.1016/j.jinf.2010.01.010
12. Batista BG, Chaves MA de, Reginatto P, Saraiva OJ, Fuentefria AM. Human fusariosis: an emerging infection that is difficult to treat. Rev Soc Bras Med Trop. 2020:53:e20200013. https://doi.org/0.1590/0037-8682-0013-2020
13. Chan TSY, Au-Yeung R, Chim CS, Wong SCY, Kwong YL. Disseminated fusarium infection after ibrutinib therapy in chronic lymphocytic leukaemia. Ann Hematol. 2017;96:871–2. https://doi.org/10.1007/s00277-017-2944-7
14. Delia M, Monno R, Giannelli G, Ianora AAS, Dalfino L, Pastore D, et al. Fusariosis in a patient with acute myeloid leukemia: a case report and review of the literature. Mycopathologia. 2016;181:457–63. https://doi.org/10.1007/s11046-016-9987-5
15. Fei H, Liu X, Sun L, Shi X, Wang W, Zhao H, et al. Disseminated fusarium infection after allogeneic hematopoietic stem cell transplantation after CART: a case report. Medicine (Baltimore). 2022;101:e31594. https://doi.org/10.1097/MD.0000000000031594
16. Nucci M, Anaissie EJ, Queiroz-Telles F, Martins CA, Trabasso P, Solza C, et al. Outcome predictors of 84 patients with hematologic malignancies and *Fusarium* infection. Cancer. 2003;98:315–9. https://doi.org/10.1002/cncr.11510

17. Pérez-Nadales E, Alastruey-Izquierdo A, Linares-Sicilia MJ, Soto-Debrán JC, Abdala E, García-Rodríguez J, et al.; Spanish Fusariosis Study Group. Invasive fusariosis in nonneutropenic patients, Spain, 2000–2015. Emerg Infect Dis. 2021;27:24–36. https://doi.org/10.3201/eid2701.190782
18. Thomas B, Audonneau NC, Machouart M, Debourgogne A. *Fusarium* infections: epidemiological aspects over 10 years in a university hospital in France. J Infect Public Health. 2020;13:1089–93. https://doi.org/10.1016/j.jiph.2020.06.007
19. Girmenia C, Pagano L, Corvatta L, Mele L, Del Favero A, Martino P. The epidemiology of fusariosis in patients with haematological diseases. Br J Haematol. 2000;111:272–6. https://doi.org/10.1111/j.1365-2141.2000.02312.x
20. Le Gall JR, Lemeshow S, Saulnier F. A new simplified acute physiology score (SAPS II) based on a European/North American multicenter study. JAMA. 1993;270:2957–63. https://doi.org/10.1001/jama.1993.03510240069035
21. Vincent JL, de Mendonça A, Cantraine F, Moreno R, Takala J, Suter PM, et al. Use of the SOFA score to assess the incidence of organ dysfunction/failure in intensive care units: results of a multicenter, prospective study. Crit Care Med. 1998;26:1793–800. https://doi.org/10.1097/00003246-199811000-00016
22. Gangneux JP, Dannaoui E, Fekkar A, Luyt CE, Botterel F, De Prost N, et al. Fungal infections in mechanically ventilated patients with COVID-19 during the first wave: the French multicentre MYCOVID study. Lancet Respir Med. 2022;10:180–90. https://doi.org/10.1016/S2213-2600(21)00442-2
23. Boutati EI, Anaissie EJ. *Fusarium*, a significant emerging pathogen in patients with hematologic malignancy: ten years' experience at a cancer center and implications for management. Blood. 1997;90:999–1008. https://doi.org/10.1182/blood.V90.3.999
24. Hotchkiss RS, Monneret G, Payen D. Immunosuppression in sepsis: a novel understanding of the disorder and a new therapeutic approach. Lancet Infect Dis. 2013;13:260–8. https://doi.org/10.1016/S1473-3099(13)70001-X
25. Nucci F, Nouér SA, Capone D, Nucci M. Invasive mould disease in haematologic patients: comparison between fusariosis and aspergillosis. Clin Microbiol Infect. 2018;24:1105.e1–4. https://doi.org/10.1016/j.cmi.2018.05.006
26. Marom EM, Holmes AM, Bruzzi JF, Truong MT, O'Sullivan PJ, Kontoyiannis DP. Imaging of pulmonary fusariosis in patients with hematologic malignancies. AJR Am J Roentgenol. 2008;190:1605–9. https://doi.org/10.2214/AJR.07.3278
27. Sassi C, Stanzani M, Lewis RE, Vianelli N, Tarsi A, Poerio A, et al. Radiologic findings of *Fusarium* pneumonia in neutropenic patients. Mycoses. 2017;60:73–8. https://doi.org/10.1111/myc.12538
28. Naesens M, Kuypers DRJ, Sarwal M. Calcineurin inhibitor nephrotoxicity. Clin J Am Soc Nephrol. 2009;4:481–508. https://doi.org/10.2215/CJN.04800908
29. Al-Hatmi AMS, Bonifaz A, Ranque S, Sybren de Hoog G, Verweij PE, Meis JF. Current antifungal treatment of fusariosis. Int J Antimicrob Agents. 2018;51:326–32. https://doi.org/10.1016/j.ijantimicag.2017.06.017
30. Kontoyiannis DP, Bodey GP, Hanna H, Hachem R, Boktour M, Girgaway E, et al. Outcome determinants of fusariosis in a tertiary care cancer center: the impact of neutrophil recovery. Leuk Lymphoma. 2004;45:139–41. https://doi.org/10.1080/1042819031000149386

Address for correspondence: Lara Zafrani, Department of Medical Intensive Care, Hôpital Saint-Louis, AP-HP, 1 avenue Claude Vellefaux, 75010 Paris, France; email: lara.zafrani@aphp.fr

Salmonella Vitkin Outbreak Associated with Bearded Dragons, Canada and United States, 2021–2022

Katherine Paphitis, Caroline A. Habrun, G. Sean Stapleton, Alexandra Reid, Christina Lee, Anna Majury, Allana Murphy, Heather McClinchey, Antoine Corbeil, Ashley Kearney, Katharine Benedict, Beth Tolar, Russell O. Forrest

We identified 2 cases of *Salmonella enterica* serovar Vitkin infection linked by whole-genome sequencing in infants in Ontario, Canada, during 2022. Both households of the infants reported having bearded dragons as pets. The outbreak strain was also isolated from an environmental sample collected from a patient's bearded dragon enclosure. Twelve cases were detected in the United States, and onset dates occurred during March 2021–September 2022 (isolates related to isolates from Canada within 0–9 allele differences by core-genome multilocus sequence typing). Most US patients (66.7%) were <1 year of age, and most (72.7%) had reported bearded dragon exposure. Hospitalization was reported for 5 (38.5%) of 13 patients. Traceback of bearded dragons identified at least 1 potential common supplier in Southeast Asia. Sharing rare serovar information and whole-genome sequencing data between Canada and the United States can assist in timely identification of outbreaks, including those that might not be detected through routine surveillance.

Nontyphoidal *Salmonella* are consistently among the most commonly reported bacterial pathogens linked to enteric illness in Canada and the United States (*1,2*). In most cases, human infection is ultimately attributed to consumption of specific foods or to contact with animals (*1,3,4*). Persons usually show development of illness within 12–36 hours after exposure (range 6 hours–16 days), and most recover without treatment (*5,6*). However, children <5 years of age, adults >65 years of age, and persons with weakened immune systems are more likely to show development of invasive infections (*5–7*).

There are >2,600 serovars of *Salmonella*, more than half of which belong to subspecies I (*S. enterica* subsp. *enterica*) and can cause human and animal illness (*8–10*). Although many *Salmonella* serovars are predominantly associated with reptiles and amphibians, most of these have low-to-moderate zoonotic potential and are believed to account for <1% of human salmonellosis, mainly affecting persons with weakened immune systems and small children (*11*). The burden of *Salmonella* caused by specific serovars varies by country and region, partially because of the distribution of reservoir animal species and because of local food preparation and dietary preferences. Although some serovars, such as Typhimurium and Enteritidis, are globally distributed, others, such as Heidelberg and Newport, are more commonly found in North America (*10,12*).

In June 2022, Public Health Ontario (PHO) noted 2 cases of a rare *Salmonella* serovar (*Salmonella enterica* serovar Vitkin [*Salmonella* Vitkin]) reported by a local public health unit. The cases were closely related (within 2 alleles based on core-genome multilocus sequence typing [cgMLST]), and onset dates were 4 weeks apart, suggestive of a common exposure.

No cases of *Salmonella* Vitkin were reported in Ontario or elsewhere in Canada for at least 14 years

Author affiliations: Public Health Ontario, Toronto, Ontario, Canada (K. Paphitis, C. Lee, A. Majury, A. Murphy, A. Corbeil); Centers for Disease Control and Prevention, Atlanta, Georgia, USA (C.A. Habrun, G.S. Stapleton, K. Benedict, B. Tolar); Ontario Ministry of Agriculture, Food, and Rural Affairs, Guelph, Ontario, Canada (A. Reid); Ontario Ministry of Health, Toronto (H. McClinchey); Public Health Agency of Canada, Winnipeg, Manitoba, Canada (A. Kearney); Public Health Agency of Canada, Guelph (R.O. Forrest)

DOI: https://doi.org/10.3201/eid3002.230963

before these 2 cases (the extent of the data available for review), and the Vitkin serovar had only been seen 23 times in PulseNet USA (https://www.cdc.gov/pulsenet/index.html) before 2021 (*13*). Similarly, no outbreaks associated with *Salmonella* Vitkin were documented within the US Centers for Disease Control and Prevention (CDC) National Outbreak Reporting System during 1971–2020 (*14*).

Given the rarity of this serovar in North America, the Public Health Agency of Canada (PHAC) coordinated communication between PHO and CDC to explore whether CDC had recently identified any cases of this rare serovar in the United States. CDC confirmed that several US isolates of *Salmonella* Vitkin had been reported to PulseNet USA by multiple US states over the previous year. Analysis of whole-genome sequencing data showed that isolates from the United States and Canada were related within 0–9 cgMLST allele differences. We report the multinational outbreak investigation performed by PHO, PHAC, CDC, and partner agencies to identify the source of this rare outbreak.

Figure 1. Bearded dragon rock cave, source of the environmental isolates that were closely related to the outbreak strain of *Salmonella enterica* serovar Vitkin found in patients in Ontario, Canada, 2022. The environmental isolates were within 1 and 2 alleles by core-genome multilocus sequence typing to those from the patients.

Methods

Epidemiology

In Ontario, public health units use standardized questionnaires for case interviewing and data collection (*15*). Using the questionnaire for *Salmonella* spp., local investigators interviewed a proxy respondent (parent or guardian) for each case and collected data on symptoms and relevant exposures during the 7 days before symptom onset. PulseNet Canada cluster codes for *Salmonella* spp. are assigned when ≥2 isolates occur within a 60-day period and are related within 0–10 alleles by whole-genome multilocus sequence typing (wgMLST) (*16*).

The range of 0–10 wgMLST allele differences might expand or narrow during an investigation on the basis of available laboratory, epidemiologic, and traceback evidence. Wider allele ranges have been previously observed in *Salmonella* outbreaks linked to zoonotic sources (*17*,*18*). Ontario case-patients were defined as patients infected with laboratory-confirmed *Salmonella* Vitkin who had an isolate matching the PulseNet Canada cluster code (2206VitkinWGS-1ON) by whole-genome sequencing (WGS) and had illness onset during April–September 2022. Data were shared with PHO through the integrated Public Health Information System reporting platform.

In July 2022, PHAC notified CDC of the Ontario case cluster and provided investigators with relevant case demographics, reptile exposure, and laboratory information. CDC queried PulseNet USA, the national molecular subtyping network for foodborne disease surveillance in the United States to confirm relatedness and identify genetically related cases. PulseNet USA cluster codes for *Salmonella* spp. are typically assigned when ≥7 clinical isolates occur within a 60-day period and are related within 10 alleles by cgMLST.

US case-patients were defined as patients infected with laboratory-confirmed *Salmonella* Vitkin that was genetically related within 0–9 allele differences based on cgMLST who had an illness onset of March 2021–September 2022. State and local public health investigators interviewed patients (or their proxies) about possible food or animal exposures before illness onset; those data were shared with CDC through the System for Enteric Disease Response, Investigation, and Coordination platform (*19*). In September 2022, CDC requested that state health departments collect additional information on bearded dragon husbandry behaviors, purchase locations, and feed.

Laboratory Investigation

We analyzed 4 environmental swab specimens collected from the bearded dragon enclosure in 1 Ontario case household (Figure 1) and a fresh fecal specimen (collected in July 2022) from the bearded dragon (Figure 2) by using routine aerobic culture at the PHO laboratory (*20*). We also analyzed open samples of dried, pelleted reptile feed and a reptile calcium supplement by routine culture at the PHO laboratory (*20*). PHO runs WGS for all *S. enterica* by using the standardized PulseNet Canada protocol (*21*). WGS data are analyzed locally and then uploaded to a centralized BioNumerics version 7.6 (bioMérieux, https://www.biomerieux.com) database, where it is compared with data from other jurisdictions in Canada to identify multijurisdictional clusters by using wgMLST. PulseNet Canada uses wgMLST as a primary method for identifying genetically related isolates but also has the ability to use cgMLST for comparison with other jurisdictions that use this method. Canada and the United States routinely share genomic data under a bilateral information sharing agreement for comparison between the 2 countries because Canada does not yet upload WGS data to a public repository, such as the National Center for Biotechnology Information (NCBI; https://www.ncbi.nlm.nih.gov), in real time.

In this investigation, sequence data from a representative *Salmonella* Vitkin isolate was requested from PulseNet USA and added to the Canada database, where it was determined to be related to the Ontario cases within 1–3 cgMLST allele differences. A representative sequence from Canada was shared with PulseNet USA for comparison by cgMLST to identify related isolates in the United States. For Canada isolates, WGS data were deposited retrospectively in NCBI in the PulseNet Canada Salmonella BioProject (PRJNA543337). US sequences were uploaded to NCBI under the PulseNet *Salmonella* BioProject (PRJNA230403).

We reviewed veterinary isolate data, representing specimens collected from sick or deceased reptiles and tested by the Animal Health Laboratory (AHL) in Ontario during 2013–2022 to determine whether *Salmonella* Vitkin had been detected in reptiles in Ontario by this surveillance program. Reptile species tested at the AHL reflect common pet species as well as samples from private zoologic institutions. No US patients permitted investigators to screen their bearded dragons for *Salmonella* spp.

Traceback of Reptiles

We conducted a traceback investigation for each of the patient's bearded dragons to identify a potential common supplier or breeder. Where applicable, local pet stores, and intermediary suppliers were interviewed to obtain information on the source(s) of their reptiles and whether they were acquired by local breeders or imported.

Figure 2. Female bearded dragon belonging to household of 1 of 2 case-patients infected with *Salmonella enterica* serovar Vitkin, Ontario, Canada, 2022.

Ethics

This study did not require research ethics committee approval because activities described herein were conducted in fulfillment of the legislated mandate of PHO "to provide scientific and technical advice and support to the health care system and the Government of Ontario in order to protect and promote the health of Ontarians" and are therefore considered public health practice, not research (*22*). Similarly, this activity was conducted consistent with applicable federal law and CDC policy (see e.g., 45 C.F.R. part 46, 21 C.F.R. part 56; 42 U.S.C. §241(d); 5 U.S.C. §552a; 44 U.S.C. §3501 et seq.).

Results

Epidemiology

Both Ontario case-patients were <1 year of age and had isolates related within 3 alleles. Onset dates were reported to be ≈4 weeks apart, in April and May 2022. No hospitalization or death was reported for either of the Ontario patients.

Table. Patient demographics for 14 *Salmonella enterica* serovar Vitkin cases in Canada and the United States, March 2021–October 2022*

Characteristic	Value
Median age, y	<1 (range <1–28)
Female sex	8 (57.1)
Contact with bearded dragons†	10 (76.9)
Hospitalization	5 (38.5)

*Values are no. (%) except as indicated. Of the 14 cases, 2 were reported in Canada and 12 in the United States.
†Of 13 cases with exposure information available.

We did not identify any common food exposures (including infant formula) among the Ontario patients. However, the proxy respondent for each patient reported ≥1 bearded dragons in the household (Table). We noted no commonalities between households with respect to bearded dragon diet. One household reported feeding their reptile(s) feeder mice.

Twelve cases of *Salmonella* Vitkin were identified in the United States, were considered genetically related to the outbreak strain, and had illness onset dates ranging from March 2021 to September 2022 (Figure 3). The US cases were identified across 10 states (Figure 4). Of 11 patients with additional information available, 5 (45%) were hospitalized and no deaths were reported. The median age of US case-patients was the same as that of the Ontario case-patients, including 8 (67%) children <1 year of age (Table).

Among the 11 US patients who had available exposure information, 8 (73%) reported either having direct contact with bearded dragons or having one in their household (Table). No common food exposures were identified among patients.

Laboratory Investigation

One environmental swab specimen, collected from the entrance to the bearded dragon's rock cave (Figure 2), was positive for *Salmonella* Vitkin. Two isolates from this swab specimen were related to the outbreak strain by WGS (Figure 3). *Salmonella* spp. were not detected from the other 3 environmental swab specimens, the fresh fecal specimen collected from the same reptile enclosure, the open sample of reptile feed, or the reptile calcium supplement. Canada human isolates and 2 environmental isolates were genetically related within 0–3 cgMLST allele differences; they also were genetically related within 0–9 cgMLST allele differences to 12 US clinical cases. The 4 Canada *Salmonella* Vitkin isolates linked to this investigation were the only Vitkin isolates in the Canada database. Therefore, no additional strains were analyzed outside the US isolates.

Traceback of Reptiles

Ontario patients reported purchasing bearded dragons from 2 different pet store locations in Ontario, and US patients reported purchases from 4 different US pet store locations and an online source. Both Ontario pet stores were supplied by a single common intermediary supplier, which imported bearded dragons from various suppliers, including an international supplier located in Southeast Asia. This intermediary supplier reported that they did not ship bearded dragons from or to the United States and that they had ceased importing reptiles from the international supplier in late 2021. The US pet stores were supplied by 1 of 3 common intermediary suppliers, 1 of which purchased bearded dragons from the same international supplier. No single breeder was identified as the source for all bearded dragons implicated in this investigation.

Reptile Isolate Data

A review of reptile veterinary isolate data compiled by the AHL found that, although most of the specimens

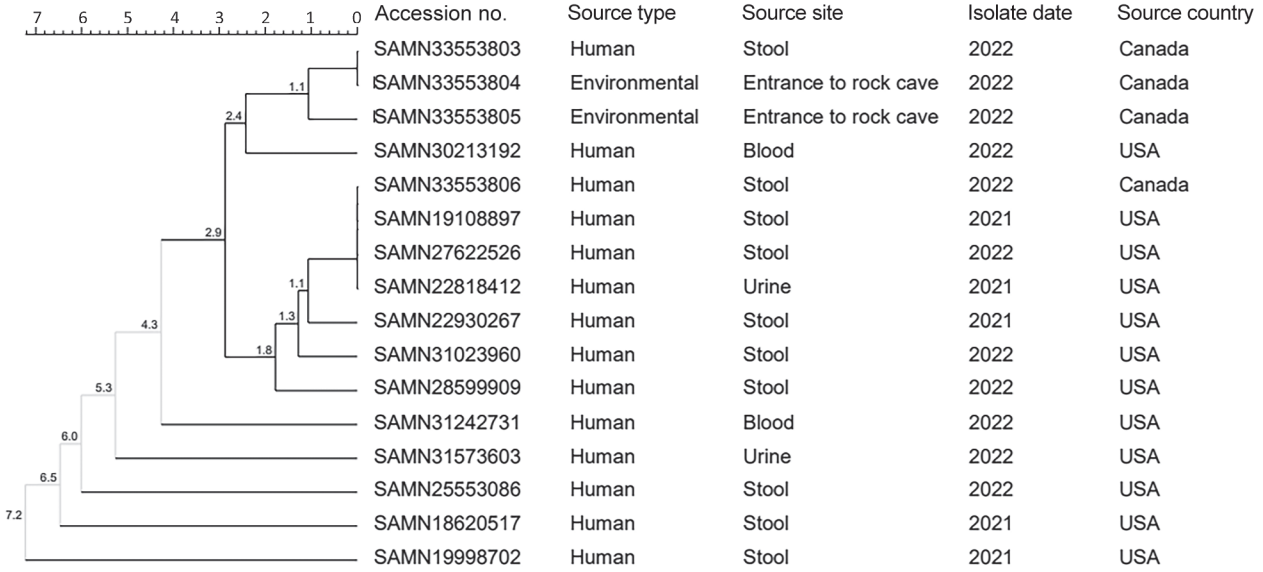

Figure 3. Unweighted pair group method with arithmetic mean dendrogram of core-genome multilocus sequence typing results for human and environmental isolates included in the Canada and the United States *Salmonella enterica* serovar Vitkin outbreak investigation, 2020–2022. Tree was generated by using BioNumerics version 7.6 (bioMérieux, https://www.biomerieux.com). Numbers along branches are median allele differences. Shown are GenBank accession numbers.

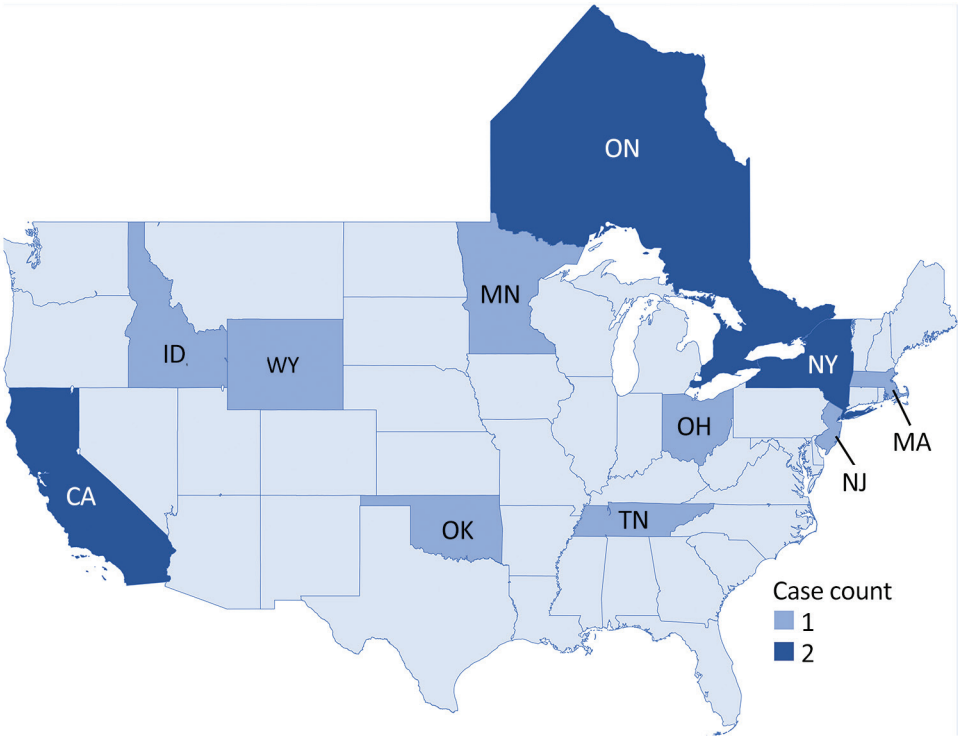

Figure 4. *Salmonella enterica* serovar Vitkin infection case counts, by state (United States) and province (Canada), 2021–2022.

tested from 2013–2022 were from bearded dragons (by reptile species, 21.3%, n = 13), *Salmonella* Vitkin was not isolated from any of these, or from any other reptile species. The serovars most commonly isolated from bearded dragons were *Salmonella* Amsterdam (23.1%, n = 3) and *Salmonella* Kisarawe (23.1%, n = 3).

Public Health Response

Local public health investigators visited each pet store identified by the Ontario case-patients as the location of bearded dragon purchase and provided pet store operators with fact sheets summarizing information on *Salmonella* infection and prevention associated with reptiles for distribution to future customers. Information provided by fact sheets included recommendations for pet owners to wash their hands after handling reptiles, to clean and disinfect any surfaces that come into contact with their reptile, and to supervise children during interactions with reptiles, while noting that these animals are not recommended as pets for households with ≥1 persons at increased risk for severe illness (*23*). Canada and US public health partners shared their outbreak findings with public health officials located in the country of the common Southeast Asia bearded dragon supplier, as well as educational resources on preventing *Salmonella* transmission from bearded dragons.

CDC first communicated to the public regarding this outbreak on October 18, 2022. The website post highlighted investigation details and information for actions to take to minimize the risk for reptile-associated *Salmonella* infections (*24*). Similar general preventative information in the form of a public-facing factsheet is available on the PHAC webpage (*23*). The investigations in Canada and the United States were closed in December 2022.

Discussion

Salmonella Vitkin infections linked to this outbreak disproportionately affected infants and often resulted in severe illness, as shown by 78% of reported case-patients being <1 year of age and almost 40% of patients reporting hospitalization because of illness. Contact with bearded dragons was the source of this outbreak. Reporting of indirect or direct contact with bearded dragons by most case-patients and isolation of the same serovar from a reptile enclosure supported bearded dragons as the most likely source of exposure. Many infants likely were indirectly exposed to infection by the contaminated clothing or hands of caregivers or by contact with contaminated environmental surfaces within the home.

Reptiles, including bearded dragons, lizards and snakes, are among several animal species that are becoming more common in Canada and elsewhere as household pets (*25*–*27*). Reptiles can carry *Salmonella* spp. in their gastrointestinal tract without displaying signs of illness and can intermittently shed the

bacteria in their feces (*28*). Fecal shedding can be prompted or exacerbated by stressors, such as handling, transportation, or illness (*28*). Persons might become ill with *Salmonella* infections if they have direct or indirect contact with reptiles or their environment, particularly if they do not wash their hands after handling or caring for their reptiles or if they do not clean and disinfect contaminated surfaces (*26*,*29*).

A study found that, although most cases of human salmonellosis in Ontario during 2010–2012 were attributed to foodborne transmission, 35.5% (n = 107) of reported cases were attributed to contact with reptiles or amphibians (*3*). This finding is notable because, according to the most recent Canadian Foodbook Report, produced by the Public Health Agency of Canada in 2015 after a population-based telephone survey of the Canadian population, only 2.1% of Ontario respondents reported having any contact with reptiles in the previous 7 days, indicating the relatively small proportion of the population who might keep these reptiles as pets (*30*). In comparison, 31.0% of Ontario respondents reported having contact with a cat and 42.2% reported having contact with a dog during the same time period (*30*). Similarly, a recent national pet owner survey found that ≈90.5 million US homes reported owning ≥1 pet. Among households that owned a pet, ≈6% (5.7 million) owned a reptile, compared with 76% (69.0 million) that owned a dog and 50% (45.3 million) that owned a cat (*31*).

Captive bearded dragons have higher rates of *Salmonella* carriage compared with those in the wild, and stress can increase the frequency of *Salmonella* shedding (*32*). Awareness and consideration of steps that can be taken by owners and breeders of bearded dragons to reduce stressors (such as avoiding overcrowding during transport, and provision of adequate space and enrichment items within enclosures) could theoretically reduce *Salmonella* shedding and subsequent human exposure (*33*). Bearded dragon owners should be encouraged to restrict roaming of their bearded dragons outside of their enclosure to surfaces and items that are able to be cleaned and disinfected afterwards.

If reptile owners are not aware that their reptiles can carry and shed *Salmonella* spp., they might fail to take appropriate preventive measures, increasing the risk for illness among household members, including those who do not have direct contact with reptiles. Because some *Salmonella* serovars can survive on surfaces for several days to months, surfaces might serve as a source of indirect exposure if they are not cleaned and disinfected after coming into contact with bearded dragons or other reptiles (*34*,*35*). Previous studies have noted that *Salmonella* carriage is common among captive reptiles and that a high-density population of animals (e.g., in breeding facilities, during transport or at point of sale) can promote the transfer of *Salmonella* spp. between reptiles, particularly if the reptiles are fed with rodents (*26*,*36*).

There have been several reported outbreaks of *Salmonella* infections linked to contact with reptiles in Canada and the United States, including outbreaks specifically linked to bearded dragons. Those outbreaks have involved several different serovars, including Uganda (2022), Muenster (2020), Apapa (2018), and Cotham (2014) (*27*,*37*–*40*). Although those outbreaks affected persons of all age groups, children were overrepresented.

To date, there has been minimal published literature on *Salmonella* Vitkin infections in humans; we identified only 1 article summarizing a case of meningitis caused by *Salmonella* Vitkin infection in an infant (1 month of age) after exposure to a pet turtle (*29*). Children, particularly those <5 years of age, might be at increased risk for exposure to *Salmonella* infections and other enteric infections because of poor hand hygiene, developing immune systems, and a tendency to mouth objects (*41*). Children might also be more susceptible to less virulent strains of the bacteria, which might explain the relatively young median age of those involved in reported outbreaks involving reptiles (*25*). Because transmission can occur by direct and indirect contact with reptiles, parents might not recognize indirect reptile contact as a risk. As such, they might fail to take appropriate preventive measures, including keeping children away from the reptiles and any potentially contaminated surfaces. Furthermore, parents and caregivers might not think to change potentially contaminated clothing or wash their hands between handling reptiles and interacting with children (*11*). Infants could be at increased risk for indirect exposure by the clothing of adult household members because they are more likely to be held or carried than independently mobile toddlers and older children.

Although a fresh fecal specimen from 1 bearded dragon was collected during the *Salmonella* Vitkin investigation and found to be negative for *Salmonella* spp., this specimen was collected 3 months after the onset of illness in the child within the same household, and the bearded dragon might have no longer (or only intermittently) been shedding *Salmonella* spp. in its stool at the time. A previous study of household *Salmonella* transmission associated with pet reptiles in Germany found that in 15 (78.9%) of 19 households with a child with confirmed *Salmonella* infection, an

identical serovar was confirmed in both the infected case and ≥1 reptile in the household (*42*). The authors further noted that, although reptiles might be simultaneously colonized with multiple *Salmonella* serovars, shedding may be intermittent, and a negative cloacal or fecal specimen does not mean that the reptile is free from *Salmonella* spp. (*42*). Instead, persons should assume that all reptiles could be carrying *Salmonella* spp. (*42*).

Although the intermediary reptile supplier in Canada in this investigation did not report US importation or exportation of reptiles, it is unknown whether cross-border importation or export of reptiles is common practice or the extent to which importation of reptiles to North America might occur. Ontario has no record-keeping requirements for persons who breed, import, export or sell reptiles. Bearded dragons within the pet trade are entirely maintained by captive breeding operations that might operate at a small scale (i.e., a person with 2 bearded dragons) or at a commercial scale (*33*). The stress and close confinement during transport is associated with an increased risk for *Salmonella* shedding and transmission (*11*). Although cases of *Salmonella* Vitkin infection linked to this outbreak were reported in the United States until November 2022, no additional cases were reported in Ontario (or elsewhere in Canada) after the intermediary supplier in Canada ceased importing bearded dragons from the common international breeder that was identified in this investigation.

Because reptile supply chains in Canada and the United States might be integrated for some species, communication between international public health investigators can assist in identification of multijurisdictional outbreaks associated with reptiles and can help to identify a potentially causative exposure, particularly in situations with rare serovars. Furthermore, environmental sampling can provide microbiological evidence to confirm source identification.

Providing reptile owners with information on the risks of *Salmonella* infection associated with reptiles at the point of purchase/acquisition could support informed decisions about pet choices and necessary precautions. Information could include steps that can be taken to minimize the risk for infection transmission from reptiles to humans, including details on persons who might be at increased risk for illness if exposed and who should ideally avoid reptile contact (*43*). In particular, potential reptile owners who have children <5 years of age should be aware that reptile ownership or contact is discouraged for this age group because, although handwashing and environmental disinfection can reduce the risk for *Salmonella* transmission from reptiles to humans, the increased susceptibility of children to infection and the risk for severe illness if infected make these high-risk pets. Further education for persons and businesses involved in reptile breeding, distribution, and sale could also focus on the need for preventive veterinary care, biosecurity, and environmental cleaning practices (*43*).

Record-keeping requirements for persons involved in the breeding, distribution, and sale of reptiles would assist in traceback investigations and support investigators in identifying the source of infection during outbreak investigations (*43*). Timely collaboration and information sharing can assist in identifying the potential source of a multijurisdictional outbreak, enabling rapid rollout of public health interventions and dissemination of information to the public to prevent illnesses.

Acknowledgments

We thank all persons involved in case investigation, case follow-up, and reptile traceback, including state/local public health partners in California, Idaho, Massachusetts, Minnesota, New Jersey, New York, Ohio, Oklahoma, Tennessee, and Wyoming, and particularly the Ontario public health unit investigators who conducted a comprehensive investigation, including environmental sampling; the Public Health Ontario laboratory for their work isolating, identifying, and sequencing *Salmonella* during this outbreak; Tim Pasma for providing the reptile isolate data used for reference in this outbreak; and Lauren Gollarza and Kaylea Nemechek for providing communication and epidemiologic technical input on enteric zoonoses during this investigation.

About the Author

Dr. Paphitis is the Enteric Zoonotic Specialist at Public Health Ontario, Toronto, Ontario, Canada. Her primary research interests are One Health and the epidemiology of enteric and zoonotic diseases, including salmonellosis.

References

1. Scallan E, Hoekstra RM, Angulo FJ, Tauxe RV, Widdowson MA, Roy SL, et al. Foodborne illness acquired in the United States—major pathogens. Emerg Infect Dis. 2011;17:7–15. https://doi.org/10.3201/eid1701.P11101
2. Thomas MK, Murray R, Flockhart L, Pintar K, Fazil A, Nesbitt A, et al. Estimates of foodborne illness-related hospitalizations and deaths in Canada for 30 specified pathogens and unspecified agents. Foodborne Pathog Dis. 2015;12:820–7. https://doi.org/10.1089/fpd.2015.1966

3. Whitfield Y, Johnson K, Hobbs L, Middleton D, Dhar B, Vrbova L. Descriptive study of enteric zoonoses in Ontario, Canada, from 2010–2012. BMC Public Health. 2017;17:217. https://doi.org/10.1186/s12889-017-4135-9
4. Beshearse E, Bruce BB, Nane GF, Cooke RM, Aspinall W, Hald T, et al. Attribution of illnesses transmitted by food and water to comprehensive transmission pathways using structured expert judgment, United States. Emerg Infect Dis. 2021;27:182–95. https://doi.org/10.3201/eid2701.200316
5. Heymann DL. Control of communicable diseases manual. 20th ed. Washington: American Public Health Association; 2015.
6. Shane AL, Mody RK, Crump JA, Tarr PI, Steiner TS, Kotloff K, et al. 2017 Infectious Diseases Society of America clinical practice guidelines for the diagnosis and management of infectious diarrhea. Clin Infect Dis. 2017;65:e45–80. https://doi.org/10.1093/cid/cix669
7. Centers for Disease Control and Prevention. *Salmonella*: information for healthcare professionals and laboratories [cited 2023 Jan 12]. https://www.cdc.gov/salmonella/general/technical.html
8. Jajere SM. A review of *Salmonella enterica* with particular focus on the pathogenicity and virulence factors, host specificity and antimicrobial resistance including multidrug resistance. Vet World. 2019;12:504–21. https://doi.org/10.14202/vetworld.2019.504-521
9. Guibourdenche M, Roggentin P, Mikoleit M, Fields PI, Bockemühl J, Grimont PA, et al. Supplement 2003–2007 (No. 47) to the White-Kauffmann-Le Minor scheme. Res Microbiol. 2010;161:26–9. https://doi.org/10.1016/j.resmic.2009.10.002
10. Ferrari RG, Rosario DK, Cunha-Neto A, Mano SB, Figueiredo EE, Conte-Junior CA. Worldwide epidemiology of *Salmonella* serovars in animal-based foods: a meta-analysis. Appl Environ Microbiol. 2019;85:e00591–19. https://doi.org/10.1128/AEM.00591-19
11. Hoelzer K, Moreno Switt AI, Wiedmann M. Animal contact as a source of human non-typhoidal salmonellosis. Vet Res (Faisalabad). 2011;42:34. https://doi.org/10.1186/1297-9716-42-34
12. Hendriksen RS, Vieira AR, Karlsmose S, Lo Fo Wong DM, Jensen AB, Wegener HC, et al. Global monitoring of *Salmonella* serovar distribution from the World Health Organization global foodborne infections network country data bank: results of quality assured laboratories from 2001 to 2007. Foodborne Pathog Dis. 2011;8:887–900. https://doi.org/10.1089/fpd.2010.0787
13. Tolar B, Joseph LA, Schroeder MN, Stroika S, Ribot EM, Hise KB, et al. An overview of PulseNet USA databases. Foodborne Pathog Dis. 2019;16:457–62. https://doi.org/10.1089/fpd.2019.2637
14. Centers for Disease Control and Prevention. National Outbreak Reporting System (NORS) [cited 2022 Dec 18]. https://wwwn.cdc.gov/norsdashboard
15. Ontario Agency for Health Protection and Promotion (Public Health Ontario). Ontario investigation tools (OIT). Toronto: King's Printer for Ontario; 2019 Dec [cited 2022 Dec 6]. https://www.publichealthontario.ca/en/diseases-and-conditions/infectious-diseases/ccm/oit
16. Public Health Agency of Canada. Outbreak toolkit: cluster code; 2020 [cited 2022 Dec 6]. https://outbreaktools.ca/case-study-overview/module-1-cluster-detection-and-initial-investigation-2/cluster-code
17. Fagan-Garcia K, Denich L, Tataryn J, Janicki R, Van Osch O, Kearney A, et al. A multi-provincial *Salmonella* Typhimurium outbreak in Canada associated with exposure to pet hedgehogs, 2017–2020. Can Commun Dis Rep. 2022;48:282–90. https://doi.org/10.14745/ccdr.v48i06a06
18. Gerner-Smidt P, Besser J, Concepción-Acevedo J, Folster JP, Huffman J, Joseph LA, et al. Whole genome sequencing: bridging One-Health surveillance of foodborne diseases. [Erratum in: Front Public Health. 2019;7:365.]. Front Public Health. 2019;7:172. https://doi.org/10.3389/fpubh.2019.00172
19. Centers for Disease Control and Prevention. SEDRIC: System for Enteric Disease Response, Investigation and Coordination [cited 2023 Jan 17]. https://www.cdc.gov/foodsafety/outbreaks/tools/sedric.html
20. Reed A. Isolation and identification of *Salmonella* from foods and environmental samples. MFHPB-20. Health Products and Food Branch, Food Directorate, Health Canada; 2009 [cited 2023 Jan 13]. https://www.canada.ca/en/health-canada/services/food-nutrition/research-programs-analytical-methods/analytical-methods/compendium-methods/methods-microbiological-analysis-foods-compendium-analytical-methods.html
21. Rumore J, Tschetter L, Kearney A, Kandar R, McCormick R, Walker M, et al. Evaluation of whole-genome sequencing for outbreak detection of Verotoxigenic *Escherichia coli* O157:H7 from the Canadian perspective. BMC Genomics. 2018;19:870. https://doi.org/10.1186/s12864-018-5243-3
22. Ontario Agency for Health Protection and Promotion Act. SO 2007, c 10 s 6. Sect. c 10, s 6 Jun 4, 2007 [cited 2023 Dec 19]. https://www.canlii.org/en/on/laws/stat/so-2007-c-10-sch-k/latest/so-2007-c-10-sch-k.html
23. Public Health Agency of Canada. *Salmonella* and reptiles. 2022 [cited 2022 Dec 13]. https://www.canada.ca/en/public-health/services/food-safety/fact-sheet/salmonella-reptiles.html
24. Centers for Disease Control and Prevention. *Salmonella* homepage. 2022. *Salmonella* outbreak linked to pet bearded dragons (*S.* Vitkin) [cited 2022 Dec 5]. https://www.cdc.gov/salmonella/beardeddragon-10-22/details.html
25. Harker KS, Lane C, De Pinna E, Adak GK. An outbreak of *Salmonella* Typhimurium DT191a associated with reptile feeder mice. Epidemiol Infect. 2011;139:1254–61. https://doi.org/10.1017/S0950268810002281
26. Zając M, Skarżyńska M, Lalak A, Kwit R, Śmiałowska-Węglińska A, Pasim P, et al. *Salmonella* in captive reptiles and their environment—can we tame the dragon? Microorganisms. 2021;9:1012. https://doi.org/10.3390/microorganisms9051012
27. Valdez JW. Using Google trends to determine current, past, and future trends in the reptile pet trade. Animals (Basel). 2021;11:676. https://doi.org/10.3390/ani11030676
28. Bjelland AM, Sandvik LM, Skarstein MM, Svendal L, Debenham JJ. Prevalence of *Salmonella* serovars isolated from reptiles in Norwegian zoos. Acta Vet Scand. 2020;62:3. https://doi.org/10.1186/s13028-020-0502-0
29. Ricard C, Mellentin J, Ben Abdallah Chabchoub R, Kingbede P, Heuclin T, Ramdame A, et al. *Salmonella* meningitis in an infant due to a pet turtle [in French]. Arch Pediatr. 2015;22:605–7. https://doi.org/10.1016/j.arcped.2013.09.019
30. Public Health Agency of Canada. Foodbook report. Ottawa (ON, Canada): Government of Canada; 2015 Nov [cited 2022 Dec 6]. https://www.canada.ca/en/public-health/services/publications/food-nutrition/foodbook-report.html
31. American Pet Products Association. Pet industry market size, trends and ownership statistics. 2022 [cited 2022 Dec 16]. https://www.americanpetproducts.org/press_industrytrends.asp

32. Whiley H, Gardner MG, Ross K. A review of *Salmonella* and squamates (lizards, snakes and amphibians): implications for public health. Pathogens. 2017;6:38. https://doi.org/10.3390/pathogens6030038
33. Johnson R, Adwick S. Central bearded dragons (*Pogona vitticeps*). In: Yeates J, editor. Companion animal care and welfare. Chichester (UK): John Wiley & Sons, Ltd; 2018. p. 395–411.
34. Bauwens L, Vercammen F, Bertrand S, Collard JM, De Ceuster S. Isolation of *Salmonella* from environmental samples collected in the reptile department of Antwerp Zoo using different selective methods. J Appl Microbiol. 2006;101:284–9. https://doi.org/10.1111/j.1365-2672.2006.02977.x
35. Pedersen K, Lassen-Nielsen AM, Nordentoft S, Hammer AS. Serovars of *Salmonella* from captive reptiles. Zoonoses Public Health. 2009;56:238–42. https://doi.org/10.1111/j.1863-2378.2008.01196.x
36. Lee KM, McReynolds JL, Fuller CC, Jones B, Herrman TJ, Byrd JA, et al. Investigation and characterization of the frozen feeder rodent industry in Texas following a multi-state *Salmonella* Typhimurium outbreak associated with frozen vacuum-packed rodents. Zoonoses Public Health. 2008;55:488–96. https://doi.org/10.1111/j.1863-2378.2008.01165.x
37. Government of Canada. Public health notice: outbreak of *Salmonella* infections linked to snakes and rodents. 2021 [cited 2022 Dec 5]. https://www.canada.ca/en/public-health/services/public-health-notices/2019/outbreak-salmonella-infections-snakes-rodents.html
38. Kiebler CA, Bottichio L, Simmons L, Basler C, Klos R, Gurfield N, et al. Outbreak of human infections with uncommon *Salmonella* serotypes linked to pet bearded dragons, 2012–2014. Zoonoses Public Health. 2020;67:425–34. https://doi.org/10.1111/zph.12701
39. Centers for Disease Control and Prevention. Reports of selected *Salmonella* outbreak investigations. 2022 [cited 2023 Jan 26]. https://www.cdc.gov/salmonella/outbreaks.html
40. Waltenburg MA, Perez A, Salah Z, Karp BE, Whichard J, Tolar B, et al. Multistate reptile- and amphibian-associated salmonellosis outbreaks in humans, United States, 2009–2018. Zoonoses Public Health. 2022;69:925–37. https://doi.org/10.1111/zph.12990
41. Sockett PN, Rodgers FG. Enteric and foodborne disease in children: A review of the influence of food- and environment-related risk factors. Paediatr Child Health. 2001;6:203–9. https://doi.org/10.1093/pch/6.4.203
42. Pees M, Rabsch W, Plenz B, Fruth A, Prager R, Simon S, et al. Evidence for the transmission of *Salmonella* from reptiles to children in Germany, July 2010 to October 2011. Euro Surveill. 2013;18:20634. https://doi.org/10.2807/1560-7917.ES2013.18.46.20634
43. Varela K, Brown JA, Lipton B, Dunn J, Stanek D, Behravesh CB, et al.; NASPHV Committee Consultants, et al. A review of zoonotic disease threats to pet owners: a compendium of measures to prevent zoonotic diseases associated with non-traditional pets such as rodents and other small mammals, reptiles, amphibians, backyard poultry, and other selected animals. Vector Borne Zoonotic Dis. 2022;22:303–60. https://doi.org/10.1089/vbz.2022.0022

Address for correspondence: Katherine Paphitis, Public Health Ontario, 661 University Ave, Ste 1701, Toronto, ON M5G 1M1, Canada; email: katherine.paphitis@oahpp.ca

Parechovirus A Circulation and Testing Capacities in Europe, 2015–2021

Laura Bubba, Eeva K. Broberg, Thea K. Fischer, Peter Simmonds, Heli Harvala; European Non-polio Enterovirus Network working group

Parechovirus infections usually affect neonates and young children; manifestations vary from asymptomatic to life-threatening. We describe laboratory capacity in Europe for assessing parechovirus circulation, seasonality, and epidemiology. We used retrospective anonymized data collected from parechovirus infection case-patients identified in Europe during January 2015–December 2021. Of 21 laboratories from 18 countries that participated in the study, 16 (76%) laboratories with parechovirus detection capacity reported 1,845 positive samples; 12/16 (75%) with typing capability successfully identified 517 samples. Parechovirus A3 was the most common type (n = 278), followed by A1 (153), A6 (50), A4 (13), A5 (22), and A14 (1). Clinical data from 1,269 participants highlighted correlation of types A3, A4, and A5 with severe disease in neonates. We observed a wide capacity in Europe to detect, type, and analyze parechovirus data. To enhance surveillance and response for PeV outbreaks, sharing typing protocols and data on parechovirus-positive cases should be encouraged.

Parechoviruses are small, nonenveloped, single-stranded RNA viruses belonging to the large Picornaviridae family that circulate worldwide; primary infections occur mainly in children <2 years of age (*1*,*2*). Parechoviruses are transmitted by fecal-oral and respiratory routes (*2*,*3*). Most infections are asymptomatic or have mild general gastrointestinal or respiratory symptoms, but they can occasionally lead to sepsis, meningitis or other neurologic manifestations, or even death (*2*–*6*).

Nineteen human parechovirus types have been classified as species types PeV-A1–A19 (*7*); the most commonly reported are A1, A3, and A6 (*2*,*3*). PeV-A1 and A6 infections are generally associated with mild outcomes, but PeV-A3 can cause severe neurologic disease in infants <3 months of age (*2*,*4*–*6*,*8*,*9*). More recently, PeV-A4 and A5 also have been associated with severe clinical manifestations in children (*10*,*11*). Recorded genotype distribution might vary on the basis of study design, including testing strategy, geographic location, and timing of sampling, because epidemiology can differ by virus type (*3*). Data collected from nonpolio enterovirus (NPEV) surveillance and childhood prevalence studies showed worldwide parechovirus distribution differs by genotype; PeV-A1 is the most prevalent type in the United States, Asia, and Europe, followed by A3 and A4 (*12*). PeV-A6 is reported as second most common in Australia and in some studies in Europe (*2*,*12*). Additional genotypes, including A2 and A7–A19, that are rare in Europe and the United States have been reported in India, Pakistan, and Africa (*12*).

Parechovirus studies in Europe have mostly focused on children or specific symptoms, with no data from dedicated surveillance and limited data from the NPEV surveillance system. The lack of systematically collected data limits full understanding of the impact and circulation of parechovirus infections. Clarifying the epidemiology, clinical implications, and phylogeny of parechovirus would help laboratories and national health authorities make decisions about the clinical relevance of infections. We therefore conducted a retrospective study to assess the presence of surveillance and laboratory capacity for parechovirus detection and typing in Europe during 2015–2021. We

Author affiliations: European Non-Polio Enterovirus Network, Geneva, Switzerland (L. Bubba); European Centre for Disease Prevention and Control, Solna, Sweden (E.K. Broberg); University Hospital of Nordsjaelland Department of Clinical Research, Hilleroed, Denmark (T.K. Fischer); University of Copenhagen Department of Public Health, Copenhagen, Denmark (T.K. Fischer); University of Oxford Nuffield Department of Medicine, Oxford, UK (P. Simmonds); National Health Service Blood and Transplant, London, UK (H. Harvala); University College London Division of Infection and Immunity, London (H. Harvala)

DOI: https://doi.org/10.3201/eid3002.230647

also described the seasonality, clinical manifestations, and molecular epidemiology of parechovirus infections during the 7-year study period (2015–2021).

Methods

Data Collection

In March 2022, the European Non-polio Enterovirus Network (ENPEN) invited the national focal point agencies that constitute the European Centre for Disease Prevention and Control (ECDC) public health network, regional reference laboratories from all 30 member states within the European Union (EU), European Economic Area, the United Kingdom, and local laboratories affiliated with ENPEN to join the study. We sent a reminder letter about participation 15 days before the deadline.

We used data collected during January 1, 2015–December 31, 2021 as part of an EU survey (*13*). The survey included questions for each participating laboratory on their extent of and approach to parechovirus detection and surveillance and their screening policies and capacity for detection and typing. We also requested information on methods used in each laboratory (Appendix Table 1, https://wwwnc.cdc.gov/EID/article/30/2/32-0647-App1.pdf). When available, we collected anonymized aggregated data on monthly and yearly parechovirus detection, associated clinical symptoms, age group, sample type, sex, and total number of samples tested for each study year by parechovirus type (Appendix Figure 1). Each laboratory collected data from various sources, such as NPEV, acute flaccid paralysis, and influenza-like illness (ILI) surveillance; screening of hospital admissions records; and cerebrospinal fluid (CSF) samples.

For each laboratory we summarized the capacity for parechovirus detection and what triggers they used to initiate testing (Table). We included laboratories reporting the absence of parechovirus testing, to better understand the extent of testing capacity in Europe. We asked participating laboratories to share nucleotide sequences of PeV-A3 strains that had been typed; in cases of outbreaks or clusters, we requested only nonidentical (i.e., differing by ≥2%) sequences.

Data Analysis

We reported the number of parechovirus infections by month/year and country of study, and analyzed data by clinical symptoms, age group, sample type, and parechovirus type when information was available. We calculated overall parechovirus detection rate when total number of samples tested was reported. Because some laboratories did not implement parechovirus detection testing until after the study had begun, we reported proportions of positive samples for the entire 2015–2021 study period and for the specific timeframes 2015–2017 and 2018–2021. We calculated parechovirus type distribution by year, clinical symptoms, age group, sample type, and month, and calculated the proportion of detections and types of samples. We performed χ^2 testing using Vassar stat (*14*) to compare proportions; $p<0.05$ indicates statistical significance.

For PeV-A3 analysis, we summarized 106 sequences with >80% completeness in viral protein (VP) 3/VP1 junction region positions 2182–2437 (as numbered in the echovirus 22 prototype sequence L02971) (Appendix Table 2). We aligned sequences using MUSCLE 3 (*15*) and compared them with 630 publicly available PeV-A3 nucleotide sequences from this region retrieved from GenBank database in December 2022 using sequence editor version 1.4 (*16*). In addition, participating laboratories provided 30 sequences from a second region in VP1 (positions 2336–3038; Appendix Table 2), which we compared with 856 available GenBank sequences. We performed neighbor-joining phylogenetic analysis (Jukes-Cantor model) and calculated maximum likelihood using the optimal substitution model, Tamura-Nei with γ correction, using MEGA package version 7 (*17*). When sampling dates were available, we inspected phylogenetic trees for country-specific clustering and temporal trends.

Results

In total, 21 laboratories from 18 EU and European Economic Area member states participated in the study; 16/21 participating laboratories performed parechovirus testing (76%). Of those not testing, 1 laboratory each in the Slovak Republic and Bulgaria planned to introduce parechovirus in routine diagnostics, but the remaining 3 laboratories, in the Czech Republic, Estonia, and Hungary, had no plans to implement nationwide parechovirus testing (Table). Of the 16 laboratories performing testing, 11 (69%) provided data for 2015–2021; 2, in Norway and the United Kingdom (Scotland), provided data only for 2015–2017, and 3, in Luxemburg, Poland, and Slovenia, reported data for 2017–2021 after commencing testing.

Twelve (75%) of 16 laboratories initially performing testing reported capacity to type parechovirus-positive samples and provided type information for this study (Table). Of those, 5 performed sequencing routinely and 7 sequenced viruses only from selected

clinically detected cases. Most (11/12) laboratories analyzed sequences in the VP3/VP1 junction region positions 2182–2437, but 1 laboratory, in the Netherlands, performed sequencing from the start of VP1 (positions 2336–3038). To perform the analysis of this region, we alternatively used data from Denmark, Poland, and the United Kingdom (England) because they provided data from a longer portion of the parechovirus genome that included VP1 (Appendix Table 2).

Parechovirus Detection

Sixteen laboratories from 13 countries reported 1,845 parechovirus-positive samples. Finland, the Netherlands, Spain, and England added parechovirus data based on voluntarily reporting positive cases to the national laboratory, to existing enterovirus surveillance (Table). Those 4 countries reported the most (65%, n = 1,200) parechovirus-positive samples. One laboratory each in Slovenia and in the Lombardy region of Italy (Italy/Lombardy) that introduced parechovirus screening into ILI surveillance provided ≈130 parechovirus-positive respiratory samples. The same laboratory in Italy/Lombardy detected parechovirus-positive samples from cases identified through an acute flaccid paralysis surveillance network, which routinely screens for polioviruses. Remaining cases were identified after clinician requests for testing not based on existing NPEV, ILI, or other surveillance systems (Table). Ireland reported the highest number of parechovirus-positive samples (26%, n = 488), followed by Denmark (17%, n = 322) and England (14%, n = 264) (Figure 1). Unfortunately, those countries provided no denominator information, so we could not calculate positivity rates.

Parechovirus testing capacity, measured by samples tested in 9 laboratories (3 in Italy and 1 each in Austria, Finland, Luxemburg, Poland, Slovenia, and the Netherlands), increased from 8,665 during 2015–2017 to 14,263 during 2018–2021; those laboratories reported 309 positive samples, 100 in 2015–2017 and 209 in 2018–2021. Although parechovirus-positive samples increased over that time, parechovirus detections per number of screened samples remained unchanged: 100/8,665 (1.3%) during 2015–2017 and 209/14,263 (1.5%) during 2018–2021. Detection rate for the entire 2015–2021 study period was 1.4% (309/22,928).

Seasonality

All participating laboratories reported month and year of collection of parechovirus-positive samples (Table; Figure 1). Infections were reported every year; 2016 accounting for 24% and 2018 for 25% of detections. Most cases were detected during June–November each year.

Distribution of Parechovirus Types

Twelve laboratories, 10 of which supplied data for the whole study period (Table), reported 517 (45%) of the 1,139 successfully sequenced parechovirus-positive samples, corresponding to 28% (517/1,845) of all positive samples reported in this study. Among 6 parechovirus types detected, PeV-A3 (54%, n = 278) was the most frequently reported, followed by A1 (30%, n = 153), A6 (10%, n = 50), A5 (4%, n = 22), A4 (2%, n = 13), and A14 (0.2%, n = 1) (Figure 2). Positive PeV-A1 and A3 samples were reported each year during 2015–2021. PeV-A3 accounted for most typed samples in 5/7 study years: 71% in 2015, 75% in 2016, 61% in 2017, 61% in 2019, and 50% in 2020; A5 accounted for 23/31 (74%) of typed samples in 2018 and A1 for 44/52 (85%) in 2021.

Geographic Distribution of Parechovirus Types

Spain (35%) and Denmark (33%) provided the most parechovirus case reports with typing information (Figure 2). All laboratories performing typing reported PeV-A3 cases, the most being from Spain (n = 138), Denmark (72), and Italy/Lombardy (17). PeV-A3 exhibits a biannual cycle; most parechovirus cases reported by Denmark were identified in even years (2016 and 2018), whereas most cases reported by Spain occurred in uneven years (2015, 2017, and 2019). Denmark and the Netherlands reported the most PeV-A1 and A6 cases; the Netherlands (35.3%, n = 6), Austria (29.4%, n = 5), and Spain (17.6%, n = 3) reported the most A5 cases. Spain reported 8/13 (62%) A4 cases and Poland reported 1 A14 case.

Sample Types

Sample type information was available for 1,294 positive samples from 13 laboratories. Fecal (n = 447; 35%), CSF (391; 30%), and respiratory (259; 20%) specimens were the sample types most often collected for parechovirus testing; in some cases patients might have provided >1 sample type for testing. CSF was the most common specimen type collected in Austria, Luxemburg, Spain, England, and Scotland; feces in Denmark, Ireland, and the Netherlands; and respiratory specimens in Italy/Lombardy and Slovenia.

From the 136 successfully typed CSF samples, PeV-A3 (40%), A4 (44%), and A5 (22.7%) were the only types reported, whereas PeV-A1 (50%), A6 (41%), and A5 (52%) were identified from 208 fecal

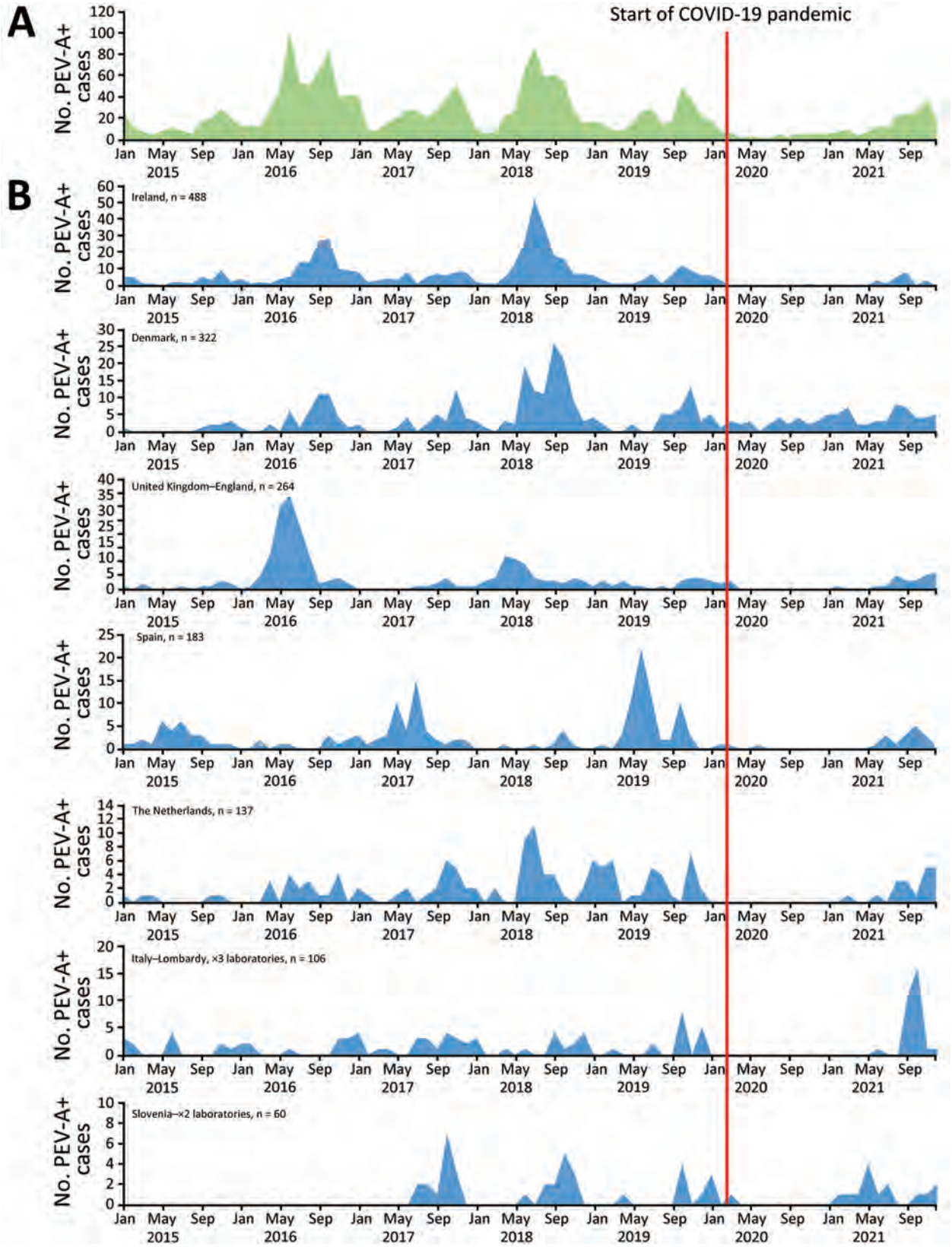

Figure 1. Monthly distribution of parechovirus in Europe, overall and by country, 2015–2021. A) Overall monthly distribution. B) Monthly distribution for countries reporting >50 infections.

samples. From the 90 respiratory samples typed, PeV-A1 (61%) was the most commonly reported, followed by A3 (20%), A6 (12%), and A5 (7%); no type A4 was reported in respiratory samples.

Demographic Information and Clinical Manifestations

Demographic information was available for 1,299 and clinical information for 1,269 parechovirus case-patients reported from 14 laboratories in 11 countries.

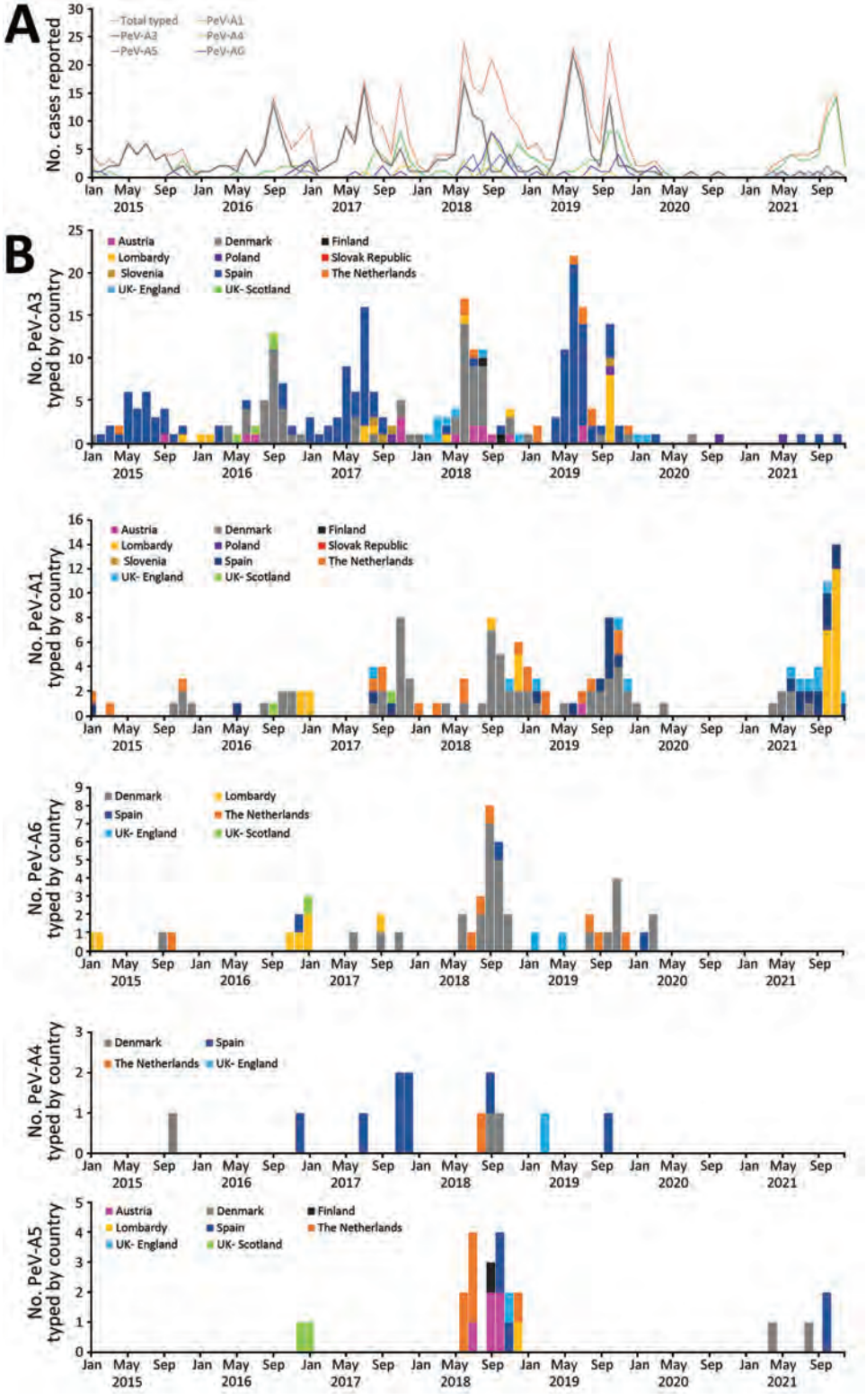

Figure 2. Monthly distribution of typed parechoviruses in Europe, by type and country, 2015–2021. A) Overall monthly distribution. B) Monthly distribution of each detected type by country of detection. Poland reported 1 type A14 infection in June 2021 (not shown).

Male patients (61%, n = 763) and infants <1 year of age (76%, n = 987) accounted for most reported cases; infants <3 months of age accounted for 777 (60%) of reported cases. Symptoms were reported for 1,232/1,479 (83%) cases; fever (23%, n = 305) and neurologic signs (21%, n = 280) were the most common, followed by respiratory symptoms (13%, n = 170). Among patients with less common signs and symptoms, 45 (3.4%) children manifested sepsis, 2 were diagnosed with cardiomyopathy, and 1 with hepatitis. Three children diagnosed with PeV-A1 infection in the Netherlands in 2017 died, but it is unknown whether death was related to parechovirus infection.

Information on age groups and symptoms were available for 509/518 (98%) successfully typed cases. The most-reported symptom was fever in children infected with PeV-A3 (44%), A4 (50%), and A5 (30%); among children infected with PeV-A6, gastrointestinal (35%) and respiratory (25%) symptoms were the most commonly reported. Respiratory symptoms (37%) were also common among children infected with PeV-A1 (Figure 3). Most children infected with PeV-A3 (87%), A4 (92%), and A5 (91%) were <3 months of age, whereas >82% of children infected with PeV-A1 were >3 months of age (p<0.0001). Parechovirus infections were rare (n = 68) in children and persons >15 years of age; in that age range, only 1/68 viruses was successful typed and identified as PeV-A3. All detected parechovirus types were associated with neurologic symptoms, of which 72% were typed as PeV-A3, followed by A1 (11%), A5 (7%), A6 (6%), and A4 (1%). The sole PeV-A14 case was detected in a fecal specimen collected from a child with neurologic symptoms from the 6–15-year age group.

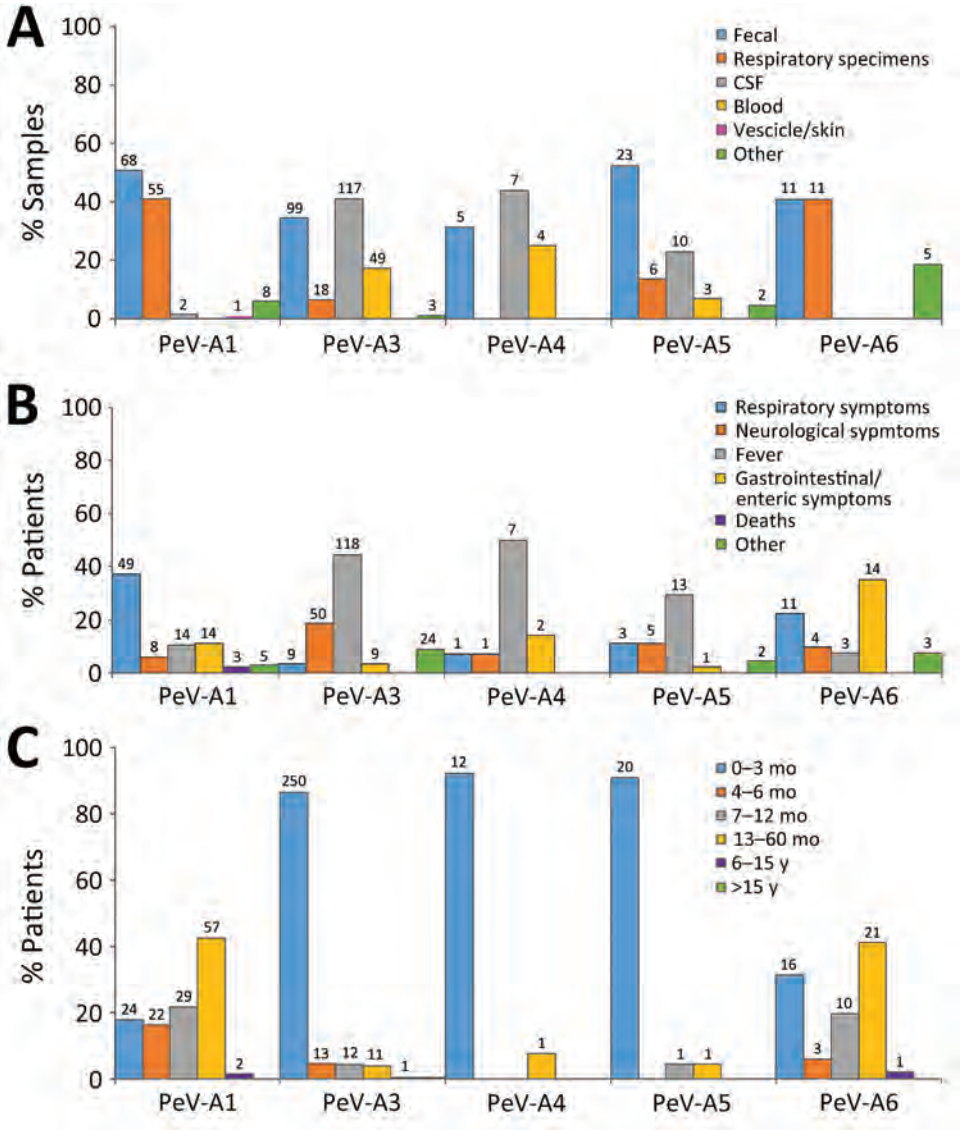

Figure 3. Detection frequencies of different parechovirus types in Europe, 2015–2021, by sample type (A), disease manifestation (B), and patient age (C). Numbers above bars indicate numbers of cases. CSF, cerebrospinal fluid; PeV, parechovirus type.

Phylogenetic Analysis

PeV-A3 was the type most frequently reported by participating laboratories. We performed phylogenetic analysis of 106 available study sequences in the VP3/VP1 junction region to compare relationships between potential country- or region-specific groups of strains and available previously published PeV-A3 variants (Figure 4; Appendix Figure 2). Whereas the resolution of the tree was limited by the relatively short length of sequences analyzed (256 bp), variants from different study regions showed some evidence of clustering, possibly representing local geographic spread (e.g., in Denmark), although there was no evidence for specific variants circulating exclusively in just 1 or a few countries. Numerous separate older lineages of PeV-A3 circulating during 2010–2014 or earlier have largely become extinct (Appendix Figure 2).

Discussion

We report the laboratory capacity, type-related temporal dynamics, epidemiology, and clinical manifestations of parechovirus infections reported from 21 laboratories in 18 countries in Europe over a 7-year study period, 2015–2021. We documented extensive capacity for parechovirus detection in northern, western, and some central European countries participating in our study; no parechovirus testing was reported in Bulgaria, the Czech Republic, the Slovak Republic, Estonia, or Hungary. Those findings were consistent with literature in which limited capacity for parechovirus detection and typing was reported outside western and northern European countries (*18*–*22*).

A total of 1,845 parechovirus infections, most identified through NPEV surveillance systems, were reported by 16 laboratories from 13 countries in Europe that participated in the study. Four national laboratories incorporated parechovirus detection into NPEV passive surveillance, collecting data on positive cases from other laboratories that send samples for sequencing after identifying parechovirus. A similar passive surveillance system, in which laboratories report positive NPEV and parechovirus cases to the Centers for Disease Control and Prevention

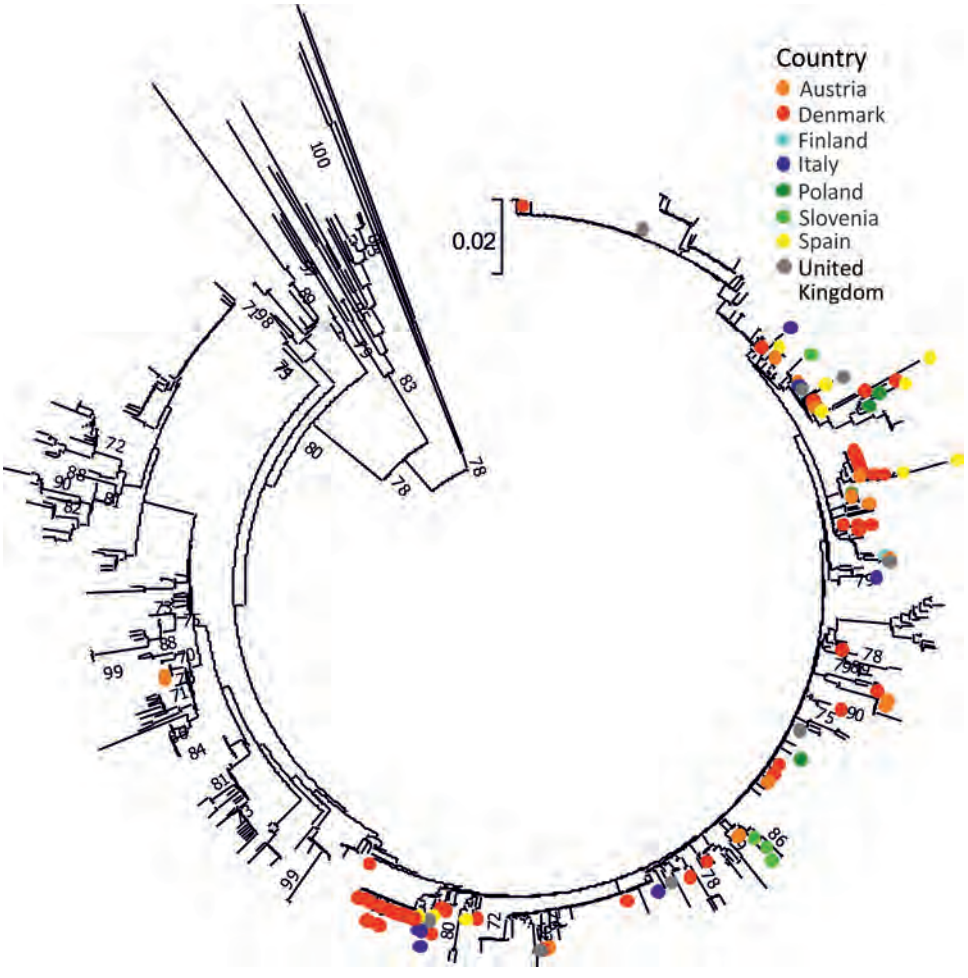

Figure 4. Phylogenetic analysis of the VP3/VP1 region of PeV-3 sequences, Europe, 2015–2021. Neighbor-joining phylogenetic tree of the VP3/VP1 junction region obtained from the study samples (n = 106) is labeled by country of sample origin and compared with 630 available sequences spanning the analyzed region from GenBank. The tree was constructed using MEGA 7 (*17*) using Jukes-Cantor corrected distances, with bootstrap resampling; branches showing 70% or greater supports were labeled. Scale bar indicates substitutions per site. A maximum-likelihood analysis of the same sequence dataset is provided in Appendix Figure 2 (https://wwwnc.cdc.gov/EID/article/30/2/23-0647-App1.pdf). PeV, parechovirus type; VP, viral protein.

(CDC), was implemented in the United States (*23*). During 2014–2016 in the United States, ≈100 domestic parechovirus cases were reported to CDC (*24*); in Europe, 540 cases from Finland, the Netherlands, Spain, and England, were reported over a comparable 3-year timeframe, 2015–2017. Those figures highlight the current volume and likely benefits of the data collected in Europe, along with the potential capacity to implement similar systems in additional countries within and beyond our region.

The capacity for parechovirus testing increased during the study period from ≈9,000 samples tested for parechovirus during 2015–2017 to >14,000 during 2018–2021. Luxemburg, Poland, and Slovenia successfully introduced parechovirus testing in 2017, but some 2018–2021 increases in detection capacity attributable to new data sources were likely offset by several laboratories substantially reducing diagnostic and surveillance testing capacity for pathogens not related to SARS-CoV-2 during the COVID-19 pandemic. The overall detection rate of 1.3% (309/22,928) was lower than previously observed rates of 2%–3% in Denmark (*21*) and 13% in Northern Ireland (*22*). However, it is difficult to compare results from our study with results from studies that focused mainly on select populations, such as children and infants needing intensive care unit admission (*4*).

Besides countries with passive surveillance, laboratories in 2 countries introduced parechovirus testing for respiratory samples collected during ILI surveillance; because samples were implicitly collected from persons with respiratory symptoms only, persons with other parechovirus symptoms would not have been captured through those means. Although ILI surveillance covered all age groups, young infants were likely underrepresented because only 12/130 parechovirus-positive samples were collected from children <3 months of age, which might explain why most of the parechovirus infections captured through ILI surveillance were identified as PeV-A1, a type uncommon among the youngest infants. Based on this finding, ILI surveillance is less likely to capture PeV-A3 infections in children, especially those <3 months of age, because A3 infection manifests with only respiratory symptoms very rarely. Using only ILI surveillance therefore might not be the best option for identifying parechovirus (*25*).

Twelve laboratories that reported typing capacity successfully sequenced ≈45% of their positive samples, so 28% of total parechovirus-positive samples reported in this study were typed. PeV-A3, the most common type identified in this study, was mostly associated with neurologic infections in infants <3 months of age. The association of PeV-A3 with severe disease, especially in young children, has been well documented elsewhere (*4*,*5*,*8*,*26*–*29*). Our study confirmed both PeV-A3 detection in infants <3 months of age (77% of all typed cases were from this age group) and its severity of infection (73% of infants <3 months of age manifested neurologic signs). Detection of PeV-A3 in sterile samples, such as CSF and blood, confirms its likely systemic nature, which often leads to severe infection. Most PeV-3 cases were originally identified in even-numbered years (2008, 2010, 2012, 2014, and 2016) in northern Europe, the United States, and Australia (*18*,*19*,*30*,*31*). That biannual seasonal pattern was observed for PeV-A3 in Denmark in spring/summer of 2016–2018, but A3 infections appeared to follow a different 2-year cycle in Spain, with peaks in 2017 and 2019. PeV-A1, on the other hand, appeared to follow an annual cycle peaking later each year. Phylogenetic analysis revealed no notable geographic or seasonal clustering of PeV-A3.

A 2022 increase in PeV-A3 infections affecting newborns and young infants and often resulting in severe outcomes was noted in the United States using data from its passive surveillance system (*32*–*34*). Those data were used to encourage clinicians to consider parechovirus as a differential diagnosis in cases of fever, sepsis-like syndrome, seizures, or meningitis without another known cause (*32*,*33*). Although our findings demonstrate that passive parechovirus surveillance and diagnostic capacities are already available in Europe, no upsurge in recorded parechovirus infections has been noted to date. In future, better harmonization of data collection could be used to monitor the spread of parechovirus infections across Europe, complement early warning systems, and provide the bases for public health recommendations during upsurges.

Despite ongoing collection and testing of samples during the COVID-19 pandemic, parechovirus detection frequencies for A3–A6 declined dramatically in 2020–2021 during periods of lockdown, comparable to previously documented decreases observed for enteroviruses, such as enterovirus D68 (*35*). An upsurge in PeV-A1 but not in other types in autumn 2021 mirrored the timing of the reappearance of enterovirus D68 and coincided with the end of COVID-19 lockdown restrictions and increased testing of respiratory samples (*35*). This suggests that PeV-A1 more likely spreads through respiratory routes than other parechovirus types.

In terms of clinical associations, our large-scale description of cases provides evidence for differentiating disease patterns between parechovirus types. A4 and A5 infections were detected largely in infants <3

months of age and more often in sterile samples, such as CSF and blood (Figure 3), both features comparable to previously described epidemiologic and clinical properties of PeV-A3 (*11*,*36*,*37*). Strikingly, parechovirus types A4 and A5 were also primarily detected in children <3 months of age, but PeV-A1 and A6 infections occurred mainly in children 1–5 years of age.

Fever and a higher frequency of neurologic symptoms were associated with higher percentages of PeV-A3 (44%), A4 (50%), and A5 (30%) than A1 or A6 cases. Further patient characterization is required to evaluate whether PeV-A4 and A5 might be more likely to cause neurologic diseases resembling those from PeV-A3 (*10*,*31*–*33*). Although clinical profiles in our study indicate similar neurologic manifestations for PeV-A3 and A4, another study reported that only 9% of A4 infections resulted in neurologic symptoms, much lower than for A3 (91%) (*10*). It should be noted that almost all PeV-A5 infections in our study were reported by Austria, the Netherlands, and Spain in 2018, and more recently by Italy/Lombardy. Therefore, clinical attributes related to neurologic effects might reflect biologic characteristics of circulating strains rather than differences in parechovirus type.

Collected data were reported as aggregated information, limiting the possibility of calculating risk ratios for associations between specific parechovirus types and clinical symptoms. In addition, each country used different case definitions and criteria for collecting and testing samples. Those limitations should inform interpretation of results and their use as baseline information for future systematic approaches.

In conclusion, we demonstrate that multiple laboratories located in 13 countries in Europe have been collecting and analyzing data on parechovirus infections, including demographic information, clinical features, specimen types, and type sequences. Results of investigating parechovirus epidemiology and collecting and analyzing an increasing amount of data suggest that this virus causes severe infections, especially in very young children. Those findings highlight the need to expand parechovirus diagnostics and typing beyond current participating laboratories and share protocols to develop and initiate more efficient systematic approaches for identifying parechovirus-positive cases in Europe. Future approaches should also include a wider spectrum of age-groups and clinical symptoms. Integrating parechovirus with NPEV surveillance would enable better characterization of parechovirus types and seasonality across and beyond Europe and support outbreak detection to improve clinical and public health awareness and provide resources to limit the spread of parechovirus in Europe.

ENPEN working group: Monika Redlberger–Fritz, Stephan Aberle (Medical University Vienna Center for Virology, Vienna, Austria); Lubomira Nikolaeva-Glomb (National Center of Infectious and Parasitic Diseases, Sofia, Bulgaria); Petra Rainetova (National Institute Public Health, Prague, Czech Republic); Sofie E. Midgley, Kristina Træholt Franck (Statens Serum Institut, Copenhagen, Denmark); Annemarjut J. Jääskeläinen (Helsinki University Hospital HUS Diagnostic Center, Helsinki, Finland); Teemu Smura (University of Helsinki, Helsinki, Finland); Agnes Farkas (National Public Health Center, Budapest, Hungary); Ursula Morley, Cillian De Gascun (University College National Virus Reference Laboratory, Dublin, Ireland); Elena Pariani, Laura Pellegrinelli (University of Milan Department of Biomedical Sciences for Health, Milan, Italy); Fausto Baldanti, Antonio Piralla (Università degli Studi di Pavia Department of Clinical Surgical Diagnostic and Paediatric Sciences, Pavia, Italy); Massimo Oggioni (Azienda Socio-Sanitaria Territoriale della Brianza Microbiologia e Virologia Clinica, Vimercate, Italy); Sara Uceda Renteria (Fondazione IRCCS Ca' Granda Ospedale Maggiore Policlinico Virology Unit, Milan, Italy); Trung Nguyen, Sibel Berger (Laboratoire national de Santé, Dudelange, Luxembourg); Kimberley Benschop, (National Institute for Public Health and the Environment [RIVM], Bilthoven, the Netherlands), Katja Wolthers (OrganoVIR Labs, Department of Medical Microbiology, Amsterdam UMC, Amsterdam, the Netherlands); Svein Nordbo, Susanne Gjeruldsen Dudman (St. Olavs University Hospital Department of Medical Microbiology, Trondheim, Norway); Magdalena Wieczorek, Arleta Krzysztoszek (National Institute of Public Health NIH–NRI Department of Virology, Warsaw, Poland); Katarína Pastuchová (Public Health Authority of the Slovak Republic, Bratislava, Slovak Republic); Nataša Berginc (National Laboratory for Health, Environment and Food, Laboratory for Public Health Virology, Maribor, Slovenia); Mario Poljak, Maja M. Lunar (University of Ljubljana Institute of Microbiology and Immunology, Ljubljana, Slovenia); Maria Cabrerizo, M. Dolores Fernandez-Garcia (National Centre for Microbiology Instituto de Salud Carlos III and Center for Biomedical Network Research on Epidemiology and Public Health [CIBERESP], Madrid, Spain); Cristina Calvo (La Paz University Hospital Department of Paediatric Infectious Diseases, and Translational Research Network in Paediatric Infectious Diseases [IDIPAZ], Madrid, Spain) Cristina Celma, Yasmin Mohammadi (UK Health Security Agency, London, UK); Kate Templeton (University of Edinburgh, Edinburgh, Scotland, UK).

Acknowledgments

We thank the European Centre of Control and Diseases training office for the opportunity to conduct this project as part of the European Public Health Microbiology fellowship. We also thank Sandro Binda and Cristina Galli for support and help with this study; Federica Giardina for sequencing support; Spanish Study Group for Pediatric Enterovirus and Parechovirus Infections; and G. Megias, J. Valencia, M. Aranzamendi, A. Gutierrez-Arroyo, C. Muñoz-Almagro, C. Launes, A. Moreno Docón, N. Rabella, C. Berengua, A. Navascués, S. Rey Cao, and M.C. Nieto.

A.P. and B.F. were supported by EU funding within the NextGeneration EU-MUR PNRR Extended Partnership initiative on Emerging Infectious Diseases (Project no. PE00000007, INF-ACT); M.W. and A.K. were supported by the National Institute of Public Health NIH–NRI (BW-1/2023).

About the Author

Dr. Bubba is a public health microbiologist who is a consultant for the World Health Organization and collaborating with ENPEN. Her research interests include syndromic-sentinel surveillance, wastewater surveillance, molecular epidemiology, phylogeny, and laboratory capacity building on both viral and bacterial infections.

Reference

1. Harvala H, Wolthers KC, Simmonds P. Parechoviruses in children: understanding a new infection. Curr Opin Infect Dis. 2010;23:224–30. https://doi.org/10.1097/QCO.0b013e32833890ca
2. Wang CYT, Ware RS, Lambert SB, Mhango LP, Tozer S, Day R, et al. Parechovirus A infections in healthy Australian children during the first 2 years of life: a community-based longitudinal birth cohort study. Clin Infect Dis. 2020;71:116–27. https://doi.org/10.1093/cid/ciz761
3. Olijve L, Jennings L, Walls T. Human parechovirus: an increasingly recognized cause of sepsis-like illness in young infants. Clin Microbiol Rev. 2017;31:e00047–17.
4. Harvala H, Robertson I, Chieochansin T, McWilliam Leitch EC, Templeton K, Simmonds P. Specific association of human parechovirus type 3 with sepsis and fever in young infants, as identified by direct typing of cerebrospinal fluid samples. J Infect Dis. 2009;199:1753–60. https://doi.org/10.1086/599094
5. Wolthers KC, Benschop KS, Schinkel J, Molenkamp R, Bergevoet RM, Spijkerman IJ, et al. Human parechoviruses as an important viral cause of sepsislike illness and meningitis in young children. Clin Infect Dis. 2008;47:358–63. https://doi.org/10.1086/589752
6. Harvala H, Calvert J, Van Nguyen D, Clasper L, Gadsby N, Molyneaux P, et al. Comparison of diagnostic clinical samples and environmental sampling for enterovirus and parechovirus surveillance in Scotland, 2010 to 2012. Euro Surveill. 2014;19:20772. https://doi.org/10.2807/1560-7917.ES2014.19.15.20772
7. Zell R, Delwart E, Gorbalenya AE, Hovi T, King AMQ, Knowles NJ, et al.; ICTV Report Consortium. ICTV virus taxonomy profile: *Picornaviridae*. J Gen Virol. 2017;98:2421–2. https://doi.org/10.1099/jgv.0.000911
8. Harvala H, McLeish N, Kondracka J, McIntyre CL, McWilliam Leitch EC, Templeton K, et al. Comparison of human parechovirus and enterovirus detection frequencies in cerebrospinal fluid samples collected over a 5-year period in Edinburgh: HPeV type 3 identified as the most common picornavirus type. J Med Virol. 2011;83:889–96. https://doi.org/10.1002/jmv.22023
9. Harvala H, Robertson I, McWilliam Leitch EC, Benschop K, Wolthers KC, Templeton K, et al. Epidemiology and clinical associations of human parechovirus respiratory infections. J Clin Microbiol. 2008;46:3446–53. https://doi.org/10.1128/JCM.01207-08
10. Sasidharan A, Harrison CJ, Banerjee D, Selvarangan R. Emergence of parechovirus A4 central nervous system infections among infants in Kansas City, Missouri, USA. J Clin Microbiol. 2019;57:e01698–18. https://doi.org/10.1128/JCM.01698-18
11. Chamings A, Liew KC, Reid E, Athan E, Raditsis A, Vuillermin P, et al. An emerging human parechovirus type 5 causing sepsis-like illness in infants in Australia. Viruses. 2019;11:913. https://doi.org/10.3390/v11100913
12. Sridhar A, Karelehto E, Brouwer L, Pajkrt D, Wolthers KC. Parechovirus A pathogenesis and the enigma of genotype A-3. Viruses. 2019;11:1062. https://doi.org/10.3390/v11111062
13. EUSurvey. HPeV circulation in EU/EEA & UK, 2015–2021 [cited 2022 Mar 10]. https://ec.europa.eu/eusurvey/runner/HPeV_circulation_in_EU-EEA_UK_2015-2021
14. Campbell I. Chi-squared and Fisher-Irwin tests of two-by-two tables with small sample recommendations. Stat Med. 2007;26:3661–75. https://doi.org/10.1002/sim.2832
15. Edgar RC. MUSCLE: multiple sequence alignment with high accuracy and high throughput. Nucleic Acids Res. 2004;32:1792–7. https://doi.org/10.1093/nar/gkh340
16. Simmonds P. SSE: a nucleotide and amino acid sequence analysis platform. BMC Res Notes. 2012;5:50. https://doi.org/10.1186/1756-0500-5-50
17. Kumar S, Stecher G, Tamura K. MEGA7: Molecular Evolutionary Genetics Analysis version 7.0 for bigger datasets. Mol Biol Evol. 2016;33:1870–4. https://doi.org/10.1093/molbev/msw054
18. Marchand S, Launay E, Schuffenecker I, Gras-Le Guen C, Imbert-Marcille BM, Coste-Burel M. Severity of parechovirus infections in infants under 3 months of age and comparison with enterovirus infections: a French retrospective study. Arch Pediatr. 2021;28:291–5. https://doi.org/10.1016/j.arcped.2021.02.014
19. Elling R, Böttcher S, du Bois F, Müller A, Prifert C, Weissbrich B, et al. Epidemiology of human parechovirus type 3 upsurge in 2 hospitals, Freiburg, Germany, 2018. Emerg Infect Dis. 2019;25:1384–8. https://doi.org/10.3201/eid2507.190257
20. Linhares MI, Brett A, Correia L, Pereira H, Correia C, Oleastro M, et al. Parechovirus genotype 3 outbreak among young infants in Portugal. Acta Med Port. 2021;34:664–8. https://doi.org/10.20344/amp.15032
21. Fischer TK, Midgley S, Dalgaard C, Nielsen AY. Human parechovirus infection, Denmark. Emerg Infect Dis. 2014;20:83–7. https://doi.org/10.3201/eid2001.130569
22. Davis J, Fairley D, Christie S, Coyle P, Tubman R, Shields MD. Human parechovirus infection in neonatal intensive care. Pediatr Infect Dis J. 2015;34:121–4. https://doi.org/10.1097/INF.0000000000000510

23. Centers for Disease Control and Prevention. National Enterovirus Surveillance System (NESS): surveillance data [cited 2023 Aug 28]. https://www.cdc.gov/surveillance/ness/surv-data.html
24. Abedi GR, Watson JT, Nix WA, Oberste MS, Gerber SI. Enterovirus and parechovirus surveillance—United States, 2014–2016. MMWR Morb Mortal Wkly Rep. 2018;67:515–8. https://doi.org/10.15585/mmwr.mm6718a2
25. Kadambari S, Harvala H, Simmonds P, Pollard AJ, Sadarangani M. Strategies to improve detection and management of human parechovirus infection in young infants. Lancet Infect Dis. 2019;19:e51–8. https://doi.org/10.1016/S1473-3099(18)30288-3
26. Benschop KS, Schinkel J, Minnaar RP, Pajkrt D, Spanjerberg L, Kraakman HC, et al. Human parechovirus infections in Dutch children and the association between serotype and disease severity. Clin Infect Dis. 2006;42:204–10. https://doi.org/10.1086/498905
27. Piralla A, Furione M, Rovida F, Marchi A, Stronati M, Gerna G, et al. Human parechovirus infections in patients admitted to hospital in northern Italy, 2008–2010. J Med Virol. 2012;84:686–90. https://doi.org/10.1002/jmv.23197
28. Harvala H, Griffiths M, Solomon T, Simmonds P. Distinct systemic and central nervous system disease patterns in enterovirus and parechovirus infected children. J Infect. 2014;69:69–74. https://doi.org/10.1016/j.jinf.2014.02.017
29. Esposito S, Rahamat-Langendoen J, Ascolese B, Senatore L, Castellazzi L, Niesters HG. Pediatric parechovirus infections. J Clin Virol. 2014;60:84–9. https://doi.org/10.1016/j.jcv.2014.03.003
30. van der Sanden S, de Bruin E, Vennema H, Swanink C, Koopmans M, van der Avoort H. Prevalence of human parechovirus in the Netherlands in 2000 to 2007. J Clin Microbiol. 2008;46:2884–9. https://doi.org/10.1128/JCM.00168-08
31. Nelson TM, Vuillermin P, Hodge J, Druce J, Williams DT, Jasrotia R, et al. An outbreak of severe infections among Australian infants caused by a novel recombinant strain of human parechovirus type 3. Sci Rep. 2017;7:44423. https://doi.org/10.1038/srep44423
32. Centers for Disease Control and Prevention. Emergency preparedness and response: recent reports of human parechovirus (PeV) in the United States—2022 [cited 2022 Jul 11]. https://emergency.cdc.gov/han/2022/han00469.asp
33. South Carolina Department of Health and Environmental Control; South Carolina Health Alert Network. CDC health advisory: recent reports of human parechovirus (PeV) in the United States—2022 [cited 2022 Jul 13]. https://scdhec.gov/sites/default/files/media/document/10523-CHA-07-13-2022-PeV.pdf
34. Victoria Department of Health. Human parechovirus type 3 in Victoria [cited 2022 Nov 7]. https://www.health.vic.gov.au/health-advisories/human-parechovirus-type-3-in-victoria
35. Benschop KS, Albert J, Anton A, Andrés C, Aranzamendi M, Armannsdóttir B, et al. Re-emergence of enterovirus D68 in Europe after easing the COVID-19 lockdown, September 2021. Euro Surveill. 2021;26:2100998. https://doi.org/10.2807/1560-7917.ES.2021.26.45.2100998
36. Kolehmainen P, Jääskeläinen A, Blomqvist S, Kallio-Kokko H, Nuolivirta K, Helminen M, et al. Human parechovirus type 3 and 4 associated with severe infections in young children. Pediatr Infect Dis J. 2014;33:1109–13. https://doi.org/10.1097/INF.0000000000000401
37. Piralla A, Perniciaro S, Ossola S, Giardina F, De Carli A, Bossi A, et al. Human parechovirus type 5 neurological infection in a neonate with a favourable outcome: a case report. Int J Infect Dis. 2019;89:175–8. https://doi.org/10.1016/j.ijid.2019.10.006

Address for correspondence: Laura Bubba, European Non-polio Enterovirus Network (ENPEN), Milan 20133, Italy; email: lauretta.bubba@gmail.com

Prevalence of SARS-CoV-2 Infection among Children and Adults in 15 US Communities, 2021[1]

Jessica Justman, Timothy Skalland, Ayana Moore, Christopher I. Amos, Mark A. Marzinke, Sahar Z. Zangeneh, Colleen F. Kelley, Rebecca Singer, Stockton Mayer, Yael Hirsch-Moverman, Susanne Doblecki-Lewis, David Metzger, Elizabeth Barranco, Ken Ho, Ernesto T.A. Marques, Margaret Powers-Fletcher, Patricia J. Kissinger, Jason E. Farley, Carrie Knowlton, Magdalena E. Sobieszczyk, Shobha Swaminathan, Domonique Reed, Jean De Dieu Tapsoba, Lynda Emel, Ian Bell, Krista Yuhas, Leah Schrumpf, Laura Mkumba, Jontraye Davis, Jonathan Lucas, Estelle Piwowar-Manning, Shahnaz Ahmed, and the CoVPN 5002 COMPASS Study Team

Medscape CME Activity

In support of improving patient care, this activity has been planned and implemented by Medscape, LLC and Emerging Infectious Diseases. Medscape, LLC is jointly accredited with commendation by the Accreditation Council for Continuing Medical Education (ACCME), the Accreditation Council for Pharmacy Education (ACPE), and the American Nurses Credentialing Center (ANCC), to provide continuing education for the healthcare team.

Medscape, LLC designates this Journal-based CME activity for a maximum of 1.00 ***AMA PRA Category 1 Credit(s)™***. Physicians should claim only the credit commensurate with the extent of their participation in the activity.

Successful completion of this CME activity, which includes participation in the evaluation component, enables the participant to earn up to 1.0 MOC points in the American Board of Internal Medicine's (ABIM) Maintenance of Certification (MOC) program. Participants will earn MOC points equivalent to the amount of CME credits claimed for the activity. It is the CME activity provider's responsibility to submit participant completion information to ACCME for the purpose of granting ABIM MOC credit.

All other clinicians completing this activity will be issued a certificate of participation. To participate in this journal CME activity: (1) review the learning objectives and author disclosures; (2) study the education content; (3) take the post-test with a 75% minimum passing score and complete the evaluation at http://www.medscape.org/journal/eid; and (4) view/print certificate. For CME questions, see page 411.

NOTE: It is Medscape's policy to avoid the use of brand names in accredited activities. However, in an effort to be as clear as possible, the use of brand names should not be viewed as a promotion of any brand or as an endorsement by Medscape of specific products.

Release date: January 23, 2024; Expiration date: January 23, 2025

Learning Objectives

Upon completion of this activity, participants will be able to:

- Distinguish the rate of seropositivity against SARS-CoV-2 in a community-based sample of US residents in 2021.
- Evaluate variables which affected the rate of seropositivity against SARS-CoV-2.
- Assess the prevalence and clinical implications of positive PCR tests for SARS-CoV-2 in the current study.
- Analyze study participants' willingness to receive the COVID-19 vaccine.

CME Editor

P. Lynne Stockton Taylor, VMD, MS, ELS(D), Technical Writer/Editor, Emerging Infectious Diseases. *Disclosure: P. Lynne Stockton Taylor, VMD, MS, ELS(D), has no relevant financial relationships.*

CME Author

Charles P. Vega, MD, Health Sciences Clinical Professor of Family Medicine, University of California, Irvine School of Medicine, Irvine, California. *Disclosure: Charles P. Vega, MD, has the following relevant financial relationships: served as a consultant or advisor for Boehringer Ingelheim; GlaxoSmithKline; Johnson & Johnson Services, Inc.*

Authors

Jessica Justman, MD; Timothy Skalland, PhD; Ayana Moore, PhD; Christopher Amos, PhD; Mark Marzinke, PhD; Sahar Zangeneh, PhD; Colleen Kelley, MD; Rebecca Singer, DNP; Yael Hirsch-Moverman, PhD; Susanne Doblecki-Lewis, MD; David Metzger, PhD; Elizabeth Barranco, MD; Ken Ho, MD; Ernesto Marques, MD, PhD; Margaret Powers-Fletcher, PhD; Patricia Kissinger, PhD; Jason Farley, PhD; Carrie Knowlton, DNP; Magdalena Sobieszczyk, MD; Shobha Swaminathan, MD; Domonique Reed, MPH; Jean De Dieu Tapsoba, PhD; Lynda Emel, PhD; Ian Bell, BA; Krista Yuhas, MS; Leah Schrumpf, MSc; Laura Mkumba, MSc; Jontraye Davis, MHA; Jonathan Lucas, MPH; Estelle Piwowar-Manning, BS, MT; Shahnaz Ahmed, BS.

During January–August 2021, the Community Prevalence of SARS-CoV-2 Study used time/location sampling to recruit a cross-sectional, population-based cohort to estimate SARS-CoV-2 seroprevalence and nasal swab sample PCR positivity across 15 US communities. Survey-weighted estimates of SARS-CoV-2 infection and vaccine willingness among participants at each site were compared within demographic groups by using linear regression models with inverse variance weighting. Among 22,284 persons ≥2 months of age and older, median prevalence of infection (prior, active, or both) was 12.9% across sites and similar across age groups. Within each site, average prevalence of infection was 3 percentage points higher for Black than White persons and average vaccine willingness was 10 percentage points lower for Black than White persons and 7 percentage points lower for Black persons than for persons in other racial groups. The higher prevalence of SARS-CoV-2 infection among groups with lower vaccine willingness highlights the disparate effect of COVID-19 and its complications.

As of May 2023, ≈104 million confirmed SARS-CoV-2 cases had been reported in the United States (*1*). That case count is certainly an underestimate, given the occurrence of asymptomatic disease; self-testing and unreported cases; and limited initial diagnostic testing, especially among children. The true case count may be gleaned from SARS-CoV-2 seroprevalence studies. In most parts of the world, including the United States, many prevalence estimates have been based on convenience samples of adults (*2*), including samples from healthcare settings (*3*) or from US commercial laboratories (*4*). According to those approaches, seroprevalence has varied from 10% to 58%, depending on the type of serologic test used, calendar time in relation to the pandemic, population sampling strategy, and characteristics of the population (e.g., demographic, clinical, and healthcare seeking) (*3*,*4*).

Population-based seroprevalence estimates from nonclinical general populations have been few (*5*), reflecting challenges posed by the COVID-19 pandemic with regard to rigorous sampling strategies for reaching representative populations (*6*–*9*). Some strategies have used social media to recruit diverse populations but lacked a well-defined sampling frame (*10*), and regional studies with random sampling schemes have lacked diverse participation (*11*–*13*). In addition, many seroprevalence studies have not included detailed demographic and socioeconomic information about the participants despite the association of those factors with SARS-CoV-2 infection (*14*–*17*).

We report the results of the Community Prevalence of SARS-CoV-2 Study (COMPASS), which was conducted in the first half of 2021 to assess prevalence of prior and current SARS-CoV-2 infection among the general population of adults and children in largely urban communities surrounding established clinical research sites in the United States. We based determination of infection on antibody and PCR positivity. We also describe the population-level factors associated with increased risk for SARS-CoV-2 infection. COMPASS used time/location sampling (TLS) as a rigorous method of nonprobability sampling of public venues near the participating research sites to enroll persons from the community (*18*,*19*). To improve the representativeness of the general population sample given the mobility restrictions of the pandemic, COMPASS also recruited a clinical cohort from outpatient healthcare facilities and a nursing home cohort from residential facilities for older adults.

Methods

Study Design and Setting

COMPASS (ClinicalTrials.gov identifier NCT04658121, https://clinicaltrials.gov) was a cross-sectional survey sponsored by the National Institute of Allergy and Infectious Diseases (NIAID)–funded COVID-19 Prevention Network (*20*). A total of 68 existing US-based

Author affiliations: Columbia University, New York, New York, USA (J. Justman, Y. Hirsch-Moverman, M.E. Sobieszczyk, D. Reed); Fred Hutchinson Cancer Center, Seattle, Washington, USA (T. Skalland, S.Z. Zangeneh, J. De Dieu Tapsoba, L. Emel, I. Bell, K. Yuhas); FHI 360, Durham, North Carolina, USA (A. Moore, L. Schrumpf, L. Mkumba, J. Davis, J. Lucas); Baylor College of Medicine, Houston, Texas, USA (C.I. Amos); Johns Hopkins University, Baltimore, Maryland, USA (M.A. Marzinke, J.E. Farley, E. Piwowar-Manning, S. Ahmed); Emory University, Atlanta, Georgia, USA (C.F. Kelley); University of Illinois Chicago, Chicago, Illinois, USA (R. Singer, S. Mayer); University of Miami, Miami, Florida, USA (S. Doblecki-Lewis); University of Pennsylvania, Philadelphia, Pennsylvania, USA (D. Metzger); Ponce Health Sciences University, Ponce, Puerto Rico (E. Barranco); University of Pittsburgh, Pittsburgh, Pennsylvania, USA (K. Ho, E.T.A. Marques); University of Cincinnati, Cincinnati, Ohio, USA (M. Powers-Fletcher); Tulane University, New Orleans, Louisiana, USA (P.J. Kissinger); University of Colorado, Aurora, Colorado, USA (C. Knowlton); Rutgers Medical School, Newark, New Jersey, USA (S. Swaminathan); RTI International, Research Triangle Park, North Carolina, USA (S.Z. Zangeneh)

DOI: https://doi.org/10.3201/eid3002.230863

[1]Preliminary results from this study were presented virtually at the 2022 Conference on Retroviruses and Opportunistic Infections, February 2022 (abstract 46).

NIAID clinical research sites (hereafter called sites) were invited to conduct the study with the goal of enhancing representative sampling in multiple regions across the United States. The 15 participating sites (Appendix, https://wwwnc.cdc.gov/EID/article/30/2/23-0863-App1.pdf) were located in the southern, midwestern, mid-Atlantic, and northeastern United States as well as Puerto Rico.

Ethics approvals were obtained from a central (Advarra) and participating sites' institutional review boards (Appendix). All participants or their representatives provided written informed consent or assent for persons 7–17 years of age with parental/guardian consent; remote electronic consent for persons 15–17 years of age was permissible for parents not physically present. For adults with mental incapacity, consent was provided by a legally authorized representative.

Participants and Sampling

The study population consisted of adults and children recruited from the catchment area of each site (*18*). TLS was used to recruit participants in the community and outpatient clinic cohorts, and because of pandemic restrictions to access, convenience sampling was used to recruit the nursing home cohort. Ethnographic mapping of community venues in each catchment area (e.g., supermarkets, parks, commercial streets, and interviews with venue managers when relevant) identified time venues (i.e., times when venues were available and likely to have foot traffic). Clinical venues where persons visiting outpatient facilities were recruited to the clinical cohort were distinct from community venues. The catchment area of each site was defined as the postal (ZIP) code of the site plus all contiguous ZIP codes, encompassing a population of ≈150,000 (Appendix).

Research teams visited time venues randomly selected on the basis of sampling frames updated weekly by each site and attempted to recruit all persons at each time venue (Appendix). They collected the number of persons approached versus enrolled at each time venue, and the resulting ratio was used to adjust for nonresponse. Adults ≥18 years of age and children ≥2 months of age who were recruited in the community were eligible for the community cohort; adults who were recruited at a selected outpatient healthcare facility were eligible to join the clinical cohort; and those recruited at a senior living facility were eligible to join the nursing home cohort. For all cohorts (community, outpatient, senior living facility), potential participants were excluded if they had previously enrolled in the study or if there was any condition that, in the opinion of the study staff, would interfere with achieving the study objectives. COVID-19 vaccination was not exclusionary. Study participants received a cash gift card consistent with local standards as compensation for time and effort.

We collected demographic, socioeconomic, geographic, clinical, and household SARS-CoV-2 exposure and infection history information from each consenting participant (or a parent of participants <9 years of age) via an interviewer-administered questionnaire conducted in English or Spanish in a relatively private location at the venue (e.g., to the side of the tent). The questionnaire assessed COVID-19 symptoms and willingness to receive an approved COVID-19 vaccine. At the end of March 2021, the questionnaire was updated to allow participants to self-report whether they had received an approved vaccine (i.e., a US Food and Drug Administration–authorized COVID-19 vaccine).

Participants provided whole blood samples via venipuncture and mid-turbinate samples via nasal swabbing. For participants ≤2 years of age, blood was collected by heel or finger stick, and dried blood spots were prepared at study sites. Serum was isolated from blood, and serologic evidence of prior SARS-CoV-2 infection was evaluated by using the Abbott Architect SARS-CoV-2 IgG nucleocapsid antibody assay (Abbott Diagnostics), for which, according to manufacturer claims, specificity was 99.6% and sensitivity was 100% (*21*). To reduce interassay and interlaboratory variability, testing was performed at a central laboratory (Quest Diagnostics) by use of a single assay. To determine the prevalence of active SARS-CoV-2 infections, PCR analysis was performed on midturbinate nasal swab samples by using validated, approved assays (Appendix). SARS-CoV-2 PCR results, but not serologic results, were returned to study participants.

Outcomes

The primary outcome was the proportion of participants with prior SARS-CoV-2 infection, based on presence of SARS CoV-2 IgG nucleocapsid antibody (Ab+). A secondary outcome was the proportion of participants with active SARS-CoV-2 infection, based on results of SARS-CoV-2 RNA testing (PCR+). A combined outcome of the proportion with prior or active SARS-CoV-2 infection was based on having a status of Ab+, PCR+, or both. Vaccine willingness was defined as the proportion of participants who reported on a 5-point scale that they were likely or very likely to receive an approved vaccine or responded that they had already received an approved vaccine. The proportion of Ab+ participants who reported being asymptomatic was based on the number of

participants who responded no to all 13 yes/no questions about experiencing upper respiratory or systemic symptoms since November 2019. The proportion of PCR+ participants who reported being asymptomatic was similarly based on the number who responded no when asked about each of the same 13 symptoms currently or in the past 14 days (Appendix).

Power Calculation and Statistical Analyses

The target sample size for each of the 4 target age groups (<18, 18–39, 40–59, ≥60 years) in the community cohort was 730, based on a prespecified margin of error of 2.5% for seroprevalence of <5% and a 5% margin of error for seroprevalence of 10%–25% (*18*). Each site therefore sought to enroll 2,920 participants from community venues, as well as an additional 500 adults from outpatient health facilities and 500 adults from nursing homes.

We constructed estimates for the 3 laboratory-based prevalence outcomes as well as vaccine willingness for each of the 15 clinical research site communities overall; for each target age group; and by sex assigned at birth (female, male), race (Black, White, other), and ethnicity (Hispanic, non-Hispanic). Other race categories were Asian, Native Hawaiian or other Pacific Islander, and other, as well as those answering don't know/not sure and prefer not to answer. Prevalence by gender identity was not estimated because 68% of enrolled participants did not respond to a question about current gender identity. Survey weights accounted for sampling design (*18*), nonresponse, and, per data from the American Community Survey (https://data.census.gov/table/?d=ACS%205-Year%20Estimates%20Detailed%20Tables), poststratification (Appendix).

We limited analyses of cross-site summary measures of the combined endpoint (Ab+, PCR+, or both) and vaccine willingness to sites that had enrolled ≥25 participants in the specific demographic group and described those measures as medians with interquartile ranges (IQRs). We separately compared combined prevalence outcome (active infection, prior infection, or both) and vaccine willingness within demographic groups (age, sex, race, and ethnicity) by using linear regression models with inverse variance weighting. We used a robust heteroskedasticity-consistent type sandwich variance estimation approach to account for potential nonconstant error variances in the weighted linear regression models that included the proportion (e.g., vaccine willingness) as an outcome and the demographic variable of interest as a covariate while accounting for site.

Results

We enrolled 26,201 adults and children in the study from January 12, 2021, through August 12, 2021; median recruitment period per site was 164 days (range 84–199 days, IQR 150–185 days). During that time, ≈69,000 persons were approached from a cumulative total of ≥450 unique community venues surrounding the 15 clinical research sites; 22,284 (≈32%) participants enrolled (Figure 1), resulting in a median enrollment per community of 1,246 (range 508–2,924, IQR 997–1,682) participants. Sites intended to enroll one quarter of the community cohort into each of the 4 age groups; however, only 2,113 (9.5%) enrolled participants were <18 years, and the median number of children per site was 48 (IQR 24–100). Most sites enrolled similar proportions of male and female participants from community venues (Appendix Table 2). A total of 3,111 participants were enrolled in the clinical cohort and 806 in the nursing home cohort (Appendix Tables 1, 3, 4, Figures 1, 2).

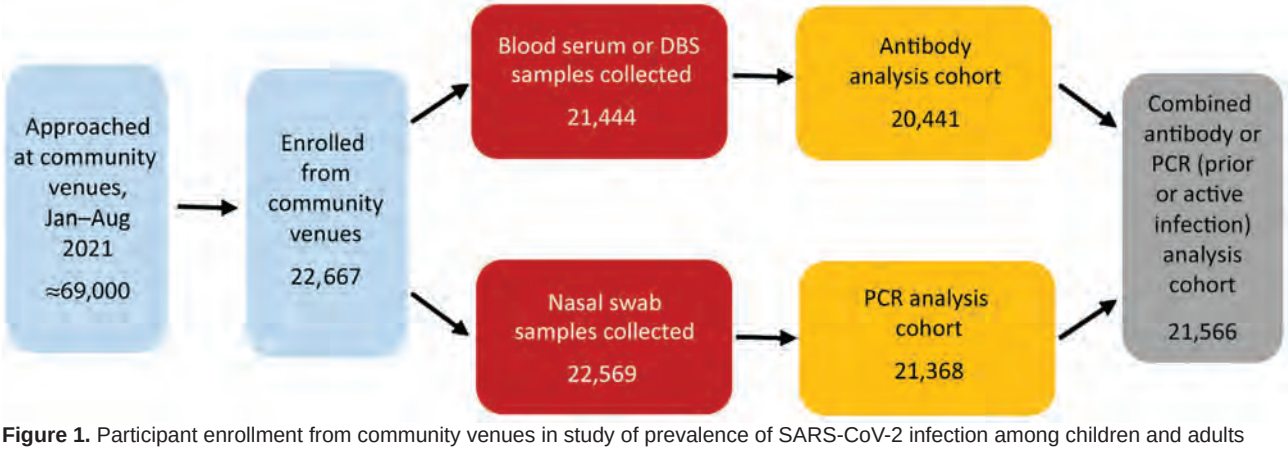

Figure 1. Participant enrollment from community venues in study of prevalence of SARS-CoV-2 infection among children and adults in 15 US communities (COMPASS 2021). Each site completed community enrollment from a median of 30 (interquartile range 24–35) venues. At each site, 80% of community enrollments were completed at a median of 13 (interquartile range 8.5–15.5) venues. DBS, dried blood spot.

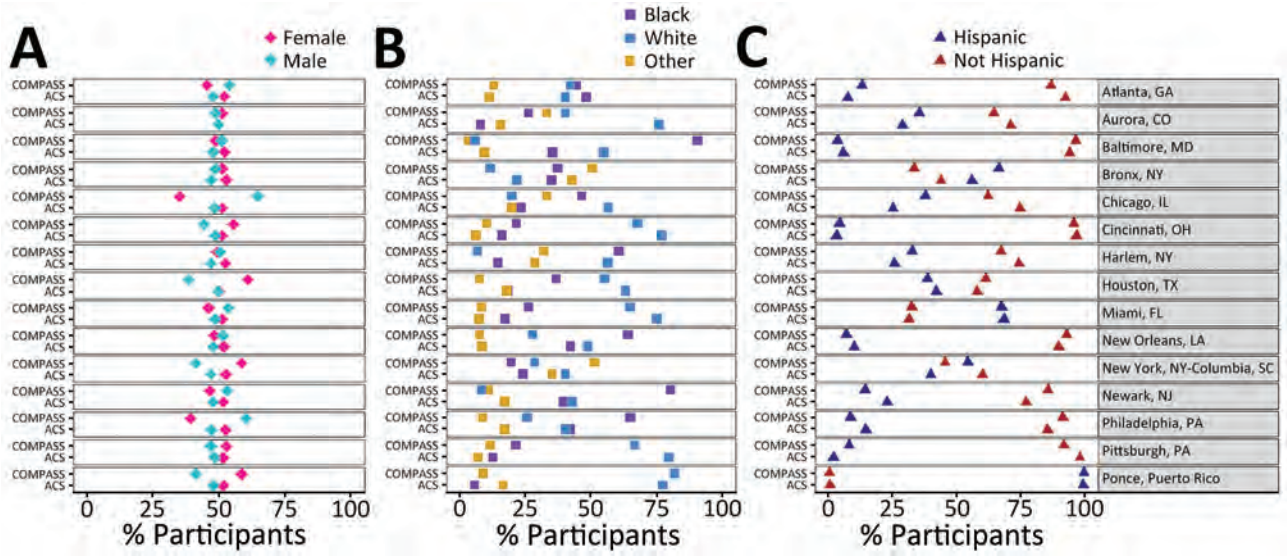

Figure 2. Demographic characteristics of community cohort (n = 21,189) in study of prevalence of SARS-CoV-2 infection among children and adults in 15 US communities (COMPASS 2021) and the 2020 US Census American Community Survey (https://www.census.gov/programs-surveys/acs) for each site.A) sex; B) race; C) ethnicity.

A total of 22,284 participants of the targeted 43,800 were enrolled from community venues; of those, 95% provided a blood sample for SARS-CoV-2 antibody testing and 99% provided a nasal swab sample for SARS-CoV-2 PCR testing (Figure 1). Complete data were available for 21,189 (95%) community cohort enrollees for analysis of a combined endpoint of Ab+, PCR+, or both (i.e., evidence of prior or active infection). The remainder of the findings about the community cohort pertain to the group of 21,189.

The unadjusted demographic profile for sex and ethnicity of the community cohort was similar to the estimated demographic profiles for most communities according to corresponding county-level data from the American Community Survey (Figure 2); however, the profile by race differed at several sites. In addition, prevalence of race varied widely, from 9% to 89% for Black persons (median 37% [IQR 24%–62%] across sites) and from 6% to 80% for White persons (median 28% [IQR 15%–60%] across sites). Hispanic ethnicity varied from 3% to 98% (median 33% [IQR 9%–47%] across sites).

Median seropositivity of the community cohort (Appendix Table 5, Figure 3), determined according to 2,272 Ab+ participants, was 12.4% (IQR 9.1%–14%); seropositivity was similar for the clinical cohort (11.3% [IQR 7.7%–15.5%]) but lower for the nursing home cohort (3.3% [IQR 2.4%–7.7%]). Of note, 50% of the nursing home cohort participants were recruited in Puerto Rico, where seroprevalence for all age groups was 3%–5% (Figure 3, panel B). The median overall prevalence of active infection (PCR positivity) in the community cohort across all sites (Appendix Table 5, Figure 3), determined according to 189 PCR+ participants, was 0.8% (IQR 0.2%–1.5%) A total of 64 participants enrolled in COMPASS were both PCR+ and Ab+ (52 from the community cohort and 12 from the clinical cohort).

In the community cohort, overall median prevalence across all 15 site-level estimates of the combined endpoint, based on PCR+ or Ab+ status, was 12.9% (range 4.9%–18%, IQR 9.2%–14%) (Figure 3, panel A). Although prevalence varied widely, when we looked at demographic differences within each site, we found no difference in average prevalence of prior or active infection by age, whether considering the 4 age groups at all sites (Figure 3, panel A) or comparing children (<18 years of age) with adults (≥18 years of age) at each of the 10 sites that enrolled ≥25 children (Figure 3, panel B). We also found no difference in average prevalence by participant sex or ethnicity (Figure 3, panel A). Within each site, however, the average prevalence estimate for Black participants was 3 percentage points higher than for White participants ($p<0.01$) and 2.4 percentage points higher than for those with race identified as other ($p = 0.11$). Among participants ≥18 years of age, we found a nonsignificant association between a higher prevalence of active or prior SARS-CoV-2 infection and a lower level of attained education (Appendix Figure 4). We found no association between COVID-19 and income level; however, many (32.8%) participants reported their household income as don't know or prefer not to answer (data not shown).

About half of seropositive persons in the community cohort reported that they had not ever experienced COVID-19 symptoms (median 50.0%

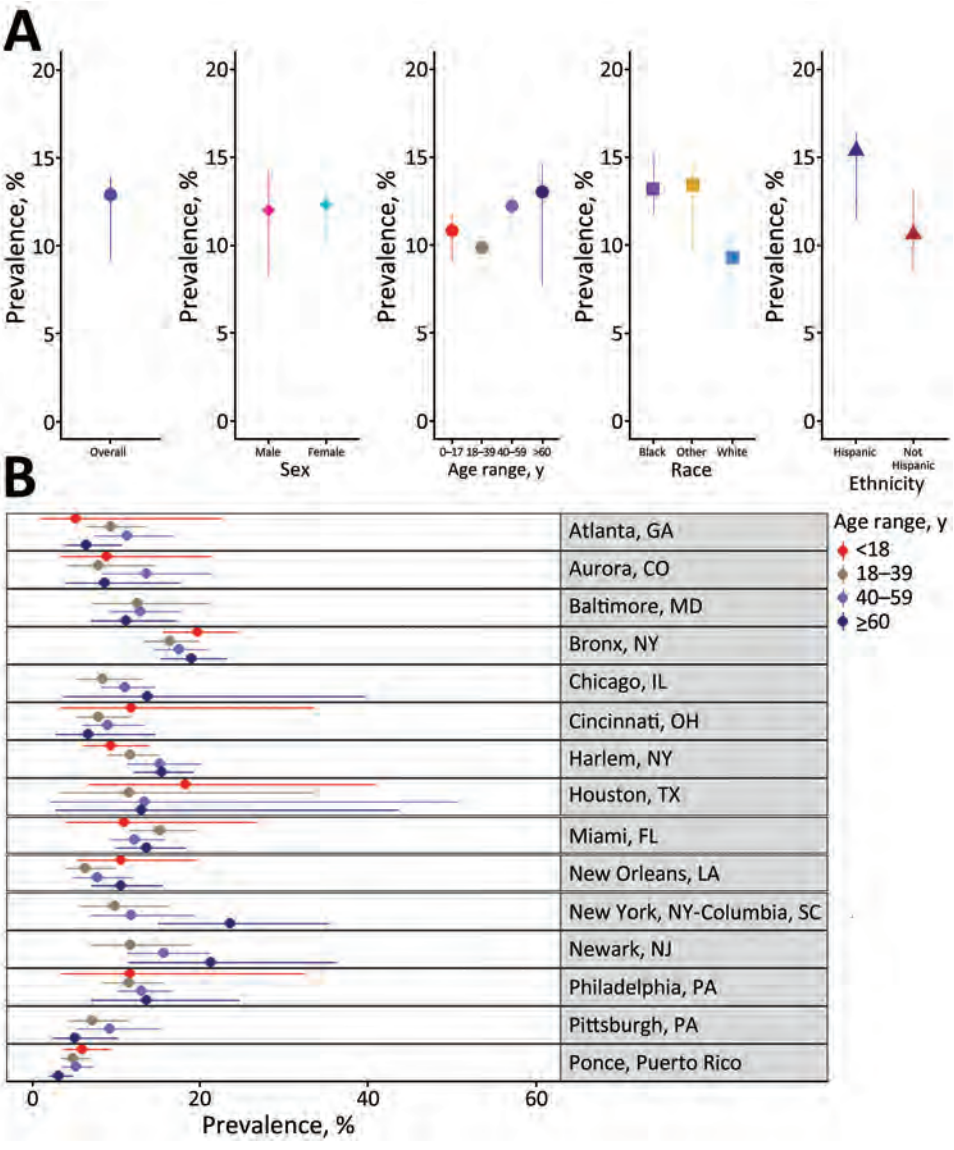

Figure 3. Prevalence of active or prior COVID-19 infection in 15 US communities, community cohort (n = 21,189), COMPASS 2021. A) By demographic characteristic across all sites. B) By age and site. Error bars indicate interquartile ranges. Note: Analysis of age limited to communities with >25 children who had complete data.

[IQR 45.3%–63.8%]; data not shown). Similarly, about half of PCR+ persons in the community cohort reported not having experienced symptoms within the 14 days before their participation in the survey (median 52.4% [IQR 50.0%–62.4%]; data not shown). In contrast, among the seronegative persons in the community cohort, a median of 80.9% (IQR 75.7%–83.4%; data not shown) reported they had not ever experienced COVID-19 symptoms. Similarly, a median of 79.8% of PCR-negative persons (IQR 75.7–83.1%; data not shown) in the community cohort reported not having experienced symptoms within the 14 days before the survey.

In a separate analysis of self-reported PCR and antibody results among the 21,940 persons who enrolled and tested antibody negative in COMPASS (18,629 from the community cohort), prevalence of a self-reported prior positive COVID-19 test (nasal swab sample) was 4.9% (n = 1,067) and prevalence of a self-reported prior positive antibody test was 2.4% (n = 526) (data not shown). By contrast, among the 2,792 who enrolled and tested antibody positive in COMPASS (2,380 from the community cohort), prevalence of a self-reported prior positive COVID-19 test (nasal swab sample) was 33.4% (n = 933) and prevalence of a self-reported prior positive antibody test was 7.9% (n = 221) (data not shown).

Overall, across 15 site-level estimates, the median percentage of persons in the community cohort who reported being willing to receive a COVID-19 vaccine was 78% (IQR 72%–82%); the percentage was higher among participants ≥60 years of age (median 89%,

IQR 84%–92%) compared with those 18–39 years of age (median 74%, IQR 67%–83%) and 40–59 years of age (median 76%, IQR 74%–81%) (Figure 4). The median percentage of participants who reported being willing to receive a vaccine was 71.4% (IQR 64.8%–76.3%) for Black, 78% (IQR 68.8%–82.5%) for other race, and 84.2% (IQR 73.6%–87.0%) for White participants (Appendix Table 6). We found no differences in willingness to receive a vaccine by sex or ethnicity across the sites. When looking at demographic differences within each site, we found that vaccine willingness among those ≥60 years of age was an average of 10 percentage points higher than among those 40–59 ($p<0.01$) years of age, 11 percentage points higher than those 18–39 ($p<0.01$) years of age, and 22 percentage points higher than those <18 years of age ($p<0.01$). Similarly, the average difference among participants who reported being willing to receive a vaccine was 10 percentage points lower for Black compared with White participants ($p<0.01$) and 7 percentage points lower for Black participants than for persons in other racial groups ($p<0.01$).

Discussion

COMPASS, a population-based cross-sectional serosurvey, enrolled ≈22,000 adults and children from community venues in 15 largely urban US settings in the first half of 2021 and found that the overall prevalence of prior and active SARS-CoV-2 infection was 12.9%. TLS, typically used to recruit hard-to-reach populations (*19*), was an innovative way to randomly sample populations representative of diverse communities amid pandemic restrictions to access and movement, based on demographic comparisons with the American Community Survey. Contrasting with initial reports of COVID-19 (*22*–*24*), population-based prevalence did not vary by age, indicating that acquisition was similar for all age groups. In addition, despite prevalence of prior or active COVID-19 being higher among Black participants, fewer Black participants in the sampled communities were willing to receive an approved COVID-19 vaccine compared with participants who were from White or other racial groups, a finding that may have magnified the disparate burden of COVID-19 and associated outcomes in these communities.

Compared with our findings, studies conducted in healthcare settings may have arrived at higher estimates of COVID-19 prevalence (*3*,*4*), reflecting the symptomatic status, healthcare access, and healthcare-seeking behavior of clinical populations. For example, a commercial laboratory seroprevalence study conducted in the United States during the second half of 2021 assessed at 4-week intervals convenience samples of blood specimens collected for clinical testing and found an overall US seroprevalence of 33.5% in December 2021 (*4*). Similar to our findings with regard to age, the study of commercial laboratory samples also found that seroprevalence among children and adults did not differ. Whether for COVID-19 or other widespread outbreaks, such as mpox, seroprevalence estimates from population-based studies that include those who are less likely to engage in care, combined with estimates from healthcare settings, may offer the most comprehensive picture of outbreak effects at that point in time.

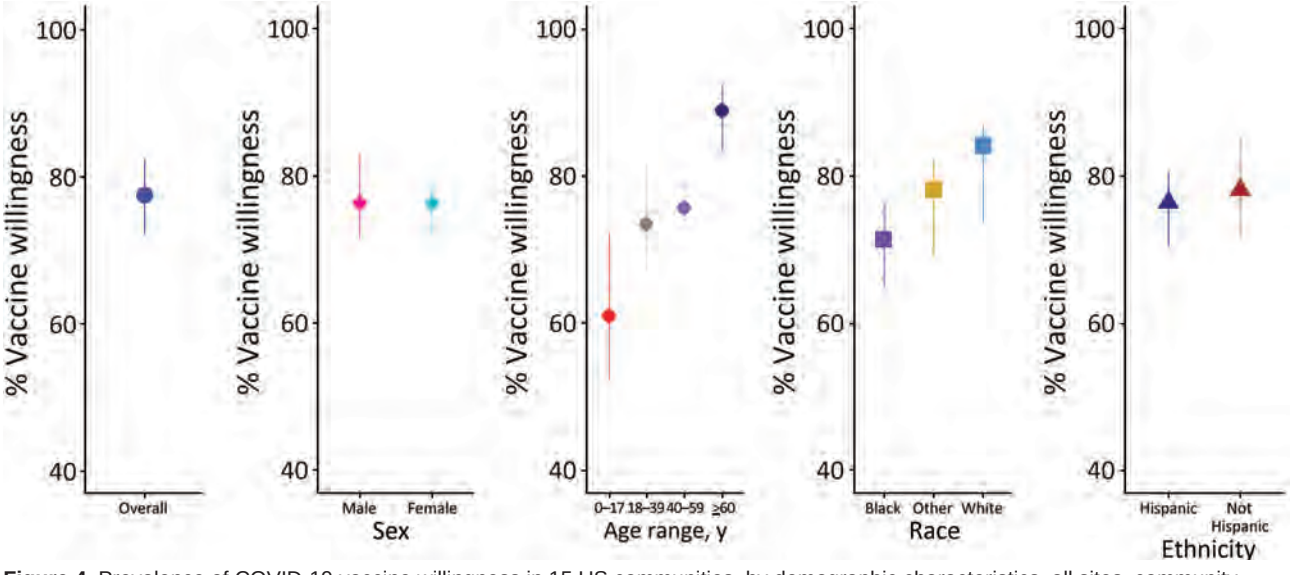

Figure 4. Prevalence of COVID-19 vaccine willingness in 15 US communities, by demographic characteristics, all sites, community cohort, COMPASS 2021. Note: Analysis of age limited to communities with >25 children who had complete data.

COMPASS found that willingness to receive a vaccine during the first half of 2021, during the earliest stages of vaccine availability in the United States, was 10 percentage points lower among Black participants and 7 percentage points lower among other race participants than among White participants. Monthly telephone surveys of immunization practices, conducted during December 2020–November 2021, found a similar level of racial disparity in April 2021 (*25*). By November 2021, racial disparities in COVID-19 vaccine uptake in the United States were no longer evident (*26*); nonetheless, 1 year later, by December 2022, Black race and Hispanic ethnicity remained associated with higher rate ratios of age-adjusted hospitalization and death compared with White race (*26*,*27*), indicating that vaccine uptake alone did not explain disparities in outcomes.

Strengths of our study included collection of biological samples and detailed demographic, behavioral, and self-reported clinical data from randomly sampled persons from the general population, including children. COMPASS used a centrally managed approach to TLS to ensure a participant population that reflected the communities surrounding clinical research sites participating in COVID-19 vaccine trials. The weekly systematic updating of community venue sampling frames was a novel way to adapt to changing COVID-19 guidelines and restrictions as well as to fluctuating weather (*18*). The prevalence of active infection was based on validated laboratory assays performed on approved platforms. Although we did not assess serologic evidence of vaccine immunity (SARS-CoV-2 spike antibody), the serologic assessment of prior infection through a single assay conducted at a centralized laboratory yielded rigorous seroprevalence findings.

Limitations of our study included conducting it in the first half of 2021, just before the Delta variant became dominant in the United States, when vaccines were becoming available, home-based rapid test kits were not yet widely available, and even PCR testing was often not easily available. Although enrollment targets, especially for children, were not fully achieved, the study had sufficient power to compare both seroprevalence and the combined endpoint of seroprevalence, PCR positivity, or both, by age group. The results do not reflect the entire US population but do reflect persons who were well enough to attend commonly frequented venues in diverse, largely urban communities surrounding the participating clinical research sites, who represent those who had more exposure to COVID-19 compared with those who were homebound. Sampling largely urban settings was relevant, given that the US population is 80% urban (*28*) and that, globally, COVID-19 cases had a large effect in urban settings, especially in the earlier stages of the epidemic (*29*). Serologic testing may have underestimated seroprevalence because of either absent or low titers after a mild infection (*30*) or waning antibody titers after a distant (>6 months) infection (*31*). Last, recall and social desirability biases may have affected the accuracy of replies to some sections of the questionnaire.

In our population-based survey, we used TLS to recruit members of the general population who were relatively hard to reach because of the status of the COVID-19 pandemic. Our findings demonstrate that prior and active SARS-CoV-2 infection varied widely by community but, contrasting with initial reports, not by age. Half of Ab+ and PCR+ participants reported no symptoms, underscoring the limitations of case-based reporting and the potential for asymptomatic transmission (*32*,*33*). Our findings of higher prevalence of prior or active COVID-19 among persons who were less willing to get vaccinated highlight the value of tailoring public health efforts to the communities most likely to continue to experience disparate effects COVID-19 and its complications.

Acknowledgments

We thank all the COMPASS study participants as well as the key study staff and their institutions for their contributions to the COMPASS study: The Ponce de Leon Center CRS, Atlanta, GA: Aryn Prince, Jessica Swiniarski, Santiago Tovar; Johns Hopkins CRS Baltimore, MD: Kelly Lowenson, Jess LaRicci, Adam Bocek, Woudase Gallo; Bronx Prevention Research Center CRS, New York, NY: Nandita Sugandhi, Rita Sondengam, Saranya Naidu, Kyle Eiffler; UIC Project Wish Clinical Research Site (CRS), Chicago, IL: Scott Lea, Taylor Ellis; Cincinnati CRS, Cincinnati, OH: Delia P. Miller, Sylvere Mukunzi, Sydnei Simpson, Madison Riddell, Kristin N. Weghorn, Justin Benoit, Diego F. Cuadros; Harlem Prevention Center CRS, New York, NY: Sharon B Mannheimer, Julie Franks, Avelino Jun Loquere, Kamesha Martin, Ibrahima Cisse, Vidhi Patel, Elvis Ndansi; Baylor College of Medicine, Houston, TX: Hana M. El Sahly, Maria Carmenza Mejia, Abiodun Oluyomi, Winnifred Hamilton, Catherine Mary Healy, Merin Thomas, Pedro A. Piedra, Kathryn Edwards, Gloria Liao, Dakai Zhu, Sarah Selleck; University of Miami, IDRU at Jackson Memorial Hospital CRS, Miami, FL: Stefani Butts, Mariano Kanamori, Zinzi Bailey; New Orleans Adolescent Trials Unit CRS, New Orleans, LA: Julie H. Hernandez, Susan E. Abdalian, Ratnayake, Susan Abdalian, Norine Schmidt; Columbia P&S CRS, New York, NY: Jorge Benitez, Henry Peralta,

Jackie Wu, Ariana Pazmino, Renee Roberts, Tae Y. Kim, Marvin Castellon, Jonathan Kunkel-Jure, Sade Tukuru, Mascha Elskamp; New Jersey Medical School CRS, Newark, NJ: Rondalya Deshields, Christie Lyn Costanza, Naema Milead, Zoraida Cruz-Barahona, Charles Oh, Sivanne Mendelson, Briana Brodie, Megan Shanahan, Ashley Zenerovitz, Pansy Law, Andrew Morero, Xena Agbolou, Travis Love; Penn Prevention CRS, Philadelphia, PA: Juan Diego Ramirez, Victoria Milano, Meredith Page Miller; University of Pittsburgh, Pittsburgh, PA: Stacey Edick, Jim Gavel, Jenn Oakley, Angel Servillo, Justin Mondry, Linda Frank, Todd Bear, Wendy King, Dara Mendez, Gabby Yearwood; St. Louis University VTEU, CAIMED-PHSU, Ponce, Puerto Rico: Lydiet Dedos, Nancy Jimenez, Velma Franceschini, Frances Figueroa, Luisa I. Alvarado, Odette Oliveri.

This research was supported by the National Institutes of Health (Office of the Director, National Institute of Allergy and Infectious Disease, National Institute on Drug Abuse, National Institute of Mental Health, and the Eunice Kennedy Shriver National Institute of Child Health and Human Development). All authors were supported by UM1AI068619 except as follows: UM1AI068617 (T.S., S.Z., J.D.T., L.E., I.B., and K.Y.), UM1AI068613 (M.A.M., E.P.-M., and S.A.); and T32AI114398 (D.R). The content is solely the responsibility of the authors and does not necessarily represent the official views of the National Institutes of Health.

About the Author

Dr. Justman is an infectious disease specialist, global health expert, and professor of medicine in epidemiology and senior technical director at ICAP, a global public health center at the Mailman School of Public Health at Columbia University. Her research interests include HIV prevention, care, and treatment in sub-Saharan Africa and the United States as well as COVID-19.

References

1. Centers for Disease Control and Prevention. Trends in United States COVID-19 hospitalizations, deaths, emergency department (ED) visits, and test positivity by geographic area [cited 2023 May 2]. https://covid.cdc.gov/covid-data-tracker/#trends_weeklydeaths_select_00
2. Akinbami LJ, Kruszon-Moran D, Wang CY, Storandt RJ, Clark J, Riddles MK, et al.SARS-CoV-2 serology and self-reported infection among adults—National Health and Nutrition Examination Survey, United States, August 2021–May 2022. MMWR Morb Mortal Wkly Rep. 2022;71:1522–5. https://doi.org/10.15585/mmwr.mm7148a4
3. Anand S, Montez-Rath M, Han J, Bozeman J, Kerschmann R, Beyer P, et al. Prevalence of SARS-CoV-2 antibodies in a large nationwide sample of patients on dialysis in the USA: a cross-sectional study. Lancet. 2020;396:1335–44. https://doi.org/10.1016/S0140-6736(20)32009-2
4. Clarke KEN, Jones JM, Deng Y, Nycz E, Lee A, Iachan R, et al. Seroprevalence of infection-induced SARS-CoV-2 antibodies—United States, September 2021–February 2022. MMWR Morb Mortal Wkly Rep. 2022;71:606–8. https://doi.org/10.15585/mmwr.mm7117e3
5. Sullivan PS, Siegler AJ, Shioda K, Hall EW, Bradley H, Sanchez T, et al. Severe acute respiratory syndrome coronavirus 2 cumulative incidence, United States, August 2020–December 2020. Clin Infect Dis. 2022;74:1141–50. https://doi.org/10.1093/cid/ciab626
6. Blumberg SJ, Parker JD, Moyer BC. National Health Interview Survey, COVID-19, and online data collection platforms: adaptations, tradeoffs, and new directions. Am J Public Health. 2021;111:2167–75. https://doi.org/10.2105/AJPH.2021.306516
7. Paulose-Ram R, Graber JE, Woodwell D, Ahluwalia N. The National Health and Nutrition Examination Survey (NHANES), 2021–2022: adapting data collection in a COVID-19 environment. Am J Public Health. 2021;111:2149–56. https://doi.org/10.2105/AJPH.2021.306517
8. Ward JA, Stone EM, Mui P, Resnick B. Pandemic-related workplace violence and its impact on public health officials, March 2020–January 2021. Am J Public Health. 2022;112:736–46. https://doi.org/10.2105/AJPH.2021.306649
9. Shook-Sa BE, Boyce RM, Aiello AE. Estimation without representation: early severe acute respiratory syndrome coronavirus 2 seroprevalence studies and the path forward. J Infect Dis. 2020;222:1086–9. https://doi.org/10.1093/infdis/jiaa429
10. Kreuter F, Barkay N, Bilinski A, Bradford A, Chiu S, Eliat R, et al. Partnering with a global platform to inform research and public policy making: what needs to be in place to make a global COVID-19 survey work? Surv Res Methods. 2020;14:159–63.
11. Snyder T, Ravenhurst J, Cramer EY, Reich NG, Balzer L, Alfandari D, et al. Serological surveys to estimate cumulative incidence of SARS-CoV-2 infection in adults (Sero-MAss study), Massachusetts, July-August 2020: a mail-based cross-sectional study. BMJ Open. 2021;11:e051157. https://doi.org/10.1136/bmjopen-2021-051157
12. Cardenas VM, Kennedy JL, Williams M, Nembhard WN, Zohoori N, Du R, et al. State-wide random seroprevalence survey of SARS-CoV-2 past infection in a southern US state, 2020. PLoS One. 2022;17:e0267322. https://doi.org/10.1371/journal.pone.0267322
13. Cowgill KD, Erosheva EA, Elder A, Miljacic L, Buskin S, Duchin JS. Anti-SARS-CoV-2 seroprevalence in King County, WA—cross-sectional survey, August 2020. PLoS One. 2022;17:e0272783. https://doi.org/10.1371/journal.pone.0272783
14. Etti M, Fofie H, Razai M, Crawshaw AF, Hargreaves S, Goldsmith LP. Ethnic minority and migrant underrepresentation in Covid-19 research: causes and solutions. EClinicalMedicine. 2021;36:100903. https://doi.org/10.1016/j.eclinm.2021.100903
15. Karmakar M, Lantz PM, Tipirneni R. Association of social and demographic factors with COVID-19 incidence and death rates in the US. JAMA Netw Open. 2021;4:e2036462. https://doi.org/10.1001/jamanetworkopen.2020.36462
16. Lackland DT, Sims-Robinson C, Jones Buie JN, Voeks JH. Impact of COVID-19 on clinical research and inclusion of diverse populations. Ethn Dis. 2020;30:429–32. https://doi.org/10.18865/ed.30.3.429
17. Aliseda-Alonso A, Lis SB, Lee A, Pond EN, Blauer B, Rutkow L, et al. The missing COVID-19 demographic data: a statewide analysis of COVID-19-related demographic

data from local government sources and a comparison with federal public surveillance data. Am J Public Health. 2022;112:1161–9. https://doi.org/10.2105/AJPH.2022.306892
18. Zangeneh SZ, Skalland T, Yuhas K, Emel L, Tapsoba JD, Reed D, et al. Adaptive time location sampling for COMPASS, a SARS-COV-2 prevalence study in fifteen diverse communities in the United States. Epidemiology. 2023. Epub ahead of print https://doi.prg/. 10.1097/EDE.0000000000001705
19. Muhib FB, Lin LS, Stueve A, Miller RL, Ford WL, Johnson WD, et al.; Community Intervention Trial for Youth Study Team. A venue-based method for sampling hard-to-reach populations. Public Health Rep. 2001;116 (Suppl 1):216–22. https://doi.org/10.1093/phr/116.S1.216
20. NIH launches clinical trials network to test COVID-19 vaccines and other prevention tools. July 8, 2020 [cited 2022 Sep 22]. https://www.nih.gov/news-events/news-releases/nih-launches-clinical-trials-network-test-covid-19-vaccines-other-prevention-tools
21. Food and Drug Administration. EUA authorized serology test performance 2022 [cited 2023 Sep 30]. https://www.fda.gov/medical-devices/covid-19-emergency-use-authorizations-medical-devices/eua-authorized-serology-test-performance
22. Sinaei R, Pezeshki S, Parvaresh S, Sinaei R. Why COVID-19 is less frequent and severe in children: a narrative review. World J Pediatr. 2021;17:10–20. https://doi.org/10.1007/s12519-020-00392-y
23. Mehta NS, Mytton OT, Mullins EWS, Fowler TA, Falconer CL, Murphy OB, et al. SARS-CoV-2 (COVID-19): what do we know about children? a systematic review. Clin Infect Dis. 2020;71:2469–79. https://doi.org/10.1093/cid/ciaa556
24. Zimmermann P, Curtis N. COVID-19 vaccination coverage, by race and ethnicity—National Immunization Survey Adult COVID Module, United States, December 2020–November 2021. Arch Dis Child. 2020 Dec 1 [Epub ahead of print]. https://doi.org/10.1136/archdischild-2020-320338
25. Kriss JL, Hung MC, Srivastav A, Black CL, Lindley MC, Lee JT, et al. COVID-19 Vaccination Coverage, by Race and Ethnicity - National Immunization Survey Adult COVID Module, United States, December 2020–November 2021. MMWR Morb Mortal Wkly Rep. 2022;71:757–63. https://doi.org/10.15585/mmwr.mm7123a2
26. Booth A, Reed AB, Ponzo S, Yassaee A, Aral M, Plans D, et al. Population risk factors for severe disease and mortality in COVID-19: a global systematic review and meta-analysis. PLoS One. 2021;16:e0247461. https://doi.org/10.1371/journal.pone.0247461
27. Centers for Disease Control and Prevention. Hospitalization and death by race/ethnicity 2022 [cited 2023 Feb 15]. https://www.cdc.gov/coronavirus/2019-ncov/covid-data/investigations-discovery/hospitalization-death-by-race-ethnicity.htm
28. US Census Bureau. 2020 Census urban areas facts [cited 2023 May 3]. https:///www.census.gov/programs-surveys/geography/guidance/geo-areas/urban-rural/2020-ua-facts.html
29. Guterres A. COVID-19 in an urban world [cited 2023 May 3]. https://www.un.org/en/coronavirus/covid-19-urban-world#:~:text=Urban%20areas%20are%20ground%20zero,sanitation%20services%2C%20and%20other%20 challenges
30. Buss LF, Prete CA Jr, Abrahim CMM, Mendrone A Jr, Salomon T, de Almeida-Neto C, et al. Three-quarters attack rate of SARS-CoV-2 in the Brazilian Amazon during a largely unmitigated epidemic. Science. 2021;371:288–92. https://doi.org/10.1126/science.abe9728
31. Peluso MJ, Takahashi S, Hakim J, Kelly JD, Torres L, Iyer NS, et al. SARS-CoV-2 antibody magnitude and detectability are driven by disease severity, timing, and assay. Sci Adv. 2021;7:eabh3409. https://doi.org/10.1126/sciadv.abh3409
32. Johansson MA, Quandelacy TM, Kada S, Prasad PV, Steele M, Brooks JT, et al. SARS-CoV-2 transmission from people without COVID-19 symptoms. JAMA Netw Open. 2021;4:e2035057. https://doi.org/10.1001/jamanetworkopen.2020.35057
33. Ma Q, Liu J, Liu Q, Kang L, Liu R, Jing W, et al. Global percentage of asymptomatic SARS-CoV-2 infections among the tested population and individuals with confirmed COVID-19 diagnosis: a systematic review and meta-analysis. JAMA Netw Open. 2021;4:e2137257. https://doi.org/10.1001/jamanetworkopen.2021.37257

Address for correspondence: Jessica Justman, Columbia University, 722 W 168th St, Rm 1315, New York, NY 10032, USA; email: jj2158@cumc.columbia.edu

Rapid Detection of Ceftazidime/Avibactam Susceptibility/Resistance in Enterobacterales by Rapid CAZ/AVI NP Test

Patrice Nordmann, Maxime Bouvier, Adam Delaval, Camille Tinguely, Laurent Poirel, Mustafa Sadek

We developed a novel culture-based test, the Rapid CAZ/AVI NP test, for rapid identification of ceftazidime/avibactam susceptibility/resistance in Enterobacterales. This test is based on glucose metabolization upon bacterial growth in the presence of a defined concentration of ceftazidime/avibactam (128/53 μg/mL). Bacterial growth is visually detectable by a red to yellow color change of red phenol, a pH indicator. A total of 101 well characterized enterobacterial isolates were used to evaluate the test performance. This test showed positive percent agreement of 100% and negative percent agreement of 98.5% with overall percent agreement of 99%, by comparison with the MIC gradient strip test (Etest) taken as the reference standard method. The Rapid CAZ/AVI NP test had only 1.5% major errors and 0% extremely major errors. This test is rapid (result within 2 hours 45 minutes), reliable, affordable, easily interpretable, and easy to implement in clinical microbiology laboratories without requiring any specific equipment.

Ceftazidime/avibactam (CAZ/AVI), approved for clinical use in 2015, is among the latest generation of commercialized antimicrobial drugs offering a valuable feature of being active against many types of carbapenem-resistant, gram-negative organisms (*1*). CAZ/AVI is mostly used for treating severe infections caused by *Klebsiella pneumoniae carbapenemase (KPC)*–producing Enterobacterales (KPC-E), commonly associated with high illness and death rates (*2*). CAZ/AVI has also been reported to show excellent activity against producers of various clinically relevant β-lactamases, including extended-spectrum β-lactamases, AmpC β-lactamases, and some class D enzymes with carbapenemase activity (e.g., OXA-48–type enzymes), but not against the metallo-β-lactamase (MBLs) producers, such as those producing NDM, VIM, and IMP enzymes, that account for a high proportion of CAZ/AVI-resistant isolates (*3*) because MBL activities are resistant to the inhibition by AVI.

Although still uncommon, acquired resistance to CAZ/AVI is being increasingly reported and might represent a serious cause of concern (*1*). Acquired resistance to CAZ/AVI in non–MBL-producing gram-negative bacteria is attributed mostly to amino acid substitutions in β-lactamases (i.e., mutations in the bla_{KPC}, $bla_{CTX\text{-}M\text{-}14}$, $bla_{CTX\text{-}M\text{-}15}$, and $bla_{VEB\text{-}1}$ genes [*4*–*7*]), reduced expression of structural modifications, loss of outer membrane proteins (i.e., alterations in OmpK35/36 protein sequences), and overexpression of efflux pumps or mutation in the penicillin-binding proteins (*8*–*10*). Mutations or deletions in the Ω-loop region (amino acid positions 164–179) of KPC β-lactamases represent the most frequent mechanism leading to acquired resistance to CAZ/AVI resistance among KPC-producing *Klebsiella pneumoniae* isolates. KPC variants conferring CAZ/AVI resistance are usually associated with weaker carbapenemase activity and low carbapenem MICs (with recovered susceptibility to carbapenems), therefore generating relevant difficulties regarding its phenotypic detection (*1*,*2*,*11*–*18*). In addition, resistance to CAZ/AVI was reported to be associated with an increased expression of wild-type KPC-3 or even SHV-type β-lactamases in several gram-negative isolates (*19*,*20*), Hyperproduction and alterations of chromosome- or plasmid-encoded AmpC β-lactamases in *Citrobacter freundii* and *Enterobacter cloacae* (*21*–*23*) have been also reported.

Broth microdilution (BMD) is the standard method for determining CAZ/AVI resistance/susceptibility

Author affiliations: University of Fribourg, Fribourg, Switzerland (P. Nordmann, M. Bouvier, A. Delaval, C. Tinguely, L. Poirel, M. Sadek); South Valley University, Qena, Egypt (M. Sadek)

DOI: https://doi.org/10.3201/eid3002.221398

(*24*). Other techniques, such as commercially available broth microdilution panels (ThermoFisher Scientific, https://www.thermofisher.com; Merlin Diagnostika, https://www.merlin-diagnostika.de; Microscan, https://automation.omron.com; Vitek, https://vitekcctv.com; and Phoenix, https://www.bd.com/platforms), gradient diffusion tests (Liofilchem https://www.liofilchem.com; and bioMèrieux, https://www.biomerieux.com), and disk diffusion tests can alternatively be used (*25*). All those techniques are time-consuming, requiring 18 hours to obtain results. Recent studies reported that those CAZ/AVI-resistant but carbapenem-susceptible KPC producers are undetectable by the main phenotypic carbapenemase detection assays, such as lateral immunochromatographic assays, the Carba NP test (bioMèrieux), and the modified carbapenem inactivation method, because of the weak carbapenemase activity of the KPC variants (*26*–*28*). The false-negative results obtained by using immunochromatographic tests probably resulted from changes in the antigenic structure of the enzyme, leading to low-binding affinity and lack of detection consequently (*29*). In addition, failure of detection by selective screening media designed for detecting carbapenem-resistant Enterobacterales, because of their low carbapenems MICs, has been reported (*27*).

Failure to detect such acquired resistance to a last-resort therapeutic option represents a serious concern, which might be at the source of dramatic therapeutic failure, apart from preventing from early recognition of such problem eventually leading to nosocomial outbreaks. Consequently, there is a crucial need for a rapid method to accurately detect CAZ/AVI susceptibility/resistance among multidrug-resistant Enterobacterales, especially for KPC-producing isolates, to optimally adapt empirical treatment and also limit further spread by using prompt infection control measures.

In this study, we attempted to develop a novel culture-based test, namely the Rapid CAZ/AVI NP test, based on carbohydrate metabolism and detecting bacterial growth (or absence of growth) in the presence of a defined concentration of CAZ/AVI. We also determined rapid categorization of CAZ/AVI susceptibility/resistance for multidrug-resistant Enterobacterales.

Methods

Bacterial Strains

To evaluate the performance of the Rapid CAZ/AVI NP test, we used 101 nonduplicate enterobacterial isolates obtained from the Swiss National Reference Center of Emerging Antibiotic Resistance (University of Fribourg, Fribourg, Switzerland). The enterobacterial isolates included 35 CAZ/AVI–resistant strains: 16 *Escherichia coli*, 12 *K. pneumoniae*, 3 *Enterobacter cloacae*, 1 *C. freundii*, 1 *Providencia stuartii*, and 2 *Proteus mirabilis*. We also tested 66 CAZ/AVI–susceptible strains: 20 *E. coli*, 24 *K. pneumoniae*, 11 *Enterobacter cloacae*, 3 *Citrobacter freundii*, 4 *Klebsiella oxytoca*, 1 *Klebsiella aerogenes*, 1 *Citrobacter koseri*, 1 *Hafnia alvei*, and 1 *Morganella morganii* (Appendix Table, https://wwwnc.cdc.gov/EID/article/30/2/23-1398-App1.pdf). The isolates were obtained from various clinical sources (blood cultures, respiratory specimens, urinary tract infections) and from various continents (Europe, America, Asia, Africa, and Australia). The strains were all identified by using the EnteroPluri-test (Liofilchem SRL, https://www.liofilchem.com) or by whole-genome sequencing. They had previously been characterized for their major β-lactam resistance determinants by PCR and sequencing (Appendix Table).

CAZ/AVI Susceptibility Testing

We determined MICs for CAZ/AVI by using Etest strips (bioMérieux) on Mueller-Hinton agar plates at 37°C according to the manufacturer's instructions. Results were interpreted according to the latest EUCAST breakpoints for *Enterobacterales* (https://www.eucast.org/fileadmin/src/media/PDFs/EUCAST_files/Breakpoint_tables/v_12.0_Breakpoint_Tables.pdf) (i.e., susceptibility [S] ≤8 μg/mL; resistance [R] >8 μg/mL) (*24*). We used the reference strain *E. coli* ATCC 25922 as the quality control for all tests.

Rapid CAZ/AVI NP Test

On the basis of our previous experience developing several rapid diagnostic NP tests, we set and compared different parameters to determine the optimal conditions of the Rapid CAZ/AVI NP test by using 2 CAZ/AVI–susceptible isolates (1 *E. coli* ATCC 25922 and 1 KPC3-producing *K. pneumoniae* 3074) as negative controls and 2 CAZ/AVI–resistant isolates (1 NDM-5-producing *E. coli* 3031 and 1 KPC-41-producing *K. pneumoniae* 3007) as positive controls. Those parameters included bacterial inoculum, 98% ceftazidime pentahydrate (Acros Organics, Thermofisher Scientific) concentrations, avibactam sodium hydrate (MedChem Express, distributed by Lucerna-Chem, https://lucerna-chem.ch) concentrations, and incubation times with and without shaking. After comparison of the results with different parameters, all experiments were performed in triplicate by 2 persons using the optimal protocol obtained, as described below.

Rapid CAZ/AVI NP Solution

Similar to the process for the Rapid Polymyxin NP test (*30*), we prepared 250 mL of the Rapid CAZ/AVI NP solution by mixing the culture medium and the pH indicator in a glass bottle as follows: 6.25 g of Mueller-Hinton CA powder, 0.0125 g of phenol red (Sigma Aldrich, https://www.sigmaaldrich.com), 2.5 mL of 10 mol/L zinc sulfate, and 223.5 mL of distilled water. We precisely adjusted the pH of the solution to 7.3 by adding drops of 1 mol/L hydrogen chloride, then autoclaved the solution at 121°C for 15 minutes. After cooling the solution to room temperature, we added 25 mL of 10% anhydrous D-(+)-glucose (Roth, Karlsruhe, https://www.carlroth.com) sterilized by filtration. The final concentrations in the Rapid CAZ/AVI NP solution were consequently 2.5% Mueller-Hinton CA powder, 0.005% phenol red indicator, 0.1 mol/L zinc sulfate, and 1% D-(+)-glucose. This Rapid CAZ/AVI NP solution can be kept at 4°C for 1 week but must be prewarmed at 37°C before use to prevent growth delay and therefore a delayed color change.

Bacterial Inoculum Preparation

For each isolate to be tested, including the positive and negative controls, we prepared a standardized bacterial inoculum by using freshly obtained (overnight) bacterial colonies grown on UriSelect 4 agar plates (or Mueller-Hinton agar plates). We resuspended the bacterial colonies into 5 mL of sterile 0.85% saline solution to obtain a 0.5 McFarland standard optical density. The bacterial suspensions should be used within 15 minutes of preparation and for no longer than 1 hour after preparation, as recommended by the EUCAST guidelines for susceptibility testing.

Tray Inoculation

Using a sterile 96-well polystyrene microplate (round base, with lid; Sarstedt, https://www.sarstedt.com), we inoculated a bacterial suspension for each isolate in parallel into 2 wells, with and without CAZ/AVI, in separate wells. We then performed the following steps of the Rapid CAZ/AVI NP test (Figure): step 1, transferred 150 µL of CAZ/AVI–free Rapid CAZ/AVI NP solution to wells A1–A4; step 2, transferred 150 µL of the Rapid CAZ/AVI NP solution containing CAZ/AVI (final concentration of 128/53 µg/mL) to wells B1–B4; step 3, added 50 mL of 0.85% saline solution to wells A1 and B1; step 4, added 50 mL of the CAZ/AVI-resistant isolate suspension (used as a positive control) to wells A2 and B2; step 5, added 50 mL of the CAZ/AVI–susceptible isolate suspension (used as a negative control) to wells A3 and B3; step 6, added 50 mL of the tested isolate suspension to wells A4 and B4. We also mixed the bacterial suspension with the reactive medium by pipetting up and down (optional). The final concentration of bacteria was ≈10^8 CFU/mL in each well, and the final concentration of CAZ/AVI was 128/53 µg/mL.

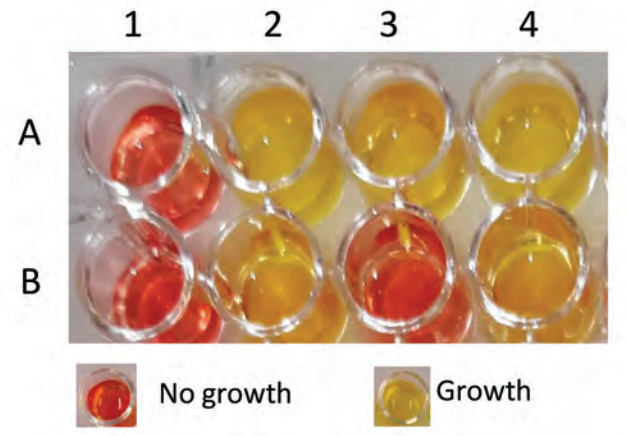

Figure. Rapid CAZ/AVI NP testing. Bacterial growth is shown by color change of the medium from red to yellow. This test was performed with a ceftazidime/avibactam (CAZ/AVI)–resistant isolate (A2 and B2) and with a CAZ/AVI/susceptible isolate (A3 and B3) in a reaction without (A) and with (B) CAZ/AVI at the defined concentration. The tested isolates (A4 and B4) that grew in the absence and presence of CAZ/AVI were considered positive (CAZ/AVI resistant). Noninoculated wells (A1 and B1) are shown as controls for possible medium contamination.

Tray Incubation and Reading

We incubated the inoculated tray for up to 2 hours 45 minutes at 35°C ± 2°C in ambient air without being sealed and without shaking. On the basis of our previous experience of development of several rapid diagnostic tests, we visually inspected the tray every 30 minutes for 3 hours. All results were obtained within 2 hours 45 minutes. We considered the test result positive if the tested isolate grew in presence of CAZ/AVI (i.e., yellow color of the culture medium), indicating CAZ/AVI resistance, and as negative if the tested isolate did not grow in presence of CAZ/AVI (remained red), indicating no growth and therefore CAZ/AVI susceptibility.

We considered the test result interpretable under 1 of 5 conditions: 1) both wells (A1 and B1) with 0.85% saline solution without bacterial suspension remained unchanged (red, indicating the absence of medium contamination); 2) CAZ/AVI-free wells (A2–A4) with bacterial suspension turned from red to yellow, confirming the metabolism of glucose and, thus, growth of the inoculated isolates; 3) the wells (A2 and B2) with the CAZ/AVI-resistant bacterial suspension (positive control) gave positive results (turned

from red to yellow), confirming the growth of this isolate; 4) the wells (A3 and B3) with the CAZ/AVI-susceptible bacterial suspension (negative control) gave negative results (remaining red), confirming the absence of growth of this isolate; and 5) the tested isolate that grew in the absence and the presence of CAZ/AVI (yellow, wells A4 and B4) was therefore reported to be CAZ/AVI resistant, or the tested isolate that grew in the absence but not in the presence of CAZ/AVI were therefore reported to be CAZ/AVI susceptible. The test result was considered positive when the well containing CAZ/AVI (well B2) and the isolate to be tested turned from red to yellow, giving exactly the same color as the well without CAZ/AVI (well A2), indicating glucose metabolism and growth in presence of CAZ/AVI (i.e., CAZ/AVI resistance) (Figure). The test result was negative when the well containing CAZ/AVI (well B3) with the isolate to be tested remained red (unchanged color) (Figure), indicating bacterial growth inhibition in presence of CAZ/AVI (i.e., CAZ/AVI susceptibility) (Figure). Results were blindly interpreted by 2 laboratory technicians.

Results

We compared results obtained with the Rapid CAZ/AVI NP test with those obtained with the MIC gradient strip test (Etest) taken as the reference method. In brief, we determined discrepancies for each method to evaluate the performance of the test to detect CAZ/AVI resistance/susceptibility. We calculated positive percent agreement (PPA), negative percent agreement (NPA), and overall percent agreement (OPA) by using standard formulas (*31*): PPA = [true positive/(true positive + false negative)] × 100%; NPA = [true negative/(true negative + false positive)] × 100%; and OPA = [(true positive + true negative)/(true positive + false positive + false negative + true negative)] × 100%. For discrepant results, we calculated errors (very major errors [VMEs] and major errors [MEs]) as described (*32*). A major error was considered for any isolates that were found to be resistant by the Rapid CAZ/AVI NP test but categorized as susceptible by using the reference method (false resistance). A VME was considered when isolates were categorized as susceptible by using the Rapid CAZ/AVI NP test but categorized as resistant by the reference method (false susceptibility).

We used 101 nonduplicate well-characterized enterobacterial isolates to evaluate the performance of the Rapid CAZ/AVI NP test (Appendix Table), among which 35 isolates were CAZ/AVI-resistant isolates (MICs of CAZ/AVI ranging from 12 to >256 μg/mL) and 66 isolates were CAZ/AVI susceptible (MICs of CAZ/AVI ranging from 0.064 to 4 μg/mL). Among the 35 CAZ/AVI-resistant isolates, resistance was caused mainly by production of metallo-β-lactamases, including NDM enzymes (n = 16, NDM-1, -4, -5, -6, -7), VIM enzymes (n = 9, VIM-1, -2, -4, -19), and IMP-1 enzymes (n = 2). In addition, previously identified KPC-3 variants (n = 5) conferring high-level resistance to CAZ/AVI among *K. pneumoniae* clinical isolates, such as KPC-41 and KPC-50, were included in this study (*11*,*12*). We also included *K. pneumoniae* and *E. coli* strains producing the extended-spectrum β-lactamase VEB-25. We have shown recently that this enzyme might confer resistance to CAZ/AVI (*33*).

The Rapid CAZ/AVI NP test correctly identified all 35 CAZ/AVI-resistant isolates (Appendix Table). Of the 66 CAZ/AVI-susceptible isolates, all but 1 showed negative results, thus being correctly categorized as susceptible; 1 isolate had an MIC for CAZ/AVI of 8 mg/L (at the susceptible breakpoint of CAZ/AVI), which gave a positive (false-positive) result with the Rapid CAZ/AVI NP test, corresponding to false resistance (Appendix Table). Overall, no VMEs (false susceptibility) and only 1 ME (false resistance) were observed. Therefore, we found excellent concordance between the results of the reference CAZ/AVI susceptibility testing method and those of the Rapid CAZ/AVI NP test for susceptible and resistant isolates. Under our conditions, the Rapid CAZ/AVI NP test showed a PPA of 100%, an NPA of 98.5%, and an OPA of 99%, in comparison with the MIC gradient strip test (Etest). The final results are best read at 2 hours 45 minutes after incubation at 35°C ± 2°C under an ambient atmosphere, with 1.5% MEs and 0% VMEs.

Discussion

Clinically, multidrug resistance is increasingly reported in enterobacterial species (e.g., *E. coli*, *K. pneumoniae*, *Enterobacter* spp.) (*34*). Delayed detection of resistance results for efficient antimicrobial drug therapy, potentially leading to clinical treatment failures or delays in isolation of corresponding carriers, eventually promotes outbreaks (*35*). Such undesired phenomena can be avoided by rapid and accurate antimicrobial susceptibility diagnostic tools to identify the possible antimicrobial drug resistance traits and consequently adapt the most effective treatment strategies (*36*).

Taking into account the increasing use of the CAZ/AVI combination and consequently the increasing isolation of CAZ/AVI-resistant gram-negative bacteria, we have developed the Rapid CAZ/AVI NP test, a fast culture-based test for detection of CAZ/AVI resistance among multidrug-resistant Enterobacterales, regardless

of their resistance mechanisms. All results were obtained within 2 hours 45 minutes, a gain of time of 18 hours (meaning 1 day earlier from a practical point of view) compared with regular testing of CAZ/AVI susceptibility by using the BMD method. The BMD method is commonly regarded as time-consuming, complex, laborious, and challenging for most routine laboratories. Other phenotypic techniques such as Etest strips are being used and showed a good correlation with the reference BMD method (*37*,*38*); however, use of those tests is much more expensive and requires the same amount of time, leading to a delay in taking timely clinical treatment measures.

Our study showed that the Rapid CAZ/AVI NP test is reliable and combines excellent sensitivity and specificity. Moreover, compared with other phenotypic methods, bacterial growth in the Rapid CAZ/AVI NP solution might be easily interpretable, which can be visually seen by a color change from red to yellow (Figure). Although few discrepancies were observed (only 1 ME), the VMEs of the Rapid CAZ/AVI NP test were as low as 0%. No false-negative results and only 1 false-positive result occurred (Appendix Table). The PPA of the test was 100% and the NPA 98.5% compared with the MIC gradient strip test (Etest) taken as the reference standard method. The Rapid CAZ/AVI NP test requires a single method step without requiring any specific equipment and is thus easy to implement in routine microbiology laboratories.

From a clinical point of view, most of the KPC-producing CAZ/AVI-resistant isolates described so far with weak carbapenemase activity and low carbapenems MICs were undetectable by the phenotypic methods commonly used for detecting carbapenem-resistant isolates (*39*). The failure to detect such CAZ/AVI-resistant carbapenem-susceptible KPC variants could lead to strains harboring those KPC mutations escaping recognition by clinical microbiology laboratories, which might result in therapeutic failure and nosocomial hospital outbreaks (*2*,*40*). Thus, use of rapid culture-based tests that do not include carbapenems as selective agents, such as the rapid CAZ/AVI NP, could represent a valuable option for detecting those mutated KPC-producing isolates. This type of test offers the possibility of a rapid susceptibility/resistance categorization, which is the information needed from clinical point of view for adequate CAZ/AVI-based treatment, particularly in countries that show endemic diffusion for KPC-producing *K. pneumoniae* strains, such as the United States, Greece, and Italy (*2*).

In conclusion, the Rapid CAZ/AVI NP test can be used to evaluate CAZ/AVI susceptibility from bacterial cultures. Additional work will evaluate its value directly from positive blood cultures. The test can also be used as a second-line screening test of CAZ/AVI resistance after use of selective media, such, as SuperCAZ/AVI medium, which is used to detect CAZ/AVI-resistant strains (*14*,*39*,*41*,*42*). Further development of the test will include the potential identification of CAZ/AVI resistance in *Pseudomonas aeruginosa*, which has different metabolic pathways.

This study was supported by the University of Fribourg and the Swiss National Science Foundation (project FNS-407240_177381).

About the Author

Dr. Nordmann is professor of medicine, chair of the Microbiology Unit, Department of Medicine, Faculty of Science, University of Fribourg, Switzerland. His primary research interests are genetics, biochemistry, and molecular epidemiology of resistance in Gram-negative bacteria, and development of rapid diagnostic tests for detection of emerging antimicrobial drug-resistant traits.

References

1. Poirel L, Sadek M, Kusaksizoglu A, Nordmann P. Co-resistance to ceftazidime-avibactam and cefiderocol in clinical isolates producing KPC variants. Eur J Clin Microbiol Infect Dis. 2022;41:677–80. https://doi.org/10.1007/s10096-021-04397-x
2. Di Bella S, Giacobbe DR, Maraolo AE, Viaggi V, Luzzati R, Bassetti M, et al. Resistance to ceftazidime/avibactam in infections and colonisations by KPC-producing Enterobacterales: a systematic review of observational clinical studies. J Glob Antimicrob Resist. 2021;25:268–81. https://doi.org/10.1016/j.jgar.2021.04.001
3. Shields RK, Clancy CJ, Hao B, Chen L, Press EG, Iovine NM, et al. Effects of *Klebsiella pneumoniae* carbapenemase subtypes, extended-spectrum β-lactamases, and porin mutations on the in vitro activity of ceftazidime-avibactam against carbapenem-resistant *K. pneumoniae*. Antimicrob Agents Chemother. 2015;59:5793–7. https://doi.org/10.1128/AAC.00548-15
4. Both A, Büttner H, Huang J, Perbandt M, Belmar Campos C, Christner M, et al. Emergence of ceftazidime/avibactam non-susceptibility in an MDR *Klebsiella pneumoniae* isolate. J Antimicrob Chemother. 2017;72:2483–8. https://doi.org/10.1093/jac/dkx179
5. Galani I, Karaiskos I, Souli M, Papoutsaki V, Galani L, Gkoufa A, et al. Outbreak of KPC-2-producing *Klebsiella pneumoniae* endowed with ceftazidime-avibactam resistance mediated through a VEB-1-mutant (VEB-25), Greece, September to October 2019. Euro Surveill. 2020;25:2000028. https://doi.org/10.2807/1560-7917.ES.2020.25.3.2000028
6. Voulgari E, Kotsakis SD, Giannopoulou P, Perivolioti E, Tzouvelekis LS, Miriagou V. Detection in two hospitals of transferable ceftazidime-avibactam resistance in *Klebsiella pneumoniae* due to a novel VEB β-lactamase variant with a Lys234Arg substitution, Greece, 2019. Euro Surveill. 2020;25:1900766. https://doi.org/10.2807/1560-7917.ES.2020.25.2.1900766

7. Compain F, Dorchène D, Arthur M. Combination of amino acid substitutions leading to CTX-M-15-mediated resistance to the ceftazidime-avibactam combination. Antimicrob Agents Chemother. 2018;62:e00357–18. https://doi.org/10.1128/AAC.00357-18
8. Zhang Y, Kashikar A, Brown CA, Denys G, Bush K. Unusual *Escherichia coli* PBP 3 insertion sequence identified from a collection of carbapenem-resistant *Enterobacteriaceae* tested *in vitro* with a combination of ceftazidime-, ceftaroline-, or aztreonam-avibactam. Antimicrob Agents Chemother. 2017;61:e00389–17. https://doi.org/10.1128/AAC.00389-17
9. Shi Q, Yin D, Han R, Guo Y, Zheng Y, Wu S, et al. Emergence and recovery of ceftazidime-avibactam resistance in bla_{KPC-33}-harboring *Klebsiella pneumoniae* sequence type 11 isolates in China. Clin Infect Dis. 2020;71(Suppl 4):S436–9. https://doi.org/10.1093/cid/ciaa1521
10. Nelson K, Hemarajata P, Sun D, Rubio-Aparicio D, Tsivkovski R, Yang S, et al. Resistance to ceftazidime-avibactam is due to transposition of KPC in a porin-deficient strain of *Klebsiella pneumoniae* with increased efflux activity. Antimicrob Agents Chemother. 2017;61:e00989–17. https://doi.org/10.1128/AAC.00989-17
11. Poirel L, Vuillemin X, Juhas M, Masseron A, Bechtel-Grosch U, Tiziani S, et al. KPC-50 confers resistance to ceftazidime-avibactam associated with reduced carbapenemase activity. Antimicrob Agents Chemother. 2020;64:e00321–20. https://doi.org/10.1128/AAC.00321-20
12. Mueller L, Masseron A, Prod'Hom G, Galperine T, Greub G, Poirel L, et al. Phenotypic, biochemical and genetic analysis of KPC-41, a KPC-3 variant conferring resistance to ceftazidime-avibactam and exhibiting reduced carbapenemase activity. Antimicrob Agents Chemother. 2019;63:e01111–9. https://doi.org/10.1128/AAC.01111-19
13. Wang Y, Wang J, Wang R, Cai Y. Resistance to ceftazidime-avibactam and underlying mechanisms. J Glob Antimicrob Resist. 2020a;22:18–27. https://doi.org/10.1016/j.jgar.2019.12.009
14. Di Pilato V, Aiezza N, Viaggi V, Antonelli A, Principe L, Giani T, et al. KPC-53, a KPC-3 variant of clinical origin associated with reduced susceptibility to ceftazidime-avibactam. Antimicrob Agents Chemother. 2020;65:e01429–20. https://doi.org/10.1128/AAC.01429-20
15. Barnes MD, Winkler ML, Taracila MA, Page MG, Desarbre E, Kreiswirth BN, et al. *Klebsiella pneumoniae* carbapenemase-2 (KPC-2), substitutions at ambler position Asp179, and resistance to ceftazidime-avibactam: unique antibiotic-resistant phenotypes emerge from β-lactamase protein engineering. MBio. 2017;8:e00528–17. https://doi.org/10.1128/mBio.00528-17
16. Haidar G, Clancy CJ, Shields RK, Hao B, Cheng S, Nguyen MH. Mutations in bla_{KPC-3} that confer ceftazidime-avibactam resistance encode novel KPC-3 variants that function as extended-spectrum β-lactamases. Antimicrob Agents Chemother. 2017;61:e02534–16. https://doi.org/10.1128/AAC.02534-16
17. Shields RK, Chen L, Cheng S, Chavda KD, Press EG, Snyder A, et al. Emergence of ceftazidime-avibactam resistance due to plasmid-borne bla_{KPC-3} mutations during treatment of carbapenem-resistant *Klebsiella pneumoniae* infections. Antimicrob Agents Chemother. 2017;61:e02097–16. https://doi.org/10.1128/AAC.02097-16
18. Venditti C, Nisii C, D'Arezzo S, Vulcano A, Capone A, Antonini M, et al. Molecular and phenotypical characterization of two cases of antibiotic-driven ceftazidime-avibactam resistance in bla_{KPC-3}-harboring *Klebsiella pneumoniae*. Infect Drug Resist. 2019;12:1935–40. https://doi.org/10.2147/IDR.S207993
19. Coppi M, Di Pilato V, Monaco F, Giani T, Conaldi PG, Rossolini GM. Ceftazidime-avibactam resistance associated with increased bla_{KPC-3} gene copy number mediated by pKpQIL plasmid derivatives in sequence type 258 *Klebsiella pneumoniae*. Antimicrob Agents Chemother. 2020;64:e01816–9. https://doi.org/10.1128/AAC.01816-19
20. Winkler ML, Papp-Wallace KM, Bonomo RA. Activity of ceftazidime/avibactam against isogenic strains of *Escherichia coli* containing KPC and SHV β-lactamases with single amino acid substitutions in the Ω-loop. J Antimicrob Chemother. 2015;70:2279–86. https://doi.org/10.1093/jac/dkv094
21. Livermore DM, Mushtaq S, Doumith M, Jamrozy D, Nichols WW, Woodford N. Selection of mutants with resistance or diminished susceptibility to ceftazidime/avibactam from ESBL- and AmpC-producing Enterobacteriaceae. J Antimicrob Chemother. 2018;73:3336–45. https://doi.org/10.1093/jac/dky363
22. Shields RK, Iovleva A, Kline EG, Kawai A, McElheny CL, Doi Y. Clinical evolution of AmpC-mediated ceftazidime-avibactam and cefiderocol resistance in *Enterobacter cloacae* complex following exposure to cefepime. Clin Infect Dis. 2020;71:2713–6. https://doi.org/10.1093/cid/ciaa355
23. Kawai A, McElheny CL, Iovleva A, Kline EG, Sluis-Cremer N, Shields RK, et al. Structural basis of reduced susceptibility to ceftazidime-avibactam and cefiderocol in *Enterobacter cloacae* due to AmpC R2 loop deletion. Antimicrob Agents Chemother. 2020;64:e00198–20. https://doi.org/10.1128/AAC.00198-20
24. EUCAST. 2022. The European Committee on Antimicrobial Susceptibility Testing. Breakpoint tables for interpretation of MICs and zone diameters. Version 12.0. 2022 [cited 2023 Dec 11]. https://www.eucast.org/fileadmin/src/media/PDFs/EUCAST_files/Breakpoint_tables/v_12.0_Breakpoint_Tables.pdf
25. Gaibani P, Giani T, Bovo F, Lombardo D, Amadesi S, Lazzarotto T, et al. Resistance to ceftazidime/avibactam, meropenem/vaborbactam and imipenem/relebactam in Gram-negative MDR bacilli: molecular mechanisms and susceptibility testing. Antibiotics (Basel). 2022;11:628. https://doi.org/10.3390/antibiotics11050628
26. Wozniak A, Paillavil B, Legarraga P, Zumarán C, Prado S, García P. Evaluation of a rapid immunochromatographic test for detection of KPC in clinical isolates of Enterobacteriaceae and *Pseudomonas* species. Diagn Microbiol Infect Dis. 2019;95:131–3. https://doi.org/10.1016/j.diagmicrobio.2019.05.009
27. Antonelli A, Giani T, Di Pilato V, Riccobono E, Perriello G, Mencacci A, et al. KPC-31 expressed in a ceftazidime/avibactam-resistant *Klebsiella pneumoniae* is associated with relevant detection issues. J Antimicrob Chemother. 2019;74:2464–6. https://doi.org/10.1093/jac/dkz156
28. Bianco G, Boattini M, Bondi A, Comini S, Zaccaria T, Cavallo R, et al. Outbreak of ceftazidime-avibactam resistant *Klebsiella pneumoniae carbapenemase (KPC)-producing Klebsiella pneumoniae* in a COVID-19 intensive care unit, Italy: urgent need for updated diagnostic protocols of surveillance cultures. J Hosp Infect. 2022;122:217–9. https://doi.org/10.1016/j.jhin.2022.02.001
29. Bianco G, Boattini M, Iannaccone M, Bondi A, Ghibaudo D, Zanotto E, et al. Carbapenemase detection testing in the era of ceftazidime/avibactam-resistant KPC-producing Enterobacterales: a 2-year experience. J Glob Antimicrob Resist. 2021;24:411–4. https://doi.org/10.1016/j.jgar.2021.02.008

30. Nordmann P, Jayol A, Poirel L. Rapid detection of polymyxin resistance in Enterobacteriaceae. Emerg Infect Dis. 2016;22:1038–43. https://doi.org/10.3201/eid2206.151840
31. Garrett PE, Lasky FD, Meier KL. User protocol for evaluation of qualitative test performance. CLSI EP12–A2. Wayne (PA): Clinical and Laboratory Standards Institute; 2008.
32. Nordmann P, Sadek M, Tinguely C, Poirel L. Rapid ResaImipenem/Acinetobacter NP test for detection of carbapenem susceptibility/resistance in *Acinetobacter baumannii*. J Clin Microbiol. 2021;59:e03025–20. https://doi.org/10.1128/JCM.03025-20
33. Findlay J, Poirel L, Bouvier M, Gaia V, Nordmann P. Resistance to ceftazidime-avibactam in a KPC-2–producing *Klebsiella pneumoniae* caused by the extended-spectrum beta-lactamase VEB-25. Eur J Clin Microbiol Infect Dis. 2023;42:639–44. https://doi.org/10.1007/s10096-023-04582-0
34. Boucher HW, Talbot GH, Bradley JS, Edwards JE, Gilbert D, Rice LB, et al. Bad bugs, no drugs: no ESKAPE! An update from the Infectious Diseases Society of America. Clin Infect Dis. 2009;48:1–12. https://doi.org/10.1086/595011
35. Decousser JW, Poirel L, Nordmann P. Recent advances in biochemical and molecular diagnostics for the rapid detection of antibiotic-resistant *Enterobacteriaceae*: a focus on ß-lactam resistance. Expert Rev Mol Diagn. 2017;17:327–50. https://doi.org/10.1080/14737159.2017.1289087
36. Burnham CD, Leeds J, Nordmann P, O'Grady J, Patel J. Diagnosing antimicrobial resistance. Nat Rev Microbiol. 2017;15:697–703. https://doi.org/10.1038/nrmicro.2017.103
37. Wang Q, Zhang F, Wang Z, Chen H, Wang X, Zhang Y, et al. Evaluation of the Etest and disk diffusion method for detection of the activity of ceftazidime-avibactam against *Enterobacterales* and *Pseudomonas aeruginosa* in China. BMC Microbiol. 2020b;20:187. https://doi.org/10.1186/s12866-020-01870-z
38. Sherry NL, Baines SL, Howden BP. Ceftazidime/avibactam susceptibility by three different susceptibility testing methods in carbapenemase-producing Gram-negative bacteria from Australia. Int J Antimicrob Agents. 2018;52:82–5. https://doi.org/10.1016/j.ijantimicag.2018.02.017
39. Bianco G, Boattini M, Comini S, Leone A, Bondi A, Zaccaria T, et al. Implementation of Chromatic Super CAZ/AVI® medium for active surveillance of ceftazidime-avibactam resistance: preventing the loop from becoming a spiral. Eur J Clin Microbiol Infect Dis. 2022;41:1165–71. https://doi.org/10.1007/s10096-022-04480-x
40. Gaibani P, Lombardo D, Foschi C, Re MC, Ambretti S. Evaluation of five carbapenemase detection assays for Enterobacteriaceae harbouring bla_{KPC} variants associated with ceftazidime/avibactam resistance. J Antimicrob Chemother. 2020;75:2010–3. https://doi.org/10.1093/jac/dkaa079
41 Sadek M, Poirel L, Tinguely C, Nordmann P. A selective culture medium for screening ceftazidime-avibactam resistance in *Enterobacterales* and *Pseudomonas aeruginosa*. J Clin Microbiol. 2020;58:e00965–20. https://doi.org/10.1128/JCM.00965-20
42. Sadek M, Poirel L, Dominguez Pino M, D'Emidio F, Pomponio S, Nordmann P. Evaluation of SuperCAZ/AVI® medium for screening ceftazidime-avibactam resistant Gram-negative isolates. Diagn Microbiol Infect Dis. 2021;101:115475. https://doi.org/10.1016/j.diagmicrobio.2021.115475

Address for correspondence: Mustafa Sadek, Medical and Molecular Microbiology Unit, Department of Medicine, Faculty of Science, University of Fribourg, Chemin du Musée 18, CH-1700 Fribourg, Switzerland; email: mustafa.sadek@unifr.ch

Public Health Impact of Paxlovid as Treatment for COVID-19, United States

Yuan Bai,[1] Zhanwei Du,[1] Lin Wang,[1] Eric H.Y. Lau,[1] Isaac Chun-Hai Fung, Petter Holme, Benjamin J. Cowling, Alison P. Galvani, Robert M. Krug, Lauren Ancel Meyers

We evaluated the population-level benefits of expanding treatment with the antiviral drug Paxlovid (nirmatrelvir/ritonavir) in the United States for SARS-CoV-2 Omicron variant infections. Using a multiscale mathematical model, we found that treating 20% of symptomatic case-patients with Paxlovid over a period of 300 days beginning in January 2022 resulted in life and cost savings. In a low-transmission scenario (effective reproduction number of 1.2), this approach could avert 0.28 million (95% CI 0.03–0.59 million) hospitalizations and save US $56.95 billion (95% CI US $2.62–$122.63 billion). In a higher transmission scenario (effective reproduction number of 3), the benefits increase, potentially preventing 0.85 million (95% CI 0.36–1.38 million) hospitalizations and saving US $170.17 billion (95% CI US $60.49–$286.14 billion). Our findings suggest that timely and widespread use of Paxlovid could be an effective and economical approach to mitigate the effects of COVID-19.

Antiviral drugs can substantially reduce illness and deaths from human infections. For example, antiretroviral therapy has prevented millions of HIV/AIDS deaths globally since the late 1980s (*1*). During the 2009 influenza A(H1N1) pandemic, oseltamivir was widely administered in the United States (28.4 prescriptions/1,000 persons) (*2*); rapid treatment after symptom onset reduced the risk for hospitalization by an estimated 63% (95% CI 17%–81%) (*3*). The reduction in viral load might reduce the risk for onward transmission while accelerating recovery. A counterfactual analysis suggests that treating even 10% of infected patients with baloxavir shortly after symptom onset would have prevented millions of infections and thousands of deaths in the United States during the severe 2017–18 influenza season (*4*). A fast-acting SARS-CoV-2 antiviral could similarly be deployed to curtail transmission on a population scale and directly save lives (*5*).

Paxlovid (Pfizer, https://www.pfizer.com), which received Food and Drug Administration Emergency Use Authorization on December 22, 2021, for treating SARS-CoV-2 infections in persons >12 years of age, combines 2 different antiviral agents, nirmatrelvir and ritonavir. Treating symptomatic COVID-19 patients with Paxlovid reduces hospitalization risks by an estimated 0.59 (95% CI 0.48–0.71) for adults 18–49 years of age, 0.40 (95% CI 0.34–0.48) for adults 50–64 years of age, and 0.53 (95% CI 0.48–0.58) for adults >64 years of age (*6*). Paxlovid has proven effective against the Omicron variant (*7*). In January 2022, the United States ordered 20 million courses of Paxlovid to be delivered within 9 months (*8*).

In this study, we analyzed the population-level benefits of expanding the clinical use of Paxlovid to treat COVID-19. By fitting a within-host model of viral replication to viral titer data from >2,000 COVID-19 patients, we provide early estimates for the efficacy of Paxlovid in curtailing viral load, depending on the timing of treatment after infection. Then, using a population-level SARS-CoV-2 transmission model, we estimated the effects of Paxlovid-based interventions on reducing the healthcare and economic burden of future COVID-19 epidemics. Specifically, we estimated the number of cases, hospitalizations,

Author affiliations: The University of Hong Kong, Hong Kong (Y. Bai, Z. Du, E.H.Y. Lau, B.J. Cowling); Hong Kong Science and Technology Park, Hong Kong, China (Y. Bai, Z. Du, E.H.Y. Lau, B.J. Cowling); University of Cambridge, Cambridge, UK (L. Wang); Deakin University, Burwood, Victoria, Australia (E.H.Y. Lau); Georgia Southern University, Statesboro, Georgia, USA (I. C.-H. Fung); Aalto University, Espoo, Finland (P. Holme); Kobe University, Kobe, Japan (P. Holme); Yale School of Public Health, New Haven, Connecticut, USA (A.P. Galvani); University of Texas at Austin, Austin, Texas, USA (R.M. Krug, L.A. Meyers); Santa Fe Institute, Santa Fe, New Mexico, USA (L.A. Meyers)

DOI: https://doi.org/10.3201/eid3002.230835

[1]These authors contributed equally to this article.

and deaths, as well as healthcare costs averted under a range of transmission scenarios, in which we vary both the between-individual transmission rate of the virus and the proportion of case-patients who receive rapid treatment with Paxlovid. This 2-level analytic framework can broadly support the rapid evaluation of antiviral-based mitigation strategies against COVID-19 and other respiratory viruses (*4*).

Materials and Methods

Within-Host Model of SARS-CoV-2 Replication Dynamics

We simulated SARS-CoV-2 virus kinetics in an infected person and the effect of Paxlovid treatment on viral growth using a standard target-cell limited virus kinetic model that tracks the number of uninfected cells, infected cells, and free viral particles (*9*,*10*) (Appendix, https://wwwnc.cdc.gov/EID/article/30/2/23-0835-App1.pdf). We used individual patient viral load data from a Paxlovid clinical trial data to estimate the 5 key parameters of the model: the infection rate of susceptible cells (b), the rate at which infected cells die (δ), the rate at which active viruses were cleared (c), the virus production rate (p), and the efficacy of Paxlovid at suppressing viral replication (ϵ). Specifically, we used a stochastic approximation expectation-maximization algorithm to fit the model to 14-day viral titer data from 1,126 infected adults treated with a placebo and 1,120 infected adults treated with Paxlovid during a clinical trial in late 2021 (*11*) (Appendix).

Modeling the Infectiousness of Treated and Untreated Cases

On the basis of previous studies (*12*,*13*), we assumed that a person's infectiousness is logarithmically related to their viral titer (Appendix). In this transmission model, we assumed that the daily infectiousness of a case-patient depends on whether they received treatment and, if so, the time at which treatment was initiated after symptom onset. To estimate the daily infectiousness of a given untreated or treated case-patient, we first used the within-host model to simulate the viral load on each day of the infection and set the viral load to zero when the estimated value dropped below the detection threshold of 100 (*14*). We then used a logarithmic equation (Appendix) to estimate the corresponding daily infectiousness.

Modeling Population-Level SARS-CoV-2 Transmission Dynamics and Effects of Antiviral Treatment

We developed a stochastic individual-based network model of SARS-CoV-2 transmission dynamics in which susceptible persons can be infected by infected contacts (Appendix Figure 1). The underlying contact network included 9,961 persons living in 5,000 households with sociodemographic characteristics provided in the 2017 National Household Travel Survey (*15*,*16*) (Appendix).

At every time point, each person was in one of 11 possible states: unvaccinated susceptible (S_U), vaccinated susceptible (S_V), exposed (E), presymptomatic (P), symptomatic infectious before becoming eligible for Paxlovid treatment (Y), symptomatic treated (Y_T), symptomatic untreated (Y_U), asymptomatic infectious (A), recovered (R), hospitalized (H), or deceased (D). We assumed that hospitalized patients were isolated and not able to infect others. Upon infection, a susceptible person progresses to the exposed state and then to either the presymptomatic state (probability ψ) or asymptomatic state (probability $1 - \psi$). Asymptomatic case-patients recover without experiencing symptoms or seeking treatment. Presymptomatic case-patients progress to the symptomatic state at a rate ω, where they might be hospitalized according to published age-specific infection hospitalization rates (h_a) and eventually recover or die from the infection, according to age-specific infection fatality rates (μ_a). A fraction ρ of symptomatic case-patients receive Paxlovid, initiated an average of 3 days after symptom onset, which is assumed to reduce the risk for hospitalization (φ_a), as well as the infectiousness of the person. The infectiousness of a case-patient depends on the timing of Paxlovid administration after infection, according to the daily infectiousness curves described in the previous section. Vaccinated persons initially have vaccine-derived immunity against infection ω_B, symptomatic disease ψ_B, and death θ_B, which wanes gradually after vaccination. Similarly, recovered persons initially have infection-derived immunity against reinfection ω_N, symptomatic disease ψ_N, and death θ_B, which wanes more slowly than vaccine-derived immunity. Persons who are vaccinated and previously infected are assumed to have the higher of the 2 levels of immunity (i.e., infection-acquired vs. immune-acquired) (Table 1; Appendix Tables 1, 2).

Antiviral Treatment and Transmission Scenarios

We analyzed 24 different scenarios, each with an effective reproduction number (R_t) (1.2, 1.5, 1.7, 2, 3, or 5) and Paxlovid treatment rate (20%, 50%, 80%, or 100%). For each scenario (s), we compared 4 variations of the antiviral strategy: no treatment (i.e., treatment rate set to zero); treatment with Paxlovid at the given treatment rate; treatment with a hypothetical antiviral that reduces infectiousness with the same efficacy as Paxlovid but does not reduce severity; and treatment with a hypothetical antiviral that reduces

Table 1. Between-host parameter estimates used in study of public health impact of Paxlovid in treatment of COVID-19, United States*

Key parameter	Estimated value
Symptomatic proportion, % (ψ)	75
Transition rate out of exposed state (d^{-1}) (σ)	1/3
Time lag between infection and recovery in days for asymptomatic patients (d^{-1}) (γ_A)	1/9
Time lag between symptom onset and recovery in days for symptomatic patients (d^{-1}) (γ_T)	1/4
Transition rate from the presymptomatic to the symptomatic stage (d^{-1}) (ω)	1/2
Age-specific efficacy of Paxlovid in reducing the hospitalization rate, y (φ_a)	
0–4	0.59 (95% CI 0.48–0.71)
5–17	0.59 (95% CI 0.48–0.71)
18–49	0.59 (95% CI 0.48–0.71)
50–64	0.40 (95% CI 0.34–0.48)
≥65	0.53 (95% CI 0.48–0.58)
Life expectancy, y, for age group *a*, adjusted assuming a 3% yearly discount rate (λ_a)	
0–4	30.3
5–17	29.3
18–49	25.8
50–64	1837
≥65	12.9

*We use the between-host model to project population-level impacts of Paxlovid treatment. Key parameter values used in the model are listed below, with more details in Appendix Table 1 (https://wwwnc.cdc.gov/EID/article/30/2/23-0835-App1.pdf).

severity with the same efficacy as Paxlovid but does not reduce infectiousness. The last 2 variations enabled us to separate the direct therapeutic benefits from the indirect transmission-blocking benefits of Paxlovid. To estimate the health and economic costs associated with each scenario, we ran 100 stochastic simulations of each of the 4 strategy variations and calculated the mean and 95% CI across simulations of the years of life lost (YLL) averted and monetary costs attributable to Paxlovid treatment.

Estimating YLL Averted and Monetary Costs

For each set of stochastic simulations, we estimated YLL averted for each antiviral strategy τ by comparing it to the no treatment strategy (Appendix). The willingness to pay per YLL averted is the maximum price a society is willing to pay to prevent the loss of 1 year of life. Health economists have inferred from healthcare expenditure that the United States is willing to pay US $100,000 per quality-adjusted life-year (*17*), of which YLL is 1 component. For a given willingness to pay for a YLL averted (θ), we calculated the net monetary benefit (NMB) of each strategy (Appendix).

Sensitivity Analyses and Model Validation

We assessed the robustness of the results with respect to the relationship between infectiousness and viral

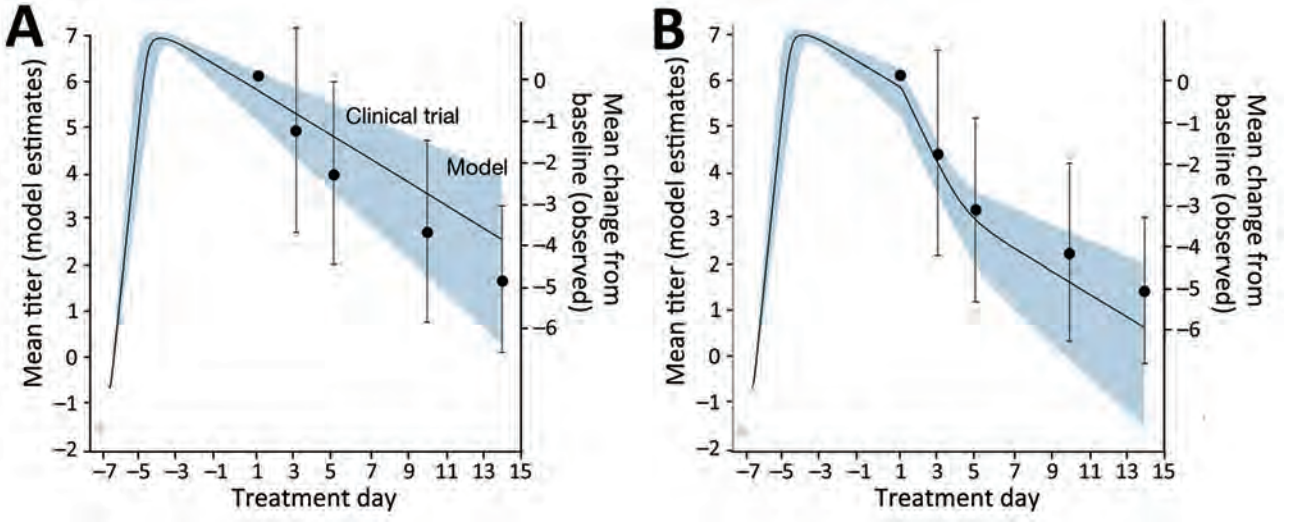

Figure 1. Estimated and observed viral load following treatment with placebo (A) or Paxlovid (B) in large-scale campaign treating COVID-19, United States. The left y-axes, black lines, and blue shading indicate the means and 95% CI of SARS-CoV-2 viral load (RNA $\log_{10}$ copies/mL) as estimated by the fitted within-host model. The right y-axes, black dots, and error bars indicate the means and 95% CI of the decrease in viral load since the initiation of treatment as reported in a clinical trial in which 1,126 patients received a placebo and 1,120 patients received Paxlovid during July 16–December 9, 2021 (*11*). Day one corresponds to the initiation of treatment. Gray circles denote the assumed initial viral load upon infection (V_0) corresponding to 1 infectious virus particle in the upper respiratory tract (*18*).

Table 2. Within-host parameter estimates used in study of public health impact of Paxlovid in treatment of COVID-19, United States*

Parameter	Mean (95% CI)
Cell infection rate in 10^{-6} mL/copies/day (b)	3.92 (2.82–5.38)
Infected cell death rate per day (δ)	0.62 (0.42–0.92)
Virus production rate in copies/mL/day/cell (p)	3.19 (2.35–4.35)
Virus death rate per day (c)	2.21 (2.10–2.33)
Antiviral efficacy (ϵ)	0.9937 (0.9917–0.9952)

*We fit the within-host model to the mean viral load dynamics reported from a clinical trial involving 2,246 infected adults treated with either Paxlovid or a placebo (*11*) using nonlinear mixed-effects model method (*19*). This method allows between-subject variability to improve the precision and accuracy of estimates (*20*). Values are means and 95% CI of parameter values in population, assuming that antiviral efficacy follows logit-normal distribution, and all other individual parameters follow log-normal distributions.

load by investigating 3 alternative functions (i.e., sigmoid, log-proportional, and step) (Appendix Tables 5, 6). To validate our within-host viral replication mode, we compared model-estimated mean viral load trajectories for untreated and treated case-patients to corresponding clinical trial data for patients receiving placebo or Paxlovid treatment (*1*). We found that the observed mean decreases in viral load fall within the estimated 95% CI and vice versa (Figure 1; Appendix Figure 3).

To validate our transmission dynamic model, we compared model projections to observed incidence data during the early 2022 and late 2022 Omicron waves in the United States (Appendix Figure 2). For each of these waves, we fitted the model to reported case data to estimate the initial R_t and then simulated the expected reported infections, assuming a 25% case-reporting rate (*7*).

Results

By fitting the within-host model to the mean viral load dynamics reported from a clinical trial (Table 2; Figure 1), we estimated that the rate at which viral particles infect susceptible cells (b) is 3.92 (95% CI 2.82–5.38) × 10^{-6} mL/copies/day), the clearance rate for infected cells (δ) is 0.62 (95% CI 0.42–0.92) per day, the rate at which infected cells release virus (p) is 3.19 (95% CI 2.35–4.35) copies/mL/day/cell, and the rate at which free virus particles are cleared (c) is 2.21 (95% CI 2.10–2.33) per day. Treatment with Paxlovid is estimated to repress viral replication by 99.37% (95% CI 99.17%–99.52%) per day.

Table 3. Projected health and economic impacts of a large-scale SARS-CoV-2 Paxlovid campaign, United States

Outcome	R_t	Treatment rate, %	Mean (95% CI)
Infections averted, millions	1.2	20	10.54 (3.03–21.12)
		50	25.65 (12.59–41.19)
	1.7	20	4.25 (0.00–8.30)
		50	10.65 (5.77–16.70)
	3	20	0.67 (−0.13 to 1.45)
		50	1.68 (0.79–2.77)
Hospitalizations averted, millions	1.2	20	0.28 (0.03–0.59)
		50	0.67 (0.33–1.25)
	1.7	20	0.48 (0.07–0.92)
		50	1.16 (0.49–1.85)
	3	20	0.85 (0.36–1.38)
		50	2.08 (1.12–2.83)
Deaths averted, thousands	1.2	20	33.85 (1.69–71.15)
		50	79.11 (35.78–146.51)
	1.7	20	59.43 (9.13–129.86)
		50	145.44 (45.60–221.34)
	3	20	109.67 (35.95–179.83)
		50	266.69 (156.71–362.77)
NMB, USD billions	1.2	20	$56.95 ($2.62–$122.63)
		50	$135.60 ($62.52–$261.32)
	1.7	20	$95.66 ($8.54–$196.23)
		50	$232.35 ($80.45–$379.51)
	3	20	$170.17 ($60.49–$286.14)
		50	$417.18 ($208.34–$580.13)
Courses of treatment used, millions	1.2	20	5.77 (4.38–7.15)
		50	12.13 (8.86–14.89)
	1.7	20	13.57 (12.42–15.12)
		50	32.85 (30.87–34.76)
	3	20	24.41 (22.34–26.56)
		50	60.21 (57.07–63.16)

*For each combination of treatment rate and reproduction number, the table provides the estimated mean and 95% CI of cases, hospitalizations, and deaths averted in the United States, NMB, and number of courses of treatment administered based on 100 pairs of stochastic simulations (treatment vs. no treatment simulations). NMB, net monetary benefit; R_t, effective reproduction number; USD, US dollars.

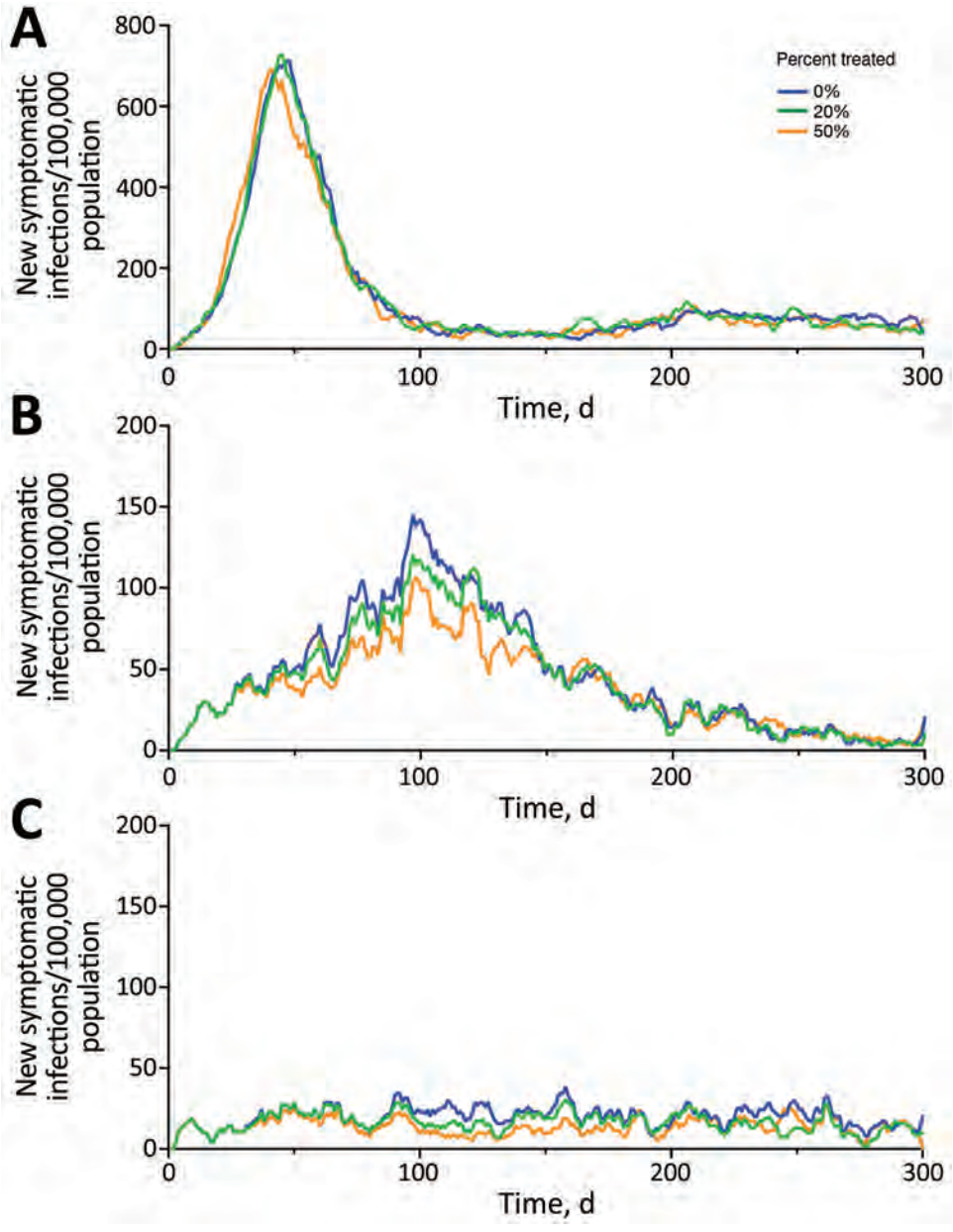

Figure 2. Projected symptomatic SARS-CoV-2 infections over 300 days in the United States across a range of transmission and Paxlovid treatment scenarios. Estimated incidence of symptomatic SARS-CoV-2 infections are shown assuming an effective reproduction number of 3.0 (A), 1.7 (B), or 1.2 (C). Colors correspond to 3 different treatment scenarios: 0% (blue), 20% (green), or 50% (orange) of symptomatic cases received a 5-day Paxlovid regimen initiated within 3 days of symptom onset.

We estimated the number of cases, hospitalizations, and deaths, as well as healthcare costs, averted under a range of transmission scenarios, in which we varied both the between-individual transmission rate of the virus and the proportion of case-patients who received rapid treatment with Paxlovid (Table 3; Figures 2, 3). Under a low-transmission scenario in which the R_t of the virus is 1.2, we estimated that treating 20% of symptomatic cases with Paxlovid would avert 10.54 million (95% CI 3.03–21.12 million) cases, 280,000 (95% CI 30,000–590,000) hospitalizations, and 33,850 (95% CI 1,690–71,150) deaths in the United States over a 300-day period (Appendix Table 4). Assuming a cost of US $530 per course of treatment (22) and willingness to pay per YLL averted of US $100,000, we estimated that the optimal strategy is always the highest achievable treatment rate. A 20% treatment rate would be expected to yield an NMB of US $56.95 billion (95% CI $2.62–$122.63 billion) averted.

To separate the direct (therapeutic) benefits of Paxlovid treatment from its indirect (transmission-reducing) effects, we conducted 2 additional analyses, 1 assuming the drug reduces severity but not infectivity and another assuming the opposite (Appendix Table 4). Assuming an R_t of 1.2, we estimated that direct therapeutic effects of treating 20% of symptomatic cases with Paxlovid would not affect the overall

attack rate but would avert 140,000 (95% CI −130,000 to 400,000) hospitalizations and 16,470 (95% CI −19,470 to 48,110) deaths over a 300-day period, resulting in an NMB of US $25.35 (95% CI −$34.98 to $84.22) billion. The reduced infectivity of the treated cases would be expected to avert an additional 10.57 (95% CI 3.03–21.19) million infections, 160,000 (95% CI −130,000 to 530,000) hospitalizations, and 19,460 (95% CI −14,140 to 58,520) deaths, resulting in an NMB of US $31.17 (95% CI −$32.77 to $103.74) billion.

Discussion

Our results show that the widespread administration of Paxlovid would not only improve outcomes in treated patients but also concomitantly reduce risks of onward transmission. In this population-level assessment of expanding rapid treatment of symptomatic COVID-19 infections with Paxlovid, we found that the direct (therapeutic) effects of treatment would substantially reduce both deaths and socioeconomic costs. Of note, the indirect (transmission-blocking) effects would be expected to reduce burden by just as much, as well as substantially reducing the overall attack rate (Appendix Table 4). We would expect mass treatment campaigns to have even greater health and economic effects in countries that have adopted zero-COVID strategies and thus have lower levels of population-level immunity than the United States (*23*).

Drugs like Paxlovid could profoundly reduce the severity of COVID-19 and enable a global transition to manageable coexistence with the virus. However, providing equitable and effective global access to SARS-CoV-2 antiviral drugs would require both ample supplies and broad-reaching test-and-treat programs. The pharmaceutical industry and global health agencies are working to produce enough Paxlovid to treat a large fraction of symptomatic cases (*8*). Online healthcare services (e.g., telemedicine) and community test-to-treat programs (*24*), such as those piloted in Pennsylvania and New Jersey (*25*), could be expanded nationally, and even globally, to accelerate and broaden access to antiviral drugs (*26*). For example, in 2020, China began an initiative to expand remote internet-based COVID-19 care (*27*). The country established 1,500 internet hospitals (either by extending existing hospitals or by opening new institutions) during 2019–2021 (*28*). The new services included follow-up consultations for common ailments (*29*) and served >239 million patients during December 2020–June 2021 (*30*). In addition, avoiding testing and treating infected individuals in person reduces the risk for SARS-CoV-2 transmission by patients to healthcare providers.

We highlight 3 limitations of our analyses that could be addressed as additional epidemiologic and clinical trial data become available. First, our fitted within-host model slightly overestimated viral levels for patients treated with placebo and underestimated those for patients receiving Paxlovid. The discrepancies might stem from limitations in the model structure or from unmodeled variation in

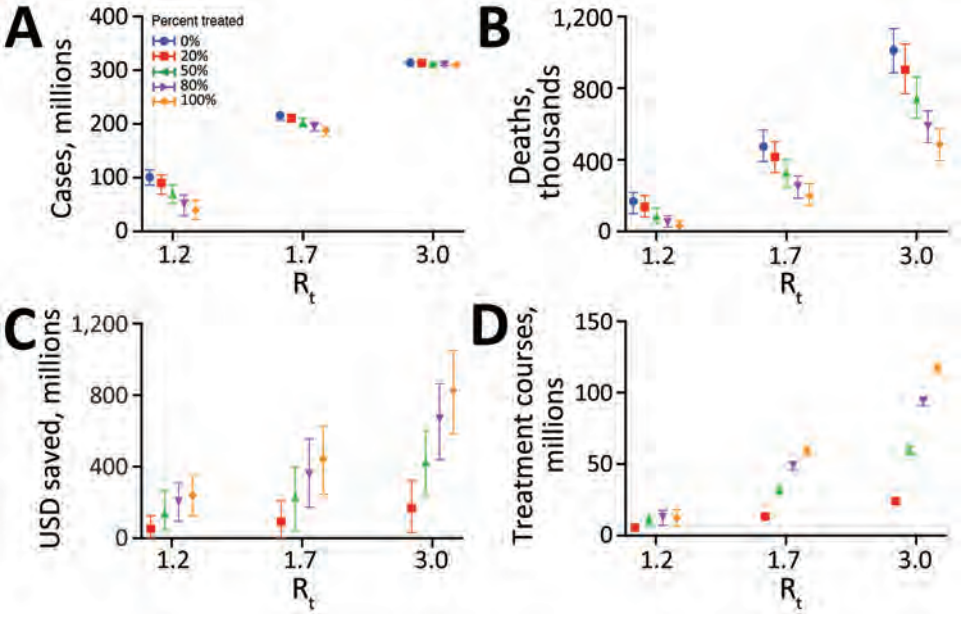

Figure 3. Projected health and economic impacts of a large-scale campaign using Paxlovid to treat COVID-19 over 300 days in the United States, across a range of transmission and treatment scenarios. Points and error bars correspond to means and 95% CI in number of infections in millions (A), number of deaths in millions (B), net monetary benefit in billions USD assuming a treatment course cost of US $530 and willingness to pay per year of life lost averted of US $100,000 (C), and number of courses of Paxlovid administered in millions (D). Each graph provides results for 3 R_t and 5 different treatment scenarios: 0% (blue), 20% (red), 50% (green), 80% (purple), or 100% (orange) of symptomatic cases started a 5-day course of Paxlovid within 3 days of symptom onset. Distributions are based on 100 stochastic simulations for each scenario. The results are scaled assuming a US population of 328.2 million (*21*). R_t, effective reproduction number; USD, US dollars.

viral kinetics and treatment efficacy across age or risk groups. In estimating model parameters, we considered only the mean in viral load of patients from 20 countries (*4*,*31*) (Figure 1). Incorporating such variability would enable us to analyze age-prioritized or risk-prioritized interventions and improve our estimates of the health and economic benefits of mass treatment. Second, we did not consider the emergence and spread of Paxlovid-resistant viruses, which could substantially undermine the utility of new drugs and exacerbate epidemics on a population level (*32*). Conversely, suppressed viral replication attributable to Paxlovid might limit viral evolution in treated patients. Depending on the immunological conditions of the individual person and population, reducing opportunities for viral growth and mutations could hinder the emergence of new variants (*33*). Third, we did not incorporate several economic, social, and logistical factors that might affect the expansion of Paxlovid treatment, including commercial impediments faced by the pharmaceutical companies that manufacture the drug (*34*); the costs of administering tests before treatment; and low levels of uptake stemming from misinformation, limited healthcare access, or pandemic fatigue. For example, in the 2009 H1N1 pandemic, only 40% of case-patients sought medical care within 3 days after symptom onset (*35*).

In conclusion, fast-acting antiviral drugs like Paxlovid can serve as invaluable tools to mitigate COVID-19 epidemics. By increasing supplies and improving infrastructure to enable rapid and equitable distribution, such drugs could substantially mitigate the health and societal burdens of COVID-19.

The computer code referenced in this study is available from Github (https://github.com/ZhanweiDU/Pax).

Financial support was provided by the AIR@InnoHK Programme from Innovation and Technology Commission of the Government of the Hong Kong Special Administrative Region, the US National Institutes of Health (grant no. R01 AI151176), the Centers for Disease Control and Prevention COVID Supplement (grant no. U01IP001136), Health and Medical Research Fund, Food and Health Bureau, Government of the Hong Kong Special Administrative Region (grant no. 21200632) and National Natural Science Foundation of China (grant no. 82304204). The funders of the study had no role in study design, data collection, data analysis, data interpretation, or writing of the report.

Y.B., Z.D., B.J.C., A.P.G., R.M.K, and L.A.M. designed research; Y.B., and Z.D. performed research; L.W., E.H.Y.L., I.C.H.F., and P.H. contributed analytic method comments. Y.B., Z.D., L.W., E.H.Y.L., I.C.H.F., P.H., B.J.C., A.P.G., R.M.K, and L.A.M. wrote the paper.

B.J.C. consults for AstraZeneca, GSK, Moderna, Roche, Sanofi Pasteur, and Pfizer.

About the Author

Dr. Bai is a postdoctoral fellow at the Laboratory of Data Discovery for Health Limited, Hong Kong Science and Technology Park, Hong Kong, China. Her research interests include optimizing infectious disease surveillance strategies, modeling disease transmission dynamics, and controlling interventions.

References

1. Dadonaite B. Antiretroviral therapy has saved millions of lives from AIDS and could save more [cited 2021 Feb 22]. https://ourworldindata.org/art-lives-saved
2. Suda KJ, Hunkler RJ, Matusiak LM, Schumock GT. Influenza antiviral expenditures and outpatient prescriptions in the United States, 2003–2012. Pharmacotherapy. 2015;35:991–7. https://doi.org/10.1002/phar.1656
3. Dobson J, Whitley RJ, Pocock S, Monto AS. Oseltamivir treatment for influenza in adults: a meta-analysis of randomised controlled trials. Lancet. 2015;385:1729–37. https://doi.org/10.1016/S0140-6736(14)62449-1
4. Du Z, Nugent C, Galvani AP, Krug RM, Meyers LA. Modeling mitigation of influenza epidemics by baloxavir. Nat Commun. 2020;11:2750. https://doi.org/10.1038/s41467-020-16585-y
5. Wahl A, Gralinski LE, Johnson CE, Yao W, Kovarova M, Dinnon KH III, et al. SARS-CoV-2 infection is effectively treated and prevented by EIDD-2801. Nature. 2021;591:451–7. https://doi.org/10.1038/s41586-021-03312-w
6. Shah MM, Joyce B, Plumb ID, Sahakian S, Feldstein LR, Barkley E, et al. Paxlovid associated with decreased hospitalization rate among adults with COVID-19—United States, April–September 2022. MMWR Morb Mortal Wkly Rep. 2022;71:1531–7. https://doi.org/10.15585/mmwr.mm7148e2
7. Pfizer. Pfizer shares in vitro efficacy of novel COVID-19 oral treatment against Omicron variant [cited 2022 Mar 21]. https://www.pfizer.com/news/press-release/press-release-detail/pfizer-shares-vitro-efficacy-novel-covid-19-oral-treatment
8. Pfizer. Pfizer to provide U.S. government with an additional 10 million treatment courses of its oral therapy to help combat COVID-19 [cited 2022 Mar 25]. https://www.pfizer.com/news/press-release/press-release-detail/pfizer-provide-us-government-additional-10-million
9. Jenner AL, Aogo RA, Alfonso S, Crowe V, Deng X, Smith AP, et al. COVID-19 virtual patient cohort suggests immune mechanisms driving disease outcomes. PLoS Pathog. 2021;17:e1009753. https://doi.org/10.1371/journal.ppat.1009753
10. Kim KS, Ejima K, Iwanami S, Fujita Y, Ohashi H, Koizumi Y, et al. A quantitative model used to compare within-host SARS-CoV-2, MERS-CoV, and SARS-CoV dynamics provides insights into the pathogenesis and treatment of SARS-CoV-2. PLoS Biol. 2021;19:e3001128. https://doi.org/10.1371/journal.pbio.3001128

11. Hammond J, Leister-Tebbe H, Gardner A, Abreu P, Bao W, Wisemandle W, et al.; EPIC-HR Investigators. Oral nirmatrelvir for high-risk, nonhospitalized adults with Covid-19. N Engl J Med. 2022;386:1397–408. https://doi.org/10.1056/NEJMoa2118542
12. Handel A, Rohani P. Crossing the scale from within-host infection dynamics to between-host transmission fitness: a discussion of current assumptions and knowledge. Philos Trans R Soc Lond B Biol Sci. 2015;370:20140302.
13. Néant N, Lingas G, Le Hingrat Q, Ghosn J, Engelmann I, Lepiller Q, et al.; French COVID Cohort Investigators and French Cohort Study groups. Modeling SARS-CoV-2 viral kinetics and association with mortality in hospitalized patients from the French COVID cohort. Proc Natl Acad Sci U S A. 2021;118:e2017962118. https://doi.org/10.1073/pnas.2017962118
14. Wölfel R, Corman VM, Guggemos W, Seilmaier M, Zange S, Müller MA, et al. Virological assessment of hospitalized patients with COVID-2019. Nature. 2020;581:465–9. https://doi.org/10.1038/s41586-020-2196-x
15. Du Z, Pandey A, Bai Y, Fitzpatrick MC, Chinazzi M, Pastore Y Piontti A, et al. Comparative cost-effectiveness of SARS-CoV-2 testing strategies in the USA: a modelling study. Lancet Public Health. 2021;6:e184–91. https://doi.org/10.1016/S2468-2667(21)00002-5
16. U.S. Federal Highway Administration. 2017 national household travel survey [cited 2020 Jun 16]. https://nhts.ornl.gov/downloads
17. Neumann PJ, Cohen JT, Weinstein MC. Updating cost-effectiveness—the curious resilience of the $50,000-per-QALY threshold. N Engl J Med. 2014;371:796–7. https://doi.org/10.1056/NEJMp1405158
18. Czuppon P, Débarre F, Gonçalves A, Tenaillon O, Perelson AS, Guedj J, et al. Success of prophylactic antiviral therapy for SARS-CoV-2: predicted critical efficacies and impact of different drug-specific mechanisms of action. PLOS Comput Biol. 2021;17:e1008752. https://doi.org/10.1371/journal.pcbi.1008752
19. Traynard P, Ayral G, Twarogowska M, Chauvin J. Efficient pharmacokinetic modeling workflow with the MonolixSuite: a case study of remifentanil. CPT Pharmacometrics Syst Pharmacol. 2020;9:198–210. https://doi.org/10.1002/psp4.12500
20. Lavielle M, Mentré F. Estimation of population pharmacokinetic parameters of saquinavir in HIV patients with the MONOLIX software. J Pharmacokinet Pharmacodyn. 2007;34:229–49. https://doi.org/10.1007/s10928-006-9043-z
21. US Census Bureau. National population by characteristics: 2010–2019 [cited 2020 Oct 1]. https://www.census.gov/data/tables/time-series/demo/popest/2010s-national-detail.html
22. Robbins R, Zimmer C. FDA clears Pfizer's Covid pill for high-risk patients 12 and older. 2021 Dec 22 [cited 2022 Apr 29]. https://www.nytimes.com/2021/12/22/health/pfizer-covid-pill-fda-paxlovid.html
23. TIME. China's approval of Pfizer pill opens door to ending COVID Zero. 2022 Feb 14 [cited 2023 Jan 21]. https://time.com/6147924/china-pfizer-covid-19-pill
24. COVID.gov. Find COVID-19 guidance for your community [cited 2022 Apr 29]. https://www.covid.gov
25. Joshi AU, Lewiss RE, Aini M, Babula B, Henwood PC. Solving community SARS-CoV-2 testing with telehealth: development and implementation for screening, evaluation and testing. JMIR Mhealth Uhealth. 2020;8:e20419. https://doi.org/10.2196/20419
26. Centers for Disease Control and Prevention. New COVID-19 test to treat initiative and locator tool [cited 2022 Apr 6]. https://emergency.cdc.gov/newsletters/coca/040422.htm
27. Huang F, Liu H. The impact of the COVID-19 pandemic and related policy responses on non-COVID-19 healthcare utilization in China. Health Econ. 2023;32:620–38. https://doi.org/10.1002/hec.4636
28. National Health Commission of the People's Republic of China. China's internet health services gathering steam amid COVID-19 [cited 2022 Dec 7]. http://en.nhc.gov.cn/2021-08/24/c_85005.htm
29. He D, Gu Y, Shi Y, Wang M, Lou Z, Jin C. COVID-19 in China: the role and activities of Internet-based healthcare platforms. Glob Health Med. 2020;2:89–95. https://doi.org/10.35772/ghm.2020.01017
30. China Internet Network Information Center. 48th statistical report on internet development in China [cited 2021 Nov 19]. https://www.cnnic.com.cn/IDR/ReportDownloads/202111/P020211119394556095096.pdf
31. Vegvari C, Hadjichrysanthou C, Cauët E, Lawrence E, Cori A, de Wolf F, et al. How can viral dynamics models inform endpoint measures in clinical trials of therapies for acute viral infections? PLoS One. 2016;11:e0158237. https://doi.org/10.1371/journal.pone.0158237
32. Iketani S, Mohri H, Culbertson B, Hong SJ, Duan Y, Luck MI, et al. Multiple pathways for SARS-CoV-2 resistance to nirmatrelvir. Nature. 2023;613:558–64. https://doi.org/10.1038/s41586-022-05514-2
33. Callaway E. How months-long COVID infections could seed dangerous new variants. Nature. 2022;606:452–5. https://doi.org/10.1038/d41586-022-01613-2
34. Herxheimer A. Relationships between the pharmaceutical industry and patients' organisations. BMJ. 2003;326:1208–10. https://doi.org/10.1136/bmj.326.7400.1208
35. Biggerstaff M, Jhung MA, Reed C, Fry AM, Balluz L, Finelli L. Influenza-like illness, the time to seek healthcare, and influenza antiviral receipt during the 2010–2011 influenza season—United States. J Infect Dis. 2014;210:535–44. https://doi.org/10.1093/infdis/jiu224

Address for correspondence: Lauren Ancel Meyers, Department of Integrative Biology, University of Texas at Austin, 2415 Speedway #C0930, Austin, TX 78712, USA; email: laurenmeyers@austin.utexas.edu

Impact of Meningococcal ACWY Vaccination Program during 2017–18 Epidemic, Western Australia, Australia

Krist Ewe,[1] Parveen Fathima,[1] Paul Effler, Carolien Giele, Peter Richmond

The rising incidence of invasive meningococcal disease (IMD) caused by *Neisseria meningitidis* serogroup W in Western Australia, Australia, presents challenges for prevention. We assessed the effects of a quadrivalent meningococcal vaccination program using 2012–2020 IMD notification data. Notification rates peaked at 1.8/100,000 population in 2017; rates among Aboriginal and Torres Strait Islander populations were 7 times higher than for other populations. Serogroup W disease exhibited atypical manifestations and increased severity. Of 216 cases, 20 IMD-related deaths occurred; most (19/20) were in unvaccinated persons. After the 2017–2018 targeted vaccination program, notification rates decreased from 1.6/100,000 population in 2018 to 0.9/100,000 population in 2019 and continued to decline in 2020. Vaccine effectiveness (in the 1–4 years age group) using the screening method was 93.6% (95% CI 50.1%–99.2%) in 2018 and 92.5% (95% CI 28.2%–99.2%) in 2019. Strategic planning and prompt implementation of targeted vaccination programs effectively reduce IMD.

Invasive meningococcal disease (IMD) remains a public health concern worldwide. The causative organism, *Neisseria meningitidis*, is differentiated into 12 distinct serogroups, of which A, B, C, W, X, and Y are most commonly associated with IMD (*1*). *N. meningitidis* is present in the nasopharynx of nearly 10% of the population without causing disease, and IMD develops in only a small proportion of those persons. IMD is characterized by sudden onset of symptoms (including stiff neck, headache, photophobia, and a characteristic spotty red-purple rash) and rapid clinical progression leading to septicemia or meningitis. IMD-associated mortality is ≈10%–15%; however, more than one third of all IMD patients experience notable long-term or permanent effects, such as skin necrosis, deafness, seizures, or other neurologic sequelae (*2*,*3*). Infants <1 year of age have the highest risk for IMD, followed by a smaller second peak in adolescents and young adults, reflecting the social behavior that increases the nasopharyngeal carriage of meningococcus.

The evolving and unpredictable epidemiology of IMD poses additional challenges to its prevention. *N. meningitidis* serogroups causing IMD are known to change over time. After meningococcal C vaccine was introduced into the Australian National Immunization Program in 2003, IMD notification rates declined from 3.5/100,000 population in 2002 to 0.6/100,000 in 2013; *N. meningitidis* serogroup B (MenB) was responsible for most cases. After 2013, IMD notification rates increased, reaching 1.5/100,000 population in 2017 (*4*). A similar trend was seen in the state of Western Australia (*4*). For many years, MenB was responsible for most IMD notifications in Australia; however, since 2013, the incidence of IMD caused by *N. meningitidis* serogroup W (MenW) has increased (*5*). Globally, MenW IMD is often associated with atypical clinical features, including gastrointestinal symptoms, septic arthritis, pneumonia, and epiglottitis (*6*), along with high rates of illness and death (*7*).

Author affiliations: Wesfarmers Centre of Vaccines and Infectious Diseases, Perth, Western Australia, Australia (K. Ewe, P. Fathima, P. Richmond); Perth Children's Hospital, Perth (K. Ewe, P. Richmond); Sydney School of Public Health, University of Sydney, Sydney, New South Wales, Australia (P. Fathima); Communicable Disease Control Directorate, Western Australia Department of Health, Perth (P. Effler, C. Giele); University of Western Australia School of Medicine, Perth (P. Richmond).

DOI: https://doi.org/10.3201/eid3002.230144

[1]These authors contributed equally to this article.

Effective vaccines against *N. meningitidis* serogroups A, B, C, W, and Y are available (*8*). Some countries have included or are considering publicly funding the quadrivalent meningococcal vaccines (ACWY) as part of their national immunization program (*8*). Those decisions are usually influenced by numerous factors, including cost-effectiveness, vaccine efficacy, and effects on public health. In Western Australia, since 2016, the state government has incrementally funded and delivered MenACWY conjugate vaccines through targeted vaccination campaigns in relevant schools, community health centers and immunization clinics. During December 2016–December 2017, the vaccines were offered free to all children 12 months–4 years of age and to teenagers 15–19 years of age in affected and at-risk communities in regional areas (*9*). During October–December 2017, the funded vaccines were extended to persons of all ages in those areas. Beginning in January 2018, the vaccine became available to all children 12 months–4 years of age. During May 2017–March 2019, funding covered students in grades 10–12 and adolescents 15–19 years of age who no longer attended school (Figures 1, 2). We reviewed the effects of the introduction of a targeted quadrivalent meningococcal (ACWY-TT) vaccination program in Western Australia following an outbreak of MenW in 2017–2018.

Methods

The Communicable Disease Control Directorate at the Western Australia Department of Health conducts enhanced surveillance for IMD statewide. All pathology laboratories within the state routinely notify the Directorate of any laboratory-confirmed or probable (suspected) diagnosis of IMD. A confirmed case is defined as one in which *N. meningitidis* is identified by standard microbiological methods from a normally sterile site (isolation of *N. meningitidis* by culture or detection of *N. meningitidis* DNA by nucleic acid amplification testing). A probable case is illness in a person experiencing clinical manifestations consistent with IMD but not confirmed by standard microbiological methods. Case data collected routinely include medical history, gender, region of residence at the time of disease onset, vaccination status, risk factors, indigenous status, clinical manifestations, serogroup information, and outcome. The data are captured on the Western Australia Notifiable Infectious Diseases Database. For this study, we extracted deidentified data on all IMD notifications in Western Australia with a date of onset during 2012–2020.

Cases were categorized into age groups of 0–4 years, 5–9 years, 10–14 years, 15–19 years, 20–24 years, 25–44 years, 45–64 years, and ≥65 years. Using annual population estimates (obtained from Rates Calculator, Epidemiology Branch, Western Australia Department of Health), we calculated age-specific and age-standardized notification rates by Aboriginal and Torres Strait Islander (hereafter referred to as Aboriginal) status. We analyzed clinical manifestations and outcomes by causative serogroup for laboratory-confirmed IMD cases. We calculated case-fatality rates (CFRs) according to year and serogroup.

We used a hierarchy of clinical manifestations to assign a single clinical syndrome category. We assigned *N. meningitidis* detected or isolated from a single normally sterile site to that site. *N. meningitidis* detected or isolated from 2 normally sterile sites was assigned the site of isolation other than blood. For example, if *N. meningitidis* was detected in blood and cerebrospinal fluid, then meningitis would be

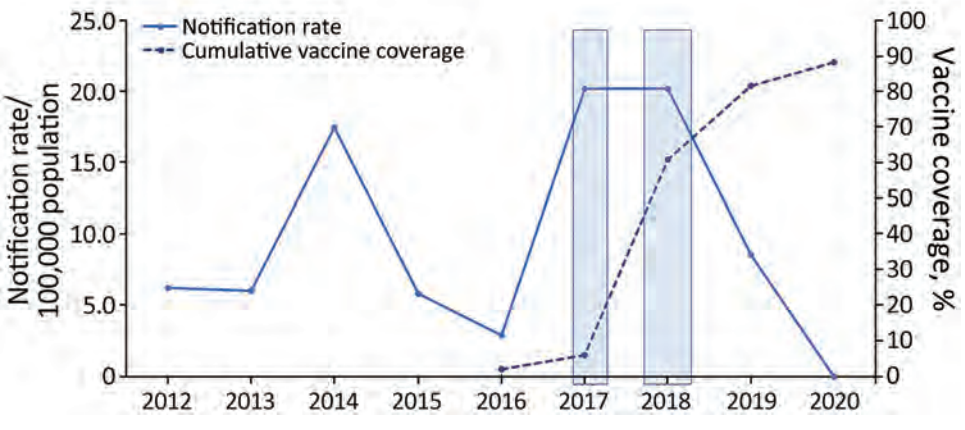

Figure 1. Invasive meningococcal disease notification rates (solid line) and cumulative meningococcal ACWY vaccine coverage rates (dotted line) among children 12 months–4 years of age, Western Australia, 2012–2020. First shaded box indicates the period of December 2016–March 2017, during which the local Western Australia government funded the meningococcal ACWY conjugate vaccine for children 12 months–4 years of age and adolescents 15–19 years of age in selected affected and at-risk regional areas. Second shaded box indicates period of October–December 2017, during which vaccine was funded for people of all ages in selected affected and at-risk regional areas. Beginning in January 2018, the vaccine was funded and available to all children 12 months–4 years of age.

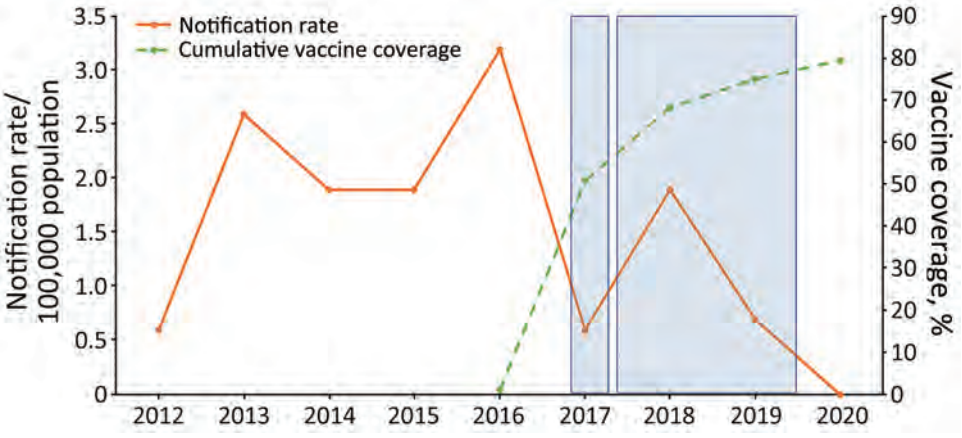

Figure 2. Invasive meningococcal disease notification rates (solid line) and cumulative meningococcal ACWY vaccine coverage rates (dotted line) among adolescents 15–19 years of age, Western Australia, 2012–2020. First shaded box indicates the period of December 2016–March 2017, during which the local Western Australia government funded the meningococcal ACWY conjugate vaccine for children 12 months–4 years and adolescents 15–19 years in selected affected and at-risk regional areas. Second shaded box indicates period of May 2017–March 2019, during which vaccine was funded for students in grades 10–12 and adolescents 15–19 years of age no longer enrolled in school.

assigned. *N. meningitidis* was not isolated from ≥3 sites in any of the cases in this study.

We collected patient or parental recall regarding previous receipt of meningococcal vaccinations for all IMD notifications. Where available, we validated data on vaccine uptake using the Australian Immunization Register (*10*). We reported vaccination status of persons with IMD as fully vaccinated (received all recommended doses of the meningococcal vaccine according to the state or regionally funded vaccination program), not vaccinated (vaccine available, but not received), unknown (vaccination status not known or documented) or nonapplicable (vaccine not publicly available or funded for the relevant groups). IMD notification rates were assessed against data on MenACWY vaccination coverage; we compared rates before and after the introduction of the target meningococcal vaccination program in Western Australia.

Using the screening method (*11*), we estimated the effectiveness of meningococcal vaccine against notified IMD for the vaccine-eligible age-groups (i.e., 1–4 years, 5–14 years and 15–19 years) using the following formula:

$$\text{Vaccine effectiveness} = 1 = \left[\frac{\text{PCV}}{1-\text{PCV}} \times \frac{1-\text{PPV}}{\text{PPV}}\right] \times 100\%$$

where PCV is the proportion of IMD case-patients who were vaccinated and PPV is the proportion of population vaccinated.

Results

During January 2012–December 2020, a total of 216 cases of IMD were reported; 113 (52%) patients were male and 103 (48%) female. Of the 216 cases, 213 (98.6%) were laboratory-confirmed cases, and the remainder (n = 3) were diagnosed on the basis of a high index of clinical suspicion. Sixty-one percent of cases (131/216) occurred in residents of the Perth Metropolitan area, home to ≈80% of the Western Australia population (*12*). The age-standardized IMD notification rate rose from a baseline of 0.8/100,000 population (n = 19) in 2012 to a peak of 1.8/100,000 (n = 46) in 2017, then declined to 0.9/100,000 in 2019, an incidence rate ratio of 0.53 (CI 0.31–0.88; p = 0.011). In 2020, the IMD notification rate declined further to 0.4/100,000 population (Figure 3).

MenB accounted for 79% (n = 15/19) of all IMD cases in 2012, in contrast to 2 cases of MenC, 1 case of MenY, and 0 cases of MenW in the same year (the remaining case was nongroupable). The proportion of IMD notifications caused by MenB waned over the years, but the number of IMD cases caused by MenW gradually increased (Figure 3); MenW overtook MenB as the dominant serogroup in 2016, accounting for 61% (n = 14/23) of all IMD notifications in Western Australia.

As expected, the highest IMD notification rates overall during 2012–2020 were among children 0–4 years of age (4.4/100,000 notifications) (Figure 4), followed by a second, smaller peak in adolescents 15–19 years and young adults 20–24 years (1.5/100,000 notifications). Notification rates were lower in other age groups, rising slightly for those ≥60 years of age. In total, 63/216 cases (29.2%) of IMD occurred among the Aboriginal population. The overall (2012–2020) age-standardized notification rate for IMD among the Aboriginal population (4.9/100,000 population) was 7 times higher than in the non-Aboriginal population (0.7/100,000 population). This difference was largely because of an IMD outbreak among the Aboriginal population in 2017–2019, beginning in Central Australia and spreading to neighboring states;

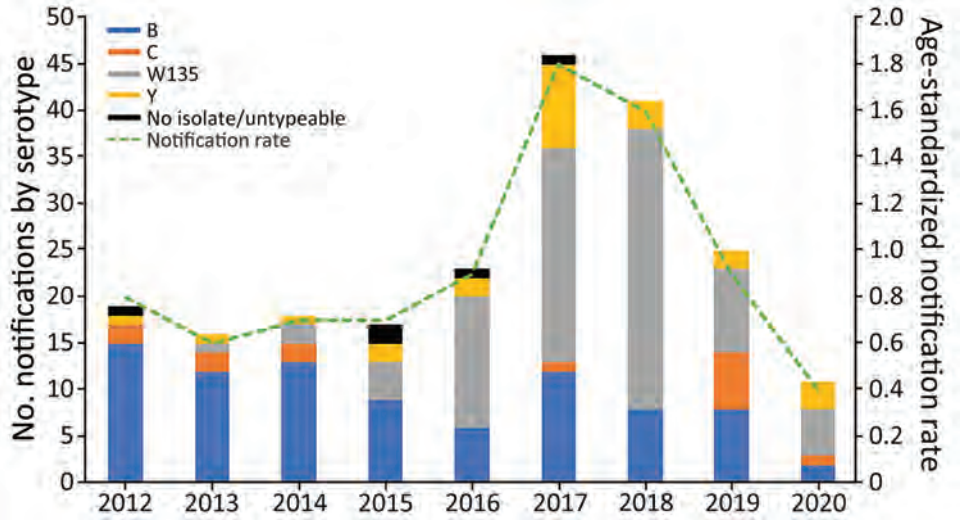

Figure 3. Invasive meningococcal disease notifications (N = 216) and age-standardized notification rates (per 100,000 population), by year and serogroup, Western Australia, 2012–2020.

65% (n = 41/63) of IMD cases in the Aboriginal population occurred during this period, and most (63%; n = 26) occurred in children <5 years of age. Overall, 76.2% (n = 48) of all IMD notifications among Aboriginal persons occurred in the 0–9 years age group, and most of those were in the 0–4 years age group (n = 40) (Figure 5).

The overall clinical manifestations ranged from typical septicemia (47.4%; n = 100/211) and meningitis (34.1%; n = 72/211) to more atypical symptoms, such as septic arthritis (6%), pneumonia (5%), epiglottitis/pharyngitis (2%), pericarditis (0.5%), and chorioamnionitis (0.5%) (Figure 6). Our study showed that 27% (24/88) of MenW case-patients and 50% (12/24) of MenY case-patients displayed atypical symptoms. The overall CFR was 9.3% (n = 20); MenW was identified in most IMD-related deaths (60%; n = 12/20), followed by MenB (35%; n = 7). With the exception of 1 case-patient whose meningococcal vaccination status was unknown, the rest of the IMD-related deaths (19/20) were in persons who were not vaccinated.

Overall, rates of meningococcal ACWY vaccine uptake were high in the targeted groups (the vaccine publicly funded for persons 12 months–4 years, 15–19 years, and for all ages in select affected or at-risk regional areas). Since the introduction of the quadrivalent meningococcal ACWY (Nimenrix) vaccination program in December 2016, uptake rates among children 1–4 years increased rapidly, reaching 90% of all children in this age group by 2020 (Figure 1). A similar trend was noted in the 15–19-year age group, in which rates reached 80% by 2020 (Figure 2). The incidence of IMD declined from 1.6/100,000 population in 2018 to 0.9/100,000 population in 2019

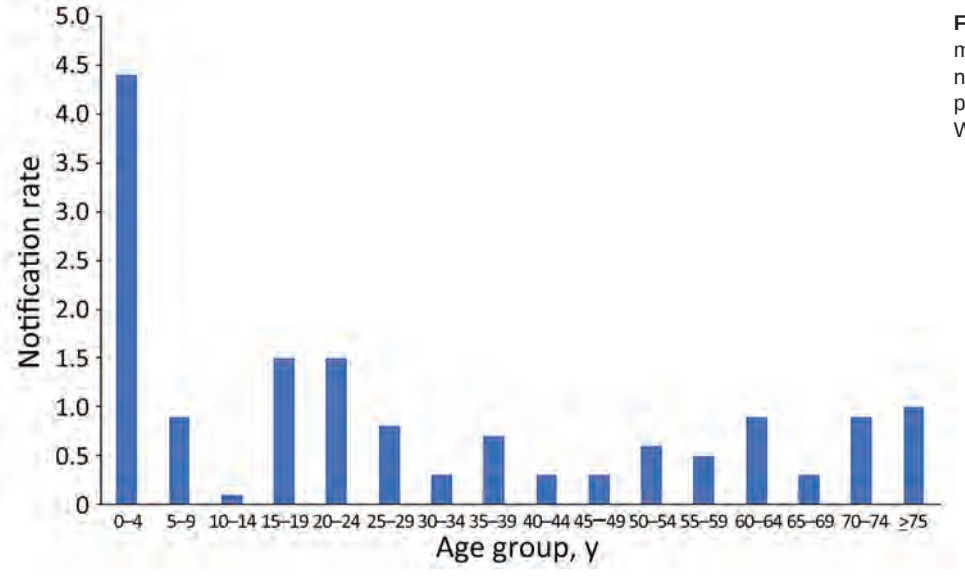

Figure 4. Invasive meningococcal disease notification rates (per 100,000 population), by age group, Western Australia, 2012–2020.

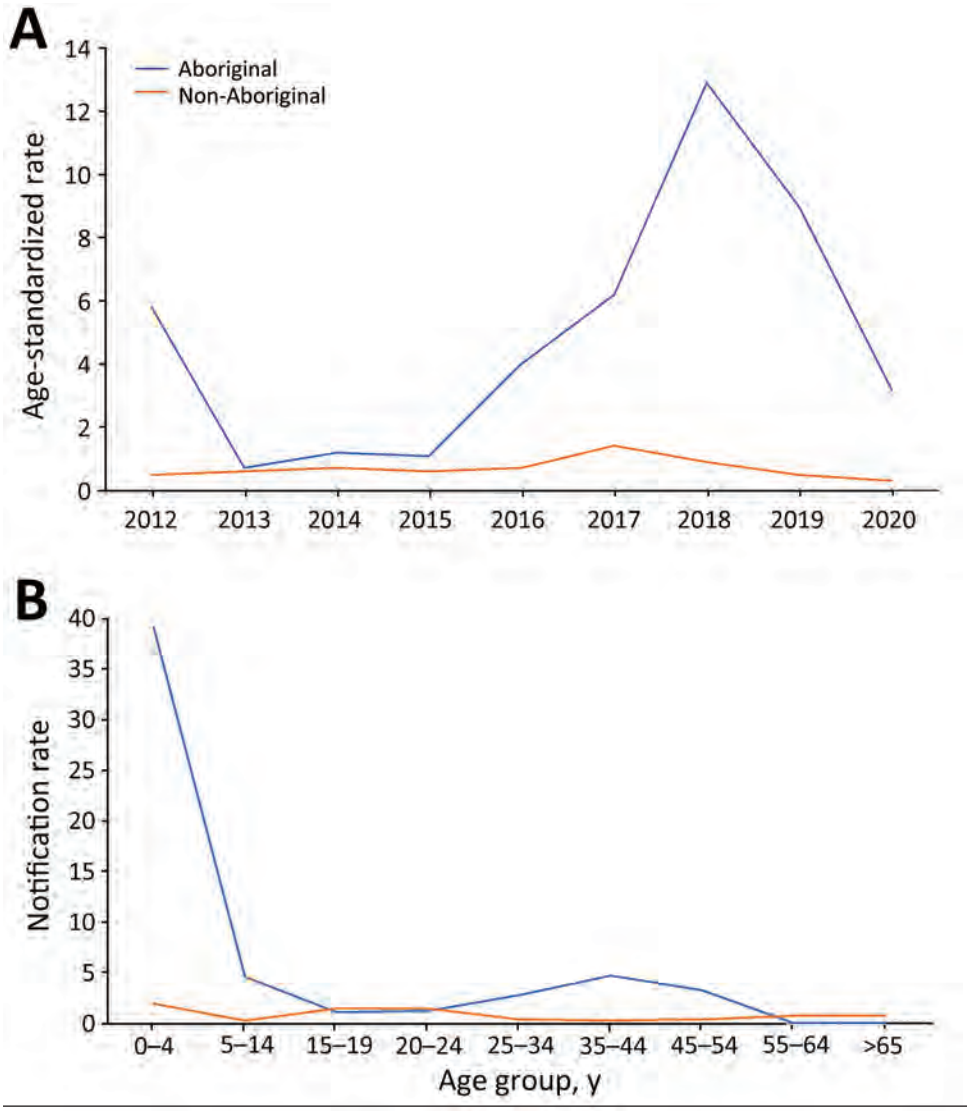

Figure 5. Invasive meningococcal disease notification rates (per 100,000 population) by population group in Western Australia (Aboriginal vs. non-Aboriginal), 2012–2020, by year (A) and age group (B).

(corresponding to 30 cases in 2018 and 9 cases in 2019) after the introduction of the targeted vaccination program. In 2020, no notifications of IMD caused by serogroups A, C, W and Y in the age cohorts targeted for vaccination were recorded.

In the highest-risk age group (12 months–4 years), the vaccine effectiveness calculated using the screening method was 93.6% (95% CI 50.1%–99.2%) for 2018 and 92.5% (95% CI 28.2%–99.2%) for 2019. Power was inadequate to generate a meaningful interpretable value for the 5–14- and 15–19-year age groups for whom the vaccine was available.

Discussion

IMD incidence data show a change in the epidemiology of IMD in Western Australia from 2012 to 2020. The dominance of MenB as the primary cause of IMD was succeeded by a rise in the number of notifications of IMD caused by MenW and, to a lesser extent, MenY. The rise in MenW notifications in Western Australia and Australia as a whole is not an isolated occurrence. Over the past 2 decades, increases in the incidence of IMD caused by MenW have been reported in other settings (*3*,*13*–*20*).

In Western Australia, the rise in IMD notifications eventually led to an IMD outbreak in 2017 and 2018, disproportionately affecting Aboriginal populations. Elevated rates of IMD have been described previously among Aboriginal Australian populations (*21*–*23*) and in other specific populations outside Australia, such as African American persons (*24*) and Pacific Islanders (*25*). Up to 1 in 5 Aboriginal Australians live in remote or very remote areas (*26*). A similar proportion of Aboriginal Australians live in overcrowded households and are more likely to live in suboptimal conditions, such as having limited access

to essential services and sanitation (*27*). The higher incidence rates of IMD disease in Aboriginal populations in Australia have been attributed to specific risk factors, whereas higher mortality rates are thought to be linked to limited timely access to healthcare services. Younger Aboriginal children experience higher rates of IMD than the general population, potentially because of a combination of risk factors, such as the immaturity of their immune system, frequent viral upper respiratory tract infections, exposure to passive smoking, household crowding (*28*), and lower vaccination rates (*29*).

Atypical clinical manifestations and higher CFR in our cohort were seen more frequently with IMD caused by MenW and MenY than for other serogroups, consistent with findings from other countries where severe cases were caused by a hypervirulent strain belonging to the sequence type 11 clonal complex (cc11) (*20*,*30*). The 2017 Australian Meningococcal Surveillance Programme reported that, among the MenW strains that were able to be genotyped, 59% (74/125) were sequence type 11, the same strain circulating in the United Kingdom and South America since 2009 (*31*). Advances in sequencing technology have enabled further characterization of this clonal complex into distinct lineages and sublineages, revealing an evolution of genetically (and geotemporally) diverse global cc11 populations that exhibit different epidemiologic properties (*32*).

Although the hypervirulent MenW cc11 strains have been shown to diverge from a MenC cc11 ancestral strain by capsular switching (*33*,*34*), some appear unrelated to the contemporary MenC cc11 strains (*35*). Furthermore, certain variants, particularly the cc11/non–ET-15 variants, lack the virulence factors present in cc11/ET-15 strains associated with more aggressive infections in the cc11/ET-15 strains (*36*). In our cohort, IMD caused by MenW was also associated with a high mortality rate, consistent with a systematic review and metaanalysis of CFR of IMD (*37*).

The clinical manifestations of IMD caused by MenY are less well characterized, but a retrospective observational study performed on a large cohort in Sweden reported atypical symptoms, such as pneumonia (19%) and septic arthritis (10%), particularly in older patients (*38*). The implications of the rise of IMD caused by MenW and MenY ultimately manifesting with more atypical symptoms might lead to delayed diagnosis or misdiagnosis even by experienced clinicians and to use of antibiotics that are ineffective against *N. meningitidis*, leading to rapid progression of disease and death.

Vaccination remains the most effective strategy for preventing IMD and its complications. The 2017–18 outbreak of MenW, and to a lesser extent MenY, in Western Australia led to the rapid implementation of a targeted vaccination program with the quadrivalent meningococcal ACWY vaccine (Nimenrix) in December 2016, starting with high-risk groups in communities located in geographic areas with increased IMD incidence.

Success stories abound of meningococcal vaccine programs responding to IMD outbreaks across the globe. In 2004, the introduction of mass vaccinations

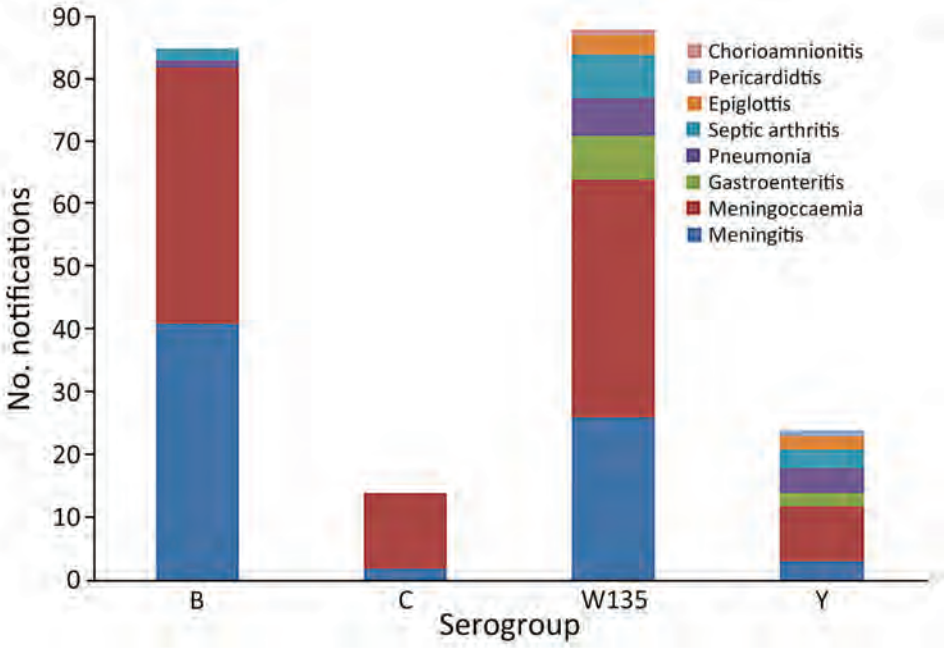

Figure 6. Clinical manifestations of invasive meningococcal disease by serogroup, Western Australia, 2012–2020. Categories of clinical manifestation include only meningococcal isolates that were typable.

with the outer membrane vesicle vaccine against the serogroup B epidemic strain in New Zealand (MeNZB) reduced the risk for infection by 4-fold, and by 2009 the incidence rate of IMD had declined to 3.3/100,00 population, compared with 17.4/100,000 population at its peak (*39*). Similarly, the use of the recombinant meningococcal serogroup B vaccine in the United States (4CMenB) in response to a university campus outbreak saw no further cases linked to the university after the initiation of the vaccine program (*40*). More impressive was the prophylactic use of the MenA conjugate vaccine in Burkina Faso, Mali, and Niger (MenAfriVac). A 10-day vaccination campaign in Burkina Faso saw ≈11 million residents get vaccinated (*41*), 3 million residents were vaccinated in Niger in 10 days (*42*), and a 14-day campaign in Mali saw 4.5 million residents get vaccinated. The success of that vaccination campaign cannot be understated; 5 years after the mass vaccination campaign, Burkina Faso had gone from a hyperendemic state to only recording sporadic cases of IMD caused by MenA (*43*). In a separate targeted vaccination program, the introduction of a 2-dose 4CMenB infant schedule as part of a publicly funded UK immunization program resulted in a 50% reduction in the incidence of MenB cases among the vaccine-eligible cohort within 10 months (*44*).

Our data show that IMD is uncommon among those who are fully vaccinated, and fatal cases occur primarily in those who are not vaccinated. The rapid implementation of a targeted vaccination program in 2017–2018 in young children most at risk (those 1–4 years of age), as well as in adolescents and young adults (15–24 years) who have the highest carriage rates, led to a dramatic reduction in the number of notifications for Western Australia in 2019 that continued into 2020. The rapid and high vaccination uptake rate reflects effective public health communication and strong awareness of the outbreak among the Aboriginal population in remote or socially disadvantaged areas, which traditionally have lower vaccination uptake than the general population (*45*). The absence of cases in the vaccinated cohort supports the notion that vaccination is effective in preventing disease and death.

Lockdowns related to COVID-19 in 2020 were thought to affect the reduction in the number of IMD notifications in that year. A study from France showed that the overall number of IMD notifications, particularly of hyperinvasive strains, reduced during the lockdown period during January 2020–May 2020, but the proportion of cases associated with respiratory symptoms (MenY) increased during that period (*46*). Analysis of surveillance data submitted from laboratories in 26 countries and territories across 6 continents demonstrated a substantial reduction of invasive diseases caused by respiratory pathogens, including *N. meningitidis*, during the same lockdown period, likely because of strict containment policies (*47*). As part of the national response to the COVID-19 pandemic in Western Australia, international borders were closed to nonresidents on March 20, 2020, and subsequent restrictions were placed on interstate travel on April 6, 2020. A statewide stay-at-home restriction, including an extended school holiday, was imposed from March 27 through April 27, 2020; schools resumed at near capacity after that. Those restrictions could arguably have affected opportunities for exposure to *N. meningitidis*. Of note, however, a substantive reduction in the number of IMD notifications was already evident in 2019, and the effect persisted throughout 2020. The statewide restrictions on interstate travel and Western Australia school closures were thought to be too brief to have any long-term effect on transmission of *N. meningitidis*, and, in our opinion, increases in handwashing and surface cleaning and physical distancing measures would not likely fully explain the absence of IMD cases caused by serogroups A, C, W, and Y among persons 0–4 years of age and adolescents in 2020.

In conclusion, the epidemiology of IMD is constantly changing. Both direct and herd protection are essential because of the atypical manifestation and high mortality associated with some serogroups, which leads to delayed diagnosis and potentially increased case fatality. The vaccine effectiveness was high in the most at-risk group using the screening method. Rapidly implementing meningococcal vaccination programs with high coverage in at-risk populations is effective in reducing the incidence of IMD in an outbreak setting. Vaccination against meningococcal disease, particularly MenW and MenY, should continue to be encouraged.

Acknowledgments

We acknowledge and thank PathWest Laboratory Medicine for their role in providing prompt laboratory diagnosis and information regarding isolate typing to the Communicable Disease Control Directorate at Western Australia Department of Health.

About the Author

Dr. Ewe is a pediatric doctor completing his infectious disease and microbiology training at PathWest Laboratory Medicine, Western Australia, who previously worked in the field of immunisation at Perth Children's

Hospital and has been involved in numerous vaccine clinical trials with the Vaccine Trials Group at Telethon Kids Institute. He intends to extend his research in pediatric infectious diseases and vaccinations. Dr. Fathima is an infectious diseases epidemiologist and postdoctoral fellow at the Sydney School of Public Health, University of Sydney. Her research interests include vaccine preventable diseases, vaccine effectiveness and safety, linked data, and causal inference methods.

References

1. Dwilow R, Fanella S. Invasive meningococcal disease in the 21st century—an update for the clinician. Curr Neurol Neurosci Rep. 2015;15:2. https://doi.org/10.1007/s11910-015-0524-6
2. Pace D, Pollard AJ. Meningococcal disease: clinical presentation and sequelae. Vaccine. 2012;30(Suppl 2):B3–9. https://doi.org/10.1016/j.vaccine.2011.12.062
3. Booy R, Gentile A, Nissen M, Whelan J, Abitbol V. Recent changes in the epidemiology of *Neisseria meningitidis* serogroup W across the world, current vaccination policy choices and possible future strategies. Hum Vaccin Immunother. 2019;15:470–80. https://doi.org/10.1080/21645515.2018.1532248
4. Australian Government Department of Health. Invasive meningococcal disease 2020 [cited 2020 Nov 19]. https://www1.health.gov.au/internet/main/publishing.nsf/Content/ohp-meningococcal-W.htm
5. Martin NV, Ong KS, Howden BP, Lahra MM, Lambert SB, Beard FH, et al.; Communicable Diseases Network Australia MenW Working Group. Rise in invasive serogroup W meningococcal disease in Australia 2013–2015. Commun Dis Intell Q Rep. 2016;40:E454–9.
6. Stinson C, Burman C, Presa J, Abalos M. Atypical presentation of invasive meningococcal disease caused by serogroup W meningococci. Epidemiol Infect. 2020;148:e12. https://doi.org/10.1017/S0950268819002152
7. Ladhani SN, Beebeejaun K, Lucidarme J, Campbell H, Gray S, Kaczmarski E, et al. Increase in endemic *Neisseria meningitidis* capsular group W sequence type 11 complex associated with severe invasive disease in England and Wales. Clin Infect Dis. 2015;60:578–85. https://doi.org/10.1093/cid/ciu881
8. Pizza M, Bekkat-Berkani R, Rappuoli R. Vaccines against meningococcal diseases. Microorganisms. 2020;8:1521. https://doi.org/10.3390/microorganisms8101521
9. National Centre from Immunisation Research and Surveillance. Significant events in meningococcal vaccination practice in Australia [cited 2023 Nov 27]. https://ncirs.org.au/health-professionals/history-immunisation-australia
10. Peterson ME, Mile R, Li Y, Nair H, Kyaw MH. Meningococcal carriage in high-risk settings: a systematic review. Int J Infect Dis. 2018;73:109–17. https://doi.org/10.1016/j.ijid.2018.05.022
11. Farrington CP. Estimation of vaccine effectiveness using the screening method. Int J Epidemiol. 1993;22:742–6. https://doi.org/10.1093/ije/22.4.742
12. Australian Bureau of Statistics. National, state and territory population, March 2022 [cited 2022 Oct 12]. https://www.abs.gov.au/statistics/people/population/national-state-and-territory-population/mar-2022
13. Ibarz-Pavón AB, Lemos AP, Gorla MC, Regueira M, Gabastou JM; SIREVA Working Group II. Laboratory-based surveillance of *Neisseria meningitidis* isolates from disease cases in Latin American and Caribbean countries, SIREVA II 2006–2010. PLoS One. 2012;7:e44102. https://doi.org/10.1371/journal.pone.0044102
14. Araya P, Fernández J, Del Canto F, Seoane M, Ibarz-Pavón AB, Barra G, et al. *Neisseria meningitidis* ST-11 clonal complex, Chile 2012. Emerg Infect Dis. 2015;21:339–41. https://doi.org/10.3201/eid2102.140746
15. Koutangni T, Boubacar Maïnassara H, Mueller JE. Incidence, carriage and case-carrier ratios for meningococcal meningitis in the African meningitis belt: a systematic review and meta-analysis. PLoS One. 2015;10:e0116725. https://doi.org/10.1371/journal.pone.0116725
16. MacNeil JR, Medah I, Koussoubé D, Novak RT, Cohn AC, Diomandé FV, et al. *Neisseria meningitidis* serogroup W, Burkina Faso, 2012. Emerg Infect Dis. 2014;20:394–9. https://doi.org/10.3201/eid2003.131407
17. Stefanelli P, Fazio C, Neri A, Rezza G, Severoni S, Vacca P, et al. Imported and Indigenous cases of invasive meningococcal disease W:P1.5,2:F1-1: ST-11 in migrants' reception centers. Italy, June–November 2014. Adv Exp Med Biol. 2016;897:81–3. https://doi.org/10.1007/5584_2015_5006
18. Krone M, Gray S, Abad R, Skoczyńska A, Stefanelli P, van der Ende A, et al. Increase of invasive meningococcal serogroup W disease in Europe, 2013 to 2017. Euro Surveill. 2019;24:1800245. https://doi.org/10.2807/1560-7917.ES.2019.24.14.1800245
19. Knol MJ, Hahné SJM, Lucidarme J, Campbell H, de Melker HE, Gray SJ, et al. Temporal associations between national outbreaks of meningococcal serogroup W and C disease in the Netherlands and England: an observational cohort study. Lancet Public Health. 2017;2:e473–82. https://doi.org/10.1016/S2468-2667(17)30157-3
20. Eriksson L, Hedberg ST, Jacobsson S, Fredlund H, Mölling P, Stenmark B. Whole-genome sequencing of emerging invasive *Neisseria meningitidis* serogroup W in Sweden. J Clin Microbiol. 2018;56:e01409-17. https://doi.org/10.1128/JCM.01409-17
21. Massey P, Durrheim D. Aboriginal and Torres Strait Islander peoples at higher risk of invasive meningococcal disease in NSW. N S W Public Health Bull. 2008;19:100–3. https://doi.org/10.1071/NB07047
22. Archer BN, Chiu CK, Jayasinghe SH, Richmond PC, McVernon J, Lahra MM, et al.; Australian Technical Advisory Group on Immunisation (ATAGI) Meningococcal Working Party. Epidemiology of invasive meningococcal B disease in Australia, 1999–2015: priority populations for vaccination. Med J Aust. 2017;207:382–7. https://doi.org/10.5694/mja16.01340
23. Sudbury EL, O'Sullivan S, Lister D, Varghese D, Satharasinghe K. Case manifestations and public health response for outbreak of meningococcal W disease, Central Australia, 2017. Emerg Infect Dis. 2020;26:1355–63. https://doi.org/10.3201/eid2607.181941
24. Sharip A, Sorvillo F, Redelings MD, Mascola L, Wise M, Nguyen DM. Population-based analysis of meningococcal disease mortality in the United States: 1990–2002. Pediatr Infect Dis J. 2006;25:191–4. https://doi.org/10.1097/01.inf.0000202065.03366.0c
25. Dyet K, Devoy A, McDowell R, Martin D. New Zealand's epidemic of meningococcal disease described using molecular analysis: implications for vaccine delivery. Vaccine. 2005;23:2228–30. https://doi.org/10.1016/j.vaccine.2005.01.050
26. Australian Institute of Health and Welfare. Indigenous housing: Australian Government; 2019 [cited 2021 May 9].

https://www.aihw.gov.au/reports/australias-welfare/indigenous-housing
27. Australian Institute of Health and Welfare. Profile of First Nations people [cited 2021 Jan 8]. https://www.aihw.gov.au/reports/australias-welfare/profile-of-indigenous-australians
28. Olesch CA, Knight GJ. Invasive meningococcal infection in Western Australia. J Paediatr Child Health. 1999;35:42–8. https://doi.org/10.1046/j.1440-1754.1999.t01-1-00337.x
29. Australian Institute of Health and Welfare. Historical coverage data tables for Aboriginal and Torres Strait Islander children [cited 2023 Sep 25]. https://www.health.gov.au/topics/immunisation/immunisation-data/childhood-immunisation-coverage/historical-coverage-data-tables-for-aboriginal-and-torres-strait-islander-children
30. Taha MK, Achtman M, Alonso JM, Greenwood B, Ramsay M, Fox A, et al. Serogroup W135 meningococcal disease in Hajj pilgrims. Lancet. 2000;356:2159. https://doi.org/10.1016/S0140-6736(00)03502-9
31. Lahra MM, Enriquez RP, George CRR. Australian Meningococcal Surveillance Programme annual report, 2017. Commun Dis Intell. 2018;2019:43.
32. Lucidarme J, Hill DM, Bratcher HB, Gray SJ, du Plessis M, Tsang RS, et al. Genomic resolution of an aggressive, widespread, diverse and expanding meningococcal serogroup B, C and W lineage. J Infect. 2015;71:544–52. https://doi.org/10.1016/j.jinf.2015.07.007
33. Mustapha MM, Marsh JW, Krauland MG, Fernandez JO, de Lemos AP, Dunning Hotopp JC, et al. Genomic epidemiology of hypervirulent serogroup W, ST-11 *Neisseria meningitidis*. EBioMedicine. 2015;2:1447–55. https://doi.org/10.1016/j.ebiom.2015.09.007
34. Honskus M, Krizova P, Okonji Z, Musilek M, Kozakova J. Whole genome analysis of *Neisseria meningitidis* isolates from invasive meningococcal disease collected in the Czech Republic over 28 years (1993–2020). PLoS One. 2023;18:e0282971. https://doi.org/10.1371/journal.pone.0282971
35. Tsang RSW, Ahmad T, Tyler S, Lefebvre B, Deeks SL, Gilca R, et al. Whole genome typing of the recently emerged Canadian serogroup W *Neisseria meningitidis* sequence type 11 clonal complex isolates associated with invasive meningococcal disease. Int J Infect Dis. 2018;69:55–62. https://doi.org/10.1016/j.ijid.2018.01.019
36. Santos DRS, Bianco K, Clementino MBM, Dávila AMR, de Filippis I. Characterisation of *Neisseria meningitidis* cc11/ET-15 variant by whole genome sequencing. Mem Inst Oswaldo Cruz. 2022;117:e220118. https://doi.org/10.1590/0074-02760220118
37. Wang B, Santoreneos R, Giles L, Haji Ali Afzali H, Marshall H. Case fatality rates of invasive meningococcal disease by serogroup and age: a systematic review and meta-analysis. Vaccine. 2019;37:2768–82. https://doi.org/10.1016/j.vaccine.2019.04.020
38. Säll O, Stenmark B, Glimåker M, Jacobsson S, Mölling P, Olcén P, et al. Clinical presentation of invasive disease caused by *Neisseria meningitidis* serogroup Y in Sweden, 1995 to 2012. Epidemiol Infect. 2017;145:2137–43. https://doi.org/10.1017/S0950268817000929
39. Kelly C, Arnold R, Galloway Y, O'Hallahan J. A prospective study of the effectiveness of the New Zealand meningococcal B vaccine. Am J Epidemiol. 2007;166:817–23. https://doi.org/10.1093/aje/kwm147
40. National Meningitis Association. Serogroup B meningococcal disease [cited 2021 May 9]. https://nmaus.org/nma-disease-prevention-information/serogroup-b-meningococcal-disease
41. Djingarey MH, Barry R, Bonkoungou M, Tiendrebeogo S, Sebgo R, Kandolo D, et al. Effectively introducing a new meningococcal A conjugate vaccine in Africa: the Burkina Faso experience. Vaccine. 2012;30(Suppl 2):B40–5. https://doi.org/10.1016/j.vaccine.2011.12.073
42. LaForce FM, Okwo-Bele JM. Eliminating epidemic Group A meningococcal meningitis in Africa through a new vaccine. Health Aff (Millwood). 2011;30:1049–57. https://doi.org/10.1377/hlthaff.2011.0328
43. Diallo AO, Soeters HM, Yameogo I, Sawadogo G, Aké F, Lingani C, et al.; MenAfriNet Consortium. Bacterial meningitis epidemiology and return of *Neisseria meningitidis* serogroup A cases in Burkina Faso in the five years following MenAfriVac mass vaccination campaign. PLoS One. 2017;12:e0187466. https://doi.org/10.1371/journal.pone.0187466
44. Parikh SR, Andrews NJ, Beebeejaun K, Campbell H, Ribeiro S, Ward C, et al. Effectiveness and impact of a reduced infant schedule of 4CMenB vaccine against group B meningococcal disease in England: a national observational cohort study. Lancet. 2016;388:2775–82. https://doi.org/10.1016/S0140-6736(16)31921-3
45. Mak DB, Bulsara MK, Wrate MJ, Carcione D, Chantry M, Efller PV. Factors determining vaccine uptake in Western Australian adolescents. J Paediatr Child Health. 2013;49:895–900. https://doi.org/10.1111/jpc.12030
46. Taha MK, Deghmane AE. Impact of COVID-19 pandemic and the lockdown on invasive meningococcal disease. BMC Res Notes. 2020;13:399. https://doi.org/10.1186/s13104-020-05241-9
47. Brueggemann AB, Jansen van Rensburg MJ, Shaw D, Mc Carthy ND, Jolley KA, Maiden MCJ, et al. Changes in the incidence of invasive disease due to Streptococcus pneumoniae, Haemophilus influenzae, and Neisseria meningitidis during the COVID-19 pandemic in 26 countries and territories in the Invasive Respiratory Infection Surveillance Initiative: a prospective analysis of surveillance data. Lancet Digit Health. 2021;3:e360–70. https://doi.org/10.1016/S2589-7500(21)00077-7

Address for correspondence: Krist Ewe, PathWest Laboratory Medicine, Fiona Stanley Hospital, Level 1, Pathology Bldg, Barry Marshall Parade, Murdoch, WA 6150, Australia; email: yean.ewe@health.wa.gov.au

Ring Vaccination

[rɪŋ-væk-sɪ′-neɪ-ʃn]]

Vijay Sharma, Rajnish Sharma, Balbir B. Singh

Ring vaccination (expanding ring, surveillance and containment) is a public health measure designed to prevent spread of disease from infected persons to others. This approach targets persons who have had close contact with confirmed or suspected cases and are at a higher risk of infection by vaccinating them first.

This strategy has shown remarkable success in combating smallpox caused by respiratory droplet/direct contact–based transmission and shortened incubation for the vaccine. The concept of protecting persons closely exposed to smallpox cases might have its origins in the late 18th century, when the London Small-Pox and Inoculation Hospital was established in 1746. Haygarth (1793) and Carl (1799) suggested systematic variolation of the population and isolation of smallpox cases. In 1877, the Leicester Method, which involved prompt notification, isolation, and quarantine of smallpox cases, was introduced in Leicester (a town in East Midlands, England), and was advocated by local anticompulsory vaccinationists. In 1896, the Royal Commission on Vaccination recommended infant vaccination to control smallpox, although C. Killick Millard, Medical Officer of the Health, appealed for reconsideration. The Leicester method was later supplemented with vaccination or revaccination of contacts in the early 20th century.

After World War II in 1946, despite limited vaccine supplies, Dixon eliminated a smallpox outbreak in the Tripolitania (a former province of Libya) using a method termed expanding ring vaccination. In 1967, Foege and colleagues introduced this concept as surveillance and containment in the smallpox eradication campaign in Nigeria. The strategy proved successful for smallpox because of the disease's relatively slow spread, mostly through face-to-face contact. The term ring vaccination is now universally used for this process.

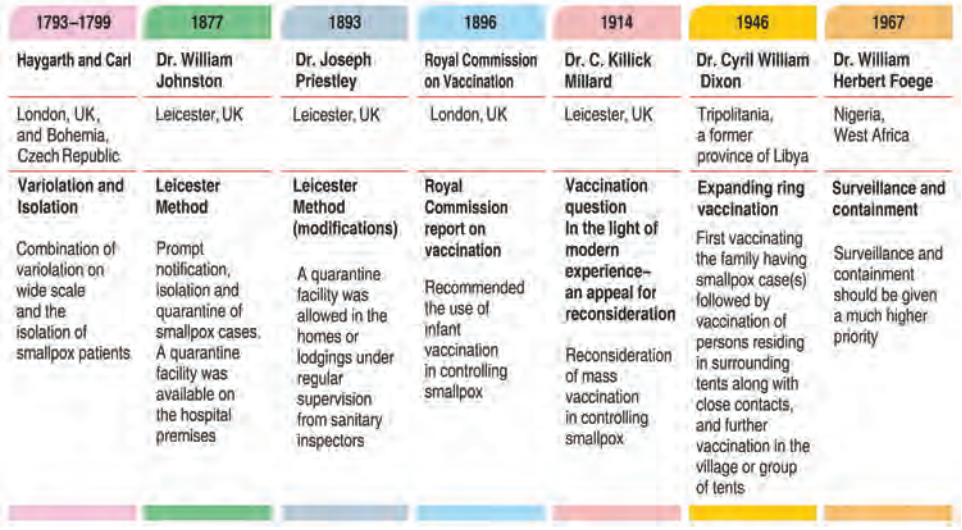

Figure. Historical concepts and persons associated with development of ring vaccination strategy.

Sources

1. Dixon CW. Smallpox in Tripolitania, 1946; an epidemiological and clinical study of 500 cases, including trials of penicillin treatment. J Hyg (Lond). 1948;46:351–77.
2. Fenner F, Henderson DA, Arita I, Jezek Z, Ladnyi ID. Chapter VI: Early efforts at control: variolation, vaccination and isolation and quarantine. In: Fenner F, Henderson DA, Arita I, Jezek Z, Ladnyi ID, editors. Smallpox and its eradication. Geneva: World Health Organization; 1988. p. 245–75.
3. Foege WH, Millar JD, Henderson DA. Smallpox eradication in West and Central Africa. Bull World Health Organ. 1975;52:209–22.
4. Fraser SM. Leicester and smallpox: the Leicester method. Med Hist. 1980;24:315–32. https://doi.org/10.1017/S0025727300040345
5. Millard CK. Chapter XII: Conclusions. In: Millard CK, editor. The vaccination question in the light of modern experience: an appeal for reconsideration. London: H.K. Lewis and Company; 1914. p. 185–92.

Author affiliation: Guru Angad Dev Veterinary and Animal Sciences University, Punjab, India

DOI: https://doi.org/10.3201/eid3002.221909

Address for correspondence: Balbir B. Singh, Centre for One Health, Guru Angad Dev Veterinary and Animal Sciences University, Ludhiana, Punjab 141004, India; email: bbsdhaliwal@gmail.com

Piscichuvirus-Associated Severe Meningoencephalomyelitis in Aquatic Turtles, United States, 2009–2021

Weerapong Laovechprasit, Kelsey T. Young, Brian A. Stacy, Steven B. Tillis, Robert J. Ossiboff, Jordan A. Vann, Kuttichantran Subramaniam, Dalen W. Agnew, Elizabeth W. Howerth, Jian Zhang, Shayna Whitaker, Alicia Walker, Andrew M. Orgill, Lyndsey N. Howell, Donna J. Shaver, Kyle Donnelly, Allen M. Foley, James B. Stanton

Viruses from a new species of piscichuvirus were strongly associated with severe lymphocytic meningoencephalomyelitis in several free-ranging aquatic turtles from 3 coastal US states during 2009–2021. Sequencing identified 2 variants (freshwater turtle neural virus 1 [FTuNV1] and sea turtle neural virus 1 [STuNV1]) of the new piscichuvirus species in 3 turtles of 3 species. In situ hybridization localized viral mRNA to the inflamed region of the central nervous system in all 3 sequenced isolates and in 2 of 3 additional nonsequenced isolates. All 3 sequenced isolates phylogenetically clustered with other vertebrate chuvirids within the genus *Piscichuvirus*. FTuNV1 and STuNV1 shared ≈92% pairwise amino acid identity of the large protein, which narrowly places them within the same novel species. The in situ association of the piscichuviruses in 5 of 6 turtles (representing 3 genera) with lymphocytic meningoencephalomyelitis suggests that piscichuviruses are a likely cause of lymphocytic meningoencephalomyelitis in freshwater and marine turtles.

Wild populations of aquatic turtles are imperiled because of anthropogenic activities (e.g., consumption, collection, fisheries bycatch) (*1*); more than half (186/357) of the recognized species of aquatic turtles in the world are designated as critically endangered, endangered, or vulnerable (*2*). In addition to anthropogenic threats, infectious agents also negatively affect free-ranging turtles. For example, chelonid herpesvirus 5 (*Scutavirus chelonidalpha5*: *Alphaherpesvirinae*) is associated with transmissible fibropapillomatosis in sea turtles around the world (*3*), and epizootic outbreaks of meningoencephalitis in Florida freshwater turtles have been attributed to the recently discovered turtle fraservirus 1 (*Fraservirus testudinis*: *Tosoviridae*) (*4*). However, learning about infectious agents in such turtles is complicated by their aquatic nature and cryptic lifestyles, which prevents full appreciation of the threat posed by viruses to free-ranging turtles.

Recently, numerous viruses in captive and free-ranging nondomesticated animals have been identified. Among the newly discovered viruses, chuvirids (class Monjiviricetes, order Jingchuvirales, family Chuviridae) (*5*) are of particular interest. First, they have a broad host range (e.g., phototrophs, a wide array of invertebrates, and vertebrates [fish and snakes]) (*5*–*10*). Second, the genomic structure of viruses in that family is unusual (*11*,*12*). Although other jingchuvirals have nonsegmented linear genomes, chuvirids have been reported to have circular segmented, circular nonsegmented, linear segmented, and linear nonsegmented genomes (*7*,*12*). Phylogenetic analysis of the large (L) protein suggests that jingchuvirals have a unique history among viruses in the class Monjiviricetes (*6*,*12*). Although recent discover-

Author affiliations: University of Georgia, Athens, Georgia, USA (W. Laovechprasit, K.T. Young, E.W. Howerth, J. Zhang, J.B. Stanton); National Oceanic and Atmospheric Administration, Pascagoula, Mississippi, USA (B.A. Stacy, L.N. Howell); University of Florida, Gainesville, Florida, USA (S.B. Tillis, R.J. Ossiboff, J.A. Vann, K. Subramaniam); Michigan State University, Lansing, Michigan, USA (D.W. Agnew); Amos Rehabilitation Keep at University of Texas Marine Science Institute, Port Aransas, Texas, USA (S. Whitaker, A. Walker, A.M. Orgill); National Park Service at Padre Island National Seashore, Corpus Christi, Texas, USA (D.J. Shaver); Brevard Zoo and Sea Turtle Healing Center, Melbourne, Florida, USA (K. Donnelly); Florida Fish and Wildlife Conservation Commission, Jacksonville, Florida, USA (A.M. Foley)

DOI: https://doi.org/10.3201/eid3002.231142

ies of chuvirids and their varying genomic structures draw interest from a virologic standpoint, the pathogenicity of chuvirids and jingchuvirals has not been confirmed (*12*). To our knowledge, only 1 published study has demonstrated any jingchuviral from an ill animal: a piscichuvirus (Herr Frank virus 1 [HFrV1]; *Chuviridae*: *Piscichuvirus franki*) in clinically ill snakes (3 of 4 boa constrictors [*Boa constrictor constrictor*] with boid inclusion body disease; all 4 boas were positive for reptarenaviruses) (*13*). However, because no piscichuviral in situ studies were performed with those snakes and meningoencephalitis was not reported, clinical significance of chuvirids remains unresolved.

To identify the potential cause of lymphocytic meningoencephalomyelitis in several aquatic turtles, we randomly sequenced central nervous system (CNS) tissues from 3 affected turtles and performed in situ hybridization (ISH) on CNS tissues of 6 turtles. We obtained complete genomes for 3 isolates, providing phylogenetic classification and in silico identification of conserved secondary structures at the genome termini and a hypothetical fourth open reading frame (ORF). The relative dissimilarity between the freshwater and sea turtle piscichuviruses raises questions regarding jingchuviral speciation criteria.

Materials and Methods

Samples and Pathologic Examination

We examined isolates from 6 aquatic turtles with idiopathic CNS inflammation (meningoencephalitis to meningoencephalomyelitis): 1 freshwater (alligator snapping turtle, morphologically consistent with either *Macrochelys temminckii* or *M. apalachicolae*) and 5 marine (1 Kemp's ridley [*Lepidochelys kempii*] and 4 loggerhead [*Caretta caretta*]), by using sequencing (turtles 1–3), ISH (turtles 1–6), or both (Table 1; Figure 1). We used 6 additional retrospective cases as controls: 2 loggerhead turtles with spirorchiid-induced mononuclear meningoencephalitis, 1 Kemp's ridley turtle with bacterial encephalitis, and 3 turtles lacking meningoencephalomyelitis (1 of each species).

All turtles died spontaneously or were euthanized via pentobarbital overdose if their illness was advanced. Gross necropsy included systematic evaluation of all organ systems. We determined sexual maturity by evaluating the reproductive system. We aseptically collected fresh tissue samples, including from the brain and spinal cord (turtles 1–3), and stored them at –80°C. We preserved samples in neutral-buffered 10% formalin fixative for 24–48 hours before processing for histopathologic analysis.

Random Sequencing

We homogenized a section of cerebrum from the alligator snapping turtle (turtle 1) and a section of the brainstem from the loggerhead turtle (turtle 3) in 450 μL 1× phosphate-buffered saline by using a QIAGEN TissueLyser LT (https://www.qiagen.com) at 35 Hz for 2 minutes with a 5-mm sterile stainless-steel bead (QIAGEN). Homogenized samples underwent viral enrichment (*14*,*15*). We extracted RNA by using Trizol LS Reagent (Thermo Fisher Scientific, https://www.thermofisher.com) and prepared the cDNA library as previously described (*16*,*17*), using manufacturer-suggested kits for ligation-based sequencing of amplicons (SQK-LSK110 with EXP-PBC096) and sequencing on a FLO-MIN106 R9.4.1 flow cell in a MinION Mk1B sequencing device (Oxford Nanopore Technologies, https://nanoporetech.com). The postsequencing analysis workflow followed the randomly primed, MinION-based sequencing as previously described (*16*,*17*). We first accomplished screening for potential pathogens by pairwise alignment of reads (BLAST, https://blast.ncbi.nlm.nih.gov/Blast.cgi]) to the National Center for Biotechnology Information (NCBI, https://

Table 1. Biographical information and results summary of 5 turtles positive for FTuNV1 or STuNV1, United States, 2009–2021*

Animal no., common name (taxonomic name)	Sex	SCL, cm	Life stage†	Stranding location‡ Latitude, °N	Stranding location‡ Longitude, °W	Clinical signs	Sequencing	ISH (FTuNV1/STuNV1)
1, Alligator snapping turtle (*Macrochelys* sp.)	M	56.5	M	29.524879	82.300594	Weak and lethargic	FTuNV1	(+/−)
2, Kemp's ridley turtle (*Lepidochelys kempii*)	F	60.3	I	27.67338	97.16880	Persistent circling and asymmetric buoyancy	STuNV1	(–/+)
3, Loggerhead turtle (*Caretta caretta*)	M	94.0	M	30.230591	87.910237	Unresponsive	STuNV1	(ND/+)
4, Loggerhead turtle (*C. caretta*)	F	81.8	M	28.04815	80.57892	Weak	ND	(ND/+)
5, Loggerhead turtle (*C. caretta*)	F	83.7	I	28.20726	80.65725	Head tremor and cervical ventroflexion	ND	(ND/+)

*FTuNV1, freshwater turtle neural virus 1; I, immature; ISH, in situ hybiridization; M, mature; ND, not done; SCL, straight carapace length; STuNV1, sea turtle neural virus 1.
†Life stage estimation was based on the maturation of the reproductive system.
‡Latitude and longitude values correspond to the stranding locations as shown in Figure.1.

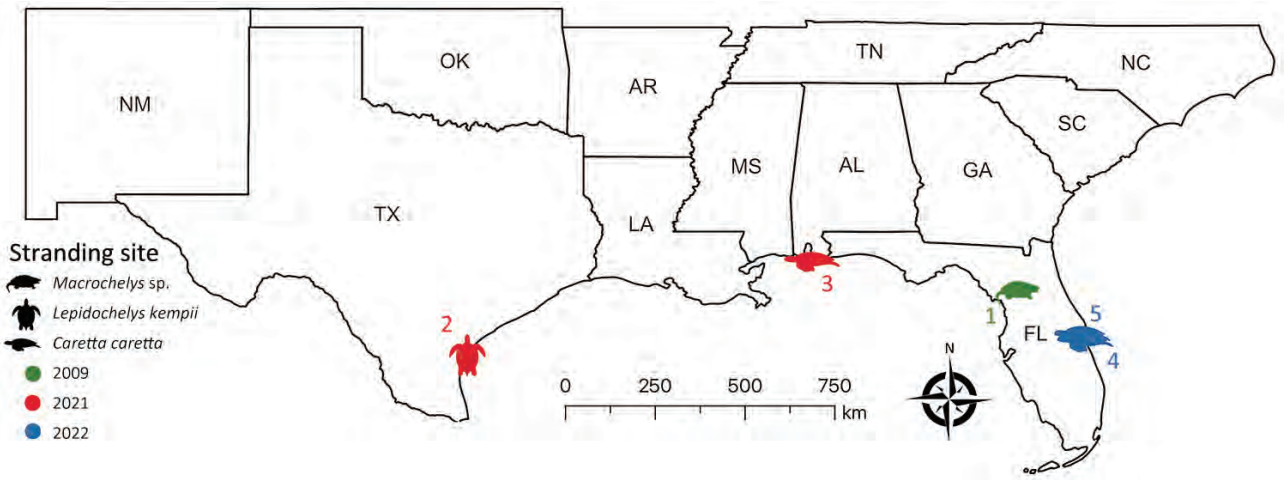

Figure 1. Geographic location and year found for 5 stranded piscichuvirus-infected aquatic turtles with meningoencephalomyelitis, United States, 2009–2021.

www.ncbi.nlm.nih.gov) nonredundant nucleotide database (updated June 4, 2022) through the Georgia Advanced Computing Research Center (https://gacrc.uga.edu) by using default settings. After identifying piscichuvirus-like reads, we used a long-read aligner (Centrifuge version 1.0.4) (*18*) with a custom index to filter out host reads by using the green sea turtle genome (GCF_015237465.1_rCheMyd.pri.v2, accessed July 2021) combined with a publicly available Centrifuge index for bacteria and archaea (https://ccb.jhu.edu/software/centrifuge/manual.shtml). We mapped the remaining reads >50 nt to the closest piscichuviral genome to iteratively assemble the turtle virus genomes in Geneious Prime 2019.1.3 (https://www.geneious.com). We confirmed assembly with de novo assembly by using Flye (*19*).

We extracted RNA from turtle 2 by using an RNeasy Mini kit (QIAGEN) and generated a cDNA library by using a NEBNext Ultra RNA Library Prep Kit (Illumina, https://www.illumina.com), which we sequenced on the iSeq 100 Sequencing System (Illumina). We processed raw data to remove host reads by first running Kraken version 2 (*20*) against a custom database created by using the green sea turtle genome (NCBI assembly GCA_000344595, accessed March 2020). We assembled the remaining paired-end reads (742,979) by using SPAdes version 3.15.3 with default parameters (*21*). We then subjected the assembled contigs to BLASTX searches in OmicsBox version 2.0 (BioBam Bioinformatics, https://www.biobam.com) against the NCBI nonredundant protein database.

Genome Analysis

We annotated the ORFs by using the NCBI ORFfinder (https://www.ncbi.nlm.nih.gov/orffinder) and by manually comparing them with the annotations of other piscichuviruses. We filled the gaps in the consensus sequences by PCR for MinION (turtles 1 and 3) or Sanger (turtle 2) sequencing. To predict RNA secondary structures at genomic termini, we used the Vienna package RNAfold tool (*22*).

ISH

We used ISH to localize turtle piscichuviral mRNA in all 6 turtles with idiopathic meningoencephalomyelitis and 6 control turtles. RNAscope 2.5 HD double z-probes (Advanced Cell Diagnostics, Inc., http://acdbio.com) were designed by using the large protein gene (*L*) gene (of freshwater turtle neural virus 1 [FTuNV1] probe: 1375–2368, sea turtle neural virus 1 [STuNV1] probe: 1535–2585). We used probes targeting testudine rRNA as positive probe controls and the *Bacillus subtilis* dihydrodipicolinate reductase (DapB) gene as negative probe controls (Advanced Cell Diagnostics, Inc.). RNAscope (Advanced Cell Diagnostics, Inc.) ISH was performed by following the manufacturer's protocols and analyzed by light microscopy.

Phylogenetic Analyses

To infer evolutionary relationships, we phylogenetically analyzed the translated *L* ORFs from FTuNV1, 2 isolates of STuNV1, and 56 other complete jingchuvirals in MEGA X (*23*). We performed multiple sequence alignments of each coding sequence separately by using ClustalW (https://www.clustal.org) and MUSCLE (http://www.ebi.ac.uk/Tools/msa/muscle) with default settings. We based selection of the best substitution model of aligned amino acid sequences on the lowest Bayesian information

criterion and Akaike scores and used the best substitution model analysis for maximum-likelihood analysis. We constructed phylogenetic analyses by using the maximum-likelihood method and the Le Gascuel matrix plus observed amino acid frequencies plus 5 discrete gamma categories distribution plus invariant sites substitution model with 500 bootstrap replicates. We used subtree-pruning-regrafting level 3 (MEGA X) for maximum-likelihood tree inference and used all gaps and missing data to construct the phylogenetic tree.

Results

Animal Histories and Pathologies

Six test turtles (turtles 1–6) with histories of persistent neurologic signs (e.g., weakness, lethargy, asymmetric buoyancy, circling, head tremors, cervical ventroflexion, and unresponsiveness) were collected from the southeastern United States; 5 were piscichuvirus-positive (Table 1; Figure 1). The CNSs of all turtles were grossly normal; however, those turtles had moderate to severe, multifocal to diffuse mononuclear meningoencephalomyelitis with severe lymphoplasmacytic cuffs. Most severely affected were the cerebrum, optic tectum, and cerebellum (Figure 2, panels A, C). The associated neuroparenchyma was vacuolated, and some neurons exhibited central chromatolysis (Figure 2, panel C). Subsequent results from ancillary testing (i.e., Ziehl-Neelsen staining [turtles 2–4] or PCR for herpesvirus [turtle 1] [*24*] and turtle fraservirus 1 [turtle 4] [*4*]) were negative. Turtles 1–3 were used for metagenomic sequencing; turtles 1–6, along with 6 control turtles, were used for ISH.

Viral Genomes

FTuNV1/Alligator Snapping Turtle

Through reference-based alignment of all reads that passed quality filtering when BLASTN was used, we detected only a few piscichuviral-like reads, including hits to Wēnlǐng fish chu-like virus (WFClV; *Piscichuvirus wenlingense*, GenBank accession no. MG600011) and HFrV1 (GenBank accession nos. MN567051, MN567057, MN56703). Mapping filtered reads to WFClV in Geneious resulted in 1,491 piscichuviral reads and a draft FTuNV1 genome. After targeted sequencing to close gaps, we obtained a 10,781-nt complete FTuNV1 genome with at least 10 times coverage: (Table 2; isolate FTuNV1/Alligator_snapping_turtle/Florida/ST0994/2009, GenBank accession no, OQ547744).

STuNV1/Kemp's Ridley Turtle

Using BLASTX, we identified 4 de novo contigs with highest similarity to HFrV1 (GenBank accession no. MN567051) and Guǎngdōng red-banded snake chuvirus-like virus (GRSCV; *Piscichuvirus lycodontis*, GenBank accession no. MG600009). After performing targeted sequencing to close gaps, we obtained a 10,839-nt complete genome (GenBank accession no. OQ547745).

STuNV1/Loggerhead Turtle

After initially detecting piscichuvirus-like reads by using Centrifuge (with a custom index [*16*] containing FTuNV1 and STuNV1), we identified piscichuviral reads by mapping to the Kemp's ridley STuNV1 consensus sequence. That process resulted in 258 reads building a 10,839-nt complete genome with at

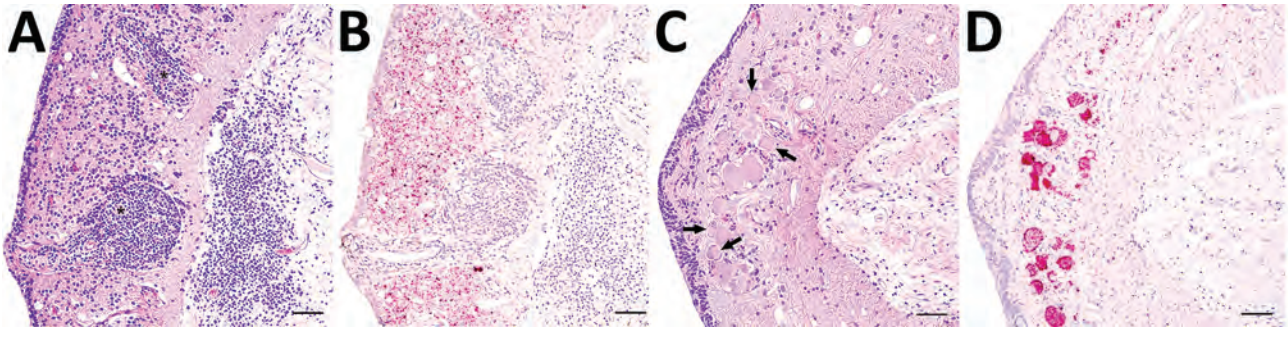

Figure 2. Representative tissue sections from the central nervous system of an alligator snapping turtle (*Macrochelys* sp.) with meningoencephalomyelitis, United States, 2009. A) Cerebellum; lymphoplasmacytic perivascular cuffs (asterisk) and infiltrates are widely disseminated in the gray matter and the adjacent leptomeninges. Hematoxylin and eosin stain. B) Replicate section of the same tissue shown in panel A. There is strong in situ hybridization signal (red) against freshwater turtle neural virus 1 (FTuNV1) in the cytoplasm of small neurons and glial cells throughout the gray matter and associated with the lymphoplasmacytic infiltrates. Hematoxylin counterstain. C) Optic tectum; several neurons have central chromatolysis (arrows). Hematoxylin and eosin stain. D) A replicate section of the tissue shown in panel C. Intense in situ hybridization signal (red) against FTuNV1 was within the neuronal and glial cytoplasm. Scale bars indicate 50 µm.

Table 2. Genome comparison of piscichuviruses from 5 turtles positive for FTuNV1 or StuNV1, United States, 2009–2021, and reference sequences*

Virus	GenBank accession no.	Genome, nt	3′ UTR, nt	ORF4, nt	N, nt	G, nt	L, nt	5′ UTR, nt
FTuNV1	OQ547744	10,781	89	318	1,446	2,052	6,438	91
STuNV1 (Kemp's ridley)	OQ547745	10,839	93	318	1,500	2,052	6,438	91
STuNV1 (Loggerhead)	OQ547746	10,839	93	318	1,500	2,052	6,438	91
GRSCV	MG600009	10,625	>59	276‡	1,482	1,995	6,423	>67
WFClV	MG600011	10,385	>64	225‡	1,344	1,929	6,348	>45
HFrV1	MN567051	10,718	79	255‡	1,509	1,983	6,435	204
HhCV	MW645030–2	10,858	NA	NA	1,566	1,956	6,363	NA
SxASC4	KX884439	11,270	>177	234†	1,794	2,046	6,468	>97
FMCV1	ON125109	10,991	25	396	1,395	2,178	6,615	104

*FMCV1, freshwater macrophyte associate chu-like virus 1; FTuNV1, freshwater turtle neural virus 1; G, glycoprotein; GRSCV, Guǎngdōng red-banded snake chuvirus-like; HFrV1, Herr Frank virus 1; HhCV, hardyhead chuvirus; L, large protein; N, nucleoprotein; NA, data not available; ORF, open reading frame; STuNV1, sea turtle neural virus 1; SxASC4, Sānxiá atyid shrimp virus 4; UTR, untranslated region; WFClV, Wēnlǐng fish chu-like virus.
†Annotations were performed in this study because ORF4 was not originally annotated in the National Center for Biotechnology Information.

least 10 times coverage, except for the first 9 bases of 5′ terminus, which had 6–9 times coverage (GenBank accession no. OQ547746.)

Genome Comparison of Piscichuviruses

The genomic structures of FTuNV1 and STuNV1 were linear, nonsegmented, and had the following ORF orientation: ORF orientation: 3′-ORF4, nucleoprotein (N), glycoprotein (G), large protein (L)-5′. In addition, we identified that the genomic termini were complementary (i.e., inverted terminal repeat sequences), and in silico modeling predicted the formation of a genomic panhandle structure for each virus (Figure 3).

To taxonomically classify FTuNV1 and STuNV1, we used the recent jingchuviral taxonomic classification, which is based on the L protein amino acid identity (*21*). The percentage pairwise amino acid identities <90%, <31%, and <21% support the differentiation of jingchuvirals as novel species, genera, and families, respectively (*12*). We determined that the L protein of the STuNV1 isolates had the same predicted length (2,145 aa; Table 2) and were 99.3% identical (Appendix, https://wwwnc.cdc.gov/EID/article/30/2/23-1142-App1.xlsx); thus, they were considered to be 2 isolates of a single variant. The FTuNV1 and STuNV1 L protein sequences had the same predicted length but were ≈92% identical (Appendix), which is close to the initially proposed speciation cutoff criterion. Thus, all 3 isolates are considered to be within the same new species, but FTuNV1 and STuNV1 are proposed as variants within this species.

We identified a fourth ORF4 in FTuNV1 and STuNV1. The predicted ORF4 amino acid sequence length was the same in all 3 turtle isolates (105 aa; Table 2), and the predicted amino acid sequences were identical for the 2 isolates of STuNV1. Predicted identity between FTuNV1 and STuNV1 was ≈77.36% (Appendix). Of note, we also identified putative, but unannotated, ORF4s in previously NCBI-deposited piscichuviral sequences (Table 2). Among the ORFs, ORF4 is predicted to have the most amino acid variation across piscichuviruses (Appendix). For piscichuviruses that were previously deposited in GenBank, the putative ORF4 was 225–276 nt (74–91 aa) long and 3′ prime of the N ORF (Table 2). In addition, ORF4 lacked evidence of transmembrane domains (https://services.

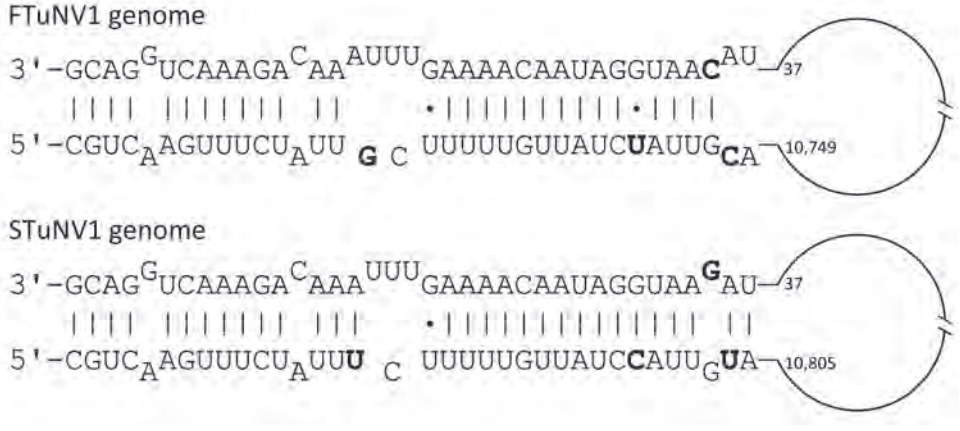

Figure 3. Terminal structure showing panhandle sequences for the 3′ and 5′ termini of FTuNV1 and STuNV1 genomes from piscichuvirus-infected aquatic turtles with meningoencephalomyelitis, United States, 2009–2021. Sequences were predicted by using the Vienna package RNAfold tool on Geneious (https://www.geneious.com). Offset bases indicate mispairing. Boldface bases indicate nucleotide differences between FTuNV1 and STuNV1. Dots indicate G/U pairings. The remaining genome is indicated by the loop structure (not to scale). FTuNV1, freshwater turtle neural virus 1; STuNV1, sea turtle neural virus 1.

healthtech.dtu.dk/TMHMM-2.0), signal sequences (https://services.healthtech.dtu.dk/SignalP-5.0), and N-linked glycosylation sites (https://services.healthtech.dtu.dk/NetNGlyc-1.0).

Phylogeny of Jingchuvirals

Phylogenetic analysis of the predicted L protein amino acid sequences from 59 chuvirids demonstrated that FTuNV1 and both STuNV1 isolates clustered with other piscichuviruses; bootstrap value was 100%. All piscichuviruses detected from reptiles form a single branch with a 92% bootstrap value (Figure 4). Similarly, all piscichuviruses detected from vertebrates form a single branch with a 100% bootstrap value (Figure 4).

Localization of FTuNV1 and STuNV1 Nucleic Acid

To more definitively associate piscichuviral infection with the clinical and histopathologic findings, we conducted RNAscope ISH on all 3 isolates that were positive for piscichuvirus by sequencing (from turtles 1–3), all 3 of which demonstrated viral RNA within inflamed areas of the CNS (Figure 2, panels C, D). ISH testing of 3 additional turtles (turtles 4–6), in which no sequencing was performed indicated that 2 of the 3 were positive. Thus, 5 of 6 cases that were originally considered idiopathic were proposed to be associated with piscichuvirus (Table 1).

ISH demonstrated disseminated, strong, punctate reactivity for piscichuviral RNA in areas of inflammation throughout the CNS. Piscichuviral RNA was detected predominantly in the gray matter (Figure 2, panel B), most notably within the cytoplasm of large neurons (often chromatolytic), small neurons, glial cells, but occasionally in ependymal cells with subtle intensity (Figure 2, panel D). Testing of nonneural tissues of turtles 1 (tested for FTuNV1 nucleic acid) and 2 (tested for STuNV1 nucleic acid) did not demonstrate viral mRNA staining.

None of the control brain tissues demonstrated viral RNA staining. The host control probe reacted appropriately in all tissues that were virus negative by ISH. Neither probe detected the other variants.

Discussion

According to the current criteria of using the L protein amino acid sequence similarity for jingchuviral speciation (*12*), these novel turtle jingchuvirals represent a new species within the genus *Piscichuvirus.* However, the original speciation criteria might need to be revisited to determine if the 2 variants (i.e., FTuNV1 and STuNV1) actually represent 2 different piscichuviral species given their relative dissimilarity (92%) and host differences. For example, although sea turtles are known to forage within tidal areas of rivers (*25*) and freshwater turtles, including alligator snapping turtles, are occasionally documented in estuarine and marine waters (*26*), those ecosystems are relatively nonoverlapping. As additional studies reveal more about the diversity within and between chuvirids, their evolutionary timeline, and their host restrictions, it is foreseeable that these 2 turtle variants might ultimately be divided into at least 2 species (e.g., freshwater [chelydroid] and marine [chelonioid] turtle).

The predicted terminal panhandle structures of the turtle neural virus genomes are similar to those of many other viruses of phylum Negarnaviricota, including bunyavirals, orthomyxovirids, paramyxovirids, and rhabdovirids (*27*–*29*) but have not been reported for jingchuvirals. In orthomyxovirids, those structures serve as promoters for transcription (*30*–*32*), but by creating double-stranded RNA, they also induce the antiviral activity of retinoic acid-inducible gene I. Although the biological effect of this structure remains to be determined, the putative panhandle-forming untranslated regions could be used for the in silico identification of genomic ends in chuvirids discovered in the future through metagenomics and might provide more insight into the development of genomic structure diversity within Chuviridae.

Recent viral zoonoses (e.g., severe acute respiratory syndrome, Ebola virus disease, AIDS) demonstrate that wildlife species can be reservoirs (*33*); thus, it is imperative to fully document the repertoire of viruses in wildlife and their association with disease. Chuvirids are the only jingchuvirals that have been identified in vertebrates, including fish and reptiles (*9*,*13*). However, any associations with the disease have been weak and lacked in situ viral localization (*13*). Our study successfully localized chuvirid mRNA within the areas of inflammation in multiple individuals across 3 turtle species from 2 different ecosystems. Because sequence-based approaches have become a common platform for disease detection and characterization, modifications to Koch's postulates have been proposed to establish the causal association of a novel agent in which Koch's postulates cannot be fulfilled (e.g., infection of novel agents in endangered species and a likely irreversible condition [meningoencephalomyelitis]) (*34*). The 2 turtle piscichuviral variants have met 3 of the 7 proposed criteria: 1) FTuNV1 and STuNV1 nucleic acid sequences were detected in diseased tissues, 2) no nucleic acid sequence was detected in tissues without disease, and 3) infection was confirmed at the cellular level via ISH. Although further research on this disease is required to

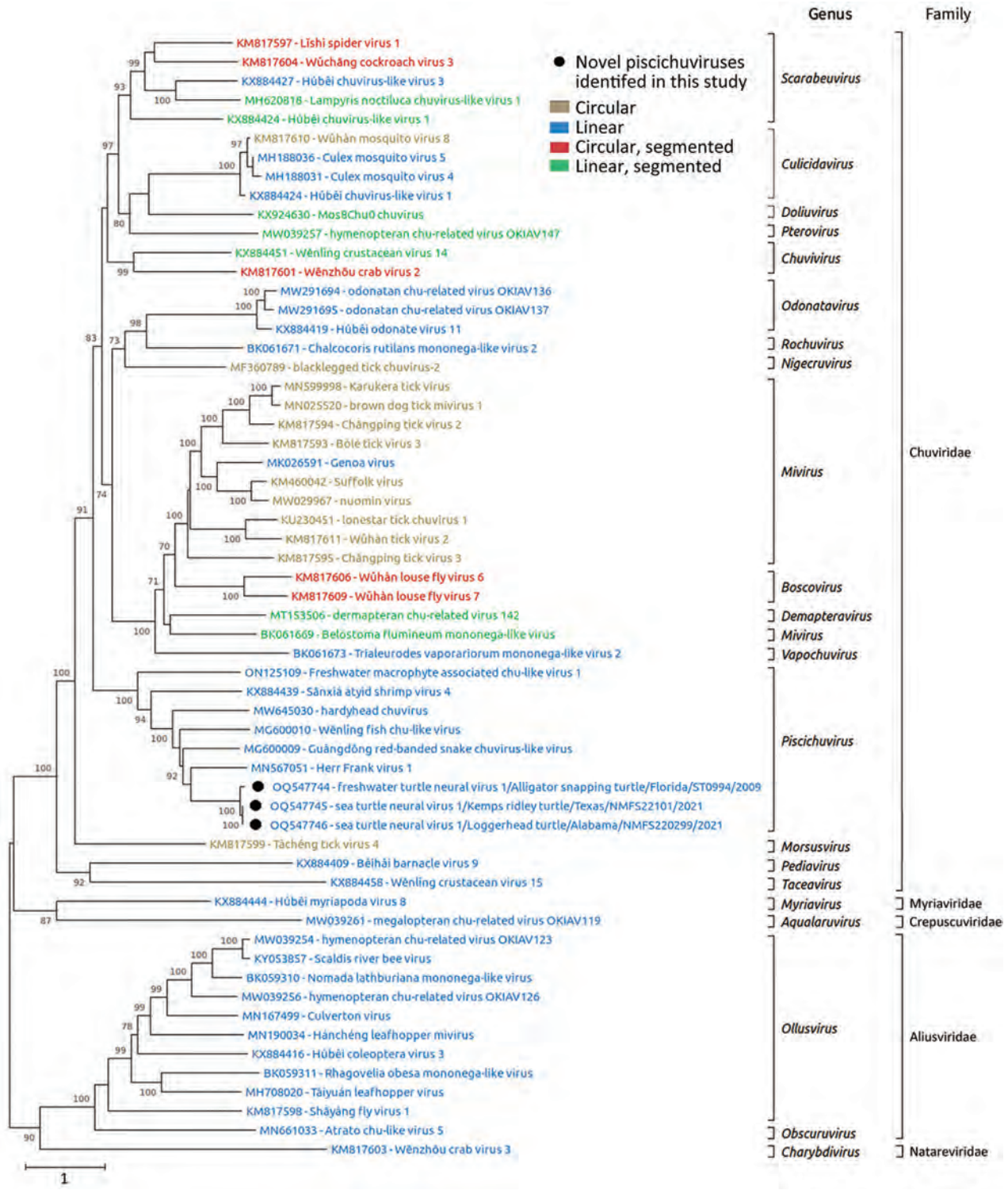

Figure 4. Phylogenetic analysis of jingchuviral large protein (L) amino acid sequences from piscichuvirus-infected aquatic turtles with meningoencephalomyelitis, United States, 2009–2021 (black dots), and reference sequences**.** Complete L amino acid sequences were aligned by using ClustalW (https://www.clustal.org) and refined by using MUSCLE (http://www.ebi.ac.uk/Tools/msa/muscle) with default settings. The phylogenetic analysis was performed on MEGA X (*23*) by using the maximum-likelihood method and Le Gascuel matrix plus observed amino acid frequencies plus 5 discrete gamma categories distribution with parameter of 1.0728 plus invariant sites with 0.65% sites. The substitution model was constructed with 500 bootstrap replicates. The tree is drawn to scale; bootstrap values are measured in the number of substitutions per site. This analysis included 59 aa sequences. Sequences are color coded based on their genomic structure.

verify reproducibility and to identify similar biological properties in other hosts, those findings strongly suggest that FTuNV1 and STuNV1 are a cause of severe mononuclear meningoencephalomyelitis in aquatic turtles in multiple ecosystems throughout the southeastern United States. The identification of closely related chuvirids in other reptiles and fish suggests that chuvirids should be considered as potential emerging viruses in at least fish and reptiles, if not mammals. Further surveillance is needed to better determine the effect of chuvirids on those and other turtles.

All of the turtle species in which a chuvirid was found are considered imperiled. Affected turtles included mature adults, which are especially vital to the stability and recovery of turtle populations (*35*). Of note, all 3 turtles with known body condition scores (turtles 1, 4, and 5) were in good nutritional condition at the time of death, and all infected turtles lacked any predisposing conditions that would increase susceptibility to virus infection. In addition, 2 STuNV1-infected loggerhead turtles (turtles 4 and 5) were stranded ≈1 month apart within the same geographic region. The potential to infect and cause disease in relatively healthy individuals and the identification of multiple diseased turtles from the same areas and time indicate a serious wildlife health concern. In addition, an observation associated with 1 of the cases reported here raises the possibility of human-mediated pathogen pollution. The genus *Macrochelys* is proposed to include either 2 or 3 species (*36*,*37*). The alligator snapping turtle infected by FTuNV1 was morphologically consistent with the more western member(s) of the genus, either *M. temminckii* or *M. apalachicolae*, neither of which should be located where that turtle was found. Thus, the discovery of that turtle outside of its natural range suggests that it may have been transported and released. Future studies are needed to understand the diversity and prevalence of chuvirids among turtles, the pathogenesis of chuvirid infections, and the effects of environment on disease susceptibility.

In summary, we identified 2 variants of a new piscichuviral species in 5 aquatic turtles that died of idiopathic meningoencephalomyelitis. FTuNV1 and STuNV1 most likely cause lymphocytic meningoencephalomyelitis in multiple aquatic turtle species.

Acknowledgments

We thank Paula Baker and staff and volunteers of the Amos Rehabilitation Keep and the University of Florida College of Veterinary Medicine Zoological Medicine Service for their contributions to veterinary care and husbandry; the participants in the Sea Turtle Stranding and Salvage Network for response to and documentation of stranded sea turtles; Paul Moler for his expertise in species identification of the alligator snapping turtle; and Nicole Stacy for the cytologic analysis and interpretation of cerebrospinal fluid.

Raw sequence data are available in the NCBI Sequence Read Archive (PRJNA936591). Complete viral genome sequences are available in GenBank (OQ547744–6).

About the Author

Dr. Laovechprasit is a marine-life veterinarian and PhD candidate in comparative biomedical sciences at the University of Georgia, Athens, GA. His primary research interests focus on metagenomic viral discovery, viral characterization, and pathology in free-ranging aquatic turtles.

Reference

1. Senko JF, Burgher KM, Del Mar Mancha-Cisneros M, Godley BJ, Kinan-Kelly I, Fox T, et al. Global patterns of illegal marine turtle exploitation. Glob Change Biol. 2022;28:6509–23. https://doi.org/10.1111/gcb.16378
2. Rhodin AGJ, Iverson JB, Bour R, Fritz U, Georges A, Shaffer HB, et al.; Turtle Taxonomy Working Group. Turtles of the world: annotated checklist and atlas of taxonomy, synonymy, distribution, and conservation status. In: Rhodin AGJ, Iverson JB, van Dijk PP, Stanford CB, Goode EV, Buhlmann, KA, et al., editors. Conservation Biology of Freshwater Turtles and Tortoises: a Compilation Project of the IUCN/SSC Tortoise and Freshwater Turtle Specialist Group. 9th ed. Chelonian Research Monographs. Rochester (NY): Mercury Print Productions. 2021;8:1–472. https://doi.org/10.3854/crm.8.checklist.atlas.v9.2021
3. Greenblatt RJ, Work TM, Dutton P, Sutton CA, Spraker TR, Casey RN, et al. Geographic variation in marine turtle fibropapillomatosis. J Zoo Wildl Med. 2005;36:527–30. https://doi.org/10.1638/04-051.1
4. Waltzek TB, Stacy BA, Ossiboff RJ, Stacy NI, Fraser WA, Yan A, et al. A novel group of negative-sense RNA viruses associated with epizootics in managed and free-ranging freshwater turtles in Florida, USA. PLoS Pathog. 2022; 18:e1010258. https://doi.org/10.1371/journal.ppat.1010258
5. Harding EF, Russo AG, Yan GJH, Mercer LK, White PA. Revealing the uncharacterised diversity of amphibian and reptile viruses. ISME Commun. 2022;2:95. https://doi.org/10.1038/s43705-022-00180-x
6. Li CX, Shi M, Tian JH, Lin XD, Kang YJ, Chen LJ, et al. Unprecedented genomic diversity of RNA viruses in arthropods reveals the ancestry of negative-sense RNA viruses. eLife. 2015;4:1–26. https://doi.org/10.7554/eLife.05378
7. Han X, Wang H, Wu N, Liu W, Cao M, Wang X. Leafhopper *Psammotettix alienus* hosts chuviruses with different genomic structures. Virus Res. 2020;285:197992. https://doi.org/10.1016/j.virusres.2020.197992
8. Shi M, Lin XD, Tian JH, Chen LJ, Chen X, Li CX, et al. Redefining the invertebrate RNA virosphere. Nature. 2016;540:539–43. https://doi.org/10.1038/nature20167
9. Shi M, Lin XD, Chen X, Tian JH, Chen LJ, Li K, et al. The evolutionary history of vertebrate RNA viruses. Nature. 2018;556:197–202. https://doi.org/10.1038/s41586-018-0012-7

10. Hahn MA, Rosario K, Lucas P, Dheilly NM. Characterization of viruses in a tapeworm: phylogenetic position, vertical transmission, and transmission to the parasitized host. ISME J. 2020;14:1755–67. https://doi.org/10.1038/s41396-020-0642-2
11. Dezordi FZ, Vasconcelos CRDS, Rezende AM, Wallau GL. In and outs of *Chuviridae* endogenous viral elements: origin of a potentially new retrovirus and signature of ancient and ongoing arms race in mosquito genomes. Front Genet. 2020;11:542437. https://doi.org/10.3389/fgene.2020.542437
12. Di Paola N, Dheilly NM, Junglen S, Paraskevopoulou S, Postler TS, Shi M, et al. *Jingchuvirales*: a new taxonomical framework for a rapidly expanding order of unusual monjiviricete viruses broadly distributed among arthropod subphyla. Appl Environ Microbiol. 2022;88:e0195421. https://doi.org/10.1128/aem.01954-21
13. Argenta FF, Hepojoki J, Smura T, Szirovicza L, Hammerschmitt ME, Driemeier D, et al. Identification of reptarenaviruses, hartmaniviruses and a novel chuvirus in captive Brazilian native boa constrictors with boid inclusion body disease. J Virol. 2020;94:1–19. https://doi.org/10.1128/JVI.00001-20
14. Conceição-Neto N, Yinda KC, Van Ranst M, Matthijnssens J. NetoVIR: modular approach to customize sample preparation procedures for viral metagenomics. In: Moya A, Pérez Brocal V, editors. The Human Virome In Molecular Biology. Totowa (NJ): Humana Press Inc.; 2018. p. 85–95. https://doi.org/10.1007/978-1-4939-8682-8_7
15. Vibin J, Chamings A, Collier F, Klaassen M, Nelson TM, Alexandersen S. Metagenomics detection and characterisation of viruses in faecal samples from Australian wild birds. Sci Rep. 2018;8:8686. https://doi.org/10.1038/s41598-018-26851-1
16. Young KT, Stephens JQ, Poulson RL, Stallknecht DE, Dimitrov KM, Butt SL, et al. Putative novel avian paramyxovirus (AMPV) and reidentification of APMV-2 and APMV-6 to the species level based on wild bird surveillance (United States, 2016–2018). Appl Environ Microbiol. 2022;88:e0046622. https://doi.org/10.1128/aem.00466-22
17. Young KT, Lahmers KK, Sellers HS, Stallknecht DE, Poulson RL, Saliki JT, et al. Randomly primed, strand-switching, MinION-based sequencing for the detection and characterization of cultured RNA viruses. J Vet Diagn Invest. 2021;33:202–15. https://doi.org/10.1177/1040638720981019
18. Kim D, Song L, Breitwieser FP, Salzberg SL. Centrifuge: rapid and sensitive classification of metagenomic sequences. Genome Res. 2016;26:1721–9. https://doi.org/10.1101/gr.210641.116
19. Kolmogorov M, Yuan J, Lin Y, Pevzner PA. Assembly of long, error-prone reads using repeat graphs. Nat Biotechnol. 2019;37:540–6. https://doi.org/10.1038/s41587-019-0072-8
20. Wood DE, Lu J, Langmead B. Improved metagenomic analysis with Kraken 2. Genome Biol. 2019;20:257. https://doi.org/10.1186/s13059-019-1891-0
21. Bankevich A, Nurk S, Antipov D, Gurevich AA, Dvorkin M, Kulikov AS, et al. SPAdes: a new genome assembly algorithm and its applications to single-cell sequencing. J Comput Biol. 2012;19:455–77. https://doi.org/10.1089/cmb.2012.0021
22. Hofacker IL. Vienna RNA secondary structure server. Nucleic Acids Res. 2003;31:3429–31. https://doi.org/10.1093/nar/gkg599
23. Kumar S, Stecher G, Li M, Knyaz C, Tamura K. MEGA X: Molecular Evolutionary Genetics Analysis across computing platforms. Mol Biol Evol. 2018;35:1547–9. https://doi.org/10.1093/molbev/msy096
24. VanDevanter DR, Warrener P, Bennett L, Schultz ER, Coulter S, Garber RL, et al. Detection and analysis of diverse herpesviral species by consensus primer PCR. J Clin Microbiol. 1996;34:1666–71. https://doi.org/10.1128/jcm.34.7.1666-1671.1996
25. Byles RA. Behavior and ecology of sea turtles from Chesapeake Bay, Behavior and ecology of sea turtles from Chesapeake Bay, Virginia [dissertation]. Williamsburg (VA): College of William and Mary; 1988. https://doi.org/doi:10.25773/v5-h9nv-c205
26. Jackson GJ, Jr, Ross A. The occurrence of barnacles on the alligator snapping turtle, *Macrochelys temminckii* (Troost). J Herpetol. 1971;5(3–4):188–189. https://doi.org/10.2307/1562744
27. Obijeski JF, McCauley J, Shekei JJ. Nucleotide sequences at the terminal of La Crosse virus RNAs. Nucleic Acids Res. 1980;8:2431–8. https://doi.org/10.1093/nar/8.11.2431
28. Hsu MT, Parvin JD, Gupta S, Krystal M, Palese P. Genomic RNAs of influenza viruses are held in a circular conformation in virions and in infected cells by a terminal panhandle. Proc Natl Acad Sci U S A. 1987;84:8140–4. https://doi.org/10.1073/pnas.84.22.8140
29. Auperin DD, Romanowski V, Galinski M, Bishop DH. Sequencing studies of pichinde arenavirus S RNA indicate a novel coding strategy, an ambisense viral S RNA. J Virol. 1984;52:897–904. https://doi.org/10.1128/jvi.52.3.897-904.1984
30. Fodor E, Pritlove DC, Brownlee GG. The influenza virus panhandle is involved in the initiation of transcription. J Virol. 1994;68:4092–6. https://doi.org/10.1128/jvi.68.6.4092-4096.1994
31. Neumann G, Hobom G. Mutational analysis of influenza virus promoter elements in vivo. J Gen Virol. 1995;76:1709–17. https://doi.org/10.1099/0022-1317-76-7-1709
32. Flick R, Neumann G, Hoffmann E, Neumeier E, Hobom G. Promoter elements in the influenza vRNA terminal structure. RNA. 1996;2:1046–57.
33. Keatts LO, Robards M, Olson SH, Hueffer K, Insley SJ, Joly DO, et al. Implications of zoonoses from hunting and use of wildlife in North American arctic and boreal biomes: pandemic potential, monitoring, and mitigation. Front Public Health. 2021;9:627654. https://doi.org/10.3389/fpubh.2021.627654
34. Fredericks DN, Relman DA. Sequence-based identification of microbial pathogens: a reconsideration of Koch's postulates. Clin Microbiol Rev. 1996;9:18–33. https://doi.org/10.1128/CMR.9.1.18
35. Heppell SS. Application of life-history theory and population model analysis to turtle conservation. Copeia. 1998;1998:367–75. https://doi.org/10.2307/1447430
36. Thomas TM, Granatosky MC, Bourque JR, Krysko KL, Moler PE, Gamble T, et al. Taxonomic assessment of alligator snapping turtles (Chelydridae: *Macrochelys*), with the description of two new species from the southeastern United States. Zootaxa. 2014;3786:141–65. https://doi.org/10.11646/zootaxa.3786.2.4
37. Folt B, Guyer C. Evaluating recent taxonomic changes for alligator snapping turtles (Testudines: Chelydridae). Zootaxa. 2015;3947:447–50. https://doi.org/10.11646/zootaxa.3947.3.11

Address for correspondence: James Stanton, Department of Pathology, College of Veterinary Medicine, University of Georgia, 501 D.W. Brooks Dr, Athens, GA 30605, USA; email: jbs@uga.edu

Multiple Introductions of *Yersinia pestis* during Urban Pneumonic Plague Epidemic, Madagascar, 2017

Voahangy Andrianaivoarimanana,[1] Cyril Savin,[1] Dawn N. Birdsell,[1] Amy J. Vogler, Anne-Sophie Le Guern, Soloandry Rahajandraibe, Sylvie Brémont, Soanandrasana Rahelinirina, Jason W. Sahl, Beza Ramasindrazana, Rado Jean Luc Rakotonanahary, Fanjasoa Rakotomanana, Rindra Randremanana, Viviane Maheriniaina, Vaoary Razafimbia, Aurelia Kwasiborski, Charlotte Balière, Maherisoa Ratsitorahina, Laurence Baril, Paul Keim, Valérie Caro, Voahangy Rasolofo, André Spiegel, Javier Pizarro-Cerda,[2] David M. Wagner,[2] Minoarisoa Rajerison[2]

Pneumonic plague (PP) is characterized by high infection rate, person-to-person transmission, and rapid progression to severe disease. In 2017, a PP epidemic occurred in 2 Madagascar urban areas, Antananarivo and Toamasina. We used epidemiologic data and *Yersinia pestis* genomic characterization to determine the sources of this epidemic. Human plague emerged independently from environmental reservoirs in rural endemic foci ≥20 times during August–November 2017. Confirmed cases from 5 emergences, including 4 PP cases, were documented in urban areas. Epidemiologic and genetic analyses of cases associated with the first emergence event to reach urban areas confirmed that transmission started in August; spread to Antananarivo, Toamasina, and other locations; and persisted in Antananarivo until at least mid-November. Two other *Y. pestis* lineages may have caused persistent PP transmission chains in Antananarivo. Multiple *Y. pestis* lineages were independently introduced to urban areas from several rural foci via travel of infected persons during the epidemic.

Madagascar reports more human plague (causative agent: *Yersinia pestis*) cases annually than any other country (*1*), often several hundred each season (typically September–March) (*2*). *Y. pestis* persists in multiple rural foci in the central and northern highlands of Madagascar (regions >800 m elevation), wherein it cycles primarily among nonnative rat hosts via nonnative and native flea vectors (*3*,*4*). Occurrence and seasonality of human plague is closely tied to rice cultivation in rural areas (*3*,*4*), which increases contact between humans and rats carrying *Y. pestis*–infected fleas. Most human cases in Madagascar are bubonic plague (BP), which originates from a flea bite (*2*). Fleaborne transmission of *Y. pestis* between humans has not been documented in Madagascar, so all BP cases are considered independently acquired from the environment. Pneumonic plague (PP) is not obtained from the environment but results from untreated BP that progresses to secondary PP (SPP), which subsequently can be passed human-to-human as primary PP. Increases in Madagascar in the proportion of BP cases progressing to PP is attributed to the deteriorating healthcare system (*2*). Human-to-human transmission of PP occurs in Madagascar (*4*–*8*) but is less common. Human plague in urban areas of Madagascar is rare because the rodents and fleas in those areas seldom carry *Y. pestis*.

Y. pestis was introduced to Madagascar in 1898, during the third plague pandemic (*9*). Phylogeographic analyses of *Y. pestis* have identified multiple distinct subgroups that occur and persist in specific

Author affiliations: Institut Pasteur de Madagascar, Antananarivo, Madagascar (V. Andrianaivoarimanana, S. Rahelinirina, B. Ramasindrazana, R.J.L. Rakotonanahary, F. Rakotomanana, R. Randremanana, M. Ratsitorahina, L. Baril, V. Rasolofo, A. Spiegel, M. Rajerison); Institut Pasteur, Paris, France (C. Savin, A.-S. Le Guern, S. Brémont, A. Kwasiborski, C. Balière, V. Caro, J. Pizarro-Cerda); Northern Arizona University, Flagstaff, Arizona, USA (D.N. Birdsell, A.J. Vogler, J.W. Sahl, P. Keim, D.M. Wagner); Madagascar Ministry of Public Health, Antananarivo (S. Rahajandraibe, V. Maheriniaina, V. Razafimbia)

DOI: http://doi.org/10.3201/eid3002.230759

[1]These authors contributed equally to this article.

[2]These senior authors contributed equally to this article.

geographic locations in Madagascar; subgroups are occasionally dispersed between rural foci but rarely become established (*10*–*12*). Given this high fidelity between specific *Y. pestis* molecular subgroups and particular geographic locations in Madagascar, assigning isolates to known molecular subgroups can identify *Y. pestis* dispersal events and likely geographic areas where BP cases were acquired from the environment (*10*).

The 2017–18 human plague season in Madagascar was characterized by a typical number of suspected BP and PP human cases reported from rural endemic foci but an atypically large number of suspected cases, primarily PP, reported from Antananarivo, the capital city, and Toamasina, the main seaport, which are the largest urban areas in Madagascar. We noted a dramatic increase in notified PP cases starting in September 2017, continuing until this urban PP epidemic was officially declared over on November 27, 2017 (*13*). The true number of infections associated with this event remains unknown, as well as whether this urban PP epidemic was caused by an extended chain of transmission of a single clone of *Y. pestis* or by multiple independent introduction events from endemic rural foci (*14*). We prepared detailed case histories for the first documented transmission chain (29 cases) from the PP epidemic and used molecular characterization of *Y. pestis* isolates and human sputum samples obtained from urban areas and rural endemic foci in 2017 to determine the sources of this urban PP epidemic.

Methods

Definitions and Investigation

In August–December 2017, plague cases in Madagascar were notified to the plague national surveillance system, which is mandatory; no ethics approval is required to use those public health data. We classified cases as suspect, probable, or confirmed as previously defined (*13*) and as urban if they occurred within cities with population ≥150,000. We considered disease onset as the first day plague symptoms occurred. We conducted an epidemiologic description for the 29 initial human cases. We have anonymized information for all cases.

Sample Analysis

Y. pestis was isolated from human samples and tested for susceptibility to multiple antimicrobial drugs as previously described (Appendix 1 sections 1, 2, https://wwwnc.cdc.gov/EID/article/30/2/23-0759-App1.pdf) (*13*); we generated whole-genome sequences (WGSs) for isolates (Appendix 1 section 3, Table 1). We conducted 2 rounds of targeted capture and enrichment of *Y. pestis* DNA from DNA extracted from sputum samples positive for *Y. pestis* via PCR, and then sequenced the enriched samples (Appendix 1 sections 5,6, Table 2). We inferred a maximum-likelihood phylogeny using single nucleotide polymorphisms (SNPs) identified from 36 WGSs from 2017 isolates and 54 other isolates representative of the overall phylogenetic diversity of *Y. pestis* in Madagascar (*10*) (Appendix 1 section 4, Table 1; Appendix 2, https://wwwnc.cdc.gov/EID/article/30/2/23-0759-App2.xlsx). SNPs identified in the phylogeny as specific to 2017 isolates, or to clades containing 2017 isolates, were queried in sequence data from enriched sputum samples (Appendix 1, section 7, Table 2).

Emergence Events

We determined that multiple 2017 human isolates resulted from the same emergence of *Y. pestis* from environmental reservoirs into humans if they differed by ≤2 SNPs in the phylogeny. We defined an emergence as independent from other emergences if there was no epidemiologic association and if the isolates from that emergence were more closely related to older isolates than to other 2017 emergences or differed from other 2017 emergences by ≥5 SNPs.

Results

Cases, Isolates, and Samples

A total of 2,549 suspected plague cases were notified throughout Madagascar during August–December 2017, including 1,347 from urban areas and 1,241 classified as PP. Confirmed or probable PP cases were reported from Antananarivo during August 28–November 20 and from Toamasina during September 12–October 27, 2017. We obtained and sequenced *Y. pestis* isolates from 36 cases from 2017 (Appendix 1 sections 1, 3, Table 1). We identified SNPs specific to 2017 isolates or to clades containing 2017 isolates in 7 enriched sputum samples (Appendix 1 section 7, Table 5).

Multiple Emergences of Human Plague in Rural Endemic Foci

Starting in Miarinarivo District in August, human plague emerged independently from environmental reservoirs ≥20 times in multiple rural endemic foci in Madagascar during August–November 2017 (Table 1; Appendix 1 section 8). Those events occurred in 19 different communes located in 12 different districts in the central and northern highlands (Table 1; Figure 1). Clinical *Y. pestis* isolates obtained from them

were closely related to previous isolates from those locations (Figure 2), confirming *Y. pestis* continues to persist in the environment in these regions (*10*). PP arose from BP in at least 6 of these events; confirmed human cases originating from 5 events, including 4 PP cases, were documented in urban areas during the epidemic (Table 1).

Initial 29 Cases Associated with the First Urban PP Transmission Chain

Case-patient 1 exhibited PP symptoms (fever, gastrointestinal and respiratory distress, but no cough) on August 25, 2017, in Ankazobe District (Tables 1, 2; Figures 1, 3) where he had been living and working and elected to travel to his permanent home in Toamasina. His employer drove him by car to Antananarivo, where he boarded a shared bush taxi to Toamasina on August 27; case-patient 2 sat beside him; case-patient 3 immediately behind; and case-patient 5, wife of case-patient 3, beside her spouse. That same day near Moramanga, case-patient 1 experienced a deteriorated health status, including respiratory distress, and died; case-patients 2 and 3 cared for him while he was dying. The corpse was removed

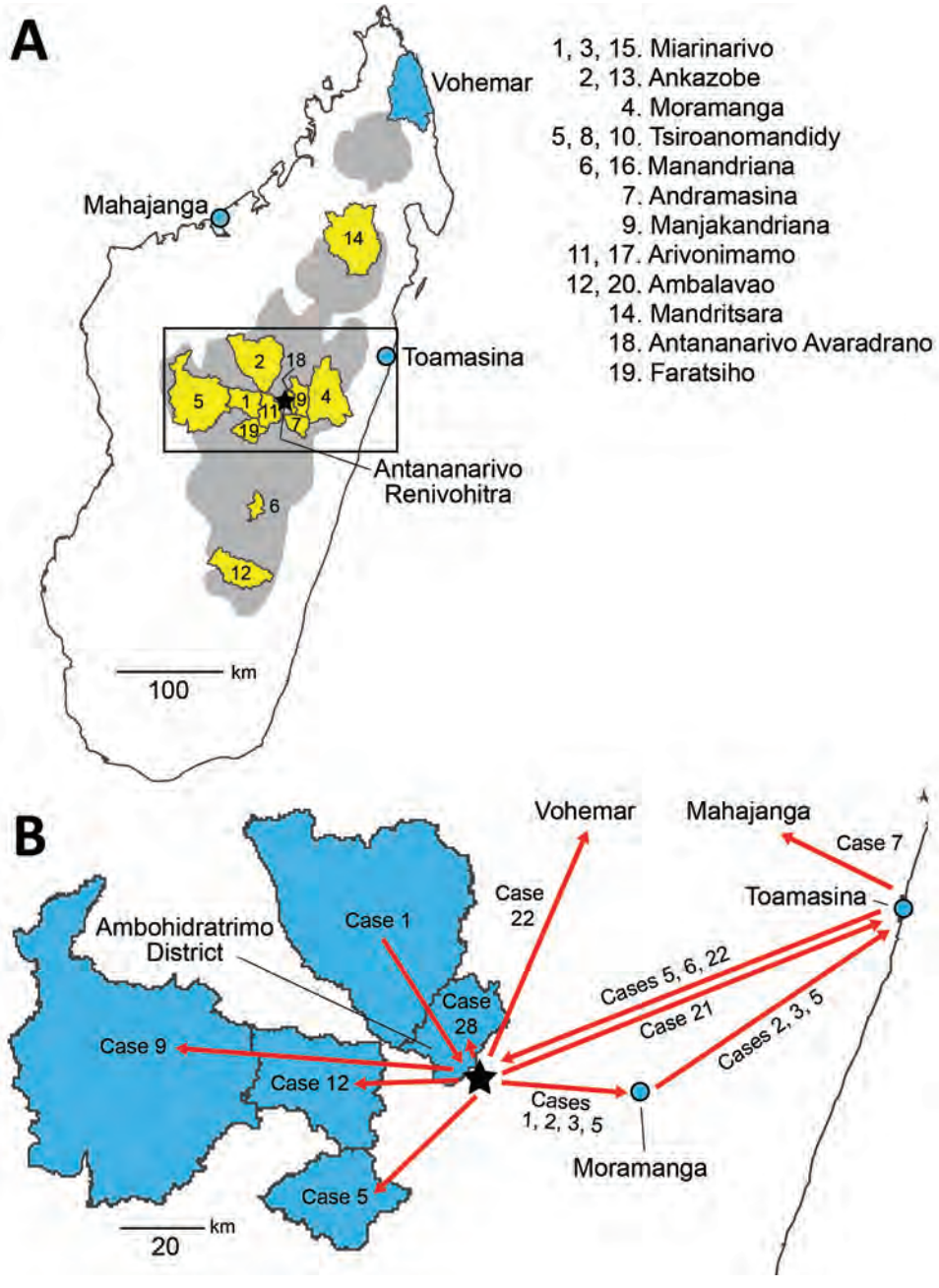

Figure 1. Plague emergence in Madagascar, August–November 2017. A) Locations of emergences. Gray shading indicates plague-endemic regions in the central and northern highlands; yellow shading indicates 12 districts from which human plague emerged from environmental reservoirs 20 times during August–November 2017. Districts are listed in chronological order of emergences. Multiple numbers in the list correspond to different independent emergences from the same district (Table 1); only the first number is indicated on the map. Black box indicates the area shown in panel B. B) Movements (red arrows) of some of the cases (Table 2) associated with the first urban pneumonic plague transmission chain (emergence 2 in Table 1). Blue polygons indicate districts of origin/destination for travel; blue circles indicate the cities of Moramanga and Toamasina.

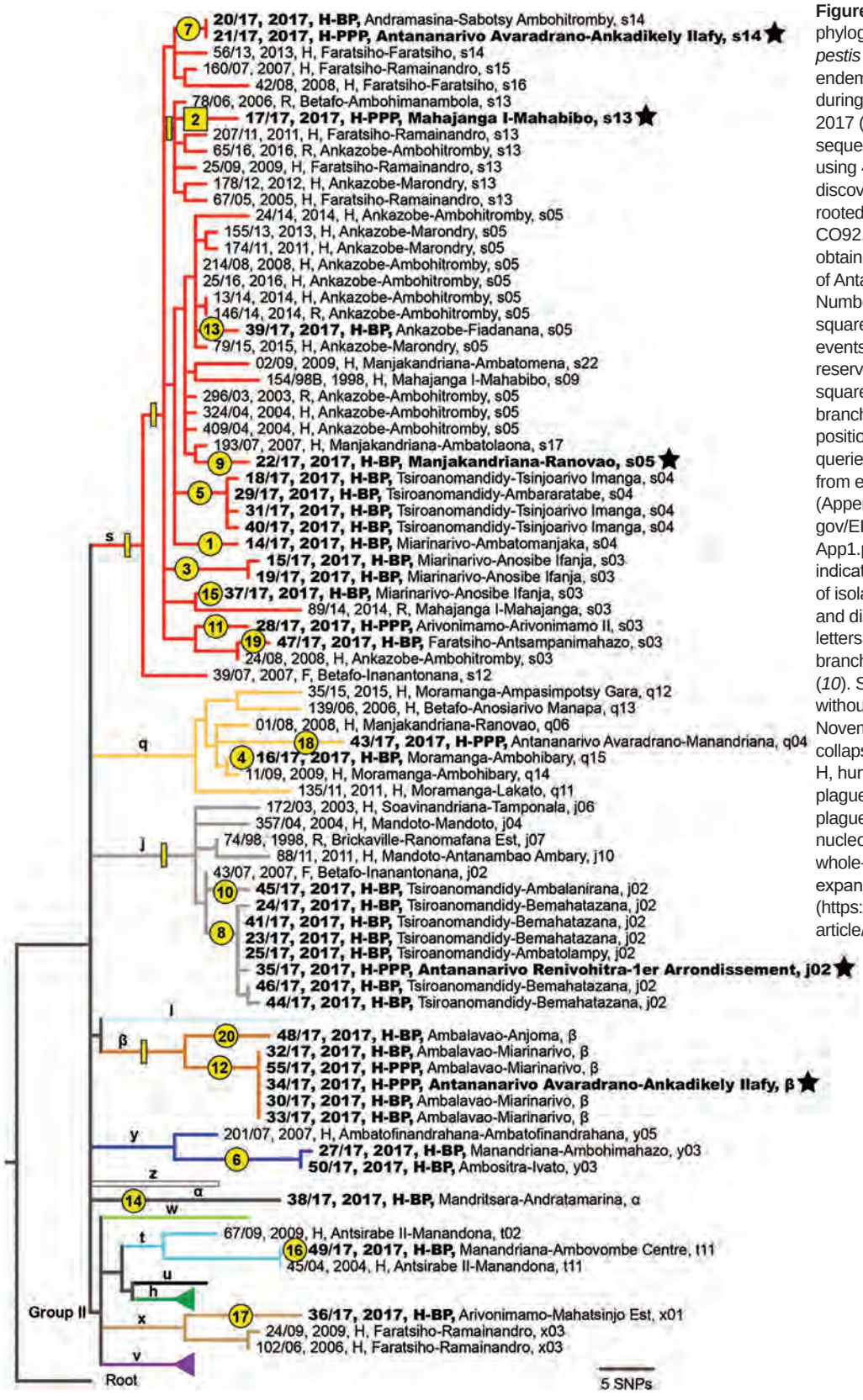

Figure 2. Maximum-likelihood phylogeny of 90 *Yersinia pestis* isolates obtained in rural endemic foci from Madagascar during August–November 2017 (boldface) and reference sequences. Tree was created using 483 core-genome SNPs discovered from WGSs and rooted using North American strain CO92. Stars indicate 5 isolates obtained within the urban areas of Antananarivo or Mahajanga. Numbers in yellow circles and squares indicate 20 emergence events from environmental reservoirs (Table 1); yellow squares and rectangles along branches indicate phylogenetic position of SNPs that were queried in *Y. pestis* sequence data from enriched sputum samples (Appendix 1, https://wwwnc.cdc.gov/EID/article/30/2/23-0759-App1.pdf). Labels for each isolate indicate identification number, year of isolation, host-disease form, and district-commune of isolation; letters on branches and colors of branches indicate known lineages (*10*). Some known lineages without isolates during August–November 2017 are unlabeled or collapsed. BP, bubonic plague; H, human; F, flea; PP, pneumonic plague; PPP, primary pneumonic plague; R, rat; SNP, single-nucleotide polymorphism; WGS, whole-genome sequencing. An expanded figure is available online (https://wwwnc.cdc.gov/EID/article/30/2/23-0759-F2.pdf).

Table 1. Twenty emergence events of *Yersinia pestis* bacteria from environmental reservoirs into humans in rural plague foci, Madagascar, August–November 2017

Event	Major *Y. pestis* group	District/Commune	Earliest recorded onset date	Progression from BP to PP?	Travel	Spread to urban areas (evidence)
1	s	Miarinarivo/Ambatomanjaka	Aug 13	No	No	
2	s	Ankazobe/Marondry	Aug 25	Yes	Yes	Toamasina (sputum 135–2017), Mahajanga (isolate 17/17), Antananarivo (sputum 2093–2017)
3	s	Miarinarivo/Anosibe Ifanja	Aug 26	No	No	
4	q	Moramanga/Ambohibary	Sep 2	No	No	
5	s	Tsiroanomandidy/Tsinjoarivo Imanga	Sep 16	No	No	
6	y	Manandriana/Ambohimahazo	Sep 17	No	No	
7	s	Andramasina/Sabotsy Ambohitromby	Sep 21	Yes	Yes	Antananarivo (isolate 21/17)
8	j	Tsiroanomandidy/Bemahatazana	Sep 26	Yes	Yes	Antananarivo (isolate 35/17, possibly sputum 819–2017)
9	s	Manjakandriana/Ranovao	Oct 2	No	Yes	Antananarivo (isolate 22/17)
10	j	Tsiroanomandidy/Ambalanirana	Oct 3	No	No	Antananarivo (possibly sputum 819–2017)
11	s	Arivonimamo/Arivonimamo II	Oct 5	Yes	No	
12	β	Ambalavao/Miarinarivo	Oct 7	Yes	Yes	Antananarivo (isolate 34/17, sputum 1494–2017)
13	s	Ankazobe/Fiadanana	Oct 8	No	No	
14	α	Mandritsara/Andratamarina	Oct 14	No	No	
15	s	Miarinarivo/Anosibe Ifanja	Oct 17	No	No	
16	t	Manandriana/Ambovombe Centre	Oct 18	No	No	
17	x	Arivonimamo/Mahatsinjo Est	Oct 23	No	No	
18	q	Antananarivo Avaradrano/Manandriana	Oct 30	Yes	Yes	
19	s	Faratsiho/Antsampanimahazo	Nov 7	No	No	
20	β	Ambalavao/Anjoma	Nov 9	No	No	

at the Moramanga health center, and the bush taxi continued to Toamasina.

Case-patient 2 experienced PP symptoms in Toamasina on September 1 and died there September 2. His brother (case-patient 22) transferred the corpse by car from Toamasina to Antananarivo, by plane from Antananarivo to Sambava-Vohemar, and then by car and on foot to their native village at Ambodisakoa, Vohemar District, where case-patient 2 was buried on September 6. Case-patient 22 sought care for PP symptoms on September 6 and was admitted to a hospital at Vohemar, where he recovered. Case-patient 23, brother-in-law of case-patient 2, sought care for PP symptoms at Vohemar on September 15 and was successfully treated. No other cases were reported from Vohemar. Case-patient 20, a friend of case-patient 2 who had direct contact with him during his disease, was admitted to a hospital at Toamasina with PP symptoms on September 12; case-patient 2 might have also had contact with case-patient 22 in Toamasina.

Case-patient 3 was admitted to hospital at Toamasina with PP symptoms on September 2 and died on September 3; a wake was held that night at Toamasina. Case-patients 5 and 7 (sister of case-patient 3, resident of Mahajanga) attended the wake. Case-patient 4, a nurse who cared for case-patient 3, exhibited PP symptoms on September 5 and fully recovered after treatment; no secondary cases were identified from case-patient 4. Case-patient 7 returned to Mahajanga, where she experienced PP symptoms on September 6; she fully recovered after treatment and no additional cases were reported from Mahajanga.

On September 4, case-patients 5 and 6 (another sister of case-patient 3) transferred the corpse of case-patient 3 by car from Toamasina to Antohomadinika-Antananarivo, where another night wake was held from September 4–6, followed by burial in Andramasina on September 6. Case-patients 5, 6, 8, 9, 12, 21, and 28 attended the night wake, funeral, or both; case-patient 5 exhibited PP symptoms on September 6. Case-patient 8 exhibited PP symptoms in Antananarivo on September 9, case-patient 9 in Tsiroanomandidy District on September 5, case-patient 12 in Miarinarivo District on September 11, case-patient 21 in Toamasina on September 12, and case-patient 28 in Ambohidratrimo District on September 17. Case-patients 8, 9, 12, 21, and 28 recovered after treatment, and no secondary cases were reported from them.

Case-patient 5 started travel to Faratsiho on September 9 but died on the way. It is unknown who was traveling with her. Her corpse was transported to Alatsinainy Bandroka, Faratsiho District, and buried

after a traditional funeral. Case-patients 13–19 and 24, all Faratsiho residents, helped prepare the corpse, participated in the funeral, or both; all exhibited PP symptoms starting on September 12 (case-patients 13–19) or 13 (case-patient 24). Case-patients 26 and 27 had documented but unspecified contacts with ≥1 of the

Table 2. Information on 29 case-patients associated with the first known urban pneumonic plague transmission chain, Madagascar, August–November 2017*

Case-patient no.	Age, y/sex	Outcome	Onset date	Onset district	Onset location	Travel	Documented contact with other case-patients	Sample/positive *Y. pestis* result	Case definition
1	32/M	Died	Aug 25	Ankazobe	Rural	Yes	2, 3, 5	None collected	Suspected
2	26/M	Died	Sep 1	Toamasina I	Urban	Yes	1, 3, 5, 20, 22	None collected	Suspected
3	36/M	Died	Sep 2	Toamasina I	Urban	Yes	1, 2, 4, 5, 7	None collected	Suspected
4	23/F	Recovered	Sep 5	Toamasina I	Urban	No	3, 5, 7	Sputum 135–2017/RDT, PCR	Probable
5	16/F	Died	Sep 6	Antananarivo-Renivohitra	Urban	Yes	1, 3, 4, 6, 7, 8, 9, 12, 13, 14, 15, 16, 17, 18, 19, 21, 24, 28	None collected	Suspected
6	47/F	Died	Sep 9	Antananarivo-Renivohitra	Urban	Yes	5, 8, 9, 10, 11, 12, 21, 25, 28, 29	Sputum 118–2017/RDT, PCR	Probable
7	40/F	Recovered	Sep 6	Mahajanga I	Urban	Yes	3, 4, 5	Sputum 121–2017/cultured isolate 17/17	Confirmed
8	45/M	Recovered	Sep 9	Antananarivo-Renivohitra	Urban	No	5, 6, 9, 12, 21, 28	Sputum 150–2017/RDT	Probable
9	30/M	Recovered	Sep 5	Tsiroanomandidy	Rural	Yes	5, 6, 8, 12, 21, 28	Sputum 143–2017/RDT	Probable
10	21/F	Recovered	Sep 11	Antananarivo-Renivohitra	Urban	No	6, 11, 29	Sputum 119–2017/none	Suspect
11	15/M	Recovered	Sep 11	Antananarivo-Renivohitra	Urban	No	6, 10, 29	Sputum 120–2017/none	Suspected
12	37/M	Recovered	Sep 11	Miarinarivo	Rural	Yes	5, 6, 8, 9, 21, 28	Sputum 153–2017/RDT	Probable
13	11/F	Recovered	Sep 12	Faratsiho	Rural	No	5, 14, 15, 16, 17, 18, 19, 24	None collected	Suspected
14	52/M	Recovered	Sep 12	Faratsiho	Rural	No	5, 13, 15, 16, 17, 18, 19, 24	Sputum 124–2017/RDT, PCR	Probable
15	48/F	Recovered	Sep 12	Faratsiho	Rural	No	5, 13, 14, 16, 17, 18, 19, 24	Sputum 125–2017/RDT, PCR	Probable
16	9/F	Recovered	Sep 12	Faratsiho	Rural	No	5, 13, 14, 15, 17, 18, 19, 24	None collected	Suspected
17	39/F	Recovered	Sep 12	Faratsiho	Rural	No	5, 13, 14, 15, 16, 18, 19, 24	None collected	Suspected
18	38/F	Recovered	Sep 12	Faratsiho	Rural	No	5, 13, 14, 15, 16, 17, 19, 24	Sputum 129–2017/RDT	Probable
19	19/M	Recovered	Sep 12	Faratsiho	Rural	No	5, 13, 14, 15, 16, 17, 18, 24	None collected	Suspected
20	25/M	Recovered	Sep 12	Toamasina I	Urban	No	2	Sputum 136–2017/RDT	Probable
21	31/M	Recovered	Sep 12	Toamasina I	Urban	Yes	5, 6, 8, 9, 12, 28	Sputum 149–2017/RDT, PCR	Probable
22	30/M	Recovered	Sep 6	Vohemar	Rural	Yes	2, 23	Sputum 184–2017/RDT	Probable
23	33/M	Recovered	Sep 15	Vohemar	Rural	No	22	Sputum 185–2017/RDT	Probable
24	UNK/F	Recovered	Sep 13	Faratsiho	Rural	No	5, 13, 14, 15, 16, 17, 18, 19	Sputum 131–2017/none	Suspected
25	49/M	Recovered	Sep 14	Antananarivo-Renivohitra	Urban	No	6	Blood 188–2017/RDT	Probable
26	13/M	Recovered	Sep 14	Faratsiho	Rural	No	≥1 of 13, 14, 15, 16, 17, 18, 19, 24	Sputum 133–2017/RDT, PCR	Probable
27	39/M	Recovered	Sep 14	Faratsiho	Rural	No	≥1 of 13, 14, 15, 16, 17, 18, 19, 24	Sputum 134–2017/none	Suspected
28	25/F	Recovered	Sep 17	Ambohidratrimo	Rural	Yes	5, 6, 8, 9, 12, 21	Sputum 164–2017/none	Suspected
29	46/F	Recovered	Sep 10	Antananarivo-Renivohitra	Urban	No	6, 10, 11	Sputum 181–2017/RDT	Probable

*UNK, unknown.

above cases and exhibited PP symptoms on September 14. All case-patients in Faratsiho recovered after treatment.

Case-patient 6 experienced PP symptoms on September 9 in Antananarivo, sought care at a private clinic with a physically altered state on September 11, and was transferred to a military hospital where she died on September 11; this case was the first identified case from the epidemic that triggered the subsequent public health response (*13*). Four secondary cases in Antananarivo resulted from contact with case-patient 6: case-patients 10 and 11 (daughter and son of case patient 6; PP onset September 11), case-patient 29 (daughter-in-law of case-patient 6; PP onset September 19), and case-patient 25. Case-patient 25 (onset September 14), who had septicemic plague, was a health agent and handled and disinfected the corpse of case-patient 6.

Sample 121–2017, collected in Mahajanga from case-patient 7, yielded the only *Y. pestis* isolate obtained from this transmission chain, 17/17, which is most closely related to older isolates from Ankazobe, Faratsiho, and Betafo districts (Figure 2). This result is consistent with Ankazobe District as the geographic source of this transmission chain; case-patient 1 was living and working there but had no recent travel to Faratsiho or Betafo Districts. Enrichment and sequencing of sputum samples obtained from case-patient 4 in Toamasina (135–2017), case-patient 15 in Faratsiho (125–2017), and case-patient 22 in Vohemar (184–2017) (Table 2) revealed the presence in those samples of 1–5 SNPs specific to isolate 17/17 (Appendix 1 section 7, Table 5), documenting that those cases were all part of a single transmission chain that was spread to multiple urban areas and regions in Madagascar. On November 8, sputum sample 2093–2017 was collected from an Antananarivo resident with no recent travel outside the city (Table 1). After we enriched and sequenced this sample, we determined that it contained 3 SNPs specific to isolate 17/17 that were also present in sputum sample 125–2017 from case-patient 15 (Appendix

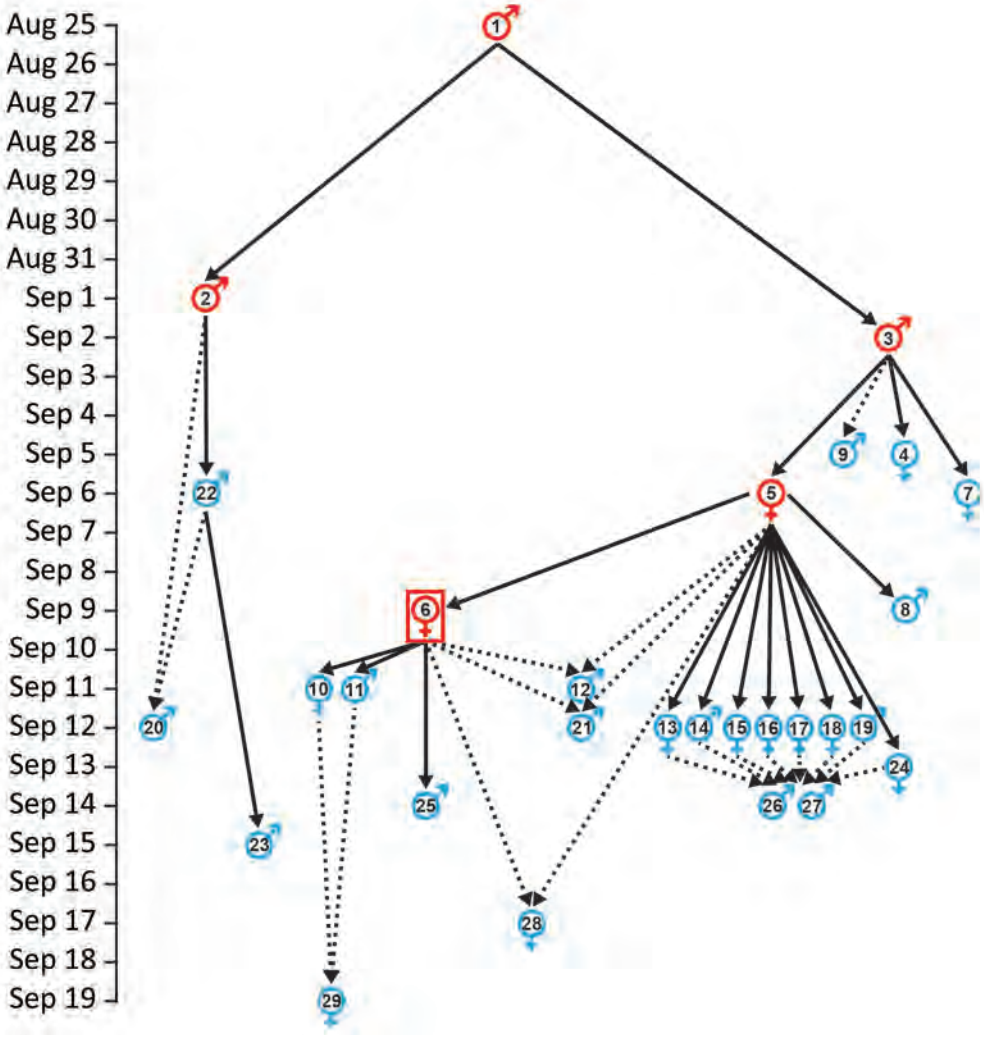

Figure 3. Transmission patterns among the initial 29 cases associated with the first urban PP transmission chain in Madagascar, August–November 2017 (emergence 2 in Table 1). Dates are illness onset dates. Solid arrows indicate likely infection sources based on known contact (Table 2); dotted arrows indicate hypothetical infection sources inferred from genetic data, epidemiologic data, or both. Symbols for individual cases indicate male or female sex; red indicates persons who died and blue indicates survivors. Red box indicates the first identified case from the epidemic that triggered the subsequent public health response.

1 section 7, Table 5), suggesting possible community spread of this transmission chain in Antananarivo and persistence there until at least November 2017.

Introduction of Other *Y. pestis* Lineages to Antananarivo

Isolate 21/17 was obtained from a sputum sample collected on September 29 from an Antananarivo resident. It is distinct from isolate 17/17 but identical to isolate 20/17 (Figure 2), which was obtained from a bubo aspirate collected on September 22 from a resident of a rural area of Andramasina District (Table 1; Appendix 1 section 8). There was no known relationship between those 2 persons, and neither reported travel. The person yielding isolate 20/17 had clinical signs consistent with SPP, including cough for <5 days. Although unknown, this person may have initiated an undocumented PP outbreak in Andramasina District; another person infected from that outbreak may have traveled to Antananarivo, leading to a transmission chain there that infected the person who yielded 21/17.

A foreign tourist sought care at a hospital in Antananarivo on October 1 for PP symptoms; he had traveled outside Antananarivo but the specific details are unknown. His sputum sample yielded isolate 35/17, which is distinct from isolate 17/17 but closely related to multiple human isolates obtained from BP cases in Tsiroanomandidy District starting in September (Table 1; Figure 2). This finding suggests plague activity in this rural focus as the ultimate source of the infection in the tourist, from whom no known secondary cases were reported. However, sequencing of enriched sputum sample 819–2017, collected on October 12 from an Antananarivo resident with no recent travel, contained 1 SNP specific to the j phylogenetic group of *Y. pestis* in Madagascar (Appendix 1 section 7, Table 5), which suggested the possibility of additional undocumented cases associated with this transmission chain in Antananarivo. Emergence 10 was also assigned to phylogenetic group j (Table 1; Figure 2), so it is possible the patient who yielded sputum sample 819–2017 could have been infected through a transmission chain from that event involving undocumented travel to Antananarivo.

Isolate 22/17 (Table 1) was obtained on October 2 from a bubo aspirate collected in Antananarivo from a girl who died the next day. She resided in a rural region of Manjakandriana District; her family brought her to Antananarivo for treatment when she became ill. Upon sequencing, isolate 22/17 was distinct from isolate 17/17 and most closely related to a 2007 human isolate from Manjakandriana District (Figure 2). No secondary cases were reported from this person, which is not unexpected because it was BP.

Isolate 34/17 was reportedly collected from a newborn baby in Antananarivo on October 15; his parents were residents of Antananarivo with no recent travel. The baby was febrile and transferred to a children's hospital as a suspect plague case; staff collected a sputum sample using a bronchoscope. The sputum sample attributed to this newborn yielded isolate 34/17, which is distinct from isolate 17/17 but identical to multiple human isolates obtained from plague activity in a rural region of Ambalavao District (Table 1; Figure 2; Appendix 1 section 8). The earliest documented case there (onset date October 7) yielded isolate 32/17 and was diagnosed as BP, but PP symptoms were also present. Subsequent PP cases were reported from this rural area into late November. No secondary cases were reported from the baby, but SNP data suggest subsequent community spread of closely related *Y. pestis* in Antananarivo.

On October 24, sputum sample 1494–2017 was collected from an Antananarivo resident with no travel history. Enrichment and sequencing of that sample determined it contained an SNP specific to human isolates 30/17, 32/17, 33/17, 34/17, and 55/17 obtained in Ambalavao District as part of the investigation of emergence 12 (Appendix 1 section 8).

Discussion

Our epidemiologic and genomic analyses of 29 human plague cases associated with the first emergence event to reach urban areas of Madagascar document that the transmission chain started in late August 2017 in rural Ankazobe District and subsequently spread to ≥8 other districts by mid-September, including the urban areas of Antananarivo, Toamasina, and Mahajanga, as well as multiple rural districts (Table 2; Figure 1). This transmission chain demonstrates that movements of infected persons can rapidly spread PP across large distances. Prompt public health responses prevented subsequent spread of this transmission chain in Mahajanga and Vohemar, but it apparently persisted into mid-November 2017 in Antananarivo. Although we did not identify genetic data to confirm continued presence of this transmission chain in Toamasina, it is located well outside the plague-endemic region in Madagascar; confirmed and probable PP cases continued to be reported there through mid-October, which suggests possible community spread. Similar to previous reports from Madagascar and elsewhere in Africa (*4*,*6*–*8*,*15*–*17*), this PP transmission chain was associated with traditional funeral practices.

PP transmission requires close contact with an infected person in the end stage of disease (*14*,*18*). On the day he died, case-patient 1 traveled both in a car

with his employer and in a bush taxi. Bush taxis in Madagascar are extremely crowded environments, typically loaded beyond the original capacity of the vehicle and departing only when completely full (*19*). Despite this close contact, only 2 secondary cases, case-patients 2 and 3 (Figure 1), appear to have resulted directly from the presence of case-patient 1 in the bush taxi and none from travel in the car. This result is likely because of his lack of cough; transmission of PP is thought to occur from either inhalation of respiratory droplets expelled by coughing persons or by direct contact (*14*,*18*), and only those 2 secondary cases were known to have had direct contact with case-patient 1 in the bush taxi.

Assessing the true number of plague cases associated with the 2017 urban PP epidemic in Madagascar has been challenging for multiple reasons (*13*,*20*). One reason is that sputum is a poor-quality sample type; isolating *Y. pestis* from sputum is always complicated by commensal flora and sample quality, and the large number of sputum samples collected during this epidemic overwhelmed public health laboratories (*13*). The associated delay in culturing sputum samples, as well as evidence that many patients may have been self-administering antimicrobial drugs effective against *Y. pestis* (*13*,*20*), likely further explains why so few *Y. pestis* isolates were obtained from this epidemic. It is also possible that many of the suspected and probable cases were not true infections (*14*,*21*). Regardless, only 4 isolates were obtained from sputum samples collected from urban areas during this epidemic: 17/17 from Mahajanga and 35/17, 21/17, and 34/17 from Antananarivo. Isolate 22/17 also was collected in Antananarivo from a BP case. All 5 of the isolates obtained in urban areas are highly distinct from each other (Figure 2) and associated with 5 different independent emergence events in rural foci (Table 1). Those patterns document that *Y. pestis* was introduced to Antananarivo ≥5 times during the epidemic, with evidence that 3 of those introductions may have led to subsequent community transmission. The patterns also suggest there may have been more introductions of *Y. pestis* to Antananarivo, Toamasina, or both that could not be documented because there were no isolates.

Movement of infected persons from rural disease-endemic regions to urban areas may have been caused by panic that arose in the Malagasy population in response to the PP epidemic (*1*). The number of notified cases associated with this epidemic increased dramatically in late September and early October 2017 (*13*), coinciding with the timing of the first situation report from the World Health Organization (*22*) and widespread coverage in the media; this increase in cases was probably caused in part from fear and panic in urban inhabitants unfamiliar with plague (*20*). Residents of rural regions are much more aware of plague and perceive it to be rapidly fatal; however, they are less familiar with PP than BP (*23*). The increased public communications regarding the PP epidemic in urban areas, as well as the increased availability there of public health resources from mobilization of substantial domestic and international public health resources (*1*), may have led some infected persons from rural areas to travel to Antananarivo to seek treatment. A previous study (*11*) described evidence of plague-infected persons moving from the central highlands to Mahajanga and from Mahajanga to Antananarivo.

In conclusion, the 2017 urban PP epidemic in Madagascar involved the introduction of multiple independent lineages of *Y. pestis* from several rural foci, which may partly explain why this epidemic was so difficult to control. Because PP spreads person-to-person, control of PP outbreaks and epidemics is focused on identifying cases and their known contacts and providing antimicrobial treatment. Those types of investigations were largely impossible in this instance, given the extent of the epidemic, which likely hampered control efforts. Our results suggest that control efforts also might have been diminished by the presence of multiple independent transmission chains that may have resulted in continuation or expansion of the epidemic. Our findings highlight the importance of using existing genotyping tools (*24*) and developing genomics capabilities in Madagascar, elsewhere in Africa, and other global locations (*25*) so they can be used during outbreaks of plague and other diseases to promptly identify multiple sources and transmission chains to better inform control efforts.

Funding for this work was provided by LabEx Integrative Biology of Emerging Infectious Diseases (grant no. ANR LBX-62 IBEID), the US Department of Defense's Defense Threat Reduction Agency (contract no. HDTRA1-20-C-0007), the Department of International Affairs of the Institut Pasteur via a cooperative agreement with the Office of the Assistant Secretary for Preparedness and Response in the US Department of Health and Human Services (grant no. IDSEP140020-01-00), the Institut Pasteur via the ANR Investissement d'Avenir Program (grant no. 10-LABX-62-IBEID), and the US Agency for International Development (grant no. AID-687-G-13-0003). The World Health Organization assisted with transport of biological samples from healthcare facilities.

About the Author

Dr. Andrianaivoarimanana is a researcher in the Plague Unit at the Institut Pasteur de Madagascar. Her research interests are immune response between *Y. pestis* and its hosts and plague epidemiology.

References

1. Bertherat E. World Health Organization. Plague around the world in 2019. Wkly Epidemiol Rec. 2019;94:289–92.
2. Andrianaivoarimanana V, Piola P, Wagner DM, Rakotomanana F, Maheriniaina V, Andrianalimanana S, et al. Trends of human plague, Madagascar, 1998–2016. Emerg Infect Dis. 2019;25:220–8. https://doi.org/10.3201/eid2502.171974
3. Andrianaivoarimanana V, Kreppel K, Elissa N, Duplantier JM, Carniel E, Rajerison M, et al. Understanding the persistence of plague foci in Madagascar. PLoS Negl Trop Dis. 2013;7:e2382. https://doi.org/10.1371/journal.pntd.0002382
4. Duplantier J-M, Duchemin J-B, Chanteau S, Carniel E. From the recent lessons of the Malagasy foci towards a global understanding of the factors involved in plague reemergence. Vet Res. 2005;36:437–53. https://doi.org/10.1051/vetres:2005007
5. Chanteau S, Ratsitorahina M, Rahalison L, Rasoamanana B, Chan F, Boisier P, et al. Current epidemiology of human plague in Madagascar. Microbes Infect. 2000;2:25–31. https://doi.org/10.1016/S1286-4579(00)00289-6
6. Migliani R, Chanteau S, Rahalison L, Ratsitorahina M, Boutin JP, Ratsifasoamanana L, et al. Epidemiological trends for human plague in Madagascar during the second half of the 20th century: a survey of 20,900 notified cases. Trop Med Int Health. 2006;11:1228–37. https://doi.org/10.1111/j.1365-3156.2006.01677.x
7. Ratsitorahina M, Chanteau S, Rahalison L, Ratsifasoamanana L, Boisier P. Epidemiological and diagnostic aspects of the outbreak of pneumonic plague in Madagascar. Lancet. 2000;355:111–3. https://doi.org/10.1016/S0140-6736(99)05163-6
8. Andrianaivoarimanana V, Wagner DM, Birdsell DN, Nikolay B, Rakotoarimanana F, Randriantseheno LN, et al. Transmission of antimicrobial resistant *Yersinia pestis* during a pneumonic plague outbreak. Clin Infect Dis. 2022;74:695–702. https://doi.org/10.1093/cid/ciab606
9. Morelli G, Song Y, Mazzoni CJ, Eppinger M, Roumagnac P, Wagner DM, et al. *Yersinia pestis* genome sequencing i dentifies patterns of global phylogenetic diversity. Nat Genet. 2010;42:1140–3. https://doi.org/10.1038/ng.705
10. Vogler AJ, Andrianaivoarimanana V, Telfer S, Hall CM, Sahl JW, Hepp CM, et al. Temporal phylogeography of *Yersinia pestis* in Madagascar: insights into the long-term maintenance of plague. PLoS Negl Trop Dis. 2017;11:e0005887. https://doi.org/10.1371/journal.pntd.0005887
11. Vogler AJ, Chan F, Nottingham R, Andersen G, Drees K, Beckstrom-Sternberg SM, et al. A decade of plague in Mahajanga, Madagascar: insights into the global maritime spread of pandemic plague. MBio. 2013;4:e00623–12. https://doi.org/10.1128/mBio.00623-12
12. Vogler AJ, Chan F, Wagner DM, Roumagnac P, Lee J, Nera R, et al. Phylogeography and molecular epidemiology of *Yersinia pestis* in Madagascar. PLoS Negl Trop Dis. 2011;5:e1319. https://doi.org/10.1371/journal.pntd.0001319
13. Randremanana R, Andrianaivoarimanana V, Nikolay B, Ramasindrazana B, Paireau J, Ten Bosch QA, et al. Epidemiological characteristics of an urban plague epidemic in Madagascar, August–November, 2017: an outbreak report. Lancet Infect Dis. 2019;19:537–45. https://doi.org/10.1016/S1473-3099(18)30730-8
14. Mead P. Epidemics of plague past, present, and future. Lancet Infect Dis. 2019;19:459–60. https://doi.org/10.1016/S1473-3099(18)30794-1
15. Apangu T, Acayo S, Atiku LA, Apio H, Candini G, Okoth F, et al. Intervention to stop transmission of imported pneumonic plague—Uganda, 2019. MMWR Morb Mortal Wkly Rep. 2020;69:241–4. https://doi.org/10.15585/mmwr.mm6909a5
16. Begier EM, Asiki G, Anywaine Z, Yockey B, Schriefer ME, Aleti P, et al. Pneumonic plague cluster, Uganda, 2004. Emerg Infect Dis. 2006;12:460–7. https://doi.org/10.3201/eid1203.051051
17. Jullien S, de Silva NL, Garner P. Plague transmission from corpses and carcasses. Emerg Infect Dis. 2021;27:2033–41. https://doi.org/10.3201/eid2708.200136
18. Kool JL, Weinstein RA. Risk of person-to-person transmission of pneumonic plague. Clin Infect Dis. 2005;40:1166–72. https://doi.org/10.1086/428617
19. Wulf V, Misaki K, Randall D, Rohde M. Travelling by taxi brousse in Madagascar. An investigation into practices of overland transportation. Media in Action Interdisciplinary Journal on Cooperative Media. 2018;1:57–97.
20. Salam AP, Raberahona M, Andriantsalama P, Read L, Andrianarintsiferantsoa F, Razafinambinintsoa T, et al. Factors influencing atypical clinical presentations during the 2017 Madagascar pneumonic plague outbreak: a prospective cohort study. Am J Trop Med Hyg. 2020;102:1309–15. https://doi.org/10.4269/ajtmh.19-0576
21. Ten Bosch Q, Andrianaivoarimanana V, Ramasindrazana B, Mikaty G, Rakotonanahary RJL, Nikolay B, et al. Analytical framework to evaluate and optimize the use of imperfect diagnostics to inform outbreak response: application to the 2017 plague epidemic in Madagascar. PLoS Biol. 2022;20:e3001736. https://doi.org/10.1371/journal.pbio.3001736
22. World Health Organization. Plague outbreak Madagascar: external situation report 01. 2017 [cited 2023 May 20]. https://iris.who.int/bitstream/handle/10665/259181/Ext-PlagueMadagascar4102017.pdf
23. Rakotosamimanana S, Rakotoarimanana FJ, Raharimanga V, Taglioni F, Ramamonjisoa J, Randremanana RV, et al. Influence of sociospatial determinants on knowledge, attitudes and practices related to the plague in a population living in endemic areas in the central highlands, Madagascar. BMC Public Health. 2021;21:1102. https://doi.org/10.1186/s12889-021-11101-3
24. Mitchell CL, Andrianaivoarimanana V, Colman RE, Busch J, Hornstra-O'Neill H, Keim PS, et al. Low cost, low tech SNP genotyping tools for resource-limited areas: plague in Madagascar as a model. PLoS Negl Trop Dis. 2017;11:e0006077. https://doi.org/10.1371/journal.pntd.0006077
25. Inzaule SC, Tessema SK, Kebede Y, Ogwell Ouma AE, Nkengasong JN. Genomic-informed pathogen surveillance in Africa: opportunities and challenges. Lancet Infect Dis. 2021;21:e281–9. https://doi.org/10.1016/S1473-3099(20)30939-7

Address for correspondence: Minoarisoa Rajerison, Plague Unit, Institut Pasteur de Madagascar, BP 1274 Ambatofotsikely, Antananarivo 101, Madagascar; email: mino@pasteur.mg

Evolution and Spread of Highly Pathogenic Avian Influenza A(H5N1) Clade 2.3.4.4b Virus in Wild Birds, South Korea, 2022–2023

Ye-Ram Seo,[1] Andrew Y. Cho,[1] Young-Jae Si,[1] Song-I Lee, Dong-Ju Kim, Hyesung Jeong, Jung-Hoon Kwon, Chang-Seon Song, Dong-Hun Lee

During October 2022–March 2023, highly pathogenic avian influenza (HPAI) A(H5N1) clade 2.3.4.4b virus caused outbreaks in South Korea, including 174 cases in wild birds. To understand the origin and role of wild birds in the evolution and spread of HPAI viruses, we sequenced 113 HPAI isolates from wild birds and performed phylogenetic analysis. We identified 16 different genotypes, indicating extensive genetic reassortment with viruses in wild birds. Phylodynamic analysis showed that the viruses were most likely introduced to the southern Gyeonggi-do/northern Chungcheongnam-do area through whooper swans (*Cygnus cygnus*) and spread southward. Cross-species transmission occurred between various wild bird species, including waterfowl and raptors, resulting in the persistence of HPAI in wild bird populations and further geographic spread as these birds migrated throughout South Korea. Enhanced genomic surveillance was an integral part of the HPAI outbreak response, aiding in timely understanding of the origin, evolution, and spread of the virus.

Since the first detection highly pathogenic avian influenza (HPAI) virus A/goose/Guangdong/1/1996 (Gs/Gd) in China in 1996, the Gs/Gd lineage of HPAI H5Nx virus has spread globally, infecting various species and posing a threat to animal and human health (*1*). Outbreaks caused by 1 Gs/Gd strain, clade 2.3.4.4, have occurred worldwide, and the clade has further evolved into 8 subclades (2.3.4.4a–2.3.4.4h) (*2*). Since 2013, ancestral HPAI H5 viruses of clade 2.3.4.4, in combination with different neuraminidase subtypes (e.g., H5N1, H5N6, and H5N8), have been circulating in Southeast Asia. Clade 2.3.4.4b H5N8 viruses were first detected in China in late 2013 and in South Korea in early 2014 (*3*). H5N8 viruses were detected in wild birds in Qinghai Lake, China, and Lake Uvs-Nuur, Russia, in May 2016 (*4*), and were then disseminated to Europe by wild birds (*5*). In 2020, a new variant of the clade 2.3.4.4b H5N1 virus emerged in Europe and spread predominantly through wild birds to various regions including Europe, Asia, and Africa (*6*–*8*). In late 2021, that 2.3.4.4b H5N1 virus spread to North America and subsequently to South America in 2022 (*9*). As of September 2023, H5N1 clade 2.3.4.4b virus is widespread in all regions except Antarctica and Oceania, causing infections and deaths in various wild birds and mammals (*10*) and posing major threats to public health and wildlife conservation.

In South Korea, 10 outbreaks of Gs/Gd-lineage H5Nx HPAI viruses have been recorded to date: clade 2.5 H5N1 outbreak during 2003–2004, clade 2.2 H5N1 during 2006–2007, clade 2.3.2 H5N1 in 2008, clade 2.3.2.1 H5N1 during 2010–2011, clade 2.3.4.4c H5N8 during 2014–2016, clade 2.3.4.4e H5N6 and clade 2.3.4.4c H5N8 during 2016–2017, clade 2.3.4.4b H5N6 during 2017–2018, clade 2.3.4.4b H5N8 during 2020–2021, clade 2.3.4.4b

Author affiliations: Konkuk University, Seoul, South Korea (Y.-R. Seo, A.Y. Cho, C.-S. Song, D.-H. Lee); National Institute of Wildlife Disease Control and Prevention, Gwangju, South Korea (Y.-J. Si, S.-I Lee, D.-J. Kim, Hyesung Jeong); Kyungpook National University College of Veterinary Medicine, Daegu, South Korea (J.-H. Kwon)

DOI: https://doi.org/10.3201/eid3002.231274

[1]These first authors contributed equally to this article.

H5N1 during 2021–2022, and clade 2.3.4.4b H5N1 during 2022–2023 (*11*–*15*). Of those, the most recent H5N1 2.3.4.4b HPAI virus was first detected in a wild Mandarin duck in October 2022, and multiple outbreaks occurred in wild birds and poultry before their absence of detection after March 2023. During October 2022–March 2023, a total of 75 cases of HPAI infection in poultry farms and 174 cases of HPAI infection in wild birds were reported (*16*). The higher number of HPAI viruses detected in wild birds than in poultry probably reflected the higher level of virus circulation in wild birds, highlighting the need for further investigating the process underlying virus emergence and spread in wild birds. Therefore, we sequenced and analyzed 113 H5N1 HPAI virus isolates, which were collected by the Korean National Institute of Wildlife Disease Control and Prevention (NIWDC) under the national wild bird surveillance program in South Korea during 2022–2023, to identify the origin and reconstruct the evolutionary and transmission dynamics of H5N1 HPAI viruses in South Korea.

Materials and Methods

Samples and Spatial Distribution

The national wild bird surveillance program in South Korea has reported 174 HPAI H5N1 viruses during 2022–2023. We isolated HPAI H5N1 viruses from wild bird habitats and major streams during September 2022–February 2023 in South Korea during the Avian Influenza National Surveillance for the Protection and Management of Wildlife Animals and Plants, conducted by the Ministry of Environment. For active surveillance, we collected oropharyngeal, or cloacal swabs from captured wild birds and fecal samples from wild bird habitats. We tested carcasses of wild birds submitted voluntarily to NIWDC for HPAI. We transported, checked, and inoculated all samples in the allantoic cavities of 9–11-day-old specific-pathogen–free embryonated eggs at 37°C for 96 hours. We performed avian host identification for avian influenza–positive fecal samples by using DNA barcoding as previously described (*17*). For this study, we selected 113 HPAI H5N1 isolates for phylogenetic and phylodynamic analyses on the basis of their geographic locations and collection dates (Appendix Table 1, https://wwwnc.cdc.gov/EID/article/30/2/23-1274-App1.pdf). We analyzed spatial distribution of 113 HPAI H5N1 isolates by using the kernel model in ArcGIS software (ESRI, https://www.esri.com) to identify areas with a high density (Appendix Table 1).

Genome Sequencing and Phylogenetic Analysis

We conducted next-generation sequencing (NGS) as previously described (*18*), and we deposited consensus genome sequences into the GISAID database (isolate nos. EPI_ISL 1824572–1824583 and EPI_ISL 18242686). To determine the genotypes, we constructed the maximum-likelihood phylogeny of each gene segment. We performed Bayesian phylodynamic analysis of geographic location and wild bird species. First, to investigate virus transmission between geographic locations, we defined geographic regions as 10 discrete nominal categories: Russia, Japan, China, and 7 locations in South Korea—Gyeonggi-do (GG), Gangwon-do (GW), Chungcheongbuk-do (CB), Chungcheongnam-do (CN), Gyeongsangbuk-do (GB), Gyeongsangnam-do (GN), and Jeolla-do (JL). Second, to infer the transmission dynamics between host species, host species were divided into 8 discrete nominal categories as follows: bean goose, crane, egret and heron, gull and crow, raptor, swan, white-fronted goose, and wild duck (Appendix).

Results

Overview of 2022–23 HPAI H5N1 Viruses from Wild Birds in South Korea

In South Korea, the 2022–23 H5N1 HPAI outbreak started with virus detection in a wild Mandarin duck in October 2022 and lasted in wild birds until March 2023 (Figure 1). A total of 174 cases of infections in wild birds were reported in 132 carcasses, 31 fecal droppings, and 11 captured wild birds. The HPAI H5N1 virus was detected in 22 wild bird species, including 16 eastern spot-billed ducks (*Anas zonorhyncha*), 28 hooded cranes (*Grus monacha*), 44 greater white-fronted geese (*Anser albifrons*), 11 whooper swans (*Cygnus cygnus*), 10 Eastern great egrets (*Ardea modesta*), and 5 unspecified bird species.

Two major waves of outbreaks occurred, a peak in the third week of December, and the second highest number of outbreaks in the first week of January. The first wave of outbreaks mainly affected the GG and JL regions and involved species such as wild duck and crane. The second wave of outbreaks mainly affected the GW region and involved white-fronted goose species (Figure 1).

We examined the spatial distribution of all HPAI outbreaks that occurred during 2022–2023 by using the kernel density estimation method. The results showed a clear geographic distribution of high-density areas around inland water bodies. We observed the peak distribution of kernel density values in GW and the highest concentration of

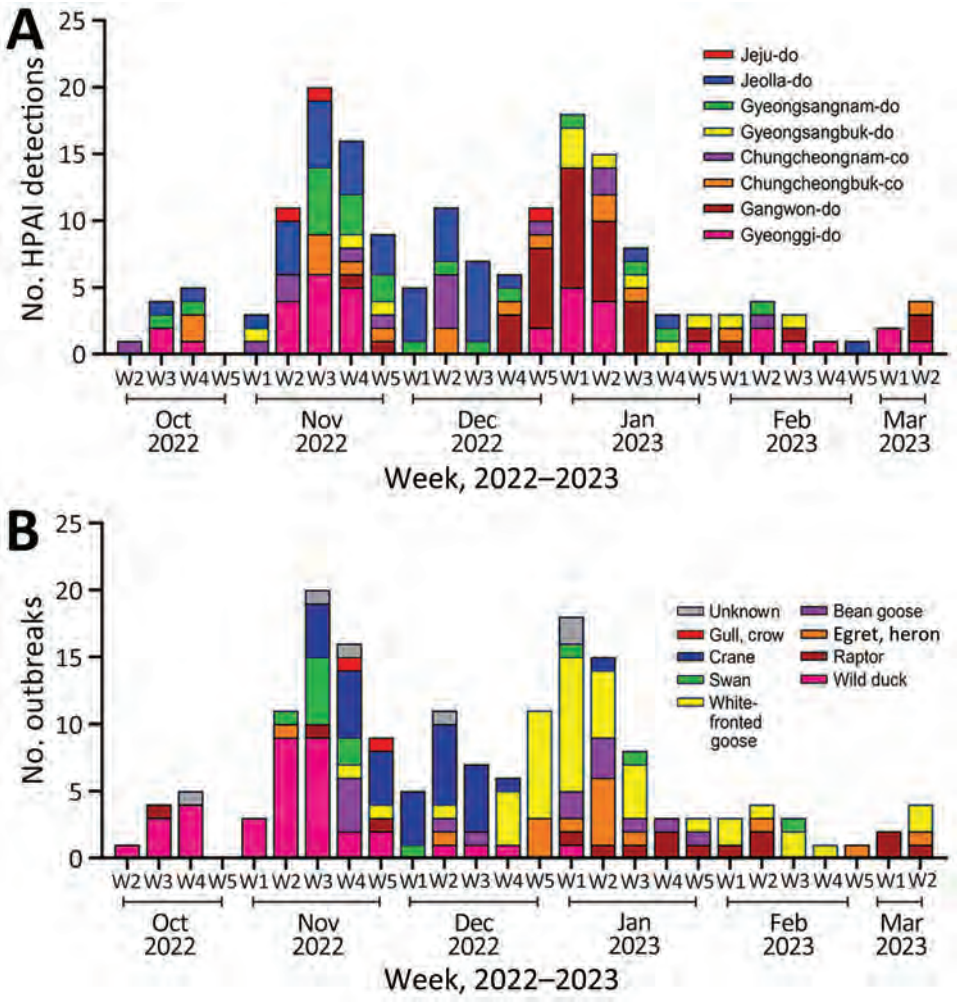

Figure 1. HPAI A(H5N1) clade 2.3.4.4b viruses and outbreaks, South Korea, October 2022–March 2023. A) Number of HPAI viruses detected in wild birds, by week, month, and geographic region. Geographic regions were determined according to a discrete trait analysis conducted for the study. B) Number of HPAI outbreaks, by week, month, and host species category. HPAI, highly pathogenic avian influenza.

cases in JL (Figure 2). Southern GG, northern CN, and northern CB, which are adjacent provinces that share inland water bodies, form a single high-density area.

Origin of H5N1 HPAI Viruses

The phylogenetic analysis of the hemagglutinin (HA) gene showed that all HPAI viruses sequenced in this study belonged to the 2.3.4.4b HPAI lineage. All of them carried a multi-basic amino acid motif at the HA cleavage site: PLREKRRKR/GLF (n = 106), PLRERRRKR/GLF (n = 2), PLRENRRKR/GLF (n = 2), PLREERRKRR/GLF (n = 1), PLREKRRRR/GLF (n = 1), and PLREKGRKR/GLF (n = 1). We hypothesized that the origin of clade 2.3.4.4b H5N1 viruses that caused outbreaks during 2022–23 was because of the reemergence of 2021–22 HPAI H5N1 viruses that persisted in wild bird populations in South Korea throughout the summer of 2022 or the introduction of the novel clade 2.3.4.4b H5N1 HPAI virus from outside South Korea. Our phylogenetic analysis results suggested that the latter assumption was the most likely one because the source-sink dynamics support that HPAI H5N1 virus was newly introduced into South Korea from Russia during the fall of 2022 (Figure 3; Appendix Table 2). The molecular dating analysis of the HA gene estimated the time to the most recent common ancestor of HPAI H5N1 viruses in South Korea to be July 14, 2022 (95% Bayesian credible interval [BCrI] May 11–September 5, 2022). The A/Em/Korea/22WF118–15P/2022 (H5N1) virus, which was detected on November 1, 2022, was not clustered with other H5N1 viruses identified in South Korea, suggesting a point-source introduction. The most closely related virus was A/Jiangsu/NJ210/2023 (H5N1), which infected humans in February 2023 in the Jiangsu region of China (Appendix Figure 1) (*19*).

Genotypes

The maximum-likelihood phylogenetic analysis of the 8 gene segments helped identify the genotypes

of H5N1 viruses. We identified 16 unique genotypes, which were most likely produced by multiple reassortment events with low pathogenic avian influenza viruses in wild birds. We assigned each genotype an alphabet letter based on the Kor22–23 nomenclature, which indicated the region of origin (Kor) and year of origin (2022–2023). The 16 genotypes were as follows: Kor22–23A (n = 4), Kor22–23B (n = 2), Kor22–23C (n = 18), Kor22–23D (n = 65), Kor22–23E (n = 6), Kor22–23F (n = 1), Kor22–23G (n = 1), Kor22–23H (n = 1), Kor22–23I (n = 1), Kor22–23J (n = 2), Kor22–23K (n = 6), Kor22–23L (n = 1), Kor22–23M (n = 1), Kor22–23N (n = 1), Kor22–23O (n = 2), and Kor22–23P (n = 1) (Appendix Table 4). The predominant genotype was Kor22–23D, accounting for 57.5% of cases, followed by Kor22–23C, accounting 15% of cases. In those predominant genotypes (Kor22–23D and Kor22–23C), we observed reassortment in all internal genes, except for the matrix protein gene, compared with the early genotype, Kor22–23A. The most frequently identified internal genotypes were polymerase basic 2 (d), polymerase basic 1 (d), polymerase acidic (d), HA (a), nucleoprotein (d), neuraminidase (a), matrix protein (a), and nonstructural (d), which corresponded to the internal genes of the Kor22–23D genotype (Appendix Figure 1). Genotype diversity decreased from late December 2022, in particular as a consequence of the disappearance of Kor22–23C and Kor22–23B (Figure 4, panel A). Kor22–23D exhibited the highest proportions in

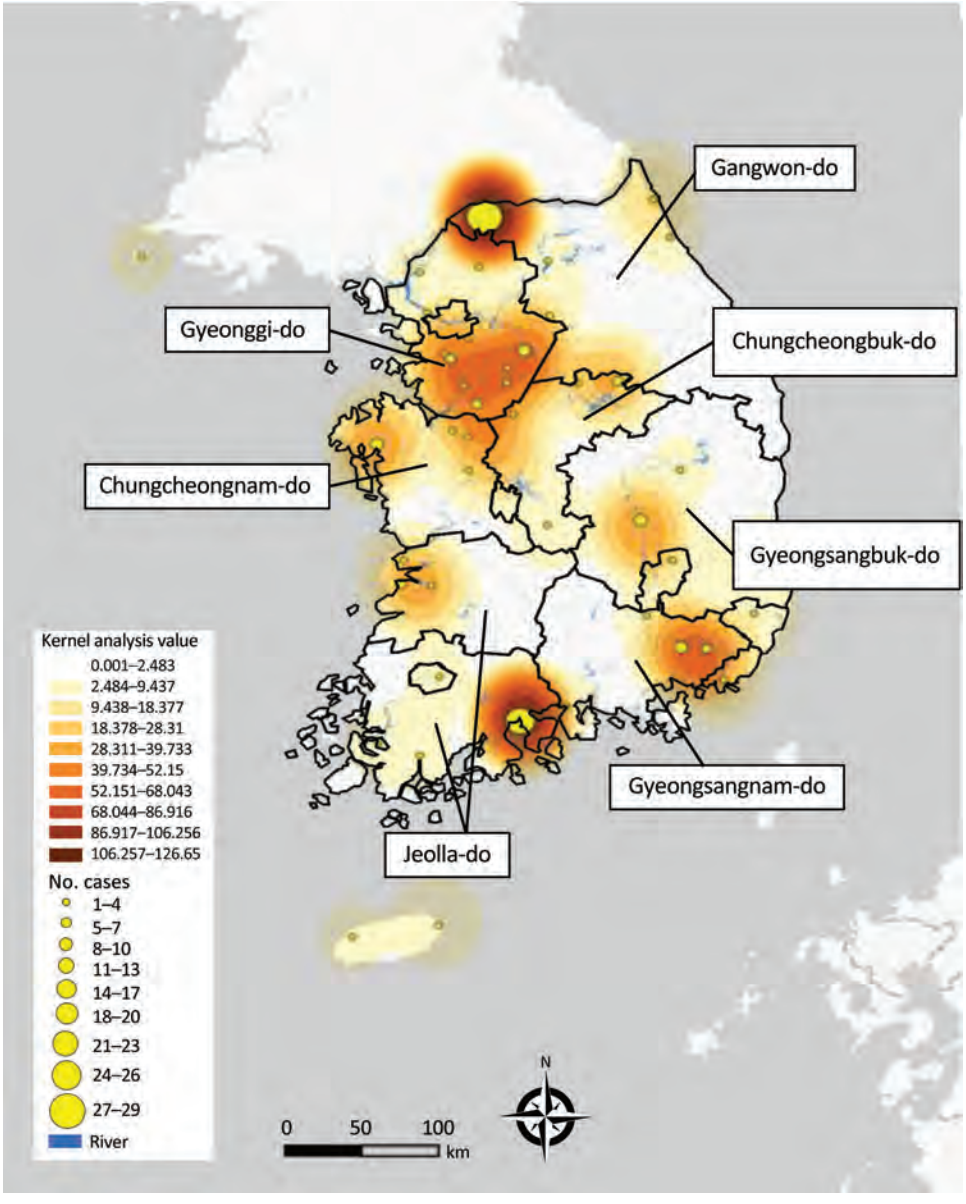

Figure 2. Kernel density map of epizootic cases of highly pathogenic avian influenza, by geographic region, South Korea, October 2022–March 2023. Geographic regions determined according to a discrete trait analysis conducted for the study.

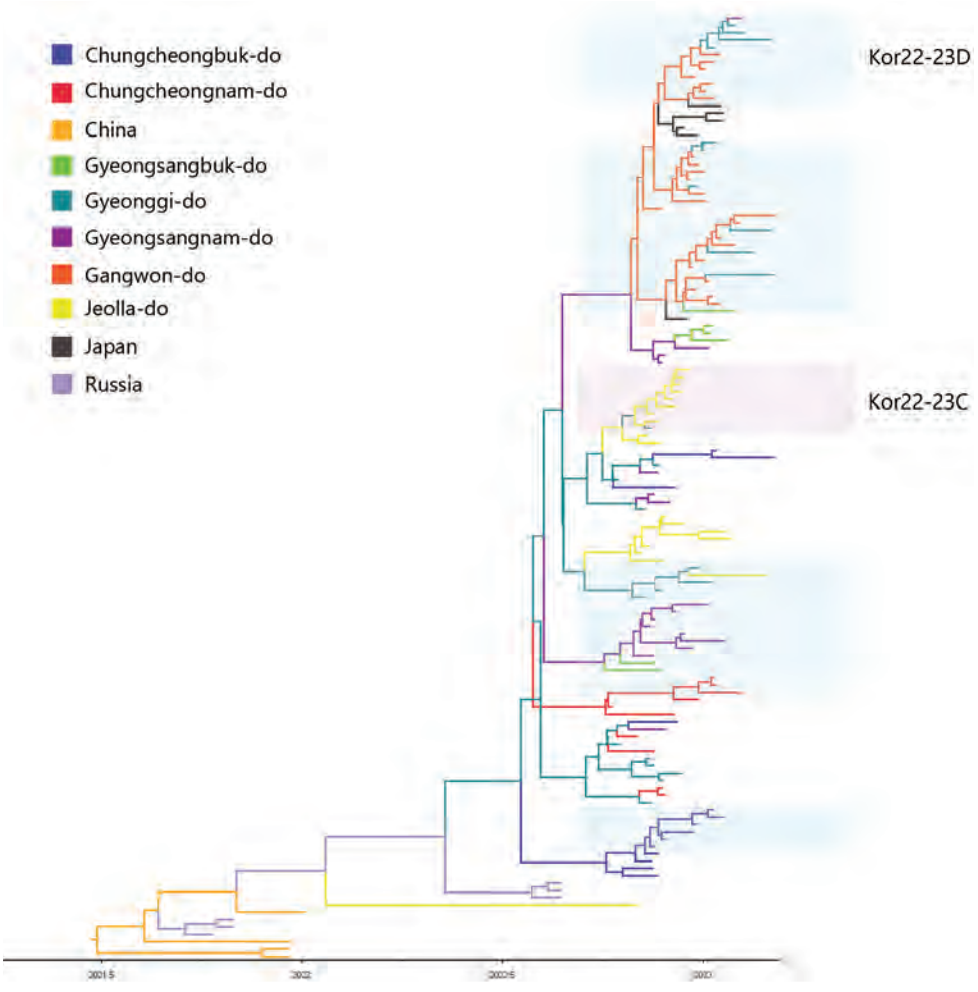

Figure 3. Maximum clade credibility tree constructed using the hemagglutinin gene of highly pathogenic avian influenza A(H5N1) clade 2.3.4.4b virus, with geographic region as a discrete trait, South Korea, June 2022–January 2023. Each branch is colored according to the geographic region specified in the legend. Each genotype was assigned an alphabet letter based on the Kor22–23 nomenclature, which indicated the region of origin (Kor) and year of origin (2022–2023). Orange shade represents Kor22–23B genotype viruses. Violet shades represent Kor22–23C genotype viruses. Blue shades represent Kor22–23D genotype viruses. The x-axis is in decimal year format.

GW, CN, and GN. Kor22–23C showed the highest proportion in JL. Kor22–23B was sporadically distributed across various regions.

Transmission Dynamics of HPAI H5N1 Viruses in South Korea during 2022–23

The discrete trait phylodynamic analyses (DTA) between geographic regions suggested that the virus was most likely dispersed from China to Russia during 2021–2022, then introduced from Russia to the GG of South Korea during 2022. In South Korea, the DTA supported the virus spread from GW to GG (transition rate [TR] 2.508, Bayes factor [BF] 212524.514, and posterior probability [PP] 1.00), GG to GN (TR 1.711, BF 35413.848, and PP 1.00), and GG to CN (TR 1.293, BF 284.057, and PP 0.97) (Appendix Table 2). We visualized the inferred transmission networks in South Korea on a map (Figure 5). We also inferred the time spent on each discrete state by estimating the Markov reward. The estimated total Markov reward time for locations in South Korea was highest in GG (3.407 [95% BCrI 2.237–4.6073]), followed by GW (2.371 [95% BCrI 1.4939–3.6048]), indicating the contribution of wild birds in GG and GW to virus persistence and circulation in South Korea (Figure 6, panel A).

On the basis of the DTA between wild bird species, the most probable transmission pathway was from white-fronted goose to raptor (TR 1.804, BF 710.953, and PP 0.99), followed by swan to bean goose (TR 1.041, BF 21.822, and PP 0.78) and swan to white-fronted goose (TR 1.233, BF 17.182, and PP 0.73) (Figure 7; Appendix Table 3). For genotypes, Kor22–23D was the predominant genotype, and its highest proportion was detected in white-fronted goose, egret, and heron, whereas the highest proportion of Kor22–23C was detected in crane. The raptor and bean goose contained highly diverse genotypes compared with those genotypes contained by other host species (Figure 4, panel B). Collectively, those results indicate that the white-fronted goose and swan played a major role in the HPAI H5N1 virus spread in South Korea. In addition, the estimated total Markov reward time by

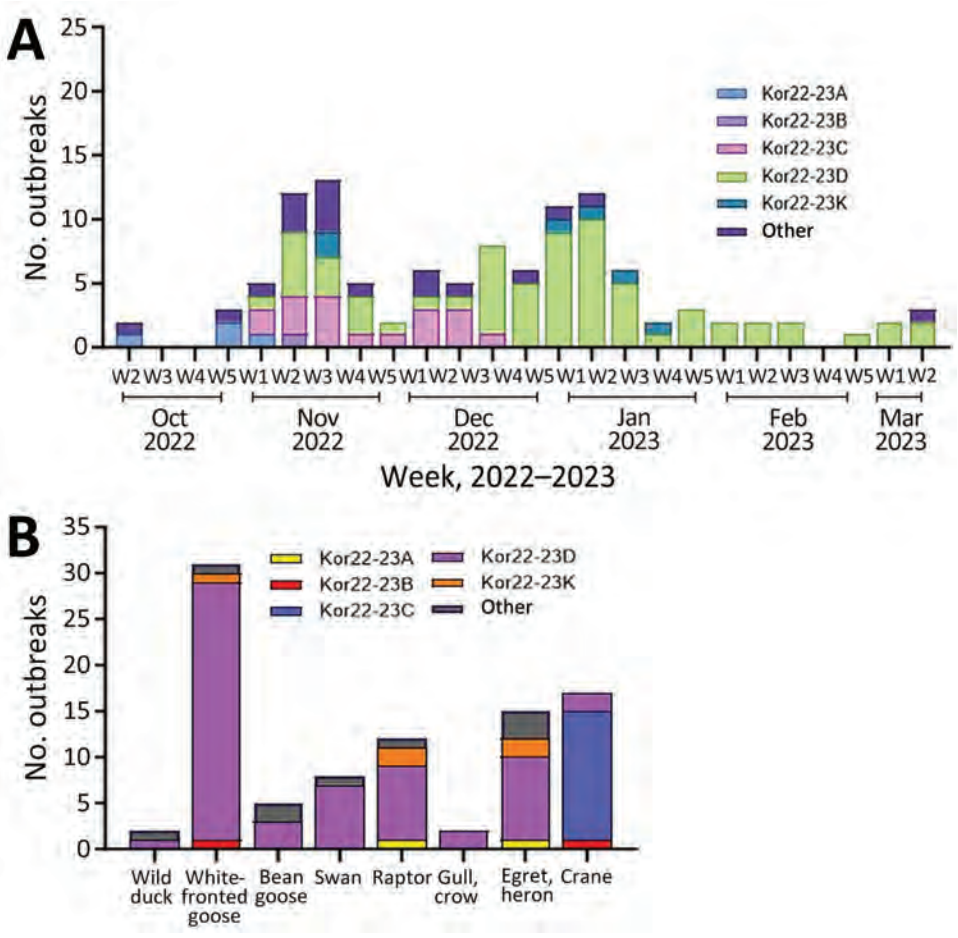

Figure 4. HPAI A(H5N1) clade 2.3.4.4b viruses and outbreaks, South Korea, October 2022–March 2023. A) Number of HPAI outbreaks by week, month, and genotype. B) Number of HPAI outbreaks, by week, month, and host species category. Each genotype was assigned an alphabet letter based on the Kor22–23 nomenclature, which indicated the region of origin (Kor) and year of origin (2022–2023). HPAI, highly pathogenic avian influenza.

host species was the highest in white-fronted goose (3.428 [95% BCrI 1.7149–5.8995]) (Figure 6, panel B). Those findings suggest that the white-fronted goose contributed to virus maintenance and spread in South Korea during 2022–2023.

Discussion

Understanding the movement and host characteristics of migratory waterfowl, which are natural hosts of avian influenza, is crucial for understanding the evolution and transmission pathways of HPAI virus. Migratory birds play a critical role in virus transmission because they have vast ranges, undertake long-distance migrations across borders to and from wintering and breeding sites, and interact with different species at each site (*20*). Some bird species can carry the virus without showing clinical signs of disease, which makes them long-distance carriers of the virus (*21*). Moreover, migratory waterfowl can potentially bring diverse strains of viruses, facilitating the emergence of new reassortant strains. Clade 2.3.4.4 HPAI viruses have undergone frequent reassortment events, especially in wild birds (*7*). The high genetic diversity of avian influenza viruses in wild birds has contributed to the generation of multiple genotypes of clade 2.3.4.4. HPAI H5Nx viruses as a donor gene pool of different genetic lineages (*22*). In our study, the genotyping of the 113 wild bird–origin HPAI H5N1 clade 2.3.4.4b viruses observed during October 2022–March 2023 revealed 16 different genotypes. Most of these newly reassorted genotypes were transient and did not show sustained transmission in wild bird populations, except for Kor22–23D and Kor22–23C. We assume that those 2 genotypes were predominant during the outbreak because they had better viral fitness than other transient genotypes for sustained transmission in wild birds.

The DTA between geographic locations indicated that most probable location for initial virus introduction to South Korea was GG. DTA is used in molecular epidemiology to study the geographic spread of infectious diseases across regions. When applied at the provincial or state level, a major limitation of this approach is its reliance on manmade borders as a proxy for the geographic structure. Manmade borders, such as provinces or state lines, do not necessarily

align with the natural distribution of wild bird populations or movement patterns of viruses. Using such borders may lead to oversimplification and inaccuracies in analyses because they may not reflect the actual transmission routes or wild bird movements. Our DTA results suggest that the virus was introduced from Russia to GG; however, the actual index case in South Korea was identified in the northern part of the CN. The kernel density analysis showed that southern GG and northern CN were classified as single high HPAI-density areas. Based on these findings, the virus was most likely introduced into the southern GG and northern CN areas initially and then spread to other regions. In addition, an HPAI H5N1 virus originating from the North American lineage was detected in October 2022, which is most likely a point-source introduction of virus (*23*).

Monitoring the geographic distribution of HPAI viruses in wild birds and locations of poultry farms is vital for assessing the risk for virus spillover. A previous study analyzed the geographic distribution of HPAI H5N1 outbreaks in poultry farms in South Korea during 2013–2017 and found high number of cases in southern GG, northern CN, and JL (*24*), which

Figure 5. Inferred transmission networks of highly pathogenic avian influenza A(H5N1) viruses from wild birds, South Korea, October 2022–March 2023. Arrows show the well-supported transitions in discrete trait phylogeography. Line colors indicate the overall Bayes factor test support for epidemiologic linkage. White arrows indicate statistical support with Bayes factor > 100 (very strong support), gray arrows indicate support with 10 < Bayes factor < 100 (strong support), and cyan arrows indicate support with 3 < Bayes factor < 10. Numbers next to arrows indicate transition rates.

were also high-density areas of HPAI detections in wild birds during 2022–2023. In particular, JL is the region with the highest poultry farm density in South Korea (*25*). JL is also the region with the highest number of HPAI H5N1 outbreaks in poultry farms during winter 2022–2023, according to the South Korean Animal and Plant Quarantine Agency (*16*). In addition, most HPAI H5N8 transmissions occurred during 2014–2015 within the western provinces, including GG, CN, and JL, which are characterized by high domestic duck densities and high numbers of overwintering waterfowl (*26*). On the basis of those findings, we suggest that integrative analysis of real-time surveillance data in wild birds and spatial distribution data of poultry farms can serve as an early warning system for forecasting the risk for avian influenza spillover from wild birds to poultry.

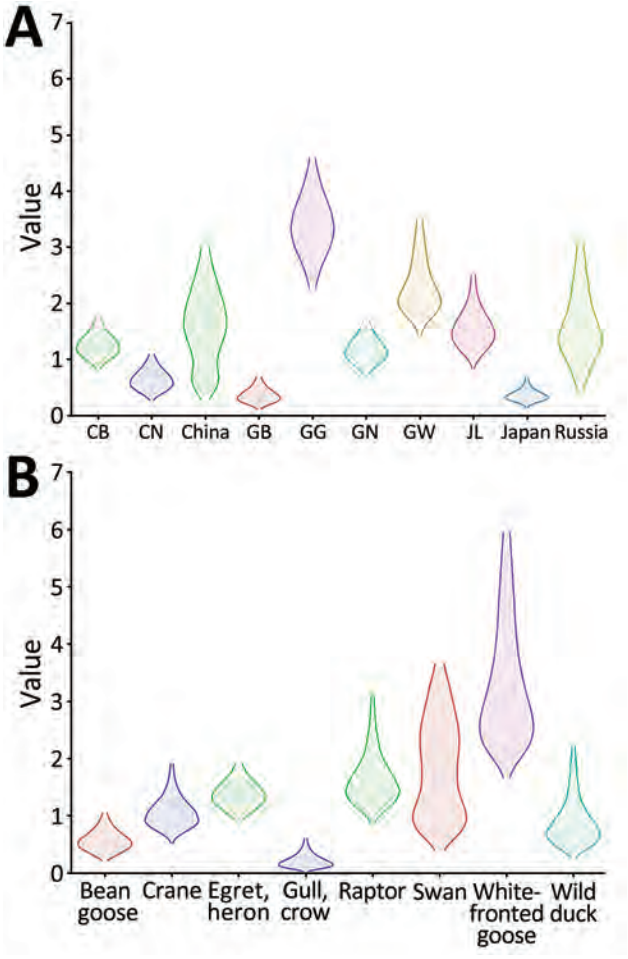

Figure 6. Markov time spent for geographic location (A) and host type (B) among highly pathogenic avian influenza A(H5N1) viruses from wild birds, South Korea, October 2022–March 2023. CB, Chungcheongbuk-do; CN, Chungcheongnam-do; GB, Gyeongsangbuk-do; GG, Gyeonggi-do; GN, Gyeongsangnam-do; GW, Gangwon-do; JL, Jeolla-do.

A previous study suggested the dissemination of HPAI viruses between South Korea and Japan through wild birds (*11*); however, the means by which the virus spreads between these 2 countries remains unclear. Of note, our DTA suggests that, after the virus spread to GW, it migrated from GW to central Japan, including Yamagata, Tochigi, Miyagi, and Shizuoka Prefectures, which have similar latitudes to that of GW. Further studies on the virus spread through migratory birds between GW and central Japan may provide valuable insights into the transboundary spread of HPAI viruses between these countries.

The initial entry of the virus through whooper swans was highly supported by DTA of host species. Whooper swans have been previously reported as long-distance migratory birds that can transmit HPAI viruses along their migration route. Previous studies on satellite GPS data showed that whooper swans bred in Mongolia and Russia were positive for HPAI viruses and subsequently migrated to South Korea, which coincides with the viral movement observed in our study (*27*). Considering the limitations of sampling in our surveillance study, an alternative explanation for this finding could be that the high susceptibility and distinctive morphology of whooper swans facilitated their early detection and subsequent sampling, potentially leading to the identification of HPAI viruses during the initial stages of the outbreak. Given that the most samples used in our surveillance study were wild bird carcasses collected by NIWDC through voluntary reports, asymptomatic wild bird carriers of HPAI viruses might not have been detected or included in our study. Of note, among the wild bird species affected by HPAI H5 virus, whooper swans have been reported as a frequently affected species thus recognized as a sentinel species for the presence of HPAI virus within the wild bird population (*27*). The frequent detections of swans found dead from HPAI infection can be attributed to their pathobiologic and morphologic characteristics compared with other wild bird species, including their high susceptibility to HPAI H5 virus infection and their substantial size and white color, which make them readily noticeable and identifiable when they are found dead from HPAI infection (*28*). Although passive surveillance of wild birds is considered the most effective method for monitoring HPAI associated with high mortality rates, active surveillance should be expanded in asymptomatic host species to improve our understanding of the behavior of these viruses in the wild-bird population. The DTA results

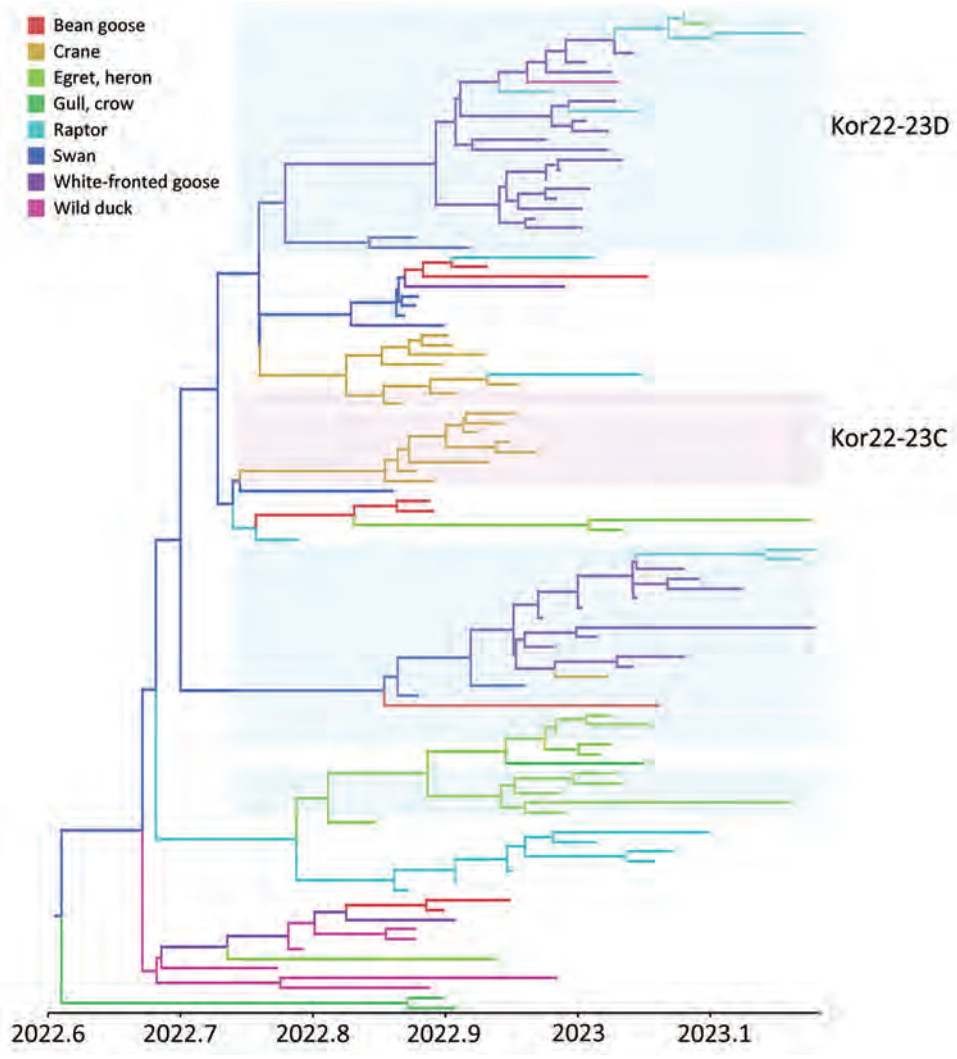

Figure 7. Maximum clade credibility tree constructed using the hemagglutinin gene of HPAI A(H5N1) clade 2.3.4.4b virus, with host types as a discrete trait, South Korea, June 2022–January 2023. Each branch is colored according to the host type specified in the legend. Each genotype was assigned an alphabet letter based on the Kor22–23 nomenclature, which indicated the region of origin (Kor) and year of origin (2022–2023). Orange shade represents Kor22–23B genotype viruses. Violet shades represent Kor22–23C genotype viruses. Blue shades represent Kor22–23D genotype viruses. The x-axis is in decimal year format.

suggested that geese (bean goose and white-fronted goose) played a crucial role in the virus spread in South Korea after these viruses were introduced by swans. Transmission was relatively frequent among swans, geese, and cranes, likely because those species share habitats around inland water bodies in South Korea (*29*). In addition, transmission of viruses from geese to raptors suggests possible upward food chain transmission during the predation of possibly infected geese.

NGS is a useful tool for obtaining complete genome sequences that can be used for outbreak analysis, combined with epidemiologic investigation data, to identify the possible origins and understand the transmission dynamics of viruses rapidly and accurately. During the 2022–23 HPAI virus outbreak, NIWDC attempted to sequence all available HPAI virus isolates from wild birds by using NGS and performed a comparative phylogenetic analysis to facilitate the rapid screening of HPAI and effective genomic surveillance. The 113 genome sequences identified in our study greatly expanded the existing dataset of the genome sequences of clade 2.3.4.4b HPAI virus from South Korea and helped us investigate the evolutionary history and molecular epidemiology of the virus outbreak across spatial and temporal scales. Immediate genome sequencing and analysis during outbreaks are recommended as an integral part of the HPAI virus outbreak response because this information can provide valuable insights into the origin, evolution, and spread of the virus. The precise and detailed genomic surveillance data can be especially beneficial to outbreak control and prevention efforts by helping public health officials and researchers monitor the emergence of new variants, trace the transmission of HPAI virus, tailor interventions and recommendations for the public, and develop countermeasures. Sharing genomic data with the global scientific

community and international health organizations can foster collaboration and a coordinated response to global HPAI outbreaks.

Acknowledgment

We acknowledge the Avian Influenza Research and Diagnostic Division of Animal and Plant Quarantine Agency, South Korea, for genome sequencing in this study.

This research was funded by South Korea's National Institute of Wildlife Disease Control and Prevention and the Ministry of Environment (grant no. 2023-007).

About the Author

Ms. Ye-Ram Seo is a veterinary student at the College of Veterinary Medicine, Konkuk University. Her research focuses on the molecular epidemiology of animal diseases. Mr. Cho is a PhD candidate at the College of Veterinary Medicine, Konkuk University. His research interests include molecular epidemiology and vaccine development of avian diseases.

References

1. Wan XF. Lessons from emergence of A/goose/Guangdong/1996-like H5N1 highly pathogenic avian influenza viruses and recent influenza surveillance efforts in southern China. Zoonoses Public Health. 2012;59(Suppl 2):32–42. https://doi.org/10.1111/j.1863-2378.2012.01497.x
2. World Health Organization. Antigenic and genetic characteristics of zoonotic influenza A viruses and development of candidate vaccine viruses for pandemic preparedness. Wkly Epidemiol Rec. 2020;95:525–39.
3. Lee YJ, Kang HM, Lee EK, Song BM, Jeong J, Kwon YK, et al. Novel reassortant influenza A(H5N8) viruses, South Korea, 2014. Emerg Infect Dis. 2014;20:1087–9. https://doi.org/10.3201/eid2006.140233
4. Lee DH, Sharshov K, Swayne DE, Kurskaya O, Sobolev I, Kabilov M, et al. Novel reassortant clade 2.3.4.4 avian influenza A(H5N8) virus in wild aquatic birds, Russia, 2016. Emerg Infect Dis. 2017;23:359–60. https://doi.org/10.3201/eid2302.161252
5. Beerens N, Heutink R, Bergervoet SA, Harders F, Bossers A, Koch G. Multiple reassorted viruses as cause of highly pathogenic avian influenza A(H5N8) virus epidemic, the Netherlands, 2016. Emerg Infect Dis. 2017;23:1974–81. https://doi.org/10.3201/eid2312.171062
6. Bevins SN, Shriner SA, Cumbee JC Jr, Dilione KE, Douglass KE, Ellis JW, et al. Intercontinental movement of highly pathogenic avian influenza A(H5N1) clade 2.3.4.4 virus to the United States, 2021. Emerg Infect Dis. 2022;28:1006–11. https://doi.org/10.3201/eid2805.220318
7. Baek YG, Lee YN, Lee DH, Shin JI, Lee JH, Chung DH, et al. Multiple reassortants of H5N8 clade 2.3.4.4b highly pathogenic avian influenza viruses detected in South Korea during the winter of 2020–2021. Viruses. 2021;13:490. https://doi.org/10.3390/v13030490
8. Wu H, Peng X, Xu L, Jin C, Cheng L, Lu X, et al. Novel reassortant influenza A(H5N8) viruses in domestic ducks, eastern China. Emerg Infect Dis. 2014;20:1315–8. https://doi.org/10.3201/eid2008.140339
9. Ruiz-Saenz J, Martinez-Gutierrez M, Pujol FH. Multiple introductions of highly pathogenic avian influenza H5N1 clade 2.3.4.4b into South America. Travel Med Infect Dis. 2023;53:102591. https://doi.org/10.1016/j.tmaid.2023.102591
10. Wille M, Klaassen M. No evidence for HPAI H5N1 2.3.4.4b incursion into Australia in 2022. Influenza Other Respir Viruses. 2023;17:e13118. https://doi.org/10.1111/irv.13118
11. Jeong S, Lee DH, Kwon JH, Kim YJ, Lee SH, Cho AY, et al. Highly pathogenic avian influenza clade 2.3.4.4b subtype H5N8 virus isolated from Mandarin duck in South Korea, 2020. Viruses. 2020;12:1389. https://doi.org/10.3390/v12121389
12. Shin J, Kang S, Byeon H, Cho SM, Kim SY, Chung YJ, et al. Highly pathogenic H5N6 avian influenza virus subtype clade 2.3.4.4 indigenous in South Korea. Sci Rep. 2020;10:7241. https://doi.org/10.1038/s41598-020-64125-x
13. Sagong M, Lee YN, Song S, Cha RM, Lee EK, Kang YM, et al. Emergence of clade 2.3.4.4b novel reassortant H5N1 high pathogenicity avian influenza virus in South Korea during late 2021. Transbound Emerg Dis. 2022;69:e3255–60. https://doi.org/10.1111/tbed.14551
14. Baek YG, Lee YN, Park YR, Chung DH, Kwon JH, Si YJ, et al. Evolution, transmission, and pathogenicity of high pathogenicity avian influenza virus A (H5N8) clade 2.3.4.4, South Korea, 2014–2016. Front Vet Sci. 2022;9:906944. https://doi.org/10.3389/fvets.2022.906944
15. Song BM, Lee EK, Lee YN, Heo GB, Lee HS, Lee YJ. Phylogeographical characterization of H5N8 viruses isolated from poultry and wild birds during 2014–2016 in South Korea. J Vet Sci. 2017;18:89–94. https://doi.org/10.4142/jvs.2017.18.1.89
16. Animal and Plant Quarantine Agency (South Korea). Highly pathogenic avian influenza detection status. 2023 [cited 2023 Nov 5]. https://www.qia.go.kr/viewwebQiaCom.do?id=60620&type=2_12qlgzls
17. Lee DH, Lee HJ, Lee YJ, Kang HM, Jeong OM, Kim MC, et al. DNA barcoding techniques for avian influenza virus surveillance in migratory bird habitats. J Wildl Dis. 2010;46:649–54. https://doi.org/10.7589/0090-3558-46.2.649
18. Lee DH. Complete genome sequencing of influenza A viruses using next-generation sequencing. Methods Mol Biol. 2020;2123:69–79. https://doi.org/10.1007/978-1-0716-0346-8_6
19. World Health Organization. Genetic and antigenic characteristics of zoonotic influenza A viruses and development of candidate vaccine viruses for pandemic preparedness. Wkly Epidemiol Rec. 2023;98:111–25.
20. Olsen B, Munster VJ, Wallensten A, Waldenström J, Osterhaus AD, Fouchier RA. Global patterns of influenza a virus in wild birds. Science. 2006;312:384–8. https://doi.org/10.1126/science.1122438
21. Tian H, Zhou S, Dong L, Van Boeckel TP, Cui Y, Newman SH, et al. Avian influenza H5N1 viral and bird migration networks in Asia. Proc Natl Acad Sci U S A. 2015;112:172–7. https://doi.org/10.1073/pnas.1405216112
22. Claes F, Morzaria SP, Donis RO. Emergence and dissemination of clade 2.3.4.4 H5Nx influenza viruses—how is the Asian HPAI H5 lineage maintained. Curr Opin Virol. 2016;16:158–63. https://doi.org/10.1016/j.coviro.2016.02.005
23. Kang Y-M, Heo G-B, An S-H, Lee Y-N, Cha RM, Cho H-K, et al. Introduction of multiple novel high pathogenicity avian influenza (H5N1) virus of clade 2.3.4.4 b into South Korea in 2022. Transbound Emerg Dis. 2023;2023. https://doi.org/10.1155/2023/8339427
24. Yoo DS, Chun BC, Hong K, Kim J. Risk prediction of three different subtypes of highly pathogenic avian influenza

outbreaks in poultry farms: based on spatial characteristics of infected premises in South Korea. Front Vet Sci. 2022;9:897763. https://doi.org/10.3389/fvets.2022.897763
25. Koh K-Y, Ahmad S, Lee J-i, Suh G-H, Lee C-M. Hierarchical clustering on principal components analysis to detect clusters of highly pathogenic avian influenza subtype H5N6 epidemic across South Korean Poultry Farms. Symmetry (Basel). 2022;14:598. https://doi.org/10.3390/sym14030598
26. Hill SC, Lee YJ, Song BM, Kang HM, Lee EK, Hanna A, et al. Wild waterfowl migration and domestic duck density shape the epidemiology of highly pathogenic H5N8 influenza in the Republic of Korea. Infect Genet Evol. 2015; 34:267–77. https://doi.org/10.1016/j.meegid.2015.06.014
27. Li S, Meng W, Liu D, Yang Q, Chen L, Dai Q, et al. Migratory whooper swans *Cygnus cygnus* transmit H5N1 virus between China and Mongolia: combination evidence from satellite tracking and phylogenetics analysis. Sci Rep. 2018;8:7049. https://doi.org/10.1038/s41598-018-25291-1
28. Li X, Lv X, Li Y, Xie L, Peng P, An Q, et al. Emergence, prevalence, and evolution of H5N8 avian influenza viruses in central China, 2020. Emerg Microbes Infect. 2022;11:73–82. https://doi.org/10.1080/22221751.2021.2011622
29. Moores N. Wetlands: Korea's most threatened habitat. Oriental Bird Club Bulletin. 2002;36:54–60.

Address for correspondence: Dong-Hun Lee, Wildlife Health Laboratory, College of Veterinary Medicine, Konkuk University, 120 Neungdong-ro, Gwangjin-gu, Seoul, 05029, South Korea; email: donghunlee@konkuk.ac.kr

Evidence of Zika Virus Reinfection by Genome Diversity and Antibody Response Analysis, Brazil

Marcia da Costa Castilho, Ana Maria Bispo de Filippis, Lais Ceschini Machado, Thaise Yasmine Vasconcelos de Lima Calvanti, Morganna Costa Lima, Vagner Fonseca, Marta Giovanetti, Cassia Docena, Armando Menezes Neto, Camila Helena Aguiar Bôtto-Menezes, Edna Oliveira Kara, Rafael de La Barrera, Kayvon Modjarrad, Silvana Pereira Giozza, Gerson Fernando Pereira, Luiz Carlos Junior Alcantara, Nathalie Jeanne Nicole Broutet, Guilherme Amaral Calvet,[1] Gabriel Luz Wallau,[1] Rafael Freitas Oliveira Franca[1]

We generated 238 Zika virus (ZIKV) genomes from 135 persons in Brazil who had samples collected over 1 year to evaluate virus persistence. Phylogenetic inference clustered the genomes together with previously reported ZIKV strains from northern Brazil, showing that ZIKV has been remained relatively stable over time. Temporal phylogenetic analysis revealed limited within-host diversity among most ZIKV-persistent infected associated samples. However, we detected unusual virus temporal diversity from ≥5 persons, uncovering the existence of divergent genomes within the same patient. All those patients showed an increase in neutralizing antibody levels, followed by a decline at the convalescent phase of ZIKV infection. Of interest, in 3 of those patients, titers of neutralizing antibodies increased again after 6 months of ZIKV infection, concomitantly with real-time reverse transcription PCR re-positivity, supporting ZIKV reinfection events. Altogether, our findings provide evidence for the existence of ZIKV reinfection events.

Zika virus (ZIKV) is an arthropodborne virus belonging to the Flaviviridae family. Virions are enveloped for a single-stranded positive-sense RNA genome of ≈10.8-kb (*1*). ZIKV is transmitted through the bite of infected *Aedes* spp. mosquitoes, mainly *A. aegypti*, which are widely distributed throughout the tropical and subtropical regions of the world.

In 2015, a large ZIKV epidemic was documented in Brazil, resulting in an estimated 440,000–1.3 million cases (*2*). Of great concern, the epidemic was preceded by a dramatic increase in the number of congenital anomalies, including newborn microcephaly (*3*,*4*). However, since the largest outbreak in 2015, ZIKV has decreased its circulation; novel cases are only sporadically reported (*5*).

ZIKV infections are usually asymptomatic, although a small proportion of persons may experience mild symptoms such as fever, rash, nonpurulent conjunctivitis, muscle pain, and joint pain. During pregnancy, ZIKV infection may result in microcephaly and other congenital abnormalities in the developing fetus (*3*). Suspected cases are diagnosed by detection of viral RNA in blood and urine during the acute phase of the disease and in other body fluids with variable frequency and duration by reverse transcription PCR (RT-PCR) (*6*). As previously reported, ZIKV infection may result in a persistent viral infection, as demonstrated by the prolonged detection of viral RNA in semen; the longest detection was up to 370 days after symptom onset (*7*). Virus compartmentalization and persistence are common features of ZIKV infection; however, the clinical and immunological aspects of ZIKV persistence, reactivation, and reinfection are still unknown.

Author affiliations: Tropical Medicine Foundation Doctor Heitor Vieira Dourado, Manaus, Brazil (M. da Costa Castilho, C.H.A. Bôtto-Menezes); Oswaldo Cruz Foundation, Rio de Janeiro, Brazil (A.M.B. de Filippis, M. Giovanetti, L.C.J. Alcantara); Oswaldo Cruz Foundation, Recife, Brazil (L.C. Machado, T.Y.V. de L. Calvanti, M.C. Lima, C. Docena, A.M. Neto, G.A. Calvet, G.L. Wallau, R.F.O. Franca); Organização Pan-Americana da Saúde/Organização Mundial da Saúde, Brasília, Brazil (V. Fonseca); University of Campus Bio-Medico di Roma, Rome, Italy (M. Giovanetti); World Health Organization, Geneva, Switzerland (E.O. Kara, N.J.N. Broutet); Walter Reed Army Institute of Research, Silver Spring, Maryland, USA (R. de La Barrera, K. Modjarrad); Department of Chronic Condition Diseases and Sexually Transmitted Infections, Brasília, Brazil (S.P. Giozza, G.F. Pereira); National Reference Center for Tropical Infectious Diseases, Hamburg, Germany (G.L. Wallau)

DOI: http://doi.org/10.3201/eid3002.230122

[1]These authors contributed equally to this article.

ZIKV phylogenetic studies have described the circulation of 2 distinct African and Asian lineages (*8*). The initial genetic analysis of the first ZIKV isolates from Brazil revealed the circulation of the Asian genotype during the 2015–2016 epidemic (*9*). Asian-derived strains that currently circulate in the Americas are now named ZIKV American strains and are well known for their capacity to infect neuronal progenitor cells, disrupting cell development, proliferation, and differentiation (*10*,*11*). Because the genomic replication of ZIKV is based on an error-prone RNA-dependent RNA polymerase (RdRp), which leads to nucleotide misincorporation during viral replication, ZIKV infection behaves as viral populations composed of genetically related sequences, similar to other RNA virus infections. As the viral replication progresses in an infected person, mutations start to accumulate, resulting in more heterogeneous viral genomic populations. Those viral population clouds are the foundation of the quasispecies theory, which posits that RNA viruses produce larger, highly variable population clouds that can evade the host immune system more efficiently (*12*). Furthermore, accumulating data show that viral cloud variability is able to interfere with disease progression (*13*,*14*). In this context, next-generation sequencing (NGS) provides a powerful tool to gain a deeper understanding of viral diversity by increasing the depth of sequencing coverage, defined as the number of reads for a given nucleotide). Therefore, the assessment of viral diversity is key to better understand virulence, evolution, and host-specific adaptations providing a direct translational information to mitigate effects of viral pathogens.

In this study, we deployed an NGS protocol to gain insight into the genetic diversity of ZIKV in naturally infected patients. Specifically, we used a previously established cohort study conducted in northern Brazil to assess virus diversity from patients with prolonged ZIKV infection (*15*–*17*). Since 2016, we have observed limited virus diversity and decreasing ZIKV transmission over the years, which was likely because of population immunity elicited during the first outbreak waves. We also found that virus diversity was limited in longitudinally sequenced samples from persons persistently infected with ZIKV, indicating restrained evolutionary rates and selection pressures acting on RNA arthropod-borne viruses; our results were consistent with previously published findings (*18*,*19*). However, we also detected the existence of divergent genomes within the same patient in a small number of samples analyzed; those participants responded to infection with alterations in neutralizing antibodies levels concomitantly with ZIKV redetection by real-time RT-PCR (rRT-PCR) several months after the initial virus exposure.

The study protocol and procedures have been reviewed and approved by the World Health Organization Research Ethics Review Committee (protocol ID: ERC.0002786); Brazilian National Research Ethics Commission (CAAE: 62.518.016.6.1001.0008); Institutional Ethics and Research Committee of the Evandro Chagas National Institute of Infectious Diseases, Fiocruz, Rio de Janeiro (CAAE: 62.518.016.6.2002.5262); Institutional Ethics and Research Committee of the Aggeu Magalhães Research Center, Fiocruz, Recife (CAAE: 62.518.016.6.2001.5190) and Institutional Ethics and Research Committee of the Tropical Medicine Foundation, Manaus, Amazonas (CAAE: 62.518.016.6.2003.0005).

Methods

Study Participants and Specimen Collection

Participants comprised men and women ≥18 years of age with a confirmed diagnosis of ZIKV infection by RT-PCR, as described previously (*15*,*16*,*20*). Participants were persons with symptomatic cases diagnosed at the study collaborating clinics (index case-patients) and their asymptomatic or symptomatic household and sexual contacts. After ZIKV infection confirmation performed 48 hours after study recruitment, we collected other specimens at established intervals, or visits (Table 1), and routinely tested for molecular screening using a multiplex rRT-PCR assay to detect ZIKV, dengue virus, and chikungunya virus.

NGS and Analysis

We processed all specimens with a positive ZIKV rRT-PCR result, defined as a cycle threshold (Ct) value ≤38, using a previously established NGS protocol (*21*). For this study, we processed plasma, urine, and

Table 1. Study visits and sample collection for participants in study of Zika virus reinfection, Brazil

Visit no.	Days after rash, range*
V0	–7 to 0
V1	0–2
V2	3–4
V3	5–8
V4	9–10
V5	11–20
V6	21–30
V7	31–60
V8	61–90
V9	91–120
V10	121–150
V11	151–180
V12	181–210
V13	211–240
V14	241–270
V15	271–300
V16	301–330
V17	331–360

*As reported by study participants.

semen samples (semen is more frequently associated with persistence). For sequencing, we first obtained a complementary DNA employing the ProtoScript II Reverse transcription kit (New England Biolabs, https://www.neb.com) and a set of random primers (random sequence [d(N)6]). We obtained whole-genome amplicons from a multiplex PCR reaction using a set of ZIKV designed primers, as described by Quick et al. (*21*); we purified amplicons using the Q5 High-Fidelity DNA Polymerase kit (New England Biolabs) and performed library preparation with the Nextera XT Library Prep kit (Illumina, https://www.illumina.com) using 2 ng of DNA. We sequenced the obtained libraries using the MiSeq Reagent kit version 3 (Illumina) on an Illumina MiSeq. We processed raw fastq data to generate consensus files (base calls only at regions with ≥5×) and to call SNVs and iSNVs (only regions with a coverage depth of ≥100×) using ViralFlow version 0.0.6 (*22*) and a reference ZIKV genome (GenBank accession no. KX197192.1).

Phylogenetic and Bayesian Analysis

The new genomic sequences reported in this study were initially submitted to a genotyping analysis using the ZIKV typing tool (http://genomedetective.com/app/typingtool/zika). We aligned genomic data generated in this study (238 genomes with coverage breadth ≥70 and average coverage depth of 100×) with a worldwide dataset of ZIKV genome sequences (n = 840 for all known ZIKV genotypes and n = 481 for ZIKV American strains). We aligned sequences using MAFFT (https://mafft.cbrc.jp/alignment/software) and inferred a preliminary maximum-likelihood tree using IQ-TREE version 2 (http://www.iqtree.org). Before conducting temporal analysis, we assessed our dataset for molecular clock signal in TempEst version 1.5.3 (http://tree.bio.ed.ac.uk/software/tempest) after removing any potential outliers that might violate the molecular clock assumption. To estimate a time-calibrated phylogeny, we used the Bayesian software package BEAST version 1.10.4 (https://beast.community) with the Bayesian skyline tree prior with an uncorrelated relaxed clock and the lognormal distribution. We ran analyses in duplicate in BEAST for 100 million Markov chain Monte Carlo (MCMC) steps, sampling parameters, and trees every 10,000th step. We checked convergence of MCMC chains using Tracer version 1.7.1 (https://beast.community/tracer). We summarized maximum clade credibility trees using TreeAnnotator (https://beast.community/treeannotator) after discarding 10% as burn-in. We submitted the genomes from this study to the Genome Detective for the analysis of the mutational pattern profile using the annotated genome aligner AGA (https://www.genomedetective.com/app/aga). We plotted results in R Studio version 4.2.1 (https://posit.co) using the Lollipop plot.

ZIKV Neutralization Assays

We measured ZIKV neutralizing antibody titers by a high-throughput ZIKV 50% microneutralization assay (MN_{50}), using a wild-type live virus as described previously (*22*). We defined seropositivity as a titer ≥1:10.

Results

Cohort Definition and Sample Assessment for NGS

During June 2017–June 2019, our study recruited a total of 255 persons with ZIKV-confirmed infection in Manaus, Brazil. Among the participants, 99% were enrolled within 1 week after the onset of illness. For this study, genomic analysis included 135 persons with confirmed ZIKV infection experiencing rash, itching, fever, and arthralgia; mean age was 38.27 (±12.97) years (Table 2). Of those 135 persons, 56 participants had ≥1 sample available, defined as a different specimen at the same visit (5/135) or any specimen at a different study visit (51/135). We sequenced those samples, which yielded a total of 238 ZIKV genomes with a median genome coverage breadth of 90%. Most of these genomes were obtained from plasma and urine samples; a minor proportion (n = 20) were obtained from semen specimens.

Phylogenetic Characterization

Initially, our objective was to thoroughly characterize ZIKV circulating from northern Brazil. We observed that all ZIKV strains circulating in Manaus since the

Table 2. Characteristics of participants included in study of genomic analysis of Zika virus reinfection, Brazil

Characteristics at enrollment	No. (%) participants, n = 135
Age group, y	
18–30	45 (33.2)
31–60	84 (62.2)
>60	6 (4.4)
Sex	
M	45 (33.3)
F	90 (66.7)
Days after symptom onset*	
0–2	44 (32.6)
3–5	68 (50.4)
6–8	22 (16.3)
9–11	1 (0.7)
Clinical signs*	
Macular or papular rash	133 (98.5)
Itching	126 (93.3)
Fever	116 (85.9)
Arthralgia	108 (80)
Nonpurulent conjunctivitis	100 (74.1)
Periarticular edema	92 (68.1)

*Reported at screening visit, which did not require enrollment.

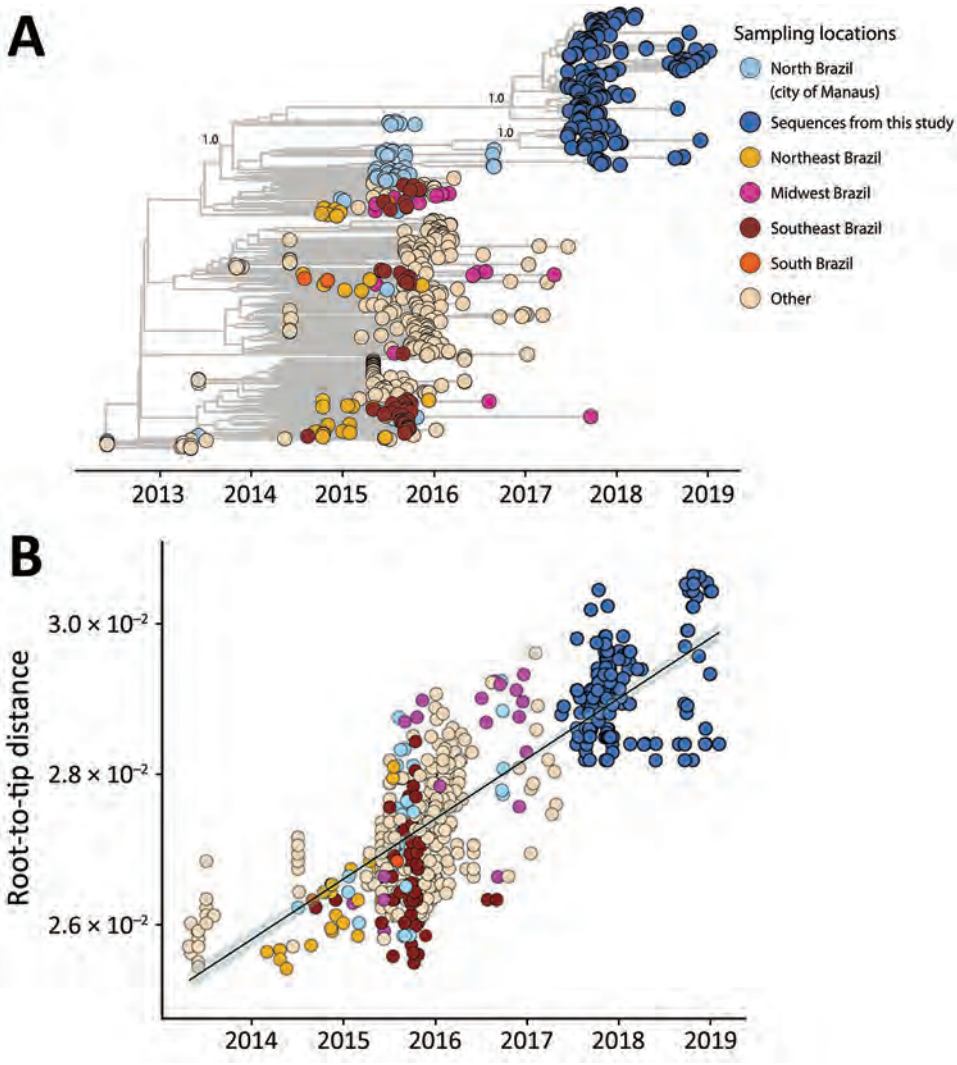

Figure 1. Genomic epidemiology of Zika virus strains obtained from study participants in northern Brazil and reference sequences. A) Time-scaled maximum clade credibility tree of Zika virus Asian lineage in Brazil, including the 238 new genomes generated in this study (dark blue) plus 481 reference strains sampled worldwide. Tips are colored according to the sample source location. Values at nodes represent posterior probability support of the tree nodes inferred under Bayesian evolutionary analysis using a relaxed molecular clock approach. B) Root-to-tip regression of sequence sampling date against genetic divergence from the root of the outbreak clade.

beginning of the outbreak, including our newly generated genomes, grouped together in a unique clade within the ZIKV Asian lineage (Appendix 1 Figure 1, https://wwwnc.cdc.gov/EID/article/30/2/23-0122-App1.pdf). In addition, our maximum clade credibility (MCC) tree clustered our generated ZIKV genomes together with viral strains previously isolated in northern Brazil (Figure 1, panel A). From this analysis, we estimated the time of the most recent common ancestor (tMRCA) occurred in late March 2014 (95% highest posterior density range January–August 2014) (Figure 1, panel B). We also explored the collective mutational pattern found in the consensus genomes obtained in this study. Most of the mutations were observed in nonstructural protein (NS) 1 protein (5 in total) and NS5, which also has 5 mutations, although with a lower frequency than NS1 (Figure 2).

Next, we searched for the total number of ZIKV cases reported in Manaus from DATASUS (https://datasus.saude.gov.br/informacoes-de-saude-tabnet), the national health information system that compiles clinical and laboratory-confirmed cases across all the states of Brazil. Our analysis revealed that the initial occurrence of ZIKV cases in Manaus dates to 2016, a significant surge of 6,033 cases that marked the peak of the ZIKV epidemic in northern Brazil. However, after the initial surge in 2016, subsequent waves experienced a significant decrease in the overall number of reported ZIKV cases. That downward trend persisted and reached a notable low point in 2019, when only 126 cases were documented (Figure 3). We concluded that the ZIKV circulating strains in northern Brazil exhibited stability over time, undergoing minimal mutations, contributing to the decline of the epidemic.

ZIKV Within-Host Genetic Diversity

We followed our study protocol, specifically designed to investigate the persistence of ZIKV in body fluids,

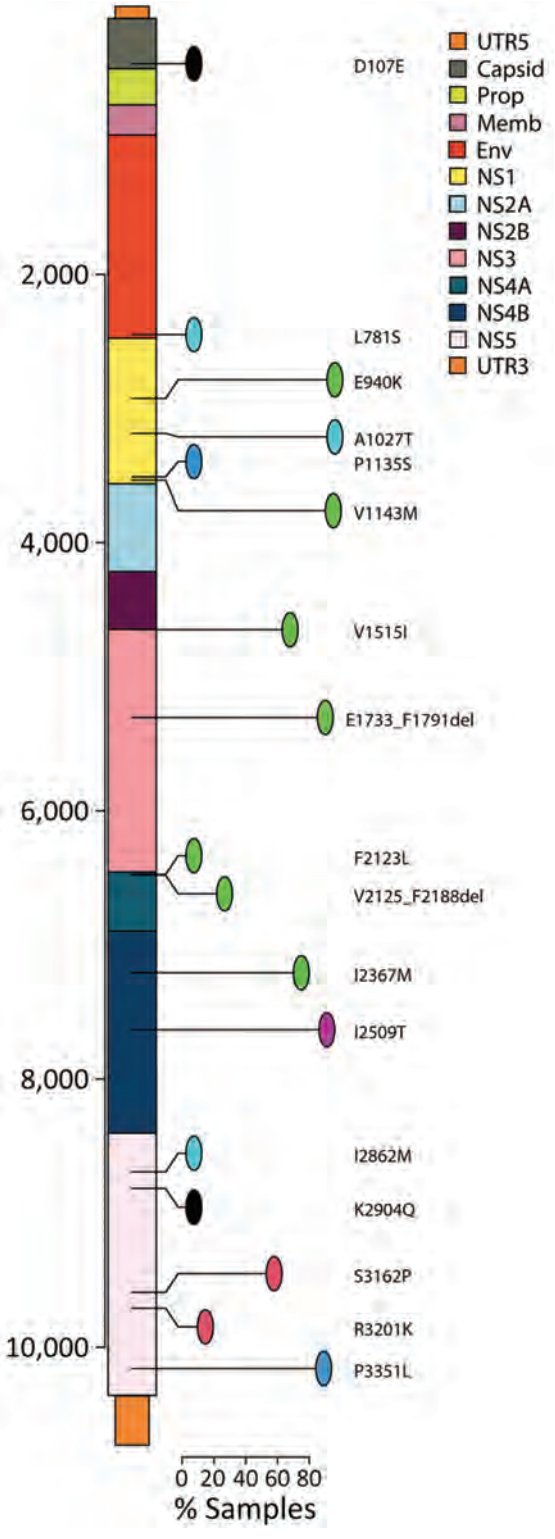

Figure 2. Single-nucleotide variants per gene for Zika virus strains obtained from study participants in northern Brazil. Amino acid changes in the polyprotein are allocated along the genome. Only mutations that appear in >10% (lines) of sequences are shown. Env, envelope; Prop, propeptide; Memb, membrane; NS, nonstructural; UTR, untranslated region.

to assess virus diversity among persons who remained persistently infected. Although there is no consensus in the literature, we defined ZIKV persistence as any participant with ZIKV-positive rRT-PCR detection within 30 days after its initial ZIKV confirmation. By applying this criterion, we identified 10 patients who had ≥1 positive persistent sample from plasma, urine, or semen. Individual temporal phylogenetic analysis grouped those ZIKV-persistent genomes into 2 major clades. For 5 of the patients, all their samples grouped into a single clade in the tree (Figure 4, panel A); those clusters indicated limited viral diversity and maintenance of a single viral lineage through time in these persistently infected persons, independent of the type of specimen analyzed. Because ZIKV neutralizing antibodies (ZIKV-NAb) are highly protective and increasing titers from acute to convalescent phase are usually linked to viral clearance, we then assessed the levels of ZIKV-NAb. Our results showed that almost all the 10 persistently ZIKV-infected participants responded with higher levels (>2,000) of ZIKV-NAb by 30 days after disease onset (Figure 4, panel B), indicating a strong neutralizing antibody response at the convalescent phase. Those results eliminated the possibility of a dysregulated immune response as a cause of persistent ZIKV infections.

Our phylogenetic analysis also showed 5 participants with ZIKV genomes clustering in distinct clades or subclades in the tree (Figure 4, panel A; Figure 5; Appendix 1 Figure 2), which suggests the presence of divergent viral genomes within the same participant over time. Those participants had highly supported minor variants (approximate likelihood ratio test >70%) that were not consistently found among all samples from the same person and showed no consistent pattern of minor variant sites accumulation over time (Appendix 2, https://wwwnc.cdc.gov/EID/article/30/2/23-0122-App2.xlsx). We hypothesize that the presence of such temporally divergent ZIKV genomes in the same person suggests a reinfection event by a distinct ZIKV clade. Thus, to further assess whether those participants were reinfected, we checked their rRT-PCR results. We observed that 1 participant (ID251064) had a continuous rRT-PCR–positive result up to 8 days after the initial ZIKV infection; viral RNA was not detected until study visit 8 (61–90 days after disease onset), when a ZIKV rRT-PCR result was again positive in plasma (Figure 6). Two participants (ID251069 and ID151035) tested positive for ZIKV RNA in either plasma or urine for up to 21 days after ZIKV confirmation. Those participants then remained ZIKV-negative for 10 months but returned to positivity at the last study visit, performed 311–360 days after disease onset (Figure 6). The rRT-PCR–positive samples indicating

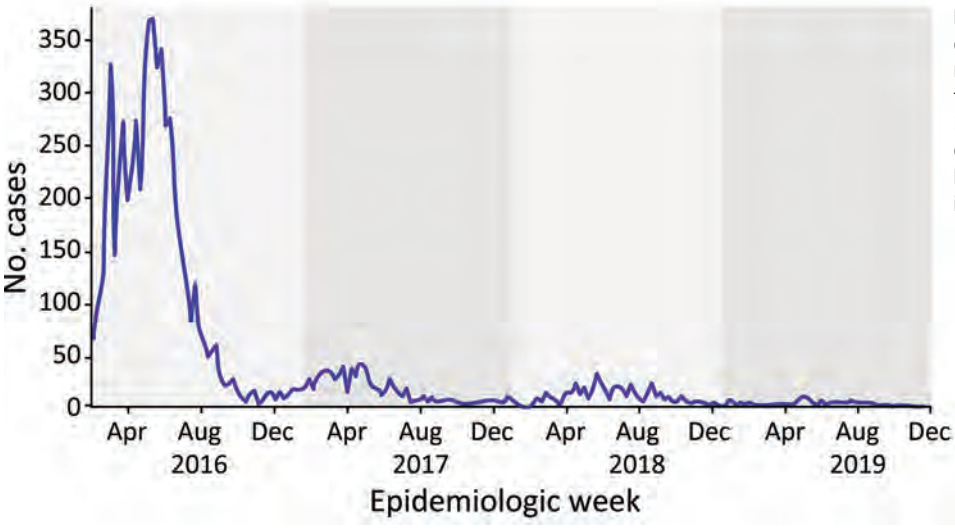

Figure 3. Notified Zika virus cases per week in Manaus municipality, Brazil, 2016–2019, from the Brazilian Ministry of Health. Shading reflects each epidemic year. Data source: https://datasus.saude.gov.br/informacoes-de-saude-tabnet.

reinfection exhibited the highest degree of divergence in terms of the ZIKV genome compared with the acute phase–sequenced samples obtained from the same participants (Figure 5).

Because reports on the genomic characteristics of ZIKV isolates from 2017 onward in northern Brazil are lacking, we conducted a complementary analysis of our own dataset that revealed the presence of these exact genomes associated with reinfection within the population. Of note, we observed the presence of these same genomes in multiple samples from our cohort (Appendix 1 Figure 2), providing strong evidence that the viruses were circulating both temporally and geographically. Finally, to support the assumption of reinfection, we analyzed the levels of ZIKV-NAb at 7, 30, 180, and 360 days after disease onset, assuming that antibody titers would vary among initial infection and reinfection, mirroring rRT-PCR results. We observed that all but 1 participant (ID251069) responded with increased levels of ZIKV-NAb at the convalescent phase of the disease (30 days after symptom onset) (Figure 7). At 180 days after onset we observed a decay in ZIKV-NAb levels at an interval when the primary infection was already cleared. All 3 potentially reinfected participants (ID251069, ID151035, ID251064) responded with a second increase in the levels of ZIKV-NAb at the last interval analyzed (Figure 7), which was preceded by viral RNA redetection in plasma or urine specimens. We also discarded other arbovirus infections as an inducer of ZIKV-NAb response because our study protocol was based on a validated multiplex rRT-PCR and none of the participants tested positive for either dengue or chikungunya virus. Other well-known circulating arboviruses in northern Brazil are Oropouche virus (OROV) (*23*) and yellow fever virus (YFV) (*24*). To date, no documented reports have indicated that OROV is capable of eliciting a ZIKV-specific antibody response. Furthermore, most study participants had prior YFV vaccination, so it is unlikely that they had become infected; thus, we have effectively ruled out YFV as a potential confounding factor in relation to the antibody response associated with ZIKV reinfection. Of note, none of the 3 potential reinfection cases reported symptoms typically associated with ZIKV infection, as confirmed through a comprehensive anamnesis conducted during each study visit at our study clinic. Collectively, our data strongly support the occurrence of reinfection events in at least 3 healthy persons residing in a ZIKV-endemic area in Brazil.

Discussion

Given the number of ZIKV cases registered at the peak of the 2016 epidemic in the northern and other regions of Brazil (*5*), added to the risk for new outbreaks, it is critical to study ZIKV evolution and its potential for adaptation to vertebrate hosts. Moreover, virus persistence may exert high evolutive pressures that contribute to virus evolution and transmission. In our study, we showed that the obtained ZIKV genomes clustered together with other ZIKV Asian strains previously isolated from northern Brazil, suggesting that this strain persisted locally through natural transmission and was kept circulating among humans until August 2019 or later. We also found that the temporal circulation of ZIKV in Manaus started a descending curve, supported by a decreasing number of cases registered after the peak of the epidemic in 2016. Thus, based on a seroprevalence study from northeastern Brazil showing that the ZIKV antibody prevalence reached a peak of 63% from 2015 to 2016 (*25*), in addition to other studies showing a high (>60%) seroprevalence of ZIKV antibodies in the general population (*26*–*28*), we

hypothesize that, within a single year, community immunity was enough to constrain virus circulation. In fact, our findings are consistent with a lower reproduction number (R0) since late 2016 in Salvador (*25*), corroborating mathematical modeling studies showing that ZIKV epidemics would be over in 3 years from its introduction in 2016 (*29*).

Long-term cohort studies can provide longitudinal data on individual virus diversity, virus evolution, clinical symptoms, and immunological outcomes, and so are crucial to better understanding ZIKV natural history. We found evidence of limited virus diversity over time from persistently ZIKV-infected persons, a feature that has also been observed by other independent studies (*18*,*19*). Thus, we can suggest that the evolutionary rates and selection pressures acting on ZIKV are moderate, affecting virus evolution and adaptation to local populations. In fact, similar to a previous report (*30*), we estimated the ZIKV whole-genome evolutionary rate at around 1.18×10^{-3} substitutions/site/year. Arboviruses primarily spread through horizontal transmission between arthropod vectors and vertebrate hosts. As a result, virus evolution is restricted by the need for optimal replication in one host, which may compromise their adaptation in the other (*31*), contributing to the short-term and long-term reduced number of adaptative mutations observed. In addition, various factors, including the

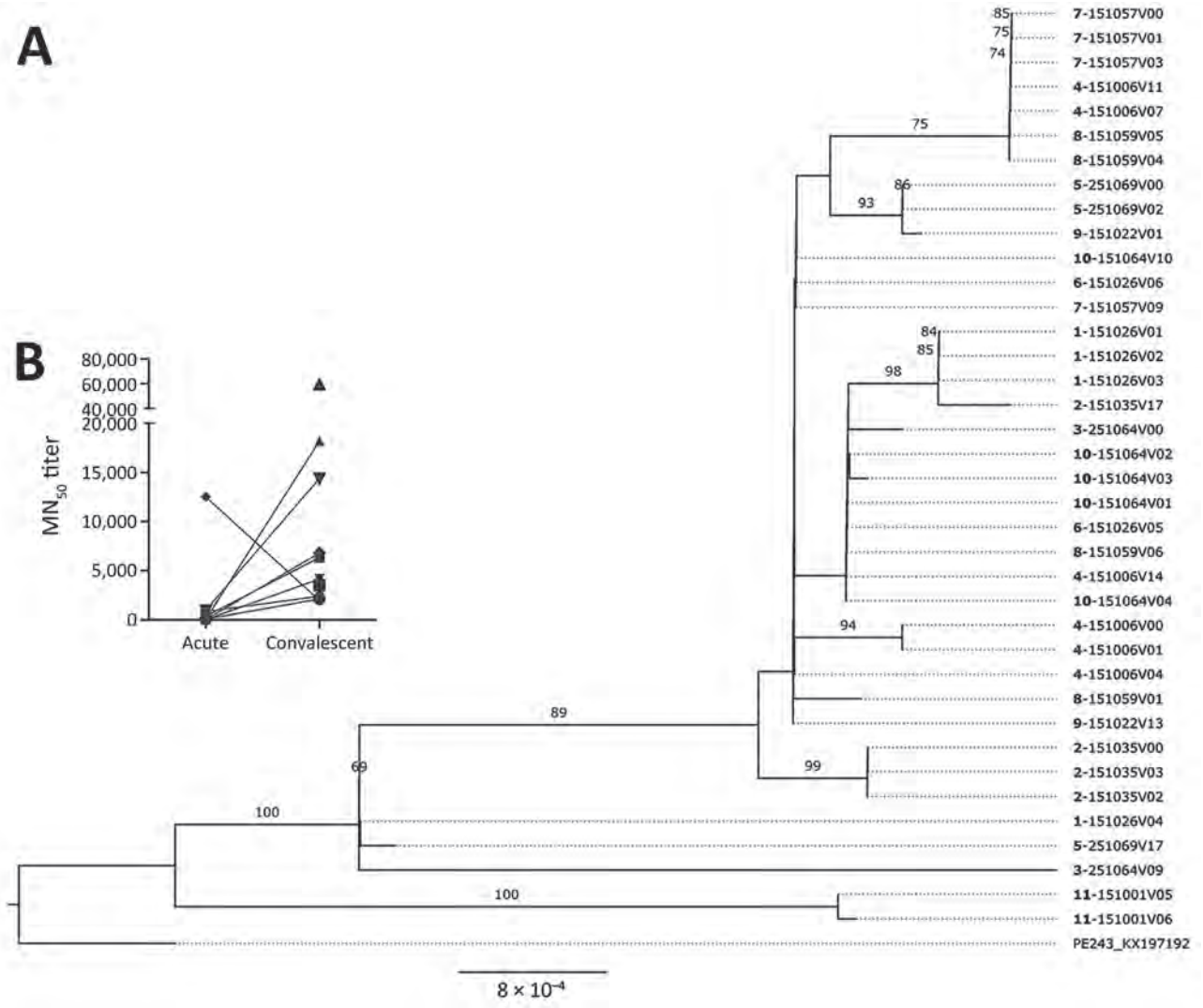

Figure 4. Phylogenetic analysis of study participants persistently infected with Zika virus, Brazil. A) Maximum-likelihood phylogenetic tree of persistent samples. The phylogenetic tree shows all 10 participants with confirmed persistent infection. Boldface indicates participant identification numbers; visit numbers (V) are indicated. Multiple identification numbers represent multiple genomes obtained from the same participant at different time points. Scale bar indicates number of nucleotide substitutions per site. Numbers on the branches indicate Shimodaira–Hasegawa approximate likelihood ratio test after 1,000 replicates. B) Neutralizing antibody titers from acute and convalescent samples, as analyzed from persistently infected participants. MN_{50}, 50% microneutralization.

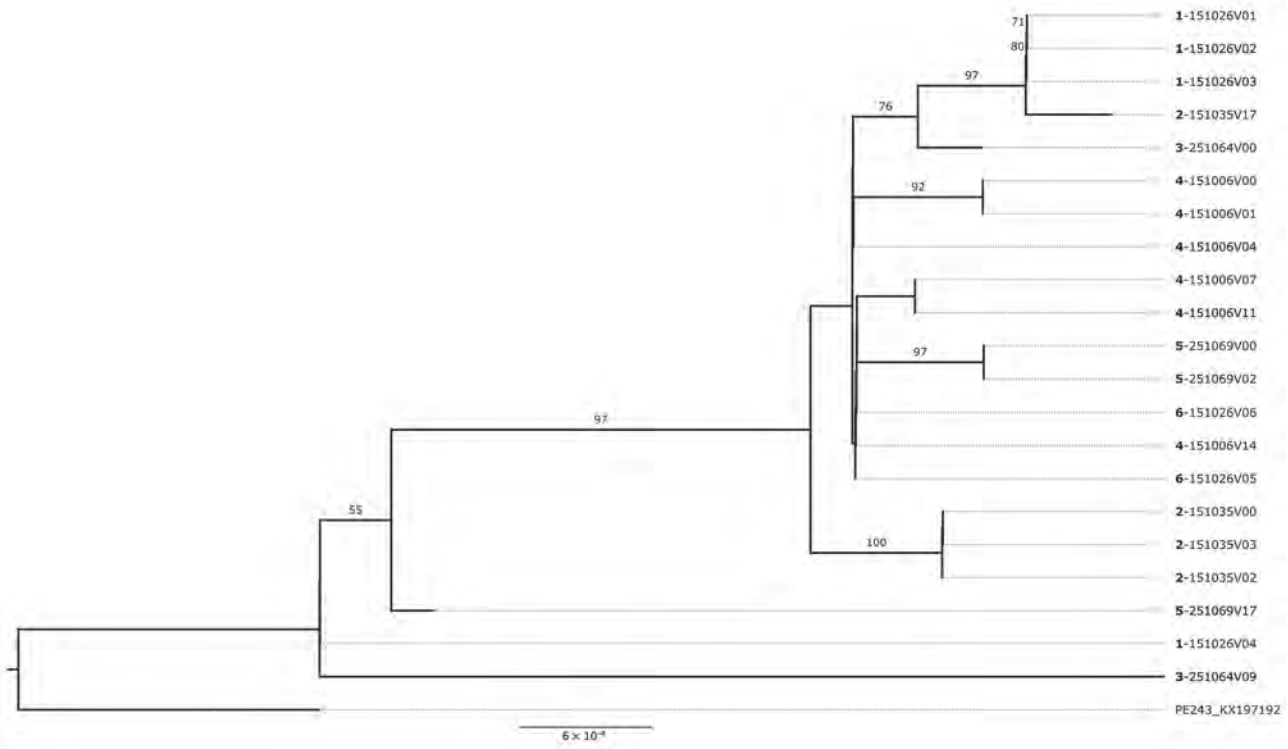

Figure 5. Maximum-likelihood phylogenetic tree supporting Zika virus reinfection among study participants in northern Brazil. The tree shows the 5 participants with divergent samples in which coinfection by different ZIKV genomes was inferred by phylogenetic reconstruction. Divergent samples from the same participant were grouped separately in the tree. Boldface indicates participant identification numbers; visit numbers (V) are indicated. Scale bar indicates number of nucleotide substitutions per site. Numbers on the branches indicate Shimodaira–Hasegawa approximate likelihood ratio test after 1,000 replicates.

short duration and low viremia observed in naturally infected persons (*32*), contribute to limiting ZIKV diversity. Consequently, our findings indicate that ZIKV displayed a relatively stable genome evolution over time and did not undergo rapid changes or diversification during the epidemic in northern Brazil.

The most notable finding of our study is the identification of reinfection events, which is highly intriguing. Given that the ZIKV epidemic in Brazil originated from a single virus strain, and combined with the observation that the virus has remained relatively stable over time, tracking reinfections becomes a challenging task. Complicating matters further, most infections are asymptomatic or cause only mild symptoms, such as fever, rash, and itching (*33*). As a result, persons who have been potentially reinfected may have gone unnoticed, especially considering that mild symptoms often do not prompt persons to seek medical attention. Although reinfections are extremely difficult to confirm when there are only very similar phylogenetically strains causing an outbreak, we detected divergent viruses in ZIKV-infected persons who provided longitudinal samples, which suggests a subsequent and distinct infection event.

Monitoring community virus circulation plays a crucial role in confirming infections within a population. As extensively explored for several other viruses (*34*), mapping diversity in a community can provide valuable information for confirming infection cases and understanding the dynamics of an outbreak. Thus, by sequencing viral genomes, it is possible to identify an specific strain or variant of the virus present in an individual or a community (*35*). Despite detecting the presence of these same reinfection-associated ZIKV genomes in other participants of our cohort, temporally and geographically confirming the circulation of these genomes in that population, there is a notable absence of independent studies validating the presence of these genomes at the time we detected potential reinfection cases. Most of the investigations from other groups were conducted during the early stages of the ZIKV outbreak; therefore, the literature lacks reports that describe the characteristics of the viruses circulating from late 2017 onward.

Confirmation of reinfection events based solely on molecular detection may introduce uncertainties because of the possibility of cross-contamination during sample processing. To address this concern, we

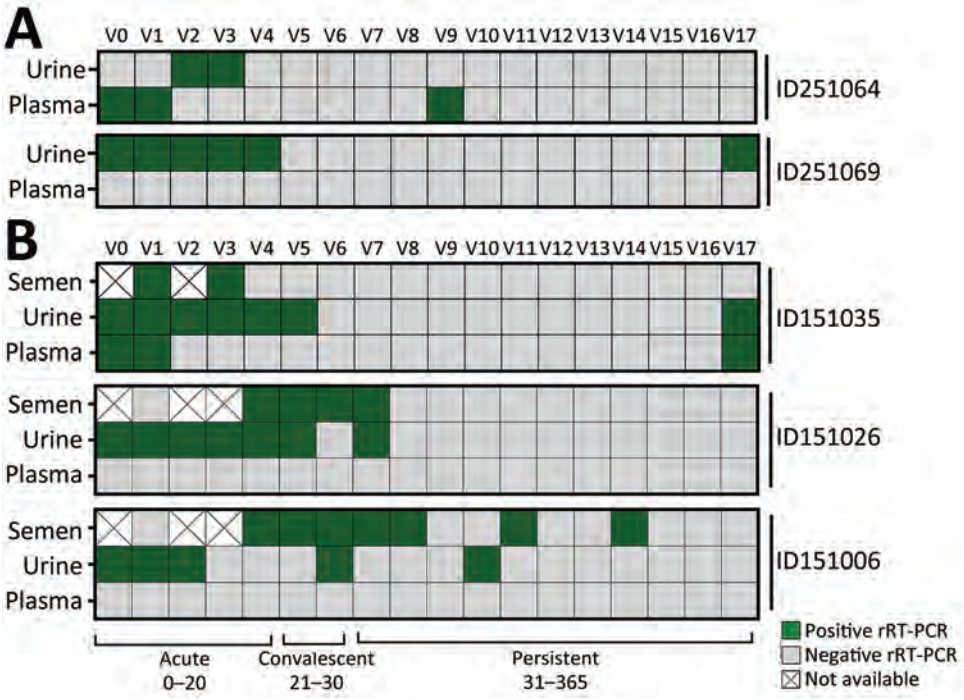

Figure 6. Zika virus rRT-PCR results from plasma, urine, and semen (when applicable) specimens supporting reinfection among female (A) and male (B) study participants in northern Brazil. Each square represents an analyzed specimen according to the schedule from study visits (Table 2). ID, participant identification; r-RT-PCR, real-time reverse transcription PCR; V, visit number.

conducted an assessment of ZIKV antibody response. By measuring the levels of ZIKV-NAb over time, we can add a deeper understanding of ZIKV infection dynamics, immune response effectiveness, and the potential for future reinfections (*36*). Here, we observed that 3 persons responded with a second increase in ZIKV-NAb levels, which was temporarily associated with rRT-PCR positivity at a late time point after the initial infection. We discarded other arbovirus infections as a cause of secondary ZIKV-NAb increase because all

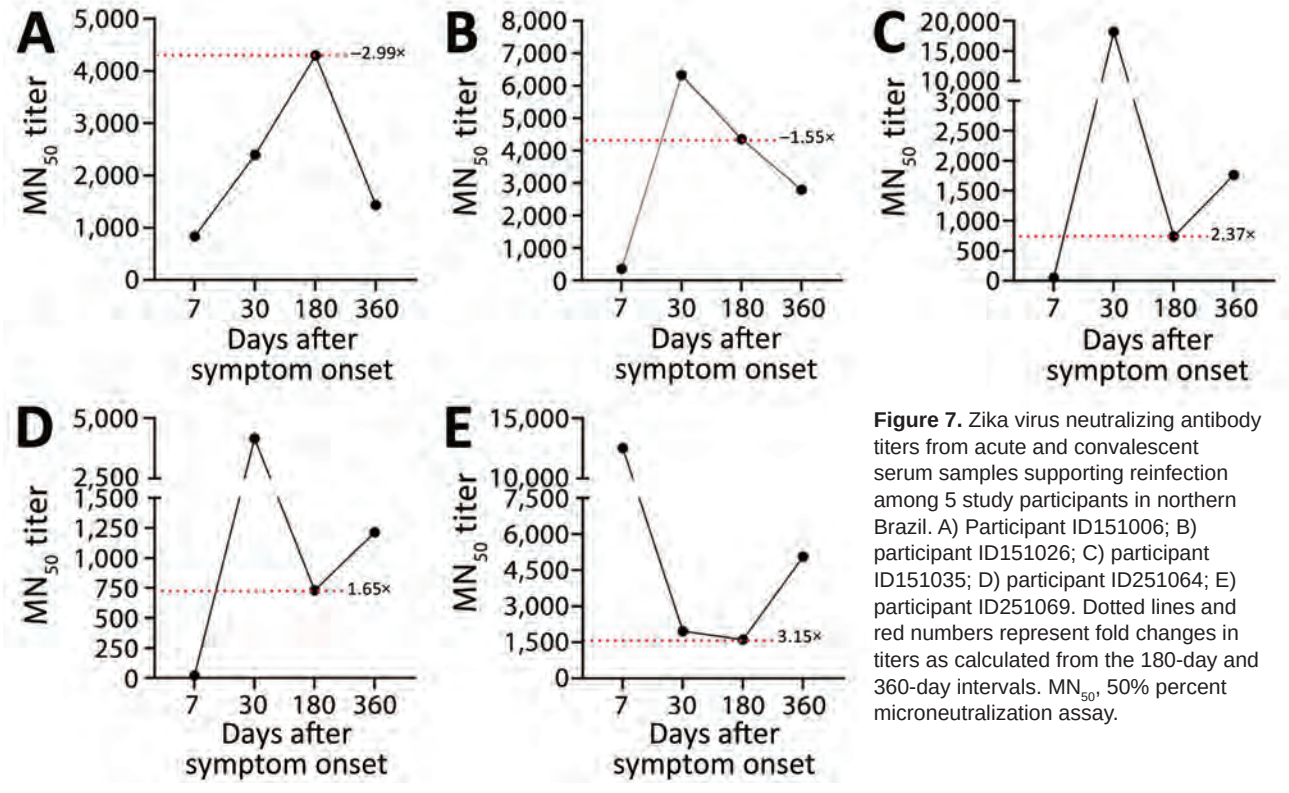

Figure 7. Zika virus neutralizing antibody titers from acute and convalescent serum samples supporting reinfection among 5 study participants in northern Brazil. A) Participant ID151006; B) participant ID151026; C) participant ID151035; D) participant ID251064; E) participant ID251069. Dotted lines and red numbers represent fold changes in titers as calculated from the 180-day and 360-day intervals. MN_{50}, 50% percent microneutralization assay.

the participants from our cohort were tested in a multiplex rRT-PCR and none of them were positive for dengue or chikungunya virus. We also discarded YFV infection and YFV vaccination because our study participants were previously vaccinated against YFV. We also assumed that these reinfection events were very mild, mostly manifesting as an asymptomatic disease, because no symptoms were reported.

Our findings hold significant implications for public health, epidemiology, clinical practice, and diagnostics. However, the frequency of reinfections during the latest ZIKV outbreaks remains uncertain. Our study emphasizes the critical role of ongoing genomic surveillance in viral infections to enhance public health interventions. Therefore, we underscore the necessity of implementing continuous surveillance strategies, which are vital for monitoring the evolutionary changes of viruses over time and gaining a comprehensive understanding of arbovirus diversity.

Acknowledgments

We thank the ZIKABRA Study Team: André Luiz de Abreu, Ximena Pamela Diaz Bermudez, Patrícia Brasil, Carlos Alexandre Antunes Brito, Tatiana Jorge Fernandes, Ndema Habib, Marcus Vinicius Guimarães Lacerda, Cristina Pimenta, Lydie Trautman.

Complete data set is available upon request. All the ZIKV genomes generated in this study are publicly available at the European Nucleotide Archive (https://www.ebi.ac.uk/ena/browser/home) under project no. PRJEB63302.

The research leading to these results received funding from the Wellcome Trust (grant no. 206522/Z/17/Z); UNDP-UNFPA-UNICEF-WHO-World Bank Special Programme of Research, Development and Research Training in Human Reproduction (HRP), a cosponsored program executed by the World Health Organization (WHO) (WHO-SRH/HRP; grant nos. 2017/720873-0 and 2017/731359-0); Brazilian Ministry of Health (Convênio 837059/2016, Processo 25000162039201616); US National Institute of Allergy and Infectious Diseases of the National Institutes of Health: (award no. R21AI139777); and the Henry M. Jackson Foundation for the Advancement of Military Medicine (prime award no. W81XWH-18-2-0040). G.L.W. is supported by the Conselho Nacional de Desenvolvimento Científico e Tecnológico through their productivity research fellowships (no. 303902/2019-1). The funders had no role in the study design, data collection, analysis, the decision to publish, or the preparation of the manuscript.

The authors alone are responsible for the views expressed in this article and they do not necessarily represent the views, decisions, or policies of the institutions with which they are affiliated.

Author contributions: A.M.B.F., M.G., V.F., L.C.J.A., L.C.M., and C.D. performed sequencing assays and data analysis, M.C.C., C.H.A.B.-M., and A.M-N. laboratory procedures and clinical data collection; G.A.C., E.K., and N.B. performed data analysis and clinical support; R.L.B. performed microneutralization assays, K.M. performed study supervision and data analysis, G.L.W. performed phylogenetic analysis and manuscript editing, R.F.O.F. conceived and supervised the study and wrote the manuscript. All authors reviewed and approved the final version of the manuscript. The authors declare they have no conflict of interests, and the funders had no role in study design, data collection, analysis, decision to publish, or preparation of the manuscript.

About the Author

Dr. Castilho has a PhD in tropical infectious diseases and works at the Tropical Medicine Foundation Doctor Heitor Vieira Dourado, Manaus, Brazil. Her research interests include arbovirus and epidemiology.

References

1. Kuno G, Chang GJ. Full-length sequencing and genomic characterization of Bagaza, Kedougou, and Zika viruses. Arch Virol. 2007;152:687–96. https://doi.org/10.1007/s00705-006-0903-z
2. Bogoch II, Brady OJ, Kraemer MUG, German M, Creatore MI, Kulkarni MA, et al. Anticipating the international spread of Zika virus from Brazil. Lancet. 2016;387:335–6. https://doi.org/10.1016/S0140-6736(16)00080-5
3. Miranda-Filho DB, Martelli CM, Ximenes RA, Araújo TV, Rocha MA, Ramos RC, et al. Initial description of the presumed congenital Zika syndrome. Am J Public Health. 2016;106:598–600. https://doi.org/10.2105/AJPH.2016.303115
4. Mlakar J, Korva M, Tul N, Popović M, Poljšak-Prijatelj M, Mraz J, et al. Zika virus associated with microcephaly. N Engl J Med. 2016;374:951–8. https://doi.org/10.1056/NEJMoa1600651
5. Yakob L. Zika virus after the public health emergency of international concern period, Brazil. Emerg Infect Dis. 2022;28:837–40. https://doi.org/10.3201/eid2804.211949
6. Paz-Bailey G, Rosenberg ES, Doyle K, Munoz-Jordan J, Santiago GA, Klein L, et al. Persistence of Zika virus in body fluids—final report. N Engl J Med. 2018;379:1234–43. https://doi.org/10.1056/NEJMoa1613108
7. Barzon L, Percivalle E, Pacenti M, Rovida F, Zavattoni M, Del Bravo P, et al. Virus and antibody dynamics in travelers with acute Zika virus infection. Clin Infect Dis. 2018;66:1173–80. https://doi.org/10.1093/cid/cix967
8. Beaver JT, Lelutiu N, Habib R, Skountzou I. Evolution of two major Zika virus lineages: implications for pathology, immune response, and vaccine development. Front Immunol. 2018;9:1640. https://doi.org/10.3389/fimmu.2018.01640
9. Faria NR, Azevedo RDSDS, Kraemer MUG, Souza R, Cunha MS, Hill SC, et al. Zika virus in the Americas: early epidemiological and genetic findings. Science. 2016;352:345–9. https://doi.org/10.1126/science.aaf5036

10. Tang H, Hammack C, Ogden SC, Wen Z, Qian X, Li Y, et al. Zika virus infects human cortical neural progenitors and attenuates their growth. Cell Stem Cell. 2016;18:587–90. https://doi.org/10.1016/j.stem.2016.02.016
11. Nguyen HN, Qian X, Song H, Ming GL. Neural stem cells attacked by Zika virus. Cell Res. 2016;26:753–4. https://doi.org/10.1038/cr.2016.68
12. Andino R, Domingo E. Viral quasispecies. Virology. 2015;479-480:46–51. https://doi.org/10.1016/j.virol.2015.03.022
13. Miura M, Maekawa S, Takano S, Komatsu N, Tatsumi A, Asakawa Y, et al. Deep-sequencing analysis of the association between the quasispecies nature of the hepatitis C virus core region and disease progression. J Virol. 2013;87:12541–51. https://doi.org/10.1128/JVI.00826-13
14. Vignuzzi M, Stone JK, Arnold JJ, Cameron CE, Andino R. Quasispecies diversity determines pathogenesis through cooperative interactions in a viral population. Nature. 2006;439:344–8. https://doi.org/10.1038/nature04388
15. Calvet GA, Kara EO, Giozza SP, Bôtto-Menezes CHA, Gaillard P, de Oliveira Franca RF, et al.; ZIKABRA Study Team. Study on the persistence of Zika virus (ZIKV) in body fluids of patients with ZIKV infection in Brazil. BMC Infect Dis. 2018;18:49. https://doi.org/10.1186/s12879-018-2965-4
16. Calvet GA, Kara EO, Landoulsi S, Habib N, Bôtto-Menezes CHA, Franca RFO, et al.; ZIKABRA Study Team. Cohort profile: study on Zika virus infection in Brazil (ZIKABRA study). PLoS One. 2021;16:e0244981. https://doi.org/10.1371/journal.pone.0244981
17. Calvet GA, Kara EO, Bôtto-Menezes CHA, Castilho MDC, Franca RFO, Habib N, et al. Detection and persistence of Zika virus in body fluids and associated factors: a prospective cohort study. Sci Rep. 20236;13:21557. https://doi.org/10.1038/s41598-023-48493-8
18. Oliveira DBL, Durigon GS, Mendes EA, Ladner JT, Andreata-Santos R, Araujo DB, et al. Persistence and intra-host genetic evolution of Zika virus infection in symptomatic adults: a special view in the male reproductive system. Viruses. 2018;10:615. https://doi.org/10.3390/v10110615
19. Holmes EC. Patterns of intra- and interhost nonsynonymous variation reveal strong purifying selection in dengue virus. J Virol. 2003;77:11296–8. https://doi.org/10.1128/JVI.77.20.11296-11298.2003
20. Bôtto-Menezes CHA, Neto AM, Calvet GA, Kara EO, Lacerda MVG, Castilho MDC, et al.; ZIKABRA Study Team. Zika virus in rectal swab samples. Emerg Infect Dis. 2019;25:951–4. https://doi.org/10.3201/eid2505.180904
21. Quick J, Grubaugh ND, Pullan ST, Claro IM, Smith AD, Gangavarapu K, et al. Multiplex PCR method for MinION and Illumina sequencing of Zika and other virus genomes directly from clinical samples. Nat Protoc. 2017;12:1261–76. https://doi.org/10.1038/nprot.2017.066
22. Modjarrad K, Lin L, George SL, Stephenson KE, Eckels KH, De La Barrera RA, et al. Preliminary aggregate safety and immunogenicity results from three trials of a purified inactivated Zika virus vaccine candidate: phase 1, randomised, double-blind, placebo-controlled clinical trials. Lancet. 2018;391:563–71. https://doi.org/10.1016/S0140-6736(17)33106-9
23. Vasconcelos HB, Azevedo RS, Casseb SM, Nunes-Neto JP, Chiang JO, Cantuária PC, et al. Oropouche fever epidemic in Northern Brazil: epidemiology and molecular characterization of isolates. J Clin Virol. 2009;44:129–33. https://doi.org/10.1016/j.jcv.2008.11.006
24. Possas C, Lourenço-de-Oliveira R, Tauil PL, Pinheiro FP, Pissinatti A, Cunha RVD, et al. Yellow fever outbreak in Brazil: the puzzle of rapid viral spread and challenges for immunisation. Mem Inst Oswaldo Cruz. 2018;113:e180278. https://doi.org/10.1590/0074-02760180278
25. Netto EM, Moreira-Soto A, Pedroso C, Höser C, Funk S, Kucharski AJ, et al. High Zika virus seroprevalence in Salvador, northeastern Brazil limits the potential for further outbreaks. MBio. 2017;8:e01390-17. https://doi.org/10.1128/mBio.01390-17
26. Duffy MR, Chen TH, Hancock WT, Powers AM, Kool JL, Lanciotti RS, et al. Zika virus outbreak on Yap Island, Federated States of Micronesia. N Engl J Med. 2009;360:2536–43. https://doi.org/10.1056/NEJMoa0805715
27. Castanha PMS, Souza WV, Braga C, Araújo TVB, Ximenes RAA, Albuquerque MFPM, et al.; Microcephaly Epidemic Research Group. Perinatal analyses of Zika- and dengue virus–specific neutralizing antibodies: a microcephaly case-control study in an area of high dengue endemicity in Brazil. PLoS Negl Trop Dis. 2019;13:e0007246. https://doi.org/10.1371/journal.pntd.0007246
28. Aubry M, Teissier A, Huart M, Merceron S, Vanhomwegen J, Roche C, et al. Zika virus seroprevalence, French Polynesia, 2014–2015. Emerg Infect Dis. 2017;23:669–72. https://doi.org/10.3201/eid2304.161549
29. Ferguson NM, Cucunubá ZM, Dorigatti I, Nedjati-Gilani GL, Donnelly CA, Basáñez MG, et al. Countering the Zika epidemic in Latin America. Science. 2016;353:353–4. https://doi.org/10.1126/science.aag0219
30. Faria NR, Quick J, Claro IM, Thézé J, de Jesus JG, Giovanetti M, et al. Establishment and cryptic transmission of Zika virus in Brazil and the Americas. Nature. 2017;546:406–10. https://doi.org/10.1038/nature22401
31. Coffey LL, Vasilakis N, Brault AC, Powers AM, Tripet F, Weaver SC. Arbovirus evolution in vivo is constrained by host alternation. Proc Natl Acad Sci U S A. 2008;105:6970–5. https://doi.org/10.1073/pnas.0712130105
32. Fontaine A, de Laval F, Belleoud D, Briolant S, Matheus S. Duration of Zika viremia in serum. Clin Infect Dis. 2018;67:1143–4. https://doi.org/10.1093/cid/ciy261
33. Musso D, Gubler DJ. Zika virus. Clin Microbiol Rev. 2016;29:487–524. https://doi.org/10.1128/CMR.00072-15
34. Roux S, Emerson JB, Eloe-Fadrosh EA, Sullivan MB. Benchmarking viromics: an in silico evaluation of metagenome-enabled estimates of viral community composition and diversity. PeerJ. 2017;5:e3817. https://doi.org/10.7717/peerj.3817
35. Grubaugh ND, Ladner JT, Lemey P, Pybus OG, Rambaut A, Holmes EC, et al. Tracking virus outbreaks in the twenty-first century. Nat Microbiol. 2018;4:10–9. https://doi.org/10.1038/s41564-018-0296-2
36. Robbiani DF, Bozzacco L, Keeffe JR, Khouri R, Olsen PC, Gazumyan A, et al. Recurrent potent human neutralizing antibodies to Zika virus in Brazil and Mexico. Cell. 2017;169:597–609.e11. https://doi.org/10.1016/j.cell.2017.04.024

Address for correspondence: Rafael F.O. Franca, Fundacao Oswaldo Cruz Virology and Experimental Therapy, Av. Prof. Moraes Rego s/n Recife/PE 50740-465, Recife 50740465, Brazil; email: rafael.franca@fiocruz.br, rafaelfreitasfranca@gmail.com

Residual Immunity from Smallpox Vaccination and Possible Protection from Mpox, China

Yu Huang,[1] Li Guo,[1] Yanan Li,[1] Lili Ren,[1] Jiqin Nie,[1] Fengwen Xu,[1] Tingxuan Huang, Jingchuan Zhong, Zhangling Fan, Yin Zhang, Yu Xie, Qiao Zhang, Shan Mei, Yan Xiao, Xinming Wang, Liuhui Xu, Fei Guo,[2] Jianwei Wang[2]

Among persons born in China before 1980 and tested for vaccinia virus Tiantan strain (VVT), 28.7% (137/478) had neutralizing antibodies, 71.4% (25/35) had memory B-cell responses, and 65.7% (23/35) had memory T-cell responses to VVT. Because of cross-immunity between the viruses, these findings can help guide mpox vaccination strategies in China.

On July 23, 2022, the World Health Organization declared the global mpox outbreak to be a public health emergency of international concern (https://www.who.int/europe/news/item/23-07-2022-who-director-general-declares-the-ongoing-monkeypox-outbreak-a-public-health-event-of-international-concern). No specific treatment is currently approved for mpox. Vaccines such as JYNNEOS (Bavarian Nordic, https://www.bavarian-nordic.com) and ACAM2000 (Emergent BioSolutions Inc., https://www.emergentbiosolutions.com) are available for preexposure protection from mpox (*1*), and tecovirimat can be used for patients who are at risk for severe disease (*2*).

Vaccinia virus Tiantan strain (VTT) was historically used for vaccines in the smallpox virus eradication campaign in China. Given the high level of sequence homology among their surface proteins, smallpox vaccination provided ≈85% protection against mpox (*3*). Because the World Health Organization declared that smallpox had been eradicated and routine use of vaccinia vaccine was terminated in most countries by 1980–1981, most persons born after 1980 do not have vaccinia virus–elicited immunity. Vaccinia-derived protection wanes in the vaccinated population over time, which may lead to an increase in susceptibility to monkeypox virus (MPXV) infection because of cross-immunity between the 2 viruses.

After the first mpox case imported from Europe to mainland China on September 14, 2022 (*4*), investigation of the level of residual VTT-specific immunity in the population of China became pressing, as researchers assessed susceptibility to mpox and guided development of appropriate protective strategies. Different patterns of residual immunity against vaccinia suggest different strategies in responding to mpox transmission. However, levels of residual immunity to poxviruses in the population in China are not well assessed. We measured VTT-specific humoral and cellular immune responses in a diverse population born during 1930–2008 in China.

Author affiliations: NHC Key Laboratory of Systems Biology of Pathogens, National Institute of Pathogen Biology, Chinese Academy of Medical Sciences & Peking Union Medical College, Beijing, China (Y. Huang, L. Guo, Y. Li, L. Ren, J. Nie, F. Xu, T. Huang, J. Zhong, Z. Fan, Y. Zhang, Y. Xie, Q. Zhang, S. Mei, Y. Xiao, X. Wang, L. Xu, F. Guo, Beijing (J. Wang); Key Laboratory of Respiratory Disease Pathogenomics, Chinese Academy of Medical Sciences, Beijing (L. Guo, L. Ren Beijing (J. Wang); National Institute of Pathogen Biology and Center for AIDS Research, Chinese Academy of Medical Sciences and Peking Union Medical College, Beijing (Y. Huang, F. Xu, Z. Fan, Y. Xie, S. Mei, F. Guo); Christophe Mérieux Laboratory, National Institute of Pathogen Biology, Chinese Academy of Medical Sciences and Peking Union Medical College, Beijing (L. Guo, Y. Li, L. Ren, J. Nie, T. Huang, J. Zhong, Y. Zhang, Q. Zhang, Y. Xiao, X. Wang, L. Xu, J. Wang); Key Laboratory of Pathogen Infection Prevention and Control (Ministry of Education), State Key Laboratory of Respiratory Health and Multimorbidity, National Institute of Pathogen Biology, Chinese Academy of Medical Sciences and Peking Union Medical College, Beijing (L. Guo, L. Ren, F. Guo, National Key Laboratory of Immunity and Inflammation, Beijing (J. Wang))

DOI: https://doi.org/10.3201/eid3002.230542

[1]These first authors contributed equally to this article.

[2]These senior authors contributed equally to this article.

Table 1. Characteristics of 1,070 participants in a cross-sectional cohort study to determine IgG titers against vaccinia virus Tiantan strain, China*

Characteristic	Decade of birth, no. (%)							
	1930–1939	1940–1949	1950–1959	1960–1969	1970–1979	1980–1989	1990–2008	Total
Overall	106 (9.91)	104 (9.72)	76 (7.10)	95 (8.88)	97 (9.07)	84 (7.85)	508 (47.48)	1,070 (100)
Sex								
M	63 (5.89)	61 (5.70)	39 (3.64)	53 (4.95)	40 (3.74)	42 (3.93)	285 (26.64)	583 (54.49)
F	43 (4.02)	43 (4.02)	37 (3.46)	42 (3.93)	57 (5.33)	42 (3.93)	223 (20.84)	487 (45.51)

*Participants lived in Beijing, Shanxi Province, Heilongjiang Province, Hubei Province, or Shenzhen..

The Study

In this cross-sectional cohort study, we collected blood specimens from 1,070 healthy donors who lived in Beijing, Shanxi Province, Heilongjiang Province, Hubei Province, or Shenzhen during regular health check-ups. Among the participants (Table 1), 478 were born during 1930–1979 and 592 were born during 1980–2008; ages ranged from 1 month to 90 years. The study was approved by the institutional review boards of the Chinese Academy of Medical Sciences' Institute of Pathogen Biology (approval no. 2013-IPB-03, IPB-2021-15).

We tested serum samples from all participants to determine IgG titers against VTT by using ELISA. We performed a Gaussia luciferase-based vaccinia neutralization assay to determine the presence of neutralizing antibodies (NAbs). We performed memory B-cell and memory T-cell enzyme-linked immunospot (ELISpot) assays (Charles River Laboratories, https://www.criver.com) by using cryopreserved peripheral blood mononuclear cells (PBMCs). Because of insufficient PBMC samples, we evaluated memory B- and T-cell responses in a subgroup of the enrolled participants (Appendix Figure 1, https://wwwnc.cdc.gov/EID/article/30/2/23-0542-App1.pdf).

Overall VTT seropositivity was 50.2% (240/478) in participants born before 1980. Persons born during 1970–1979 had the lowest seropositivity, 29.9% (29/97), compared with 61.3% (65/106 [p<0.0001]) among persons born during 1930–1939, 57.7% (60/104 [p<0.0001]) among persons born during 1940–1949, 50.0% (38/76 [p = 0.0042]) among persons born during 1950–1959, 50.5% (48/95 [p = 0.0018]) among persons born during 1960–1969. By comparison, ≈4.8% (4/84) participants born during 1980–1989 had VTT-specific IgG, and VTT-specific IgG was not detectable in persons born after 1990 (Figure 1, panel A). The VTT-specific IgG titers were not significantly different among participants born during 1930–1939, 1940–1949, 1950–1959, and 1960–1969 (p = 0.11), but all were higher than in persons born during 1970–1979 (Appendix Figure 2, panel A).

We examined distribution of NAb levels in relation to year of birth (Table 2; Figure 1, panel B). Of the 478 serum samples from persons born before 1980, most (341 [71.3%]) had an NAb titer of <1/4. Of the remaining samples, NAb titers were 1/4 for 62 (13.0%), 1/8 for 51 (10.7%), 1/16 for 15 (3.1%), and 1/32 for 9 (1.9%), suggesting the lack or low titers of NAb against VTT. VTT NAbs were detectable in 35.8% (38/106) of persons born during 1930–1939, 33.7% (35/104) born during 1940 –1949, 22.4% (17/76) born during 1950–1959, 28.4% (27/95) born during 1960–1969, and 20.6% (20/97) born during 1970–1979 but were detectable in only 3.6% (3/84) born during 1980–1989 (≥1/4) (Appendix Figure 2, panel B). We observed a significant correlation between NAb and IgG titers in persons born before 1990 (Spearman r = 0.54; p<0.0001) (Appendix Figure 2, panel C).

We measured VTT-specific memory B-cell responses in 45 participants whose PBMCs were isolated successfully (Appendix Figure 3). Approximately 71.4% (25/35) of persons born before 1980 showed VTT-specific memory B-cell responses; positivity

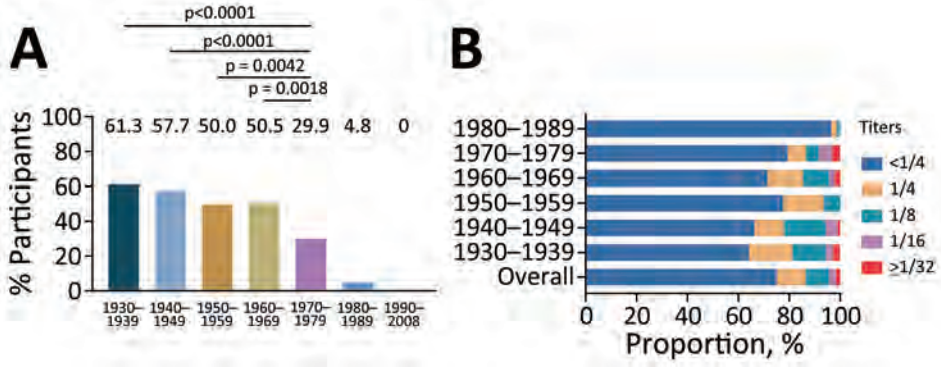

Figure 1. Serum IgG and neutralizing antibody responses against vaccinia virus Tiantan strain (VTT) among 1,070 participants in a cross-sectional cohort study, China. A) Seropositivity of VTT-specific IgG by birth cohort in 1,070 persons born during 1930–2008, conducted with χ^2 or Fisher exact test as appropriate. B) Prevalence of neutralizing antibody by birth cohort in 562 persons born before 1990.

Table 2. Neutralizing antibody titers against vaccinia virus Tiantan strain in persons born during 1930–1979, by birth cohort, China*

Decade of birth	Neutralizing antibody titers, no. (%)				
	<1/4	1/4	1/8	1/16	≥1/32
1930–1939, n = 106	68 (64.2)	18 (17.0)	14 (13.2)	3 (2.8)	3 (2.8)
1940–1949, n = 104	69 (66.3)	12(11.5)	17 (16.3)	5 (4.8)	1 (0.96)
1950–1959, n = 76	59 (77.6)	12 (15.8)	5 (6.6)	0 (0)	0 (0)
1960–1969, n = 95	68 (71.6)	13 (13.7)	10 (10.5)	2 (2.1)	2 (2.1)
1970–1979, n = 97	77 (79.4)	7 (7.2)	5 (5.2)	5 (5.2)	3 (3.1)
Overall, N = 478	341 (71.3)	62 (13.0)	51 (10.7)	15 (3.1)	9 (1.9)

*Participants lived in Beijing, Shanxi Province, Heilongjiang Province, Hubei Province, or Shenzhen.

across the 4 birth decades was 80% (4/5) for 1940–1949, 70% (7/10) for 1950–1959, 80% (8/10) for 1960–1969, and 60% (6/10) for 1970–1979. PBMCs of all persons born after 1980 were negative for VTT-specific memory B-cells (Figure 2, panel A). We observed no significant correlations between VTT-specific memory B-cell magnitude and VTT IgG (Appendix Figure 4, panel A) or NAb (Appendix Figure 4, panel B) titers.

We further evaluated interferon-γ (IFN-γ) responses to VTT in the same 45 participants (Appendix Figure 5). We detected VTT-specific memory T-cell responses in 65.7% (23/35) of persons across the 4 birth decades, distributed as 80% (4/5) for 1940–1949, 50% (5/10) for 1950–1959, 70% (7/10) for 1960–1969, and 70% (7/10) for 1970–1979. In contrast, T-cell IFN-γ responses were below the detection limit in the 10 persons born after 1980 (Figure 2, panel B). We observed no correlations between the magnitude of VTT-specific memory T-cell responses and IgG (Appendix Figure 6, panel A) or NAb (Appendix Figure 6, panel B) titers.

As a control, we tested for influenza virus and Epstein Barr virus–specific memory T-cell responses, which we detected in persons born during 1940–2008 (Appendix Figure 7, panel A). Among the 35 persons born before 1980 and found to be positive for specific cellular immune responses, 28 (80%) had no detectable NAb (<1/4). However, 67.9% (19/28) persons showed IFN-γ responses in the ELISpot assay (Appendix Figure 7, panel B).

Conclusions

We evaluated residual VTT immunity in the population of China across >5 birth decades. Our and other studies suggest that antibody responses against vaccinia virus after vaccination can be long-lived (*5*–*7*). We observed a low prevalence (28.7% [137/478]) of NAb against VTT in persons born before 1980, which is consistent with a previous study in the population of China (*8*). Our data demonstrate that 71.4% of the 35 tested participants

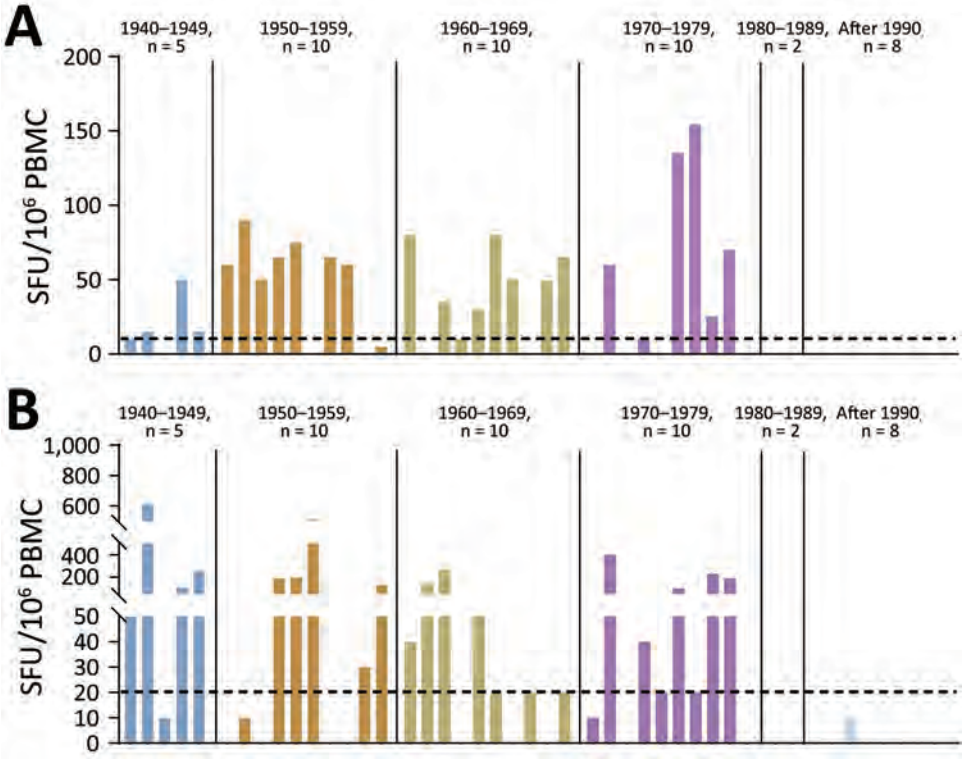

Figure 2. Vaccinia virus–specific memory B- and T-cell responses among 45 participants in a cross-sectional cohort study to determine IgG titers against vaccinia virus Tiantan strain (VTT), China. A) Magnitude of memory B-cell responses against VTT for each person. B) Magnitude of interferon-γ T-cell responses against VTT for each person. Dotted lines indicate detection limit of assay. PBMC, peripheral blood mononuclear cells; SFU, spot-forming units.

born before 1980 had VTT-specific memory B-cell responses. Those memory B-cells can still rapidly differentiate into plasma cells and produce protective antibodies upon reinfection (*9*).

Smallpox vaccine–induced antibodies may protect against MPXV (*10*). Approximately 65.7% of the 35 participants born before 1980 that we tested had VTT-specific T-cell responses, which is consistent with previous reports that T-cell responses against vaccinia virus were maintained up to 51–75 years postimmunization and had a half-life of 8–15 years (*5*,*7*).

One limitation of our study is that it is a cross-sectional study. In addition, no information regarding smallpox vaccination or smallpox infection was available for the persons enrolled. Moreover, a small number of samples were tested for T- and B-memory cell responses.

In summary, we evaluated residual immune responses to VTT in the population of China and found that >65% of 35 tested persons born before 1980 showed memory B- and T-cell responses. However, the prevalence and NAb titers against VTT were low in this population. To protect the population from infection by MPXV and any other related pathogenic orthopoxviruses, safe and effective vaccines will be needed for all age groups.

Acknowledgments

We are grateful to all the persons who participated in this study and their families.

This study was funded by the National Natural Science Foundation of China (grant nos. 81930063, 82241075, 82271802, 82072288, and 32200718), the Science Fund for Creative Research Groups of the National Natural Science Foundation of China (grant no. 82221004), the National Key R&D program of China (grant no. 2022YFE0203100), the Chinese Academy of Medical Sciences Innovation Fund for Medical Sciences (grant nos. 2021-I2M-1-038 and 2021-I2M-1-047), and the Special Research Fund for Central Universities, Peking Union Medical College (grant no. 3332021092).

Author contributions: J.W. and F.G. conceived and designed the study, had full access to all the data in the study, and take responsibility for the integrity of the data and the accuracy of the data analysis. Y.H., L.G., F.X., and S.M. did the literature review. L.G., Y.H., F.X., Y.L., L.R., T.H., J.Z., Z.F., Y.Z., Y.X., and Q.Z. did the laboratory analysis. L.G., Y.H., F.X., F.G., and J.W. drafted the paper. Y.X. and X.W. collected the data. L.G., Y.H., F.X., L.R., L.X., and J.N. verified the underlying data in the study. All authors read and edited the manuscript. All authors approved the final version, had full access to all the data, and had final responsibility for the decision to submit for publication.

About the Author

Dr. Huang is a postdoctoral fellow at the Institute of Pathogen Biology, Chinese Academy of Medical Sciences. Her primary research interests include antiviral innate immunity, epidemic pathogens infectious disease surveillance, and applying these research to the prevention of epidemics.

References

1. Ghaseminia M. Preventing monkeypox outbreaks: focus on diagnosis, care, treatment, and vaccination. J Clin Transl Sci. 2023;7:e60. https://doi.org/10.1017/cts.2023.11
2. Frenois-Veyrat G, Gallardo F, Gorgé O, Marcheteau E, Ferraris O, Baidaliuk A, et al. Tecovirimat is effective against human monkeypox virus in vitro at nanomolar concentrations. Nat Microbiol. 2022;7:1951–5. https://doi.org/10.1038/s41564-022-01269-8
3. Fine PE, Jezek Z, Grab B, Dixon H. The transmission potential of monkeypox virus in human populations. Int J Epidemiol. 1988;17:643–50. https://doi.org/10.1093/ije/17.3.643
4. Zhao H, Wang W, Zhao L, Ye S, Song J, Lu R, et al. The first imported case of monkeypox in the mainland of China—Chongqing Municipality, China, September 16, 2022. China CDC Wkly. 2022;4:853–4.
5. Crotty S, Felgner P, Davies H, Glidewell J, Villarreal L, Ahmed R. Cutting edge: long-term B cell memory in humans after smallpox vaccination. J Immunol. 2003;171:4969–73. https://doi.org/10.4049/jimmunol.171.10.4969
6. Pütz MM, Alberini I, Midgley CM, Manini I, Montomoli E, Smith GL. Prevalence of antibodies to vaccinia virus after smallpox vaccination in Italy. J Gen Virol. 2005;86:2955–60. https://doi.org/10.1099/vir.0.81265-0
7. Hammarlund E, Lewis MW, Hansen SG, Strelow LI, Nelson JA, Sexton GJ, et al. Duration of antiviral immunity after smallpox vaccination. Nat Med. 2003;9:1131–7. https://doi.org/10.1038/nm917
8. Liu Q, Huang W, Nie J, Zhu R, Gao D, Song A, et al. A novel high-throughput vaccinia virus neutralization assay and preexisting immunity in populations from different geographic regions in China. PLoS One. 2012;7:e33392. https://doi.org/10.1371/journal.pone.0033392
9. Laidlaw BJ, Ellebedy AH. The germinal centre B cell response to SARS-CoV-2. Nat Rev Immunol. 2022;22:7–18. https://doi.org/10.1038/s41577-021-00657-1
10. Edghill-Smith Y, Golding H, Manischewitz J, King LR, Scott D, Bray M, et al. Smallpox vaccine–induced antibodies are necessary and sufficient for protection against monkeypox virus. Nat Med. 2005;11:740–7. https://doi.org/10.1038/nm1261

Address for correspondence: Jianwei Wang or Fei Guo, No. 9 Dong Dan San Tiao, Dongcheng District, Beijing 100730, China, email: wangjw28@163.com or guofei@ipb.pumc.edu.cn

Inferring Incidence of Unreported SARS-CoV-2 Infections Using Seroprevalence of Open Reading Frame 8 Antigen, Hong Kong

Shi Zhao,[1] Chris Ka Pun Mok,[1] Yun Sang Tang, Chunke Chen, Yuanxin Sun, Ka Chun Chong, David S.C. Hui

We tested seroprevalence of open reading frame 8 antigens to infer the number of unrecognized SARS-CoV-2 Omicron infections in Hong Kong during 2022. We estimate 33.6% of the population was infected, 72.1% asymptomatically. Surveillance and control activities during large-scale outbreaks should account for potentially substantial undercounts.

Hong Kong controlled the spread of COVID-19 caused by the SARS-CoV-2 Delta variant with stringent border control, effective contact tracing, and social distancing measures; only a small number of local SARS-CoV-2 infections had been reported in the 4 months before the Omicron variant appeared in late December 2021 (*1*). During the almost 2 years of pandemic before the Omicron outbreak, only ≈0.16% of the 7.5 million persons in Hong Kong were confirmed to be infected with SARS-CoV-2, among whom 200 persons died. An earlier investigation estimated that >99.5% of the population (>7 million persons) were naive to SARS-CoV-2 after the first 3 waves of community transmissions arising from imported cases (*2*).

Author affiliations: School of Public Health, Tianjin Medical University, Tianjin, China (S. Zhao); JC School of Public Health and Primary Care, Chinese University of Hong Kong, Hong Kong, China (S. Zhao, C.K.P. Mok, Y.S. Tang, C. Chen, Y. Sun, K.C. Chong); Centre for Health Systems and Policy Research, Chinese University of Hong Kong, Hong Kong, China (S. Zhao, K.C. Chong); CUHK Shenzhen Research Institute, Shenzhen, China (S. Zhao, K.C. Chong); Li Ka Shing Institute of Health Sciences, Chinese University of Hong Kong, Hong Kong, China (C.K.P. Mok, Y.S. Tang, C. Chen, Y. Sun); S.H. Ho Research Centre for Infectious Diseases, Chinese University of Hong Kong, Hong Kong, China (C.K.P. Mok, D.S.C. Hui)

DOI: https://doi.org/10.3201/eid3002.231332

However, after the advent of the Omicron outbreak in Hong Kong, COVID-19 became uncontrolled in early 2022. The huge upsurge in cases, including daily COVID-19 death rates among the highest recorded globally, overwhelmed hospitals and led to an extreme shortage in critical care facilities (*3*). To maintain comprehensive disease surveillance, the government launched an online system for persons to self-report positive cases identified by self-administrated rapid antigen tests (RAT); RAT results were included in official surveillance reports beginning February 26, 2022 (*4*). Although reporting positive self-test results was compulsory in accordance with a local disease prevention and control ordinance, a large number of infections likely went untested and unreported because of a high proportion of asymptomatic or mild cases.

Few empirical investigations have assessed the actual number of unrecognized infections during the Omicron epidemic, and estimates were mainly generated by modeling studies based on limited data. In previous studies, presence of open reading frame (ORF) 8 protein antibodies in blood samples was reported as a reliable serologic marker of natural SARS-CoV-2 infection (*5*,*6*). Given that ORF8 proteins are expressed only during the SARS-CoV-2 replication cycle, serologic testing for antibodies is able to determine whether a patient had been previously infected.

In this study, we used the seroprevalence of ORF8 antigen antibodies to infer the actual number of unrecognized infections in an infection-naive population during the Omicron outbreak in Hong Kong. Our study was approved by the Joint Chinese University of Hong Kong/New Territories East Cluster Clinical Research Ethics Committee (ref no. 2020.229). All participants who completed interview questionnaires

[1]These authors contributed equally to the article.

or provided blood samples for this study signed informed consent forms.

The Study

We obtained plasma samples from 1,028 volunteers ≥18 years of age during March 1–June 29, 2022, in the course of the Omicron BA.2 epidemic wave. All participants reported that, before the sampling date, they had never tested positive for COVID-19 by reverse transcription PCR test or RAT. We tested plasma samples using ELISA with ORF8 protein as an antigen for detection (Appendix, https://wwwnc.cdc.gov/EID/article/30/2/23-1332-App1.pdf). We obtained daily numbers of reported cases confirmed by PCR or RAT from the Hong Kong Department of Health. On the basis of the rates of ORF8 ELISA–positive test results relative to the number of reported cases at different time points, we estimated the true daily numbers of SARS-CoV-2 infections and infection attack rates by fitting a multinomial-distribution model, accounting for sensitivity and specificity of RAT and PCR tests. We assumed an initial infection attack rate of 0.2% before 2022, given Hong Kong's stringent infection control measures before the Omicron outbreak (*2*,*7*). We also reconstructed the time-varying reproduction number by renewal equation (*8*). We used Markov chain Monte Carlo method to estimate the posterior distributions of model parameters, summarized by medians with 95% credible intervals (CrIs) (Appendix).

Of the 1,028 self-reported uninfected persons in our study, 371 (36.1%) were male and 657 (63.9%) female, and median age was 50 (range 18–88) years; 1,027 reported having received ≥2 doses of COVID-19 vaccines. Overall positivity rate of ORF8 ELISA testing among our cohort was 2.5% (26 positive/1,028 tested). We found positivity rates were unlikely to vary on the basis of sex, age, or calendar date among self-reported uninfected persons in our cohort (Table).

Among the total population in Hong Kong, 16.2% were reported to have tested positive by RAT (6.1%) or reverse transcription PCR (10.1%). On the basis of estimates from our statistical model (Appendix), we inferred that 33.6% (95% CrI 32.1%–34.8%) of the 7.5 million persons in Hong Kong were infected during January 1–June 20, 2022 (Figure, panels A, B), corresponding to ≈2.5 million persons. We calculated percentages of asymptomatic cases of 41.8% among reported SARS-CoV-2 infections and 72.1% (95% CrI 70.8%–73.0%) among total (reported and unreported) infections. Reproduction numbers obviously dropped after positive RAT result reporting was implemented in Hong Kong on February 26, 2022 (Figure, panel C), consistent with findings about changes in transmission dynamics reported elsewhere (*9*).

Conclusions

Using the seroprevalence of ORF8 antigens, we inferred that 16.2% of 33.6% (≈1/2) SARS-CoV-2 infections during the Omicron epidemic in Hong Kong were unrecognized, despite RATs being widely disseminated and reporting of positive results made locally compulsory. Our estimates of asymptomatic proportions were generally higher than estimates previously reported for earlier variants (*10*). With such a large number of unrecognized cases circulating the virus in the community, it was not surprising that the Omicron outbreak was uncontrollable, even though stringent measures, such as contact tracing and quarantine for close contacts, continued to be in effect. Our study findings highlight the usefulness of testing for ORF8 seroprevalence among efforts to monitor COVID-19 outbreaks, especially for

Table. Summary of testing status of SARS-CoV-2 ORF8 ELISA among 1,028 self-claimed uninfected persons, China, 2022*

Stratification	ORF8 test, no. (%)		Positivity rate, %	p value†
	Positive	Negative		
Overall	26 (100)	1,002 (100)	2.5	NA
Sex				
F	12 (46.2)	645 (64.4)	1.8	0.062
M	14 (53.8)	357 (35.6)	3.8	
Age, y				
<40	6 (23.1)	305 (30.4)	1.9	0.715
40–65	16 (61.5)	566 (56.5)	2.7	
≥65	4 (15.4)	131 (13.1)	3.0	
Test month				
March	2 (7.7)	97 (9.7)	2.0	0.608
April	2 (7.7)	137 (13.7)	1.4	
May	4 (15.4)	92 (9.2)	4.2	
June	18 (69.2)	676 (67.5)	2.6	

*NA, not applicable; ORF, open reading frame.
†By 2-sided Fisher exact test.

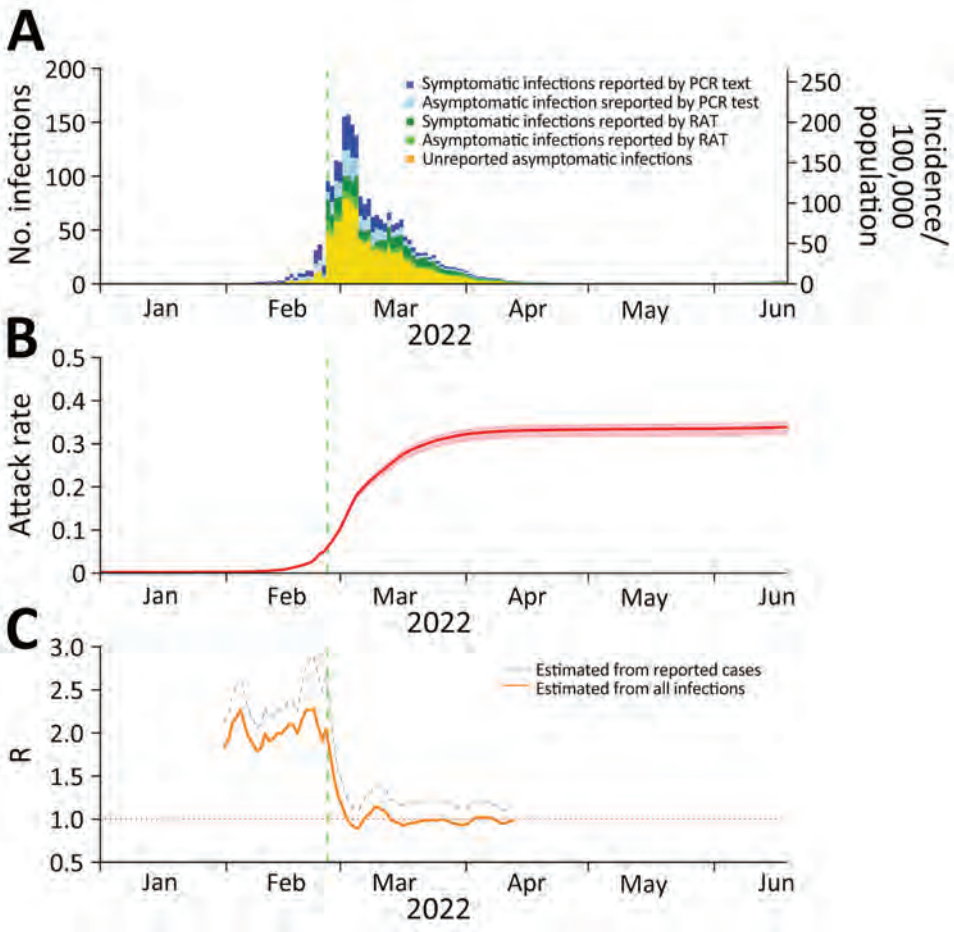

Figure. Reported SARS-COV-2 incidence versus estimates based on open reading frame 8 antigen testing, Hong Kong, China, January 1–June 20, 2022. A) Daily numbers and incidence of all reported infections and estimated asymptomatic infections by test type and presence or absence of symptoms. B) Estimated infection attack rate; shading indicates 95% credible intervals (CrIs). C) Estimated time-varying R for reported cases compared with estimated cases. Green vertical dashed lines indicate date (February 26, 2022) when compulsory reporting of positive RAT results was implemented in Hong Kong. Because of the large number of cases, 95% CrIs for R were extremely narrow, and thus we omitted CrIs in panel C. R, reproduction number; RAT, rapid antigen test.

emerging new variants of concern. Public health agencies need to take into account the potential for substantial undercount of actual numbers of infections when considering the commitment of resources to prevent and control outbreaks.

Acknowledgments

The authors thank all participants from the Prince of Wales Hospital, Hong Kong, who contributed to blood sample collection during the period when SARS-COV-2 Omicron infections were increasing rapidly around them.

This research was supported by grants from the Health and Medical Research Fund Commissioned Research on the Novel Coronavirus Disease (COVID-19), Hong Kong (COVID1903003), Hong Kong Research Grants Council (RGC) theme-based research schemes (T11-705/21-N), Emergency Key Program of Guangzhou Laboratory (EKPG22-30-6), Chinese University of Hong Kong (CUHK) direct grant (2021.015), RGC Collaborative Research Fund (C4139-20G), group research scheme from CUHK, and a donation from the S.H. Ho Foundation.

Author contributions: C.K.P.M., D.S.C.H., and K.C.C. planned, coordinated, and obtained funding for the study. K.C.C., S.Z., and C.K.P.M. wrote manuscript. C.K.P.M., Y.S.T., C.C., and Y.S. coordinated laboratory testing. S.Z. and K.C.C. contributed modeling and statistical analysis. All authors commented on the manuscript draft and agreed with its submission.

About the Author

Dr. Shi Zhao is a professor at School of Public Health, Tianjin Medical University, who previously was a postdoctoral fellow at JC School of Public Health and Primary Care, Chinese University of Hong Kong. His research interests focus on computational epidemiology, and emerging infectious disease transmission dynamics.

References

1. Chong KC, Chan PK, Hung CT, Wong CK, Xiong X, Wei Y, et al. Changes in all-cause and cause-specific excess mortality before and after the Omicron outbreak of COVID-19 in Hong Kong. J Glob Health. 2023;13:06017. https://doi.org/10.7189/jogh.13.06017

2. Boon SS, Wong MCS, Ng RWY, Leung DTM, Chen Z, Lai CKC, et al. Seroprevalence of unidentified SARS-CoV-2 infection in Hong Kong during 3 pandemic waves. JAMA Netw Open. 2021;4:e2132923. https://doi.org/10.1001/jamanetworkopen.2021.32923
3. Ma A, Parry J. When Hong Kong's "dynamic zero" covid-19 strategy met omicron, low vaccination rates sent deaths soaring. BMJ. 2022;377:o980. https://doi.org/10.1136/bmj.o980
4. Hong Kong Government. Selecting and using rapid antigen tests [cited 2022 Feb 27]. https://www.info.gov.hk/gia/general/202202/27/P2022022600796.htm
5. Hachim A, Kavian N, Cohen CA, Chin AWH, Chu DKW, Mok CKP, et al. ORF8 and ORF3b antibodies are accurate serological markers of early and late SARS-CoV-2 infection. Nat Immunol. 2020;21:1293–301. https://doi.org/10.1038/s41590-020-0773-7
6. Hachim A, Gu H, Kavian O, Mori M, Kwan MYW, Chan WH, et al. SARS-CoV-2 accessory proteins reveal distinct serological signatures in children. Nat Commun. 2022;13:2951. https://doi.org/10.1038/s41467-022-30699-5
7. Leung K, Lau EHY, Wong CKH, Leung GM, Wu JT. Estimating the transmission dynamics of SARS-CoV-2 Omicron BF.7 in Beijing after adjustment of the zero-COVID policy in November–December 2022. Nat Med. 2023;29:579–82. https://doi.org/10.1038/s41591-023-02212-y
8. Cori A, Ferguson NM, Fraser C, Cauchemez S. A new framework and software to estimate time-varying reproduction numbers during epidemics. Am J Epidemiol. 2013;178:1505–12. https://doi.org/10.1093/aje/kwt133
9. Du Z, Tian L, Jin DY. Understanding the impact of rapid antigen tests on SARS-CoV-2 transmission in the fifth wave of COVID-19 in Hong Kong in early 2022. Emerg Microbes Infect. 2022;11:1394–401. https://doi.org/10.1080/22221751.2022.2076616
10. Oran DP, Topol EJ. Prevalence of asymptomatic SARS-CoV-2 infection: a narrative review. Ann Intern Med. 2020;173:362–7. https://doi.org/10.7326/M20-3012

Address for correspondence: Ka Chun Chong, JC School of Public Health and Primary Care, Prince of Wales Hospital, 30-32 Ngan Shing Street, Shatin, New Territories, Hong Kong, China; email: marc@cuhk.edu.hk; David SC Hui, Department of Medicine and Therapeutics, Prince of Wales Hospital, 30-32 Ngan Shing Street, Shatin, New Territories, Hong Kong, China; email: dschui@cuhk.edu.hk

Rebound of Gonorrhea after Lifting of COVID-19 Preventive Measures, England

Holly Fountain,[1] Stephanie J. Migchelsen,[1] Hannah Charles, Tika Ram, Helen Fifer, Hamish Mohammed, Katy Sinka

After lifting of all COVID-19 preventive measures in England in July 2021, marked, widespread increases in gonorrhea diagnoses, but not testing numbers, were observed, particularly in persons 15–24 years of age. Continued close surveillance and public health messaging to young persons are needed to control and prevent gonorrhea transmission.

The COVID-19 pandemic caused a substantial disruption of sexual health services (SHS) in England (including reduced testing), contributing to a 33.5% decrease in new sexually transmitted infection (STI) diagnoses in 2020 (n = 311,480) compared with 2019 (n = 468,260) (*1*). In July 2021, all COVID-19 restrictions associated with the third and final lockdown in England were lifted (*2*), normal social mixing was permitted, and a rebound in SHS occurred; a 23.8% increase in new STI diagnoses was observed in 2022 (n = 392,453) compared with those in 2021 (n = 317,022) (*1*). Of the most commonly diagnosed STIs, the largest proportional increase occurred for gonorrhea, caused by infection with *Neisseria gonorrhoeae* bacteria. The number of new gonorrhea diagnoses increased by 50.3% in 2022 (n = 82,592) compared with 2021 (n = 54,961) (*1*). We describe trends for gonorrhea testing and diagnosis in England after all COVID-19 control measures were lifted and explore how those differed among populations.

The Study

In England, all STI tests and diagnoses from SHS are captured by the Genitourinary Medicine Clinic Activity Dataset STI Surveillance System (*3*). We analyzed data on gonorrhea tests and diagnoses during January 1, 2019–December 31, 2022. To prevent double counting, we only counted 1 test or diagnosis per SHS user within a 42-day period. We examined quarterly trends, disaggregated by age group (15–24, 25–34, 35–44, and ≥45 years of age), gender and sexual orientation (gay, bisexual, and other men who have sex with men [MSM]; heterosexual men; women who have sex with men [WSM]; and women who only have sex with women), and local authority districts of residence. We did not include records with missing demographic data in their respective analysis. We analyzed data by using Stata version 16.1 software (StataCorp LLC, https://www.stata.com). No ethics approval was needed for this study because we used routine surveillance data.

After lifting of COVID-19–related restrictions, the number of gonorrhea tests increased by 5.6% from quarter (Q) 3 of 2021 (n = 483,717) to the end of Q4 of 2022 (n = 510,792). Gonorrhea diagnoses increased by 63.8% (13,715 to 22,471) during the same period (Figure 1, panel A). The total number of gonorrhea diagnoses in 2022 was the highest on record, although testing remained just below 2019 levels. Test positivity increased to the highest point within the 4-year study period during 2022 Q4 (4.4%) from a low point in 2021 Q3 (2.8%) (Figure 1, panel B).

Increases in gonorrhea diagnoses began immediately after COVID-19–related restrictions were lifted and were most notable in young persons, 15–24 years of age, who saw a 141.3% increase (3,747 diagnoses in 2021 Q3, 9,041 in 2022 Q4) (Figure 2, panel A); a 34.8% increase was observed for persons ≥25 years of age. Persons 19–20 years of age had the highest increase in diagnoses, 229.0% (930 in 2021 Q3, 3,060 in 2022 Q4). During the same period, testing remained relatively steady among young persons (1.5% increase). Overall, testing returned to or exceeded numbers from 2019 in all age groups except the 15–24-year group (12.4% decrease from 2019 Q4 to 2022 Q4) (Figure 2,

Author affiliation: UK Health Security Agency, London, UK

DOI: https://doi.org/10.3201/eid3002.231148

[1]These first authors contributed equally to this article.

panel B). Test positivity increased >2-fold in persons 15–24 years of age from 2021 Q3 (2.2%) to 2022 Q4 (5.3%); positivity increased at a lower rate in older age groups.

Of all gender and sexual orientation groups, MSM had the largest numbers of gonorrhea diagnoses during the 4-year study period. However, proportionally, increases in gonorrhea diagnoses from 2021 Q3 to 2022 Q4 were largest among WSM (104.7% increase; 2,577 to 5,274) and heterosexual men (90.4%; 2,152 to 4,097); diagnoses among MSM increased 39.7% (7,107 to 9,932) (Table 1). Testing increased by 21.8% among MSM from 2019 Q4 to 2022 Q4; however, testing decreased by 20.3% for WSM and by 8.1% for heterosexual men during the same period. Among persons 15–24 years of age, the increase in gonorrhea diagnoses from 2021 Q3 to 2022 Q4 was greater among heterosexual persons (179.6%; 2,092 to 5,850) than among MSM (63.2%; 1,035 to 1,689). For persons ≥25 years of age, diagnoses increased similarly among heterosexual persons (33.7%) and MSM (35.8%).

Gonorrhea diagnoses increased in all regions of England after COVID-19–related restrictions were removed, most notably in South West England (226.0% increase; 407 in 2021 Q3 to 1,327 in 2022 Q4) and North East England (194.0% increase; 285 in 2021 Q3 to 838 in 2022 Q4). Most (91.3%) local authority districts showed an increase in diagnoses during this same period.

Conclusions

National surveillance data showed an increase in gonorrhea diagnoses in England after the cessation of social restrictions in summer 2021. Increases were observed among persons of all age groups, genders, and sexual orientations but particularly among persons 15–24 years of age and those who identified as heterosexual.

Testing did not increase as markedly as diagnoses after the removal of COVID-19 lockdown restrictions, suggesting that a true increase in gonorrhea transmission existed within the population. Changes in diagnosis numbers could potentially represent a delay in gonorrhea detection because of decreased testing during the lockdown periods; however, this difference is unlikely to be a main factor

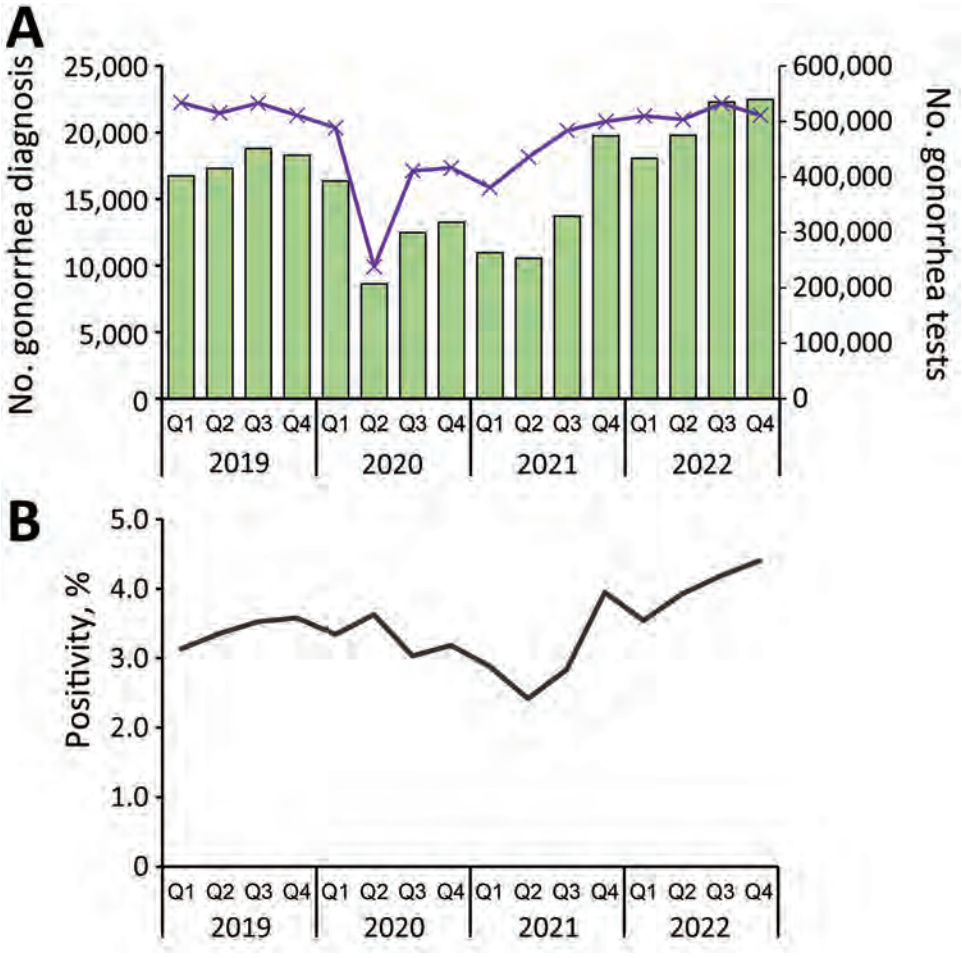

Figure 1. Total number of gonorrhea diagnoses and tests and percent test positivity in study of rebound of gonorrhea after lifting of COVID-19 preventive measures in England, January 1, 2019–December 31, 2022. A) Total number of diagnoses and tests. Bars indicate the total number of gonorrhea diagnoses; purple line indicates the total number of gonorrhea tests. B) Percent positivity of gonorrhea tests. Q, quarter. Scales for the y-axes differ substantially to underscore patterns but do not permit direct comparisons.

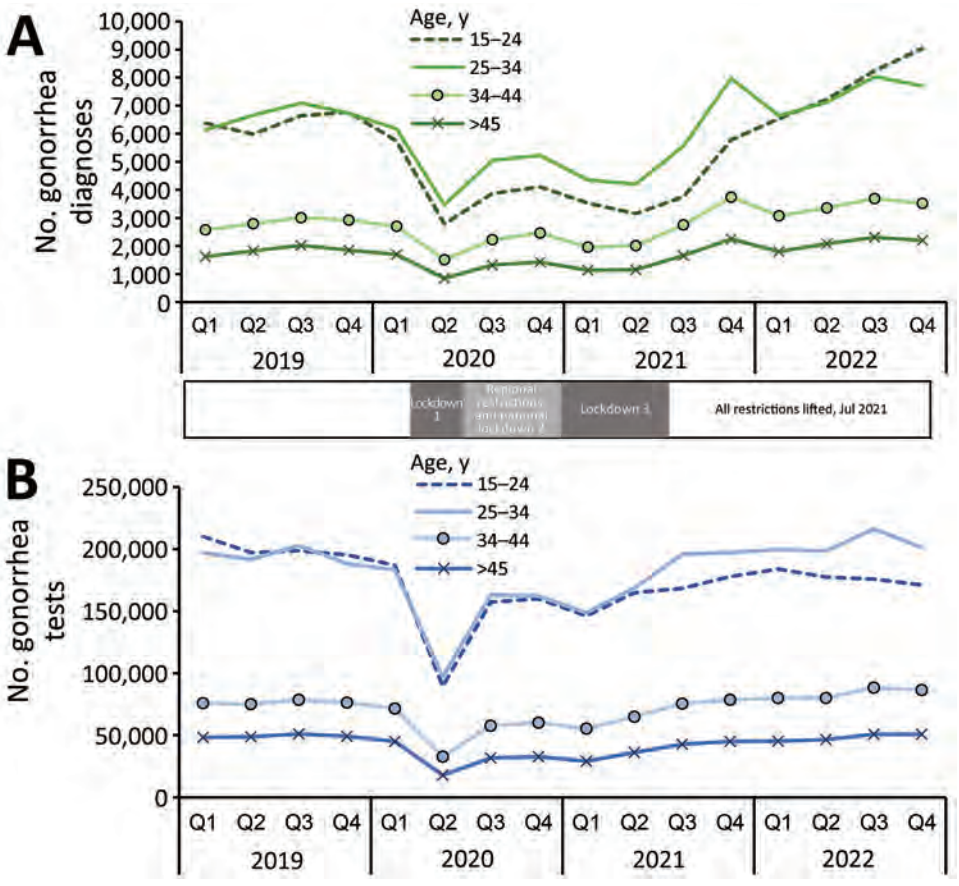

Figure 2. Total number of gonorrhea diagnoses (A) and tests (B) according to age groups in study of rebound of gonorrhea after lifting of COVID-19 preventive measures in England, January 1, 2019–December 31, 2022. Shaded bars between panels indicate dates of COVID-19 lockdowns. Q, quarter.

for the observed increase in diagnoses because the largest increases in testing primarily occurred before all lockdown restrictions were removed (i.e., from 2020 Q2 to Q3 and 2021 Q1 to Q3; Figure 1, panel A). Furthermore, 18 months after lockdowns ended, increases in gonorrhea diagnoses continued to outpace increases in testing, corresponding to increasing test positivity. In addition, gonorrhea

Table. Numbers of persons with gonorrhea diagnoses who attended sexual health services according to gender and sexual orientation in study of rebound of gonorrhea after lifting of COVID-19 preventive measures, England*

Year	No. persons with gonorrhea diagnosis				
	MSM	Heterosexual men	WSM	WOSW	Not known
2019					
Quarter 1	7,851	3,678	4,280	44	889
Quarter 2	8,341	3,692	4,205	64	1,005
Quarter 3	9,249	3,832	4,498	55	1,152
Quarter 4	8,466	3,909	4,757	47	1,119
2020					
Quarter 1	8,040	3,356	3,883	60	1,005
Quarter 2	4,352	1,681	1,962	39	580
Quarter 3	6,194	2,436	2,832	59	956
Quarter 4	6,491	2,585	2,964	69	1,134
2021					
Quarter 1	5,184	2,041	2,392	52	1,305
Quarter 2	5,251	1,674	2,076	77	1,456
Quarter 3	7,107	2,152	2,577	69	1,810
Quarter 4	8,724	2,674	3,665	85	4,590
2022					
Quarter 1	8,809	2,916	3,809	109	2,419
Quarter 2	9,684	3,224	4,182	127	2,560
Quarter 3	10,498	3,684	5,032	115	2,953
Quarter 4	9,932	4,097	5,274	123	3,045

*Preventive measures were lifted in July (quarter 3) of 2021. MSM, gay, bisexual and other men who have sex with men; WOSW, women who only have sex with women; WSM, women who have sex with men.

in heterosexual men is likely to cause symptomatic urethritis, which might cause those persons to seek earlier treatment at SHS. Although we did not have access to data on symptoms for confirmation, the increase in diagnoses observed in heterosexual men suggests an increase in incident infection and not just a delay in detection.

The sexual behavior of young persons was most adversely affected by COVID-19–related restrictions (*4*). After all lockdown restrictions were removed during summer 2021, the return of in-person attendance at higher education institutions might have provided increased opportunities for new and frequent changing of sexual partners. The potential change to higher STI risk behaviors could perhaps help explain the observed increases and is similar to reports from other countries in Europe in which gonorrhea diagnoses increased in 2022 among young persons of average university age (*5*–*8*).

Young persons were affected the most by disruptions to SHS caused by lockdown measures (*9*). Testing by using online services increased, but evidence of access inequality existed; those 15–19 years of age were less likely to access testing through this route (*10*). We have shown that testing levels in young persons remained lower in 2022 than during the prepandemic period, suggesting that potential undiagnosed cases contributed to observed increases in gonorrhea. Messaging focused on the importance of regular STI testing, especially for young persons with new partners, could help address disease transmission resulting from undiagnosed cases. Public health messaging directed at young persons was published to coincide with the start of the 2023–24 academic year (*11*).

In conclusion, the increase in gonorrhea diagnoses was widespread in England after removal of all COVID-19 lockdown restrictions. It remains to be seen whether increases in gonorrhea diagnoses will be short-lived because of restrictions removal, whether pre–COVID-19 pandemic diagnoses levels will resume, or whether another trend will be observed. Continued close surveillance, a better understanding of the factors leading to the increase in gonorrhea diagnoses, and public health messaging (particularly to young persons) are needed to focus efforts on gonorrhea transmission control and prevention.

About the Author

Ms. Fountain is a senior STI surveillance and prevention scientist at the UK Health Security Agency. Her research is focused on real-time and enhanced surveillance of STIs in England and responding to changes in baseline circulation.

References

1. Migchelsen SJ, Enayat Q, Harb AK, Daahir U, Slater L, Anderson A, et al.; UK Health Security Agency. Sexually transmitted infections and screening for chlamydia in England, 2022. 2023 [cited 2023 Jun 23]. https://www.gov.uk/government/statistics/sexually-transmitted-infections-stis-annual-data-tables/sexually-transmitted-infections-and-screening-for-chlamydia-in-england-2022-report
2. United Kingdom Government Cabinet Office. COVID-19 response: summer 2021 [cited 2023 Jun 20]. https://www.gov.uk/government/publications/covid-19-response-summer-2021-roadmap/covid-19-response-summer-2021
3. Savage EJ, Mohammed H, Leong G, Duffell S, Hughes G. Improving surveillance of sexually transmitted infections using mandatory electronic clinical reporting: the genitourinary medicine clinic activity dataset, England, 2009 to 2013. Euro Surveill. 2014;19:20981. https://doi.org/10.2807/1560-7917.ES2014.19.48.20981
4. Mercer CH, Clifton S, Riddell J, Tanton C, Freeman L, Copas AJ, et al. Impacts of COVID-19 on sexual behaviour in Britain: findings from a large, quasi-representative survey (Natsal-COVID). Sex Transm Infect. 2022;98:469–77. https://doi.org/10.1136/sextrans-2021-055210
5. Public Health Scotland. Gonorrhoea infection in Scotland 2013–2022. 2023 [cited 2023 Jun 23]. https://publichealthscotland.scot/publications/gonorrhoea-infection-in-scotland/gonorrhoea-infection-in-scotland
6. Norwegian Institute of Public Health. Annual surveillance report 2022 for sexual transmitted infections [in Norwegian] [cited 2023 Jun 23]. https://www.fhi.no/publ/2023/overvakning-av-seksuelt-overforbare-infeksjoner.-arsrapport-2022
7. Kayaert L, Sarink D, Visser M, van Wees DA, Willemstein IJM, Op de Coul ELM, et al. Sexually transmitted diseases in the Netherlands in 2022. RIVM report 2023-0161. Bilthoven (the Netherlands): National Institute for Public Health and the Environment; 2023
8. Health Protection Surveillance Centre. Sexually transmitted infections (STIs) in Ireland: trends to the end of 2022. Slide set. April 20, 2023 [cited 2023 Aug 1]. https://www.hpsc.ie/a-z/sexuallytransmittedinfections/publications/stireports
9. Dema E, Gibbs J, Clifton S, Copas AJ, Tanton C, Riddell J, et al. Initial impacts of the COVID-19 pandemic on sexual and reproductive health service use and unmet need in Britain: findings from a quasi-representative survey (Natsal-COVID). Lancet Public Health. 2022;7:e36–47. https://doi.org/10.1016/S2468-2667(21)00253-X
10. Sonubi T, Sheik-Mohamud D, Ratna N, Bell J, Talebi A, Mercer CH, et al. STI testing, diagnoses and online chlamydia self-sampling among young people during the first year of the COVID-19 pandemic in England. Int J STD AIDS. 2023;34:841–53. https://doi.org/10.1177/09564624231180641
11. UK Health Security Agency. University freshers urged to use condoms amid record levels of gonorrhoea. September 15, 2023 [cited 2023 Nov 7]. https://www.gov.uk/government/news/university-freshers-urged-to-use-condoms-amid-record-levels-of-gonorrhoea

Address for correspondence: Holly Fountain, UK Health Security Agency, 61 Colindale Ave, London, NW9 5EQ, UK; email: holly.fountain@ukhsa.gov.uk

Adapting COVID-19 Contact Tracing Protocols to Accommodate Resource Constraints, Philadelphia, Pennsylvania, USA, 2021

Seonghye Jeon,[1] Lydia Watson-Lewis,[1] Gabriel Rainisch, Chu-Chuan Chiu, François M. Castonguay, Leah S. Fischer, Patrick K. Moonan, John E. Oeltmann, Bishwa B. Adhikari, Hannah Lawman,[2,3] Martin I. Meltzer[2]

Because of constrained personnel time, the Philadelphia Department of Public Health (Philadelphia, PA, USA) adjusted its COVID-19 contact tracing protocol in summer 2021 by prioritizing recent cases and limiting staff time per case. This action reduced required staff hours to prevent each case from 21–30 to 8–11 hours, while maintaining program effectiveness.

Case investigation and contact tracing (CICT) were among the primary nonpharmaceutical interventions for COVID-19 before vaccines became widely available. Previous studies estimated that CICT played an important role in mitigating the COVID-19 pandemic in the United States (*1*,*2*). However, CICT programs were resource-intensive and required trained personnel, testing capacity, and technology to support successful implementation (*3*,*4*). Health departments had to make decisions about how to best allocate limited resources to CICT and other competing mitigation strategies, such as vaccination, testing programs, and community outreach.

Because of a surge in cases associated with the SARS-CoV-2 Delta variant (B.1.617.2) during summer 2021 (*5*) and the redirection of staff hours from CICT to other activities, the Philadelphia Department of Public Health (PDPH; Philadelphia, PA, USA) adjusted its existing CICT protocol on August 18, 2021. The new protocol prioritized cases with the most recent specimen collection dates rather than on the basis of time registered in the surveillance system. In addition, instead of making multiple attempts to reach case-patients and contacts within ≈4 days, staff made 1 attempt to reach each case-patient and contact. The new protocol prioritized persons in the early stages of infection, aiming to prevent secondary transmission by allocating resources more effectively. In addition, by limiting the time allocated to each case, CICT staff could expand their reach to more persons. This redistribution of staff resources also supported the redirection of staff to other important response efforts.

The Study

To assess the effect of the CICT protocol change, we defined two 8-week evaluation periods; period 1 was before the CICT protocol change (June 23–August 17, 2021), and period 2 was after the protocol change (September 1–October 26, 2021) (Figure). We employed a 2-week gap between the 2 periods to allow sufficient time for the effects of the new protocol to be reflected in reported cases. PDPH routinely collected the daily number of new COVID-19 cases (*6*), daily vaccination records (*6*), and CICT program metrics (*7*), including staff hours (Table 1). PDPH had a separate team responsible for overseeing contact tracing in select high-risk groups, such as nursing homes and other congregate living facilities; the effect of that team is not considered in the analysis. The PDPH Institutional Review Board determined that this work did not constitute human subjects research and was therefore not subject to institutional review board review.

Author affiliations: Centers for Disease Control and Prevention, Atlanta, Georgia, USA (S. Jeon, G. Rainisch, F.M. Castonguay, L.S. Fischer, P.K. Moonan, J.E. Oeltmann, B.B. Adhikari, M.I. Meltzer); Philadelphia Department of Public Health, Philadelphia, Pennsylvania, USA (L. Watson-Lewis, C.-C. Chiu, H. Lawman); University of Montreal School of Public Health, Montreal, Quebec, Canada (F.M. Castonguay)

DOI: https://doi.org/10.3201/eid3002.230988

[1]These first authors contributed equally to this article.

[2]These senior authors contributed equally to this article.

[3]Current affiliation: Novo Nordisk, Philadelphia, Pennsylvania, USA.

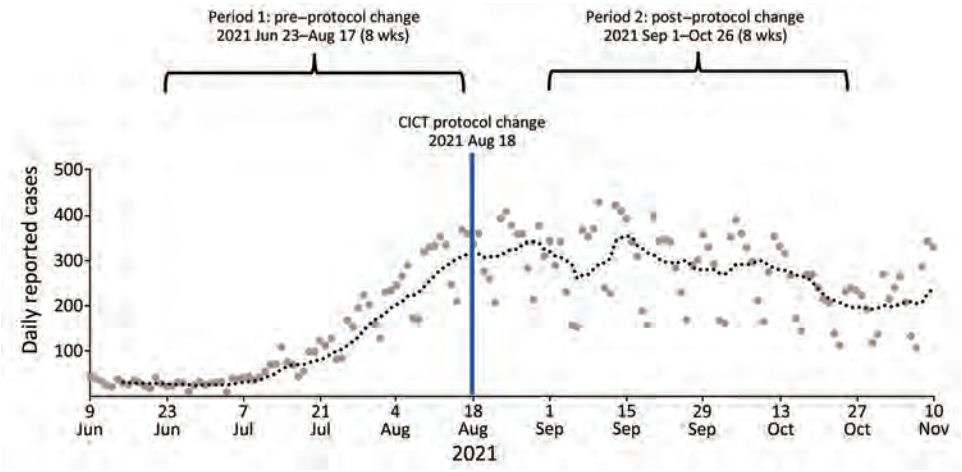

Figure. Daily reported COVID-19 cases and 2 evaluation periods before and after CICT protocol change, Philadelphia, Pennsylvania, June–November 2021. The large dots represent daily case counts, and the dotted line represents the 7-day moving average case count. CICT, case investigation and contact tracing.

We combined data collected by PDPH with the Centers for Disease Control and Prevention COVIDTracer modeling tool (https://www.cdc.gov/ncezid/dpei/resources/covid-tracer-Advanced-Special-edition.xlsm) to estimate cases averted before and after the protocol change. COVIDTracer is a spreadsheet-based tool that uses a susceptible–exposed–infectious–recovered epidemiologic model to illustrate the spread of COVID-19 and the effects of community interventions such as CICT (*8*). We measured CICT effectiveness by calculating the proportion of case-patients and contacts isolated or quarantined in response to PDPH's CICT efforts and the number of days needed for them to enter isolation or quarantine (Table 2). We then estimated the combined effects of other community interventions, such as masking, social distancing, and vaccination, by fitting the model-generated cumulative case curve to the observed one. Finally, to simulate a scenario without CICT, we removed CICT's effects in the model and calculated the difference between this hypothetical curve and the reported cases as the cases averted by CICT (Appendix, https://wwwnc.cdc.gov/EID/article/30/2/23-0988-App1.pdf).

The percentage of cases interviewed declined from 42% to 29% after the protocol change, mainly because of a doubling of reported cases in period 2 (Table 1). However, a larger absolute number of case-patients were interviewed in period 2, resulting in more contacts being notified and monitored.

Table 1. COVID-19 incidence, reported CICT program metrics, and CICT staff hours before and after CICT protocol change, Philadelphia, Pennsylvania, USA, 2021*

Characteristic	Period 1, before protocol change	Period 2, after protocol change
Evaluation dates	Jun 23–Aug 17	Sep 1–Oct 26
COVID-19 incidence		
Mean daily incidence, cases/100,000 persons†	9	18
Total no. reported cases	7,544	15,681
% Population fully vaccinated	58	65
CICT program performance metrics		
No. case-patients reached for interviews‡	5,685	9,351
No. case-patients who completed interviews (% all case-patients)	3,172 (42)	4,537 (29)
No. interviewed case-patients naming ≥1 contact	852	1,074
No. contacts identified	1,922	2,375
No. contacts notified	1,372	1,853
No. contacts monitored§	883	1,234
Timing of case-patient interview, days after specimen collection¶	3	2
Timing of contact notification, days after specimen collection#	4	3
CICT staff hours		
Average no. CICT staff per week	83	85
Total staff hours over the 8-wk period**	19,890	12,788

*CICT, case investigation and contact tracing.
†Mean daily incidence for each of the 8-week evaluation periods.
‡Include case-patients who completed interviews, those who were reached but refused interview, and those who were reached but were unable to be interviewed because of other reasons (e.g., incarcerated, deceased, and language barriers).
§Contacts who agreed to share symptom updates with the health department through text or phone calls.
¶Reported median days from specimen collection to positive test results reported to health departments.
#Reported median days from specimen collection to contact notification.
**On average, CICT staff spent 80% of their work (i.e., 30 h/wk) dedicated to CICT during period 1 and 50% during period 2 (i.e., 18.75 h/wk).

Table 2. Calculated CICT effectiveness values and model-estimated CICT effectiveness before and after CICT protocol change, Philadelphia, Pennsylvania, USA, 2021*

Characteristic	Period 1, before protocol change	Period 2, after protocol change
Calculated CICT effectiveness values		
% Case-patients and contacts isolated because of CICT (range)†	17 (11.7–21.9)	10 (6.7–12.5)
Days from infection to isolation‡	9	8
Model-estimated CICT effectiveness		
No. cases averted by CICT	657–968	1,156–1,609
No. hospitalizations averted by CICT	16–24	28–40
% Disease prevalence averted by CICT	8.4–12.0	6.8–9.2
Average staff hours per case averted§	21–30	8–11
Average staff hours per 1% disease prevalence averted¶	1,661–2,358	1,397–1,892

*CICT, case investigation and contact tracing.
†Including contacts who later become case-patients. Calculated as follows using the observed performance metrics (Table 1), assumed compliance with isolation and quarantine guidance among cases and contacts (Appendix Table 1, https://wwwnc.cdc.gov/EID/article/30/2/23-0988-App1.pdf), and an assumed $k = 1.2$: [(% case-patients interviewed × compliance) + k × % contacts identified × (% contacts monitored × compliance + % contacts notified but not monitored × compliance)] / (1 + k), where k is approximated from the effective reproduction number (R_t), because undetected infected contacts will infect R_t additional persons on average. During the evaluation period, the average R_t in Philadelphia was 1.29 during periods 1 and 0.99 during period 2. If the assumed compliance was 100%, the estimated effectiveness could be as high as 26% for period 1 and 15% for period 2.
‡The average length of time from infection to isolation and quarantine between case-patients and contacts who later became case-patients. We assumed a 5-day presymptomatic period. We further assumed that interviewed case-patients and notified contacts began isolation and quarantine the day after their interactions with the health department (Appendix).
§Calculated by dividing the total staff hours by the estimated number of cases averted by CICT. Lower value represents a more cost-effective program, given that it requires fewer staff hours to prevent each case.
¶Calculated by dividing the total staff hours by the estimated proportion of disease prevalence averted by CICT. Lower value represents a more cost-effective program, given that it requires fewer staff hours to prevent each percentage of disease prevalence.

Notification speed improved; case-patient interviews and contact notifications occurred 1 day faster after the protocol change (Table 1). We estimated that the percentage of case-patients and contacts isolated or quarantined because of CICT decreased after the protocol change, from 17% (range 11.7%–21.9%) to 10% (range 6.7%–12.5%). These ranges reflect different levels of assumed compliance with isolation and quarantine recommendations (Appendix Table 1). However, the number of days after specimen collection needed to start case-patient isolation and contact quarantine improved by 1 day, decreasing from 9 to 8 days (Table 2).

CICT efforts averted an estimated 657–968 cases during June 23–August 17 (period 1) and 1,156–1,609 cases during September 1–October 26 (period 2) (Table 2; Appendix Table 2). The estimate ranges consider various time values for exposed persons to become infectious, accounting for circulating COVID-19 variants (Appendix). The higher number of cases averted in period 2 may be influenced by the higher prevalence (Table 1); a larger number of cases in the community increases the potential for averting additional cases. The estimates of averted cases represent ≈8.4%–12.0% of the total disease prevalence in period 1 and ≈6.8%–9.2% of the total disease prevalence in period 2 (Table 2; Appendix Table 2).

When we calculated the effect of the protocol change by estimating cases averted in period 2 by using the CICT effectiveness values from period 1, the new protocol resulted in 93–189 fewer cases averted than would have occurred if the protocol had not changed (Appendix Table 3). This result indicates that, during the evaluation period, the benefits of increased notification speed were not sufficient to fully offset the negative effects of the lower coverage. Of note, factors beyond the implementation of the CICT program, such as variations in staff experience and efficiency between the 2 periods, and inherent errors associated with case-patient interviews may have influenced the results.

Similar numbers of staff were assigned to the CICT program during the 2 periods (an average of 83 staff per week in period 1 and 85 staff per week in period 2). However, on average, staff spent 80% of their time on CICT during period 1 (totaling 19,890 hours) and 50% of their time on CICT in period 2 (totaling 12,788 hours), which allowed staff to assist with vaccinations, testing, and other emergency response activities (e.g., influx of refugees from Afghanistan). Although CICT averted relatively more disease cases before the protocol change, average staff hours per case averted decreased after the protocol change (21–30 vs. 8–11 hours per case averted) (Table 2).

Conclusions

PDPH's new CICT protocol exemplifies the tradeoffs public health agencies in resource-limited settings encounter while working to fulfill their missions. Under the new protocol, the proportion of disease cases averted because of CICT decreased. However, the new protocol reduced staff hours needed to prevent each additional case by 63%. Throughout both periods,

the estimated number of disease cases averted by CICT was meaningful, reducing the potential caseload by an estimated 300–800/month, depending on case levels and protocol changes.

Prioritizing more recently tested case-patients and limiting staff hours dedicated to each case-patient and contact resulted in increased efficiency of the CICT program. The staff time saved by the protocol change (7,103 staff hours saved over an 8-week period) (Table 1) was directed toward other meaningful mitigation efforts as the response evolved, including vaccination, testing, and outreach services.

Although resource-intensive, the CICT program collected valuable surveillance data on contextual, demographic, occupational, and exposure trends related to COVID-19. Furthermore, the direct interactions between CICT staff and residents provided essential health information and resources, encouraging positive behavioral changes that prevented further community transmission (*9*,*10*). In addition, CICT has proven effective in controlling outbreaks of Middle East respiratory syndrome and Ebola (*11*) and will serve as an important tool for managing other infectious diseases with pandemic potential. The inherent value of CICT underscores the need to implement more resource-efficient strategies, such as those used in PDPH's protocol change, to sustain the program during future pandemics.

Acknowledgments

We are grateful to the COVID-19 Response Team of the Philadelphia Department of Public Health for their tireless work to protect the lives and wellbeing of the public during the pandemic.

H.L. contributed to this article in her own capacity and not on behalf of Novo Nordisk.

About the Author

Dr. Jeon is a senior statistician in the Health Economics and Modeling Unit, Division of Preparedness and Emerging Infections, National Center for Zoonotic and Emerging Infectious Diseases, Centers for Disease Control and Prevention. Her research interest includes leveraging statistical and mathematical models to estimate the effect of public health interventions.

References

1. Jeon S, Rainisch G, Lash RR, Moonan PK, Oeltmann JE Jr, Greening B Jr, et al.; Contact Tracing Impact Group. Estimates of cases and hospitalizations averted by COVID-19 case investigation and contact tracing in 14 health jurisdictions in the United States. J Public Health Manag Pract. 2022;28:16–24. https://doi.org/10.1097/PHH.0000000000001420
2. Rainisch G, Jeon S, Pappas D, Spencer KD, Fischer LS, Adhikari BB, et al. Estimated COVID-19 cases and hospitalizations averted by case investigation and contact tracing in the US. JAMA Netw Open. 2022;5:e224042. https://doi.org/10.1001/jamanetworkopen.2022.4042
3. Ruebush E, Fraser MR, Poulin A, Allen M, Lane JT, Blumenstock JS. COVID-19 case investigation and contact tracing: early lessons learned and future opportunities. J Public Health Manag Pract. 2021;27(Suppl 1):S87–97. https://doi.org/10.1097/PHH.0000000000001290
4. Harper-Hardy P, Ruebush E, Allen M, Carlin M, Plescia M, Blumenstock JS. COVID-19 case investigation and contact tracing programs and practice: snapshots from the field. J Public Health Manag Pract. 2022;28:353–7. https://doi.org/10.1097/PHH.0000000000001488
5. CDC. SARS-CoV-2 variant classifications and definitions. 2023 [cited 2023 Jul 1]. https://www.cdc.gov/coronavirus/2019-ncov/variants/variant-classifications.html
6. OpenDataPhilly. COVID tests and cases. 2022 [cited 2023 Jul 1]. https://opendataphilly.org/datasets/covid-tests-and-cases
7. Lash RR, Moonan PK, Byers BL, Bonacci RA, Bonner KE, Donahue M, et al. COVID-19 contact tracing in the United States, 2020. JAMA Netw Open. 2021;4:e2115850. https://doi.org/10.1001/jamanetworkopen.2021.15850
8. Adhikari BB, Arifkhanova A, Coronado F, Fischer LS Jr. BG, Jeon S, et al. COVIDTracer Advanced: a planning tool to illustrate the resources needed to conduct contact tracing and monitoring of coronavirus disease 2019 (COVID-19) cases and the potential impact of community interventions and contact tracing efforts on the spread of COVID-19 2020 [cited 2023 Jul 1]. https://www.cdc.gov/coronavirus/2019-ncov/php/contact-tracing/COVIDTracerTools.html
9. Oeltmann JE, Vohra D, Matulewicz HH, DeLuca N, Smith JP, Couzens C, et al. Isolation and quarantine for COVID-19 in the United States, 2020–2022. Clin Infect Dis. 2023;77:212–9. https://doi.org/10.1093/cid/ciad163
10. DeLuca N, Caruso E, Gupta R, Kemmerer C, Coughlin R, Chan O, et al. Experiences with COVID-19 case investigation and contact tracing: a qualitative analysis. SSM Qual Res Health. 2023;3:100244.
11. Kwok KO, Tang A, Wei VWI, Park WH, Yeoh EK, Riley S. Epidemic models of contact tracing: systematic review of transmission studies of severe acute respiratory syndrome and Middle East respiratory syndrome. Comput Struct Biotechnol J. 2019;17:186–94. https://doi.org/10.1016/j.csbj.2019.01.003

Address for correspondence: Seonghye Jeon, Centers for Disease Control and Prevention, 1600 Clifton Rd NE, Mailstop H24-11, Atlanta, GA 30333-4018, USA; email: sjeon@cdc.gov

Power Law for Estimating Underdetection of Foodborne Disease Outbreaks, United States

Laura Ford,[1] Julie L. Self,[1] Karen K. Wong, Robert M. Hoekstra, Robert V. Tauxe, Erica Billig Rose, Beau B. Bruce

We fit a power law distribution to US foodborne disease outbreaks to assess underdetection and underreporting. We predicted that 788 fewer than expected small outbreaks were identified annually during 1998–2017 and 365 fewer during 2018–2019, after whole-genome sequencing was implemented. Power law can help assess effectiveness of public health interventions.

Each year in the United States, >800 foodborne outbreaks are reported, causing >14,000 illnesses and >800 hospitalizations (*1*–*3*). Foodborne outbreaks range from small, localized outbreaks, such as those associated with a locally contaminated meal shared by family or friends, to large, multistate outbreaks associated with a contaminated food that is widely distributed. Selection and information biases, pathogen testing methods, and outbreak size can affect detection, investigation, and reporting (*4*). However, few methods are available to estimate the extent of outbreak underdetection and underreporting.

Outbreaks can be considered natural occurrences with a mathematical relationship between frequency and size. Several studies have used a power law distribution, where one variable is proportional to the power of another, to help describe disease outbreaks or transmission (*5*–*9*). We examined the mathematical relationship between foodborne outbreak frequency and size to estimate the number of expected outbreaks of different sizes, comparing power law, log-normal, and exponential distributions by using censored and complete data to clarify underdetection and underreporting.

The Study

Local, state, and federal public health agencies in the United States identify and investigate foodborne outbreaks and report them to the Foodborne Disease Outbreak Surveillance System (FDOSS; https://www.cdc.gov/fdoss). In FDOSS, a foodborne outbreak is defined as ≥2 similar illnesses associated with a common food source. We used FDOSS data from 1998–2019 and defined outbreak size as the number of laboratory-confirmed cases. We also included outbreaks with ≥2 similar illnesses that had only 1 confirmed case. We evaluated the fit of power law, log-normal, and exponential distributions by applying the Kolmogorov-Smirnov (KS) statistic (*10*) to the number of outbreaks by size.

We estimated medians and 90% credible intervals (CrIs) for the minimum threshold, slope, and difference between expected and actual outbreak frequency by bootstrapping 5,000 random samples with replacement from the dataset of all outbreaks of the same size. We defined outbreaks of <10 confirmed cases as small and outbreaks of >100 confirmed cases as large. We conducted all analyses in R (The R Foundation for Statistical Computing, https://www.r-project.org) by using the poweRlaw package version 0.70.6 (*11*). We provide additional methods and R script (Appendix 1, https://wwwnc.cdc.gov/EID/article/30/2/23-0342-App1.pdf) and the dataset used (Appendix 2, https://wwwnc.cdc.gov/EID/article/30/2/23-0342-App2.xlsx).

During 1998–2019, a total of 10,026 foodborne outbreaks were reported in the United States, ranging from 1 to 1,500 laboratory-confirmed cases. The data appeared linear on a log-log scale, consistent with a power law distribution (Figure 1, panel A). We rejected the exponential and log-normal distributions because they fit poorly based on the KS statistic (exponential 0.109, p<0.001; log-normal 0.0101, p<0.001). The power law distribution fit the data (KS = 0.00985, p = 0.15).

Foodborne outbreaks with ≥4 (90% CrI 4–8) cases followed a power law distribution of $\alpha = 2.15$ (90%

Author affiliation: Centers for Disease Control and Prevention, Atlanta, Georgia, USA

DOI: https://doi.org/10.3201/eid3002.230342

[1]These first authors contributed equally to this article.

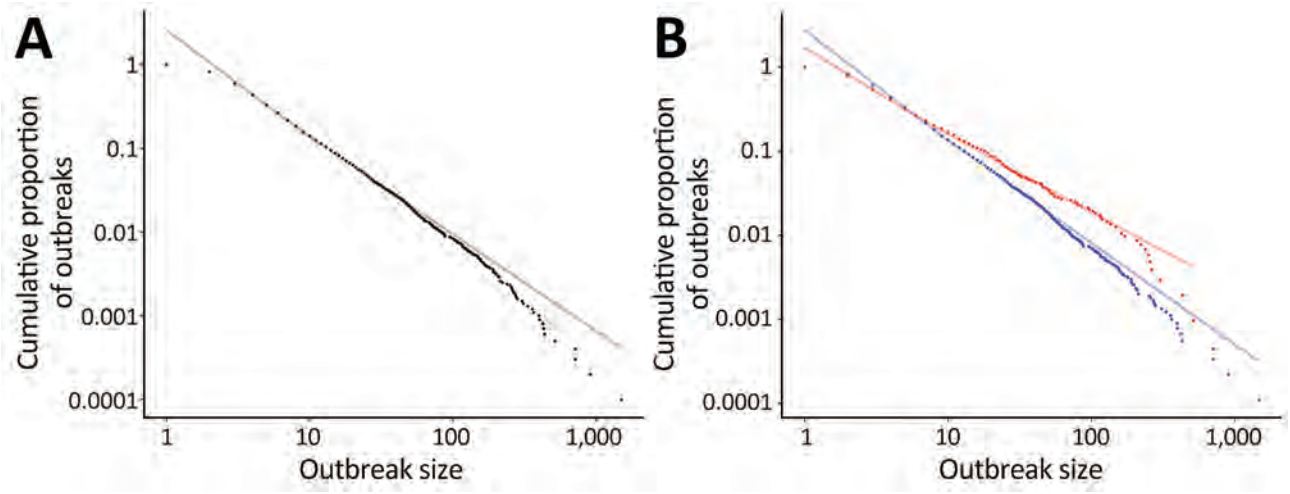

Figure 1. Log-log scale of foodborne outbreak size versus frequency from a power law for estimating underdetection of foodborne disease outbreaks, United States. A) Actual (black points) versus expected from the power law distribution (gray line) 1998–2019; B) actual (blue points) versus expected (light blue line) 1998–2017 and actual (red points) versus expected (light red line) 2018–2019. Estimates for the difference between the number of expected and actual small (<10 cases) and large (>100 cases) outbreaks were calculated by the sum of the differences between each of the relevant actual points and the expected line at the same x-value. Annual estimates were then calculated by dividing the number of years represented.

CrI 2.12–2.19) (Figure 2). We estimated 718 (90% CrI 594–783) fewer than expected small outbreaks and 0.4 (90% CrI −0.07–0.9) fewer than expected large outbreaks occurred annually, representing 841 (90% CrI 669–932) fewer than expected small outbreak-associated illnesses and 574 (90% CrI 325–871) fewer than expected large outbreak-associated illnesses.

By 2018, most US public health laboratories were using whole-genome sequencing (WGS) to subtype some bacteria that cause foodborne illness, including *Salmonella enterica*, *Escherichia coli*, and *Listeria monocytogenes*. WGS has helped public health practitioners detect more outbreaks and determine the food or other source while outbreaks are still small (*12*).

A power law distribution fit the outbreak data for both the 1998–2017 (8,993 outbreaks; KS = 0.00949, p = 0.37) and the 2018–2019 (1,033 outbreaks; KS = 0.0211, p = 0.43) periods (Figure 1, panel B). The minimum threshold was ≥5 cases (90% CrI 4–9) and α = 2.20 (90% CrI 2.16–2.25) during 1998–2017, compared with

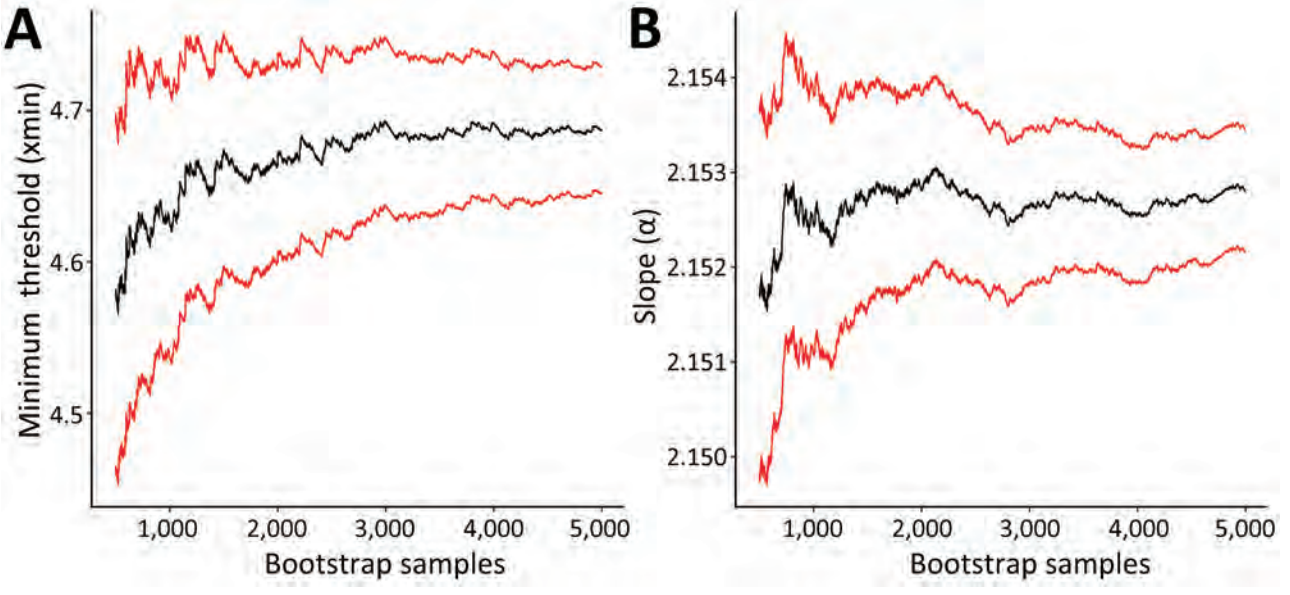

Figure 2. Parameter estimates from a power law for estimating underdetection of foodborne disease outbreaks, United States. Graphs display distribution of foodborne outbreak size and frequency for the minimum threshold (A) and slope (B) for outbreaks during 1998–2019. Black lines represent bootstrapped parameter estimate; red lines represent 90% credible intervals.

a minimum threshold of ≥3 cases (90% CrI 2–6) and α = 1.91 (90% CrI 1.83–2.00) during 2018–2019. We estimate 788 (90% CrI 665–888) fewer than expected small outbreaks and 0.4 (90% CrI −0.06 to 0.9) fewer than expected large outbreaks were identified annually during 1998–2017, compared with 365 (90% CrI 277–475) fewer than expected small outbreaks and 1 (90% CrI −3 to 2) more than expected large outbreak annually during 2018–2019.

Conclusions

We found that foodborne disease outbreak data fit a power law distribution. On the basis of that finding, we quantified the unobserved burden of foodborne outbreaks in the United States during 1998–2019, predicting that 718 fewer than expected small outbreaks are detected, investigated, and reported every year and 1 fewer than expected large outbreak was detected and reported about every 3 years. Detection and reporting of foodborne outbreaks have improved; during 2018–2019, we estimate that underreporting of small outbreaks decreased by 54% (365/year) compared with 1998–2017 (788/year). The power law distribution quantifies improvements in detection and reporting, which could in part be explained by WGS.

Many factors affect outbreak and case detection, investigation, and reporting, including whether the outbreak is caused by a common molecular strain, how many persons ate the contaminated food, clinical manifestations, care-seeking, diagnostic testing, and laboratory or health department outbreak investigation and response capacity. Natural limitations to outbreak size are also likely, including the geographic distribution of a contaminated food product, food safety policies that control contamination in the food system, and product recalls or other disease control efforts that end large outbreaks before natural limitations are reached.

Power law distribution parameters should be stable over time, but changes in the slope or minimum threshold or deviations from the estimated power law might indicate perturbations of concern. Understanding the different power law parameters that underlie outbreak size and frequency can also be useful for exploring how detection of foodborne outbreaks differs by pathogen or food vehicle. In addition, those parameter changes can reflect public health interventions.

The power law distribution has applications beyond foodborne outbreaks and has been applied to COVID-19, measles, and gonorrhea (*5*–*9*). By predicting outbreak frequency and the extent of underdetection, we can plan outbreak response needs for routine and surge scenarios, assess the effects of outbreak prevention efforts, and improve estimates of the proportion of illnesses that are outbreak-associated versus sporadic.

A limitation of this analysis is that failure to statistically reject the power law distribution does not ensure that the data follow a power law. The KS statistic also might miss systematic patterns that differ between distributions because it uses only the largest difference. However, we used a hypothesis-driven rationale to censor data by establishing a minimum threshold, tested alternative distributions, and characterized uncertainty by using the bootstrap. Another limitation is that we only include reported outbreaks with laboratory confirmed cases, which could underestimate cases but also reduces variation from comparing across multiple types of outbreaks. Laboratory-confirmed cases also could be an underestimate for the largest outbreaks because public health laboratories might run out of resources to subtype patient samples or be faced with other constraints due to the overwhelming size of the outbreak.

In conclusion, we used the power law distribution on foodborne disease outbreak data to quantify underdetection and how foodborne disease reporting has improved. The improvement in underdetection during 2018–2019 could in part be explained by improved detection or investigation from the implementation of WGS. The power law distribution can be used to assess the impact of past and future public health interventions and as a tool for resource planning.

This work was supported by the Centers for Disease Control and Prevention. The study did not receive dedicated funding.

About the Author

Dr. Ford is an epidemiologist in the Division of Foodborne, Waterborne, and Environmental Diseases, National Center for Emerging and Zoonotic Infectious Diseases, Centers for Disease Control and Prevention, Atlanta, Georgia, USA. Her primary research interests include surveillance and outbreak response for foodborne diseases.

References

1. Centers for Disease Control and Prevention (CDC). Surveillance for foodborne disease outbreaks, United States, 2015, annual report. Atlanta: US Department of Health and Human Services, CDC; 2017.
2. Centers for Disease Control and Prevention (CDC). Surveillance for foodborne disease outbreaks, United States, 2016, annual report. Atlanta: US Department of Health and Human Services, CDC; 2018.
3. Centers for Disease Control and Prevention (CDC). Surveillance for foodborne disease outbreaks, United States,

2017, annual report. Atlanta: US Department of Health and Human Services, CDC; 2019.
4. Mouly D, Goria S, Mounié M, Beaudeau P, Galey C, Gallay A, et al. Waterborne disease outbreak detection: a simulation-based study. Int J Environ Res Public Health. 2018;15:1505. https://doi.org/10.3390/ijerph15071505
5. Beare BK, Toda AA. On the emergence of a power law in the distribution of COVID-19 cases. Physica D. 2020;412:132649. https://doi.org/10.1016/j.physd.2020.132649
6. Komarova NL, Schang LM, Wodarz D. Patterns of the COVID-19 pandemic spread around the world: exponential versus power laws. J R Soc Interface. 2020;17:20200518. https://doi.org/10.1098/rsif.2020.0518
7. Blasius B. Power-law distribution in the number of confirmed COVID-19 cases. Chaos. 2020;30:093123. https://doi.org/10.1063/5.0013031
8. Keeling M, Grenfell B. Stochastic dynamics and a power law for measles variability. Philos Trans R Soc Lond B Biol Sci. 1999;354:769–76. https://doi.org/10.1098/rstb.1999.0429
9. Whittles LK, White PJ, Didelot X. A dynamic power-law sexual network model of gonorrhoea outbreaks. PLOS Comput Biol. 2019;15:e1006748. https://doi.org/10.1371/journal.pcbi.1006748
10. Chakravarti IM, Laha RG, Roy J. Handbook of methods of applied statistics, volume I. New York: John Wiley & Sons; 1967.
11. Gillespie CS. Fitting heavy tailed distributions: the poweRlaw package. J Stat Softw. 2015;64:1–16. https://doi.org/10.18637/jss.v064.i02
12. Besser JM, Carleton HA, Trees E, Stroika SG, Hise K, Wise M, et al. Interpretation of whole-genome sequencing for enteric disease surveillance and outbreak investigation. Foodborne Pathog Dis. 2019;16:504–12. https://doi.org/10.1089/fpd.2019.2650

Address for correspondence: Laura Ford, Centers for Disease Control and Prevention, 1600 Clifton Rd NE, MS H24-11, Atlanta, GA 30329-4018, USA; email: qdz4@cdc.gov

Tick-Borne Encephalitis, Lombardy, Italy

Alessandra Gaffuri, Davide Sassera, Mattia Calzolari, Lucia Gibelli, Davide Lelli, Alessandra Tebaldi, Nadia Vicari, Alessandro Bianchi, Claudio Pigoli, Monica Cerioli, Luca Zandonà, Giorgio Varisco, Irene Bertoletti, Paola Prati

Tick-borne encephalitis was limited to northeast portions of Italy. We report in Lombardy, a populous region in the northwest, a chamois displaying clinical signs of tickborne encephalitis virus that had multiple virus-positive ticks attached, as well as a symptomatic man. Further, we show serologic evidence of viral circulation in the area.

Tick-borne encephalitis (TBE) is a considerable public health concern caused by the tick-borne encephalitis virus (TBEV), a member of the Flaviviridae family. This virus is classified into 5 genotypes; European, Siberian, and Far Eastern are the main types, each exhibiting distinct epidemiologic patterns and clinical manifestations (*1*). TBEV infection is mainly attributed to the bite of *Ixodes* ticks, most notably *Ixodes ricinus* in Europe (*1*). The virus primarily affects the central nervous system, leading to a range of neurologic symptoms and potential long-term complications, including death. Clinical manifestations of TBE consist of a first phase characterized by headache and fever and a second phase, where myelitis can cause altered consciousness, tremors, ataxia, and paresis (*1*).

TBEV is distributed across several regions of Europe and Asia. European TBEV is prevalent in Austria, Germany, Sweden, Switzerland, and the Russian Federation (*2*). This strain is endemic in northeastern Italy (*3*), but the rest of the country has been considered virus-free, with the exception of a single autochthonous case in Emilia-Romagna (*4*). A recent serologic screening of wild ungulates confirmed the absence of TBEV in the Piedmont region (*5*). No data on TBEV in the most populous region of Italy, Lombardy, have been published recently. Considering Lombardy's position, bordering states (Switzerland) and regions where the pathogen is endemic, and the abundant presence of *I. ricinus* ticks (*6*,*7*), Lombardy represents an area at risk for expansion of TBEV.

The Study

The Experimental Zooprophylactic Institute of Lombardy and Emilia Romagna (IZSLER) is responsible for the surveillance of the wild fauna in the Lombardy region. Considering the potential risk for TBEV expansion, the Institute started molecular screening of ticks retrieved from humans in Lombardy in 2019 (*8*). Since 2021, serologic analysis of wild ungulates (*9*) was added to the surveillance program, including serum samples collected in the previous year. A total of 3,555 ticks have been subjected to molecular surveillance since the start of the program (2,556 from humans, 999 from wildlife), and none were found to be positive. Out of the 1,954 examined samples from wild ungulates, 47 samples tested positive for TBEV antibodies (Table; Figure 1, https://wwwncdc.eid.gov/EID/articles/30/2/23-1016-F1.htm). Albeit not fully conclusive, those results prompted an increased alert, with attention to possible cases of neurologic symptoms compatible with TBE in animals and humans in the region.

Author affiliations: Bergamo Unit, Experimental Zooprophylactic Institute of Lombardy and Emilia Romagna, Bergamo, Italy (A. Gaffuri, L. Zandonà, G. Varisco); University of Pavia, Italy, and The I.R.C.C.S. Policlinico San Matteo Foundation, Pavia, Italy (D. Sassera); Reggio Emilia Unit, Experimental Zooprophylactic Institute of Lombardy and Emilia Romagna, Reggio Emilia, Italy (M. Calzolari); Milano Unit, Experimental Zooprophylactic Institute of Lombardy and Emilia Romagna, Milano, Italy (L. Gibelli, C. Pigoli); Virology Unit, Experimental Zooprophylactic Institute of Lombardy and Emilia Romagna, Brescia, Italy (D. Lelli); ASST Papa Giovanni XXIII Hospital, Bergamo, Italy (A. Tepaldi); Pavia Unit, Experimental Zooprophylactic Institute of Lombardy and Emilia Romagna, Pavia, Italy (N. Vicari, P. Prati); Sondrio Unit, Experimental Zooprophylactic Institute of Lombardy and Emilia Romagna, Sondrio, Italy (A. Bianchi, I. Bertoletti); Epidemiology Unit, Experimental Zooprophylactic Institute of Lombardy and Emilia Romagna, Brescia (M. Cerioli).

DOI: http://doi.org/10.3201/eid3002.231016

Table. Results of testing for tick-borne encephalitis virus antibodies among serum samples taken from wild ungulate species, Italy*

Year	Wild ungulate species, no. positive/no. tested			
	Chamois	Roe deer	Red deer	Mouflon
2020	8/216	1/145	11/194	NA
2021	6/222	0/187	4/217	0/25
2022	4/114	3/154	7/255	0/30
2023	1/4	0/7	2/184	NA
Total	19/556	4/493	24/850	0/55

*NA, not available.

On November 28, 2022, a 49-year-old male hunter sought treatment at the Pope John XXIII Hospital in Bergamo, Lombardy, displaying clinical symptoms compatible with TBE. The man reported a tick bite in the previous month while in Val Brembana valley (Figure 1), with no recent history of travel outside of the region, but multiple mountain excursions in the study area. He reported clinical manifestations that included fever and fatigue, followed a few days later by neurologic symptoms (lack of coordination and equilibrium), which supported a 2-phase clinical picture compatible with TBE (*1*). Serologic exam for TBEV resulted in positive readings for both IgG and IgM. The patient's clinical picture improved spontaneously, and he was discharged on December 12, 2022. Since that time, he has reported myalgia, fatigue, impairment of concentration, and memory lapses.

On May 12, 2023, in Carona, Bergamo Province, Lombardy region (Figure 1), a hunter encountered a chamois (European goat-antelope) that had neurologic symptoms of ataxia, muscle tremors, incoordination, and frequent swallowing. The chamois was killed and conferred to the IZSLER, where we performed necropsy and collected blood and organs for further examination. Postmortem examination revealed poor general condition, absence of adipose tissue, and incomplete molt. Necropsy did not reveal mechanical trauma or ingestion of poisonous food. A massive tick infestation was presen; some ticks were clustered, but others were scattered on various areas of the body. At the lung level, pleuro-costal adhesions and parasitic nodular lesions were evident. Other observations included gastrointestinal nematodes, pallor of the kidney parenchyma and cribrous appearance of the cortical surface, hypertrophy of the adrenals, and pallor of the liver, including focal irregular, whitish lesions on the surface. Histopathology revealed severe, chronic, nonpurulent meningoencephalitis, characterized by perivascular lymphohistiocytic cuffs, neuronal necrosis, and satellitosis (Figure 2, panel A). Immunohistochemical analysis showed neuronal positivity for TBEV (Figure 2, panel B). An attempt to culture the virus from brain tissue on Vero E6 cells (IZSLER Biobank code BSCL87, http://www.ibvr.org) was unsuccessful.

The animal's blood was used for molecular and serologic investigations, which both showed evident TBEV positivity, as did a pool of organs and brain. The threshold cycle of the PCR of the organ pool was low, suggesting a high viraemia. A total of 26 ticks were found attached to the body, all identified morphologically as adult *I. ricinus* ticks, 12 of them male and 14 partially engorged female. All retrieved ticks were subjected to TBEV PCR; 4 male and 8 female ticks showed clear positivity. We Sanger sequenced PCR products (224 nt) from the chamois and from the ticks; sequences were all identical (Genbank accession nos. OR473050–4) so we used 1 representative for phylogenetic reconstruction (Figure 3). The phylogenetic tree shows that the novel sequence falls within sequences representing the European genotype (*10*).

In parallel, we performed bacteriologic examination of the viscera of the chamois and tested for *Anaplasma phagocytophilum*, *Babesia* spp., and pestiviruses. All test results were negative. We also

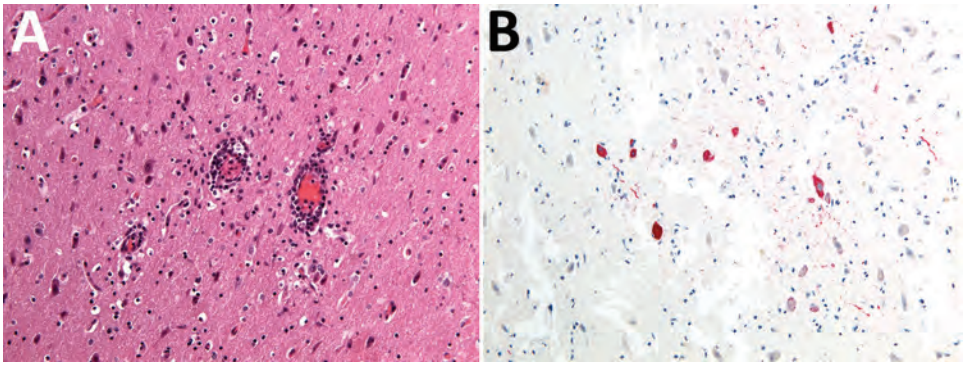

Figure 2. Histopathologic findings from the brain of a wild chamois with tick-borne encephalitis virus found in the Lombardy region of Italy in May 2023. A) Severe, chronic, nonpurulent meningoencephalitis characterized by perivascular lymphohistiocytic cuffs. Hematoxylin-eosin stain; original magnification ×20. B) Neuronal positivity for tick-borne encephalitis virus. Immunohistochemistry; original magnification ×20.

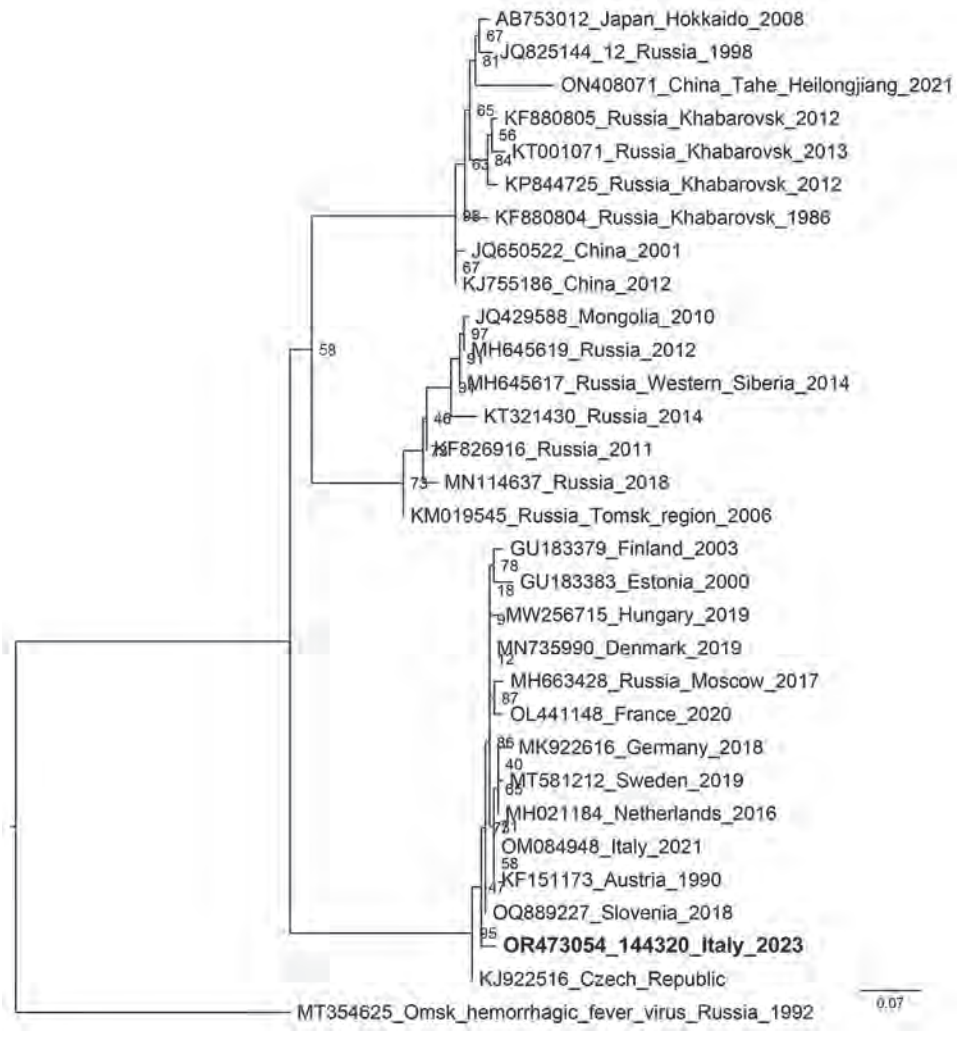

Figure 3. Phylogenetic tree of a representative tick-borne encephalitis virus (boldface) from samples collected from a wild chamois and ticks in the Lombardy region of Italy. Tree shows the relationship between the obtained sequence of a 224-bp portion of the nonstructural 5 gene and reference sequences from GenBank (accession numbers, country, and year of isolation provided). The phylogenetic analysis was performed on the homologous sequences by the maximum-likelihood method using IQ-TREE software (http://www.iqtree.org), after alignment.

screened the ticks for other pathogens, namely *Borrelia* spp., *Babesia* spp., *Rickettsia* spp., *Francisella* spp., *Coxiella burnetii*, and *Anaplasma*, as previously performed (*11*,*12*). All results were negative, except for 2 females found positive for *Rickettsia helvetica* and 1 found positive for *Borrelia miyamotoi,* all confirmed by Sanger sequencing.

Conclusions

We report TBE cases in a human and in a chamois in the Lombardy region of Italy, as well as molecular positivity in *I. ricinus* ticks. A clinical case in a chamois is especially noteworthy given recently reported clinical cases of TBEV in other wild and domestic animals, including ruminants (*13*), and the steady increase of wild ruminants in the Alps (*14*). The high viraemia of the chamois we studied, together with the TBEV positivity of multiple attached ticks, suggests a potential role in the maintenance of the virus, one generally not considered (*13*,*15*). Our finding of TBE-positive *I. ricinus* male ticks with sequences identical to female ticks is compatible with transstadial and venereal transmission; female tick positivity could also be explained by cofeeding. When considered alongside the high amount of virus detected in the chamois, the findings from our analysis of the attached ticks corroborate the existence of a complete cycle of infection and a potential role of this animal as reservoir.

Results from our investigation indicate the presence of TBE in northwestern Italy and suggest the need for increased awareness of the westward spread of TBEV, now present in most of the central Alps. The severity of the reported human case highlights the importance of raising the awareness of stakeholders and high-risk portions of the population (e.g., hunters, excursionists, and farmers) to promote vaccination and control of raw milk and traditional cheesemaking. Taking immediate preventive measures in the most at-risk areas will help prevent subsequent clinical cases of TBEV in humans.

Work was funded by the Extended Partnership Project INF-ACT (PE_00000007), which is part of the National Recovery and Resilience Plan, and by the Italian Ministry of Health, Directorate–General for animal health and veterinary medicinal products (grant no. IZSLER 2021/014).

About the Author

Dr. Gaffuri is a graduate in veterinary medicine in Milan, Italy, and works at the Istituto Zooprofilattico Sperimentale della Lombardia e dell'Emilia Romagna, Bergamo. She is involved in research and surveillance in microbiology, and animal and wildlife health.

References

1. Chiffi G, Grandgirard D, Leib SL, Chrdle A, Růžek D. Tick-borne encephalitis: a comprehensive review of the epidemiology, virology, and clinical picture. Rev Med Virol. 2023;33:e2470. https://doi.org/10.1002/rmv.2470
2. Wondim MA, Czupryna P, Pancewicz S, Kruszewska E, Groth M, Moniuszko-Malinowska A. Epidemiological trends of trans-boundary tick-borne encephalitis in Europe, 2000–2019. Pathogens. 2022;11:704. https://doi.org/10.3390/pathogens11060704
3. Alfano N, Tagliapietra V, Rosso F, Ziegler U, Arnoldi D, Rizzoli A. Tick-borne encephalitis foci in northeast Italy revealed by combined virus detection in ticks, serosurvey on goats and human cases. Emerg Microbes Infect. 2020;9:474–84. https://doi.org/10.1080/22221751.2020.1730246
4. Barp N, Cappi C, Meschiari M, Battistel M, Libbra MV, Ferri MA, et al. First human case of tick-borne encephalitis in non-endemic region in Italy: a case report. Pathogens. 2022;11:854. https://doi.org/10.3390/pathogens11080854
5. Garcia-Vozmediano A, Bellato A, Rossi L, Hoogerwerf MN, Sprong H, Tomassone L. Use of wild ungulates as sentinels of TBEV circulation in a naïve area of the Northwestern Alps, Italy. Life (Basel). 2022;12:1888. https://doi.org/10.3390/life12111888
6. Cafiso A, Olivieri E, Floriano AM, Chiappa G, Serra V, Sassera D, et al. Investigation of tick-borne pathogens in *Ixodes ricinus* in a peri-urban park in Lombardy (Italy) reveals the presence of emerging pathogens. Pathogens. 2021;10:732. https://doi.org/10.3390/pathogens10060732
7. Otranto D, Dantas-Torres F, Giannelli A, Latrofa MS, Cascio A, Cazzin S, et al. Ticks infesting humans in Italy and associated pathogens. Parasit Vectors. 2014;7:328. https://doi.org/10.1186/1756-3305-7-328
8. Schwaiger M, Cassinotti P. Development of a quantitative real-time RT-PCR assay with internal control for the laboratory detection of tick borne encephalitis virus (TBEV) RNA. J Clin Virol. 2003;27:136–45. https://doi.org/10.1016/S1386-6532(02)00168-3
9. Lelli D, Moreno A, Zanoni M, Pezzoni G, Sozzi E, Brocchi E, et al. Tick-borne encephalitis (TBE): development of a serological test for the detection of specific antibodies in animal sera [D10:132]. Presented at: Epizone 7th Annual Meeting; Brussels, Belgium; October 1–4, 2013.
10. Formanová P, Černý J, Bolfíková BČ, Valdés JJ, Kozlova I, Dzhioev Y, et al. Full genome sequences and molecular characterization of tick-borne encephalitis virus strains isolated from human patients. Ticks Tick Borne Dis. 2015;6:38–46. https://doi.org/10.1016/j.ttbdis.2014.09.002
11. Maioli G, Pistone D, Bonilauri P, Pajoro M, Barbieri I, Mulatto P, et al. Ethiological agents of rickettsiosis and anaplasmosis in ticks collected in Emilia-Romagna region (Italy) during 2008 and 2009. Exp Appl Acarol. 2012;57:199–208. https://doi.org/10.1007/s10493-012-9535-z
12. Pajoro M, Pistone D, Varotto Boccazzi I, Mereghetti V, Bandi C, Fabbi M, et al. Molecular screening for bacterial pathogens in ticks (*Ixodes ricinus*) collected on migratory birds captured in northern Italy. Folia Parasitol (Praha). 2018;65:2018.008. https://doi.org/10.14411/fp.2018.008
14. Da Rold G, Obber F, Monne I, Milani A, Ravagnan S, Toniolo F, et al. Clinical tick-borne encephalitis in a roe deer (*Capreolus capreolus* L.). Viruses. 2022;14:300. https://doi.org/10.3390/v14020300
15. Paulsen KM, das Neves CG, Granquist EG, Madslien K, Stuen S, Pedersen BN, et al. Cervids as sentinel-species for tick-borne encephalitis virus in Norway—a serological study. Zoonoses Public Health. 2020;67:342–51. https://doi.org/10.1111/zph.12675
17. Michelitsch A, Wernike K, Klaus C, Dobler G, Beer M. Exploring the reservoir hosts of tick-borne encephalitis virus. Viruses. 2019;11:669. https://doi.org/10.3390/v11070669

Address for correspondence: Davide Sassera, Department of Biology and Biotechnology, University of Pavia, Via Ferrata 9, 27100 Pavia (PV), Italy; Email: davide.sassera@unipv.it

Critically Ill Patients with Visceral *Nocardia* Infection, France and Belgium, 2004–2023

Lucas Khellaf, Virginie Lemiale, Maxens Decavèle, Marc Pineton de Chambrun, Alexandra Beurton, Toufik Kamel, Anabelle Stoclin, Djamel Mokart, Fabrice Bruneel, Clara Vigneron, Achille Kouatchet, Benoît Henry, Jean-Pierre Quenot, Grégoire Jolly, Nahema Issa, Matthieu Bellal, Julien Poissy, Claire Pichereau, Julien Schmidt, Nathalie Layios, Maxime Gaillet, Elie Azoulay, Adrien Joseph

We studied 50 patients with invasive nocardiosis treated during 2004–2023 in intensive care centers in France and Belgium. Most (65%) died in the intensive care unit or in the year after admission. *Nocardia* infections should be included in the differential diagnoses for patients in the intensive care setting.

Nocardia is a ubiquitous, filamentous, gram-positive bacillus present in soil and decaying plants (*1*), affecting immunocompromised patients by way of inhalation, with a risk of secondary dissemination. Invasive *Nocardia* infections are mainly observed in patients who have undergone organ transplantation (incidence 0.2%) and hematopoietic stem cell transplantation (incidence 1.7%). Infections also occur in persons with primary immunodeficiency, solid cancer, or autoimmune disease. Other previously identified risk factors include use of long-term steroids and calcineurin inhibitors (*2*–*4*). Pulmonary involvement constitutes the most common manifestation of *Nocardia* infection, which can potentially lead to secondary dissemination, particularly in immunocompromised populations; the central nervous system is a common site, and many cases involving asymptomatic manifestations (*5*).

Blood cultures are positive in 10%–20% of cases involving *Nocardia* infection, and lung PCR can indicate colonization, requiring such tests as bronchoalveolar lavage and abscess needle aspiration. *Nocardia* species are typically resistant to common antibiotics, which contribute to the complexity of diagnosing and managing disseminated infections (*6*,*7*). The mortality rate associated with *Nocardia* infection is substantial; 16%–40% of patients die within the first year of diagnosis, and outcomes depend largely on the underlying disease (*6*–*8*). We explored the risk factors, characteristics, and prognosis of patients with invasive nocardiosis in the context of the intensive care setting.

The Study

We conducted a retrospective, multicenter study of patients with invasive nocardiosis admitted to 22 intensive care units (ICUs) from the Groupe de Recherche Respiratoire en Réanimation Onco-Hématologique (Grrr-OH) during 2004–2023 in France and Belgium. We established inclusion criteria as unplanned ICU medical admission, age >18 years, and a documented invasive nocardiosis diagnosis (before

Author affiliations: Saint-Louis Teaching Hospital, Public Assistance Hospitals of Paris (APHP), Paris, France (L. Khellaf, V. Lemiale, E. Azoulay, A. Joseph); Pitié-Salpétière Teaching Hospital, APHP, Paris (M. Decavèle, M. Pineton de Chambrun); Hôpital Tenon, Groupe Hospitalo-Universitaire Sorbonne University, APHP, Paris (A. Beurton); Centre Hospitalier Régional d'Orléans, Orléans, France (T. Kamel); Institut Gustave Roussy, Villejuif, France (A. Stoclin); Institut Paoli Calmettes, Marseille, France (D. Mokart); Centre Hospitalier de Versailles, Hôpital André Mignot, Le Chesnay, France (F. Bruneel); Cochin Teaching Hospital, APHP, Paris (C. Vigneron); Centre Hospitalier Universitaire d'Angers, Angers, France (A. Kouatchet); Hôpital Bicêtre, APHP, France (B. Henry); Dijon Bourgogne University Hospital, Dijon, France (J.-P. Quenot); Rouen University Hospital, Rouen, France (G. Jolly); Saint-André Hospital, Bordeaux, France (N. Issa); University Hospital of Caen, Caen, France (M. Bellal); Hôpitaux Universitaires de Strasbourg, Strasbourg, France (J. Poissy); Centre Hospitalier Intercommunal de Poissy Saint Germain, Poissy, France (C. Pichereau); Avicennes Hospital, APHP, Ile de France, France (J. Schmidt); University Hospital of Liege, Liege, Belgium (N. Layios); Lyon University Hospital, Lyon, France (M. Gaillet)

DOI: http://doi.org/10.3201/eid3002.231440

Table 1. Baseline characteristics of patients in study of critically ill patients with visceral *Nocardia* infection, France and Belgium, 2004–2023*

Baseline characteristics	Nocardiosis cases, n = 50
Age, y, median (IQR)	59 (47–67)
Sex	
M	39 (78)
F	11 (22)
Charlson score, median (IQR)	4 (3–7)
Cardiovascular risk factors, median (IQR)	2 (1–3)
Immunosuppression	46 (92)
Corticosteroids at admission	34 (68)
5–10 mg/d	5 (10)
>10 mg/d	29 (58)
Tacrolimus treatment	16 (32)
Mycophenolate mofetil treatment	12 (24)
Other conventional immunosuppressive drugs†	5 (10)
Organ transplantation	18 (36)
Kidney	12 (24)
Heart	4 (8)
Liver	1 (2)
Lung	1 (2)
Systemic autoimmune disease‡	12 (24)
Hematologic malignancies	10 20)
Aggressive B cell lymphoma	6 (12)
Acute lymphoid leukemia	3 (6)
Acute myeloid leukemia	1 (2)
No. lymphocytes/mm^3, median (IQR)	552 (287–1,210)
Gamma globulin, g/L, median (IQR)	6 (4–10)
Trimethoprim/sulfamethoxazole prophylaxis	12 (24)

*Values are no. (%) except as indicated. IQR, interquartile range.
†Azathioprine, n = 4 (8%); methotrexate, n = 1 (2%).
‡Connective tissue disease, n = 2; glomerulonephritis, n = 1; periarteritis nodos, n = 1; bullous pemphigoid, n = 1; Evans syndrome, n = 1; IgA vasculitis, n = 1; type 1 diabetes, n = 1; myasthenia gravis, n = 1; sarcoidosis, n = 1; chronic inflammatory demyelinating polyradiculoneuropathy, n = 1; inflammatory bowel disease, n = 1.

or during ICU stay). We excluded cases of suspected nocardiosis without microbiological documentation or those with a lack of medical chart data.

Documented nocardiosis was determined by a positive culture for *Nocardia* species or a *Nocardia* PCR-based assay coupled with organ involvement. Disseminated nocardiosis was characterized by the infection affecting ≥2 noncontiguous sites; bacteremia constituted dissemination if 1 organ was involved. Organ failures were identified based on the Sepsis-related Organ Failure Assessment score.

We performed a comparison between patients admitted to the ICU for *Nocardia* infection and patients enrolled in the HIGH multicenter clinical trial (*9*), which included immunocompromised patients admitted to the ICU for acute respiratory failure and compared the effect of high-flow nasal oxygen versus standard oxygen on 28-day mortality. We excluded diagnoses of *Pneumocystis* infection, acute pulmonary edema, and specific lung lesions, which we assumed could be easily distinguished from nocardiosis.

We present continuous data as median (interquartile range) and categorical data as numbers and percentages. We compared characteristics between our cohort and data from the HIGH clinical trial by using a Wilcoxon rank-sum test (continuous variables) or Fisher exact test (categorical variables). We used only variables that were statistically significant ($p<0.05$) in univariate analysis in multivariate analysis and conducted an assessment of collinearity. We performed 2-sided statistical analyses by using R statistical software version 2023.03.0+386 (The R Foundation for Statistical Computing, https://www.r-project.org).

In total, we studied 50 patients with invasive nocardiosis who were admitted to the ICU. The median age was 59 (47–67) years; 39 (78%) were men, and 11 (22%) were women. We took into account such details as patient demographics, concurrent diseases, and immunosuppressive therapies (Table 1). Almost all patients (46 [92%]) were immunocompromised; the primary causes were solid organ transplantation (18 [36%]), systemic autoimmune diseases (12 [24%]), and hematologic malignancies (10 [20%]). Steroid therapy was administered to most patients (34 [68%]). Low-dose trimethoprim/sulfamethoxazole prophylaxis was given to 12 (24%) patients.

We noted disseminated infection in almost half of the patients (48%); the most frequently involved organs were lungs (98%), central nervous system (47%), and skin (20%) (Table 2). At admission to intensive care, 33 (66%) patients had acute respiratory distress and 19 (38%) experienced coma (defined by a

Table 2. Patient clinical and radiologic findings from the intensive care unit in study of critically ill patients with visceral *Nocardia* infection, France and Belgium, 2004–2023*

Findings	Nocardiosis cases, n = 50
Clinical features	
Chronic cough†	36 (72)
No. previous antibacterial therapy lines	2 (0–3)
Fever	29 (58)
Co-infection	22 (44)
Fungal‡	11 (22)
Bacterial§	8 (16)
Viral¶	5 (10)
Lung involvement	49 (98)
Oxygen therapy at admission	32 (64)
Oxygen flow, L/min, median (IQR)	8 (4–15)
Respiratory rate, L/min, median (IQR)	30 (25–36)
Hemoptysis	8 (16)
Neurologic involvement	24 (48)
Confusion	21 (42)
Coma	16 (32)
Motor deficit	13 (26)
Cranial nerve lesions	10 (20)
Meningitis	8 (16)
Epilepsy	6 (12)
Glasgow score, median (IQR)	13 (12–14)
Skin/muscle abscess	10 (20)
Disseminated infection	24 (48)
Organ failures	45 (90)
Multiorgan	25 (50)
Respiratory	33 (66)
Including acute respiratory distress syndrome	3 (8)
Acute kidney injury	11 (22)
Hemodynamic	17 (34)
Neurologic	19 (38)
Hepatic	4 (8)
Sequential organ failure assessment score, median (IQR)	5 (3–7)
Imaging findings	
Computed tomography scan	
Lung consolidation	43 (86)
Lung nodules with cavitation	26 (52)
Pleural effusion	15 (30)
Interstitial syndrome	8 (16)
Alveolar hemorrhage	6 (12)
Lung lobes involved	
1 lobe	16 (32)
Multilobe	16 (32)
Bilateral	18 (36)
Brain magnetic resonance imaging, n = 23	
Single lesion	9 (39)
Multiple lesions	14 (61)
≥10 mm	17 (74)
<10 mm	6 (26)
Brain herniation	6 (26)
Ventriculitis	2 (9)
Diagnostics methods	
Bronchoalveolar lavage analysis	42 (84)
Diagnostic yield, n = 42	25 (60)
Computed tomography–scan targeted biopsy	18 (36)
Blood culture positivity	7 (14)
Nocardia PCR-based assay positivity	26 (52)
Nocardia culture positivity	24 (48)
Diagnosis made in intensive care unit	23 (46)

*Values are no. (%) except as indicated. IQR, interquartile range.
†Chronic cough is defined as a cough persisting for >8 weeks.
‡Fungal infections (n = 11) comprised 8 invasive *Aspergillus* sp. infections, 2 *Pneumocystis jirovecii* infections, and 1 case of cutaneous candidosis.
§Comprised 7 gram-negative bacillus co-infections and 1 methicillin-resistant *Staphylococcus aureus* co-infection.
¶Virus infections (n = 5) comprised 3 influenza infections (including 1 H1N1 co-infection) and 2 respiratory syncytial virus infections.

Glasgow Coma Scale score ≤8) or septic shock. Overall, 45 (90%) patients exhibited ≥1 organ failure; the most common were respiratory failure (33 [66%]) and multiorgan dysfunction (25 [50%]). Computed tomography scans revealed alveolar consolidations in 43 (86%) patients and cavitated nodules in 26 (52%) patients. Magnetic resonance imaging of the brain in 23 (46%) patients revealed multiple lesions in 14 (61%) patients and brain herniation in 6 (26%) patients.

Most (62%) patients received dual therapy or triple therapy, including aminoglycosides (10 [20%]), most commonly trimethoprim/sulfamethoxazole (80%) and carbapenem (51%) (Appendix Table 1, https://wwwnc.cdc.gov/EID/article/30/2/23-1440-App1.pdf). Upon admission to the intensive care unit, 32 patients (63%) required oxygen support, and 19 (38%) required mechanical ventilation. The ICU mortality rate was 22%, and the all-cause mortality rate at 1 year was 44%. In multivariable analysis, factors significantly associated with 1-year mortality included vasopressor use, fungal coinfection, and neurologic involvement (Appendix Table 2).

We compared cases of *Nocardia* infection against cases of other immunocompromised pneumonia in patients admitted to the ICU (*2*,*11*) (Figure 1; Appendix Table 3). Patients with *Nocardia* infection were younger and had a higher prevalence of autoimmune diseases and solid organ transplants. Lung consolidation (86% vs. 27%; p = 0.001) and cavitated nodules (52% vs. 1%; p = 0.001) were significantly more frequent. Upon admission to the ICU, patients with nocardiosis were rated as more severe on the Sepsis-related Organ Failure Assessment and Glasgow Coma Scale compared with patients with other immunocompromised pneumonia, but there was no significant difference in ICU mortality (22% vs. 32%; p = 0.184).

Conclusions

Based on the findings for our study population, critically ill patients with nocardiosis exhibit frequent and severe pulmonary and neurologic involvement; 44% of patients die (22 of 50) and 14% (7 of 50) experience disability at the 1-year mark. Several cohorts have documented *Nocardia* infections within diverse immunocompromised populations, reporting mortality rates of 16%–40% (*3*,*4*). In our analysis, we conducted a comparative assessment with other pneumonia cases in immunocompromised patients (*9*) to elucidate situations warranting consideration of *Nocardia* infection. Cellular immunosuppression appears to be necessary for the development of a severe *Nocardia* infection, which is consistent with previous studies (*4*,*6*,*10*), particularly among organ transplant recipients, patients with systemic autoimmune diseases, and those with hematologic malignancies. Coinfections, particularly fungal ones, were reported as an independent prognostic factor for mortality in this population (*11*) and could partially explain this initial severity. Such findings highlight the burden of

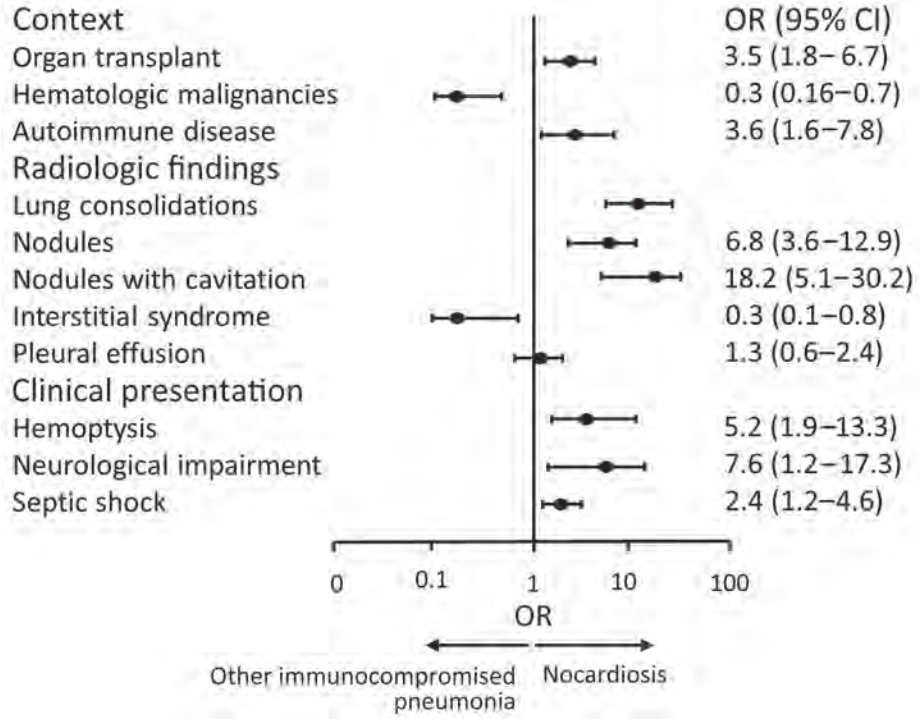

Figure. Comparison between nocardiosis and other immunocompromised pneumonia in a study of patients admitted to intensive care units in France and Belgium during 2004–2023. Other immunocompromised pneumonia data extracted from the HIGH clinical trial (*9*). OR, odds ratio.

immunosuppression and the need for vigilance in assessing concurrent infections in this population. Two recent studies suggest that trimethoprim/sulfamethoxazole could be protective against *Nocardia* infections (*11*,*12*). Because invasive *Nocardia* infections are rare, results of our study may lack statistical power, and significant prognostic or distinctive factors might have gone unnoticed. However, we believe the inclusion of patients from 22 ICUs, with few cases missing data, provides a relevant overview of nocardiosis in critically ill patients.

In summary, in this study of critically ill patients with nocardiosis, we observed high mortality rates, posing a diagnostic challenge for critical care practitioners. Our findings emphasize the need for a heightened level of vigilance in monitoring patients for *Nocardia* infection in the intensive care setting, especially among immunocompromised patients who exhibit pulmonary nodules and neurologic involvement.

This study received approval from the ethics committee of the "Société de Réanimation de langue Française" (reference 22–055). Due to the retrospective nature of the study, patient consent was waived in accordance with French law.

About the Author

Dr. Khellaf has worked in the medical intensive care unit at Saint-Louis Hospital during his residency. Research interests include medical intensive care for immunocompromised patients, systemic diseases, and opportunistic infections.

References

1. Beaman BL, Beaman L. *Nocardia* species: host-parasite relationships. Clin Microbiol Rev. 1994;7:213–64. https://doi.org/10.1128/CMR.7.2.213
2. Coussement J, Lebeaux D, van Delden C, Guillot H, Freund R, Marbus S, et al.; European Study Group for Nocardia in Solid Organ Transplantation. *Nocardia* infection in solid organ transplant recipients: a multicenter European case-control study. Clin Infect Dis. 2016;63:338–45. https://doi.org/10.1093/cid/ciw241
3. Coussement J, Lebeaux D, Rouzaud C, Lortholary O. *Nocardia* infections in solid organ and hematopoietic stem cell transplant recipients. Curr Opin Infect Dis. 2017;30:545–51. https://doi.org/10.1097/QCO.0000000000000404
4. Yagishita M, Tsuboi H, Tabuchi D, Sugita T, Nishiyama T, Okamoto S, et al. Clinical features and prognosis of nocardiosis in patients with connective tissue diseases. Mod Rheumatol. 2021;31:636–42. https://doi.org/10.1080/14397595.2020.1823070
5. Averbuch D, De Greef J, Duréault A, Wendel L, Tridello G, Lebeaux D, et al.; European Study Group for Nocardia in Hematopoietic Cell Transplantation. *Nocardia* infections in hematopoietic cell transplant recipients: a multicenter international retrospective study of the Infectious Diseases Working Party of the European Society for Blood and Marrow Transplantation. Clin Infect Dis. 2022;75:88–97. https://doi.org/10.1093/cid/ciab866
6. Rouzaud C, Rodriguez-Nava V, Catherinot E, Méchaï F, Bergeron E, Farfour E, et al. Clinical assessment of a *Nocardia* PCR-based assay for diagnosis of nocardiosis. J Clin Microbiol. 2018;56:e00002-18. https://doi.org/10.1128/JCM.00002-18
7. Lebeaux D, Bergeron E, Berthet J, Djadi-Prat J, Mouniée D, Boiron P, et al. Antibiotic susceptibility testing and species identification of *Nocardia* isolates: a retrospective analysis of data from a French expert laboratory, 2010–2015. Clin Microbiol Infect. 2019;25:489–95. https://doi.org/10.1016/j.cmi.2018.06.013
8. Brown-Elliott BA, Brown JM, Conville PS, Wallace RJ Jr. Clinical and laboratory features of the *Nocardia* spp. based on current molecular taxonomy. Clin Microbiol Rev. 2006;19:259–82. https://doi.org/10.1128/CMR.19.2.259-282.2006
9. Azoulay E, Lemiale V, Mokart D, Nseir S, Argaud L, Pène F, et al. Effect of high-flow nasal oxygen vs standard oxygen on 28-day mortality in immunocompromised patients with acute respiratory failure: the HIGH randomized clinical trial. JAMA. 2018;320:2099–107. https://doi.org/10.1001/jama.2018.14282
10. Lebeaux D, Freund R, van Delden C, Guillot H, Marbus SD, Matignon M, et al.; European Study Group for Nocardia in Solid Organ Transplantation. Outcome and treatment of nocardiosis after solid organ transplantation: new insights from a European study. Clin Infect Dis. 2017;64:1396–405. https://doi.org/10.1093/cid/cix124
11. Yetmar ZA, Thoendel MJ, Bosch W, Seville MT, Hogan WJ, Beam E. Risk factors and outcomes of nocardiosis in hematopoietic stem cell transplantation recipients. Transplant Cell Ther. 2023;29:206.e1–7. https://doi.org/10.1016/j.jtct.2022.12.004
12. Passerini M, Nayfeh T, Yetmar ZA, Coussement J, Goodlet KJ, Lebeaux D, et al. Trimethoprim-sulfamethoxazole significantly reduces the risk of nocardiosis in solid organ transplant recipients: systematic review and individual patient data meta-analysis. Clin Microbiol Infect. Oct 19:S1198-743X(23)00500-1 [Epub ahead of print]. https://doi.org/10.1016/j.cmi.2023.10.008 PMID: 37865337

Address for correspondence: Dr Lucas Khellaf, Assistance Public des Hôpitaux de Paris (AP-HP), 1 avenue Claude Vellefaux, 75010 Paris CEDEX 10, France; email: lucasremi.khellaf@aphp.fr

Confirmed Autochthonous Case of Human Alveolar Echinococcosis, Italy, 2023

Francesca Tamarozzi, Niccolò Ronzoni, Monica Degani, Eugenio Oliboni, Dennis Tappe, Beate Gruener, Federico Gobbi

In September 2023, a patient in Italy who had never traveled abroad was referred for testing for suspected hepatic cystic echinococcosis. Lesions were incompatible with cystic echinococcosis; instead, autochthonous alveolar echinococcosis was confirmed. Alveolar echinococcosis can be fatal, and awareness must be raised of the infection's expanding distribution.

The main human echinococcal infections are caused by *Echinococcus granulosus* sensu lato, which causes cystic echinococcosis (CE), and *E. multilocularis*, which causes alveolar echinococcosis (AE). The parasites have different life cycles and cause different diseases (*1*). *E. granulosus* s.l./CE is endemic worldwide in livestock-raising areas, including Italy, and accounts for most human echinococcal infections (*2*). The parasite is transmitted in a domestic cycle between dogs and livestock and causes generally benign disease in humans marked by the formation of well-defined fluid-filled cysts mostly in the liver (*1*,*2*). *E. multilocularis*/AE is endemic to the Northern Hemisphere and is transmitted in a sylvatic cycle between wild canids (e.g., foxes) and small rodents (e.g., voles) (*2*).

Humans become infected with the 2 pathogens by accidental ingestion of parasite eggs from material contaminated with infected definitive host feces. In Europe, North America, and Asia, expanding distribution has been observed in recent decades (*2*). In Europe, the historical endemic areas are Austria, France, Germany, and Switzerland, and that range has expanded to include Eastern and Northern Europe (*3*). In Italy, infected foxes have been reported over the past 20 years in the Trentino-Alto Adige region (*4*–*7*). Autochthonous animal transmission might occur in the area (*8*), and prevalence in foxes seems to be increasing (*9*). A 2017 survey conducted in the Liguria region first detected *E. multilocularis* in fecal samples of dogs and wolves, suggesting a southward expansion of the parasite (*10*) (Appendix Figure, https://wwwnc.cdc.gov/EID/article/30/2/23-1527-App1.pdf), as predicted by modeling (*3*). Surveillance of *E. multilocularis* in Europe is usually conducted voluntarily (*11*), and no structured surveillance program for animal infection in Italy occurs beside targeted surveillance through research projects.

We report a confirmed autochthonous human AE case in Italy. Ethics approval was not necessary because data were derived from routine clinical practice. The patient consented to the publication of this report.

The Study

In September 2023, a 55-year-old man in Italy was referred from his local hospital in Bolzano province, Trentino-Alto Adige region, to IRCCS Sacro Cuore Don Calabria Hospital, upon suspicion of CE. The patient was born and lived in Trentino-Alto Adige and had never traveled abroad; he worked in the tertiary sector and did not report contact with wild carnivores. He also did not report risk factors for *E. granulosus* infection.

The suspicion of CE was posed in June 2023, when he underwent abdominal ultrasound for a mild thrombocytopenia, revealing 5 recently developed small hepatic lesions (ultrasound results in 2016 were unremarkable). The lesions were described as septated and hypodense with no contrast enhancement and no calcifications on computed tomography performed in June 2023 (Figure, panels A–D),

Author affiliations: IRCCS Sacro Cuore Don Calabria Hospital, Negrar di Valpolicella, Verona, Italy (F. Tamarozzi, N. Ronzoni, M. Degani, E. Oliboni, F. Gobbi); Bernhard-Nocht-Institute, Hamburg, Germany (D. Tappe); University Hospital of Ulm, Ulm, Germany (B. Gruener); University of Brescia, Brescia, Italy (F. Gobbi)

DOI: https://doi.org/10.3201/eid3002.231527

hypointense in T1-weighted magnetic resonance imaging (MRI), and hyperintense in T2-weighted MRI (Figure, panels E–H), with no diffusion restriction. No other lesions were present on total body imaging. Results of *Echinococcus* serologic testing using Western blot method were positive, but banding pattern was not reported.

We excluded the diagnosis of CE on the basis of the lesions' morphology on ultrasound, which did not show any CE pathognomonic or compatible features. We observed 5 lesions: 1 with 2.3 cm diameter in hepatic segment I, 1 of 0.9 cm in VI, 2 subcapsular of 2.7 cm and 0.5 cm in VII, and 1 of 1.6 cm in segment VIII (adjacent to the median hepatic vein). The lesions were hypoechoic with irregular margins, particularly the lesion in segment I, which had fine and tightly packed septations (Figure, panels I–L). The lesions were not enhancing on contrast-enhanced ultrasound (Figure, panels I–L). Serologic testing using the *Echinococcus* Western Blot IgG (LDBIO Diagnostics, https://ldbiodiagnostics.com) was positive for *Echinococcus* spp., showing genus-specific 7 kDa and 26–28 kDa bands, not assignable specifically to a species. Results of an

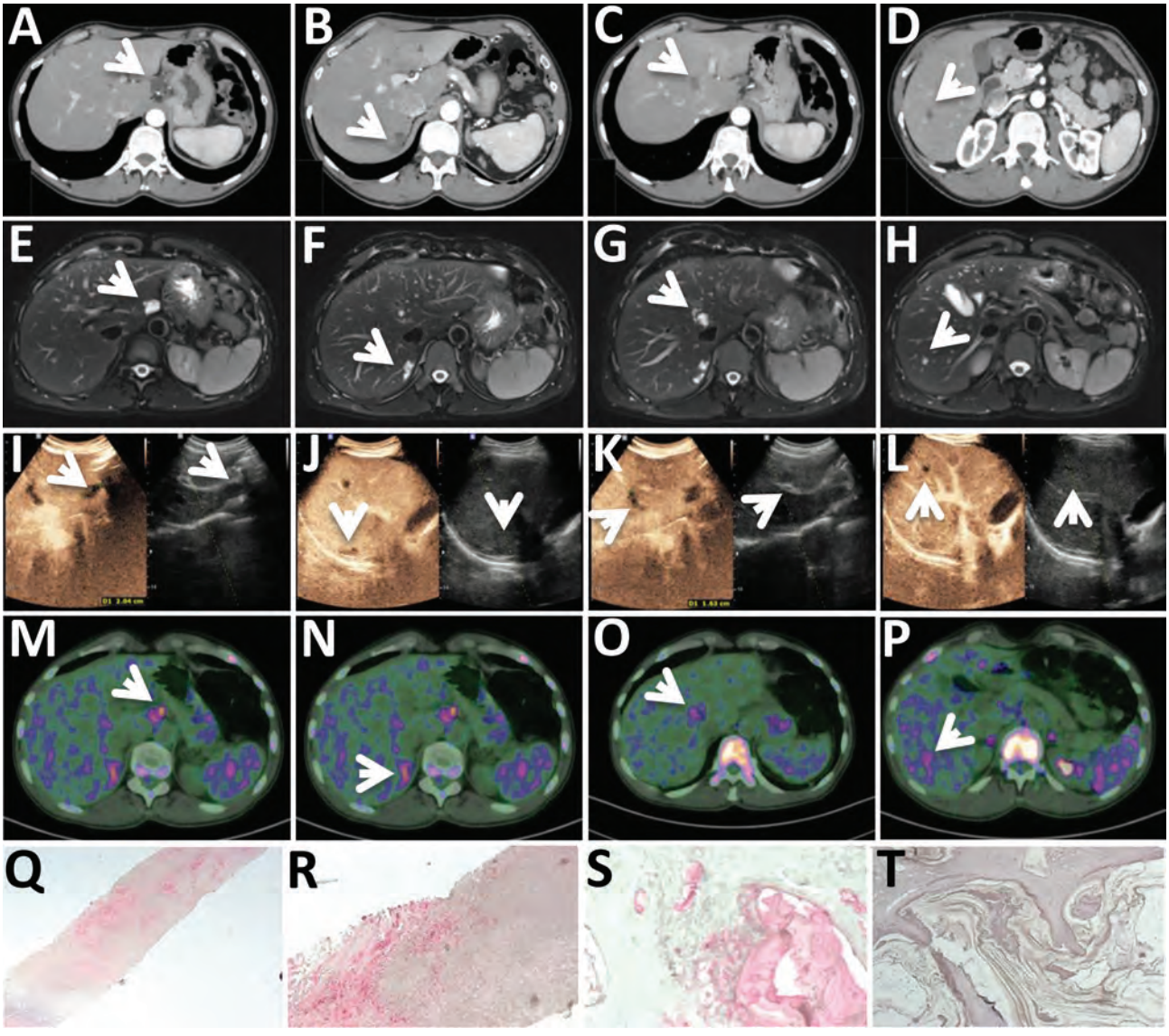

Figure. Diagnostic tests for patient in Italy with confirmed autochthonous case of human alveolar echinococcosis, 2023; white arrows indicate lesions. A–D) Contrast-enhanced computed tomography arterial phase. E–H) T2-weighted magnetic resonance imaging. I–L) Ultrasonography and contrast-enhanced ultrasonography. M–P) ^{18}F-FDG-PET scan delayed acquisition (4 hours). Q–T) Em2 immunohistochemistry indicating small particles of *Echinococcus multilocularis* (spems) stained in red in patient's sample (original magnification ×2.5 [Q] and ×20 [R]); positive alveolar echinococcosis sample control (original magnification ×20 [S]); Em2 negative control (cystic echinococcosis case, negative laminated layer; original magnification ×20) (T).

^{18}F-FDG-PET scan showed light hypermetabolism in delayed (4-hour) acquisitions (Figure, panels M–P). Taken together, those results made the lesions highly indicative of AE.

We performed a biopsy of the only accessible lesion, located in segment VI, and submitted the specimen to the German Reference Laboratory for Tropical Parasites at the Bernhard-Nocht Institute for Tropical Medicine (Hamburg, Germany). A serum sample also submitted for further serologic testing showed low antibody titers against crude antigen preparations of *E. multilocularis* and *E. granulosus* (1:40–1:80 in indirect hemagglutination [negative <1:20] and 30–40 arbitrary units in ELISA [negative <20]). Results of Em18-ELISA (*12*) were negative. Histology revealed necrotic granuloma and fibrosis without PAS-positive structures. Results of PCR testing targeting cestode cytochrome oxidase and *Echinococcus*-specific 12S rDNA (*13*) were negative. In contrast, immunohistochemistry with the monoclonal antibody Em2G11 (*14*) stained positive for small particles of *E. multilocularis* (spems) (Figure, panels Q–R). Spems consist of outer laminated layer of Em2 antigen in close proximity to AE lesions and thus confirmed the diagnosis of AE, defined by the WHO Informal Working Group on Echinococcosis (WHO-IWGE) as the presence of clinical-epidemiologic factors plus compatible imaging findings plus seropositivity for echinococcosis plus compatible histopathology (*15*). The laboratory uses Em2G11-IHC regularly for suspected AE. The immunohistochemistry has been extensively validated and is also used by other laboratories; CE lesions and other cestode lesions stain negatively (*14*), whereas lesions by neotropical *E. vogeli* stain faintly (Appendix reference *16*).

Staging according to the WHO-IWGE (*1*,*15*) was P2N0M0 (i.e., central lesions with proximal vascular and/or biliary involvement of 1 lobe, no regional involvement, no metastasis). We adopted a conservative management approach because removing the lesions would require major surgery and because the results of Em18 serologic testing and ^{18}F-FDG-PET scan suggested low-viability parasites (*1*,*13*). At the time of publication, the patient was receiving albendazole (400 mg 2×/d) with fat-containing meals and tolerating the medication well. Follow-up with contrast-enhanced ultrasound and serologic testing was scheduled every 6 months, MRI in 1 year, and ^{18}F-FDG-PET scan in 2 years (*1*).

Conclusions

AE is a complex disease with a high fatality rate (0%–25% 10-year survival) if untreated (*1*). It primarily affects the liver and is characterized by infiltrating, metastatic, tumor-like behavior (*1*). Unlike CE, AE lesions have no pathognomonic signs on imaging, and the differential diagnosis is mainly tumors (*1*). Even in AE-endemic areas, misdiagnosis and consequent incorrect treatment occurs frequently (*1*; Appendix reference *17*).

Curative treatment options include surgery and albendazole if radical resection is achievable, or albendazole alone indefinitely in other cases (*1*). Treatment interruption can be envisaged in selected cases when serologic testing and ^{18}F-FDG-PET scans become negative (*1*). In this case, the Western blot banding pattern, low antibody concentrations against crude parasite antigens, negativity of Em18 ELISA, and faint hypermetabolism on ^{18}F-FDG-PET scan indicate low parasite viability (*1*,*13*). PCR on bioptic material was negative, explained by the absence of cell-containing larval structures on histology; however, *E. multilocularis*–specific immunochemistry was positive, confirming the diagnosis (*1*,*13*).

A report from 1928 mentioned 2 human AE cases identified in South Tyrol in 1906 and 1922 (*2*), but reports of human confirmed AE in Italy are otherwise lacking; a 2019 research review identified no reports from this country (*12*). Italian Hospital Discharge Records reports cases labeled as AE according to International Classification of Diseases, 9th Edition (Appendix reference *18*). From the analysis of cases that we could examine (Appendix reference *19*), those cases seem to be CE with multiloculated cyst morphology (CE2 and CE3b stages according to WHO-IWGE), erroneously recorded as *E. multilocularis* (*1*).

An expanding area of endemicity of *E. multilocularis* in Europe has been observed and predicted by modeling (*3*). Because of the high lethality of this disease if misdiagnosed and mistreated, physicians, especially in Italy's alpine regions, must be informed about this infection and its possibility even in patients who have never lived in or traveled to known endemic areas.

Acknowledgments

We thank Andrea Angheben, Paola Rodari, Maria Luca D'Errico, and the infectious-tropical diseases ward at IRCCS Sacro Cuore Don Calabria hospital in Negrar for clinical management during the patient's hospitalization; Stefano Tais for support with sample management; Ansgar Deibel for the discussion on the case diagnosis and management; and Dora Buonfrate for critically reviewing the manuscript.

Funding was provided through Italian Ministry of Health "Fondi Ricerca Corrente –L2" to IRCCS Sacro Cuore Don Calabria hospital, Negrar di Valpolicella, Verona, Italy.

F.T., M.D., E.O., and T.D. performed and interpreted imaging and laboratory tests; F.T., N.R., B.G., and F.G. clinically managed the patient. F.T., D.T., and G.B. wrote the manuscript. All authors reviewed and approved the published version of the manuscript.

About the Author

Dr. Tamarozzi is a senior research physician and cohead of the WHO Collaborating Centre on Strongyloidiasis and other NTDs at the Department of Infectious-Tropical Diseases and Microbiology, IRCCS Sacro Cuore Don Calabria Hospital, in Negrar di Valpolicella, Verona, Italy, as well as a member of the steering committee of the WHO Informal Working Group on Echinococcosis. Her main field of work is the laboratory- and imaging-based diagnosis of neglected helminthic infections, in particular echinococcal infections.

References

1. Kern P, Menezes da Silva A, Akhan O, Müllhaupt B, Vizcaychipi KA, Budke C, et al. The echinococcoses: diagnosis, clinical management and burden of disease. Adv Parasitol. 2017;96:259–369. https://doi.org/10.1016/bs.apar.2016.09.006
2. Deplazes P, Rinaldi L, Alvarez Rojas CA, Torgerson PR, Harandi MF, Romig T, et al. Global distribution of alveolar and cystic echinococcosis. Adv Parasitol. 2017;95:315–493. https://doi.org/10.1016/bs.apar.2016.11.001
3. Cenni L, Simoncini A, Massetti L, Rizzoli A, Hauffe HC, Massolo A. Current and future distribution of a parasite with complex life cycle under global change scenarios: *Echinococcus multilocularis* in Europe. Glob Change Biol. 2023;29:2436–49. https://doi.org/10.1111/gcb.16616
4. Manfredi MT, Genchi C, Deplazes R, Trevisiol K, Fraquelli C. *Echinococcus multilocularis* infection in red foxes in italy. Vet Rec. 2002;150:757. https://doi.org/10.1136/vr.150.24.757
5. Casulli A, Manfredi MT, La Rosa G, Di Cerbo AR, Dinkel A, Romig T, et al. *Echinococcus multilocularis* in red foxes (*Vulpes vulpes*) of the Italian Alpine region: is there a focus of autochthonous transmission? Int J Parasitol. 2005;35:1079–83. https://doi.org/10.1016/j.ijpara.2005.04.005
6. Citterio CV, Obber F, Trevisiol K, Dellamaria D, Celva R, Bregoli M, et al. *Echinococcus multilocularis* and other cestodes in red foxes (*Vulpes vulpes*) of northeast Italy, 2012–2018. Parasit Vectors. 2021;14:29. https://doi.org/10.1186/s13071-020-04520-5
7. Celva R, Crestanello B, Obber F, Dellamaria D, Trevisiol K, Bregoli M, et al. Assessing red fox (*Vulpes vulpes*) demographics to monitor wildlife diseases: a spotlight on *Echinococcus multilocularis*. Pathogens. 2022;12:60. https://doi.org/10.3390/pathogens12010060
8. Casulli A, Bart JM, Knapp J, La Rosa G, Dusher G, Gottstein B, et al. Multi-locus microsatellite analysis supports the hypothesis of an autochthonous focus of *Echinococcus multilocularis* in northern Italy. Int J Parasitol. 2009;39:837–42. https://doi.org/10.1016/j.ijpara.2008.12.001
9. Obber F, Celva R, Da Rold G, Trevisiol K, Ravagnan S, Danesi P, et al. A highly endemic area of *Echinococcus multilocularis* identified through a comparative re-assessment of prevalence in the red fox (*Vulpes vulpes*), Alto Adige (Italy: 2019–2020). PLoS One. 2022;17:e0268045. https://doi.org/10.1371/journal.pone.0268045
10. Massolo A, Valli D, Wassermann M, Cavallero S, D'Amelio S, Meriggi A, et al. Unexpected *Echinococcus multilocularis* infections in shepherd dogs and wolves in south-western Italian Alps: a new endemic area? Int J Parasitol Parasites Wildl. 2018;7:309–16. https://doi.org/10.1016/j.ijppaw.2018.08.001
11. European Food Safety Authority (EFSA); European Centre for Disease Prevention and Control (ECDC). The European Union One Health 2022 zoonoses report. EFSA J. 2023;21:e8442.
12. Baumann S, Shi R, Liu W, Bao H, Schmidberger J, Kratzer W, et al.; interdisciplinary Echinococcosis Working Group Ulm. Worldwide literature on epidemiology of human alveolar echinococcosis: a systematic review of research published in the twenty-first century. Infection. 2019;47:703–27. https://doi.org/10.1007/s15010-019-01325-2
13. Siles-Lucas M, Casulli A, Conraths FJ, Müller N. Laboratory diagnosis of *Echinococcus* spp. in human patients and infected animals. Adv Parasitol. 2017;96:159–257. https://doi.org/10.1016/bs.apar.2016.09.003
14. Barth TF, Herrmann TS, Tappe D, Stark L, Grüner B, Buttenschoen K, et al. Sensitive and specific immunohistochemical diagnosis of human alveolar echinococcosis with the monoclonal antibody Em2G11. PLoS Negl Trop Dis. 2012;6:e1877. https://doi.org/10.1371/journal.pntd.0001877
15. Brunetti E, Kern P, Vuitton DA; Writing Panel for the WHO-IWGE. Expert consensus for the diagnosis and treatment of cystic and alveolar echinococcosis in humans. Acta Trop. 2010;114:1–16. https://doi.org/10.1016/j.actatropica.2009.11.001

Address for correspondence: Francesca Tamarozzi, Department of Infectious-Tropical Diseases and Microbiology, IRCCS Sacro Cuore Don Calabria Hospital, Via don A Sempreboni 5, 37024, Negrar di Valpolicella, Verona, Italy; email: francesca.tamarozzi@sacrocuore.it

Experimental SARS-CoV-2 Infection of Elk and Mule Deer

Stephanie M. Porter, Airn E. Hartwig, Helle Bielefeldt-Ohmann, Jeffrey M. Marano, J. Jeffrey Root,[1] Angela M. Bosco-Lauth[1]

To assess the susceptibility of elk (*Cervus canadensis*) and mule deer (*Odocoileus hemionus*) to SARS-CoV-2, we performed experimental infections in both species. Elk did not shed infectious virus but mounted low-level serologic responses. Mule deer shed and transmitted virus and mounted pronounced serologic responses and thus could play a role in SARS-CoV-2 epidemiology.

Natural infections and experimental studies have indicated that diverse species of mammals can be infected with SARS-CoV-2 (*1*). The angiotensin-converting enzyme 2 receptor of white-tailed deer is closely homologous to that of humans. Angiotensin-converting enzyme 2 modeling studies predict that cervids, including sika deer (*Cervus nippon*), reindeer (*Rangifer tarandus*), and Père David's deer (*Elaphurus davidianus*), are susceptible to SARS-CoV-2 (*2*–*4*). White-tailed deer are susceptible to experimental infection with SARS-CoV-2, subsequently shedding infectious virus and infecting naive conspecifics (*5*–*7*). Surveillance studies have demonstrated SARS-CoV-2 infection in free-ranging and captive white-tailed deer in the United States and Canada, determined by viral RNA detection, antibodies to SARS-CoV-2, or virus isolation (*8*–*11*). After their displacement in humans, the Alpha and Delta variants of concern persisted in white-tailed deer populations (*12*,*13*). Because SARS-CoV-2 is likely to have repeatedly spilled over from humans to white-tailed deer and circulated within North America deer populations, we assessed susceptibility of elk (*Cervus canadensis*) and mule deer (*Odocoileus hemionus*) to the Delta variant of SARS-CoV-2. All animal work was approved by the Colorado State University (Fort Collins, Colorado, USA) Institutional Animal Care and Use Committee.

Author affiliations: US Department of Agriculture, Fort Collins, Colorado, USA (S.M. Porter, J.J. Root); Colorado State University, Fort Collins (A.E. Hartwig, J.M. Marano, A.M. Bosco-Lauth); University of Queensland, St Lucia, Queensland, Australia (H. Bielefeldt-Ohmann)

DOI: https://doi.org/10.3201/eid3002.231093

The Study

We studied 6 weanling elk (all female) and 6 yearling mule deer (5 female, 1 male). Animals were procured from private vendors and group housed (3 individuals of the same species/room) in an animal Biosafety Level 3 facility at Colorado State University. Before study commencement, all animals were seronegative for SARS-CoV-2.

We passaged the Delta variant of SARS-CoV-2 (BEI Resources, National Institute of Allergy and Infectious Diseases, National Institutes of Health: isolate hCoV-19/USA/MD-HP05647/2021 [lineage B.1.617.2]) 1 time in Vero cells. We then sequenced the isolate by using a next-generation pipeline and detected a single synonymous consensus change at amino acid 410 in nonstructural protein 14 (C to T transition) (GenBank accession no. OR758451) (*14*). We then intranasally inoculated 2 animals/room with 3.7–4.5 $\log_{10}$ PFU of virus diluted in phosphate-buffered saline (confirmed by back-titration of inoculum on Vero cells); the third animal in each room served as a contact.

We assessed the animals daily for signs of clinical disease (e.g., lethargy, anorexia, nasal discharge, sneezing, coughing, and dyspnea). One mule deer (no. 3) was tachypneic and coughing at arrival, and clinical signs continued throughout the week-long acclimation period until euthanasia at 3 days postinoculation (dpi) according to the study schedule. Because that respiratory pattern was present before study commencement, we did not attribute it to SARS-CoV-2 infection. No other clinical signs were observed in any animal.

At 0, 1, 2, 3, 5, 7, and 14 dpi, we collected oral, nasal, and rectal swab samples. Because no elk shed infectious virus orally or nasally, we did not assess

[1]These senior authors contributed equally to this article.

Table 1. PCR cycle threshold values for oral and nasal swab samples from elk experimentally infected with SARS-CoV-2*

Elk no. (infection route)	Oral swab sample, postinoculation day						Nasal swab sample, postinoculation day				
	0	1	2	3	5	7	1	2	3	5	7
1 (direct)	–	36.9	–	35.2	NA	NA	–	–	–	NA	NA
2 (direct)	–	–	–	–	NA	NA	35.6	35.0	–	NA	NA
3 (contact)	–	–	–	–	NA	NA	–	–	–	NA	NA
4 (direct)	–	–	–	–	–	–	33.6	29.9	34.4	26.5	–
5 (direct)	–	–	–	–	–	–	–	–	–	–	–
6 (contact)	–	–	–	–	–	–	–	–	–	–	–

*NA, not applicable because elk were euthanized on day 3; RT-PCR, reverse transcription PCR; –, no SARS-CoV-2 RNA was detected.

elk rectal swab samples. We performed reverse transcription PCR on elk oral and nasal swab samples collected through 7 dpi. We recovered SARS-CoV-2 RNA from samples from 3 directly inoculated elk collected at 1–5 dpi; cycle threshold values for all 3 were >28 (Table 1). Plaque assay showed that 3 of the 4 directly inoculated mule deer shed infectious virus orally and nasally (Figures 1, 2). Oral shedding of virus commenced at either 2 or 3 dpi and resolved by 7 dpi for directly inoculated mule deer. One contact mule deer shed virus orally at 7 dpi (Figure 1). Nasal shedding of virus was more staggered; inoculated animals initially shed virus at 1, 2, or 3 dpi, continuing through 7 dpi (in the 2 direct inoculants remaining at that time). For contact mule deer, only 1 nasal sample per animal was positive, collected at either 3 or 7 dpi (Figure 2). Infectious virus was not recovered from any mule deer rectal samples.

At 3 dpi, we euthanized and necropsied animals from 1 room of each species (n = 3; 2 inoculants and 1 contact) and collected tissues (nasal turbinates, trachea, heart, lung, liver, spleen, kidney, small intestine) for virus isolation and histopathologic examination. Although we did not detect infectious virus in any elk tissues, we recovered infectious virus from the nasal turbinates and trachea of 1 directly inoculated mule deer.

The remaining animals were maintained until 21 dpi, when they were euthanized and underwent necropsy with the same tissues collected into formalin. Blood from those animals was collected weekly and evaluated for a serologic response to SARS-CoV-2 by plaque reduction neutralization test (*15*). A low-level antibody response developed in both directly inoculated elk; peak neutralizing titers were 1:20 at 21 dpi. The contact elk did not seroconvert. Virus-neutralizing antibodies developed in all mule deer held until 21 dpi; peak titers reached ≥1:1,280 (Table 2).

At necropsy, we observed no gross lesions in any animals. A veterinary pathologist evaluated all respiratory tissues from all mule deer. The tracheas of all mule deer were histologically unremarkable, but multifocal accumulations of mononuclear leukocytes in the absence of frank inflammation were noted in the nasal turbinates, lungs, or both from 5 mule deer. Elk tissues did not undergo histologic evaluation.

Conclusions

If wildlife populations serve as maintenance hosts for SARS-CoV-2, the implications could be substantial. The persistence of virus variants already displaced in the human population, virus evolution, and spillback into a human have all been suggested

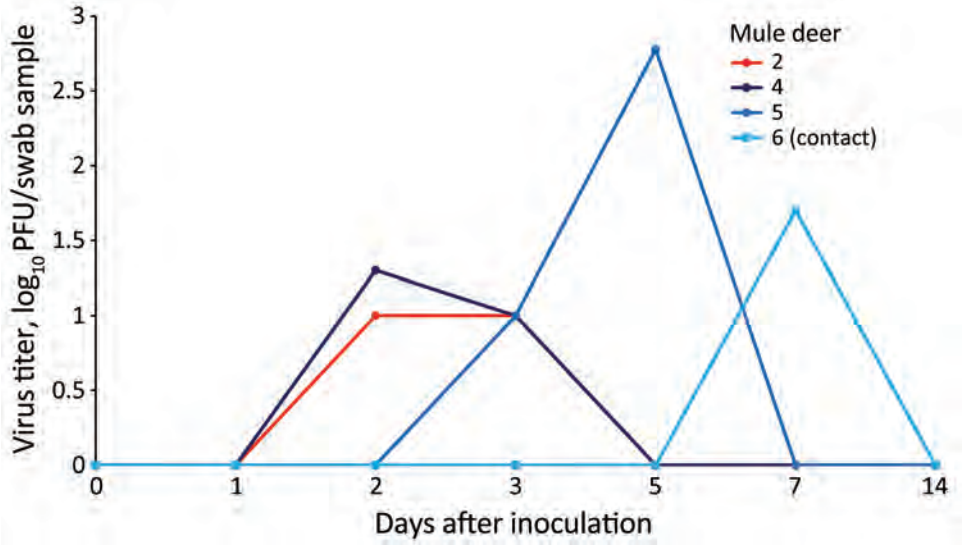

Figure 1. Oropharyngeal shedding of SARS-CoV-2 by experimentally infected mule deer as detected by plaque assay. Mule deer 2 was euthanized 3 days after infection. Mule deer 2, 4, and 5 were directly inoculated, and mule deer 6 was a contact animal.

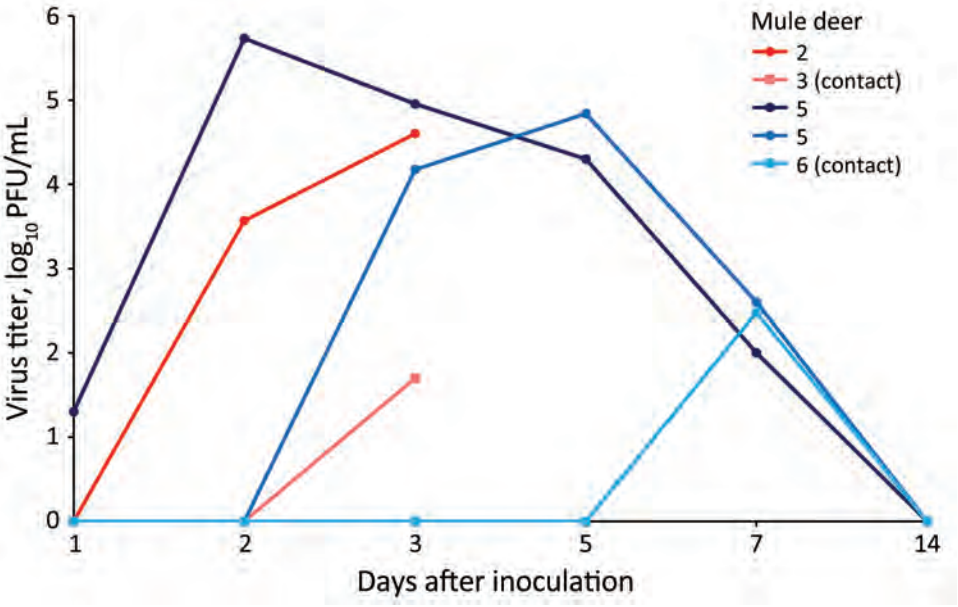

Figure 2. Nasal shedding of SARS-CoV-2 by experimentally infected mule deer as detected by plaque assay. Mule deer 2 and 3 were euthanized 3 days after infection. Mule deer 2, 4, and 5 were directly inoculated, and mule deer 3 and 6 were contact animals.

to have occurred in white-tailed deer populations (*11*,*12*), although it is still unclear whether those deer will serve as maintenance hosts of the virus. Evaluating the susceptibility of other cervid species to SARS-CoV-2 will help direct surveillance efforts among free-ranging wildlife, which are key to understanding the epidemiology of SARS-CoV-2 and implementing control measures.

We used the Delta variant of SARS-CoV-2 to challenge animals in this experiment on the basis of evidence that this variant of concern was prevalent in white-tailed deer populations (*13*). Our results indicate that although elk seem to be minimally susceptible to infection with the Delta variant, mule deer are highly susceptible and capable of transmitting the virus. Inoculated elk showed no clinical signs, did not shed infectious virus, and mounted low-level humoral titers. The genomic RNA recovered from elk could represent residual inoculum. Infection in mule deer was subclinical, and although immune activation in the absence of frank inflammation was observed in respiratory tissues from 5 of the 6 animals, that finding may or may not be linked to SARS-CoV-2 infection. Of note, all mule deer used in this study were incidentally tested to assess their chronic wasting disease (CWD) status. Animals no. 1 and 3 were CWD positive, although it is unlikely that a concurrent infection with CWD greatly affected their susceptibility to infection with SARS-CoV-2 because only 1 of those animals became infected with SARS-CoV-2 while the other was the sole mule deer in our study that did not.

Experimental infection of elk and mule deer with SARS-CoV-2 revealed that although elk are minimally susceptible to infection, mule deer become infected, shed infectious virus, and can infect naive contacts. Mule deer are less widely distributed than white-tailed deer but still represent a population of cervids that is frequently in contact with humans and domestic animals. Therefore, susceptibility of mule deer provides yet another potential source for SARS-CoV-2 spillover or spillback. At this time, there is no evidence that wildlife are a significant source of SARS-CoV-2 exposure for humans, but the potential for this virus to become established in novel host species could lead to virus evolution in which novel variants may arise. Therefore, continued surveillance of species at risk, such as white-tailed and mule deer, is needed to detect any variants quickly and prevent transmission.

Table 2. Plaque reduction neutralization test antibody titers from for elk and mule deer experimentally infected with SARS-CoV-2*

Animal	Preinfection	7 dpi	14 dpi	21 dpi
Elk 4	<10	<10	10	20
Elk 5	<10	<10	10	20
Elk 6	<10	<10	<10	<10
Mule deer 4	<20	40	5,120	1,280
Mule deer 6	<20	<20	1,280	1,280
Mule deer 5	<20	<20	1,280	640

*dpi, days postinoculation.

Acknowledgments

We thank and recognize the US Department of Agriculture, Animal and Plant Health Inspection Service Science Fellows Program for supporting the salary of S.M.P. We are very grateful to Tracy Nichols, Colorado and Kansas state veterinarians, and Colorado Parks and Wildlife for logistical support. Special thanks to Jeremy

Ellis for technical assistance; Susan Shriner for consulting; McKinzee Barker, Elizabeth Lawrence, and Hannah Sueper for their help with animal handling; and Richard Bowen for facilities support.

This work was supported by internal funding from Colorado State University and the US Department of Agriculture, Animal and Plant Health Inspection Service. This study was directly funded by the American Rescue Plan Act provision to conduct monitoring and surveillance of animals susceptible to SARS-CoV-2.

About the Author

Dr. Porter is a science fellow with the National Wildlife Research Center at the US Department of Agriculture. Her research interests include the pathogenesis and transmission of infectious diseases.

References

1. Frazzini S, Amadori M, Turin L, Riva F. SARS CoV-2 infections in animals, two years into the pandemic. Arch Virol. 2022;167:2503–17. https://doi.org/10.1007/s00705-022-05609-1
2. Lopes LR, Carvalho de Lucca Pina N, da Silva Junior AC, Bandiera-Paiva P. Evolutionary analysis of mammalian ACE2 and the key residues involved in binding to the spike protein revealed potential SARS-CoV-2 hosts. Journal of Medical Microbiology and Infectious Diseases. 2022;10:1–9. https://doi.org/10.52547/JoMMID.10.1.1
3. Fischhoff IR, Castellanos AA, Rodrigues JPGLM, Varsani A, Han BA. Predicting the zoonotic capacity of mammals to transmit SARS-CoV-2. Proc Biol Sci. 2021;288:20211651.
4. Damas J, Hughes GM, Keough KC, Painter CA, Persky NS, Corbo M, et al. Broad host range of SARS-CoV-2 predicted by comparative and structural analysis of ACE2 in vertebrates. Proc Natl Acad Sci U S A. 2020;117:22311–22. https://doi.org/10.1073/pnas.2010146117
5. Palmer MV, Martins M, Falkenberg S, Buckley A, Caserta LC, Mitchell PK, et al. Susceptibility of white-tailed deer (*Odocoileus virginianus*) to SARS-CoV-2. J Virol. 2021;95:e00083–21. https://doi.org/10.1128/JVI.00083-21
6. Martins M, Boggiatto PM, Buckley A, Cassmann ED, Falkenberg S, Caserta LC, et al. From deer-to-deer: SARS-CoV-2 is efficiently transmitted and presents broad tissue tropism and replication sites in white-tailed deer. PLoS Pathog. 2022;18:e1010197. https://doi.org/10.1371/journal.ppat.1010197
7. Cool K, Gaudreault NN, Morozov I, Trujillo JD, Meekins DA, McDowell C, et al. Infection and transmission of ancestral SARS-CoV-2 and its alpha variant in pregnant white-tailed deer. Emerg Microbes Infect. 2022;11:95–112. https://doi.org/10.1080/22221751.2021.2012528
8. Chandler JC, Bevins SN, Ellis JW, Linder TJ, Tell RM, Jenkins-Moore M, et al. SARS-CoV-2 exposure in wild white-tailed deer (*Odocoileus virginianus*). Proc Natl Acad Sci U S A. 2021;118:e2114828118. https://doi.org/10.1073/pnas.2114828118
9. Hale VL, Dennis PM, McBride DS, Nolting JM, Madden C, Huey D, et al. SARS-CoV-2 infection in free-ranging white-tailed deer. Nature. 2022;602:481–6. https://doi.org/10.1038/s41586-021-04353-x
10. Kuchipudi SV, Surendran-Nair M, Ruden RM, Yon M, Nissly RH, Vandegrift KJ, et al. Multiple spillovers from humans and onward transmission of SARS-CoV-2 in white-tailed deer. Proc Natl Acad Sci U S A. 2022;119:e2121644119. https://doi.org/10.1073/pnas.2121644119
11. Pickering B, Lung O, Maguire F, Kruczkiewicz P, Kotwa JD, Buchanan T, et al. Divergent SARS-CoV-2 variant emerges in white-tailed deer with deer-to-human transmission. Nat Microbiol. 2022;7:2011–24. https://doi.org/10.1038/s41564-022-01268-9
12. Marques AD, Sherrill-Mix S, Everett JK, Adhikari H, Reddy S, Ellis JC, et al. Multiple introductions of SARS-CoV-2 Alpha and Delta variants into white-tailed deer in Pennsylvania. MBio. 2022;13:e0210122. https://doi.org/10.1128/mbio.02101-22
13. McBride D, Garushyants S, Franks J, Magee A, Overend S, Huey D, et al. Accelerated evolution of SARS-CoV-2 in free-ranging white-tailed deer. Nat Commun. 2023;14:5105.
14. Marano JM, Weger-Lucarelli J. Replication in the presence of dengue convalescent serum impacts Zika virus neutralization sensitivity and fitness. Front Cell Infect Microbiol. 2023;13:1130749. https://doi.org/10.3389/fcimb.2023.1130749
15. Bosco-Lauth AM, Hartwig AE, Porter SM, Gordy PW, Nehring M, Byas AD, et al. Experimental infection of domestic dogs and cats with SARS-CoV-2: pathogenesis, transmission, and response to reexposure in cats. Proc Natl Acad Sci U S A. 2020;117:26382–8. https://doi.org/10.1073/pnas.2013102117

Address for correspondence: Angela Bosco-Lauth, Department of Biomedical Sciences, Colorado State University, 1683 Campus Delivery, Fort Collins, CO 80523, USA; email: angela.bosco-lauth@colostate.edu

Identification of Large Adenovirus Infection Outbreak at University by Multipathogen Testing, South Carolina, USA, 2022

Marco E. Tori, Judith Chontos-Komorowski, Jason Stacy, Daryl M. Lamson, Kirsten St. George, Avril T. Lail, Heather A. Stewart-Grant, Linda J. Bell, Hannah L. Kirking, Christopher H. Hsu

Using multipathogen PCR testing, we identified 195 students with adenovirus type 4 infections on a university campus in South Carolina, USA, during January–May 2022. We co-detected other respiratory viruses in 43 (22%) students. Continued surveillance of circulating viruses is needed to prevent virus infection outbreaks in congregate communities.

Human adenovirus (HAdV) infections can cause a range of symptoms but most commonly result in respiratory illnesses (*1*). Most HAdV infections are not clinically severe; however, more serious illness can occur (*2*,*3*). A total of 51 recognized HAdV serotypes and >100 genotypes (classified into 7 species, HAdV-A–G) have been characterized globally (*4*). Because testing does not change clinical management, persons with HAdV infections often do not receive a virus infection diagnosis. If adenovirus testing is available, it is usually performed as part of a multipathogen PCR panel. Adenovirus infection outbreaks caused by transmission through respiratory droplets and fomites have been reported in various congregate settings, including nursing homes (*5*), military recruit barracks (*6*–*8*), and college campuses (*9*–*11*). The incubation period varies from 2–14 days.

Author affiliations: South Carolina Department of Health and Environmental Control, Columbia, South Carolina, USA (M.E. Tori, L.J. Bell); Centers for Disease Control and Prevention, Atlanta, Georgia, USA (M.E. Tori, H.L. Kirking, C.H. Hsu); University of South Carolina Student Health Services, Columbia (J. Chontos-Komorowski, J. Stacy, A.T. Lail, H.A. Stewart-Grant); New York State Department of Health, Albany, NY, USA (D.M. Lamson, K. St. George)

DOI: https://doi.org/10.3201/eid3002.230623

In early February 2022, a university campus in South Carolina, USA, notified its regional health department of 4 students with HAdV infections who had sought care for respiratory symptoms the previous week at student health services (SHS). Nasopharyngeal swab specimens were collected and tested by using a multipathogen PCR panel for respiratory pathogens; HAdV was detected in all 4 patient samples. SHS contacted the South Carolina Department of Health and Environmental Control and the Centers for Disease Control and Prevention (CDC) to request typing of the HadV specimens to determine if ≥1 HadV type was circulating. Partial genomic sequencing showed that HadV was the same type in all 4 specimens. Cases of HadV infections continued to increase on campus; therefore, the university, state and local health departments, and CDC investigated the scope of the outbreak. The timing of this outbreak during the COVID-19 pandemic enabled unique observations and responses. We describe the outbreak, the university's response intended to prevent further transmission, and implications of HadV infection outbreaks in congregate settings, such as universities. The South Carolina Department of Health and Environmental Control Institutional Review Board deemed this work was non–human subjects research. This activity was reviewed by CDC and was conducted consistent with applicable federal law and CDC policy.

The Study

We analyzed laboratory and exposure data from symptomatic students who sought care at the university's health clinic during January 1–May 31, 2022. SHS staff collected nasal or nasopharyngeal swab samples from students and tested those specimens

by using BioFire RSP 2.1 multiplex PCR (bioMérieux, https://www.biomerieux.com). We defined positive cases as students who manifested respiratory or constitutional symptoms and were HadV-positive in the multipathogen PCR panel.

SHS routinely collected demographic information, symptoms, and medical history from students seeking care at the university clinic. Those data were supplemented from March 22–May 10, 2022, by using focused call-back interviews of students who

Table 1. Characteristics of university students in study identifying a large adenovirus infection outbreak by multipathogen testing, South Carolina, USA, 2022*

Characteristics	Adenovirus infections
Total no. infected students	195
Sex	
M	97 (50)
F	98 (50)
Median age, y (range)	19 (18–24)
Academic class	
Freshman	76 (39)
Sophomore	58 (30)
Junior	33 (17)
Senior	25 (13)
Graduate student	3 (1)
Residence	
On-campus dormitory	115 (59)
On-campus apartment	6 (3)
Off campus	68 (35)
Unknown	6 (3)
Area of academic study	
Prebusiness or business	41 (21)
Finance	17 (9)
Biology	17 (9)
Psychology	13 (7)
Public health	9 (5)
Sports/entertainment management	8 (4)
Undeclared	8 (4)
Political science	7 (4)
All others	75 (38)
Symptoms†	
Cough	149 (76)
Sore throat	166 (85)
Fever	146 (75)
Headache	120 (62)
GI	52 (27)
Conjunctivitis	20 (10)
Smoking or vaping	30 (15)
Comorbidities	
Asthma	14 (7)
Immunocompromised‡	2 (1)
Other or not reported	179 (92)
Co-detected respiratory viruses§	
Human rhinovirus/enterovirus	28 (14)
Seasonal coronavirus¶	9 (5)
SARS-CoV-2	8 (4)
Parainfluenza, types 2–4	6 (3)
Influenza A	1 (1)
RSV	1 (1)
Human metapneumovirus	1 (1)
Adenovirus typing by hexon gene sequencing	
Human adenovirus type 4	30 (15)
Not typed#	165 (85)

*Values are no. (%) except as indicated.
†Students could report multiple symptoms.
‡Immunocompromised because of methotrexate or immunomodulatory agent treatment.
§Other respiratory viruses were detected by using multipathogen PCR. A total of 43 students tested positive for human adenovirus (HAdV) and ≥1 other respiratory pathogen. Ten of 43 students tested positive for HAdV and ≥2 other pathogens; 5 of those students had HAdV, SARS-CoV-2, and human rhinovirus/enterovirus. One student tested positive for HAdV, SARS-COV-2, parainfluenza 2, and human rhinovirus/enterovirus. Additional testing, including typing or genomic sequencing, was not performed on specimens that were negative for HAdV.
¶Seasonal coronavirus types were OC43, 229E, NL63, and HKU1.
#Typing not attempted or not possible.

had confirmed HadV infections to identify potential transmission events and locations. We used the aggregate interview data to examine student behaviors and activities that might have been associated with transmission events.

We considered students who tested positive for HadV plus another respiratory pathogen on the multipathogen panel to have pathogen co-detections. We compared demographic characteristics, symptoms, and illness severity between students who had co-detections and those who were only infected with HadV by using *t*-tests.

During January 1–May 31, 2022, a total of 687 students were tested by using the respiratory multipathogen PCR panel after seeking care at SHS for acute respiratory or systemic symptoms. Of those 687 students, 195 (28.4%) tested positive for HadV; HadV infections were distributed evenly between men and women. The median age of infected students was 19 years (range 18–24 years) (Table 1). The most common symptoms reported by students were sore throat (85%), cough (76%), fever (75%), and headache (62%). Nausea and vomiting were reported by 27% of students; conjunctivitis was reported by 10% of students. No known emergency department visits, hospitalizations, or deaths were reported among any HadV-infected students. HadV-4 was identified in 30 swab specimens by partial genomic sequencing of the hexon gene (Appendix, https://wwwnc.cdc.gov/EID/article/30/2/23-0623-App1.pdf). We randomly selected 8 of those 30 sequences for whole-genome sequencing and performed phylogenetic analyses (Appendix Figure).

Weekly case counts increased slowly during January–February and more rapidly after the week of March 6 (university spring break) (Figure). Rapid and detailed attention to surface decontamination in academic and residential buildings on campus was reported in February and early March. Mandatory masking recommendations as part of COVID-19 mitigation efforts were lifted in March. Cases fell precipitously after students left campus for summer break

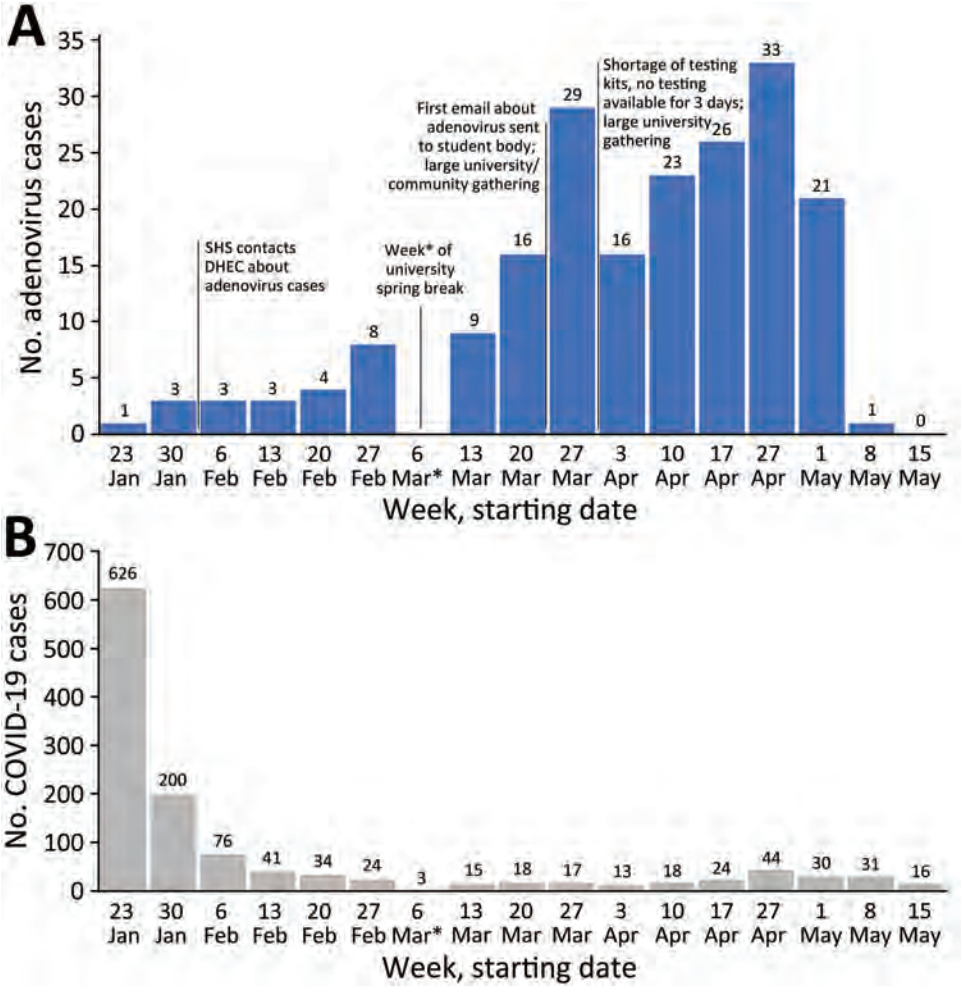

Figure. Number of adenovirus (A) and COVID-19 (B) cases at a university campus in South Carolina in study identifying a large adenovirus infection outbreak by multipathogen testing, South Carolina, USA, January 1–May 31, 2022. Numbers above bars indicate number of cases at each weekly time point. Vertical lines between bars indicate timelines of university events affecting the outbreak. Asterisks indicate the week of university spring break, after which weekly case counts began to rapidly increase. DHEC, Department of Health and Environmental Control; SHS, student health services.

Table 2. Comparison of university students with HAdV infection only and those with respiratory virus co-detections in study identifying a large adenovirus infection outbreak by multipathogen testing, South Carolina, USA, 2022*

Characteristics	HAdV infection only	HAdV + co-detected respiratory virus†	p value
No. students	152	43	NA
Sex			
F	70 (46)	28 (65)	0.002
M	82 (54)	15 (35)	0.03
Median age, y (range)	19 (18–24)	19 (18–22)	NA
Residence			
On campus dormitory	85 (56)	30 (66)	0.09
Off campus	59 (39)	11 (25)	0.09
Symptoms			
Cough	113 (74)	36 (84)	0.16
Sore throat	124 (82)	42 (98)	0.001
Fever	116 (76)	30 (70)	0.41
Headache	90 (59)	30 (70)	0.19
Nausea or vomiting	44 (29)	8 (19)	0.14
Conjunctivitis	19 (13)	1 (2)	0.001
Severe infection	6 (4)	1 (2)	0.07
Smoking or vaping	15 (11)	5 (12)	0.75

*Values are no. (%) except as indicated. p values were obtained from 2-sided *t*-tests. HAdV, human adenovirus; NA, not applicable.
†One student was HAdV positive in March, then had recurrent symptoms in early May and was found to be both HAdV and parainfluenza 3 positive. The student was included in the HAdV infection only column and not in the co-detection column. This student's clinical course and timeline were more consistent with a new parainfluenza infection; the detection of adenovirus was likely attributable to prolonged virus DNA shedding, not a new infection. This group does not include students with Epstein-Barr virus or group A *Streptococcus* infections.

(week of May 1); no cases were reported after May 10, 2022. The outbreak investigation was closed on June 7 after 2 full incubation periods (total of 28 days).

Of all HadV-infected students, infections occurred most in first-year (39%) and second-year (30%) students. Most (115 [59%]) students lived in on-campus dormitories. Three of 22 affected dormitories had ≥10 students with confirmed HadV infections during the outbreak. We did not observe a preponderance of one academic area of study that might suggest clustering according to academic departments.

Among the 195 students who tested positive for HadV, ≥1 other respiratory pathogen was also detected in 43 (22%) students (Table 2). The most common co-detected viruses were human rhinovirus/enterovirus (28 [65%]), seasonal coronaviruses (9 [21%]), and SARS-CoV-2 (8 [19%]). Most (42 [98%]) HadV-infected students who had co-detected viruses reported a sore throat, compared with 124 (82%) students infected with only HadV (p = 0.001). More HadV-only–infected students (13%) reported conjunctivitis than students who had co-detected viruses (2%; p = 0.001). We did not observe a substantial difference in disease severity (i.e., need for intravenous fluids) among HadV-only–infected students compared with those who had virus co-detections (4% vs. 2%; p = 0.07).

The university clinic staff began interviewing students with confirmed HadV infection on March 21. Interviews were completed for 96 of 121 students with HadV (79% response rate) before the end of the outbreak. Most (62 [65%]) students did not know where they had acquired infection; 9 (9%) students had a known exposure to someone with confirmed HadV infection, and 18 (19%) students had exposure to someone with similar symptoms before illness onset. Seventy-five (78%) students had not traveled away from campus before their symptoms began. We were unable to link infections to campus or off-campus locations because of limited sample size.

Conclusions

This outbreak of respiratory illness attributed to HadV-4 was among the largest described HadV outbreaks on a university campus (*9*,*12*); symptoms and transmission were similar to other large HadV outbreaks in congregate settings (*13*). Infected students were mostly freshmen and sophomores living in dormitories, highlighting increased transmission in close university settings. The outbreak occurred during the COVID-19 pandemic, and detection of HadV might have been delayed without availability of multipathogen testing. The outbreak on campus appeared to end when student density decreased during summer break, and further transmission was not observed among the limited number of students remaining on campus.

SHS was able to detect and respond quickly to a potentially serious virus infection outbreak by using multipathogen testing. Furthermore, this testing enabled identification of students who were infected with multiple pathogens. In addition to SARS-CoV-2, many other respiratory viruses can be detected in university students, including those that cause illness and outbreaks. As universities move beyond COVID-19 as the main public health priority affecting students and campuses, renewed attention to other

pathogens is needed (*14*). Continued surveillance of circulating viruses in congregate communities remains critical for ongoing risk communication and prevention efforts.

Acknowledgments

We thank Ana Endsley, William Harley, Adriana Kajon, Marie Killerby, Rachel Radcliffe, Warren Scott, and Rebecca Walker for their work in responding to the outbreak at the university.

Specimen testing at the New York State Public Health Laboratory was partially supported by the CDC's Vaccine Preventable Disease Reference Center contract (cooperative agreement no. 5NU600E000104).

This activity was reviewed by CDC and was conducted consistent with applicable federal law and CDC policy (e.g., 45 Code of Federal Regulations part 46, 21 Code of Federal Regulations part 56; 42 United States Code [U.S.C.] §241(d); 5 U.S.C. §552a; 44 U.S.C. §3501 et seq).

About the Author

Dr. Tori is a career epidemiology field officer in the Division of State and Local Readiness, Office of Readiness and Response, Centers for Disease Control and Prevention, Atlanta, Georgia, USA, stationed in South Carolina. This work was performed while he was the CDC's Epidemic Intelligence Service officer in South Carolina. His research focuses on communicable disease prevention.

References

1. Khanal S, Ghimire P, Dhamoon AS. The repertoire of adenovirus in human disease: the innocuous to the deadly. Biomedicines. 2018;6:30. https://doi.org/10.3390/biomedicines6010030
2. Lion T. Adenovirus infections in immunocompetent and immunocompromised patients. Clin Microbiol Rev. 2014;27:441–62. https://doi.org/10.1128/CMR.00116-13
3. Gutierrez Sanchez LH, Shiau H, Baker JM, Saaybi S, Buchfellner M, Britt W, et al. A case series of children with acute hepatitis and human adenovirus infection. N Engl J Med. 2022;387:620–30. https://doi.org/10.1056/NEJMoa2206294
4. Committee on Infectious Diseases. Red book: 2021–2024 report of the Committee on Infectious Diseases, 32nd ed. Kimberlin DW, Barnett ED, Lynfield R, Sawyer MH, editors. Itasca (IL): American Academy of Pediatrics; 2021.
5. Kajon AE, Lamson DM, Bair CR, Lu X, Landry ML, Menegus M, et al. Adenovirus type 4 respiratory infections among civilian adults, northeastern United States, 2011–2015. Emerg Infect Dis. 2018;24:201–9. https://doi.org/10.3201/eid2402.171407
6. Rogers AE, Lu X, Killerby M, Campbell E, Gallus L, Kamau E, et al. Outbreak of acute respiratory illness associated with adenovirus type 4 at the U.S. Naval Academy, 2016. MSMR. 2019;26:21–7.
7. Ko JH, Woo HT, Oh HS, Moon SM, Choi JY, Lim JU, et al. Ongoing outbreak of human adenovirus-associated acute respiratory illness in the Republic of Korea military, 2013 to 2018. Korean J Intern Med. 2021;36:205–13. https://doi.org/10.3904/kjim.2019.092
8. Chu VT, Simon E, Lu X, Rockwell P, Abedi GR, Gardner C, et al. Outbreak of acute respiratory illness associated with human adenovirus type 4 at the United States Coast Guard Academy, 2019. J Infect Dis. 2022;225:55–64. https://doi.org/10.1093/infdis/jiab322
9. Kujawski SA, Lu X, Schneider E, Blythe D, Boktor S, Farrehi J, et al. Outbreaks of adenovirus-associated respiratory illness on 5 college campuses in the United States, 2018–2019. Clin Infect Dis. 2021;72:1992–9. https://doi.org/10.1093/cid/ciaa465
10. Biggs HM, Lu X, Dettinger L, Sakthivel S, Watson JT, Boktor SW. Adenovirus-associated influenza-like illness among college students, Pennsylvania, USA. Emerg Infect Dis. 2018;24:2117–9. https://doi.org/10.3201/eid2411.180488
11. Lamson DM, Kajon A, Popowich M, Fuschino M, St George K. Human adenovirus 7d strains associated with influenza-like illness, New York, USA, 2017–2019. Emerg Infect Dis. 2020;26:1047–9. https://doi.org/10.3201/eid2605.200116
12. Sivan AV, Lee T, Binn LN, Gaydos JC. Adenovirus-associated acute respiratory disease in healthy adolescents and adults: a literature review. Mil Med. 2007;172:1198–203. https://doi.org/10.7205/milmed.172.11.1198
13. Tsou TP, Tan BF, Chang HY, Chen WC, Huang YP, Lai CY, et al.; Unknown Pathogen Discovery/Investigation Group. Community outbreak of adenovirus, Taiwan, 2011. Emerg Infect Dis. 2012;18:1825–32. https://doi.org/10.3201/eid1811.120629
14. Olsen SJ, Winn AK, Budd AP, Prill MM, Steel J, Midgley CM, et al. Changes in influenza and other respiratory virus activity during the COVID-19 pandemic—United States, 2020–2021. Am J Transplant. 2021;21:3481–6. https://doi.org/10.1111/ajt.16049

Address for correspondence: Marco E. Tori, South Carolina Department of Health and Environmental Control, 2100 Bull St, Columbia, SC 29201, USA; email: rhq2@cdc.gov

Emerging Enterovirus A71 Subgenogroup B5 Causing Severe Hand, Foot, and Mouth Disease, Vietnam, 2023

Nguyen Van Vinh Chau, Tang Chi Thuong, Nguyen Thanh Hung, Nguyen Thi Thu Hong, Du Tuan Quy, Tran Ba Thien, Cao Minh Hiep, Ngo Ngoc Quang Minh, Truong Huu Khanh, Do Duong Kim Han, Truong Hoang Chau Truc, Nguyen Thi Han Ny, Le Kim Thanh, Lam Anh Nguyet, Cao Thu Thuy, Le Nguyen Truc Nhu, Pham Van Quang, Phung Nguyen The Nguyen, Phan Tu Qui, H. Rogier van Doorn, C. Louise Thwaites, Tran Tan Thanh, Nguyen Thanh Dung, Guy Thwaites, Nguyen To Anh, Le Nguyen Thanh Nhan, Le Van Tan, for the SEACOVARIANTS[1]

We report on a 2023 outbreak of severe hand, foot, and mouth disease in southern Vietnam caused by an emerging lineage of enterovirus A71 subgenogroup B5. Affected children were significantly older than those reported during previous outbreaks. The virus should be closely monitored to assess its potential for global dispersal.

Since 1997, large outbreaks of severe hand, foot, and mouth disease (HFMD) caused by diverse enterovirus A71 (EV-A71) subgenogroups (such as B4, B5, C4, and C5) have been reported in the Asia Pacific region (*1*), resulting in millions of hospitalizations and substantial numbers of deaths. Increased EV-A71 detection and associated neurologic disease have also been documented worldwide, including in the United States in more recent years (*2*).

During January 1–June 30, 2023, a total of 12,600 HFMD cases and 7 deaths were reported in Vietnam. Of those cases, 5,383 (42.7%) infections and all 7 deaths were recorded in June 2023. We investigated the epidemiologic and virologic features of this outbreak. The study was approved by the Institutional Review Board of CH1 and the Oxford University Tropical Research Ethics Committee. Written informed consent was obtained from a parent or guardian of each enrolled patient.

The Study

This study forms part of an ongoing HFMD research program conducted at Children's Hospital 1 (CH1) in Ho Chi Minh City, Vietnam, since 2013 (Appendix, https://wwwnc.cdc.gov/EID/article/30/2/23-1024-App1.pdf) (*3*). Recruited patients had clinical data recorded and throat and rectal swab samples collected for virologic investigation of EV-A71 and other enterovirus infections (Appendix Figure 1) (*4*,*5*). We extracted complementary data from hospital records or from a clinical study conducted during 2013–2018 (*3*).

We generated EV-A71 whole-genome sequences directly from virus-positive rectal or throat swab samples that had sufficient viral loads (PCR cycle threshold values of ≤30) by using a metagenomics-based approach, as previously described (*6*). We

Author affiliations: Department of Health, Ho Chi Minh City, Vietnam (N.V.V. Chau, T.C. Thuong); Children's Hospital 1, Ho Chi Minh City (N.T. Hung, D.T. Quy, C.M. Hiep, N.N.Q. Minh, T.H. Khanh, P.V. Quang, P.N.T. Nguyen, L.N.T. Nhan); Oxford University Clinical Research Unit, Ho Chi Minh City (N.T.T. Hong, T.B. Thien, D.D.K. Han, T.H.C. Truc, N.T.H. Ny, L.K. Thanh, L.A. Nguyet, C.T. Thuy, L.N.T. Nhu, H.R. van Doorn, C.L. Thwaites, T.T. Thanh, G. Thwaites, N.T. Anh, L.V. Tan); Pham Ngoc Thach University of Medicine, Ho Chi Minh City (P.V. Quang); University of Medicine and Pharmacy at Ho Chi Minh City, Ho Chi Minh City (P.N.T. Nguyen); Hospital for Tropical Diseases, Ho Chi Minh City (P.T. Qui, N.T. Dung); University of Oxford, Oxford, UK (H.R. van Doorn, C.L. Thwaites, G. Thwaites, L.V. Tan)

DOI: https://doi.org/10.3201/eid3002.231024

[1]Members are listed at the end of this article.

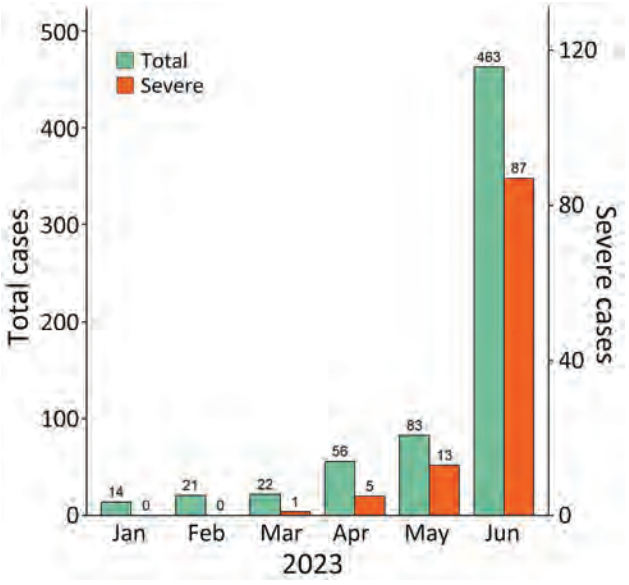

Figure 1. Admissions for and severe cases of hand, foot, and mouth disease recorded during January–June 2023 at Children's Hospital 1, Ho Chi Minh City, Vietnam, in study of emerging enterovirus A71 subgenogroup B5. Green bars indicate total number of patients admitted for hand, foot, and mouth disease. Red bars indicate the number of admitted patients who had severe disease. Numbers above bars indicate actual number of cases at each time point. Scales for the y-axes differ substantially to underscore patterns but do not permit direct comparisons.

performed recombination analysis by using the Chimera, GENECONV, Maxchi, Bootscan, and Siscan algorithms available in RDP4 software (*7*). To assess virus evolution, we constructed maximum-likelihood phylogenetic trees for enterovirus viral protein 1 (VP1) and whole-genome sequences by using IQ-TREE (*8*); we obtained representative global sequences from GenBank for comparisons (Appendix Tables 1, 2).

During January–June 2023, a total of 659 children with HFMD (including 106 with severe cases) were admitted to CH1; most admissions (463/659 [70.3%]) and severe cases (87/106 [82.1%]) occurred in June (Figure 1). Of the 659 children, 101 participated in this study. The participants resided in 15 provinces/cities in southern Vietnam (Appendix Figure 2) and were admitted to CH1 shortly after illness onset; the median number of illness days before admission was 2 (interquartile range 1–2) (Table 1). Twenty-eight (27.7%) participants had a disease severity grade of 2A, and 73 (72.3%) had grade 2B1 or worse (Table 1). Disease progressed from lower to higher severity grade in 63 (62.4%) of 101 children; clinical manifestations progressed within 1 day after admission in 47 (74.6%) children (Appendix Figure 3).

We detected enteroviruses in samples from 84 (83.2%) of 101 patients. Of those 84 patients, 83 (98.8%) were positive for EV-A71, and 1 patient was positive for coxsackievirus A5. We determined the subgenogroup for 67 samples and assigned 65 samples to subgenogroup B5 (Table 1) and 2 samples to subgenogroup C1. The 2 C1-infected patients had grade 2B1 and grade 3 disease severity. Compared with EV-A71–infected children enrolled in the clinical study during 2013–2018, those in the 2023 outbreak were significantly older (Table 2; Appendix Figure 4).

We obtained whole-genome sequences from 16 B5-positive samples (14 rectal and 2 throat swab samples from 16 individual patients) (Appendix Table 2). We did not detect recombination events. Phylogenetic analysis indicated the B5 viruses in Vietnam were most closely related to the B5 viruses from Japan, but they formed a distinct lineage from those previously isolated from Vietnam and worldwide (Figure 2; Appendix Table 3, Figure 5). In addition, 15 of 16 B5

Table 1. Demographics of patients with enterovirus infections and clinical grades of hand, foot, and mouth disease in study of emerging EV-A71 subgenogroup B5, Vietnam, 2023*

Characteristics	Total, n = 101	EV-A71, n = 83	EV-A71 B5, n = 65	PCR negative, n = 17
Sex				
M	61 (60.4)	48 (57.8)	39 (60.0)	12 (70.6)
F	40 (39.6)	35 (42.2)	26 (40.0)	5 (29.4)
Median age, mo (IQR)	26 (19–34)	27 (21–36)	28 (21–36)	20 (15–22)
Illness at admission, median d (IQR)†	2 (1–2)	2 (1–2)	2 (1–3)	2 (1–2)
Origin of patients				
Ho Chi Minh City	46 (45.5)	35 (42.2)	28 (43.1)	10 (58.8)
Other provinces/cities	55 (54.5)	48 (57.8)	37 (56.9)	7 (41.2)
Clinical grade of disease‡				
2A	28 (27.7)	17 (20.5)	15 (23.1)	10 (58.8)
2B1	15 (14.9)	12 (14.5)	11 (16.9)	3 (17.6)
2B2	16 (15.8)	15 (18.1)	12 (18.5)	1 (5.9)
3	41 (40.6)	39 (47.0)	27 (41.5)	2 (11.8)
4	1 (1.0)	0 (0.0)	0 (0.0)	1 (5.9)

*Values are no. (%) except as indicated. EV-A71, enterovirus A71; IQR, interquartile range.
†Median number of days of illness before admission.
‡Clinical grades of hand, foot, and mouth disease have been previously defined (*3*).

Table 2. Age comparisons among patient groups infected with different enterovirus subgenogroups over time in study of emerging EV-A71 subgenogroup B5 causing severe hand, foot, and mouth disease, Vietnam, 2023*

	EV-A71			EV-A71 B5			EV-A71 C4†	
Age	2023	2013–2018	p value	2023	2013–2018	p value	2013–2018	p value
Median age, mo (IQR)	27 (21–36)	21 (15–31)	<0.001	28 (21–36)	18 (13–30)	<0.001	22 (17–33)	0.042

*Wilcoxon rank-sum test with continuity correction was applied for analyses of patient ages among groups. EV-A71, enterovirus A71; IQR, interquartile range.
†Comparison was between EV-A71 subgenogroup B5 detected during 2023 vs. EV-A71 subgenogroup C4 detected during 2013–2018.

sequences from the 2023 outbreak carried a glycine residue at position 17 (G17) within the N-terminus of VP1. In the 1 remaining sample, a G17 codon was detected in 3 of 122 reads generated by the metagenomic workflow, and a serine (S17) codon was detected in the remaining 119 reads (Appendix Figure 6). In contrast, among 287 nonidentical global B5 sequences used for phylogenetic analysis, an S17 codon was observed in 285 (99.3%) and a G17 codon was observed in 2 (0.7%) sequences. However, the 2 G17-containing sequences were derived from virus isolates passaged in cultured cell lines (*9*). Because of the small number of subgenogroup C1 sequences (n = 2), we deemed a similar in-depth analysis to be uninformative, but the C1 viruses from this study were closely related phylogenetically to C1 strains isolated worldwide (Appendix Figure 7).

Conclusions

We report that the 2023 outbreak of severe HFMD in Vietnam was caused by EV-A71 subgenogroups B5 and C1; B5 is dominant, and more older children were affected than during previous outbreaks. Phylogenetic analyses suggest that both B5 and C1 viruses were derived from new introductions of EV-A71 into Vietnam. In addition, the B5 viruses likely represent

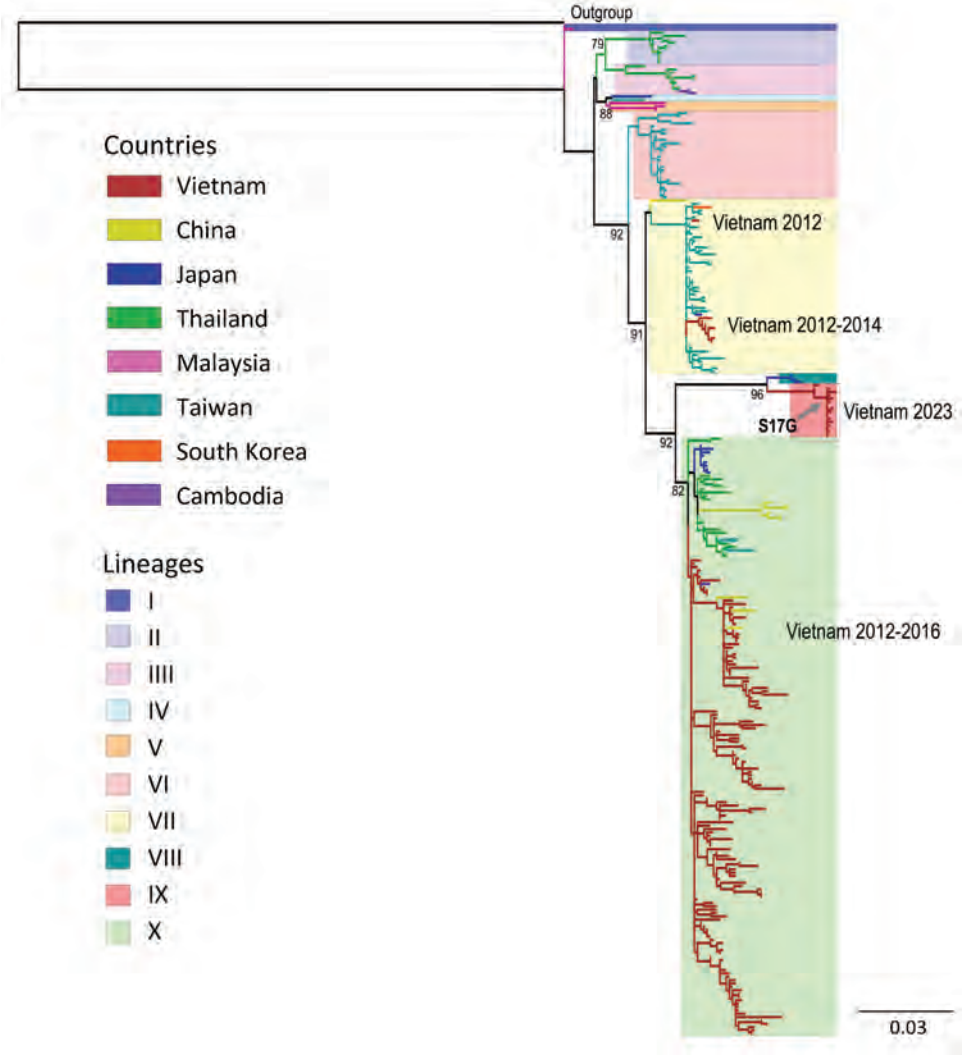

Figure 2. Phylogenetic analysis of viral protein 1 (VP1) coding sequences in study of emerging enterovirus A71 subgenogroup B5 causing severe hand, foot, and mouth disease, Vietnam, 2023. Tree was constructed for VP1 gene sequences by using the maximum-likelihood method to compare genetic relatedness among the B5 sequences from this study and global sequences obtained from GenBank. Line colors indicate the country of origin for each sequence. Box colors indicate the enterovirus lineage. Arrow indicates the emerging B5 lineage from Vietnam carrying an S17G codon substitution within the N-terminus of VP1. Similar phylogenetic tree structure was obtained when the analysis was performed by using complete genome coding sequences. Interlineage and intralineage nucleotide sequence similarities among the lineages were calculated (Appendix Table 3, https://wwwnc.cdc.gov/EID/article/30/2/23-1024-App1.pdf). Scale bar indicates nucleotide substitutions per site.

an emerging lineage because of a unique nonsynonymous amino acid substitution (S17G) in VP1 and because they form a distinct lineage within the global B5 phylogenetic tree. Further research is needed to clarify the origin and transmission network of this emerging lineage.

Underlying factors might cause the emergence of EV-A71 subgenogroups within a specific locality; the accumulation of a sufficient number of susceptible young children in the population and pathogen evolution might play critical roles (*9*,*10*). The changing epidemiology of respiratory pathogens as a consequence of COVID-19 has been documented (*11*), although EV-A71 is mainly transmitted by the oral-fecal route; thus, the effects of COVID-19 on EV-A71 transmission might be different from those of other respiratory viruses. However, the COVID-19 pandemic could have resulted in a large cohort of children who had greater susceptibility to EV-A71 infection, leading to a surge in infections among older children in the 2023 outbreak. Virus immune evasion or altered virulence might also be substantial contributing factors in the outbreak (*9*,*12*). The amino acid residue 17 in VP1 does not form part of the identified EV-A71 immune epitopes (*13*), but mutations in the N terminus of VP1 might increase cell tropism, potentially contributing to EV-A71 pathogenesis. Collectively, because VP1 is the most immunogenic protein of EV-A71, the potential effects of the nonsynonymous S17G substitution on immune escape and virulence of EV-A71 subgenogroup B5 warrant further investigation.

Previous peaks of EV-A71 outbreaks in Vietnam occurred during September–November (*3*), coinciding with school reopening after the summer holiday (June–August). As of November 2023, the outbreak in Vietnam was still ongoing and had resulted in >100,000 infections and 23 deaths across the country. The potential for severe EV-A71–associated HFMD outbreaks to spread to other parts of the world should be closely monitored.

Inactivated EV-A71 vaccines have been developed in China and Taiwan (*14*) but have only been used in China. Real-world data have shown that those vaccines substantially reduced EV-A71–associated disease transmission in China (*15*). Thus, using EV-A71 vaccines in other HFMD-endemic countries could have a similar effect. However, the extent to which EV-A71 vaccines might shape HFMD dynamics as a whole should be closely monitored. Because HFMD is transmitted through the oral-fecal route, good hygiene is critical to reduce EV-A71 transmission.

In conclusion, the 2023 outbreak of severe HFMD in Vietnam has mainly been caused by an emerging EV-A71 subgenogroup B5 lineage, and older children have been affected. Clinicians should recognize the diverse clinical manifestations of HFMD. Furthermore, enhanced EV-A71 surveillance is needed to inform the outbreak response in Vietnam and elsewhere, should the virus spread.

Members of the SEACOVARIANTS: Nguyen To Anh, Nguyen Thi Thu Hong, Truong Hoang Chau Truc, Nguyen Thi Han Ny, Do Duong Kim Han, Le Kim Thanh, Lam Anh Nguyet, Cao Thu Thuy, Le Nguyen Truc Nhu, Tran Tan Thanh, Nguyen To Anh, Lam Minh Yen, Vu Thi Ty Hang, Pham Tieu Kieu, Vo Tan Hoang, Nguyen Thi Thao, Mary Chambers, Vu Duy Thanh, Tran Chieu Hoang, C Louise Thwaites, Guy Thwaites, Le Van Tan (Oxford University Clinical Research Unit, Ho Chi Minh City, Vietnam), H. Rogier van Doorn, Trinh Son Tung (Oxford University Clinical Research Unit, Ha Noi, Vietnam), H. Rogier van Doorn, C Louise Thwaites, Guy Thwaites, Raph L Hamers, Anuraj Shankar, Juthathip Mongkolsapaya, Gavin Screaton, Aiete Dijokaite-Guraliuc, Raksha Das, Chang Liu, Piyada Supasa, Muneeswaran Selvaraj, Susanna J Dunachie, Paul Klenerman, E Yvonne Jones, David I Stuart, Barbara Kronsteiner-Dobramysl, Martha Zewdie, Priyanka Abraham, Jennifer Hill (University of Oxford, Oxford, UK), Wang Lin-Fa, Tan Chee Wah, Yap Wee Chee, Lim Beng Lee (Duke-NUS Medical School, Singapore), Raph L Hamers, Anuraj Shankar, Suwarti, Yanie Tayipto, Eva Simarmata, Ragil Dien (Oxford University Clinical Research Unit, Jakarta, Indonesia), Wanwisa Dejnirattisai, Warangkana Chantima, Narisara Chantratita, Prapassorn Poolchanuan, Vichapon Tiacharoen, Adul Dulsuk (Mahidol University, Bangkok, Thailand), Sophon Iamsirithaworn (Ministry of Public Health, Thailand), Nick Day, Phaik Yeong Cheah, Tassawan Poomchaichote, Kanpong Boonthaworn (Mahidol Oxford Tropical Medicine Research Unit, Bangkok), Nghiem My Ngoc (Hospital for Tropical Diseases, Ho Chi Minh City), Alba Grifoni, Alessandro Sette (La Jolla Institute for Immunology, California, USA).

Acknowledgments

We thank the patients and their parents for their participation in this study and all nursing and medical staff in the pediatric intensive care unit and infectious diseases wards at Children's Hospital 1 who provided care for the patients and helped collect clinical data.

This work was supported by the Wellcome Trust, United Kingdom (grant nos. 226120/Z/22/Z, 222574/Z/21/Z, and 225437/Z/22/Z). The funding body did not have any

influence on the study design, study conduct, preparation of the manuscript, or decision to publish.

About the Author

Dr. Chau is vice director of the Ho Chi Minh City Department of Health in Vietnam. His research interests focus on infectious diseases of public health importance in Vietnam, especially emerging infections.

References

1. World Health Organization Regional Office for the Western Pacific. A guide to clinical management and public health response for hand, foot and mouth disease (HFMD). 2011 [cited 2023 Jun 1]. https://apps.who.int/iris/handle/10665/207490
2. Messacar K, Burakoff A, Nix WA, Rogers S, Oberste MS, Gerber SI, et al. Notes from the field: enterovirus A71 neurologic disease in children—Colorado, 2018. MMWR Morb Mortal Wkly Rep. 2018;67:1017–8. https://doi.org/10.15585/mmwr.mm6736a5
3. Nhan LNT, Khanh TH, Hong NTT, Van HMT, Nhu LNT, Ny NTH, et al. Clinical, etiological and epidemiological investigations of hand, foot and mouth disease in southern Vietnam during 2015–2018. PLoS Negl Trop Dis. 2020;14:e0008544. https://doi.org/10.1371/journal.pntd.0008544
4. Thanh TT, Anh NT, Tham NT, Van HMT, Sabanathan S, Qui PT, et al. Validation and utilization of an internally controlled multiplex real-time RT-PCR assay for simultaneous detection of enteroviruses and enterovirus A71 associated with hand foot and mouth disease. Virol J. 2015;12:85. https://doi.org/10.1186/s12985-015-0316-2
5. Kroneman A, Vennema H, Deforche K, v d Avoort H, Peñaranda S, Oberste MS, et al. An automated genotyping tool for enteroviruses and noroviruses. J Clin Virol. 2011;51:121–5. https://doi.org/10.1016/j.jcv.2011.03.006
6. Dung NT, Hung LM, Hoa HTT, Nga LH, Hong NTT, Thuong TC, et al. Monkeypox virus infection in 2 female travelers returning to Vietnam from Dubai, United Arab Emirates, 2022. Emerg Infect Dis. 2023;29:778–81. https://doi.org/10.3201/eid2904.221835
7. Martin DP, Murrell B, Golden M, Khoosal A, Muhire B. RDP4: detection and analysis of recombination patterns in virus genomes. Virus Evol. 2015;1:vev003. https://doi.org/10.1093/ve/vev003
8. Minh BQ, Schmidt HA, Chernomor O, Schrempf D, Woodhams MD, von Haeseler A, et al. IQ-TREE 2: new models and efficient methods for phylogenetic inference in the genomic era. Mol Biol Evol. 2020;37:1530–4. https://doi.org/10.1093/molbev/msaa015
9. Kobayashi K, Nishimura H, Mizuta K, Nishizawa T, Chu ST, Ichimura H, et al. Virulence of enterovirus A71 fluctuates depending on the phylogenetic clade formed in the epidemic year and epidemic region. J Virol. 2021;95:e0151521. https://doi.org/10.1128/JVI.01515-21
10. Takahashi S, Metcalf CJE, Arima Y, Fujimoto T, Shimizu H, Rogier van Doorn H, et al. Epidemic dynamics, interactions and predictability of enteroviruses associated with hand, foot and mouth disease in Japan. J R Soc Interface. 2018;15:20180507. https://doi.org/10.1098/rsif.2018.0507
11. Eden JS, Sikazwe C, Xie R, Deng YM, Sullivan SG, Michie A, et al.; Australian RSV study group. Off-season RSV epidemics in Australia after easing of COVID-19 restrictions. Nat Commun. 2022;13:2884. https://doi.org/10.1038/s41467-022-30485-3
12. Tee KK, Lam TT, Chan YF, Bible JM, Kamarulzaman A, Tong CYM, et al. Evolutionary genetics of human enterovirus 71: origin, population dynamics, natural selection, and seasonal periodicity of the VP1 gene. J Virol. 2010;84:3339–50. https://doi.org/10.1128/JVI.01019-09
13. Yuan J, Shen L, Wu J, Zou X, Gu J, Chen J, et al. Enterovirus A71 proteins: structure and function. Front Microbiol. 2018;9:286. https://doi.org/10.3389/fmicb.2018.00286
14. Nguyen TT, Chiu CH, Lin CY, Chiu NC, Chen PY, Le TTV, et al. Efficacy, safety, and immunogenicity of an inactivated, adjuvanted enterovirus 71 vaccine in infants and children: a multiregion, double-blind, randomised, placebo-controlled, phase 3 trial. Lancet. 2022;399:1708–17. https://doi.org/10.1016/S0140-6736(22)00313-0
15. Hong J, Liu F, Qi H, Tu W, Ward MP, Ren M, et al. Changing epidemiology of hand, foot, and mouth disease in China, 2013–2019: a population-based study. Lancet Reg Health West Pac. 2022;20:100370. https://doi.org/10.1016/j.lanwpc.2021.100370

Address for correspondence: Le Van Tan, Oxford University Clinical Research Unit, 764 Vo Van Kiet, District 5, Ho Chi Minh City, Vietnam; email: tanlv@oucru.org

Obstetric and Neonatal Invasive Meningococcal Disease Caused by *Neisseria meningitidis* Serogroup W, Western Australia, Australia

Julie Hart, Gary K. Dowse, Michelle Porter, David J. Speers, Anthony D. Keil, Jane D. Bew, Shakeel Mowlaboccus, Charlene M. Kahler

Three mother-baby pairs with invasive meningococcal disease occurred over 7 months in Western Australia, Australia, at a time when serogroup W sequence type 11 clonal complex was the predominant local strain. One mother and 2 neonates died, highlighting the role of this strain as a cause of obstetric and early neonatal death.

In Western Australia, Australia, an outbreak of serogroup W meningococcal disease in 2017 caused obstetric and neonatal cases of invasive meningococcal disease (IMD). The outbreak was caused by a hypervirulent strain of *Neisseria meningitides* belonging to sequence type 11 clonal complex (MenW:cc11). We report 3 cases that occurred during this outbreak. This study was approved by the Western Australia Women and Newborn Health Service Human Research Ethics Committee.

The Study

Case 1, in June 2017, involved a 26-year-old pregnant woman (G2P1, 41 weeks) who had no concurrent conditions underwent induction with artificial rupture of membranes for fetal compromise on cardiotocography and delivered vaginally. The baby was well at birth and discharged on day 2 of life. At 5 days of age, the neonate was returned to hospital by ambulance with respiratory distress requiring intubation. Treatment with intravenous benzylpenicillin, cefotaxime, and acyclovir was given, but because of extensive hypoxic brain injury, the baby was extubated and died 2 days later. *Neisseria meningitidis* serogroup W (MenW) DNA was detected by PCR (in-house multiplex real-time PCRs for *ctrA* and *porA* genes) but was not cultured from placenta or from brain, larynx, and lung tissue at postmortem. *N. meningitidis* (not typed) was the only pathogen isolated from a maternal low vaginal swab specimen collected 1-week postdelivery to investigate vaginal discharge.

Case 2, in December 2017, involved a 36-year-old pregnant woman (G8P5, 38 weeks) who had gestational diabetes was hospitalized because of watery diarrhea and severe abdominal pain. Her condition rapidly deteriorated, and she died despite resuscitative efforts. A perimortem emergency caesarean section was performed, but the fetus was delivered without signs of life. Maternal blood culture grew MenW (isolate EXNM778, PubMLST [https://pubmlst.org/organisms/neisseria-spp] identification no. 110297), which demonstrated intermediate susceptibility to penicillin (0.25 mg/L) by Etest (bioMérieux, https://www.biomerieux.com) interpreted using Clinical and Laboratory Standards Institute (https://clsi.org) guidelines. MenW was detected by PCR from placental tissue but not from postmortem fetal blood or lung, liver, or brain tissue.

Case 3, in January 2018, involved a 22-year-old pregnant woman (G2P1, 39 weeks) who had gestational diabetes sought care in spontaneous labor with fever and fetal compromise on cardiotocography, prompting a nonelective caesarean section. The neonate had neck cord entanglement and tachypnea requiring continuous positive airway pressure. Maternal C-reactive protein (194 mg/L) and leukocyte count (34 × 10^9 cells/L) were increased. Intravenous benzylpenicillin and gentamicin were given for

Author affiliations: Queen Elizabeth II Medical Centre, Nedlands, Western Australia, Australia (J. Hart, M. Porter, D.J. Speers, A.D. Keil, J.D. Bew); Department of Health, Perth, Western Australia, Australia (G.K. Dowse); The University of Western Australia, Perth (D.J. Speers, S. Mowlaboccus, C.M. Kahler)

DOI: https://doi.org/10.3201/eid3002.230639

suspected neonatal sepsis (C-reactive protein 21 mg/L, lactate 4.9 nmol/L). Gastric aspirate, ear, and placental swab specimens (but not blood or cerebrospinal fluid) subsequently grew MenW (isolate EXNM791, PubMLST identification no. 110300) demonstrating intermediate susceptibility to penicillin (0.25 mg/L). The neonate received intravenous cefotaxime for 5 days. Testing of whole blood and cerebrospinal fluid by PCR did not detect *N. meningitidis*. The mother initially received intravenous clindamycin, gentamicin, and metronidazole (previous rash to penicillin) and then intravenous ceftriaxone for 5 days. No growth resulted from maternal blood culture collected after antimicrobial drugs were given. Mother and baby were discharged at day 7, after rapid improvement.

We performed typing of case isolates by nested PCR directed at the *porA* gene covering 2 variable regions (VR1 and VR2), followed by gel electrophoresis and Sanger sequencing analysis, with comparison to sequences in the PubMLST database. Whole-genome sequencing (*1*) of case 2 and 3 isolates demonstrated phylogenetic clustering in cluster B (penicillin resistance–associated lineage) of MenW:cc11 lineage 11.1, which is distinct from lineage 11.2, to which the US nongroupable urethritis strain belongs (*2*) (Figure 1). Only case 2 clustered with isolates from other local contemporaneous cases, part of an outbreak that began in 2014 (*1*).

Conclusions

The recent rapid global expansion of hypervirulent MenW:cc11, which emerged in the late 1990s from South America and spread to Europe, North America, and Australasia (*3*), caused a rapid increase in IMD incidence in Western Australia, from an average of <1 MenW case/year before 2014 to 30 cases among a population of 2.6 million persons in 2018

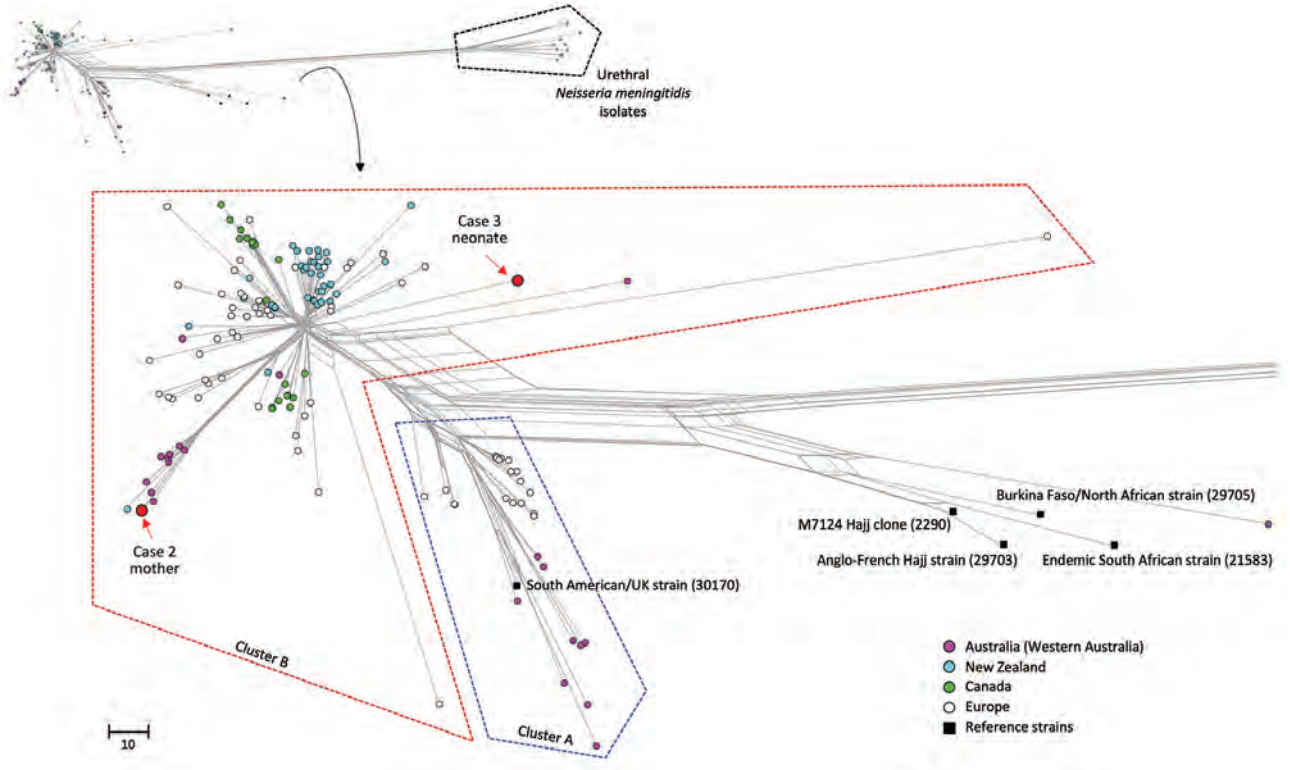

Figure 1. Phylogenetic relationship of 2 invasive *Neisseria meningitidis* serogroup W (MenW:cc11) strains from 3 mother-baby pairs with invasive meningococcal disease in Western Australia, Australia, compared with other local and international isolates. The neighbor-net phylogenetic network was constructed based on 1,605 core genome loci using the Genome Comparator tool available on the PubMLST *Neisseria* website (https://pubmlst.org/organisms/neisseria-spp). Red indicates the 2 isolates reported in this study ; pink circles indicate isolates from Western Australia reported by Mowlaboccus et al. (*1*); blue, green, and white circles indicate isolates from the Australian Penicillin Resistance–Associated Lineage reported by Willerton et al. (*3*) from New Zealand, Canada, and Europe, respectively; black squares indicate reference invasive MenW/cc11 strains characterized by Lucidarme et al. (*4*). Identification numbers in parentheses indicate PubMLST identification numbers of reference isolates. Inset at top shows full phylogenetic trees; callout at left shows urethral *N. meningitidis* strains strains from Tzeng et al. (*2*) and Ma et al. (*5*), which were isolated from urethral swabs in the United States (NM1, NM2), the United Kingdom (M11_240294, M11_241043, M13_240559), Italy (PE5, PE6, PE7), and France (LNP26948, LNP27256). Scale bar indicates number of different loci among the 1,605 compared.

(Figure 2). Some MenW:cc11 strains have been associated with a high case-fatality rate and atypical disease manifestations (*3*).

Isolates from case 2 (mother) and case 3 (neonate) belonged to the UK/South America MenW:cc11 lineage (*3*) and to the penicillin resistance–associated lineage previously described from Western Australia (*1*), which has since expanded to 8 countries (*3*). Those isolates have demonstrated intermediate penicillin resistance by Clinical and Laboratory Standards Institute guidelines and have been associated with treatment failure using low-dose penicillin regimens recommended for IMD. The 2 isolates we describe were not closely related to lineage 11.2 urethritis isolates and did not possess previously described adaptations to urogenital infection; they had intact capsule genes and did not harbor the gonococcal *aniA* and *norB* alleles that promote urethral anaerobic growth (*2*,*5*). Our cases are most likely to represent atypical disease manifestations of MenW:cc11 resulting from ascending maternal genital infection (case 1) or from maternal IMD (case 2).

N. meningitidis is primarily spread by the respiratory route, but genital meningococcal disease is reported (*5*). Although a retrospective matched case–control study (*6*) has shown a strong association between childhood IMD and coincident pregnancy of the patient's mother, increased meningococcal carriage rates in pregnant women have not been shown, and few case reports of IMD during pregnancy have been published (*7*).

National surveillance data from England (2011–2014) (*7*) included 4 cases in pregnant women but indicated that pregnant women were 5 times less likely to have IMD develop than were nonpregnant women. This finding highlights the unusual occurrence of 3 mother-baby pairs within 7 months in a much smaller population. Additional reported cases in pregnancy include 5 with meningitis and single cases with acute meningococcemia, chronic meningococcemia, and pericarditis (*8*–*12*). In total, those 12 cases in pregnant women caused 4 neonatal deaths. The England surveillance study also identified 5 cases of early-onset (<7 days) neonatal IMD, none with reported maternal illness (*7*). Fetal or early-onset neonatal IMD can occur after colonization of the maternal genital tract or by septicemic transmission in utero from maternal IMD (*13*). Early neonatal IMD is rare, presumably because of the rarity of genital tract colonization plus maternal antibody transfer across the placenta (*13*).

A review in 2017 described 23 cases of early-onset (<8 days) neonatal IMD with a high case-fatality rate (34.8%) (*14*). A 2020 review (*13*) and 2 case reports (*15*) added an additional 8 cases, with 2 neonatal deaths. In total, those 31 cases resulted in 10 neonatal deaths, although the 3 known MenW case-patients survived.

MenW incidence in Western Australia has decreased substantially, from 30 cases in 2018 to 3 cases in 2021 (Figure 2). This decrease is probably associated with MenACWY vaccination programs for adolescents 15–19 years of age and children 12 months–4 years of age, which began in Western Australia in May 2017 and January 2018, respectively, along with the effect of subsequent COVID-19–related public health restrictions.

In summary, we report a time-place cluster of 3 mother-baby pairs with *N. meningitidis* infection, ranging from vaginitis to fulminant fatal maternal

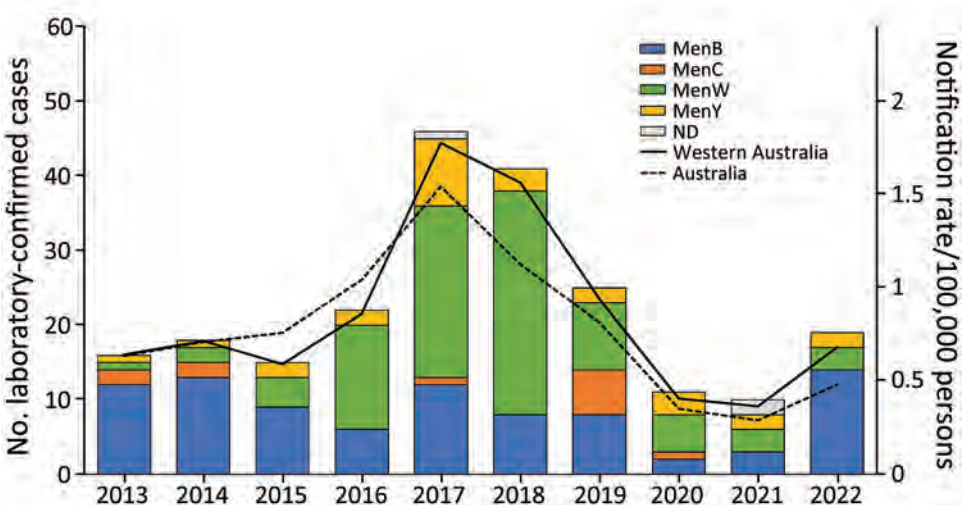

Figure 2. Notifications of laboratory-confirmed invasive meningococcal disease cases in Western Australia and Australia, by serogroup and year of onset, 2013–2022. Serogroup data were extracted from the Western Australian Notifiable Infectious Diseases Database (https://www.health.wa.gov.au), and the overall national notification data were obtained from the National Notifiable Diseases Surveillance System (https://www.health.gov.au/our-work/nndss). Rates were calculated by using estimated resident population data from the Australian Bureau of Statistics (https://www.abs.gov.au) (national, state and territory population March 2023, accessed on October 3, 2023). Men, meningococcal; ND, not determined; WA, Western Australia.

and neonatal sepsis, to highlight the potential for MenW:cc11 to cause obstetric and early neonatal infection. Because *N. meningitidis* is uncommonly isolated from the genital tract and does not necessarily cause disease, there is no current recommendation to routinely screen or treat pregnant women. However, these cases suggest the need for opportune laboratory reporting of *N. meningitidis* isolates from the genital tract; if pregnant women are found colonized, preemptive treatment should be considered to prevent subsequent neonatal infection. Our findings also highlight the need for MenACWY vaccination of adolescents and possible opportunistic catch-up vaccination in women before or during pregnancy.

Acknowledgments

We thank the families of the case-patients for their consent to publication of these case reports. We also thank our clinical, laboratory and public health colleagues for their involvement in management of case-patients.

C.M.K. was supported by the National Health and Medical Research Council (grant APP546003) and the Amanda Young Foundation, a not-for-profit charity.

About the Author

Dr. Hart is a clinical microbiologist and infectious diseases specialist at PathWest Laboratory Medicine and Sir Charles Gairdner Hospital, Perth, Western Australia. Her primary research interest is clinical infectious diseases.

References

1. Mowlaboccus S, Jolley KA, Bray JE, Pang S, Lee YT, Bew JD, et al. Clonal expansion of new penicillin-resistant clade of *Neisseria meningitidis* serogroup W clonal complex 11, Australia. Emerg Infect Dis. 2017;23:1364–7. https://doi.org/10.3201/eid2308.170259
2. Tzeng YL, Bazan JA, Turner AN, Wang X, Retchless AC, Read TD, et al. Emergence of a new *Neisseria meningitidis* clonal complex 11 lineage 11.2 clade as an effective urogenital pathogen. Proc Natl Acad Sci U S A. 2017;114:4237–42. https://doi.org/10.1073/pnas.1620971114
3. Willerton L, Lucidarme J, Walker A, Lekshmi A, Clark SA, Gray SJ, et al. Increase in penicillin-resistant invasive meningococcal serogroup W ST-11 complex isolates in England. Vaccine. 2021;39:2719–29. https://doi.org/10.1016/j.vaccine.2021.03.002
4. Lucidarme J, Hill DM, Bratcher HB, Gray SJ, du Plessis M, Tsang RS, et al. Genomic resolution of an aggressive, widespread, diverse and expanding meningococcal serogroup B, C and W lineage. J Infect. 2015;71:544–52. https://doi.org/10.1016/j.jinf.2015.07.007
5. Ma KC, Unemo M, Jeverica S, Kirkcaldy RD, Takahashi H, Ohnishi M, et al. Genomic characterization of urethritis-associated *Neisseria meningitidis* shows that a wide range of N. meningitidis strains can cause urethritis. J Clin Microbiol. 2017;55:3374–83. https://doi.org/10.1128/JCM.01018-17
6. van Gils EJ, van Woensel JB, van der Ende A, Kuijpers TW. Increased attack rate of meningococcal disease in children with a pregnant mother. Pediatrics. 2005;115:e590–3. https://doi.org/10.1542/peds.2004-2291
7. Parikh SR, Borrow R, Ramsay ME, Ladhani SN. Lower risk of invasive meningococcal disease during pregnancy: national prospective surveillance in England, 2011–2014. BJOG. 2019;126:1052–7. https://doi.org/10.1111/1471-0528.15701
8. Polayes SH, Ohlbaum C, Winston HB. Meningococcus meningitis with massive hemorrhage of the adrenals (Waterhouse-Friderichsen syndrome) complicating pregnancy with pre-eclamptic toxemia. Am J Obstet Gynecol. 1953;65:192–6. https://doi.org/10.1016/0002-9378 (53)90032-5
9. Persa OD, Jazmati N, Robinson N, Wolke M, Kremer K, Schweer K, et al. A pregnant woman with chronic meningococcaemia from *Neisseria meningitidis* with lpxL1-mutations. Lancet. 2014;384:1900. https://doi.org/10.1016/S0140-6736(14)61645-7
10. Finan MA, Smith SG, Sinnott JT, O'Brien W, Ibach M, Morales R. An interesting case presentation: peripartum meningococcal meningitis. J Perinatol. 1992;12:78–80.
11. Neubert AG, Schwartz PA. *Neisseria meningitidis* sepsis as a complication of labor. A case report. J Reprod Med. 1994;39:749–51.
12. Brandeberry KR, Vergon JM. Meningococcic meningitis in term pregnancy. Am J Obstet Gynecol. 1951;61:699–700. https://doi.org/10.1016/0002-9378(51)91427-5
13. Filippakis D, Gkentzi D, Dimitriou G, Karatza A. Neonatal meningococcal disease: an update. J Matern Fetal Neonatal Med. 2020;35:4190–5. https://doi.org/10.1080/14767058.2020.1849092
14. Basani L, Aepala R. *Neisseria meningitidis* causing multiple cerebral abscesses in early neonatal period: case report and review of literature. J Clin Diagn Res. 2017;11:SD01–03. https://doi.org/10.7860/JCDR/2017/25284.10151
15. Achten NB, Been JV, Schoenmakers S, Vermont CL, Verdijk RM, Reiss IK, et al. Fatal early-onset sepsis caused by intrauterine transmission of serogroup Y meningococcus. Pediatr Infect Dis J. 2022;41:e517–9. https://doi.org/10.1097/INF.0000000000003722

Address for correspondence: Julie Hart, PathWest Laboratory Medicine, Queen Elizabeth II Medical Centre, Hospital Ave, Nedlands, Western Australia, Australia; email: julie.hart@health.wa.gov.au

Using Insurance Claims Data to Estimate Blastomycosis Incidence, Vermont, USA, 2011–2020

Brian F. Borah, Paul Meddaugh, Veronica Fialkowski, Natalie Kwit

The epidemiology of blastomycosis in Vermont, USA, is poorly understood. Using insurance claims data, we estimated the mean annual blastomycosis incidence was 1.8 patients/100,000 persons during 2011–2020. Incidence and disease severity were highest in north-central counties. Our findings highlight a need for improved clinical awareness and expanded surveillance.

Blastomycosis is a rare but potentially fatal fungal disease caused by *Blastomyces* spp., a group of thermally dimorphic environmental mycoses found in moist soil and decaying organic matter. Human illness most often results in pulmonary conditions but can involve any organ system; clinical manifestations range from subclinical infection to life-threatening disease (*1*). Associated illness and death rates are high; among symptomatic persons, hospitalization rates are 57%–69% (*2*–*5*) and death rates 4%–22% (*1*).

Epidemiology of blastomycosis in the United States is poorly understood. Geographic areas of the United States that have historically been considered endemic, based largely on sporadic case reports and a few documented outbreaks, include midwestern, south-central, and southeastern regions of the country, particularly adjacent to the Ohio and Mississippi Rivers, Great Lakes, and St. Lawrence Seaway. In those areas, statewide annual incidence rates are ≈0.2–2.0 cases/100,000 persons (*1*–*3*). However, blastomycosis is not a nationally notifiable disease, and public health surveillance is limited to just 5 states: Arkansas, Louisiana, Michigan, Minnesota, and Wisconsin. The true burden of blastomycosis elsewhere is unknown.

Author affiliations: Centers for Disease Control and Prevention, Atlanta, Georgia, USA (B. Borah); Vermont Department of Health, Burlington, Vermont, USA (B. Borah, P. Meddaugh, N. Kwit); Green Mountain Care Board, Montpelier, Vermont, USA (V. Fialkowski)

DOI: https://doi.org/10.3201/eid3002.230825

Recent studies suggest incidence in the United States, particularly in the northeastern region, might be greater than previously understood (*6*–*9*). To assess the epidemiology of blastomycosis in the northeastern state of Vermont, we used insurance claims data and vital records to describe case-patient demographics, hospitalization rates, deaths, annual incidence, and geographic distribution of disease. This activity was reviewed by the Centers for Disease Control and Prevention and conducted consistent with applicable federal law and agency policy. Activity was determined to meet the requirements of public health surveillance as defined in 45 CFR 46.102(l)(2).

The Study

The Vermont Health Care Uniform Reporting and Evaluation System (VHCURES) is an all-payer health insurance claims database managed by the Green Mountain Care Board (Montpelier, Vermont, USA). VHCURES includes insurance claims data from medical, dental, and pharmacy encounters for all Medicare and Medicaid recipients and ≈75% of Vermont residents with commercial insurance. For this retrospective cohort analysis, we used VHCURES to identify all patients who received a primary or secondary diagnosis code of 116.0 (International Classification of Disease [ICD], 9th Edition, Clinical Modification) or B40.X (ICD, 10th Edition, Clinical Modification) for blastomycosis during a 2011–2020 medical encounter. VHCURES excludes personally identifiable information but does provide patient-level information including age, sex, insurance type (Medicare, Medicaid, or commercial), county of residence, and hospitalization status. Race and ethnicity data were unavailable. We identified blastomycosis-attributable deaths from Vermont vital records and calculated incidence rates (cases/100,000 persons) using state- and county-level census estimates.

Table. Characteristics of patients with blastomycosis, Vermont, USA, 2011–2020*

Characteristic	All patients	Hospitalized patients	Deaths
Total	114 (100)	34 (30)	4†
Sex			
M	67 (59)	20 (59)	1 (25)
F	47 (41)	14 (41)	3 (75)
Insurance type			
Commercial	48 (42)	≤10†	NA
Medicare	42 (37)	19 (56)	NA
Medicaid	24 (21)	≤10†	NA
Age category, y			
0–19	≤10‡	≤10†	0
20–39	21 (18)	≤10†	0
40–59	40 (35)	11 (32)	2 (50)
60–79	43 (38)	12 (35)	1 (25)
≥80	≤10‡	≤10†	1 (25)
Median age, y (range)	55 (0–89)	56 (3–89)	59 (45–90)

*Values are no. (%) except as indicated.
†Deaths were identified from different data source than patients and hospitalizations; death rate cannot be calculated.
‡In accordance with the Green Mountain Care Board data use agreement for the Vermont Health Care Uniform Reporting and Evaluation System, all results with a patient count ≤10 must be suppressed.

We identified 114 patients with blastomycosis diagnosed during 2011–2020, a median of 10.5 (range 6–19 cases) cases/year. Most case-patients were male (67; 59%), and median age at first diagnosis was 55 years (range: 0–89 years) (Table). At the time of first diagnosis, 48 (42%) patients had commercial insurance, 42 (37%) Medicare, and 24 (21%) Medicaid. Mean annual statewide incidence of blastomycosis was 1.8 cases/100,000 persons; incidence among male residents (2.2/100,000 population) was greater than that among female residents (1.5/100,000 population). The highest annual incidence, 3.0/100,000 persons, occurred in 2011, followed by 2019 (2.7/100,000 population) and 2020 (2.5/100,000 population) (Figure 1).

Thirty-four (30%) patients had ≥1 blastomycosis-associated hospitalization during the study period. Median age of hospitalized patients at time of diagnosis was 56 (range 3–89) years; 20 (59%) were male and 19 (56%) covered by Medicare. Risk for hospitalization was similar between male and female patients (risk ratio 1.00, 95% CI 0.57–1.78). According to vital records data, 4 deaths were attributed to blastomycosis, a mean annual death rate of 0.06/100,000 population. Three deaths were among female patients, at a median age of 59 years.

Of Vermont's 14 counties, 3 counties in north-central Vermont (Lamoille, Orleans, and Washington) had the highest mean annual incidences (Figure 2). Although the populations of those counties represent only 18% of the state population, 49% of all case-patients and 65% of hospitalized patients resided in those counties. Case-patients in those counties were ≈2 times as likely to be hospitalized with blastomycosis as patients residing elsewhere (risk ratio 1.90, 95% CI 1.04–3.46).

Although Vermont has historically not been considered an area with high relative incidence of blastomycosis, an estimated mean annual incidence of 1.8 case-patients/100,00 population suggests otherwise. That incidence is greater than the mean annual incidences during 1987–2017 in 4 of 5 states that mandate reporting of blastomycosis (Arkansas, Louisiana, Michigan, and Minnesota, but not Wisconsin) (2);

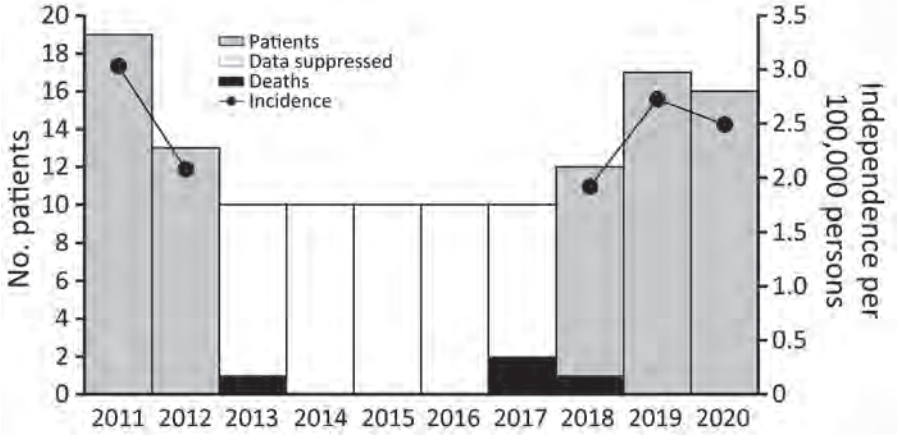

Figure 1. Numbers of patients with blastomycosis, attributable deaths per year, and annual incidence (cases/100,000 population) in Vermont, USA, 2011–2020. Results are suppressed for years with ≤10 patients, in accordance with the Green Mountain Care Board data use agreement for the Vermont Health Care Uniform Reporting and Evaluation System.

incidence in Vermont was greater than in all 5 of those states in 2019 (*3*). Missouri (*10*), Mississippi (*11*), and Illinois (*12*), also located within known endemic areas, reported mean annual incidences of 0.2–1.3/100,000 population for differing intervals during 1979–2018. Although differences in surveillance methods and case definitions among states make direct comparisons difficult, Vermont's burden of blastomycosis appears comparable to, and perhaps higher than, most states that have published blastomycosis incidences.

Consistent with other published studies, our results demonstrate that blastomycosis was more common in adults and male patients (*2*,*3*). We also found that disease incidence and hospitalization rates were greatest in north-central Vermont, a finding supported by clinician reports and at least 1 publication (*6*). Explanations for regional clustering and high statewide incidence in Vermont are unclear. Outdoor activities, climate, geographic features, and soil characteristics have all been associated with heterogeneity of blastomycosis distribution elsewhere (*1*,*2*,*4*,*13*). Like hyperendemic regions of Wisconsin, Vermont is rich in acidic spodosol soil (*14*), which is thought to support *Blastomyces* spp. growth (*2*). Although the 3 counties with the highest incidence in Vermont do not share a common waterway, proximity to waterways generally has been associated with disease (*1*,*13*). Future studies, including animal, environmental, and ecologic niche models (*13*), could further characterize these and other risk factors in Vermont.

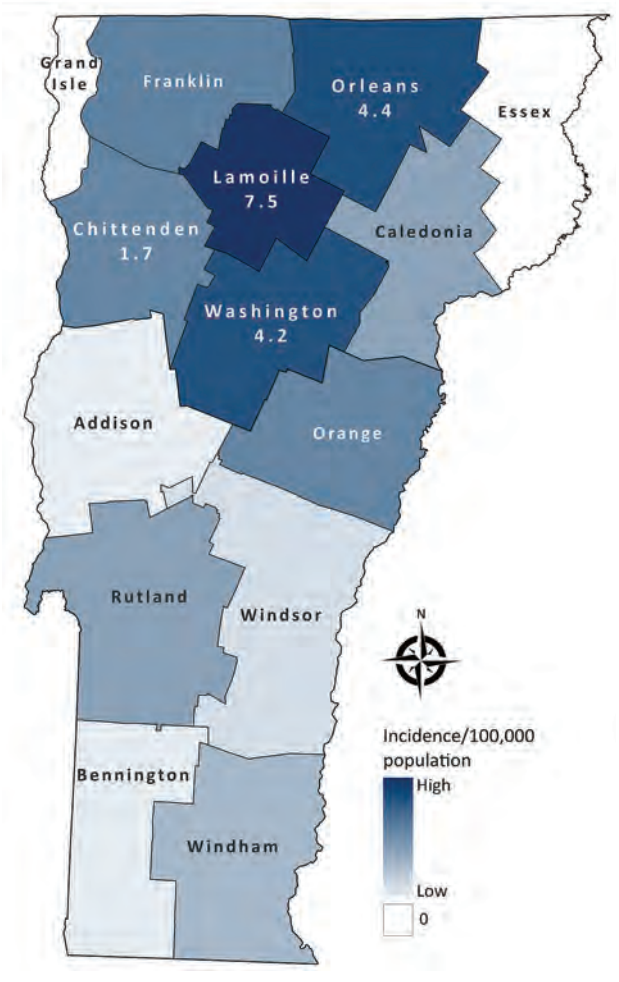

Figure 2. Geographic distribution of blastomycosis cases by county, Vermont, USA, 2011–2020. Numbers indicate incidence rates (cases/100,000 population) for counties with the highest incidence.

Among limitations in our study, blastomycosis diagnoses are commonly delayed or missed in clinical practice because of low clinical suspicion and nonspecific diagnostic tests (*1*), and laboratory-confirmed diagnoses can be missed by ICD-based queries (*10*). Next, claims data are used primarily for administrative purposes and thus have inherent limitations for public health surveillance, including coding errors and disease misclassification. We might also have undercounted diagnoses among the minority of the Vermont population who did not have claims submitted to VHCURES. Moreover, given inherent complexities in VHCURES data which limit accurate estimations of total annual VHCURES enrollees, we used census estimates of state population for incidence denominators. Those limitations likely resulted in an underestimation of blastomycosis incidence. However, other limitations might have posed some risk of overestimation. We might have included patients who were diagnosed with blastomycosis before 2011 if they had a follow-up encounter associated with the diagnosis during 2011–2020. In addition, we were unable to validate ICD-based diagnoses with external laboratory or clinical data. Our methods possibly captured mild illnesses better than passive surveillance, which is biased toward severe cases (*15*), which might explain why the hospitalization rate (30%) in our study was lower than rates elsewhere (*2*–*5*). Finally, we used county of residence of case-patients to describe geographic distribution of the disease; we could not determine whether fungal exposures were travel-associated.

Conclusions

Our findings, based on the most comprehensive assessment of blastomycosis in Vermont to date, align with a growing body of evidence suggesting that the burden of endemic blastomycosis is greater than commonly appreciated (*6*–*9*). These results challenge routine assumptions about the epidemiology and ecology of this disease and reflect a need for future studies. Clinicians should consider blastomycosis

in patients with compatible signs and symptoms. Standardized surveillance could also improve our understanding of exposures, risk factors, and clinical outcomes.

Acknowledgments

The authors thank colleagues at CDC's Mycotic Diseases Branch (Division of Foodborne, Waterborne, and Environmental Diseases, National Center for Emerging and Zoonotic Infectious Diseases), including Dallas Smith, Kaitlin Benedict, Mitsuru Toda, Samantha Williams, and Ian Hennessee, who provided valuable insight for this project. Thank you as well to Rhiannon Killian for development of the choropleth map, and to Patsy Kelso, Kris Bisgard, and Lynn Blevins for assisting with and reviewing this work. Finally, a note of appreciation to the many clinicians and public health colleagues throughout Vermont who were instrumental in this study's inception.

Analyses, conclusions, and recommendations drawn from VHCURES data are solely those of the authors and not necessarily those of Green Mountain Care Board.

About the Author

Dr. Borah is an internal medicine physician and CDC Epidemic Intelligence Service officer at the Vermont Department of Health. His research interests include public health surveillance and infectious disease prevention especially among historically disenfranchised populations.

References

1. Mazi PB, Rauseo AM, Spec A. Blastomycosis. Infect Dis Clin North Am. 2021;35:515–30. https://doi.org/10.1016/j.idc.2021.03.013
2. Benedict K, Gibbons-Burgener S, Kocharian A, Ireland M, Rothfeldt L, Christophe N, et al. Blastomycosis surveillance in 5 states, United States, 1987–2018. Emerg Infect Dis. 2021;27:999–1006. https://doi.org/10.3201/eid2704.204078
3. Smith DJ, Williams SL; Endemic Mycoses State Partners Group. Benedict KM, Jackson BR, Toda M. Surveillance for coccidiomycosis, histoplasmosis, and blastomycosis—United States, 2019. MMWR Surveill Summ. 2002;71 (No. SS-7):1–14. https://doi.org/10.15585/mmwr.ss7107a1
4. Ireland M, Klumb C, Smith K, Scheftel J. Blastomycosis in Minnesota, USA, 1999–2018. Emerg Infect Dis. 2020;26:866–75. https://doi.org/10.3201/eid2605.191074
5. Dworkin MS, Duckro AN, Proia L, Semel JD, Huhn G. The epidemiology of blastomycosis in Illinois and factors associated with death. Clin Infect Dis. 2005;41:e107–11. https://doi.org/10.1086/498152
6. Mazi PB, Sahrmann JM, Olsen MA, Coler-Reilly A, Rauseo AM, Pullen M, et al. The geographic distribution of dimorphic mycoses in the United States for the modern era. Clin Infect Dis. 2023;76:1295–301. https://doi.org/10.1093/cid/ciac882
7. Ross JJ, Koo S, Woolley AE, Zuckerman RA. Blastomycosis in New England: 5 cases and a review. Open Forum Infect Dis. 2023;10:ofad029.
8. McDonald R, Dufort E, Jackson BR, Tobin EH, Newman A, Benedict K, et al. Notes from the field: blastomycosis cases occurring outside of regions with known endemicity—New York, 2007–2017. MMWR Morb Mortal Wkly Rep. 2018;67:1077–8. https://doi.org/10.15585/mmwr.mm6738a8
9. Kiatsimkul P. Increasing incidence of blastomycosis infection in Vermont. Poster presented at: IDWeek 2017 (annual meeting of the Infectious Diseases Society of America); San Diego, CA, USA; October 4–8, 2017.
10. Cano MV, Ponce-de-Leon GF, Tippen S, Lindsley MD, Warwick M, Hajjeh RA. Blastomycosis in Missouri: epidemiology and risk factors for endemic disease. Epidemiol Infect. 2003;131:907–14. https://doi.org/10.1017/S0950268803008987
11. Chapman SW, Lin AC, Hendricks KA, Nolan RL, Currier MM, Morris KR, et al. Endemic blastomycosis in Mississippi: epidemiological and clinical studies. Semin Respir Infect. 1997;12:219–28.
12. Herrmann JA, Kostiuk SL, Dworkin MS, Johnson YJ. Temporal and spatial distribution of blastomycosis cases among humans and dogs in Illinois (2001–2007). J Am Vet Med Assoc. 2011;239:335–43. https://doi.org/10.2460/javma.239.3.335
13. Reed KD, Meece JK, Archer JR, Peterson AT. Ecologic niche modeling of *Blastomyces dermatitidis* in Wisconsin. PLoS One. 2008;3:e2034. https://doi.org/10.1371/journal.pone.0002034
14. U.S. Department of Agriculture. Natural Resource Conservation Service. Spodosols [cited 2023 Feb 27]. https://www.nrcs.usda.gov/conservation-basics/natural-resource-concerns/soils/spodosols
15. Benedict K, Beer KD, Jackson BR. Histoplasmosis-related healthcare use, diagnosis, and treatment in a commercially insured population, United States. Clin Infect Dis. 2020;70:1003–10.

Address for correspondence: Brian Borah, Vermont Department of Health, 108 Cherry St, Ste 304, Burlington, VT 05401, USA; email: bfborah@gmail.com

Introduction and Spread of Dengue Virus 3, Florida, USA, May 2022–April 2023

Forrest K. Jones,[1] Andrea M. Morrison,[1] Gilberto A. Santiago, Kristyna Rysava, Rebecca A. Zimler, Lea A. Heberlein, Edgar Kopp, Florida Department of Health Bureau of Public Health Laboratory Team,[2] Katharine E. Saunders, Samantha Baudin, Edhelene Rico, Álvaro Mejía-Echeverri, Emma Taylor-Salmon, Verity Hill, Mallery I. Breban, Chantal B.F. Vogels, Nathan D. Grubaugh, Lauren M. Paul, Scott F. Michael, Michael A. Johansson, Laura E. Adams, Jorge Munoz-Jordan, Gabriela Paz-Bailey, Danielle R. Stanek

During May 2022–April 2023, dengue virus serotype 3 was identified among 601 travel-associated and 61 locally acquired dengue cases in Florida, USA. All 203 sequenced genomes belonged to the same genotype III lineage and revealed potential transmission chains in which most locally acquired cases occurred shortly after introduction, with little sustained transmission.

Dengue virus (DENV) is not endemic in the continental United States (*1*); most cases occur among travelers to DENV-endemic areas (*2*). In Florida, USA, DENV infections are primarily reported among travelers (https://ndc.services.cdc.gov/case-definitions/dengue-virus-infections-2015); however, locally acquired cases and limited outbreaks have been reported in Monroe County in 2009–2010 (n = 88), Martin County in 2013 (n = 24), and Monroe County in 2020 (n = 72) (*3*–*5*). During 2009–2021, an annual median of 83 (range 19–413) travel-associated DENV infections and 7 (range 0–77) locally acquired cases were reported in Florida; all DENV types (DENV-1−4) occurred among both travel-associated and locally acquired cases (*6*). Previous work demonstrated the DENV vectors *Aedes aegypti* and *A. albopictus* mosquitoes are present across Florida (*7*).

In early 2022, the Florida Department of Health (FDOH) identified an increase in travel-associated DENV infections, primarily among travelers returning from Cuba. In July 2022, a DENV-3 outbreak was reported in Cuba (*8*); DENV-3 case increases were also documented in other countries in the Americas (*9*,*10*). On July 18, Miami-Dade County health officials issued a mosquito-borne illness advisory after the first locally acquired DENV infection in 2022 was confirmed in a Florida resident (*11*). We document the DENV-3 outbreak in Florida by describing the epidemiologic features of reported cases, analyzing DENV-3 genomic sequences, and reconstructing possible transmission trees.

The Study

FDOH routinely conducts active case-finding activities for DENV and conducts IgM and reverse transcription PCR testing for confirmation and DENV serotype identification. Suspected case-patients are interviewed to identify risk factors, possible mosquito exposure locations, and additional suspected cases (*3*). Ethics approval was not required because this work was part of standard public health outbreak surveillance and response.

During May 1, 2022–April 30, 2023 (52 weeks), 1,037 DENV infections were reported, 966 (93%) were travel-associated and 71 (7%) locally acquired. DENV-3 was the most frequently identified serotype

Author affiliations: Centers for Disease Control and Prevention, San Juan, Puerto Rico, USA (F.K. Jones, G.A. Santiago, M.A. Johansson, L.E. Adams, J. Munoz-Jordan, G. Paz-Bailey, K. Rysava); Centers for Disease Control and Prevention, Atlanta, Georgia, USA (F.K. Jones, K.E. Saunders); Florida Department of Health, Tallahassee, Florida, USA (A.M. Morrison, R.A. Zimler, L.A. Heberlein, E. Kopp, K.E. Saunders, S. Baudin, E. Rico, Á. Mejía-Echeverri, D.R. Stanek); Yale School of Medicine, New Haven, Connecticut, USA (E. Taylor-Salmon); Yale School of Public Health, New Haven (E. Taylor-Salmon, V. Hill, M.I. Breban, C.B.F. Vogels, N.D. Grubaugh); Florida Gulf Coast University, Fort Myers, Florida, USA (L.M. Paul, S.F. Michael)

DOI: https://doi.org/10.3201/eid3002.231615

[1]These authors shared first authorship.

[2]Team members are listed at the end of this article.

(64%, n = 662), followed by DENV-2 (10%, n = 104), DENV-1 (7%, n = 68), and DENV-4 (5%, n = 57); in 146 (14%) cases, multiple serotypes or no serotype was identified (Figure 1, panel A). Among DENV-3 cases, 601 (91%) were travel-associated and 61 (9%) were locally acquired cases (Figure 1, panel B). Most DENV-3 case-patients identified as White (n = 609; 92%) and Hispanic or Latino (n = 642, 97%).

Among 601 travel-associated DENV-3 cases, the median age was 52 (interquartile range 41–61) years; 51% of patients were male and 49% female. Most (98%, n = 589) case-patients with travel-associated DENV-3 had recently traveled from Cuba; they were reported in 21/67 Florida counties (Figure 1, panel C). Miami-Dade County had the most travel-associated DENV-3 cases (71%, n = 428). Among 61 locally acquired DENV-3 cases, the median age was 54 (interquartile range 36–58) years; 67% of patients were male and 33% female, and nearly all (93%, n = 57) were reported in Miami-Dade County. The 485 DENV-3 case-patients in Miami-Dade County were identified in 60/82 postal (ZIP) codes.

We performed genomic characterization of DENV-3 by sequencing the complete genomes of 203 cases at the Centers for Disease Control and Prevention (San Juan, Puerto Rico, USA), Yale School of Public Health (New Haven, CT, USA), and FDOH (Appendix 1, https://wwwnc.cdc.gov/EID/article/30/2/23-1615-App1.pdf) (*12*). Sequencing was prioritized and successful for 34 locally acquired cases, as well as case-patients with recent travel history to Cuba (n = 168) or Guyana (n = 1). To assess the representativeness of DENV sequences, we evaluated symptom onset dates and counties of residence for cases selected for sequencing and all cases detected (Appendix 1 Figure 1). We conducted maximum-likelihood phylogenetic analysis to infer the genetic relatedness of DENV-3 to contemporary circulation globally. Global context was provided with a subsample of 146 publicly available genomes that represent relevant genotypes.

The DENV-3 genomes identified in Florida are classified as genotype III and cluster within the novel American II lineage (*9*). We observed a close relationship with DENV-3 genomes recently identified in Arizona, Puerto Rico, and Brazil, indicating that the lineage is spreading across the Americas (Figure 2). However, the limited sampling of the new American II lineage prevented us from inferring a potential time of emergence in Florida. The short branch lengths and similarity between locally acquired and travel-associated cases in the phylogenetic tree demonstrate low genomic diversity during the sampling period, where genomes from locally acquired cases cluster randomly with travel-associated cases. The tree topology suggests frequent importation events occurred during

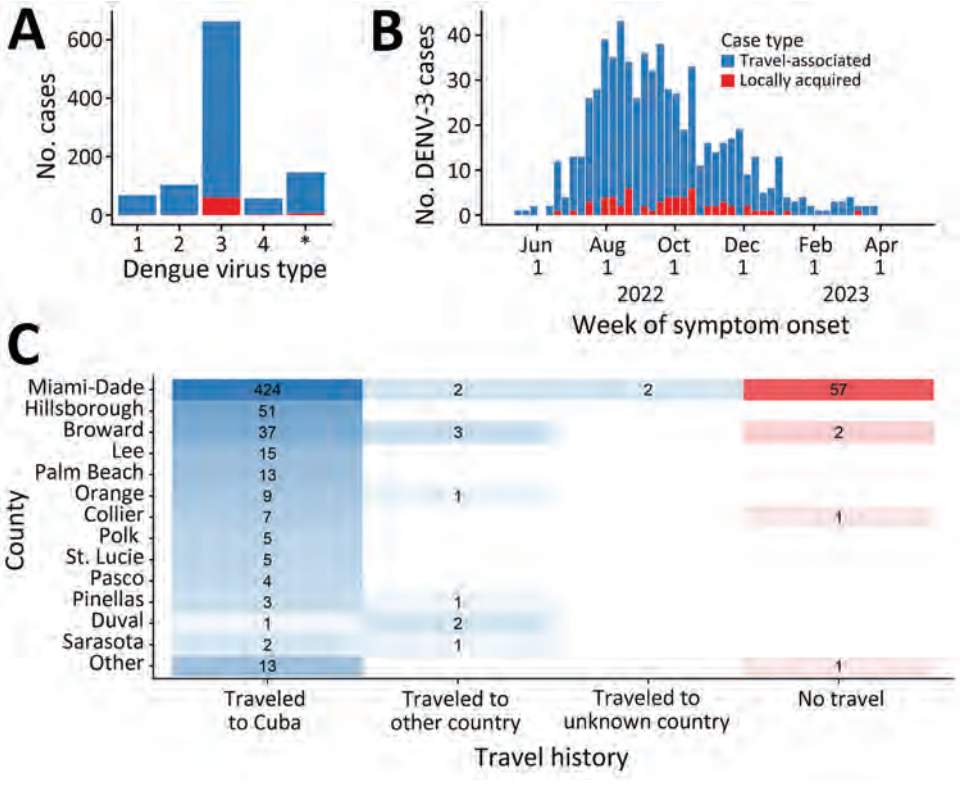

Figure 1. DENV serotype distribution and DENV-3 case distribution by week of symptom onset, county of reporting, and origin of travel, Florida, USA, May 1, 2022–April 30, 2023. A) Number of dengue cases by each virus serotype. Cases with an unknown dengue virus type (asterisk) only had a positive serologic test or multiple serotypes identified. B) Epidemic curve of reported cases of DENV-3, showing 601 travel-associated cases and 61 locally acquired cases. C) Heat map indicating number of DENV-3 cases by county and by travel history. Other countries were Bangladesh, Colombia, Guyana, India, Jamaica, Mexico, Pakistan, and Sri Lanka. The names of counties reporting ≥3 DENV-3 cases are shown and sorted by the total number of cases reported. DENV, dengue virus; DENV-3, DENV serotype 3.

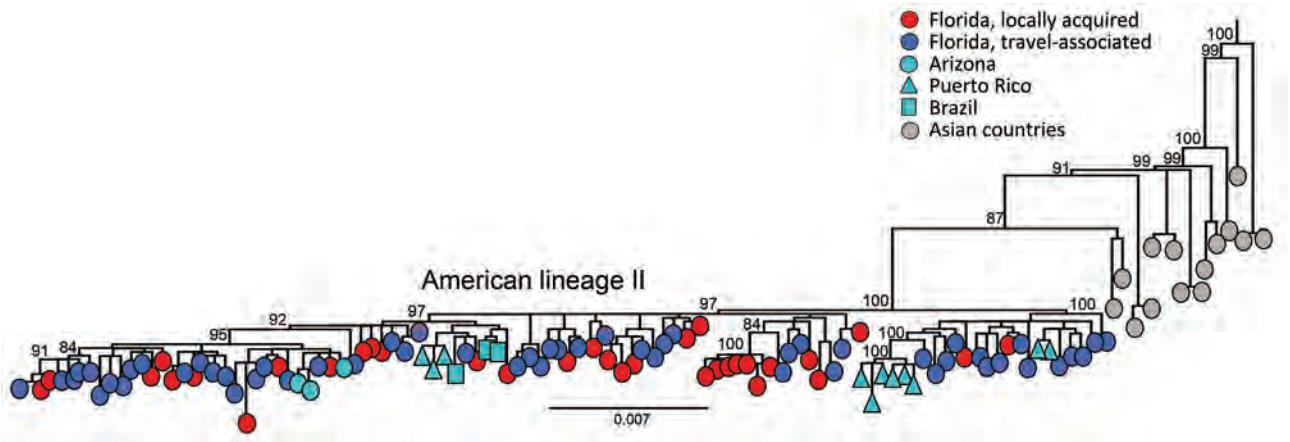

Figure 2. Evolutionary analysis of dengue virus serotype 3 sampled in Florida, USA, May 1, 2022–April 30, 2023. Maximum-likelihood phylogenetic tree was generated from a subset of 203 complete genomes from Florida (34 local cases, 168 cases in persons with recent travel history to Cuba, and 1 traveler case from Guyana) and 146 complete genomes publicly available (1985–2022) from GenBank representing genotype III, American lineage II. A subset of the sequences was used because of the low diversity in the population sample, which was limiting the phylogenetic signal and hampering the statistical analyses that supported the tree accuracy and certainty in major nodes. Sampling locations are coded by shape and color. Scale bar represents nucleotide substitutions per site.

the sampling period and indicate frequent movement of DENV between Cuba and Florida without establishing sustained local transmission in Florida.

To model a possible transmission tree, we adapted a graph-based model using genomic sequences and symptom onset dates from 31 locally acquired and 144 travel-associated cases (Appendix 1) (*13*,*14*). To account for infections in transmission chains that went undetected between reported cases, we included a surveillance reporting probability (i.e., the probability an infection was detected as a case) and performed sensitivity analyses assuming different reporting probabilities of 1%, 5%, 10%, and 15%. Assuming a 5% reporting probability, we identified 22 travel-associated cases (15%) with most compatible linkages leading to the 31 locally acquired cases (Appendix 1 Figure 2). Overall, 122 (85%) travel-associated cases had no likely linkage to locally acquired cases, 17 (11%) were linked to 1 case, 2 (1%) were linked to 2 cases, 2 (1%) were linked to 3 cases, and 1 (1%) was linked to 4 cases.

Conclusions

We documented an unprecedented number of travel-associated and locally acquired DENV-3 cases in Florida during May 2022–April 2023; circulation of the DENV-3 genotype III was recently identified in the Americas. Our investigation illustrates that local transmission and spread in Florida was limited, despite multiple introductions from outside the country. Sequencing and phylogenetic analysis revealed that cases were from the same DENV-3 genotype III lineage and were highly related to one another and to cases identified in Puerto Rico, Arizona, and Brazil. Assessment of possible linkages between sequenced cases indicated that local transmission during this outbreak was limited; most travel-associated cases did not lead to further transmission.

DENV activity in Cuba and Florida are linked given their proximity and the extensive travel between them. Our results are similar to findings in Florida in 2019 (*5*), where many DENV case-patients reported recent travel to Cuba, leading to an increase in locally acquired cases. An elevated number of locally acquired DENV cases in Florida might be expected after a high number of introductions, but our analysis suggests that DENV introductions did not result in sustained local transmission beyond small-scale outbreaks. Factors potentially reducing transmission include living conditions (e.g., use of air conditioning and screens), rapid case notification that enabled vector interventions (e.g., spraying insecticide, conducting surveillance, community education, and removing standing water), or limited availability of mosquito breeding sites (*15*).

The relatively low genetic diversity in this dataset limited our ability to estimate the timing of initial DENV-3 introductions and fully reconstruct local spread. We did not use case locations to determine the compatibility of transmission links. DENV case detection continued through 2023 in Florida; efforts to understand those transmission dynamics are ongoing.

In summary, we used epidemiologic surveillance and genomic sequencing to identify a newly emerging lineage of DENV-3 genotype III that caused an unusually large number of travel-associated and locally acquired DENV infections in

Florida, particularly in Miami-Dade County. Our analysis suggests that locally acquired cases were driven by large numbers of case-patients with recent travel to Cuba and that DENV persistence in Florida was limited. Close monitoring of DENV activity internationally, as well as increasing healthcare provider awareness about DENV identification and testing, can strengthen preparedness and response to future introductions in non–DENV-endemic areas.

Florida Department of Health Bureau of Public Health Laboratory Team: Sylvia Bunch, Natalia Cano, Amanda Davis, Yibo Dong, Rayah Jaber, Timothy Locksmith, Charles Panzera, Brittany Rowlette, Sarah Schmedes, Julieta Vergara.

Acknowledgments

We thank Joshua Wong for help with initial discussions on analysis plans. We also gratefully acknowledge the Arizona Department of Health Services and the Maricopa County Department of Public Health for contributing specimens for the phylogenetic analysis.

Code presented in this study is available at https://github.com/fjones2222/denv-3-florida-2022/.

Research reported in this publication was supported by the National Institute of Allergy and Infectious Diseases of the National Institutes of Health under award number DP2AI176740 (NDG), and by CTSA Grant Number UL1 TR001863 from the National Center for Advancing Translational Science (NCATS), a component of the National Institutes of Health (CBFV), and by the National Institute of General Medical Sciences of the National Institutes of Health under award number R21GM142011 (SFM).

About the Author

Dr. Jones is an Epidemic Intelligence Service officer stationed at the Centers for Disease Control and Prevention Dengue Branch (Division of Vector-Borne Diseases, National Center for Emerging and Zoonotic Infectious Diseases) in San Juan, Puerto Rico. His research interest is surveillance and modeling of infectious diseases.

References

1. Centers for Disease Control and Prevention. Dengue [cited 2023 Aug 19]. https://www.cdc.gov/dengue/index.html
2. Wong JM, Rivera A, Volkman HR, Torres-Velasquez B, Rodriguez DM, Paz-Bailey G, et al. Travel-associated dengue cases—United States, 2010–2021. MMWR Morb Mortal Wkly Rep. 2023;72:821–6. https://doi.org/10.15585/mmwr.mm7230a3
3. Rowe D, McDermott C, Veliz Y, Kerr A, Whiteside M, Coss M, et al.; Florida Department of Health Dengue Investigation Team. Dengue outbreak response during COVID-19 pandemic, Key Largo, Florida, USA, 2020. Emerg Infect Dis. 2023;29:1643–7. https://doi.org/10.3201/eid2908.221856
4. Graham AS, Pruszynski CA, Hribar LJ, DeMay DJ, Tambasco AN, Hartley AE, et al. Mosquito-associated dengue virus, Key West, Florida, USA, 2010. Emerg Infect Dis. 2011;17:2074–5. https://doi.org/10.3201/eid1711.110419
5. Sharp TM, Morris S, Morrison A, de Lima Corvino D, Santiago GA, Shieh WJ, et al.; 2019 Florida Dengue Investigation Team. Fatal dengue acquired in Florida. N Engl J Med. 2021;384:2257–9. https://doi.org/10.1056/NEJMc2023298
6. Centers for Disease Control and Prevention. Historic data (2010–2022) [cited 2023 Aug 19]. https://www.cdc.gov/dengue/statistics-maps/historic-data.html
7. Parker C, Ramirez D, Connelly CR. State-wide survey of *Aedes aegypti* and *Aedes albopictus* (Diptera: Culicidae) in Florida. J Vector Ecol. 2019;44:210–5. https://doi.org/10.1111/jvec.12351
8. U.S. Embassy in Cuba. Health alert for U.S. citizens in Cuba on dengue fever [cited 2023 Aug 19]. https://cu.usembassy.gov/health-alert-for-u-s-citizens-in-cuba-on-dengue-fever
9. Naveca FG, Santiago GA, Maito RM, Ribeiro Meneses CA, do Nascimento VA, de Souza VC, et al. Reemergence of dengue virus serotype 3, Brazil, 2023. Emerg Infect Dis. 2023;29:1482–4. https://doi.org/10.3201/eid2907.230595
10. Kretschmer M, Collins J, Dale AP, Garrett B, Koski L, Zabel K, et al. Notes from the field: first evidence of locally acquired dengue virus infection—Maricopa County, Arizona, November 2022. MMWR Morb Mortal Wkly Rep. 2023;72:290–1. https://doi.org/10.15585/mmwr.mm7211a5
11. Florida Health, Miami-Dade County. Health officials issue mosquito borne illness advisory following confirmation of one dengue case [cited 2023 Aug 19]. https://miamidade.floridahealth.gov/newsroom/2022/07/2022-07-18-mosquito-borne-illness-advisory.html
12. Vogels C. DengueSeq: A pan-serotype whole genome amplicon sequencing protocol for dengue virus v1 [cited 2023 Sep 27]. https://www.protocols.io/view/dengueseq-a-pan-serotype-whole-genome-amplicon-seq-kqdg39xxeg25/v2
13. Cori A, Nouvellet P, Garske T, Bourhy H, Nakouné E, Jombart T. A graph-based evidence synthesis approach to detecting outbreak clusters: an application to dog rabies. PLOS Comput Biol. 2018;14:e1006554. https://doi.org/10.1371/journal.pcbi.1006554
14. Hampson K, Dushoff J, Cleaveland S, Haydon DT, Kaare M, Packer C, et al. Transmission dynamics and prospects for the elimination of canine rabies. PLoS Biol. 2009;7:e53. https://doi.org/10.1371/journal.pbio.1000053
15. Reiter P, Lathrop S, Bunning M, Biggerstaff B, Singer D, Tiwari T, et al. Texas lifestyle limits transmission of dengue virus. Emerg Infect Dis. 2003;9:86–9. https://doi.org/10.3201/eid0901.020220

Address for correspondence: Forrest Kirby Jones, Centers for Disease Control and Prevention, 1324 Calle Cañada, San Juan, 00920, Puerto Rico, USA; email: fjones3@cdc.gov

Borrelia turicatae from Ticks in Peridomestic Setting, Camayeca, Mexico

Edwin Vázquez-Guerrero, Alexander R. Kneubehl, Patricio Pellegrini-Hernández, José Luis González-Quiroz, María Lilia Domínguez-López, Aparna Krishnavajhala, Paulina Estrada-de los Santos, J. Antonio Ibarra, Job E. Lopez

We conducted surveillance studies in Sinaloa, Mexico, to determine the circulation of tick-borne relapsing fever spirochetes. We collected argasid ticks from a home in the village of Camayeca and isolated spirochetes. Genomic analysis indicated that *Borrelia turicatae* infection is a threat to those living in resource-limited settings.

Tick-borne relapsing fever (TBRF) spirochetes are neglected pathogens in Mexico, and human infection is frequently misdiagnosed because of nonspecific symptoms (*1*). *Borrelia turicatae* infection is associated with irregular fevers, vomiting, rigors, nausea, and meningitis (*2*). The neurologic symptoms that follow infection can be misdiagnosed as Lyme disease, and the use of nonspecific serologic tests further complicates an accurate diagnosis of TBRF. Prior studies have used whole-protein lysates of *Borreliella* (*Borrelia*) *burgdorferi* in ELISAs and immunoblotting assays for disease diagnosis (*3*,*4*), but serologic cross-reactivity occurs regardless of whether patients are infected with Lyme-causing or TBRF-causing spirochetes (*5*). Another report from Mexico amplified a portion of the *flagellin* gene from a patient's blood sample, and it most closely aligned with *B. burgdorferi* (*6*). However, no other loci were sequenced, and it is unknown if the isolate causing infection exists. Additional work is needed to understand the circulation of spirochetes in Mexico.

Author affiliations: Instituto Politécnico Nacional, Mexico City, Mexico (E. Vázquez-Guerrero, J.L. González-Quiroz, M.L. Domínguez-López, P. Estrada-de los Santos, J.A. Ibarra); Baylor College of Medicine, Houston, Texas, USA (A.R. Kneubehl, A. Krishnavajhala, J.E. Lopez); Wildlife Conservation Management Unit (Macochín), El Fuerte, Sinaloa, Mexico (P. Pellegrini-Hernández).

DOI: http://doi.org/10.3201/eid3002.231053

Argasid ticks transmit most species of TBRF spirochetes, and the life cycle of those ticks further confounds a clear understanding of the disease's epidemiology. Argasids in the genus *Ornithodoros* are cavity-dwelling rapid feeders that are rarely found attached to the host. A case study from Panama noted persons who reported being bitten by insects during their sleep (*7*). An investigation identified *Ornithodoros puertoricensis* ticks under floor tiles and within cracks of windowsills (*7*). Those findings indicated that, once introduced into the dwelling, the ticks targeted human occupants as their primary blood source.

To clarify the ecologic overlap of TBRF spirochetes and humans, we initiated efforts to collect argasid ticks from peridomestic settings in Mexico. We describe identification of *Ornithodoros turicata* ticks from the village of Camayeca in Sinaloa, Mexico. We determined infection in the collected ticks by feeding them on a laboratory mouse, isolating TBRF spirochetes from the mouse blood, and confirming the pathogen as *B. turicatae* through genomic analysis.

The Study

In March 2022, we collected argasid ticks in peridomestic settings of Sinaloa, Mexico. In the village of Camayeca (Figure 1, panel A), we sampled 5 burrows using an aspirator or dry ice as a source of carbon dioxide to lure ticks. In the human dwelling where ticks were collected (Figure 1, panel B), we aspirated the dirt at the base of the home (Figure 1, panel C). We collected 3 adults and 19 nymphs. We also noted ground squirrel activity around the burrows.

In the laboratory, we speciated ticks using microscopy and by sequencing a portion of the 16S mitochondrial gene. Morphologic characterization of nymphs and adults identified them as *O. turicata.* We extracted total DNA from 3 nymphs using the DNeasy Blood

and Tissue kit (QIAGEN, https://www.qiagen.com), according to the manufacturer's protocol, and amplified ≈475 nt of the 16S mitochondrial rRNA gene by using Tm16S+1 and Tm16S-1 primers (*8*). We sequenced amplicons by using the Sanger method and trimmed the data by using ChromasPro version 2.1.5 (Technelysium Pty Ltd, https://technelysium.com.au). We performed a BLASTN analysis (https://www.ncbi.nlm.nih.gov/Blast.cgi), which indicated 99.1% nucleotide identity to *O. turicata.* We deposited sequences from this study into GenBank (accession no. OR189376–8).

We did not evaluate the remaining 19 individual *O. turicata* ticks for infection because we did not want to sacrifice them; however, we determined colonization of TBRF spirochetes by allowing them to feed on a BALB/c mouse and then assessing the animal for infection. We collected daily blood samples from the mouse and performed Giemsa staining to visualize spirochetes. Seven days after feeding ticks, we exsanguinated the mouse and centrifuged whole blood at 500 × *g* for 5 minutes. We then removed plasma and centrifuged again at 5,000 × *g* for 10 minutes. We resuspended the resulting pellet in 1 mL of Barbour-Stoenner-Kelly–IIB media and cultured in a total of 4 mL of the media formulation at 35°C (*9*). Eight days later, we placed an aliquot of the culture on a glass slide, allowed it to air dry, and performed Giemsa staining. We visualized numerous spirochetes on the slide (Figure 2, panel A). We designated the isolate CAM-1 and generated glycerol stocks.

We sequenced the CAM-1 isolate to determine the species and genomic structure. We isolated genomic DNA and performed pulsed field electrophoresis to determine DNA quality (*10*). We performed long-read sequencing with the Oxford Nanopore Technologies (https://nanoporetech.com) Mk1B platform with the SQK-RBK110.96 library preparation kit and R9.4.1 flow cell. We generated short-read sequences by using the Microbial Genome Sequencing Center (MiGS Center, https://migscenter.wordpress.com) and an Illumina 2x150 library preparation kit (Illumina, https://www.illumina.com). We produced a plasmid-resolved genome assembly by using short-reads to polish the long-read data, as done previously

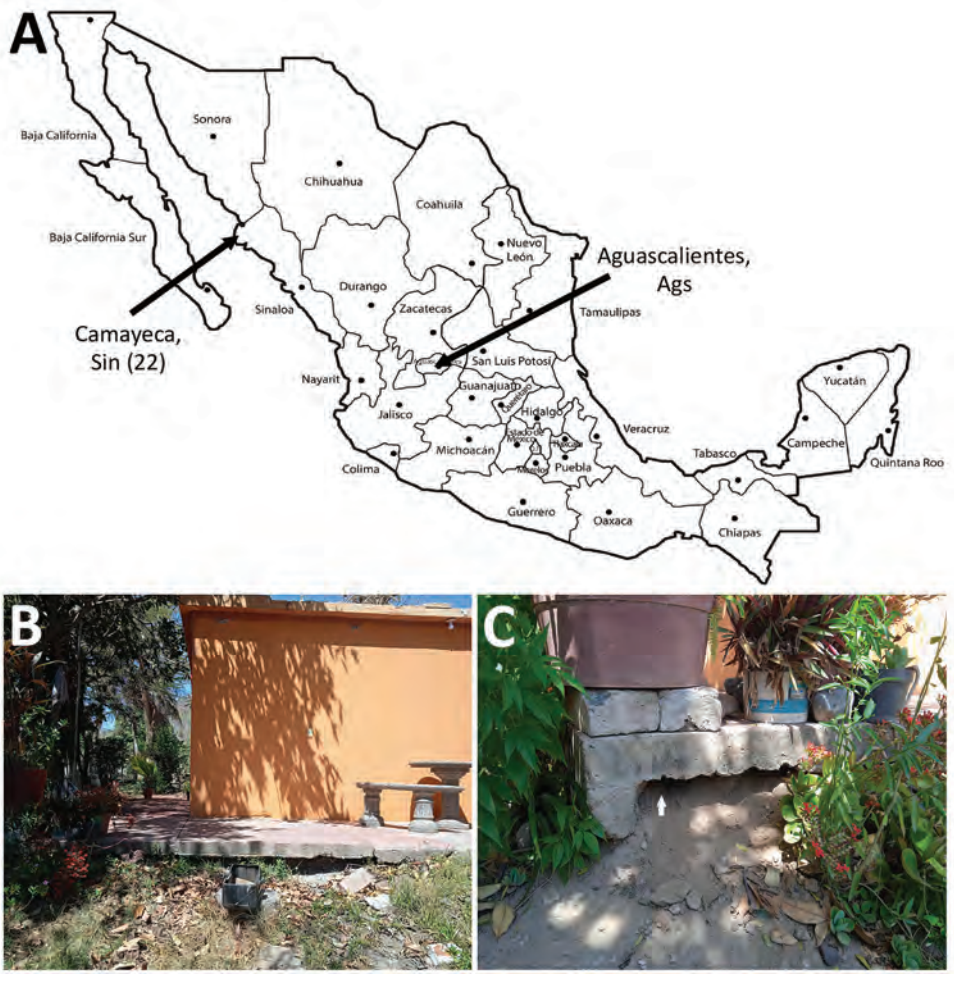

Figure 1. Collection of *Ornithodoros turicata* ticks from village of Camayeca, Mexico. A) Location in the state of Sinaloa where 22 ticks were collected (left arrow). Also labeled is the state of Aguascalientes, where we recently collected *O. turicata* ticks (right arrow). B) Collection efforts were focused in peridomestic settings C) Ticks were aspirated from the base of a human dwelling; white arrow indicates where ticks were collected.

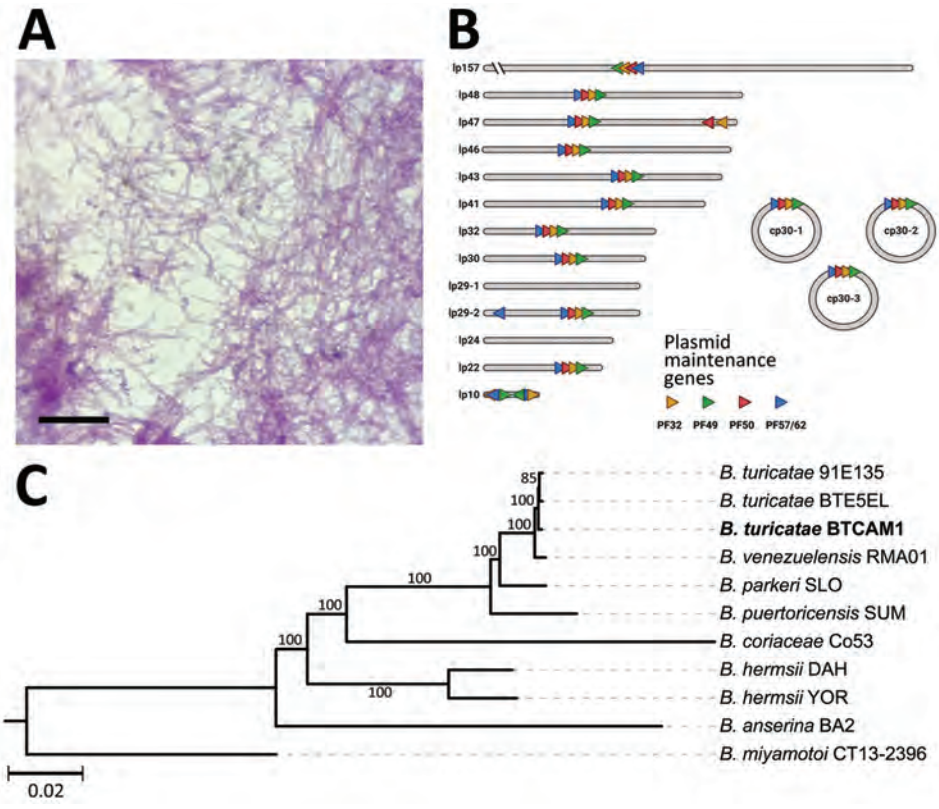

Figure 2. Isolation and genetic characterization of *Borrelia turicatae* from ticks collected in the village of Camayeca, Mexico. A) Spirochetes were isolated from murine blood in culture medium. Scale bar indicates 20 μm. B) Genome sequencing and assembly generated the plasmid repertoire of the bacteria. Plasmids were designated as lp or cp and by their respective size to the nearest kilobase. PF partitioning genes are shown in each plasmid as orange, green, red, and blue triangles. C) Maximum-likelihood species tree performed in a phylogenomic analysis of the spirochete sample we extracted, designated CAM-1 (boldface), grouped the spirochete with *B. turicatae.* The tree was generated with an edge-linked proportional partition model with 1,000 ultra-fast bootstraps. Scale bar indicates 0.02 substitutions per site. cp, circular plasmid; lp, linear plasmid; PF, plasmid family.

(*10*). The mean Oxford Nanopore Technologies coverage was 439×, and the mean Illumina coverage was 236×. Using a previously established approach (*10*), we determined a completeness score of 99.89% and a QV score (based on the Phred scale) of Q53.82. We annotated the assembly with the National Center for Biotechnology Information's Prokaryotic Genome Annotation Pipeline and submitted the assembly to GenBank (accession nos. CP129306–22). The chromosome was 925,885 bp. We noted 16 plasmids, ranging from 10,351 to 156,755 bp, 3 of which were circular (Figure 2, panel B). We used concatenated sequences from 650 core genes in our phylogenomic analysis, which encompassed 720,532 nt and grouped the CAM-1 isolate with *B. turicatae* (Figure 2, panel C).

Conclusions

O. turicata ticks were originally described in Mexico in 1876 by Alfredo Dugès (*11*) but were implicated as a vector of TBRF spirochetes until the 1930s. In 1933, Brumpt et al. detected spirochetes in *O. turicata* ticks collected from Austin, Texas, USA, and he later confirmed that the tick transmitted *B. turicatae* (*12*). At the same time, Pilz and Mooser observed human cases of relapsing fever in the city of Aguascalientes, Mexico (*13*). Their work showed that *O. turicata* ticks were in the region, and the researchers implicated that species as the vector. Since those reports, studies from Mexico on *Ornithodoros* ticks ecology or TBRF spirochetes have been negligible.

Our findings indicate that updates are needed for distribution models of *O. turicata* ticks. For example, a maximum entropy species distribution model predicted suitable habitat for *O. turicata* ticks by using georeferenced data points from tick collections and reports of *B. turicatae*, primarily from the United States (*14*). New regions of northern Mexico were predicted to have habitat for *O. turicata* ticks, but there was low probability of suitable habitat in other areas of the country. However, in addition to collecting ticks from Camayeca, Mexico, we also have recovered *O. turicata* ticks from the city of Aguascalientes, Mexico (Figure 1, panel A) (*15*). The 2 cities are >1,000 km apart. Aguascalientes is located in the middle of the country and is considered a temperate environment, ≈1,900 m in elevation, whereas Camayeca is an arid desert region at ≈150 m elevation. The environmental differences between the 2 cities show wider habitat suitability for *O. turicata* ticks than what was previously predicted.

Identifying infected *O. turicata* ticks in a peridomestic setting suggests that TBRF is likely underreported in Mexico. In support of this finding, retrospective serodiagnostic studies detected human exposure to TBRF spirochetes in populations

originally diagnosed with fever of unknown origin (*1*). Given those observations and our findings, additional studies should be conducted to determine infection frequencies of argasid ticks collected in peridomestic settings and to define the distribution and ecology of *O. turicata* ticks and other argasid ticks of human importance in Mexico to increase knowledge and awareness of these ticks and the potential threat they pose to animal and human health.

This article was preprinted at https://www.biorxiv.org/content/10.1101/2023.08.01.551332v1.

Acknowledgments

We thank Miguel Medina-Cota for putting us in contact with our collaborator in Sinaloa.

Testing performed on laboratory mice was approved by the Institutional Animal Care and Use Committee (protocol # ZOO-001–2022).

This work was supported by funds provided to JEL from the National School of Tropical Medicine at Baylor College of Medicine and by funds to JAI from Secretaría de Investigación y Posgrado-IPN (20230850 and 20232722).

About the Author

Dr. Vázquez-Guerrero is an infectious disease specialist in Mexico. His areas of interest are acarology and infectious diseases.

References

1. Vázquez-Guerrero E, Gordillo-Pérez G, Ríos-Sarabia N, Lopez JE, Ibarra JA. Case report: exposure to relapsing fever group borreliae in patients with undifferentiated febrile illness in Mexico. Am J Trop Med Hyg. 2023;108:510–2. https://doi.org/10.4269/ajtmh.22-0386
2. Cadavid D, Barbour AG. Neuroborreliosis during relapsing fever: review of the clinical manifestations, pathology, and treatment of infections in humans and experimental animals. Clin Infect Dis. 1998;26:151–64. https://doi.org/10.1086/516276
3. Gordillo-Pérez G, Solorzano F, Cervantes-Castillo A, Sanchez-Vaca G, García-Ramirez R, Díaz AM, et al. Lyme neuroborreliosis is a severe and frequent neurological disease in Mexico. Arch Med Res. 2018;49:399–404. https://doi.org/10.1016/j.arcmed.2018.11.007
4. Gordillo-Pérez G, García-Juárez I, Solórzano-Santos F, Corrales-Zúñiga L, Muñoz-Hernández O, Torres-López J. Serological evidence of *Borrelia burgdorferi* infection in Mexican patients with facial palsy. Rev Invest Clin. 2017;69:344–8. https://doi.org/10.24875/RIC.17002344
5. Lopez JE, Schrumpf ME, Nagarajan V, Raffel SJ, McCoy BN, Schwan TG. A novel surface antigen of relapsing fever spirochetes can discriminate between relapsing fever and Lyme borreliosis. Clin Vaccine Immunol. 2010;17:564–71. https://doi.org/10.1128/CVI.00518-09
6. Colunga-Salas P, Sánchez-Montes S, Volkow P, Ruíz-Remigio A, Becker I. Lyme disease and relapsing fever in Mexico: an overview of human and wildlife infections. PLoS One. 2020; 15:e0238496. https://doi.org/10.1371/journal.pone.0238496
7. Bermúdez SE, Castillo E, Pohlenz TD, Kneubehl A, Krishnavajhala A, Domínguez L, et al. New records of *Ornithodoros puertoricensis* Fox 1947 (Ixodida: Argasidae) parasitizing humans in rural and urban dwellings, Panama. Ticks Tick Borne Dis. 2017;8):466–9. https://doi.org/10.1016/j.ttbdis.2017.02.004
8. Black WC IV, Piesman J. Phylogeny of hard- and soft-tick taxa (Acari: Ixodida) based on mitochondrial 16S rDNA sequences. Proc Natl Acad Sci USA. 1994;91:10034–8. https://doi.org/10.1073/pnas.91.21.10034
9. Replogle AJ, Sexton C, Young J, Kingry LC, Schriefer ME, Dolan M, et al. Isolation of *Borrelia miyamotoi* and other Borreliae using a modified BSK medium. Sci Rep. 2021;11:1926. https://doi.org/10.1038/s41598-021-81252-1
10. Kneubehl AR, Krishnavajhala A, Leal SM, Replogle AJ, Kingry LC, Bermúdez SE, et al. Comparative genomics of the Western Hemisphere soft tick-borne relapsing fever borreliae highlights extensive plasmid diversity. BMC Genomics. 2022;23:410. https://doi.org/10.1186/s12864-022-08523-7
11. Dugès A. Turicata de Guanajuato. Artículo en el periódico "El Repertorio" de Guanajuato. 1876;Sect. 11–2.
12. Brumpt E, Brumpt LC. Identite du spirochete des fievres recurrentes a tiques des plateaux mexicains et du *Spirochaeta turicatae* agent de la fievre recurrente sporadique des Etats-Unis. Ann Parasitol Hum Comp. 1939;17:287–98. https://doi.org/10.1051/parasite/1939-1940174287
13. Pilz H, Mooser H. La fiebre recurrente en Aguascalientes. Boletín del Instituto de Higiene, México. 1936;2:295–300.
14. Donaldson TG, Pèrez de León AA, Li AY, Castro-Arellano I, Wozniak E, Boyle WK, et al. Assessment of the geographic distribution of *Ornithodoros turicata* (Argasidae): Climate variation and host diversity. PLoS Negl Trop Dis. 2016;10: e0004383. https://doi.org/10.1371/journal.pntd.0004383
15. Vázquez-Guerrero E, González-Quiroz JL, Domínguez-López ML, Kneubehl AR, Krishnavajhala A, Curtis MW, et al. New records of *Ornithodoros turicata* (Ixodida: Argasidae) in rural and urban sites in the Mexican states of Aguascalientes and Zacatecas indicate the potential for tick-borne relapsing fever. Exp Appl Acarol. 2023;91:99–110. https://doi.org/10.1007/s10493-023-00830-2

Address for correspondence: Job Lopez, Baylor University College of Medicine, One Baylor Plaza, Houston, TX 77030, USA; email: job.lopez@bcm.edu; J. Antonio Ibarra, Instituto Politécnico Nacional, ENCB-Unidad Santo Tomás Mexico City 11340, Mexico; email jibarrag@ipn.mx

Phylogenomics of Dengue Virus Isolates Causing Dengue Outbreak, São Tomé and Príncipe, 2022

Lazismino Lázaro, Doris Winter, Katia Toancha, Adjaia Borges, Anabela Gonçalves, Asmiralda Santos, Marcos do Nascimento, Nilton Teixeira, Yardlene Sacramento Sequeira, Anery Katia Lima, Bakissy da Costa Pina, Andreza Batista de Sousa, Jürgen May, Rosa Maria Afonso Neto, Kathrin Schuldt

Author affiliations: National Reference Laboratory for Tuberculosis and Emerging Diseases, Ministry of Health, São Tomé, São Tomé and Príncipe (L. Lázaro, K. Toancha, A. Borges, A. Gonçalves, A. Santos, M. do Nascimento, N. Teixeira, Y. Sacramento Sequeira, A.K. Lima, R.M. Afonso Neto); Bernhard Nocht Institute for Tropical Medicine, Hamburg, Germany (D. Winter, J. May, K. Schuldt); National Emergency Operating Center, Ministry of Health, São Tomé (B. da Costa Pina); National Surveillance Department, Ministry of Health, São Tomé (A. Batista de Sousa); German Center for Infection Research, Hamburg–Lübeck–Borstel–Riems, Germany (J. May); University Medical Center Hamburg–Eppendorf, Hamburg (J. May)

DOI: https://doi.org/10.3201/eid3002.231316

We determined that the dengue outbreak in São Tomé and Príncipe during 2022 was caused by dengue virus serotype 3 genotype III. Phylogenomic analyses showed that the outbreak strain was closely related to the newly identified GIII-American-II lineage and that the virus probably was introduced from the Americas.

Globally, dengue case numbers have increased dramatically over recent decades; an estimated 96 million clinical dengue cases per year have been reported in >100 countries (*1*). Dengue is an acute febrile disease that can evolve into a severe life-threatening disease. Dengue is caused by an infection with the dengue virus (DENV), a member of the family *Flaviviridae*, and has 4 different serotypes (DENV-1–4) and distinct infection dynamics (*2*).

In 2022, São Tomé and Príncipe, an island state with ≈210,000 inhabitants in the Gulf of Guinea in sub-Saharan Africa, reported the occurrence of dengue cases in the country. During epidemiologic weeks 15–50 in 2022, a total of 1,152 dengue fever cases confirmed by positive rapid diagnostic tests (RDTs) were reported. The first cases were reported April 15, and case numbers peaked at 178 notifications in week 24 (Appendix Figure, https://wwwnc.cdc.gov/EID/article/30/02/23-1316-App1.pdf). Among the 1,152 RDT-confirmed cases, the most frequent observed symptoms were fever (92%), headache (78%), and myalgia (38%). A total of 144 (12.5%) persons were admitted to the hospital (Appendix Table 1), and 8 persons died from infection with the virus. The presumptive index patient was described as a 27-year-old man from São Tomé and Príncipe who had traveled to the island of Guadeloupe before arriving in São Tomé on March 26, 2022, and whose onset of symptoms occurred on April 4, 2022 (*3*). A previous study analyzed the seroprevalence of DENV antibodies in the São Tomé and Príncipe population. In that study, 31 of 78 tested pregnant women were found to be seropositive for DENV, indicating that the country's population might have experienced exposure to the virus before 2003–2004, during which the collection of the analyzed serum samples took place (*4*).

This study was approved by the Health Ethics Committee for Scientific Research at the Ministry of Health of STP (approval no. 015B/2022). During May 6–16, 2022, we collected 7 plasma samples from dengue RDT–positive patients in São Tomé and Príncipe (Appendix Table 2). All 7 infections were confirmed by real-time PCR, and subtyping revealed the presence of DENV-3 (Appendix Table 2). Long-read whole-genome sequencing and subsequent assembly (reference strain GenBank accession no. NC_001475) resulted in 48–64,440 assembled reads (Appendix Table 3) with an average depth of coverage of 4–4,148× (Appendix Figure 2). We classified all 7 isolates as DENV-3 genotype III (GIII) by using a flavivirus genotyping tool (*5*) with bootstrap support of 100.

To study the evolutionary relationship of the virus isolates from São Tomé and Príncipe, we included 4 reconstructed genomes with best assembly results (>10 kb, genome coverage >98%, depth of coverage >250×) in a phylogenomic analysis together with 1,168 DENV-3 GIII genomes (Appendix Table 4) sampled worldwide. All 1,172 sequences passed the IQ-TREE2 composition test. The best-fitting evolutionary model according to Bayesian information criterion (BIC) was the general time-reversible plus empirical frequencies plus invariate sites plus FreeRate model. The reconstructed consensus tree revealed that the newly sequenced DENV-3 isolates from São Tomé and Príncipe clustered with and are closely related to the new monophyletic clade consisting of 218 DENV-3 sequences detected in the Americas during 2022–2023 (Figure). A recent study by Naveca et al. (*6*) demonstrates that this new lineage (GIII-American-II lineage) was most likely introduced to Cuba from the Indian subcontinent in

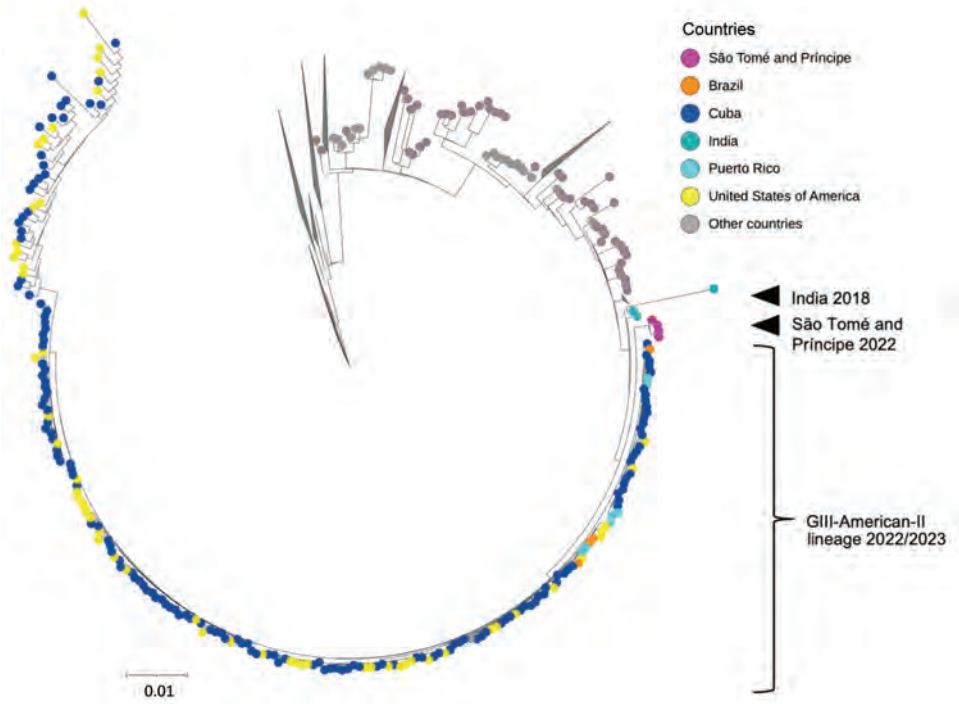

Figure. Reconstructed consensus tree of newly sequenced dengue virus serotype 3 isolates from São Tomé and Príncipe. The isolates clustered with and are closely related to a new monophyletic clade consisting of 218 dengue virus serotype 3 sequences detected in the Americas during 2022–2023. To improve visualization, several clades have been collapsed. Scale bar indicates nucleotide substitutions per site.

2019 (*6*). Consistent with their findings, our consensus tree (Figure) shows 3 DENV-3 sequences collected in India in 2018 as part of the next bigger clade comprising the GIII-American-II lineage and the 4 isolates from São Tomé and Príncipe.

Because the index patient reportedly had traveled to Guadeloupe before arriving in São Tomé and Príncipe, the likely scenario of virus importation is that after the introduction of the DENV-3-GIII lineage from Asia to America during 2018–2020, the virus might have circulated in the region, and from there it was introduced to São Tomé and Príncipe in 2022. Although we did not conduct formal phylogeographic analysis as part of this study, 2 points support our conclusions: the epidemiologic information that the index patient visited Guadalupe; and the results of the previous study from Brazil, describing the new DENV-3, GIII-American-II lineage and how it arose in America (*6*). Thus, our results suggest that the São Tomé and Príncipe outbreak originated from the new American lineage.

According to surveillance data of the Pan American Health Organization, Guadeloupe has experienced yearly dengue outbreaks since 2018, and in the year 2020, the serotypes 1–3 were detected (*7*). Unfortunately, no information is available on the DENV serotype or genomic sequences on the DENV circulating in 2022 in Guadeloupe, and only sparse information is available on dengue cases from countries in Africa.

The results of our study corroborate a possible global expansion of the new DENV-3 GIII-American-II clade previously described by Naveca et al. (*6*). Furthermore, finding this American lineage in Africa reinforces the importance of genomic surveillance of DENV in countries at risk for future outbreaks.

This research was funded by the German Federal Ministry of Health, Global Health Protection Program (grant no. FKZ 2521GHP919).

We deposited the 4 dengue virus whole-genome sequences from this study in the European Nucleotide Archive at European Molecular Biology Laboratory–European Bioinformatics Institute (accession no. PRJEB65577).

Author contributions: L.L., D.W., K.T., A.B., A.G., A.S., M.N., N.T., Y.S.S., and A.K.L. performed the RNA extraction and the laboratory analyses; B.C.P and A.B.S. contributed the public health surveillance data; J.M. contributed to obtain funds; L.L., R.M.A.N., and K.S. designed the study and performed the bioinformatic analyses; and K.S. wrote the manuscript. All authors have read and approved the manuscript.

About the Author

Mr. Lázaro is a laboratory expert from the National Reference Laboratory for Tuberculosis and Emerging Diseases in São Tomé and Príncipe. His primary research interests include molecular surveillance of pathogens by whole-genome sequencing and bioinformatic analyses.

References

1. World Health Organization. Dengue fact sheet [cited 2023 Jul 17]. https://www.who.int/news-room/fact-sheets/detail/dengue-and-severe-dengue
2. Guzman MG, Halstead SB, Artsob H, Buchy P, Farrar J, Gubler DJ, et al. Dengue: a continuing global threat. Nat Rev Microbiol. 2010;8(Suppl):S7–16. https://doi.org/10.1038/nrmicro2460
3. United Nations Office for the Coordination of Humanitarian Affairs. São Tomé and Príncipe: worsening Dengue outbreak: DREF Application (MDRST002) [cited 2023 Jul 23]. https://reliefweb.int/report/sao-tome-and-principe/sao-tome-principe-worsening-dengue-outbreak-dref-application-mdrst002
4. Yen TY, Trovoada dos Santos MJ, Tseng LF, Chang SF, Cheng CF, Carvalho AVA, et al. Seroprevalence of antibodies against dengue virus among pregnant women in the Democratic Republic of São Tomé and Príncipe. Acta Trop. 2016;155:58–62. https://doi.org/10.1016/j.actatropica.2015.12.012
5. National Institute for Public Health and the Environment. Flavivirus genotyping tool [cited 2023 Jul 18]. https://www.rivm.nl/mpf/typingtool/flavivirus
6. Naveca FG, Santiago GA, Maito RM, Ribeiro Meneses CA, do Nascimento VA, de Souza VC, et al. Reemergence of dengue virus serotype 3, Brazil, 2023. Emerg Infect Dis. 2023;29:1482–4. https://doi.org/10.3201/eid2907.230595
7. Pan American Health Organization, World Health Organization. Reported cases of dengue fever in the Americas [cited 2023 Jul 20]. https://www3.paho.org/data/index.php/en/mnu-topics/indicadores-dengue-en/dengue-nacional-en/252-dengue-pais-ano-en.html

Address for correspondence: Kathrin Schuldt, Infectious Diseases Epidemiology Department, Bernhard Nocht Institute for Tropical Medicine, Bernhard-Nocht-Str. 74, 20359 Hamburg, Germany; email: schuldt@bnitm.de

Integrating Veterinary Diagnostic Laboratories for Emergency Use Testing during Pandemics[1]

Natasha F. Hodges, McKenzie Sparrer, Tyler Sherman, Treana Mayer, Danielle R. Adney, Izabela Ragan, Molly Carpenter, Christie Mayo,[2] Tracy L. Webb[2]

Author affiliations: Colorado State University, Fort Collins, Colorado, USA (N.F. Hodges, M. Sparrer, T. Sherman, T. Mayer, I. Ragan, M. Carpenter, C. Mayo, T.L. Webb); Lovelace Biomedical, Albuquerque, New Mexico, USA (D.R. Adney)

DOI: https://doi.org/10.3201/eid3002.230562

The SARS-CoV-2 pandemic showed limitations in human outbreak testing. Veterinary diagnostic laboratories (VDLs) possess capabilities to bolster emergency test capacity. Surveys from 26 participating VDLs found human SARS-CoV-2 testing was mutually beneficial, including One Health benefits. VDLs indicated testing >3.8 million human samples during the pandemic, which included some challenges.

After emergence of SARS-CoV-2 in late January 2020, diagnostic testing was fraught with challenges. As cases increased, public health agencies struggled to provide timely support, prompting veterinary diagnostic laboratories (VDLs) to assist with processing human SARS-CoV-2 samples (*1*). VDLs regularly conduct diagnostic testing for infectious agents and maintain the necessary equipment, personnel, facilities, and protocols for animal disease testing. Currently, there are 60 university- or state-affiliated VDLs across the United States (*2*). On April 1, 2020, the World Organization for Animal Health published guidance stating that VDLs possess the resources and personnel expertise to help human diagnostic laboratories meet the demand for SARS-CoV-2 testing (*3*,*4*).

To assess VDL participation in human testing, we distributed a 14-question survey (Appendix, https://wwwnc.cdc.gov/EID/article/30/2/23-0562-App1.pdf) to 52 VDLs across the United States that had available email addresses. The study was reviewed by Colorado State University's Institutional Review Board (Protocol no. 3620), and respondent answers were deidentified before analysis. The first question queried whether human SARS-CoV-2 samples were tested and required an affirmative response to continue the survey. Subsequent questions were optional. Responses were gathered during July 7–December 22, 2022. Two follow-up reminders were sent during the open survey period. Responses were received from 26 (43.3%) of the 60 VDLs overall or 26 (50%) of the 52 VDLs that were contacted. Nine respondents indicated no human testing, and 17 (65.4%) of the 26 responding VDLs reported performing human testing. When >1 response was received from the same VDL (5 VDLs submitted >1 survey), numeric data were averaged, and all free text entries were included.

The duration of human testing across responding VDLs ranged from 5 to 31 months; average

[1]Preliminary results from this study were presented at the 65th American Association of Veterinary Laboratory Diagnosticians Conference and the 126th US Animal Health Association Annual Conference, October 6–12, 2022, Minneapolis, Minnesota, USA.

[2]These authors were co–principal investigators.

testing duration was 20 months (95% CI 15.7–24.4 months). Twelve VDLs reported testing numbers ranging from 6,000 to 200,000 samples/facility (95% CI 67,200–224,000 samples/facility). One additional facility reported 2.1 million samples tested, totaling ≈3.8 million samples. When asked to declare populations served, VDLs indicated staff and students as the largest testing group, followed by local community as the second largest and long-term care facilities as the third largest (Figure).

We asked VDLs to rank the main challenges for human SARS-CoV-2 testing by using a rank-order question with 6 predefined and 3 open-response options. The survey asked respondents to rank items from 1 to 9, where 1 represented not challenging and 9 represented most challenging; each rank was selected only once. Personnel was the biggest challenge reported (average rank 7.7). Supplies (5.7) and certification (5.4) were moderately challenging on average, and facilities (3.7), training (3.6), and funding (3.0) were less challenging.

All respondents reported that the experience was beneficial to overall work going forward, 66.7% strongly agreeing and 33.3% somewhat agreeing. When asked to elaborate, 14 respondents included opportunities to optimize personnel, optimizing testing workflows, increased recognition, and relationship building as benefits. Most (83%) surveyed VDLs responded yes to the question of whether their laboratories experienced One Health benefits related to performing human sample testing (i.e., interagency connections, interdisciplinary work, or ideas that came from testing). In a follow-up write-in question, respondents' comments included improved awareness and recognition, relationship building, resultant collaborative opportunities, and sharing of information.

Two final questions asked about lessons learned. Responses supported planning and readiness with flexible workspaces, tested workflows, available trained personnel, financial needs, quality sample management, and validated equipment. Knowledge about Clinical Laboratory Improvement Amendments regulations and certification (https://dch.georgia.gov/divisionsoffices/hfrd/facilities-provider-information/clia) was mentioned in 40% of responses. Additional comments focused on the need for staff support, challenges to managing sample requirements, balancing multiple disease outbreaks, the need for establishing relationships, and pride in accomplishments.

Challenges reported through the survey included access to supplies as supply chain disruptions contributed to difficulty in procuring instrumentation, laboratory consumables, and personal protective equipment. Challenges related to personnel included availability of staff that met state-level criteria for testing, such as Clinical Laboratory Improvement Amendments certification. Further complications experienced by many VDLs included software integration and maintenance for reporting test results, as well as coordination of sample collection and receiving and handling from collaborating entities. The SARS-CoV-2 caseload was often in addition to existing testing needs, requiring longer or irregular working hours to meet expected

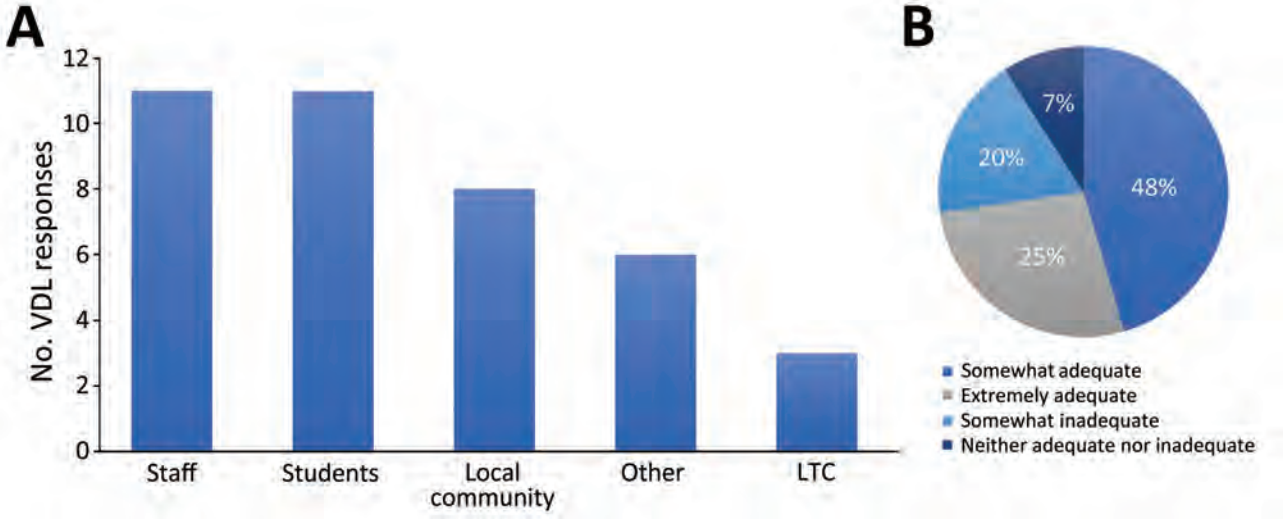

Figure. Population served (A) and perceived funding adequacy (B) of veterinary diagnostic laboratories (VDLs) conducting human SARS-CoV-2 testing, United States. A) Sum of responses for each of 5 selectable testing population types as reported by 13 of 17 VDLs performing human SARS-CoV-2 testing that responded to this optional question. VDLs could select any combination of answers that represented their specific testing populations. LTC, long-term care. B) Percentages of the 11 of 17 VDLs performing human SARS-CoV-2 testing that responded to the optional question to select 1 of 5 funding adequacy descriptions (no responses were received for inadequate).

turnaround times. For frontline pandemic workers, those conditions might have contributed to accelerated staff burnout and reported staff challenges.

The SARS-CoV-2 pandemic offers a One Health case model, given that both humans and animals may become infected and environmental detection is possible (e.g., wastewater) (*5*,*6*). As recently demonstrated, human testing facilities might struggle to meet emergency public health demands without additional support; however, laboratories that regularly test other zoonotic and nonzoonotic pathogens can help meet testing needs. Many of the responding VDLs reported mutually beneficial outcomes from participating in human SARS-CoV-2 testing, particularly in the form of new interagency relationships, shared information, and improved recognition. Similar coordinated, collaborative efforts might be particularly useful in mitigating future pandemics and improving disease response outcomes (*7*,*8*).

Acknowledgments

We thank the VDL members who graciously shared their time and expertise for this study, as well as support of the pandemic response.

About the Author

Ms. Hodges is a graduate research assistant in the Department of Microbiology, Immunology, and Pathology, at Colorado State University, Fort Collins, CO. Her primary research interests include emerging infectious diseases and zoonotic transmission.

References

1. Maxie G. The case for animal health laboratories to collaborate as One Health laboratories. J Vet Diagn Invest. 2020;32:501–2. https://doi.org/10.1177/1040638720938889
2. Nolen RS. Veterinary labs continue to support COVID-19 testing. American Veterinary Medical Association. 2020 [cited 2023 Jan 17]. https://www.avma.org/javma-news/2020-07-01/veterinary-labs-continue-support-covid-19-testing
3. Cullinane A, Al Muhairi S, Cattoli G, O'Keefe J, Fooks T, Kojima K, et al. A guidance for animal health laboratories. 2020 [cited 2023 Jan 19]. https://www.woah.org/app/uploads/2021/03/a-guidance-for-animal-health-laboratories-1april2020.pdf
4. OIE. OIE's response to COVID-19. OIE News May 2020 Special Edition COVID-19. 2020 [cited 2023 Dec 2]. https://bulletin.woah.org/wp-content/uploads/2020/05/OIE-News-May2020-Special-Edition-COVID-19-main-news-article_withoutstatement.pdf
5. Peccia J, Zulli A, Brackney DE, Grubaugh ND, Kaplan EH, Casanovas-Massana A, et al. Measurement of SARS-CoV-2 RNA in wastewater tracks community infection dynamics. Nat Biotechnol. 2020;38:1164–7. https://doi.org/10.1038/s41587-020-0684-z
6. Núñez-Delgado A. What do we know about the SARS-CoV-2 coronavirus in the environment? Sci Total Environ. 2020;727:138647. https://doi.org/10.1016/j.scitotenv.2020.138647
7. American Public Health Association. Advancing a "One Health" approach to promote health at the human-animal-environment interface. 2017 [cited 2023 Jan 19]. https://www.apha.org/policies-and-advocacy/public-health-policy-statements/policy-database/2018/01/18/advancing-a-one-health-approach
8. World Bank. People, pathogens and our planet: the economics of One Health. Washington, DC: 2012 Jun. Report No.: 69245-GLB [cited 2023 Jan 19]. https://openknowledge.worldbank.org/handle/10986/11892

Address for correspondence: Natasha F. Hodges, Colorado State University, 2450 Gillette Dr, Fort Collins, CO 80526, USA; email: natasha.hodges@colostate.edu

Model for Interpreting Discordant SARS-CoV-2 Diagnostic Test Results

Oluwaseun F. Egbelowo,[1] Spencer J. Fox,[1] Graham C. Gibson, Lauren Ancel Meyers

Author affiliations: The University of Texas at Austin, Austin, Texas, USA (O.F. Egbelowo, L.A. Meyers); University of Georgia, Athens, Georgia, USA (S.J. Fox); Los Alamos National Laboratory, Los Alamos, New Mexico, USA (G.C. Gibson); Santa Fe Institute, Santa Fe, New Mexico, USA (L.A. Meyers)

DOI: https://doi.org/10.3201/eid3002.230200

We devised a model to interpret discordant SARS-CoV-2 test results. We estimate that, during March 2020–May 2022, a patient in the United States who received a positive rapid antigen test result followed by a negative nucleic acid test result had only a 15.4% (95% CI 0.6%–56.7%) chance of being infected.

During the COVID-19 pandemic, nucleic acid amplification tests (NAATs) and rapid antigen tests (RATs) have been widely used to direct patient care and control transmission (*1*). NAATs, such as reverse transcription PCR, tend to have higher sensitivity and

[1]These first authors contributed equally to this article.

specificity than RATs (*2*) but often are more costly and take much longer to process (*3*,*4*). Thus, RATs increasingly have been used across the United States for at-home symptom-based testing and asymptomatic screening in healthcare, educational, and public event settings (*5*).

During June 2020–April 2022, healthcare providers recommended a confirmatory NAAT after a positive RAT because of high false-positive rates for RATs when community disease prevalence was low (*6*,*7*). When a patient received a negative confirmatory NAAT result, clinicians had to decide which of the results was erroneous and suggest a course of action.

In this study, we describe a statistical model that can guide the interpretation of discordant test results. The model considers test sensitivity and specificity and estimated community prevalence of the virus. By using community prevalence, the model can estimate the probability that an initial RAT result was a false-positive after a negative confirmatory NAAT result (Appendix, https://wwwnc.cdc.gov/EID/article/30/2/23-0200-App1.pdf).

As a case study, we considered BinaxNOW (Abbott Laboratories, https://www.abbott.com), a test widely used in 2021. BinaxNOW had an estimated test sensitivity of 84.6%; we also considered various NAAT false-negative rates depending on how long after BinaxNOW a NAAT was administered: 68% at 0 days, 37% at 1 day, 24% at 2 days, and 21% at 3 days (*2*). For a patient who received a positive RAT result and then a negative NAAT result, we estimated the probability that the RAT result was erroneous and the patient was not infected (Figure, panel A). That probability was >80% if community prevalence was <200 new weekly COVID-19 cases/100,000 population, the Centers for Disease Control and Prevention (CDC) threshold for low community prevalence (*8*), and generally declined as disease prevalence increased (Figure, panel A). However, a tradeoff exists between NAAT accuracy and speed of diagnosis. For instance, if RAT and NAAT were administered on the same day, the RAT false-positive probability was 89.6% (95% CI 80.5%–100%) when community COVID-19 levels were low according to CDC

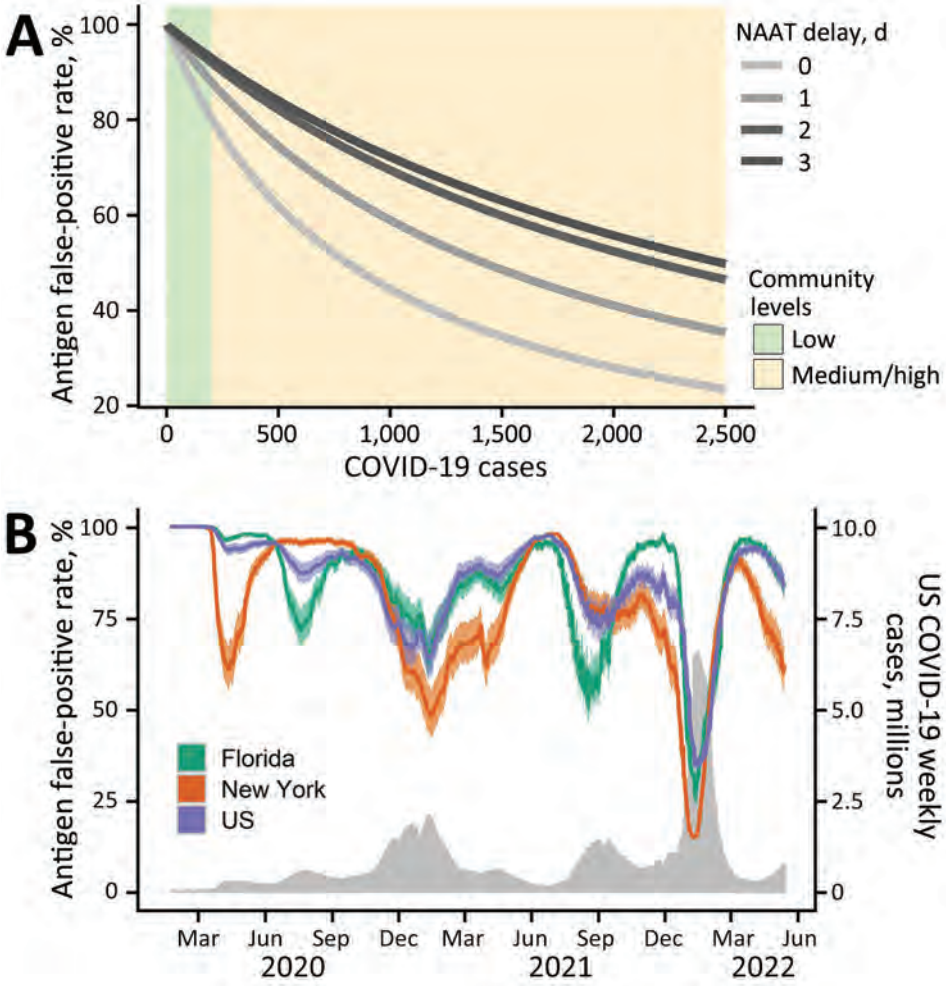

Figure. Estimated probability that a positive RAT result is erroneous given a subsequent negative NAAT in a model for interpreting discordant SARS-CoV-2 diagnostic test results. A) Estimated RAT false-positive percentages for levels of community transmission ranging from 0–2,500 COVID-19 cases per 100,000 population. Green and yellow shading correspond to the Centers for Disease Control and Prevention threshold for low and medium or high community levels (*8*). Line color corresponds to different numbers of days between the initial RAT and confirmatory NAAT, ranging from same day (lightest gray) to 3 days later (black). B) Estimated RAT false-positive percentages for the United States (purple), Florida (green), and New York (orange) during March 2020–May 2022, assuming the NAAT is administered 1 day after the RAT and that 1 in 4 cases were reported. Shading reflects uncertainty in Centers for Disease Control and Prevention estimated COVID-19 infection underreported, ranging from 1 in 3 to 1 in 5. The gray time series along the bottom indicates the daily 7-day sum of reported COVID-19 cases in the United States. NAAT, nucleic acid amplification test; RAT, rapid antigen test.

Table. Probability that a RAT is false-positive in a model for interpreting discordant SARS-CoV-2 diagnostic test results*

No. days between RAT and NAAT	Estimated RAT false-positive rate, % (95% CI)
0	73.4 (49.2–100)
1	82.5 (63.4–100)
2	88 (73.3–100)
3	89.2 (75.9–100)
4	89.6 (76.6–100)
5	88.8 (75.0–100)
6	88.4 (74.1–100)
7	86.7 (71–100)

*The model assumes that a NAAT was negative after a RAT and that NAAT was performed after specified time delay. Estimates assume that the antigen test was performed when patient symptoms first appeared and had a test sensitivity of 84.6% and specificity of 98.54%, which corresponds to the estimated values for BinaxNOW (Abbott Laboratories, https://www.abbott.com) (Appendix Table 1, https://wwwnc.cdc.gov/EID/article/30/2/23-0200-App1.pdf). The NAAT false negative rate for each delay was drawn from a previous study (*3*). NAAT, nucleic acid amplification test; RAT, rapid antigen test.

guidelines. However, if the NAAT was administered 3 days after the RAT, the corresponding probability increased to 96.4% (95% CI 93.0%–100%) (Appendix Table 4). Our confidence in the negative NAAT result peaked when the NAAT was administered 4 days after the RAT (Table; Appendix Figure 1, panel B). Barring other external information (e.g., symptomicity), clinicians can be 89.6% (95% CI 80.5%–100%) confident that the initial RAT result was false-positive when a community is in low risk according to CDC guidelines and 70.5% (95% CI 62.0%–80.5%) confident the same RAT was false-positive when the community is at medium or high risk (Appendix Tables 2–4, Figure 1, panel A).

During May 2020–May 2022, we estimate that RAT false-positive probability in the United States ranged from 34% (95% CI 29%–41%) to 97.7% (95% CI 97.2%–98.3%), assuming a 25% (95% CI 20%–33%) case reporting rate (Figure, panel B) (*9*). The probability of an erroneous RAT was lowest during the Omicron surge in the winter of 2021–22, when community prevalence was estimated to be highest. At the Omicron peak, we estimate RAT false-positive probabilities of 15% (95% CI 11%–20%) for New York, 25% (95% CI 21%–32%) for Florida, and 34% for (95% CI 29%–41%) the United States (Figure, panel B). The relative trends are similar for other commonly used antigen tests, but the estimated false-positive rates depend on test sensitivities and specificities for each test (Appendix Figures 2, 3).

Rapid and reliable diagnoses of severe infectious diseases is critical for clinical care and infection control. However, the first 2 years of the COVID-19 pandemic revealed enormous barriers to deploying inexpensive, rapid, and accurate tests to combat a newly emerging or rapidly evolving pathogen. We developed this framework during fall 2021 to guide decision-making by patients, physicians, and public health officials in the Austin, Texas, USA metropolitan area. The University of Texas used this model for decision-making regarding when patients might need to visit a clinician. Our framework is limited by the accuracy of the estimates of the RAT and NAAT test sensitivity and specificity and the estimated community disease prevalence, which we drew from transmission estimates from the first 2 years of the pandemic. If community prevalence was higher than we estimated, which could be the case in the early weeks of the pandemic, our model could overestimate the RAT false-positive rate.

In conclusion, we developed a model to estimate false-positive RAT rates during the COVID-19 pandemic. The model inputs can be readily modified to guide the interpretation of discordant tests as COVID-19 continues to evolve and as RATs become more widely used for other diseases, such as influenza or respiratory syncytial virus (*10*).

This article was preprinted at https://medrxiv.org/cgi/content/short/2023.02.07.23285547v1.

Acknowledgments

We acknowledge the financial support from the National Institutes of Health (grant no. R01 AI151176) and the Centers for Disease Control and Prevention (grant no. U01IP001136).

About the Author

Dr. Egbelowo is a postdoctoral researcher in the Department of Integrative Biology at the University of Texas at Austin. His research interests focus on the application of mathematical and statistical techniques to aid in decision-making for the control of infectious diseases. Dr. Fox is an assistant professor at the University of Georgia in the Department of Epidemiology & Biostatistics. His research interests include statistical modeling of emerging infectious diseases and outbreak forecasting.

References

1. Wong G, Liu W, Liu Y, Zhou B, Bi Y, Gao GF. MERS, SARS, and Ebola: the role of super-spreaders in infectious disease. Cell Host Microbe. 2015;18:398–401. https://doi.org/10.1016/j.chom.2015.09.013
2. Kucirka LM, Lauer SA, Laeyendecker O, Boon D, Lessler J. Variation in false-negative rate of reverse transcriptase polymerase chain reaction–based SARS-CoV-2 tests by time since exposure. Ann Intern Med. 2020;173:262–7. https://doi.org/10.7326/M20-1495

3. Yang S, Rothman RE. PCR-based diagnostics for infectious diseases: uses, limitations, and future applications in acute-care settings. Lancet Infect Dis. 2004;4:337–48. https://doi.org/10.1016/S1473-3099(04)01044-8
4. Schuit E, Veldhuijzen IK, Venekamp RP, van den Bijllaardt W, Pas SD, Lodder EB, et al. Diagnostic accuracy of rapid antigen tests in asymptomatic and presymptomatic close contacts of individuals with confirmed SARS-CoV-2 infection: cross sectional study. BMJ. 2021;374:n1676. https://doi.org/10.1136/bmj.n1676
5. Filgueiras PS, Corsini CA, Almeida NBF, Assis JV, Pedrosa MLC, de Oliveira AK, et al. COVID-19 rapid antigen test at hospital admission associated to the knowledge of individual risk factors allow overcoming the difficulty of managing suspected patients in hospitals. Fortune J Health Sci. 2022;5:211–31. https://doi.org/10.26502/fjhs.055
6. Gans JS, Goldfarb A, Agrawal AK, Sennik S, Stein J, Rosella L. False-positive results in rapid antigen tests for SARS-CoV-2. JAMA. 2022;327:485–6. https://doi.org/10.1001/jama.2021.24355
7. Kanji JN, Proctor DT, Stokes W, Berenger BM, Silvius J, Tipples G, et al. Multicenter postimplementation assessment of the positive predictive value of SARS-CoV-2 antigen-based point-of-care tests used for screening of asymptomatic continuing care staff. J Clin Microbiol. 2021;59:e0141121. https://doi.org/10.1128/JCM.01411-21
8. Centers for Disease Control and Prevention; National Center for Immunization and Respiratory Diseases (NCIRD), Division of Viral Diseases. Science brief: indicators for monitoring COVID-19 community levels and making public health recommendations. In: CDC COVID-19 science briefs. Atlanta (GA): Centers for Disease Control and Prevention (US); 2022.
9. Centers for Disease Control and Prevention. Estimated COVID-19 burden [cited 2022 May 25]. https://www.cdc.gov/coronavirus/2019-ncov/cases-updates/burden.html
10. Osterman A, Badell I, Basara E, Stern M, Kriesel F, Eletreby M, et al. Impaired detection of omicron by SARS-CoV-2 rapid antigen tests. Med Microbiol Immunol (Berl). 2022;211:105–17. https://doi.org/10.1007/s00430-022-00730-z

Address for correspondence: Lauren Ancel Meyers, The University of Texas at Austin, Department of Integrative Biology, 1 University Station C0930, Austin, TX 78712, USA: email: laurenmeyers@austin.utexas.edu

SARS-CoV-2 Infection in Beaver Farm, Mongolia, 2021

Taichiro Takemura,[1] Ulaankhuu Ankhanbaatar,[1] Tirumala Bharani K. Settypalli, Dulam Purevtseren, Gansukh Shura, Batchuluun Damdinjav, Hatem Ouled Ahmed Ben Ali, William G Dundon, Giovanni Cattoli, Charles E. Lamien

Author affiliations: International Atomic Energy Agency, Seibersdorf, Austria (T. Takemura, T.B.K. Settypalli, H.O.A.B. Ali, W.G. Dundon, G. Cattoli, C.E. Lamien); State Central Veterinary Laboratory, Ulaanbaatar City, Mongolia (U. Ankhanbaatar, D. Purevtseren, G. Shura, B. Damdinjav)

DOI: http://doi.org/10.3201/eid3002.231318

We report an outbreak of COVID-19 in a beaver farm in Mongolia in 2021. Genomic characterization revealed a unique combination of mutations in the SARS-CoV-2 of the infected beavers. Based on these findings, increased surveillance of farmed beavers should be encouraged.

The COVID-19 pandemic that began in 2019 remains uncontained, and fatalities and multiple waves of infection continue to occur worldwide (*1*). The causative agent, SARS-CoV-2, has been detected in humans and several animal species, including domestic, wild, and laboratory animals (*2*,*3*). Because SARS-CoV-2 can be transmitted from humans to animals and back to humans, understanding the dynamics of infection in animals can contribute to the creation of more comprehensive response strategies.

We identified SARS-CoV-2 infection in beavers (*Castor fiber*) farmed for conservation reasons in Mongolia and report on serologic and whole genome sequence data from this outbreak. The beaver farm, located in the Bayanzurkh district in Ulaanbaatar, Mongolia, reared 32 adults and 16 kits in 2021. They were housed indoors in a large area separated by waist-high walls, with space for multiple animals. One of the 7 employees of the farm had influenza-like symptoms for several days and was diagnosed with COVID-19 on August 6, 2021. On August 9, the beaver farm reported the death of 2 beavers (one 6 months of age and one 2 years of age) after signs of coughing, nasal discharge, rasping on auscultation of the lungs and chest cavity, sluggish movement, and aversion to food. On August 13, research investigators collected nasal swabs, saliva, and 7 tissue samples

[1]These first authors contributed equally to this article.

(lung, kidney, liver, heart, spleen, larynx, and tongue from the 2 dead animals. Researchers also collected nasal swab specimens, saliva, and blood from 7 other beavers with notable clinical signs of coughing and purulent nasal discharge. Follow-up investigation on August 18 or 19 and on September 12 included collection of additional nasal swab specimens, saliva, and blood samples from the same animals as well as from 2 healthy animals (September 12 only).

All samples were transported to a Biosafety Level 3 facility in Ulaanbaatar and were screened by quantitative reverse transcription PCR according to the Peiris protocol (*4*). The results showed that 46 of 48 specimens from 9 animals with clinical signs, including the 2 dead animals, tested positive for SARS-CoV-2 RNA. Serum was separated from the blood samples by centrifugation (2,000 × *g* for 10 min) and stored at −20°C until required. The serum samples were then subjected to antibody screening by using a commercial ELISA kit (ID Screen SARS-CoV-2 Double Antigen Multi-species ELISA; Innovative Diagnostics, https://www.innovative-diagnostics.com). Fifteen of 23 samples tested positive and 1 was intermediate, indicating that all animals became antibody positive within 1 month of confirmation of SARS-CoV-2 RNA positivity. One clinically unremarkable beaver tested positive for SARS-CoV-2 antibodies, indicating a possible subclinical infection (Table).

We shipped 5 randomly selected quantitative reverse transcription PCR–confirmed SARS-CoV-2–positive RNA samples to the Animal Production and Health Laboratory (Seibersdorf, Austria), a joint program of the International Atomic Energy Agency and the Food and Agriculture Organization of the United Nations, and subjected them to whole-genome sequencing (Appendix 1, https://wwwnc.cdc.gov/EID/article/30/2/23-1318-App1.pdf; Appendix 2, https://wwwnc.cdc.gov/EID/article/30/2/23-1318-App2.xlsx). Based on genotype analysis, all 5 genome sequences were assigned to the B.1.617.2 lineage, commonly referred to as the Delta variant. At the time of sampling, Alpha and Delta variants of SARS-CoV-2 were being identified in humans in Mongolia. The closest related sequences to those we identified in the beavers studied were from

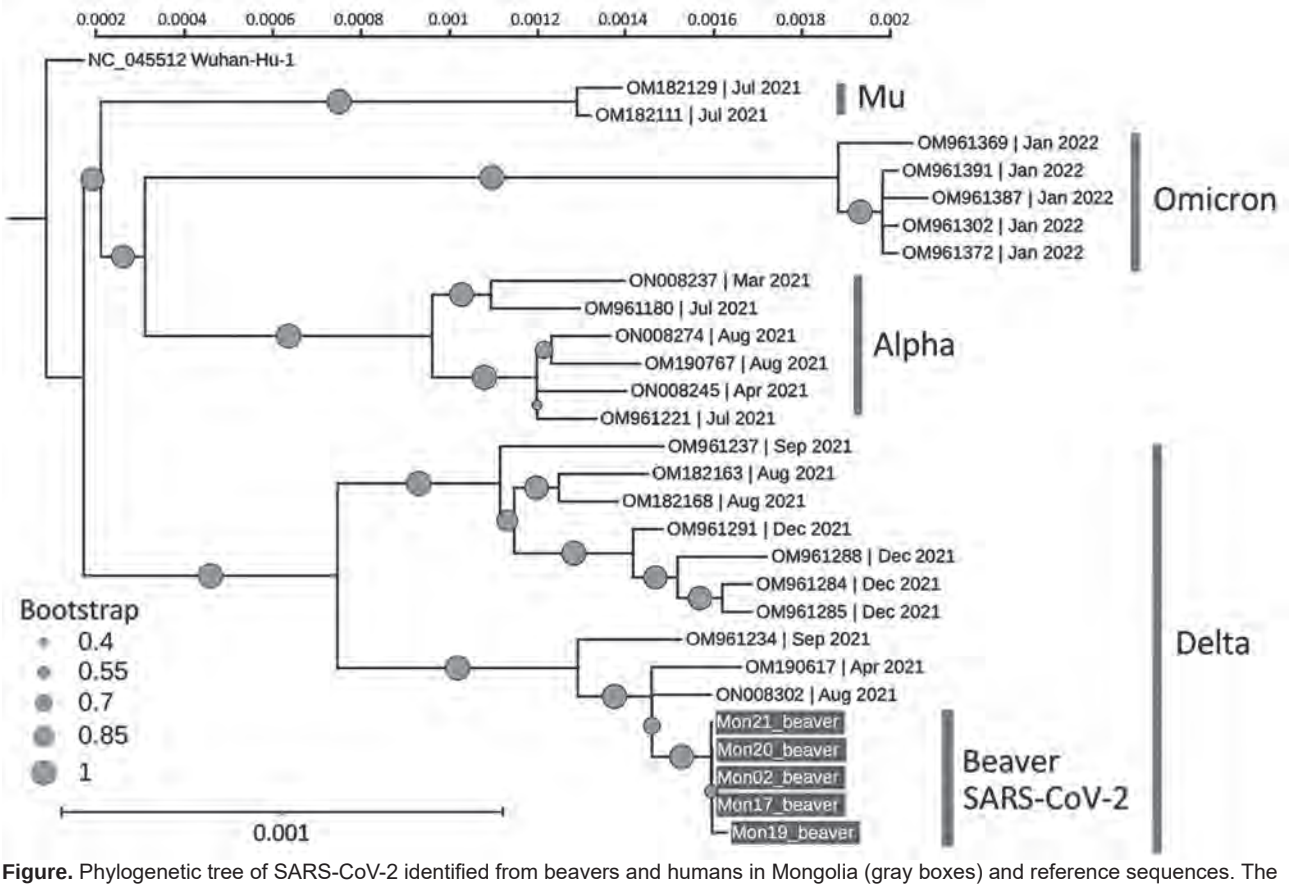

Figure. Phylogenetic tree of SARS-CoV-2 identified from beavers and humans in Mongolia (gray boxes) and reference sequences. The circle size indicates the bootstrap values at the node. The vertical bar shows the genetic distance. SARS-CoV-2 lineages are identified at right. GenBank accession numbers and date identified are shown for reference sequences; the newly obtained sequence data were deposited in GenBank (accession nos. OR389473–7).

Table. Sampling date and results of serologic analysis of SARS-CoV-2 antibodies from farmed beavers, Ulaanbaatar, Mongolia, 2021*

		Date of swab sampling and qRT-PCR results			Date of serum sampling and ELISA results†		
Animal ID	Status	2021 Aug 13	2021 Aug 19	2021 Sep 12	2021 Aug 13	2021 Aug 18	2021 Sep 12
1	Died Sep 8	Positive	NT	NT	NT	NT	NT
2	Died 2021 Sep 8	Positive	NT	NT	NT	NT	NT
3	Sick	Positive	Positive	Positive	Negative	Negative	Positive
4	Sick	Positive	Positive	Positive	Negative	Negative	Positive
5	Sick	Positive	Positive	Positive	Negative	Positive	Positive
6	Sick	Positive	Positive	Positive	Positive	Positive	Positive
7	Sick	Positive	Positive	Positive	Positive	Positive	Intermediate
8	Sick	Positive	Positive	Negative	Positive	Positive	Positive
9	Sick	Positive	Positive	Negative	Negative	Positive	Positive
10	Healthy	NT	NT	NT	NT	NT	Positive
11	Healthy	NT	NT	NT	NT	NT	Negative

*ID, identification; qRT-PCR, quantitative reverse transcription PCR; NT, not tested.
†ID Screen SARS-CoV-2 Double Antigen Multi-species ELISA (Innovative Diagnostics, https://www.innovative-diagnostics.com). The interpretation is based on the signal-to-noise (S/N) ratio, (sample optical density [OD] 450/negative control OD450) × 100, according to instruction manual. Positive: S/N>100.0; intermediate: 100.0>S/N>50.0; negative: 50.0>S/N.

human SARS-CoV-2 in Mongolia (GenBank accession nos. ON008302, OM190617, and OM961234) identified during April–September 2021 (Figure). In addition to 4 mutations in the spike region, the sequences shared 7 amino acid substitutions in open reading frame [ORF] 1a, 4 amino acid substitutions in ORF1b, and 1 amino acid substitution in nucleocapsid genes. In the beaver sequences, 4 amino acid substitutions identified were not in the human isolates from Mongolia: S2500F, A3657V in ORF1a and H604Y, T1404M in ORF1b. Although those substitutions have been identified individually in SARS-CoV-2 sequences in GenBank and the GISAID database (https://www.gisaid.org), there are no records of sequences with all 4 mutations.

Several cases of SARS-CoV-2 transmission between humans and animals have already been reported (*5*–*8*). An alarming aspect of SARS-CoV-2 infection in animals is that host animals can maintain the virus and contribute to the emergence in humans of new variants that have accumulated multiple mutations (*7*–*10*). Indeed, the specific combination of mutations observed in the beavers we studied has not been found in other SARS-CoV-2 sequences in public databases (as of November 2023). This finding suggests that the mutations might have occurred or accumulated after the introduction of the virus into the beaver population. Because the emergence of viruses with mutations not targeted by current SARS-CoV-2 vaccines is a credible possibility, more active surveillance of SARS-CoV-2 infection in animals should be encouraged to identify the appearance of mutated viruses. In intensively farmed animals, species–species and species–humans contact is more frequent than in animals dwelling in other environments, which might increase the risk for zoonotic pathogen transmission (*2*). Thus, implementing more active surveillance and infection control strategies is critical to disease prevention and containment.

Samples used in this study were those submitted to the State Central Veterinary Laboratory, Mongolia, for emergency diagnosis of SARS-CoV-2. Ethics approval was not required.

Funding came from the VETLAB network initiative of the Joint Food and Agriculture Organization of the United Nations (FAO)/International Atomic Energy Agency (IAEA) Centre through the IAEA Peaceful Uses Initiative Project ("Detection of emerging and re-emerging animal and zoonotic pathogens at the animal-human interface"), funded by the Government of Japan and the United States of America and IAEA ZODIAC Project.

About the Author

Dr Takemura is a technical expert for the ZODIAC project, Animal Production and Health Laboratory, Joint FAO/IAEA Division of Nuclear Techniques in Food and Agriculture. His main research interests are in the biology of infectious pathogens.

References

1. Coronavirus disease (COVID-19) pandemic, World Health Organization web database [cited 2023 Sep 20]. https://www.who.int/emergencies/diseases/novel-coronavirus-2019
2. Cui S, Liu Y, Zhao J, Peng X, Lu G, Shi W, et al. An updated review on SARS-CoV-2 infection in animals. Viruses. 2022;14:1527. https://doi.org/10.3390/v14071527
3. Rao SS, Parthasarathy K., Sounderrajan V, Neelagandan K, Anbazhagan P, Chandramouli V. Susceptibility of SARS Coronavirus-2 infection in domestic and wild animals: a systematic review. 3 Biotech. 2023;13:5. https://doi:10.1007/s13205-022-03416-8 *PMID: 36514483*
4. World Health Organization Detection of 2019 novel coronavirus (2019-nCoV) in suspected human cases by RT-PCR [cited 2023 Nov 1]. https://www.who.int/docs/default-source/coronaviruse/peiris-protocol-16-1-20.pdf
5. SARS-CoV-2 in animals situation update, FAO, Rome. [cited 2023 Sep 1]. https://www.fao.org/animal-health/situation-updates/sars-cov-2-in-animals

6. Oude Munnink BB, Sikkema RS, Nieuwenhuijse DF, Molenaar RJ, Munger E, Molenkamp R, et al. Transmission of SARS-CoV-2 on mink farms between humans and mink and back to humans. Science. 2021;371:172–7. https://doi.org/10.1126/science.abe5901
7. Pickering B, Lung O, Maguire F, Kruczkiewicz P, Kotwa JD, Buchanan T, et al. Divergent SARS-CoV-2 variant emerges in white-tailed deer with deer-to-human transmission. [Erratum in: Nat Microbiol. 2023:8:188; https://doi.org/10.1038/s41564-022-01298-3] Nat Microbiol. 2022;7:2011–24. https://doi.org/10.1038/s41564-022-01268-9
8. Tan CCS, Lam SD, Richard D, Owen CJ, Berchtold D, Orengo C, et al. Transmission of SARS-CoV-2 from humans to animals and potential host adaptation. Nat Commun. 2022;13:2988. https://doi.org/10.1038/s41467-022-30698-6
9. Koopmans M. SARS-CoV-2 and the human-animal interface: outbreaks on mink farms. Lancet Infect Dis. 2021;21:18–9. https://doi.org/10.1016/S1473-3099(20)30912-9
10. Sharun K, Tiwari R, Saied AA, Dhama K. SARS-CoV-2 vaccine for domestic and captive animals: An effort to counter COVID-19 pandemic at the human-animal interface. Vaccine. 2021;39:7119–22. https://doi.org/10.1016/j.vaccine.2021.10.053

Address for correspondence: Taichiro Takemura, Animal Production and Health Laboratory, International Atomic Energy Agency, Friedenstrasse 1, Seibersdorf, Austria; email: T.Takemura@iaea.org

Severe Infective Endocarditis Caused by *Bartonella rochalimae*

Edward C. Traver, Kapil Saharia, Paul Luethy, Anthony Amoroso

Author affiliation: University of Maryland School of Medicine, Baltimore, Maryland, USA

DOI: http://doi.org/10.3201/eid3001.230929

A 22-year-old man from Guatemala sought care for subacute endocarditis and mycotic brain aneurysm after living in good health in the United States for 15 months. *Bartonella rochalimae*, a recently described human and canine pathogen, was identified by plasma microbial cell-free DNA testing. The source of infection is unknown.

A 22-year-old man with a history of an unrepaired congenital ventricular septal defect (VSD) experienced 3 months of progressive dyspnea on exertion, weight loss, and fatigue and 2 weeks of debilitating weakness. He had been born in Guatemala, where he worked in construction; he had had contact with goats, horses, cattle, and chickens but reported no contact with dogs or cats. Eighteen months before he sought care, he had migrated to the mid-Atlantic region of the United States, where he lived with his uncle and a few other adults in a suburban town. He continued to work in construction, did not use illicit drugs, and had 1 female sexual partner. Six months after he arrived, his uncle took in a stray dog.

The patient was afebrile, hypotensive, bradycardic, and thin. A systolic ejection murmur and a fourth heart sound were present. He had right upper quadrant abdominal tenderness and digital clubbing. Laboratory studies revealed anemia, unremarkable creatinine levels, and elevated liver enzymes (Table). Results of 3 sets of bacterial blood cultures and 1 set of fungal blood cultures were negative. Transthoracic and transesophageal echocardiograms demonstrated a VSD with bidirectional shunting and a mobile mitral valve echodensity. We

Table. Laboratory results for patient with infective endocarditis caused by *Bartonella rochalimae*, United States*

Test	Result	Reference range
Leukocytes, K/μL	4.8	4.5–11.0
Hemoglobin, g/dL	10.9	12.6–17.4
Platelets, K/μL	168	153–367
Creatinine, mg/dL	0.77	0.66–1.25
AST, units/L	**84**	17–59
ALT, units/L	**58**	0–49
Alkaline phosphatase, units/L	109	38–126
Total bilirubin, mg/dL	0.6	0.3–1.2
CRP, mg/dL	**3.7**	≤1.0
ESR, mm/h	**81**	0–15
4th-generation HIV antigen and antibody test	Nonreactive	Nonreactive
Coxiella burnetii Phase 2 IgM	**1:32**	Negative
C. burnetii Phase 2 IgG	**1:128**	Negative
C. burnetii Phase 1 IgM	Negative	Negative
C. burnetii Phase 1 IgG	**1:16**	Negative
Brucella antibody agglutination	<1:20	<1:20
Chlamydia pneumoniae IgM	<1:20	<1:20
C. pneumoniae IgG	**1:512**	<1:64
C. trachomatis IgM	<1:20	<1:20
C. trachomatis IgG	**1:128**	<1:64
C. psittaci IgM	<1:20	<1:20
C. psittaci IgG	**1:512**	<1:64
Bartonella henselae IgG	**>1:1024**	Unknown
B. henselae IgM	**1:64**	Unknown
B. quintana IgG	**>1:1024**	Unknown
B. quintana IgM	<1:16	Unknown

*Bold text indicates abnormal values. ALT, alanine transaminase; AST, aspartate transferase; CRP, C-reactive protein; ESR, erythrocyte sedimentation rate.

initiated treatment for culture-negative infective endocarditis (Figure). A computed tomography angiogram of the brain, performed on day 2, revealed a 2–3 mm mycotic aneurysm in the right frontal middle cerebral artery; it appeared smaller by digital subtraction angiography on day 7.

On hospital day 2, we sent a plasma microbial cell-free DNA (mcfDNA) test to Karius (Redwood City, CA, USA). The result on day 4 was positive for *Bartonella rochalimae* DNA (47,501 molecules/μL; reference <10 molecules/μL). We changed the antimicrobial drug regimen to target *Bartonella* endocarditis and adjusted it over the hospital stay to avoid toxicities and interactions (Figure). We performed serologic tests for *Bartonella*, *Brucella*, *Chlamydia*, and *Coxiella* species (Table).

Thirteen days after admission, the mitral valve was surgically replaced; both valve leaflets demonstrated chronic-appearing vegetations, and the anterior leaflet was perforated. Results for bacterial culture of the valve tissue were negative; histopathology was not performed. Mitral valve tissue 16S ribosomal RNA amplicon-based next-generation sequencing (NGS) was performed by the University of Washington Department of Laboratory Medicine Molecular Diagnosis Microbiology Section (Renton, WA, USA). After mitral valve replacement, the left-to-right shunt increased, and the patient underwent a second sternotomy and open VSD repair. The amplicon-based NGS test of the mitral valve tissue result, received on hospital day 36, was positive for *B. rochalimae*. The patient was discharged and instructed to complete an additional 3-month course of oral doxycycline. However, he moved out of the region 2 months later, so no follow-up visits occurred.

B. rochalimae was first isolated from a person traveling from the United States to Peru and demonstrated to be the cause of her febrile illness in 2007 (*1*). It has since been detected in 1 other human (*2*). We report a case of *B. rochalimae* human infective endocarditis in a man with an unrepaired congenital heart disease, diagnosed by plasma mcfDNA and confirmed to the species level by NGS of the endocardial tissue. Results of serologic tests for other *Bartonella* species and *Coxiella* and *Chlamydia* species may be elevated because of co-exposure or cross-reactivity (*3*,*4*). *B. rochalimae* has not been detected in other clinical samples by the Karius test (L. Dyner, Karius, Inc., pers. comm., email, 2023 Feb 17) and was not detected among 168 *Bartonella* spp. identified to the species level by 16S PCR at the University of Washington during 2003–2021 (*5*).

A published case of human disease occurred in a traveler who had been exposed to arthropods in Peru; a closely related, possibly identical, species named AF415211, was collected from a flea in Peru in 1998 (*1*,*6*). It is unclear if *B. rochalimae* exists in Guatemala, where the patient we report lived, or if the infection was subclinical for the 15 months he was living in the United States in good health. *B. rochalimae* has caused infective endocarditis in dogs in the United States and Europe and has been detected by PCR in the fleas or blood of dogs throughout the world (*6*–*8*). Dogs, foxes, and coyotes may be natural reservoirs. Our patient did report exposure to a dog, but only after arriving in the mid-Atlantic region of the United States. The location and vector of this patient's infection require further investigation, but our findings illustrate that mcfDNA may be useful to identify of new and emerging pathogens.

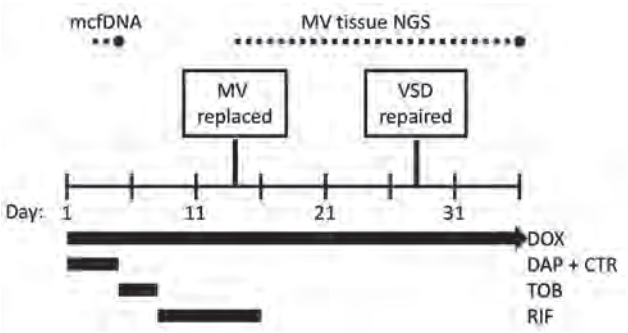

Figure. Diagnostics and treatments for *Bartonella rochalimae* endocarditis during a 36-day hospitalization. Dotted lines indicate the time between specimen collection and test result for mcfDNA and MV tissue NGS tests. CTR, ceftriaxone; DAP, daptomycin; DOX, doxycycline; mcfDNA, microbial cell-free DNA; MV, mitral valve; NGS, next-generation sequencing; RIF, rifampin; TOB, tobramycin; VSD, ventricular septal defect.

The University of Maryland, Baltimore Institutional Review Board determined that this work is not human research and does not require IRB review.

Author contributions: E.C.T.: conceptualization, writing original draft, review, and editing; K.S.: conceptualization, review, and editing; P.L.: conceptualization, review, and editing; A.A.: conceptualization, review, and editing.

About the Author

Dr. Traver practices general infectious disease and HIV medicine at the University of Maryland School of Medicine and University of Maryland Medical Center. His clinical work and research focus on bacterial infections in persons who use drugs and improving care delivery through multidisciplinary collaboration.

References

1. Eremeeva ME, Gerns HL, Lydy SL, Goo JS, Ryan ET, Mathew SS, et al. Bacteremia, fever, and splenomegaly caused by a newly recognized *Bartonella* species. N Engl J Med. 2007;356:2381–7. https://doi.org/10.1056/NEJMoa065987
2. Ramos JM, Pérez-Tanoira R, Martín-Martín I, Prieto-Pérez L, Tefasmariam A, Tiziano G, et al. Arthropod-borne bacteria cause nonmalarial fever in rural Ethiopia: a cross-sectional study in 394 patients. Vector Borne Zoonotic Dis. 2019;19:815–20. https://doi.org/10.1089/vbz.2018.2396
3. La Scola B, Raoult D. Serological cross-reactions between *Bartonella quintana*, *Bartonella henselae*, and *Coxiella burnetii*. J Clin Microbiol. 1996;34:2270–4. https://doi.org/10.1128/jcm.34.9.2270-2274.1996
4. Maurin M, Eb F, Etienne J, Raoult D. Serological cross-reactions between *Bartonella* and *Chlamydia* species: implications for diagnosis. J Clin Microbiol. 1997;35:2283–7. https://doi.org/10.1128/jcm.35.9.2283-2287.1997
5. McCormick DW, Rassoulian-Barrett SL, Hoogestraat DR, Salipante SJ, SenGupta D, Dietrich EA, et al. *Bartonella* spp. infections identified by molecular methods, United States. Emerg Infect Dis. 2023;29:467–76. https://doi.org/10.3201/eid2903.221223
6. Henn JB, Gabriel MW, Kasten RW, Brown RN, Koehler JE, MacDonald KA, et al. Infective endocarditis in a dog and the phylogenetic relationship of the associated "*Bartonella rochalimae*" strain with isolates from dogs, gray foxes, and a human. J Clin Microbiol. 2009;47:787–90. https://doi.org/10.1128/JCM.01351-08
7. Ernst E, Qurollo B, Olech C, Breitschwerdt EB. *Bartonella rochalimae*, a newly recognized pathogen in dogs. J Vet Intern Med. 2020;34:1447–53. https://doi.org/10.1111/jvim.15793
8. Roura X, Santamarina G, Tabar MD, Francino O, Altet L. Polymerase chain reaction detection of *Bartonella* spp. in dogs from Spain with blood culture-negative infectious endocarditis. J Vet Cardiol. 2018;20:267–75. https://doi.org/10.1016/j.jvc.2018.04.006

Address for correspondence: Edward C. Traver, Institute of Human Virology, 725 W Lombard St, Baltimore, MD 21201, USA; email: etraver@ihv.umaryland.edu

Fatal West Nile Virus Infection in Horse Returning to United Kingdom from Spain, 2022

Mirjam Schilling, Bettina Dunkel, Tobias Floyd, Daniel Hicks, Alex Nunez, Falko Steinbach, Arran J. Folly, Nicholas Johnson

Author affiliations: Animal and Plant Health Agency, Addlestone, UK (M. Schilling, T. Floyd, D. Hicks, A. Nunez, F. Steinbach, A.J. Folly, N. Johnson); Royal Veterinary College, Hatfield, UK (B. Dunkel); University of Surrey School of Veterinary Medicine, Guildford, UK (F. Steinbach)

DOI: https://doi.org/10.3201/eid3002.230690

We report fatal West Nile virus (WNV) infection in a 7-year-old mare returning to the United Kingdom from Spain. Case timeline and clustering of virus sequence with recent WNV isolates suggest that transmission occurred in Andalusía, Spain. Our findings highlight the importance of vaccination for horses traveling to WNV-endemic regions.

A West Nile virus (WNV) outbreak among equids occurred in Andalusia, Spain, in 2020, and subsequent cases were reported in 2021 and 2022 (*1*). Thus far, WNV originating in the United Kingdom has not been detected, and surveillance of birds is used to monitor for possible introduction. WNV was previously detected in the United Kingdom in a horse returning from Cyprus, where WNV circulates seasonally (*2*). Serologic data suggest that <30% of horses in the United Kingdom are currently vaccinated because WNV is not endemic (*3*). The risk factors that predispose horses to developing neurologic disease after WNV infection are unknown.

In November 2022, a 7-year-old mare showing clinical signs of ataxia, hyperesthesia, and reluctance to move was admitted to the Royal Veterinary College Referral Hospital (Hatfield, UK). The mare had just returned to the United Kingdom after 1 month in Andalusia and 2 days of traveling through France. Quantitative reverse transcription PCR (qRT-PCR) performed on a nasopharyngeal swab sample was negative for equine herpesviruses 1 and 4. Because of the mare's travel history and seasonal presence of WNV in Spain, serum was submitted to the Animal and Plant Health Agency for WNV antibody testing. The result of ELISA testing for detection of WNV IgM (IDvet, https://www.innovative-diagnostics.com), indicative of recent infection or vaccination, was

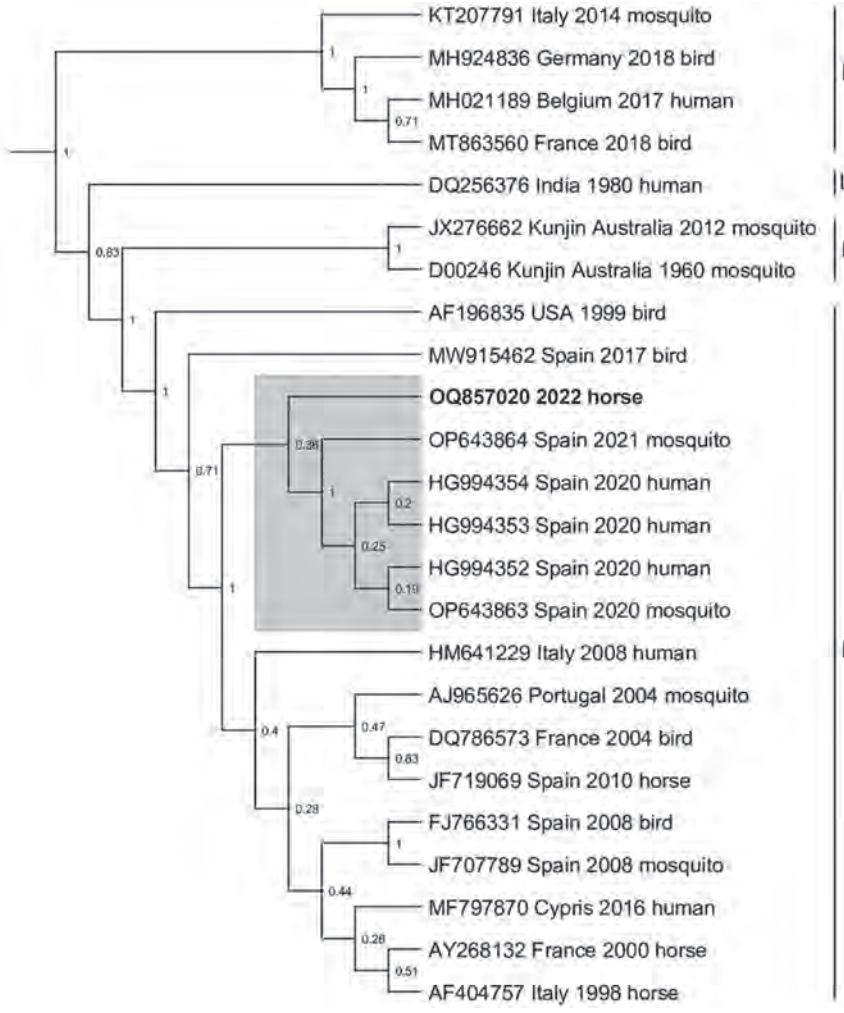

Figure 1. Next-generation sequencing data associated with fatal West Nile virus (WNV) infection in a horse returning to the United Kingdom from Spain, 2022. Bayesian phylogenetic tree analysis of a 624-bp sequence located in the nonstructural 5 gene showed that the strain from the horse (boldface; GenBank accession no. OQ857020) clusters with recent sequences from Andalusia, Spain (gray shading). Next-generation sequencing was conducted on an Illumina MiSeq sequencer (https://www.illumina.com). The sequence was aligned with 23 WNV lineage 1 and 2 reference sequences obtained from GenBank in MEGA version 11.0.13 (https://www.megasoftware.net), and a Bayesian phylogenetic analysis was undertaken in BEAST version 1.10.4 (https://beast.community) using a general time reversible plus invariant sites plus gamma nucleotide substitution model and 10,000,000 Markov chain Monte Carlo generations. Node labels represent posterior probabilities. Accession number, country, year of detection and host species are included for each sequence.

positive. The mare had no record of having received WNV vaccine. WNV-specific qRT-PCR (*4*) failed to detect virus in serum and cerebrospinal fluid samples. After receipt of anti-inflammatories (0.1 mg/kg dexamethasone), the mare's condition improved initially, allowing her discharge from hospital. However, after discharge, her condition deteriorated and she was readmitted to the referral hospital, where she was euthanized because of rapid progression of neurologic signs leading to recumbency.

A full postmortem examination performed under Biosafety Level 3 containment showed no

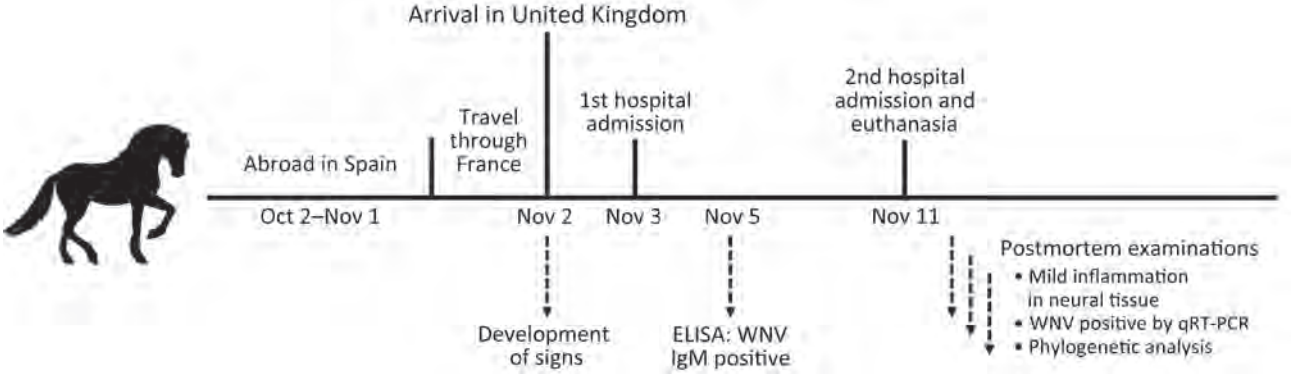

Figure 2. Timeline of events associated with fatal WNV infection in horse returning to the United Kingdom from Spain, 2022. qRT-PCR, quantitative reverse transcription PCR; WNV, West Nile virus.

substantial gross pathology. Histopathologic investigation of the central nervous system (CNS) revealed mild nonsuppurative inflammation, affecting predominantly gray matter of the brainstem and spinal cord, consistent with a viral infection. Microscopic examination of peripheral nervous tissue and a range of viscera (heart, skeletal muscle, lung, liver, kidney, spleen, and submandibular lymph node) revealed no substantial pathologic changes. Immunohistochemical staining with Kunjin virus primary antibodies (nonstructural 1, rabbit; Australian Animal Health Laboratory, https://www.csiro.au/en/about/facilities-collections/acdp) detected small amounts of virus antigen in association with inflammatory foci in the spinal cord only. No specific immunostaining was found elsewhere in the CNS or any other tissues. WNV-specific qRT-PCR detected WNV RNA in brain tissue (mesencephalon, cerebral cortex, and medulla oblongata) and in the spinal cord. A partial genomic sequence was obtained from RNA samples of the spinal cord by next-generation sequencing. The resulting phylogeny showed clustering of the retrieved virus sequence with recent isolates of lineage 1a from mosquitoes and humans in Andalusia (Figure 1) (*5*), suggesting that transmission most likely occurred in Andalusia.

In conclusion, travel history, clinical examination, laboratory testing, and postmortem examination combined indicated an acute WNV infection in this horse (Figure 2). In contrast to cases in birds and some humans, WNV infection in horses seems to be characterized by encephalitic lesions with little associated antigen, occasionally even a discrepancy between distribution of virus antigen and location of lesions (*6*). Although IgM is detectable 4–6 weeks after infection, the low levels of virus in CSF, blood, and tissue are consistent with earlier descriptions of WNV infections in horses (*7*).

Vaccination is strongly advised for all horses traveling to areas where WNV is known to circulate because treatment consists only of symptomatic support, whereas licensed vaccines providing effective protection are available (*8*). In light of the ongoing spread of WNV across the world, an increasing amount of traveling horses are at risk. Veterinary and public health bodies should therefore increase vigilance for this emerging disease and prepare for more WNV infections in the future.

About the Author

Dr. Schilling works for the Vector Borne Diseases Workgroup at the Animal and Plant Health Agency, United Kingdom. Her research interests are arboviruses and virus host interactions.

References

1. García-Bocanegra I, Franco JJ, León CI, Barbero-Moyano J, García-Miña MV, Fernández-Molera V, et al. High exposure of West Nile virus in equid and wild bird populations in Spain following the epidemic outbreak in 2020. Transbound Emerg Dis. 2022;69:3624–36. https://doi.org/10.1111/tbed.14733
2. Fooks AR, Horton DL, Phipps LP, Mansfield KL, McCracken F, Jeffries CL, et al. Suspect West Nile encephalitis in a horse imported into the UK from Europe. Vet Rec Case Rep. 2014;2:e000104. https://doi.org/10.1136/vetreccr-2014-000104
3. Folly AJ, Waller ESL, McCracken F, McElhinney LM, Roberts H, Johnson N. Equine seroprevalence of West Nile virus antibodies in the UK in 2019. Parasit Vectors. 2020;13:596. https://doi.org/10.1186/s13071-020-04481-9
4. Linke S, Ellerbrok H, Niedrig M, Nitsche A, Pauli G. Detection of West Nile virus lineages 1 and 2 by real-time PCR. J Virol Methods. 2007;146:355–8. https://doi.org/10.1016/j.jviromet.2007.05.021
5. Ruiz-López MJ, Muñoz-Chimeno M, Figuerola J, Gavilán AM, Varona S, Cuesta I, et al. Genomic analysis of West Nile virus lineage 1 detected in mosquitoes during the 2020–2021 outbreaks in Andalusia, Spain. Viruses. 2023;15:266. https://doi.org/10.3390/v15020266
6. Cantile C, Del Piero F, Di Guardo G, Arispici M. Pathologic and immunohistochemical findings in naturally occurring West Nile virus infection in horses. Vet Pathol. 2001;38:414–21. https://doi.org/10.1354/vp.38-4-414
7. Angenvoort J, Brault AC, Bowen RA, Groschup MH. West Nile viral infection of equids. Vet Microbiol. 2013;167:168–80. https://doi.org/10.1016/j.vetmic.2013.08.013
8. Ulbert S. West Nile virus vaccines - current situation and future directions. Hum Vaccin Immunother. 2019;15:2337–42. https://doi.org/10.1080/21645515.2019.1621149

Address for correspondence: Mirjam Schilling, Animal and Plant Health Agency, Virology, Woodham Ln, Addlestone KT15 3NB, UK; email: mirjam.schilling@apha.gov.uk

Lymphocytic Choriomeningitis Virus Lineage V in Wood Mice, Germany

Calvin Mehl, Olayide Abraham Adeyemi, Claudia Wylezich,[1] Dirk Höper, Martin Beer, Cornelia Triebenbacher, Gerald Heckel, Rainer G. Ulrich

Author affiliations: Friedrich-Loeffler-Institut, Greifswald-Insel Riems, Germany (C. Mehl, O.A. Adeyemi, C. Wylezich, D. Höper, M. Beer, R.G. Ulrich); German Center for Infection Research, Partner Site Hamburg-Lübeck-Borstel-Riems, Germany (C. Mehl, R.G. Ulrich); Bavarian State Institute for Forest and Forestry, Freising, Germany (C. Triebenbacher); University of Bern, Bern, Switzerland (G. Heckel)

DOI: https://doi.org/10.3201/eid3002.230868

We identified a novel lineage of lymphocytic choriomeningitis virus, tentatively named lineage V, in wood mice (*Apodemus sylvaticus*) from Germany. Wood mouse–derived lymphocytic choriomeningitis virus can be found across a substantially greater range than previously thought. Increased surveillance is needed to determine its geographic range and zoonotic potential.

Lymphocytic choriomeningitis virus (LCMV; species *Mammarenavirus choriomeningitidis*) is a single-stranded RNA virus that has a bisegmented genome and ambisense coding strategy (*1*). LCMV is a zoonotic virus that causes encephalitis, meningitis, and sudden infant death syndrome in humans (*2*,*3*) and callitrichid hepatitis in New World primates (family Callitrichidae) (*4*). According to phylogenetic analysis, LCMV lineages I–IV are recognized. The most common, lineages I and II, are found worldwide (the house mouse, *Mus musculus*, is a reservoir host), whereas lineage III was found in 1 patient in Georgia, USA. Lineage IV was identified by sequencing small (S) RNA segments obtained from wood mice (*Apodemus sylvaticus*) found at 3 sites in southern Spain (*5*). That same study also reported the presence of LCMV antibodies in *M. musculus*, *M. spretus*, and *Rattus norvegicus* (Norway) rats in Spain (*5*). Similarly, LCMV-reactive antibodies have been found in wood mice from Austria (*6*) and in yellow-necked field mice (*Apodemus flavicollis*) and voles from Italy (*7*). LCMV reemerged in Germany in a captive golden lion tamarin (*Leontopithecus rosalia*) and sympatric wild *M. musculus domesticus* mice (*8*). We report the discovery of LCMV RNA in wood mice from Germany.

High-throughput sequencing of pooled brain tissue from *Apodemus* spp. captured in southern Germany revealed the presence of LCMV sequence reads (Appendix, https://wwwnc.cdc.gov/EID/article/30/2/23-0868-App1.pdf). We tested brain tissue samples from each of those animals (4 yellow-necked field mice and 13 wood mice) separately by reverse transcription PCR (*9*). We found LCMV amplification products of the expected length only in 2 wood mouse samples (KS20/3119 and KS20/3122). In addition, we tested 132 rodents and shrews collected during 2005–2018, representing 5 species from the same geographic region in Bavaria, Germany, as the 2 LCMV RNA-positive animals. Those 132 animals were negative for LCMV RNA by using conventional panarenavirus reverse transcription PCR (Appendix Table 1, Figure 1).

We captured all 134 animals (132 rodents and shrews plus 2 LCMV-positive wood mice) near natural forest or reforested areas at an altitude of 366–620 m by using line trapping. We placed traps 2 m apart within lines and 10 m between lines. We trapped animals 1 time per year for 2 consecutive nights during 2005–2018.

We assembled nearly complete sequences of LCMV large (L) and S RNA segments and host mitochondrial cytochrome b DNA from brain tissue of the 2 LCMV-positive wood mice and performed phylogenetic analyses. We deposited LCMV sequences obtained in this study in GenBank (accession nos. OR135709–12). The L (7,144 nt) and S (3,342 nt) sequences contained complete coding regions except for the first ≈55 nt and last ≈18 nt of the L segment and first ≈18 nt and last ≈24 nt of the S segment. For all 3 coding regions examined (L protein, glycoprotein, and nucleocapsid protein), virus sequences from the 2 mice formed a separate monophyletic clade (tentatively named lineage V) that is ancestral to all previously published LCMV sequences (Figure; Appendix Figures 2, 3) and highly divergent at the nucleotide and amino acid sequence levels (Appendix Table 2). Phylogenetic analysis of wood mouse mitochondrial cytochrome b sequences showed that both LCMV-positive animals clustered with *Apodemus sylvaticus* subclade 2b (Appendix Figure 4), the same subclade as the mice from Spain in which LCMV lineage IV was discovered (*5*).

In conclusion, we identified a new LCMV lineage in wood mice from southern Germany. Unlike Dandenong virus, an unclassified mammarenavirus that

[1]Current affiliation: Friedrich-Loeffler-Institut, Greifswald-Insel Riems, Germany and Justus-Liebig-Universität Gießen, Gießen, Germany.

falls within lineage II (both L and S segments), sequences from lineage V constitute their own distinct clade that is basal to other known LCMV lineages. Host mitochondrial DNA sequences indicated the wood mice from Germany belonged to the same clade as those in which LCMV lineage IV was previously identified in Spain. The serologic evidence of LCMV in wood mice from Italy (*7*) and Austria (*6*) combined with LCMV RNA detection in wood mice from Spain (*5*) and this study suggest that wood mouse-derived

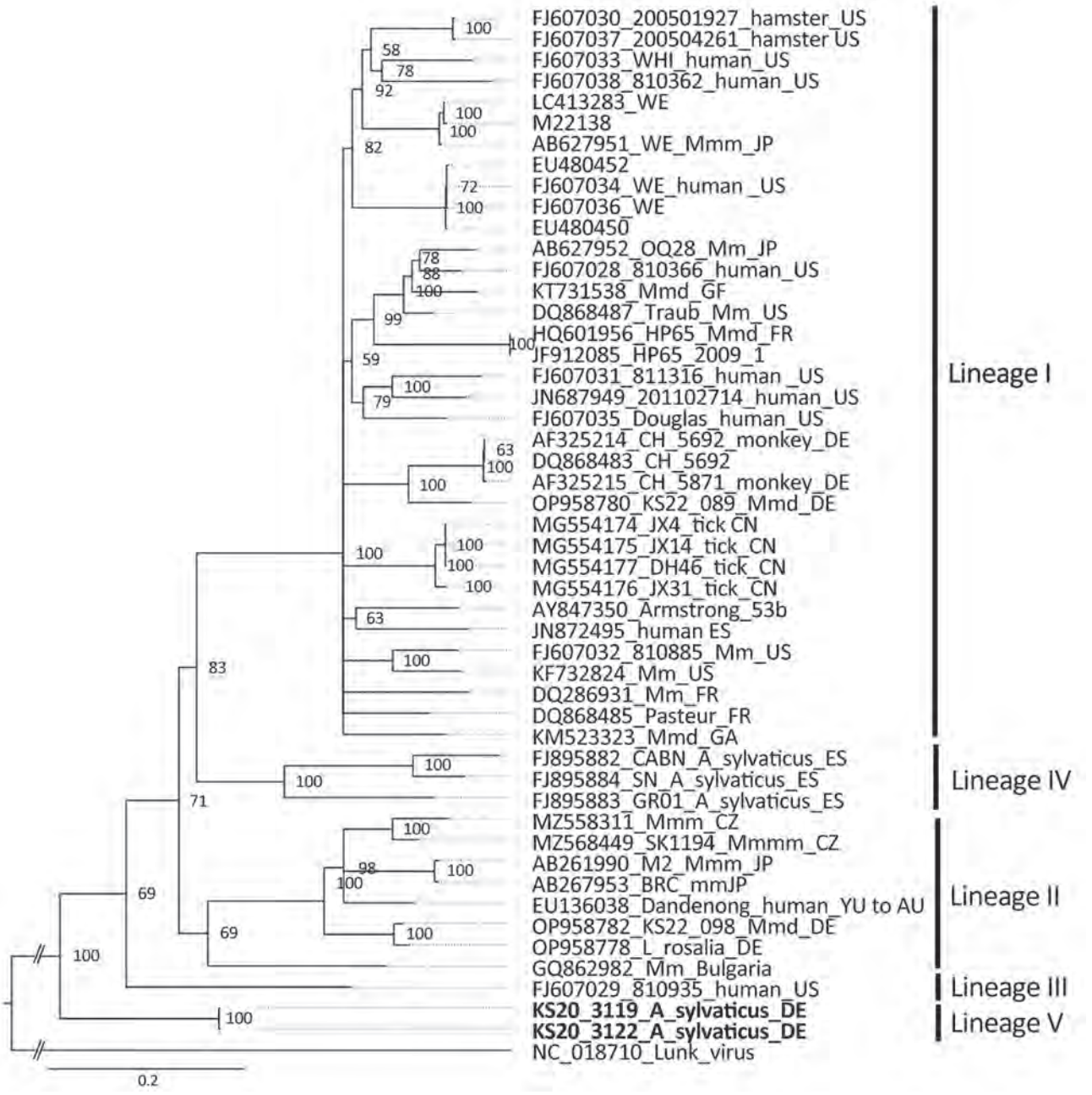

Figure. Phylogenetic analysis of the nucleocapsid protein encoding region of lymphocytic choriomeningitis virus lineage V identified in wood mice, Germany (boldface), and reference sequences. Bayesian inference method was used to analyze the 1,674-nt open reading frame corresponding to codons 1–558 without the stop codon. GenBank accession number, strain name, host species, and country of origin (if known) are shown. Roman numerals I–IV represent the different virus lineages as defined previously (*10*). Lunk virus from *Mus minutoides* mice was used as an outgroup. WE and Armstrong are laboratory strains of lymphocytic choriomeningitis virus. Scale bar indicates nucleotide substitutions per site. Asyl, *Apodemus sylvaticus*; AU, Australia; BG, Bulgaria; CN, China; CZ, Czech Republic; DE, Germany; ES, Spain; FR, France; GA, Gabon; GF, French Guiana; JP, Japan; Mm, *Mus musculus*; Mmm, *M. musculus musculus*; Mmd, *M. musculus domesticus*; SK, Slovakia; US, United States; YU, former Yugoslavia.

LCMV can be found across a substantially greater range than previously thought. Greater surveillance is needed to determine the geographic range and diversity of LCMV in small mammals and the potential infection risk to humans.

Acknowledgments

We thank Sina Nippert, Viola Haring, and Dörte Kaufmann for technical assistance.

The study was funded by the Deutsches Zentrum für Infektionsforschung, thematic translational unit Emerging Infections (grant no. 01.808_00).

About the Author

Mr. Mehl is a doctoral candidate at the Friedrich-Loeffler-Institut in Greifswald-Insel Riems, Germany. His research interests focus on how small mammal ecology, microbiome diversity, and ecotoxicology influence disease ecologies.

References

1. Meyer BJ, de la Torre JC, Southern PJ. Arenaviruses: genomic RNAs, transcription, and replication. Curr Top Microbiol Immunol. 2002;262:139–57. https://doi.org/10.1007/978-3-642-56029-3_6
2. Ackermann R, Stille W, Blumenthal W, Helm EB, Keller K, Baldus O. Syrian hamsters as vectors of lymphocytic choriomeningitis [in German]. Dtsch Med Wochenschr. 1972;97:1725–31. https://doi.org/10.1055/s-0028-1107638
3. Goldwater PN. A mouse zoonotic virus (LCMV): a possible candidate in the causation of SIDS. Med Hypotheses. 2021;158:110735. https://doi.org/10.1016/j.mehy.2021.110735
4. Asper M, Hofmann P, Osmann C, Funk J, Metzger C, Bruns M, et al. First outbreak of callitrichid hepatitis in Germany: genetic characterization of the causative lymphocytic choriomeningitis virus strains. Virology. 2001;284:203–13. https://doi.org/10.1006/viro.2001.0909
5. Ledesma J, Fedele CG, Carro F, Lledó L, Sánchez-Seco MP, Tenorio A, et al. Independent lineage of lymphocytic choriomeningitis virus in wood mice (*Apodemus sylvaticus*), Spain. Emerg Infect Dis. 2009;15:1677–80. https://doi.org/10.3201/eid1510.090563
6. Schmidt S, Essbauer SS, Mayer-Scholl A, Poppert S, Schmidt-Chanasit J, Klempa B, et al. Multiple infections of rodents with zoonotic pathogens in Austria. Vector Borne Zoonotic Dis. 2014;14:467–75. https://doi.org/10.1089/vbz.2013.1504
7. Kallio-Kokko H, Laakkonen J, Rizzoli A, Tagliapietra V, Cattadori I, Perkins SE, et al. Hantavirus and arenavirus antibody prevalence in rodents and humans in Trentino, Northern Italy. Epidemiol Infect. 2006;134:830–6. https://doi.org/10.1017/S0950268805005431
8. Mehl C, Wylezich C, Geiger C, Schauerte N, Mätz-Rensing K, Nesseler A, et al. Reemergence of lymphocytic choriomeningitis mammarenavirus, Germany. Emerg Infect Dis. 2023;29:631–4. https://doi.org/10.3201/eid2903.221822
9. Vieth S, Drosten C, Lenz O, Vincent M, Omilabu S, Hass M, et al. RT-PCR assay for detection of Lassa virus and related Old World arenaviruses targeting the L gene. Trans R Soc Trop Med Hyg. 2007;101:1253–64. https://doi.org/10.1016/j.trstmh.2005.03.018
10. Albariño CG, Palacios G, Khristova ML, Erickson BR, Carroll SA, Comer JA, et al. High diversity and ancient common ancestry of lymphocytic choriomeningitis virus. Emerg Infect Dis. 2010;16:1093–100. https://doi.org/10.3201/eid1607.091902

Address for correspondence: Rainer Ulrich, Friedrich-Loeffler-Institut, Südufer 10, Greifswald-Insel Riems 17493, Germany; email: rainer.ulrich@fli.de

No Evidence for Clade I Monkeypox Virus Circulation, Belgium

Laurens Liesenborghs,[1] Jasmine Coppens,[1] Christophe Van Dijck, Isabel Brosius, Irith De Baetselier, Koen Vercauteren,[2] Marjan Van Esbroeck[2]

Author affiliations: Institute of Tropical Medicine, Antwerp, Belgium (L. Liesenborghs, J. Coppens, C. Van Dijck, I. Brosius, I. De Baetselier, K. Vercauteren, M. Van Esbroeck); Katholieke Universiteit Leuven, Leuven, Belgium (L. Liesenborghs, C. Van Dijck)

DOI: https://doi.org/10.3201/eid3002.231746

To the Editor: As professionals involved in the mpox response in Belgium, we read with concern the report by Kibungu et al. on a clade I mpox outbreak linked to sexual transmission in the Democratic Republic of the Congo (DRC), in March 2023 (*1*). The authors and the World Health Organization (WHO) reported that the male index case had a sexual encounter with another man in Belgium before traveling to the DRC, where he developed symptoms the day he arrived and tested positive for monkeypox virus (MPXV) 8 days later (*2*). By that timeline, WHO suggested, the man likely was infected in Belgium. This conclusion raised concerns about clade I MPXV circulation within sexual networks in Belgium and Europe, regions highly affected by the 2022 clade IIb outbreak.

Mpox diagnoses in Belgium were mostly made by using a PCR that does not distinguish between clades (*3*). After the aforementioned reports, we retested stored samples from 296 mpox patients, 37% of all mpox patients in Belgium, by using a clade I–specific PCR (*4*). None tested positive.

In addition, from October 2022 onward, few mpox cases were reported in Belgium; none occurred in the 6 weeks before the DRC cluster started. Also, in the 9 months after the DRC outbreak, only 4 mpox cases were detected in Belgium, the earliest of which was diagnosed 12 weeks after the DRC index case (L. Liesenborghs et al., unpub. data). Moreover, during January–November 2023, we screened 2,415 men visiting our sexual health clinic using an MPXV-specific PCR as part of ongoing surveillance to detect undiagnosed or asymptomatic infections (*5*). We detected only 1 presymptomatic clade IIb MPXV infection.

On the basis of this information, we have no indications that clade I MPXV has been circulating in Belgium. However, sustained vigilance, clade differentiation, and timely outbreak investigations remain crucial to halting potential spread of clade I MPXV through sexual transmission.

[1]These first authors contributed equally to this article.

[2]These last authors contributed equally to this article.

Acknowledgments

This project was funded in part by the Research Foundation Flanders (grant no. G096222N to L.L.); C.V.D. is a fellow of the Research Foundation Flanders (grant no. 12B1M24N).

References

1. Kibungu EM, Vakaniaki EH, Kinganda-Lusamaki E, Kalonji-Mukendi T, Pukuta E, Hoff NA, et al.; International Mpox Research Consortium. Clade I–associated mpox cases associated with sexual contact, the Democratic Republic of the Congo. Emerg Infect Dis. 2024;30:172–6. https://doi.org/10.3201/eid3001.231164
2. World Health Organization. Mpox (monkeypox)—Democratic Republic of the Congo [cited 2023 Dec 21]. https://www.who.int/emergencies/disease-outbreak-news/item/2023-DON493
3. Coppens J, Vanroye F, Brosius I, Liesenborghs L, van Henten S, Vanbaelen T, et al.; ITM MPX study group. Alternative sampling specimens for the molecular detection of mpox (formerly monkeypox) virus. J Clin Virol. 2023;159:105372. PubMed https://doi.org/10.1016/j.jcv.2022.105372
4. Li Y, Zhao H, Wilkins K, Hughes C, Damon IK. Real-time PCR assays for the specific detection of monkeypox virus West African and Congo Basin strain DNA. J Virol Methods. 2010;169:223–7. https://doi.org/10.1016/j.jviromet.2010.07.012
5. Van Dijck C, De Baetselier I, Kenyon C, Liesenborghs L, Vercauteren K, Van Esbroeck M, et al.; ITM Monkeypox Study Group. Mpox screening in high-risk populations finds no asymptomatic cases. Lancet Microbe. 2023;4:e132–3. PubMed https://doi.org/10.1016/S2666-5247(22)00357-3

Address for correspondence: Laurens Liesenborghs, Institute of Tropical Medicine, Nationalestraat 155, 2000 Antwerp, Belgium; email: lliesenborghs@itg.be

Nonnegligible Seroprevalence and Predictors of Murine Typhus, Japan

Kentaro Iwata

Author affiliation: Kobe University Hospital, Kobe, Japan

DOI: https://doi.org/10.3201/eid3002.230827

To the Editor: I was impressed by the recent publication by Aita et al. who reported a surprisingly high seroprevalence rate for *Rickettsia typhi* within resident populations on Honshu Island, Japan (*1*). The authors pointed out the possibility of murine typhus reemergence in Japan, where the disease has been reported only sporadically (*2*). However, the conclusions might be premature because the study was cross-sectional, and only 1 timepoint was evaluated. Many cases of murine typhus could have occurred in the distant past, which might not be reflected in this type of study. A previous study in Spain showed a high incidence rate in patients who were much younger (mean age of ≈46 years) (*3*) than those reported in this study (mean age of 67 years). A study in Greece showed frequent epidemiologic links to flea exposure (*4*), but the study in Japan did not investigate this apparent risk factor. I do not believe that age-related differences in flea exposures exist in Japan; hence, it is likely that exposures might have occurred in the past, when persons in Japan had a lower standard of hygiene. According to another study, the median half-life of *R. typhi* IgG was 177 days, and the median IgG titer was 800 at day 365 postinfection, suggesting long-lasting seropositivity (*5*). Therefore, the relatively stringent cutoff value of *R. typhi* serology in this study (*1*) could have overestimated the prevalence. To demonstrate that murine typhus is indeed a reemerging disease in Japan, further actual cases in Japan need to be identified, or similar seroprevalence studies should be repeated in other regions to determine trends in *R. typhi* seropositivity.

References

1. Aita T, Sando E, Katoh S, Hamaguchi S, Fujita H, Kurita N. Nonnegligible seroprevalence and predictors of murine typhus, Japan. Emerg Infect Dis. 2023;29:1438–42. https://doi.org/10.3201/eid2907.230037
2. Sakaguchi S, Sato I, Muguruma H, Kawano H, Kusuhara Y, Yano S, et al. Reemerging murine typhus, Japan. Emerg Infect Dis. 2004;10:964–5. https://doi.org/10.3201/eid1005.030697
3. Rodríguez-Alonso B, Almeida H, Alonso-Sardón M, Velasco-Tirado V, Robaina Bordón JM, Carranza Rodríguez C, et al. Murine typhus. How does it affect us in the 21st century? The epidemiology of inpatients in Spain (1997–2015). Int J Infect Dis. 2020;96:165–71. https://doi.org/10.1016/j.ijid.2020.04.054
4. Labropoulou S, Charvalos E, Chatzipanagiotou S, Ioannidis A, Sylignakis P, Taka S, et al. Sunbathing, a possible risk factor of murine typhus infection in Greece. PLoS Negl Trop Dis. 2021;15:e0009186. https://doi.org/10.1371/journal.pntd.0009186
5. Phakhounthong K, Mukaka M, Dittrich S, Tanganuchitcharnchai A, Day NPJ, White LJ, et al. The temporal dynamics of humoral immunity to *Rickettsia typhi* infection in murine typhus patients. Clin Microbiol Infect. 2020;26:781.e9–16. https://doi.org/10.1016/j.cmi.2019.10.022

Address for correspondence: Kentaro Iwata, Professor of Infectious Diseases Therapeutics, Kobe University Hospital, Kusunokicho 7-5-2, Chuoku Kobe, Hyogo 6500017, Japan; email: kentaroiwata1969@gmail.com

Tetsuro Aita, Eiichiro Sando, Shungo Katoh, Sugihiro Hamaguchi, Hiromi Fujita, Noriaki Kurita

Author affiliations: Fukushima Medical University, Fukushima, Japan (T. Aita, E. Sando, S. Katoh, S. Hamaguchi, N. Kurita); Kita-Fukushima Medical Center, Fukushima (E. Sando, S. Katoh, H. Fujita)

DOI: https://doi.org/10.3201/eid3002.231465

In Response: We thank Dr. Iwata (*1*) for his remarks regarding our study of seroprevalence and predictors of murine typhus in Japan (*2*). In reference to long-term seropositivity, high seroprevalence of *Rickettsia typhi* might reflect distant past murine typhus (MT) infections rather than recent infections (*2*). We acknowledge the significance of this limitation in interpreting our results, which we first addressed in a preprint of the article (T. Aita et al., unpub. data, https://doi.org/10.1101/2023.01.12.2328449). Nonetheless, we posit that *R. typhi* seroprevalence would include some persons who have recently experienced MT. First, participants with remarkably high *R. typhi* IgG titers probably had recent MT infections, because *R. typhi* IgG titers generally undergo a continuous postinfection decline in diagnostic serologic assays. The percentage of persons with antibody titers of ≥1:3,200 in an indirect immunofluorescence assay was ≈85% at 4 weeks postinfection but decreased to ≈25% within 1 year (*3*). In addition, antibody titers continued to decrease over 3 years postinfection in an

enzyme-linked immunosorbent assay (*4*). In our study, using an indirect immunoperoxidase-based assay, 20 participants exhibited notably high antibody titers (1:1,280 to ≥1:40,960). Second, despite raising the diagnostic cutoff from 1:40 to 1:160, the preeminence of *R. typhi* seroprevalence persisted over that of *Orientia tsutsugamushi* (*2*), the causative agent of scrub typhus, which is the most frequent endemic rickettsiosis in Japan. Thus, excluding many persons with distant past infections did not influence the study's conclusion that *R. typhi* seroprevalence was significantly higher than that of *O. tsutsugamushi*. Therefore, the higher *R. typhi* seroprevalence indicates not only prolonged seropositivity but also recent *R. typhi* infections.

In conclusion, although Dr. Iwata's commentary is pivotal for a more precise interpretation of our results, our study indicates the occurrence of recent MT cases in Japan. We aim to elucidate this potential MT reemergence by conducting a case-based prospective study.

References

1. Iwata K. Nonnegligible seroprevalence and predictors of murine typhus, Japan. Emerg Infect Dis. 2024;30:403. https://doi.org/10.3201/eid3002.230827
2. Aita T, Sando E, Katoh S, Hamaguchi S, Fujita H, Kurita N. Nonnegligible seroprevalence and predictors of murine typhus, Japan. Emerg Infect Dis. 2023;29:1438–42. https://doi.org/10.3201/eid2907.230037
3. Phakhounthong K, Mukaka M, Dittrich S, Tanganuchitcharnchai A, Day NPJ, White LJ, et al. The temporal dynamics of humoral immunity to *Rickettsia typhi* infection in murine typhus patients. Clin Microbiol Infect. 2020;26:781.e9–16. https://doi.org/10.1016/j.cmi.2019.10.022
4. Halle S, Dasch GA. Use of a sensitive microplate enzyme-linked immunosorbent assay in a retrospective serological analysis of a laboratory population at risk to infection with typhus group rickettsiae. J Clin Microbiol. 1980;12:343–50. https://doi.org/10.1128/jcm.12.3.343-350.1980

Address for correspondence: Eiichiro Sando, Department of General Internal Medicine and Clinical Infectious Diseases, Fukushima Medical University, 1 Hikarigaoka, Fukushima city, Fukushima, 960-1295, Japan; email: e-sando@fmu.ac.jp

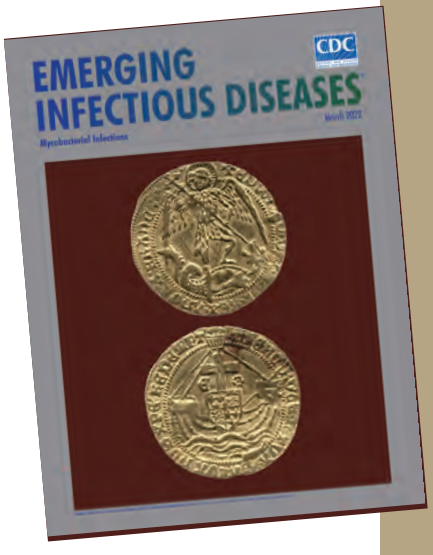

Originally published in March 2022

etymologia revisited

Schizophyllum commune

[skiz-of′-ĭ-ləm kom′-yoon]

Schizophyllum commune, or split-gill mushroom, is an environmental, wood-rotting basidiomycetous fungus. *Schizophyllum* is derived from "*Schíza*" meaning split because of the appearance of radial, centrally split, gill like folds; "*commune*" means common or shared ownership or ubiquitous. Swedish mycologist, Elias Magnus Fries (1794–1878), the Linnaeus of Mycology, assigned the scientific name in 1815. German mycologist Hans Kniep in 1930 discovered its sexual reproduction by consorting and recombining genomes with any one of numerous compatible mates (currently >2,800).

References

1. Chowdhary A, Kathuria S, Agarwal K, Meis JF. Recognizing filamentous basidiomycetes as agents of human disease: a review. Med Mycol. 2014;52: 782–97. https://doi.org/10.1093/mmy/myu047
2. Cooke WB. The genus *Schizophyllum*. Mycologia. 1961;53:575–99. https://doi.org/10.1080/00275514.1961.12017987
3. Greer DL. Basidiomycetes as agents of human infections: a review. Mycopathologia. 1978;65:133–9. https://doi.org/10.1007/BF00447184
4. O'Reilly P. *Schizophyllum commune*, split gill fungus, 2016 [cited 2021 Aug 23]. https://www.first-nature.com/fungi/schizophyllum-commune.php
5. Raper CA, Fowler TJ. Why study *Schizophyllum*? Fungal Genet Rep. 2004;51:30–6. https://doi.org/10.4148/1941-4765.1142

https//wwwnc.cdc.gov/eid/article/28/3/et-2803_article

To Catch a Virus, 2nd Edition

John Booss, Marie Louise Landry, Marilyn J. August; ASM Press, Washington, DC, USA, 2022; ISBN-10: 1683673735; ISBN-13: 978-1683673736; Pages: 416; Price: US $37.00 (E-book), US $45.95 (paperback)

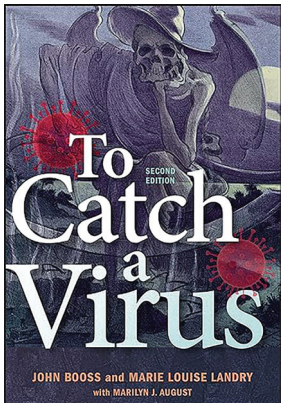

The first edition of To Catch a Virus was published in 2013. Why is a second edition needed so soon? Much has happened in virology over the past 10 years; the most notable occurrence was the COVID-19 pandemic, for which an entire new chapter was added. The title is a nod to the 1955 Hitchcock film To Catch a Thief. Rather than each chapter focusing on 1 virus or related family, the narrative is centered around discovery and diagnostics. Yellow fever is used to highlight the birth of virology and discovery of viruses as filterable agents. Polio, rabies, and influenza illustrate the use of animal models in research. Smallpox is used to elucidate the complex human immune system.

Cellular pathology is shown for several viruses; reading about the move from light microscopy to electron microscopy is riveting. Discovery of the cytopathogenic effect was a turning point in virology, leading to diagnostic use of tissue culture assays; the momentous work on poliovirus is highlighted by tissue culture assay development. Many viruses were discovered starting in the 1950s. As coined by Robert J. Huebner, the "torrent of viral isolates" was the "virologist's dilemma": which isolates are associated with disease?

Those and other discoveries led to advances in diagnostics and patient management. In particular, HIV/AIDS research was transformative. Nucleic acid extraction, amplification, and measurements are now routine automated laboratory processes. Sequencing and bioinformatics methods are also now embedded in clinical and public health laboratories. The astonishing rapidity by which SARS-CoV-2 was discovered and then tracked by those techniques was breathtaking. Within 2 weeks of the first international notice of COVID-19 in December 2019, the entire SARS-CoV-2 genome sequence was posted online. Within 10 months, clinical trials evaluating the Pfizer-BioNTech mRNA vaccine showed 95% effectiveness. The story of the eventual discovery of the hepatitis B virus and routine detection by double diffusion in agar, electron microscopy, radioimmunoassay, and enzyme immunoassay/ELISA is fascinating to read.

Many historical figures are presented throughout the book. For example, the husband-and-wife team, Werner and Gertrude Henle, were productive scientists in virology, known for their development of the first influenza vaccine, but who also worked with mumps and Epstein-Barr viruses. At the start of the COVID-19 pandemic, Dr. Li Wenliang sent a warning to colleagues regarding what he had seen clinically before the government of China had acknowledged any cases. He was forced to sign a confession that declared he had made false statements. He returned to work at Wuhan Central Hospital, contracted COVID-19, and died on February 7, 2021. He was later exonerated.

The book is well referenced; the appendix has a useful timeline for each chapter. As early as 1957, Robert J. Huebner stated, "the virologist must be just as much an epidemiologist and clinician when studying the effect of prevalent nonfatal viruses in man as he is a well-grounded experimentalist or pathologist when studying similar effects in mice." This book will appeal to virologists, microbiologists, clinicians, epidemiologists, other public health practitioners, and anyone who has an interest in the history of science or medicine. The book provides the history of virology, a dramatic story worth reading.

Richard N. Danila

Author affiliation: Retired, St. Paul, Minnesota, USA

DOI: https://doi.org/10.3201/eid3002.231576

Address for correspondence: Richard N. Danila, 1398 Midway Pkwy, St. Paul, MN 55108, USA; email: richard.danila55@gmail.com

Karl Bitter (1867–1915), *Spirit of Transportation* (1895) relief sculpture. William H. Gray III 30th Street Station (moved from Broad Street Station), Philadelphia, Pennsylvania, United States. Craig Jack Photographic/Almay Stock Photo.

The Spirit of Transportation in a Connected World

Nkuchia M. M'ikanatha, Byron Breedlove, David P. Welliver

In early 2020, concerns about the spread of SARS-CoV-2 halted all but essential travel, causing bustling seaports, airports, and railroad stations around the world to go quiet. The same scenario played out at the Philadelphia 30th Street Station, recently renamed the William H. Gray III 30th Street Station. That busy train station is the home of *Spirit of Transportation,* an exquisitely detailed 30-foot relief sculpture that has been displayed there since 1933. Completed in 1895 by Karl Bitter, the 3-dimensional work celebrates a triumphant march into modernity, depicted as a procession accompanying a carriage pulled by gallant horses. Leading the way are youths carrying representations of various modes of travel: train, ship, and—carried by the youngest child—a model of a futuristic airship. The Spirit herself, in the middle, is riding on an elaborate carriage trailed by a wagon pulled by uncooperative oxen. As Bitter's sculpture shows, transportation enables movement of people and cargo, including animals, via various vessels by land, sea, or air. Such connectivity, however, facilitates (usually unintentionally) the spread of disease-causing microbes, including emerging pathogens.

Bitter was born in 1867 in Vienna, Austria, where he studied at various institutions, including the Academy of Painting and Sculpture. He worked as an assistant to the sculptor Joseph Kaffsack, and that experience triggered his interest in architectural decorative art. In 1889, Bitter immigrated to New York, New York, where he was recruited by Richard Morris Hunt, a leading Beaux-Arts architect. They worked on various projects, such as the Administration Building exhibits for the 1893 World's Fair in Chicago

Author affiliations: Pennsylvania Department of Health, Harrisburg, Pennsylvania, USA (N.M. M'ikanantha); Centers for Disease Control and Prevention, Atlanta, Georgia, USA (B. Breedlove); Clarific Services, Rochester, Minnesota, USA (D.P. Welliver).

DOI: https://doi.org/10.3202/eid3002.AC3002

(World's Columbian Exposition). Other collaborations included decorations for the Biltmore House on the Biltmore Estate near Asheville, North Carolina—a life-size bronze fountain sculpture of a boy with geese is a prominent example.

In later years, Bitter's work shifted away from naturalism to a modernist tone inspired by Greek and Viennese elements. Notable examples are the 4 allegorical muses on the façade of New York's Metropolitan Museum of Art along 5th Avenue—the figures were carved from Indiana limestone to represent Sculpture, Painting, Architecture, and Music. Bitter served as the sculpture director for the 1901 Pan-American Exposition in Buffalo, New York, and the 1915 Panama-Pacific Exposition in San Francisco, California. His awards included the silver medal at the 1900 Paris Exposition and the gold medal at the 1904 Saint Louis Exposition. He was also a member of prestigious professional societies, including the American Academy of Arts and Letters.

In his book describing the 1901 Exposition, Professor Kerry S. Grant, former dean of the College of Arts and Sciences at the State University of New York at Buffalo, offers this perspective: "[Bitter] fervently believed that the decorative arts should do more than merely please the senses. They should also convey the purpose of the Exposition." *Abundance*, a model for the Pulitzer Fountain in front of the Plaza Hotel, at 5th Avenue and 59th Streets in New York, was Bitter's last sculpture. Bitter died on April 11, 1915, shortly after he was struck by a car as he left the Metropolitan Opera House. He was eulogized by the National Academy of Design as an adopted member honored for "representing American ideals in sculpture."

Spirit of Transportation embodies the human quest to overcome geographic barriers, culminating with the arrival of air travel. Envisaged in the hands of the youngest boy leading the Spirit, that advancement now enables an individual to move from one location on the globe to another with astonishing speed. Before the still lingering coronavirus pandemic COVID-19, the International Civil Aviation Organization estimated that 100,000 commercial flights took off and landed daily worldwide, carrying more than 12 million passengers.

Although rapid transportation has expedited travel around the world, it has also expedited movement of pathogens. Global connectivity through air and other modes of transportation enables the rapid spread of emerging infectious diseases. For instance, airline travel introduced both SARS-CoV and SARS-CoV-2 to various regions of the world, and the recent emergence of Zika virus and its subsequent spread to other regions was fueled by international travel. The movement of humans or animals can lead to transmission of other vectorborne pathogens reported in this month's issue. For example, the World Health Organization Collaborative Center for Rickettsial Diseases at Marseille, France, documented 32 cases of murine typhus among travelers returning to France from different regions during 2008–2010. S.L. Hills and colleagues reported 6 cases of travel-associated tick-borne encephalitis in the United States during 2010–2020. In addition, transportation of domesticated animals—for example, moving horses infected with the West Nile Virus—can enable emergence or reemergence of vectorborne pathogens. What is more, transportation of companion animals can equally enable the spread of zoonotic pathogens, as in the recent bearded dragon–associated *Salmonella* Vitkin outbreak reported by the Centers for Disease Control and Prevention.

International travel may also accelerate the spread of antimicrobial resistance in foodborne pathogens and drug-resistant sexually transmitted pathogens. Moreover, unvaccinated travelers have been associated with the reintroduction of measles in countries where the disease had previously been eliminated.

Sea transportation is associated with the spread of diseases within and across countries. In 1991, after Latin America had been cholera free for a century, a ship from a cholera-endemic area introduced the disease into Peru, igniting a massive epidemic (1991−1994) that resulted in more than 1 million infections and 9,600 deaths in the Western Hemisphere.

Although modern transportation has, in a sense, dissolved geographic barriers and ushered in globalization, it has inadvertently multiplied opportunities for the spread of pathogens. Measures such as vaccination to prevent typhoid, prophylaxis for malaria, screening of travelers, and isolation of sick passengers can help reduce travel-associated diseases. The Centers for Disease Control and Prevention's *CDC Yellow Book: Health Information for International Travel* offers practical evidence-based guidelines for making travel safer. In addition, the International Society for Travel Medicine provides a convenient online clinic directory for pretravel and posttravel consultation. Embracing the *Spirit of Transportation* in a connected world means welcoming innovations in transportation—as Bitter's sculpture illustrates—while simultaneously mitigating, to the extent possible, travel-associated infections.

Bibliography

1. Angelo KM, Gastañaduy PA, Walker AT, Patel M, Reef S, Lee CV, et al. Spread of measles in Europe and implications for US travelers. Pediatrics. 2019;144:e20190414. https://doi.org/10.1542/peds.2019-0414
2. Biltmore Company. Boy Stealing Geese [cited 2023 April 19] https://www.biltmore.com/blog/parkers-favorites-in-biltmore-house
3. Guthmann JP. Epidemic cholera in Latin America: spread and routes of transmission. J Trop Med Hyg. 1995;98:419–27.
4. Columbia University Digital Library Collection. No. 139–Group for Administration Building—Carl Bitter, Sculptor. Statuary for World's Columbian Exposition, Chicago [cited 2023 Apr 19]. https://dlc.library.columbia.edu/catalog/cul:2z34tmpj00
5. European Centre for Disease Prevention and Control. Zika virus disease—annual epidemiological report for 2018 [cited 2023 May 22]. https://www.ecdc.europa.eu/en/publications-data/zika-virus-disease-annual-epidemiological-report-2018
6. EverGreene. Karl Bitter's façade sculptures. Metropolitan Museum of Art, New York, New York [cited 2024 Jan 11]. https://evergreene.com/projects/bitters-facade-sculptures
7. Findlater A, Bogoch II. Human mobility and the global spread of infectious diseases: a focus on air travel. Trends Parasitol. 2018;34:772–83. 10.1016/j.pt.2018.07.004 https://doi.org/10.1016/j.pt.2018.07.004
8. Grant KS, Seiner WH. The Rainbow City: celebrating light, color, and architecture at the Pan-American Exposition, Buffalo 1901. Buffalo (NY): Canisius College Press; 2001.
9. Hills SL, Broussard KR, Broyhill JC, Shastry LG, Cossaboom CM, White JL, et al. Tick-borne encephalitis among US travellers, 2010-20. J Travel Med. 2022;29:taab167. https://doi.org/10.1093/jtm/taab167
10. Matteelli A, Carosi G. Sexually transmitted diseases in travelers. Clin Infect Dis. 2001;32:1063–7. https://doi.org/10.1086/319607
11. Morens DM, Folkers GK, Fauci AS. The challenge of emerging and re-emerging infectious diseases. Nature. 2004;430:242–9. https://doi.org/10.1038/nature02759
12. Smithsonian Archives of American Art. Karl Theodore Francis Bitter papers, 1887–circa 1977 [cited 2024 Jan 11]. https://www.aaa.si.edu/collections/karl-theodore-francis-bitter-papers-8889/biographical-note
13. New York City Public Art. Pulitzer Fountain, 1914−1916 [cited 2023 Apr 19]. http://www.blueofthesky.com/publicart/works/pulitzer.htm
14. Olsen SJ, Chang HL, Cheung TYY, Tang AFY, Fisk TL, Ooi SPL, et al. Transmission of the severe acute respiratory syndrome on aircraft. N Engl J Med. 2003;349:2416–22. https://doi.org/10.1056/NEJMoa031349
15. Porse CC, Messenger S, Vugia DJ, Jilek W, Salas M, Watt J, et al. Travel-associated Zika cases and threat of local transmission during global outbreak, California, USA. Emerg Infect Dis. 2018;24:1626–32. https://doi.org/10.3201/eid2409.180203
16. Tien V, Punjabi C, Holubar MK. Antimicrobial resistance in sexually transmitted infections. J Travel Med. 2020;27:taz101. https://doi.org/10.1093/jtm/taz101
17. Timoney PJ. Infectious diseases and international movement of horses. Equine Infectious Diseases. 2014; 544–51.e1.
18. United Nations. Department of Economic and Social Affairs Sustainable Development. International Civil Aviation Organization (ICAO) [cited 2024 Jan 11]. https://sdgs.un.org/un-system-sdg-implementation/international-civil-aviation-organization-icao-49514
19. Walter G, Botelho-Nevers E, Socolovschi C, Raoult D, Parola P. Murine typhus in returned travelers: a report of thirty-two cases. Am J Trop Med Hyg. 2012; 86:1049–53. https://doi.org/10.4269/ajtmh.2012.11-0794

Address for correspondence: Nkuchia M. M'ikanatha, Pennsylvania Department of Health, Division of Infectious Disease Epidemiology, Health and Welfare Building, Rm 933, 7th and Forster St, Harrisburg, PA 17120, USA; email: nmikanatha@pa.gov, nmm84@psu.edu

EMERGING INFECTIOUS DISEASES®

Upcoming • March 2024
Tuberculosis and Other Mycobacteria

- Systematic Review and Molecular Epidemiology of Underreported Emerging Zoonotic Pathogen Streptococcus suis, Europe
- Expansion of Neisseria meningitidis Serogroup C Clonal Complex 10217 during 2019 Meningitis Outbreak, Burkina Faso
- Population-Based Evaluation Vaccine Effectiveness against SARS-CoV-2 Infection, Severe Illness, and Death, Taiwan
- Microsporidia (Encephalitozoon cuniculi) in Patients with Degenerative Hip and Knee Disease, Czech Republic
- Estimates of Incidence and Predictors of Fatiguing Illness after SARS-CoV-2 Infection
- Highly Pathogenic Avian Influenza A(H5N1) Virus Clade 2.3.4.4b in Domestic Ducks, Indonesia, 2022
- Biphasic MERS-CoV Incidence in Nomadic Dromedaries with Putative Transmission to Humans, Kenya, 2022–2023
- Potentially Zoonotic Enteric Infections in Cameroon Gorillas and Tanzania Chimpanzees
- Betacoronavirus Outbreak, São Paulo, Brazil, Fall 2023
- Detection of Anopheles stephensi Mosquitos through Molecular Surveillance, Ghana
- Spatial Analysis of Drug-Susceptible and Multidrug-Resistant Cases of Tuberculosis, Ho Chi Minh City, Vietnam, 2020–2023
- Systematic Review of Scales for Measuring Infectious Disease–Related Stigma
- Newly Identified Mycobacterium africanum Lineage 10, Central Africa

Complete list of articles in the March issue at https://wwwnc.cdc.gov/eid/#issue-306

Earning CME Credit

To obtain credit, you should first read the journal article. After reading the article, you should be able to answer the following, related, multiple-choice questions. To complete the questions (with a minimum 75% passing score) and earn continuing medical education (CME) credit, please go to http://www.medscape.org/journal/eid. Credit cannot be obtained for tests completed on paper, although you may use the worksheet below to keep a record of your answers.

You must be a registered user on http://www.medscape.org. If you are not registered on http://www.medscape.org, please click on the "Register" link on the right hand side of the website.

Only one answer is correct for each question. Once you successfully answer all post-test questions, you will be able to view and/or print your certificate. For questions regarding this activity, contact the accredited provider, CME@medscape.net. For technical assistance, contact CME@medscape.net. American Medical Association's Physician's Recognition Award (AMA PRA) credits are accepted in the US as evidence of participation in CME activities. For further information on this award, please go to https://www.ama-assn.org. The AMA has determined that physicians not licensed in the US who participate in this CME activity are eligible for AMA PRA Category 1 Credits™. Through agreements that the AMA has made with agencies in some countries, AMA PRA credit may be acceptable as evidence of participation in CME activities. If you are not licensed in the US, please complete the questions online, print the AMA PRA CME credit certificate, and present it to your national medical association for review.

Article Title

Multicenter Retrospective Study of Invasive Fusariosis in Intensive Care Units, France

CME Questions

1. Which of the following statements regarding the bseline data of the current cohort in the study by Demonchy and colleagues is most accurate?

A. The median age of patients was 83 years
B. 80% of patients were immunocompromised
C. 4% of patients had active hematologic malignancy
D. 12% of patients had recent hematopoietic stem cell transplantation

2. Which of the following complications was most common among patients with IF in the current study?

A. Severe acute kidney injury
B. Need for renal replacement therapy
C. Severe anemia with hemoglobin 7 g/dL
D. Respiratory failure requiring mechanical ventilation

3. Which of the following methods was one of the least common for mycological diagnosis in the current study?

A. Sinus aspirate culture
B. Blood culture
C. Skin biopsy
D. Sputum culture

4. What was the most common risk factor for mortality associated with IF in the current study?

A. Higher Sequential Organ Failure Assessment (SOFA) score
B. Age > 70 years
C. Failure to apply antifungal prophylaxis
D. Need for oxygen therapy

Earning CME Credit

To obtain credit, you should first read the journal article. After reading the article, you should be able to answer the following, related, multiple-choice questions. To complete the questions (with a minimum 75% passing score) and earn continuing medical education (CME) credit, please go to http://www.medscape.org/journal/eid. Credit cannot be obtained for tests completed on paper, although you may use the worksheet below to keep a record of your answers.

You must be a registered user on http://www.medscape.org. If you are not registered on http://www.medscape.org, please click on the "Register" link on the right hand side of the website.

Only one answer is correct for each question. Once you successfully answer all post-test questions, you will be able to view and/or print your certificate. For questions regarding this activity, contact the accredited provider, CME@medscape.net. For technical assistance, contact CME@medscape.net. American Medical Association's Physician's Recognition Award (AMA PRA) credits are accepted in the US as evidence of participation in CME activities. For further information on this award, please go to https://www.ama-assn.org. The AMA has determined that physicians not licensed in the US who participate in this CME activity are eligible for AMA PRA Category 1 Credits™. Through agreements that the AMA has made with agencies in some countries, AMA PRA credit may be acceptable as evidence of participation in CME activities. If you are not licensed in the US, please complete the questions online, print the AMA PRA CME credit certificate, and present it to your national medical association for review.

Article Title

Prevalence of SARS-CoV-2 Infection among Children and Adults in 15 US Communities, 2021

CME Questions

1. What was the overall rate of seropositivity against SARS-CoV-2 in the current community-based study?

A. 3.1%
B. 12.4%
C. 35.2%
D. 51.9%

2. Which of the following trends in seropositivity against SARS-CoV-2 in the current study was most significant?

A. Higher rates in Black vs White individuals
B. Higher rates among younger vs older adults
C. Higher rates among women vs men
D. Higher rates among individuals with low income vs middle/high income

3.Which of the following statements regarding positive polymerase chain reaction (PCR) tests for SARS-CoV-2 in the current study is most accurate?

A. The prevalence of positive PCR tests was 4.9%
B. The prevalence of positive PCR tests was 11.4%
C. Only half of individuals with a positive PCR test reported symptoms in the past 14 days
D. 98% of individuals with a negative PCR test were asymptomatic in the past 14 days.

4. Which of the following statements regarding beliefs around COVID-19 vaccination in the current study is most accurate?

A. Only half of the participants were willing to receive a COVID-19 vaccine
B. Age was not significantly associated with vaccine acceptance
C. Men were less likely than women to accept a vaccine
D. Black individuals were significantly less likely than White and Other racial groups to accept a vaccine

Emerging Infectious Diseases
Photo Quiz Articles

Volume 14, Number 9
September 2008

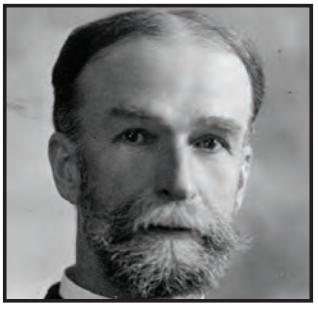

Volume 14, Number 12
December 2008

Volume 15, Number 9
September 2009

Volume 15, Number 10
October 2009

Volume 16, Number 6
June 2010

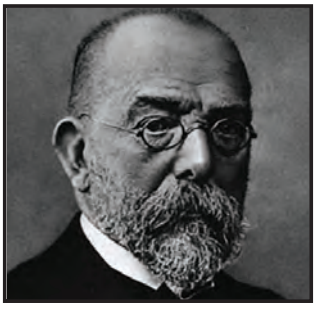

Volume 17, Number 3
March 2011

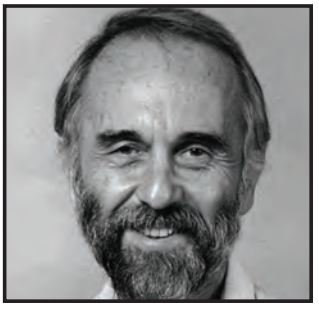

Volume 17, Number 12
December 2011

Volume 19, Number 4
April 2013

Volume 20, Number 5
May 2014

Volume 21, Number 9
September 2015

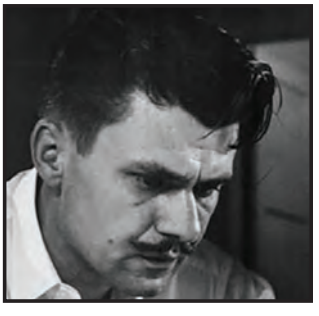

Volume 22, Number 8
August 2016

Volume 28, Number 3
March 2022

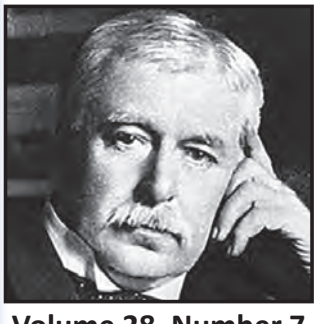

Volume 28, Number 7
July 2022

Click on the link below to read about the people behind the science.

https://bit.ly/3LN02tr

See requirements for submitting a photo quiz to EID.

https://bit.ly/3VUPqfj

EID Journal